

FUNDAMENTALS OF OCEAN ACOUSTICS

Third Edition

AIP Series in

Modern Acoustics and Signal Processing

Editor-in-Chief

ROBERT T. BEYER

Department of Physics, Brown University, Providence, Rhode Island

Editorial Board

YOICHI ANDO, Graduate School of Science and Technology, Kobe University,
Kobe, Japan

ARTHUR B. BAGGEROER, Department of Ocean Engineering,
Massachusetts Institute of Technology, Cambridge, Massachusetts

NEVILLE H. FLETCHER, Research School of Physical Science and Engineering,
Australian National University, Canberra, Australia

CHRISTOPHER R. FULLER, Department of Mechanical Engineering,
Virginia Polytechnic Institute and State University, Blacksburg, Virginia

WILLIAM M. HARTMANN, Department of Physics and Astronomy,
Michigan State University, East Lansing, Michigan

JOANNE L. MILLER, Department of Psychology, Northeastern University,
Boston, Massachusetts

JULIA DOSWELL ROYSTER, Environmental Noise Consultants, Raleigh,
North Carolina

LARRY ROYSTER, Department of Mechanical and Aerospace Engineering,
North Carolina State University, Raleigh, North Carolina

MANFRED R. SCHRÖDER, Göttingen, Germany

ALEXANDRA I. TOLSTOY, ATolstoy Sciences, Annandale, Virginia

WILLIAM A. VON WINKLE, New London, Connecticut

Books In The Series

Producing Speech: Contemporary Issues for Katherine Safford Harris, edited by
Fredericka Bell-Berti and Lawrence J. Raphael

Signals, Sound, and Sensation, by William M. Hartmann

Computational Ocean Acoustics, by Finn B. Jensen, William A. Kuperman,
Michael B. Porter, and Henrik Schmidt

*Pattern Recognition and Prediction with Applications to Signal
Characterization*, by David H. Kil and Frances B. Shin

Oceanography and Acoustics: Prediction and Propagation Models, edited by
Alan R. Robinson and Ding Lee

Handbook of Condenser Microphones, edited by George S.K. Wong and
Tony F.W. Embleton

Seismic Wave Propagation and Scattering in the Heterogeneous Earth,
by Haruo Sato and Michael C. Fehler

Architectural Acoustics, by Yoichi Ando

FUNDAMENTALS OF OCEAN ACOUSTICS

Third Edition

L.M. Brekhovskikh

Yu.P. Lysanov

Moscow, Russia

With 120 Figures

**AIP
PRESS**



Springer

L.M. Brekhovskikh
P. P. Shirshov Institute of Oceanology
Russian Academy of Sciences
Nakhimovskii pr. 36
117851 Moscow
Russia
abrekh@mail.ru

Yu.P. Lysanov
Andreev Acoustics Institute
Russian Academy of Sciences
Shverniki Street 4
117036 Moscow
Russia

Series Editors:

Robert T. Beyer
Department of Physics
Brown University
Providence, RI 02912
USA

Alexandra I. Tolstoy
ATolstoy Sciences
8610 Battailles Court
Annandale, VA 22003
USA

Library of Congress Cataloging-in-Publication Data

Brekhovskikh, L.M. (Leonid Maksimovich)

[Teoreticheskie osnovy akustiki okeana. English]

Fundamentals of ocean acoustics/L.M. Brekhovskikh, Yu.P. Lysanov.—3rd ed.
p. cm.—(Modern acoustics and signal processing)

Includes bibliographical references and index.

ISBN 0-387-95467-8 (acid-free paper)

I. Underwater acoustics. I. Lysanov, Yu.P. (Iurii Pavlovich) II. Title. III. AIP series
in modern acoustics and signal processing.

QC242.2 .B73313 2002

551.46'01—dc21

2002024159

ISBN 0-387-95467-8

Printed on acid-free paper.

© 2003, 1991, 1982 Springer-Verlag New York, Inc.

AIP Press is an imprint of Springer-Verlag New York, Inc.

All rights reserved. This work may not be translated or copied in whole or in part without the written permission of the publisher (Springer-Verlag New York, Inc., 175 Fifth Avenue, New York, NY 10010, USA), except for brief excerpts in connection with reviews or scholarly analysis. Use in connection with any form of information storage and retrieval, electronic adaptation, computer software, or by similar or dissimilar methodology now known or hereafter developed is forbidden.

The use in this publication of trade names, trademarks, service marks, and similar terms, even if they are not identified as such, is not to be taken as an expression of opinion as to whether or not they are subject to proprietary rights.

Printed in the United States of America.

9 8 7 6 5 4 3 2 1

SPIN 10872598

www.springer-ny.com

Springer-Verlag New York Berlin Heidelberg

A member of BertelsmannSpringer Science+Business Media GmbH

Preface to the Third Edition

This is the third edition of our book *Fundamentals of Ocean Acoustics*, revised and supplemented, including much new material responding to the progress in the theory of sound propagation and scattering in the ocean over the last 10 years. New topics are devoted mainly to such questions as the intrathermocline lenses and their effect on sound fields in the ocean, weakly divergent bundles of rays, ocean acoustic tomography, coupled modes, invariants of an interference pattern in a range-dependent oceanic waveguide, sound scattering by random highly anisotropic volume inhomogeneities (fluctuations of the refractive index of the sea medium) with a fractal spectrum, fractal nature of low-frequency attenuation in the underwater sound channel, small-slope approximation in treating sound scattering from the rough sea surface (Voronovich's approach), sound scattering by an air bubble near the sea surface, collective bubble behaviour, etc. Both the direct and inverse problems are considered. Some recent experimental data are also added. More than 60 new references are presented. Some new references and figures are preceded by the letter A.

The book is intended for experts in acoustics and oceanology, engineers, post-graduates, and students of universities and institutes of geophysical and hydrometeorological profiles. Thus, it can be used as a scientific monograph and textbook of advanced type.

The authors are grateful to T.I. Tsyplakova for her great help in preparing the manuscript.

Moscow, Russia
December 2001

L.M. Brekhovskikh
Yu.P. Lysanov

Preface to the Second Edition

The general structure of this second edition remains the same as the first. However, the reader will find some new material in almost every chapter, for example, Snell's law for a range-dependent environment, the hybrid ray-mode method, invariants of an interference pattern in the coordinates of range and frequency, new considerations concerning the parabolic equation method, peculiarities of the correlation function of the field scattered by a sea surface, the new phenomenon of fore-reverberation, etc. New references have also been added. Errata of the first edition have been corrected.

Moscow, Russia
October 1990

L.M. Brekhovskikh
Yu.P. Lysanov

Preface to the First Edition

The continents of our planet have already been exploited to a great extent. Therefore man is turning his sight to the vast spaciousness of the ocean whose resources—mineral, biological, energetic, and others—are just beginning to be used. The ocean is being intensively studied. Our notions about the dynamics of ocean waters and their role in forming the Earth's climate as well as about the structure of the ocean bottom have substantially changed during the last two decades.

An outstanding part in this accelerated exploration of the ocean is played by ocean acoustics. Only sound waves can propagate in water over large distances. Practically all kinds of telemetry, communication, location, and remote sensing of water masses and the ocean bottom use sound waves. Propagating over thousands of kilometres in the ocean, they bring information on earthquakes, eruptions of volcanoes, and distant storms. Projects using acoustical tomography systems for exploration of the ocean are presently being developed. Each of these systems will allow us to determine the three-dimensional structure of water masses in regions as large as millions of square kilometres.

The rapidly extending applications of ocean acoustics require a manual where the theory of sound propagation in the ocean in its most fundamental form is systematically and rather completely presented. The authors have tried to write such a book. After looking through its contents the reader can see that all the most significant aspects of the theory are presented in this book. These include a deterministic theory of the underwater sound channel whose characteristics either are constant or change with distance, the theory of anti-channel, shallow water, the problems of sound reflection from the bottom, and so on. The stochastic aspects of the theory are also presented rather completely for sound scattering at the random ocean surface and at the bottom, propagation in the presence of internal waves, turbulence, etc.

The authors are thoroughly convinced that theory cannot be developed without close connection with experiment. Hence, a book on theoretical underwater acoustics should also elucidate principal experimental data. On the other hand, mixing theory and experimental facts in the presentation is undesirable since theory is more "fundamental" and steady in time as compared with the rapidly changing

experimental background. Solving this contradiction, the authors preface the main theoretical chapters with a rather bulky first chapter where the most interesting experimental facts are presented and the main characteristics of the ocean as an acoustical medium are considered. If it were possible to revise the book continuously after its publication, then the first chapter would have to be rewritten every other year or so, while the principal content of the theoretical chapters would have to be changed approximately every ten years.

The book is intended for students, postgraduates, researchers, and practical workers dealing with ocean acoustics.

The authors are sincerely grateful to V.M. Kurtepov for his critical reading of the book, V.V. Vavilova who had the main task of translating the book into English, and I.F. Treshchetenkova and E.A. Turina for their great help in preparing the manuscript.

Moscow, Russia
January 1982

L.M. Brekhovskikh
Yu.P. Lysanov

Contents

Preface to the Third Edition	v
Preface to the Second Edition	vii
Preface to the First Edition	ix
1 The Ocean as an Acoustic Medium	1
1.1 Sound Velocity in Sea Water	1
1.2 Typical Vertical Profiles of Sound Velocity and Corresponding Conditions of Sound Propagation	2
1.2.1 Underwater Sound Channel (USC)	2
1.2.2 Surface Sound Channel	6
1.2.3 USC with Two Axes	8
1.2.4 Antiwaveguide Propagation	9
1.2.5 Propagation of Sound in Shallow Water	9
1.3 Absorption of Sound	10
1.4 Variability of the Ocean and Its Effect on Acoustics	12
1.4.1 Large-Scale Currents and Frontal Zones	12
1.4.2 Synoptic (Meso-Scale) Eddies	13
1.4.3 Internal Waves	15
1.4.4 Fine Vertical Structure of Waters	17
1.4.5 Small-Scale Turbulence	18
1.5 Ocean Surface	20
1.6 Sound Scattering at the Ocean Surface	22
1.7 Sound Scattering by Air Bubbles	25
1.8 Deep-Scattering Layers (DSL)	26
1.9 Ocean Bottom	28
1.10 Ambient Noise	30
1.11 Intrathermocline Lenses	32
2 Ray Theory of the Sound Field in the Ocean	35
2.1 Wave Equation for an Inhomogeneous Medium	35
2.1.1 Simplest Solutions of the Helmholtz Equation	37
2.2 Refraction of Sound Rays	38

2.3	Horizontal Distance Covered by a Ray	41
2.4	Constant-Gradient Approximation of the Sound Velocity Profile	42
2.5	Sound Intensity, Focusing Factor, and Caustics	43
2.6	"Three-Dimensional" Refraction	47
2.7	Snell's Law for the Range-Dependent Ocean	50
2.8	Ocean Acoustic Tomography	52
2.9	Weakly Divergent Bundles of Rays	56
3	Reflection of Sound from the Surface and Bottom of the Ocean: Plane Waves	61
3.1	Reflection and Transmission Coefficients at an Interface Separating Two Liquids	61
3.2	Transmission of a Sound Wave from Water into Air and Vice Versa	65
3.3	Sound Wave Reflection from an Ocean Bottom Consisting of Liquid Layers	67
3.3.1	Reflection from a Homogeneous Layer	67
3.3.2	Reflection from an Arbitrary Number of Layers	71
3.4	Sound Reflection from a Solid	72
3.4.1	Analysis of the Reflection Coefficient	75
3.4.2	Surface Rayleigh and Stonely Waves	76
3.5	Reflection from a Continuously Layered Medium	78
4	Reflection of Sound from the Surface and Bottom of the Ocean: Point Source	80
4.1	Sound Field of an Underwater Source Located Near the Water Surface	80
4.1.1	Wave Representations	80
4.1.2	Ray Representation	81
4.1.3	Directional Pattern	81
4.1.4	Radiated Power	84
4.2	Expansion of a Spherical Wave into Plane Waves	85
4.3	Reflected Wave	87
4.4	Lateral Wave	91
4.5	Reflection from the Layered Inhomogeneous Half-Space: Caustics	95
5	Propagation of Sound in Shallow Water	101
5.1	Ray Representation of the Sound Field in a Layer: Image Sources	101
5.2	Integral Representation of the Field in the Layer	103
5.3	Normal Modes in the Ocean with a Perfectly Reflecting Bottom	105
5.4	Relation Between the Different Representations of the Field	109

5.5	Normal Modes in a Two-Layered Liquid	110
5.6	Averaged Decay Law	113
5.6.1	Homogeneous Layer ($c = c_l = c_h$)	114
5.6.2	Layer with Negative Refraction	116
6	Underwater Sound Channel	118
6.1	Simple Ray Theory of the USC: Trapping Coefficient of the USC	118
6.1.1	“Linear” Model of the USC	119
6.1.2	Travel Time	121
6.2	Canonical Underwater Sound Channel	123
6.3	Convergence Zones	125
6.4	Field of a Point Source in the Underwater Sound Channel as a Sum of Normal Waves (Modes)	128
6.5	Integral Representation of the Sound Field in the USC	130
6.6	Transformation of the Integral Representation into the Sum of Normal Modes	131
6.6.1	Linear Waveguide	132
6.7	Normal Modes in the WKB Approximation: Phase Integral	136
6.7.1	Normal Modes and Rays	140
6.7.2	Spatial Periods of Interference	143
7	Range-Dependent Waveguide	149
7.1	Normal Modes in an Almost Stratified Medium: Reference Waveguide Method	149
7.2	Adiabatic Approximation: Ray Invariant	151
7.2.1	Ray Invariant	152
7.2.2	An Example of Using the Ray Invariant	154
7.2.3	Conditions for the Validity of the Adiabatic Approximation and Ray Invariant	157
7.2.4	Coupled Modes	159
7.3	Rays in a Horizontal Plane	161
7.3.1	The Case of a Coastal Wedge	161
7.4	Parabolic Equation Method	163
8	Antiwaveguide Sound Propagation	169
8.1	Linear Antiwaveguide Adjacent to Water Surface	169
8.2	Symmetric Antiwaveguide: Quasi-Modes	172
8.3	Symmetric Antiwaveguide: Lateral Wave	179
9	Scattering of Sound at Rough Surfaces	183
9.1	Rayleigh Parameter	183
9.2	Method of Small Perturbation (MSP)	184
9.3	Average Intensity	186
9.3.1	An Infinite Surface	186
9.3.2	Bounded Scattering Surface: Far Zone	187

9.3.3	Correlation Function of the Scattered Field	189
9.4	Scattering Coefficient for the Ocean Surface	192
9.5	Frequency Spectrum of the Scattered Field	196
9.6	Reflection Coefficient in the Specular Direction	199
9.7	Method of Tangent Plane: Basic Concept	201
9.8	Average Field	203
9.9	Scattering Coefficient of High-Frequency Sound	205
9.9.1	Scattering Pattern	207
9.10	Frequency Spectrum	210
9.11	Sound Scattering from a Surface with Two Scales of Roughness	212
9.12	Surface Channel with a Rough Boundary	215
9.12.1	Attenuation Along a Single Ray	215
9.12.2	Averaged Decay Law for a Coherent Field	217
9.13	Fore-reverberation of Sound in the Ocean	218
9.14	Small-Slope Approximation in Wave Scattering by Rough Surfaces	221
10	Sound Propagation in the Random Ocean	227
10.1	Amplitude and Phase Fluctuations	227
10.1.1	Phase Fluctuations	228
10.1.2	Amplitude Fluctuations	232
10.2	Scattering of Sound by Random Inhomogeneities	234
10.2.1	Average Intensity of a Scattered Field	235
10.2.2	Volume Scattering Coefficient	237
10.2.3	Sound Scattering by Highly Anisotropic Inhomogeneities with a Fractal Spectrum	239
10.2.4	Attenuation of Low-Frequency Sound in an Underwater Sound Channel	240
10.3	Phase Fluctuations due to Internal Waves	242
10.4	Fluctuations in Multipath Propagation	247
11	Scattering and Absorption of Sound by Gas Bubbles in Water	250
11.1	Sound Scattering by a Single Ideal Bubble	250
11.2	Scattering and Absorption of Sound by a Real Bubble	253
11.3	Dispersion of Sound Velocity	257
11.4	Sound Scattering by an Air Bubble Near a Sea Surface	259
11.5	Collective Bubble Oscillations	262
	References	265
	Index	275

The Ocean as an Acoustic Medium

The ocean is an extremely complicated acoustic medium. The most characteristic feature of the oceanic medium is its inhomogeneous nature. There are two kinds of inhomogeneities, regular and random, and both strongly influence the sound field in the ocean. For example, the regular variation of the sound velocity with depth leads to the formation of the underwater sound channel and, as a consequence, to long-range sound propagation. The random inhomogeneities give rise to scattering of sound waves and, therefore, to fluctuations in the sound field.

In this chapter the acoustic characteristics of the ocean are considered in detail, including the effects of the rough sea surface and ocean bottom, internal waves, synoptic eddies and small-scale turbulence, deep scattering layers of biological origin, and the absorption and attenuation of sound.

1.1 Sound Velocity in Sea Water

Variations of the sound velocity c in the ocean are relatively small. As a rule, c lies between 1450 and 1540 m/s. But even so, small changes of c significantly affect the propagation of sound in the ocean.

The sound velocity can be measured directly in situ using special instruments—velocimeters—or calculated by empirical formulae if the temperature T , salinity S , and hydrostatic pressure P (or depth z) are known. The error of measurements by modern velocimeters is about 0.1 m/s. The accuracy of calculations by the most complete empirical formulae is about the same. However, formulae providing such high accuracy are very cumbersome. A less accurate but simpler equation is [1.1]

$$c = 1449.2 + 4.6T - 0.055T^2 + 0.00029T^3 + (1.34 - 0.010T)(S - 35) + 0.016z. \quad (1.1.1)$$

Here the temperature is expressed in °C, salinity S in parts per thousand [‰], depth z in metres, and sound velocity c in metres per second. Equation (1.1.1) is valid for $0^\circ\text{C} \leq T \leq 35^\circ\text{C}$, $0 \leq S \leq 45\text{‰}$, and $0 \leq z \leq 1000$ m.

The sound velocity increases with temperature, salinity, and depth. According to (1.1.1) the increase of salinity by 1‰ at $T = 10^\circ\text{C}$ and of depth by 100 m

lead to an increase of the sound velocity of 1.2 m/s and 1.6 m/s, respectively. The increment of the sound velocity Δc due to a change in temperature of 1°C depends on the value of the temperature:

$T [^\circ\text{C}]$	5	10	15	20	25	30
$\Delta c [\text{m/s}]$	4.1	3.6	3.1	2.7	2.4	2.1.

When the temperature and the salinity are constant, the sound velocity increases with a rise in the hydrostatic pressure (hydrostatic gradient of the sound velocity). The relative gradient (dc/dz divided by c_0) in this case is $1.1 - 1.2 \times (10^{-5} \text{ m}^{-1})$. The vertical gradient of the sound velocity in most regions of the ocean is about a thousand times the horizontal one, except in areas of the convergence of cold and warm currents where the horizontal and vertical gradients are sometimes comparable.

Thus, in a first approximation, the ocean may be considered as a plane-stratified medium, the characteristics of which vary only with depth and are constant in the horizontal plane. The influence of internal waves, large eddies, currents, and some other factors perturbing this picture must be considered separately.

1.2 Typical Vertical Profiles of Sound Velocity and Corresponding Conditions of Sound Propagation

The form (profile) of curve $c(z)$ and the distribution of the sound velocity gradient with depth, rather than an absolute value of the sound velocity, are most important for the propagation of sound in the ocean. For one type of profile $c(z)$ the sound can propagate hundreds and thousands of kilometres, and for another type, sound of the same frequency propagates only as far as a few tens of kilometres or even less.

The $c(z)$ profiles are different in the various regions of the ocean and vary with time as well. The largest fluctuations are in the upper ocean, mainly due to seasonal and diurnal variations of temperature and salinity. At depths below 1 km vertical variations of temperature (as well as of salinity) are usually weak, and the increase of the sound velocity with depth is almost exclusively due to the increasing hydrostatic pressure. As a consequence, at great depths the sound velocity increases almost linearly with depth.

We will now consider the main forms of the profiles $c(z)$ and the corresponding types of sound propagation.

1.2.1 Underwater Sound Channel (USC)¹

In the deep-water regions the typical profile $c(z)$ is that for which the sound velocity minimum is at a certain depth z_m (Fig. 1.1a). This depth is an axis of the underwater sound channel. Above this axis the sound velocity increases mainly

¹It is often called the SOFAR channel.

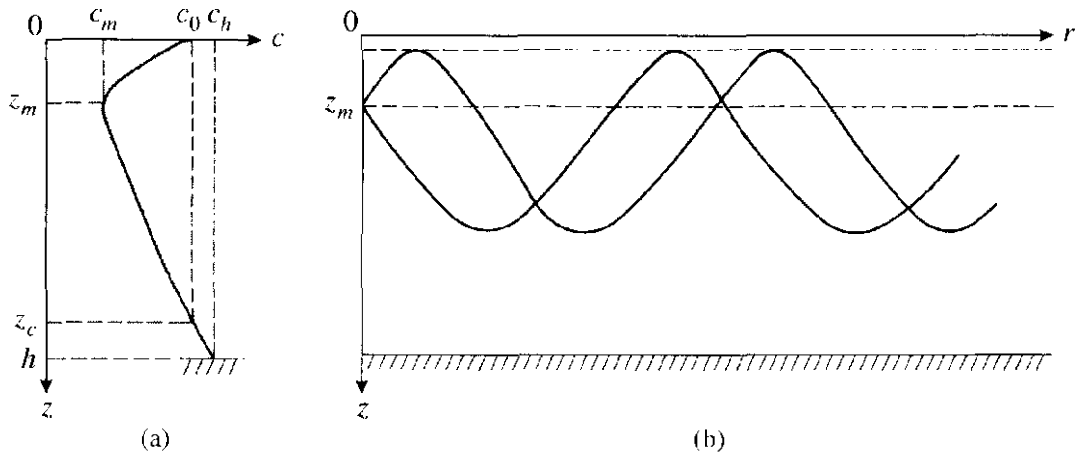


FIGURE 1.1. Underwater sound channel of the first kind ($c_0 < c_h$). (a) profile $c(z)$, (b) ray diagram

due to temperature increases; below it the increase in hydrostatic pressure is mainly responsible for increasing the sound velocity. If a sound source is on the axis of the USC or near it, some part of the sound energy is trapped in the USC and propagates within it, not reaching the bottom or surface, and, therefore, not undergoing scattering and absorption at these boundaries. The ray diagram in the USC is given in Fig. 1.1b. The rays leaving the source at a small or moderate grazing angle (angle with a horizontal plane) return to the channel axis repeatedly. This is a kind of *waveguide* propagation. The USC is one particular case of a natural waveguide. There is an analogous acoustic waveguide in the atmosphere, as well.

Waveguide propagation for the case shown in Fig. 1.1 is observed in the interval of depths $0 < z < z_c$. The depths $z = 0$ and $z = z_c$ are the boundaries of the USC. The channel traps all sound rays which leave the source (located on the axis) at grazing angles $\chi < \chi_{\max}$, where

$$\chi_{\max} = [2(c_0 - c_m)/c_m]^{1/2},$$

and where c_m and c_0 are the sound velocities at the axis and boundaries of the channel, respectively. Hence, the greater the difference $c_0 - c_m$, the larger is the interval of angles in which the rays are trapped, i.e., the waveguide is more effective.

The depth of the axis of the USC is usually 1000–1200 m. In the tropical zone it falls down to 2000 m, and rises up closer to the surface at high latitudes. At moderate latitudes (say from 60°S to 60°N) the sound velocity on the USC axis ranges from 1450 to 1485 m/s in the Pacific and from 1450 to 1500 m/s in the Atlantic Ocean.

If the sound velocity below the axis of a sound channel increases only due to the hydrostatic pressure, we say that such a sound channel is *hydrostatical*. However, in some cases in the ocean a USC arises as a result of the presence of warm waters with high salinity below the channel axis. This type of USC is called *thermal*. The typical thermal USC occurs, for example, in the Baltic and Black Seas.

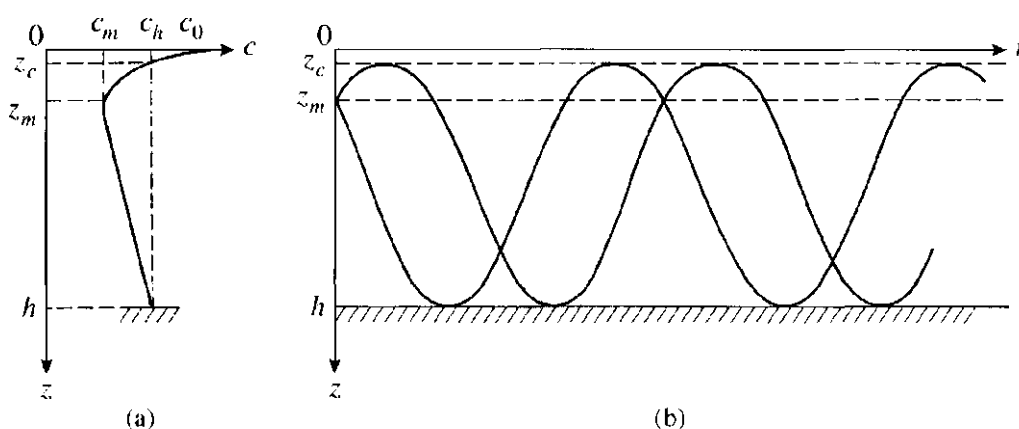


FIGURE 1.2. Underwater sound channel of the second kind ($c_0 > c_h$). (a) profile $c(z)$, (b) ray diagram

There are two types of USC depending on the ratio c_0/c_h . The case when $c_0 < c_h$ is shown in Fig. 1.1a. For regions of shallower water the opposite case $c_0 > c_h$ is true (Fig. 1.2). Here the USC extends from the bottom up to the depth z_c where the sound velocity equals c_h . Two limiting rays are shown in Fig. 1.2b for this case. Trapped rays do not extend above the depth z_c . Only the rays reflected from the bottom reach this zone.

The maximum distance of sound propagation in the USC is limited mainly by absorption in sea water. Sound of sufficiently low frequency, for which absorption is fairly small, can propagate over distances of hundreds and thousands of kilometres. For example, sound signals generated by a 57-Hz source located at a site near the Heard Island (the Indian Ocean) at a depth of 157 m (the local sound channel axis) have been detected by several receiver sites in the Indian, Atlantic, and Pacific Oceans at distances of 18,000 km (Fig. A.1.1) [1.2]. Such sound propagation is called *long-range sound propagation*.

A number of interesting features arise for the case of a source near the ocean surface. A typical case for the USC “zonal structure” of the sound field—a sequence of *insonified* and *shadow* zones—is clearly seen in the ray diagram (Fig. 1.3). Shadow zones are denoted by $A_1, A_2, \dots, B_1, B_2, \dots$. Trapped sound rays do not penetrate into them. As the source approaches the USC axis, the width of the shadow zones decreases and that of the insonified zones increases. If the depths of the source and the USC axis coincide, shadow zones disappear at this depth. Quite a number of rays arrive at the receiver in this case if the latter is not far from the USC axis. Such multipath propagation is one of the most characteristic features of the sound field in the USC.

The secondary emergence of sound rays at small depths after their refraction in deep layers is usually associated with their convergence and the formation of so-called caustics (thick lines in Fig. 1.3b). As a result, these areas are called *convergence zones*. They are characterised by high sound intensity levels.

Distinct zonal structure is sometimes observed at great distances. In the tropical Atlantic between distances of 400 and 2300 km up to 37 convergence zones were observed (frequency: 13.89 Hz) [1.3]. At greater distances the zonal structure was

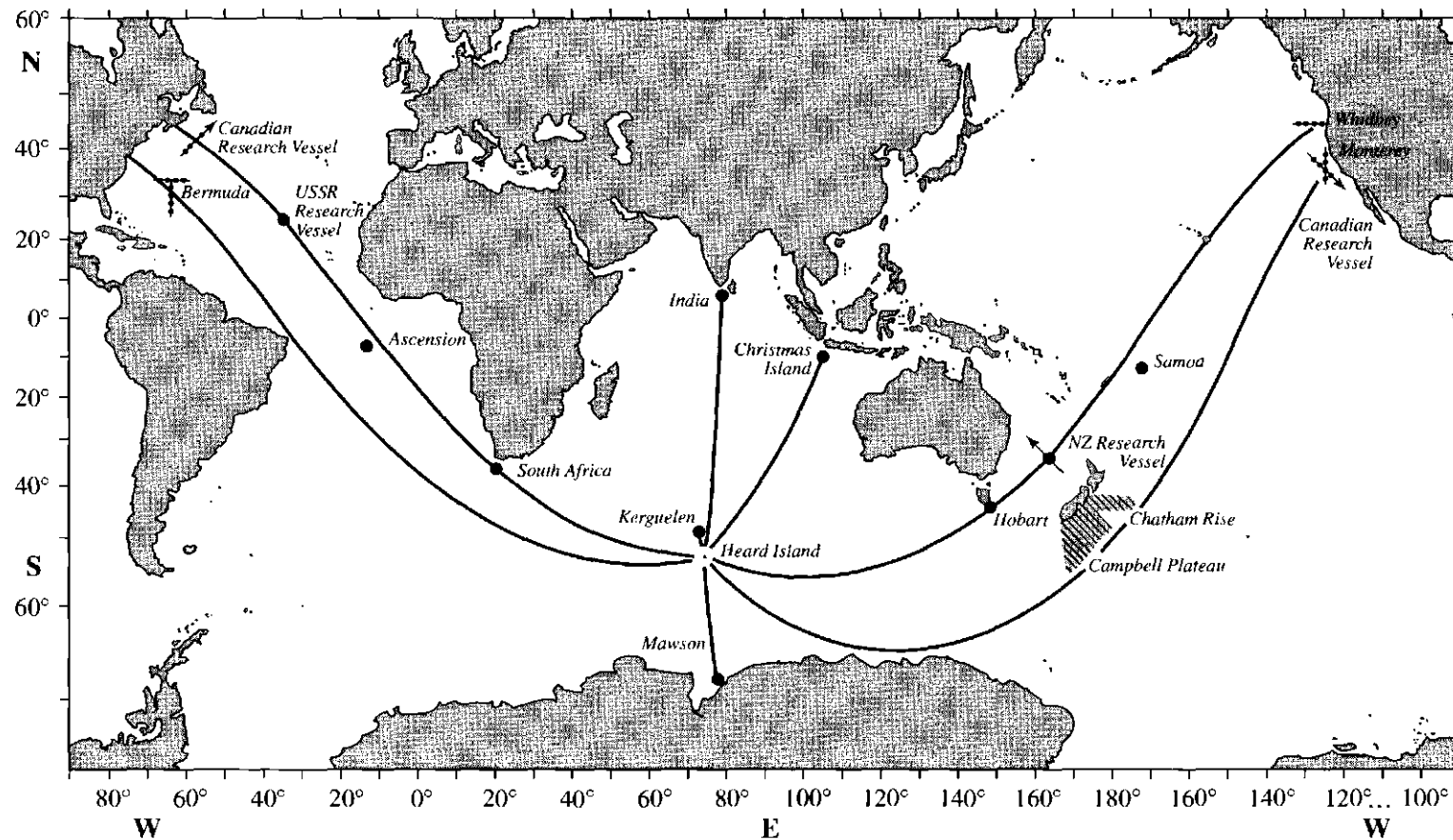


FIGURE A.1.1. Ray paths from source to receiver sites. Single dots indicate sites with single receivers. Dots connected by horizontal lines designate bottom-mounted array, vertical lines designate vertical array, and slanted lines designate arrays towed in the direction of the arrow. (Reprinted with permission from Munk et al., The Heard Island Feasibility Test, J. Acoust. Soc. Am., 1994, pp. 2330–2342.)

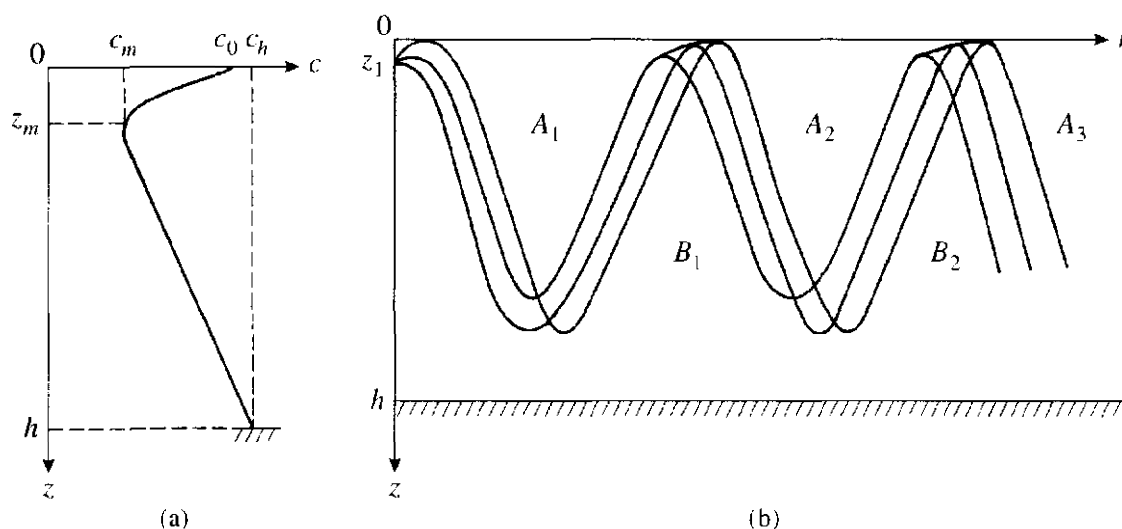


FIGURE 1.3. Typical zonal structure of a sound field in the USC. $A_1, A_2, \dots, B_1, B_2, \dots$ are shadow zones

smeared due to variations of the profile $c(z)$ along the path of sound propagation. The transmission loss of the sound field at distances from 400 to 1000 km is shown in Fig. 1.4. The two upper recordings correspond to the sound frequency of 111.1 Hz (the depth of the source is 21 m). The top recording presents the sound intensity as a function of distance after averaging over distances of 7 km, and the second from the top after averaging over 215 m. The locations of convergence zones (maxima of the sound intensity) with numbers from 7 to 15 is shown by vertical lines. The distance between convergence zones is 65 km. The two bottom recordings were obtained at the frequency 13.89 Hz (the depth of the source was 104 m) by averaging over distances of 7 km and 400 m, respectively. Convergence zones are 61.7 km apart. The difference in distances between convergence zones at various frequencies is due to wave effects.

1.2.2 Surface Sound Channel

This channel is formed when the channel axis is at the surface. A typical profile $c(z)$ for this case is shown in Fig. 1.5a. The sound velocity increases down to the depth $z = h$ and then begins to decrease. The corresponding ray diagram is shown in Fig. 1.5b. Rays leaving the source at grazing angles $\chi < \chi_b$ (where χ_b is the grazing angle of the boundary ray tangent to the lower boundary of the channel) propagate with multiple reflections from the surface. If the ocean surface is smooth, these rays remain in the sound channel regardless of distance from the source and give rise to waveguide propagation. If the ocean surface is rough, part of the sound energy is scattered into angles $\chi > \chi_b$ at each contact with the surface and, therefore, leaves the sound channel. As a result in this case, the sound field decays in the sound channel, but in the area below the channel its level increases.

The case shown in Fig. 1.5 frequently occurs in the tropical and moderate zones of the ocean, when the temperature and salinity in the upper ocean layer are almost

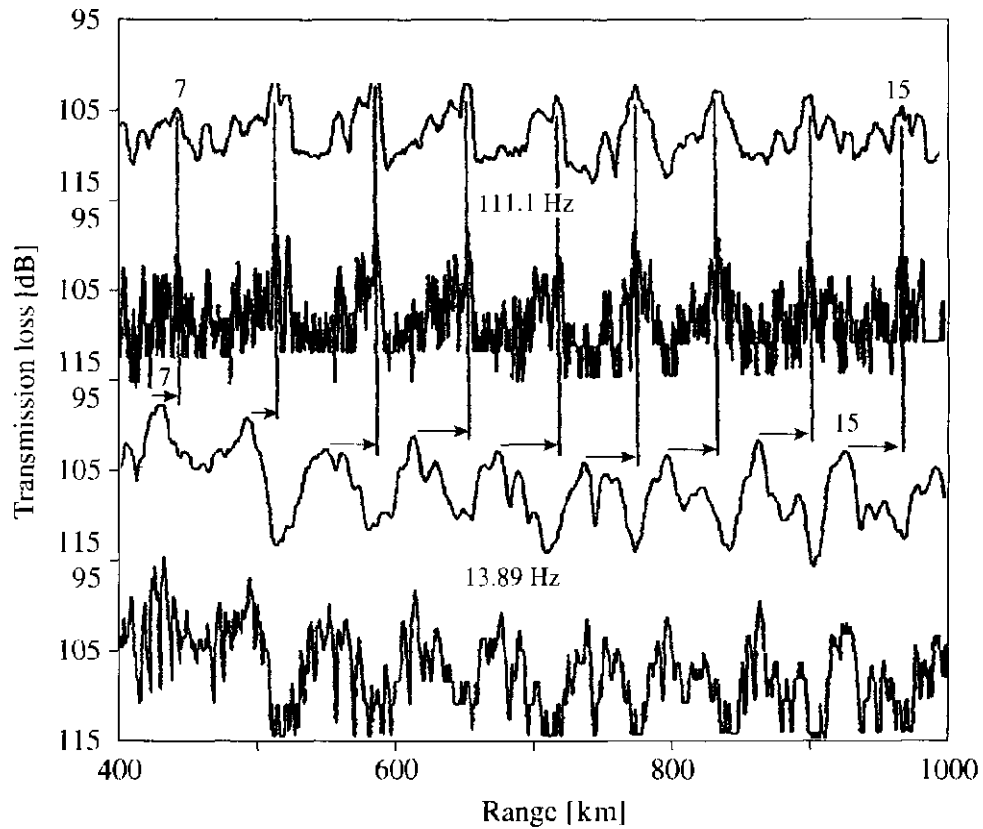


FIGURE 1.4. Transmission loss vs range in the tropical Atlantic [1.3]. The arrows show the shift in range between corresponding high- and low-frequency convergence zones

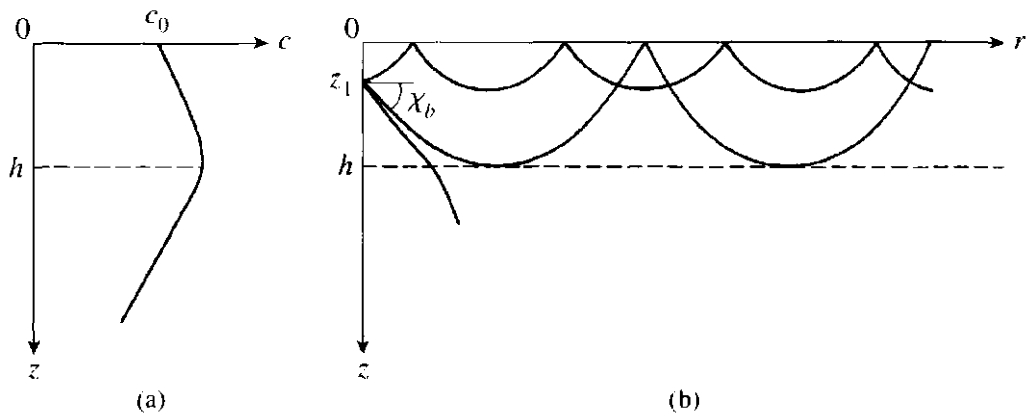
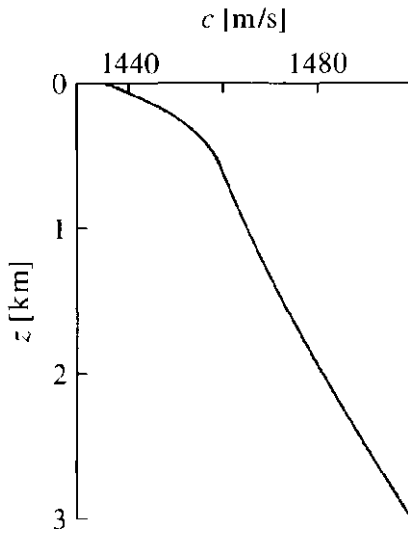
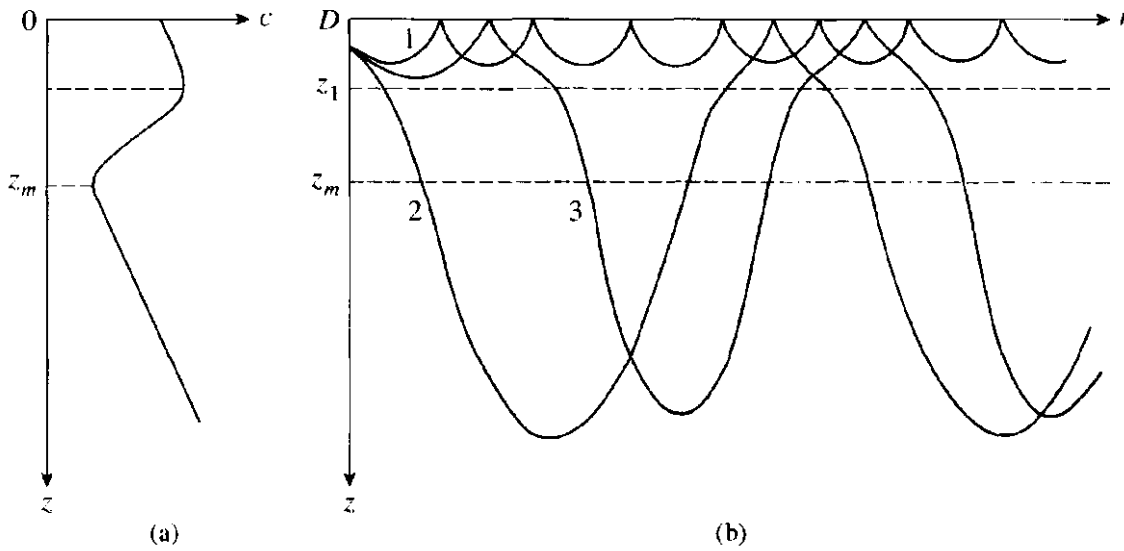


FIGURE 1.5. Surface sound channel. (a) profile $c(z)$, (b) ray diagram

constant due to wind mixing. In this case the sound velocity increases with depth due to the hydrostatic pressure gradient.

An increase in the sound velocity can be observed from the surface to the very bottom in the Arctic and Antarctic regions, in mediterranean seas in the tropical zone, and in shallow seas during autumn and winter. The typical profile $c(z)$ for the Arctic Ocean is schematically shown in Fig. 1.6. The existence of a thin

FIGURE 1.6. Typical sound velocity profile $c(z)$ for the Arctic OceanFIGURE 1.7. Two-axis sound channel. (a) profile $c(z)$, (b) ray diagram

surface layer with very low sound velocity and a large sound velocity gradient [$a \approx 4 - 5 (10^{-5} \text{ m}^{-1})$] is characteristic.

1.2.3 USC with Two Axes

This case takes place most commonly when surface and deep sound channels are present simultaneously. A typical profile $c(z)$ is shown in Fig. 1.7a. The axis of the upper channel is at the surface, and the other at depth z_m . The corresponding ray diagram for a source located in the upper channel is shown in Fig. 1.7b. Here ray 1 propagates in the upper channel, and ray 2 mainly in the lower one. Some rays initially belonging to the upper channel can also penetrate into the lower channel due to scattering at the rough surface (for example, ray 3). These are called leakages. Variations of the profile $c(z)$ along the propagation path can also give rise to leakages. A pronounced two-axial sound channel is observed in the

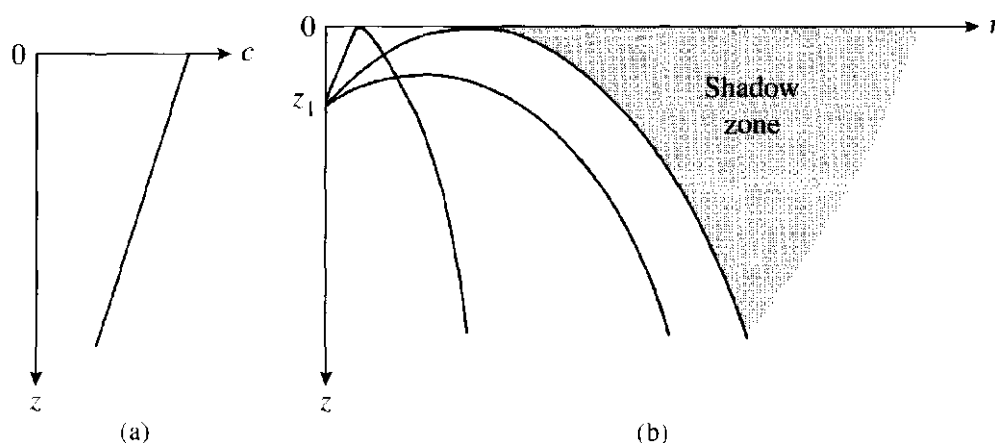


FIGURE 1.8. Formation of a geometrical shadow zone when the sound velocity monotonically decreases with depth

northern Atlantic off the coast of the Portugal peninsula. The upper axis is at a depth of 450–500 m, and the lower axis is at a depth of about 2000 m. Such a distribution of the sound velocity with depth is due to the intrusion of warmer and saltier Mediterranean waters into deep layers (~ 1200 m) of the Atlantic Ocean [A.1.1].

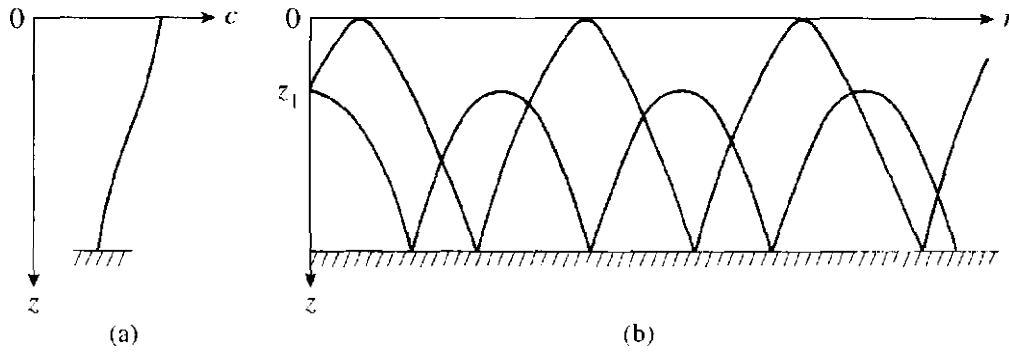
1.2.4 Antiwaveguide Propagation

The simplest kind of antiwaveguide propagation is observed when the sound velocity monotonically decreases with depth (Fig. 1.8a). This is often the result of the intensive heating of the upper layers by solar radiation. The ray diagram is shown in Fig. 1.8b. All rays refract downwards. The ray tangent to the surface is the limiting one. The shaded area represents the geometrical shadow zone. For typical conditions in the ocean, the distance from the source to the shadow zone is only a few kilometres.

The geometrical shadow zone is not a region of zero sound intensity. In the ideal case shown in Fig. 1.8 the sound energy penetrates into the shadow zone due to diffraction. In real cases sound waves reflected from the bottom and scattered by the random inhomogeneities of the medium also produce some insonification of this zone.

1.2.5 Propagation of Sound in Shallow Water

This type of sound propagation corresponds to the case when each ray from the source, when continued long enough is reflected at the bottom. A typical profile is shown in Fig. 1.9a. It is observed in shallow seas and at the ocean shelf, especially during the summer-autumn period when the upper water layers are well heated. A proper ray diagram is given in Fig. 1.9b. Since every reflection from the bottom causes a marked attenuation of sound waves, propagation of sound over large distances is associated with great losses of acoustic energy.

FIGURE 1.9. Sound propagation in a shallow sea. (a) profile $c(z)$, (b) ray diagram

1.3 Absorption of Sound

When sound propagates in the ocean, part of the acoustic energy is continuously absorbed, i.e., is transformed into heat. This absorption is partly due to the shear viscosity of the liquid. However, the volume viscosity due to some relaxation processes in sea water is mainly responsible for absorption at frequencies 100 Hz–100 kHz.

Another reason for the decay of the sound intensity with range in the ocean is the scattering of sound waves by inhomogeneities of a different kind. As a rule, it is possible to only measure the combined effect of absorption and scattering. This is called sound attenuation. On the basis of an analysis of extensive laboratory and field experimental data, *Marsh* and *Schulkin* [1.4] have obtained the following empirical formula for the attenuation coefficient in sea water at frequencies between 3 kHz and 0.5 MHz²:

$$\beta = 8.68 \cdot 10^3 \left(\frac{SAf_T f^2}{f_T^2 + f^2} + \frac{Bf^2}{f_T} \right) (1 - 6.54 \cdot 10^{-4} P) \text{ [dB/km]} \quad (1.3.1)$$

where $A = 2.34 \cdot 10^{-6}$, $B = 3.38 \cdot 10^{-6}$, S is salinity [‰], P is hydrostatic pressure [kg/cm²], f is frequency [kHz], and

$$f_T = 21.9 \cdot 10^6 - 1520/(T+273)$$

is a relaxation frequency [kHz], with T the temperature [°C]. While the temperature ranges from 0° to 30°C, f_T varies approximately from 59 to 210 kHz.

In (1.3.1) the first term in the first parentheses describes absorption due to relaxation of MgSO₄, and the second term corresponds to the viscous absorption. The expression in the second parentheses gives the dependence of absorption upon the hydrostatic pressure. However, the dependence is comparatively weak; up to 4-km depth, its variation does not exceed 30%.

² β is expressed in decibels per kilometre [dB/km]. The difference between pressures p_1 and p_2 is N decibels if $20 \log |p_1/p_2| = N$.

At low frequencies (100 Hz–3 kHz) the attenuation of sound is better described by the Thorp formula [1.5],

$$\beta = \frac{0.11 f^2}{1 + f^2} + \frac{44 f^2}{4100 + f^2} \text{ [dB/km]}, \quad (1.3.2)$$

f being the sound frequency [kHz]. Both terms have typical relaxation structures: the first (most important at the frequencies considered) describes absorption which is apparently due to the relaxation of boric acid, H_3BO_3 (relaxation frequency: 1 kHz); the second describes the relaxation of MgSO_4 (relaxation frequency: ≈ 65 kHz). The absorption coefficient due to boric acid relaxation has a marked geographic variation associated with the difference in the pH values throughout the oceans [1.6]. This pH dependence requires a modification of the first term in (1.3.2) by introducing a pH-dependent additional factor K . Its values range throughout the oceans from 0.5 to 1.1. The analysis of the regional variability of the boric acid sound absorption was carried out by *Lovett* [1.7].

According to (1.3.2) the attenuation of low-frequency sound is very small. For instance, a tenfold attenuation of the sound intensity at a frequency of 100 Hz occurs at a range of 8333 km. No other kind of radiation can compete with low-frequency sound waves for long-range propagation in the ocean. Electromagnetic waves, including those radiated by powerful lasers, are absorbed almost completely at distances of less than 1 km.

Figure 1.10 summarizes experimental data for the frequency dependence of the attenuation coefficient; they are given for the Atlantic, Indian, and Pacific Oceans, as well as for the Mediterranean and the Red Seas [1.5]. Calculations according to (1.3.1) for frequencies above 3 kHz for $z = 1240$ m, and according to (1.3.2) for the frequency range 0.1–3 kHz, give the attenuation coefficient which is in sufficiently good agreement with experiment. However, below 100 Hz experimental data significantly exceed theoretical values and have large dispersion (more than an order of magnitude). *Kibblewhite* and *Hampton* [1.8] reviewed all the relevant data on low-frequency absorption in the USC, grouped them according to water masses, and achieved consistent results within each group. Water masses were specified by the sound velocity profile $c(z)$. As a result, they proposed the following formula for the absorption coefficient in the USC below 1 kHz:

$$\beta = \beta_s + 0.11 f^2 K (1 + f^2)^{-1} + 0.011 f^2 \text{ [dB/km]}, \quad (1.3.3)$$

where K is the coefficient which accounts for the regional variation of the boron-related effects. β_s is the additional attenuation coefficient independent of the frequency. Its values depend on the type of water mass and range from $0.2 \cdot 10^{-3}$ to $4.2 \cdot 10^{-3}$ dB/km.

Though this regional grouping of the experimental data gives consistent values, physical reasons for the excess attenuation at frequencies below 100 Hz are not quite clear yet. Frequency-independent sound scattering by large-scale turbulent inhomogeneities is a possible reason for the attenuation in this frequency band. At frequencies of a few Hertz, diffraction losses associated with sound energy

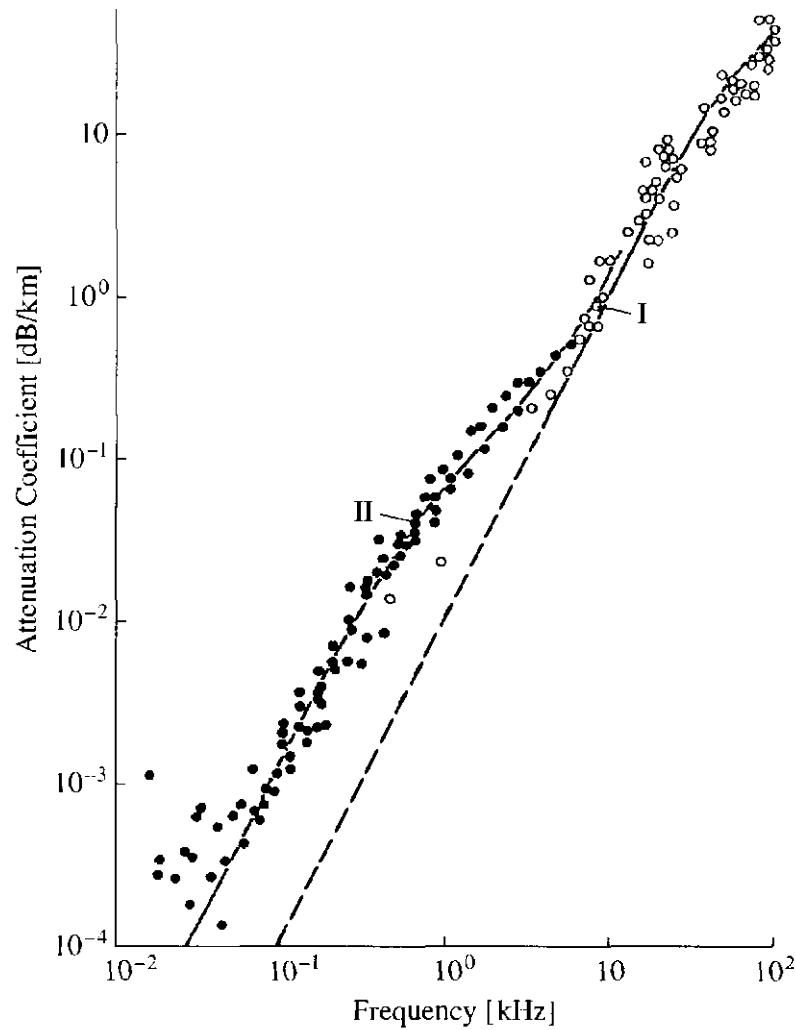


FIGURE 1.10. Experimental attenuation coefficient vs frequency. (\circ) sinusoidal measurements; (\bullet) explosive measurements. Curves I and II are predictions based on (1.3.1) and (1.3.2), respectively [1.5]

leakages from the USC are important. The attenuation due to diffraction losses increases with decreasing frequency.

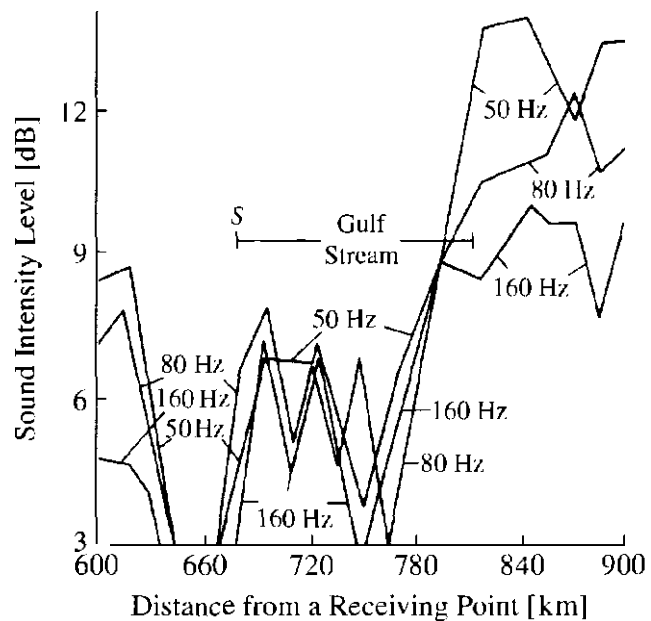
1.4 Variability of the Ocean and Its Effect on Acoustics

From the acoustical point of view the ocean is extremely variable: currents, internal waves, and small-scale turbulence perturb the horizontally stratified character of the sound velocity and cause spatial and temporal fluctuations of the propagating sound.

1.4.1 Large-Scale Currents and Frontal Zones

Boundaries of large-scale currents, such as the Gulf Stream and the Kuroshio, represent frontal zones separating water masses with essentially different physical characteristics. Within these frontal zones, temperature, salinity, density, and

FIGURE 1.11. Sound intensity levels (normalized for attenuation and cylindrical spreading) vs range in one-third octave bands centred at 50, 80, and 160 Hz for propagation across the Gulf stream [1.9]; N and S are north and south boundaries of the Gulf Stream



sound velocity suffer strong variations. For example, at the northern boundary of the Gulf Stream (northward of 35°N) the temperature drop is 10°C per 5 nautical miles. The southern boundary is represented by a weak front—the temperature drop between the Gulf Stream and the Sargasso Sea waters is about $1\text{--}2^{\circ}\text{C}$.

In Fig. 1.11 the results of experimental studies of long-range acoustic propagation along the track crossing the Gulf Stream from southeast to northwest are given. Explosive charges of TNT used as a sound source were detonated at a depth of 244 m along the part of the path covering the Gulf Stream, 600–900 km away from two deep hydrophones located on the bottom near Bermuda. Received signals were analyzed in one-third octave bands centered at 50, 80, and 160 Hz. Measurements of the profile $c(z)$ along the path were carried out nearly simultaneously with acoustical experiments.

Figure 1.11 shows that the received levels were lowest when the charges were detonated near the southern and northern boundaries of the Gulf Stream. A strong variation of the sound level (6–10 dB) caused by a small shift of the position of the explosion is noticeable. The theoretical analysis showed that the observed features of the sound field can be explained by the variation of profile $c(z)$ along the path, in particular, by the increased depth of the sound channel axis between cold slope water and the warm waters of the Sargasso Sea.

1.4.2 Synoptic (Meso-Scale) Eddies

Large eddies in the ocean are most frequently observed near intensive frontal currents, such as the Gulf Stream and the Kuroshio. The frontal eddies have the shape of rings and are formed as a result of the separation of great meanders from the main flow. Recently synoptic eddies were also found in the open ocean [1.10]. The parameters of synoptic eddies vary over a rather wide range: the diameter of an

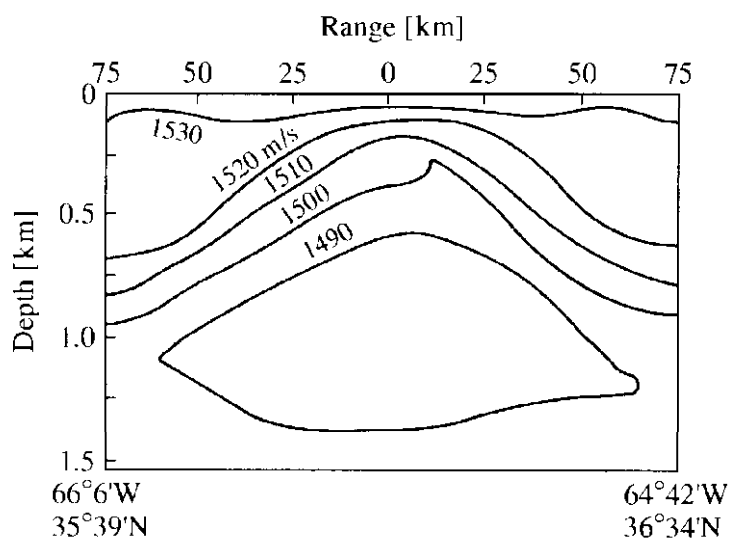


FIGURE 1.12. Sound isovel section in vertical plane passing through a cyclonic ring separated from the Gulf Stream. The numbers near curves denote the sound velocity in m/s [1.11]

eddy 25–500 km, the velocity of water in the eddy 30–150 cm/s, and the velocity of motion of the eddy centre up to 10 cm/s.

In the eddy zone the sound velocity has a complicated structure. In Fig. 1.12 the distribution of the velocity of sound is shown in the vertical plane crossing a cyclonic ring separated from the Gulf Stream. An elevation of the isovels as high as 700 m is observed in the central portion of the ring. As a result, the vertical gradient of the sound velocity markedly increases towards the centre of the ring.

In Fig. 1.13 transmission loss versus range is shown for sound propagation across the northern half of a cyclonic ring (Fig. 1.12). The data have been calculated in the ray approximation for a point omnidirectional source located in the centre of the ring at a depth of 200 m. The receiver depth is 300 m. The calculation of transmission loss takes into account wave-front spreading, absorption in the water,³ and leakage of sound energy into the bottom. For comparison, the transmission loss for the Sargasso Sea conditions outside the ring is also given here. When sound propagates through the cyclonic ring, two features are observed: first, the removal of energy from the middepth channel to the deep USC due to the increased downward refraction of rays and the decrease of the sound intensity level; second, the decrease of the horizontal extent of the convergence zones and the displacement of their position as compared with the standard position in the USC in the Sargasso Sea. At a depth of 1000 m, on the contrary, transmission loss curves show increased sound intensity levels (Fig. 1.14). Analysis of the ray diagram shows that effective sound propagation in the deep USC ($z_m = 1000$ m) arises in this case even if a sound source is located at a relatively small depth within the cyclonic ring. At a depth of 300 m, the first and second convergence zones are displaced towards the source by about 5 km, whereas at a depth of 1000 m they are displaced by 20 and 30 km, respectively. Thus, the cyclonic ring produces considerable perturbations of the sound field.

³Absorption was taken for a frequency of 100 Hz.

FIGURE 1.13. Sound intensity levels vs range for a receiver at a depth of 300 m. The solid curve corresponds to the Sargasso Sea ray diagram and the dashed curve represents the cyclonic ring ray diagram [1.11]

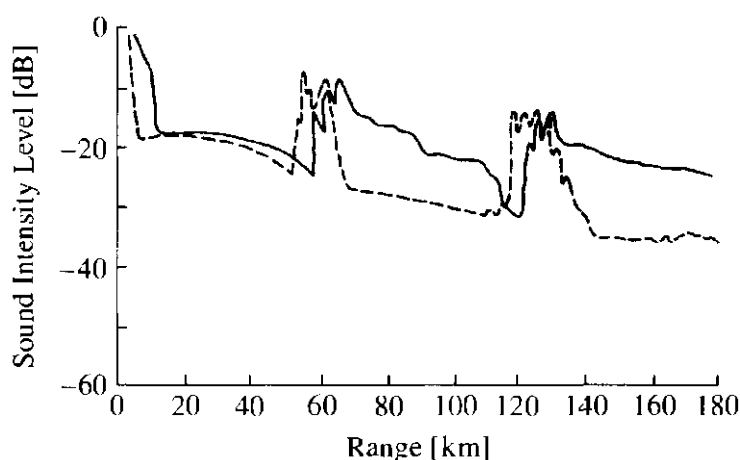
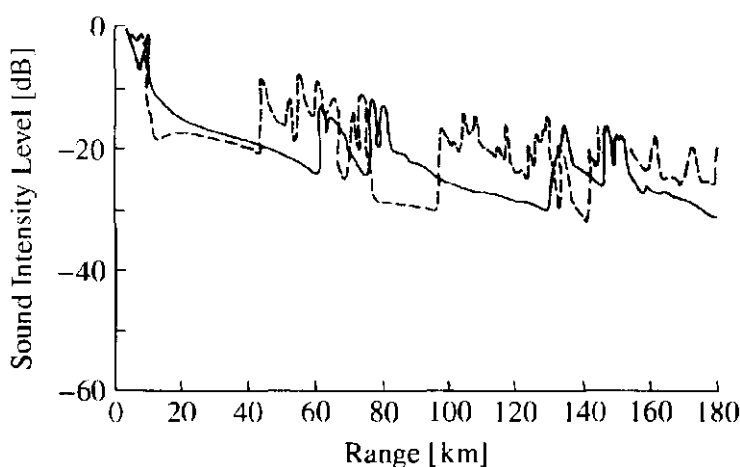


FIGURE 1.14. As in Fig. 1.13 for a receiver at a depth of 1000 m [1.11]



1.4.3 Internal Waves

Considerable fluctuations of the intensity and phase of sound waves arise in the presence of internal waves. These are wavelike motions which arise when gravitational forces act on changes from the mean density in the medium. They have periods from a dozen minutes up to an inertial period T ($T = 12 \text{ hours}/\sin \varphi$, φ denotes latitude). In Fig. 1.15 [1.12] temporal fluctuations of the amplitude (a) and the phase (b) of a 367-Hz signal recorded at the range of 1318 km are shown. The source was located at a depth of 527 m on the bottom slope near Eleuthera, and the receiver was at a depth of 1723 m on the bottom near Bermuda.

Figure 1.16 [1.13] presents spectra of fluctuations of the Cartesian pressure components X and Y (Sect. 10.4) for a 220-Hz sound signal: phase-rate spectra (on the left), spectra of the log amplitude (in the middle), and amplitude spectra (on the right). The experiment was performed southeast of Bermuda. A sound source was moored on the axis of the USC, at a depth of 1100 m near Bermuda. The signals were received by hydrophones suspended from a drifting ship at 500-, 1000-, and 1500-m depths, at a range of about 250 km from the source. The phase-rate spectra fall monotonically, at a rate between $\omega^{-0.5}$ and ω^{-1} . The spectra from

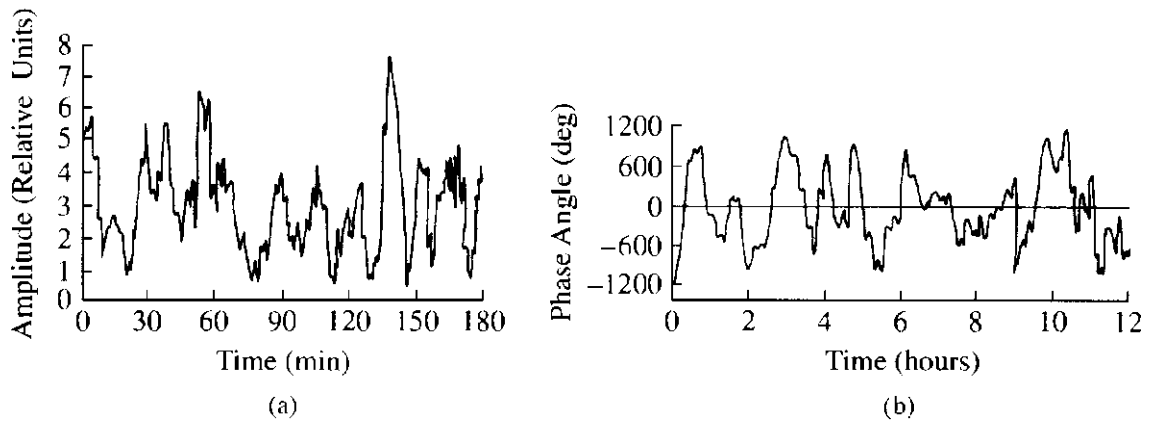


FIGURE 1.15. (a) Amplitude and (b) phase fluctuations of 367-Hz sound signal at a range of 1318 km [1.12]

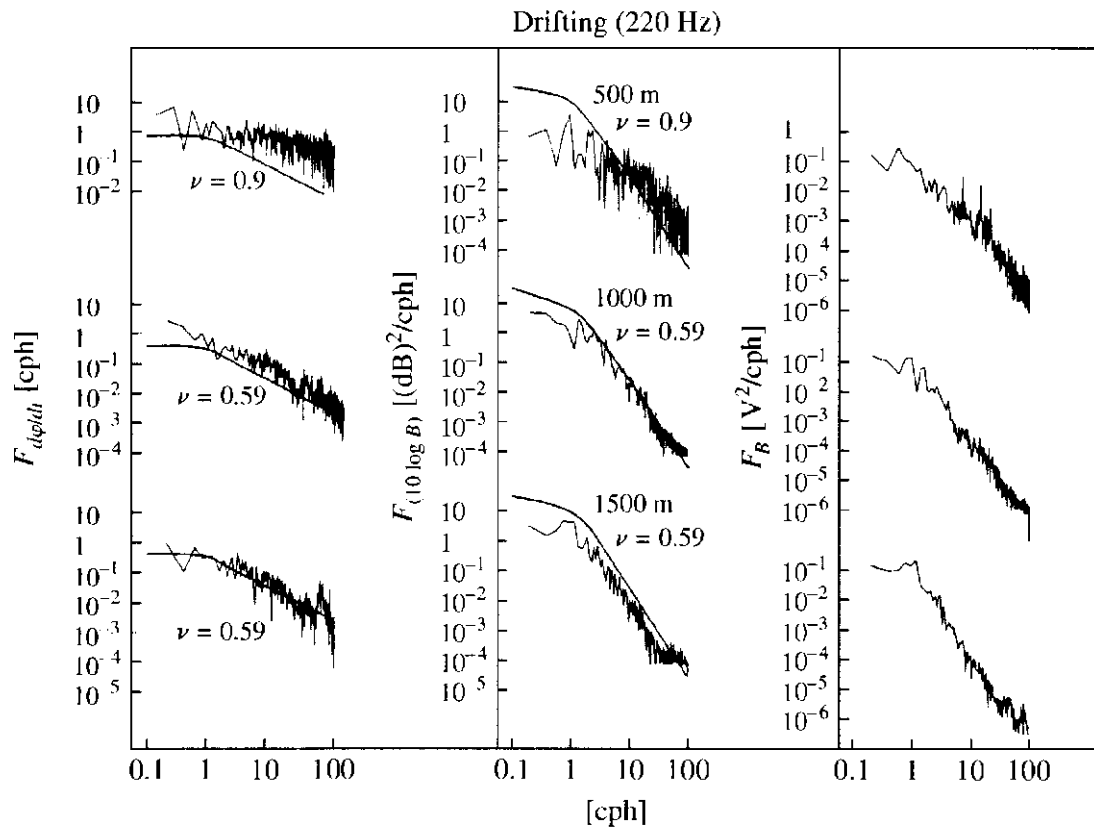


FIGURE 1.16. Frequency spectra of 220-Hz sound signal fluctuations: phase-rate ($d\phi/dt$) spectra on the left; spectra of the log amplitude ($10 \log E$) in the middle, and amplitude (E) spectra on the right [1.13]. Smooth curves are predictions based on the random multipath model in [1.14] (see also Sect. 10.4)

the deeper hydrophones fall somewhat more rapidly. The amplitude spectra fall monotonically as $\omega^{-1.5}$. Solid lines are theoretical results based on the random multipath model of sound propagation developed by *Dyson et al.* [1.14] using the Garrett-Munk model of internal waves (Chap. 10). It is seen that the theoretical results and experimental data are in good agreement.

The calculations have also shown that in the presence of the first mode of an internal wave with sufficiently large amplitude and relative small length in the seasonal thermocline, a system of additional caustics appears in the first convergence zone. These caustics appear at those moments when a crest of an internal wave passes by the source and disappear when a trough passes by. The possibility of the formation of convergence zones due to sound refraction at the crest of an internal wave near the source was also shown [1.15]. The internal waves can also cause marked horizontal refraction of sound rays, i.e., a change of the propagation direction of rays in the horizontal plane.

1.4.4 Fine Vertical Structure of Waters

Quite recently it was found that such characteristics of the ocean water as salinity, temperature, density, and current velocity do not vary smoothly with depth, but in a discontinuous fashion. They remain almost constant within certain layers and change rapidly in passing from one layer to another. The thickness of these layers varies from tens of centimetres to tens of metres; their horizontal extent may reach up to tens of kilometres. The values of vertical gradients of the temperature and salinity at boundaries of layers exceed the values of their mean gradients by 1–2 orders of magnitude. The vertical gradient of the current velocity may reach the significant value of 2 cm/s per metre of depth, and in some cases even 5–10 cm/s per metre of depth in boundary layers [1.16]. Sometimes the vertical profiles of temperature, salinity, and density look like regular steplike structures.

An example of such a steplike structure in the temperature T , salinity S and density $\sigma_t = (\rho - 1) 10^3$ fields is shown in Fig. 1.17 [1.17]. Experimental data were obtained with a STD probe in the northwest part of the tropical Atlantic.

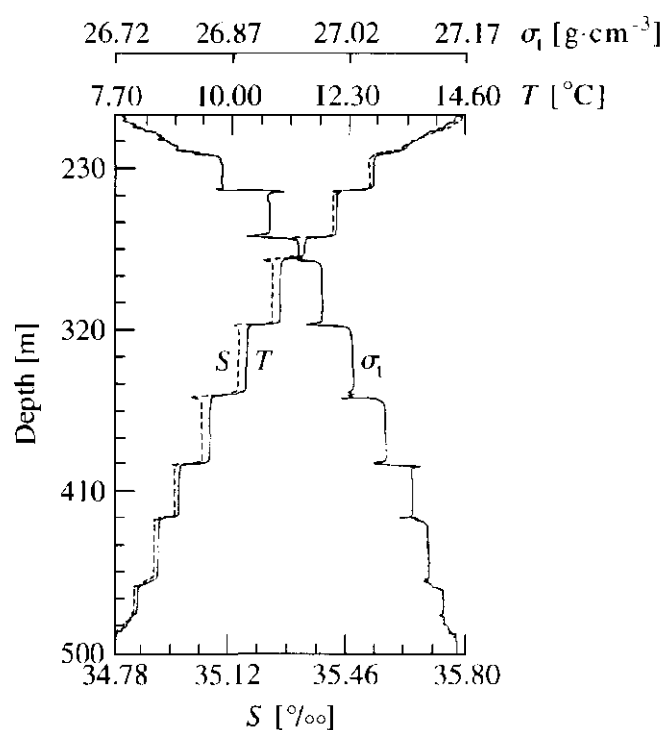


FIGURE 1.17. Steplike structure of temperature T , salinity S , and density $\sigma_t = (\rho - 1) 10^3$ in the tropical Atlantic [1.17]

The thickness of the quasi-homogeneous layers varies from 8 to 55 metres, and the thickness of interlayers from 1 to 8 metres. The analysis of possible physical reasons for the generation of the steplike structures is given in [1.17, 1.18].

The fine-layered structure of the ocean can considerably influence the sound fields. For instance, vertical gradients of the current velocity at boundaries of layers can become comparable with vertical gradients of the sound velocity. This can significantly change the trajectory of sound rays if their direction at this level is close to horizontal. In order to illustrate this, *Sanford* [1.19] has done the calculations for a simple environmental-acoustic model shown in Fig. 1.18. The profile of the sound velocity was observed in the Sargasso Sea. The current velocity is equal to zero everywhere, except in the layer of 250–400 m. A sound source is located at a depth of 350 m. In Fig. 1.19 ray diagrams for sound propagation in the direction of current and against current are shown.

The observations have shown that the fine-layered structure of water leads to the multipath mechanism of sound transmission even in the case when in the absence of the fine structure only one ray would arrive at the receiver. In turn, multipath propagation causes some additional fluctuations of phase and amplitude of the sound signal.

1.4.5 Small-Scale Turbulence

Oceanic turbulence has a fairly wide spectrum of scales. Small-scale turbulence with spatial scales from a few centimetres to dozens of metres is very important for acoustics. Due to the direct influence of the atmosphere, turbulence is permanently observed in the upper mixed layer of the ocean. At large depths it becomes apparent in the form of separate “patches” in which fast pulsations of the current velocity and fluctuations of the physical parameters (temperature, salinity, sound velocity) of the medium are observed [1.20].

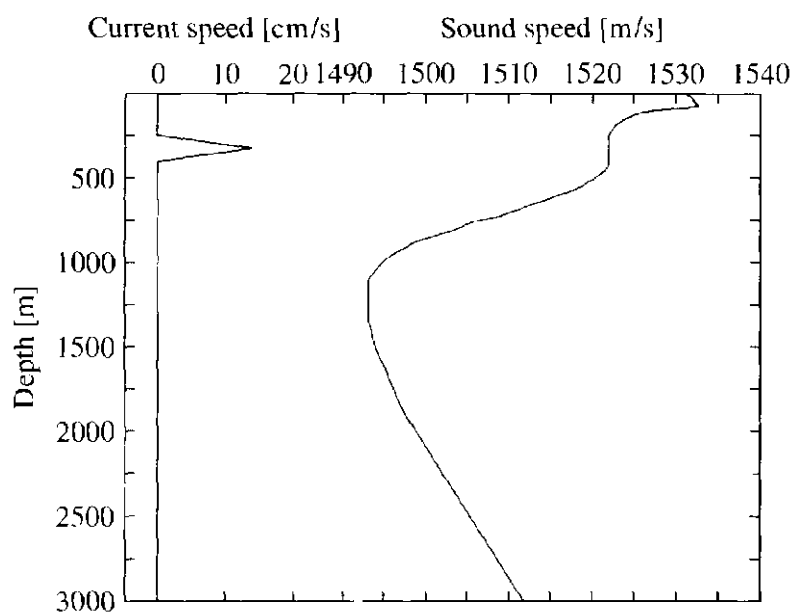


FIGURE 1.18.
Current and sound
speed model used to
compute refraction
[1.19]

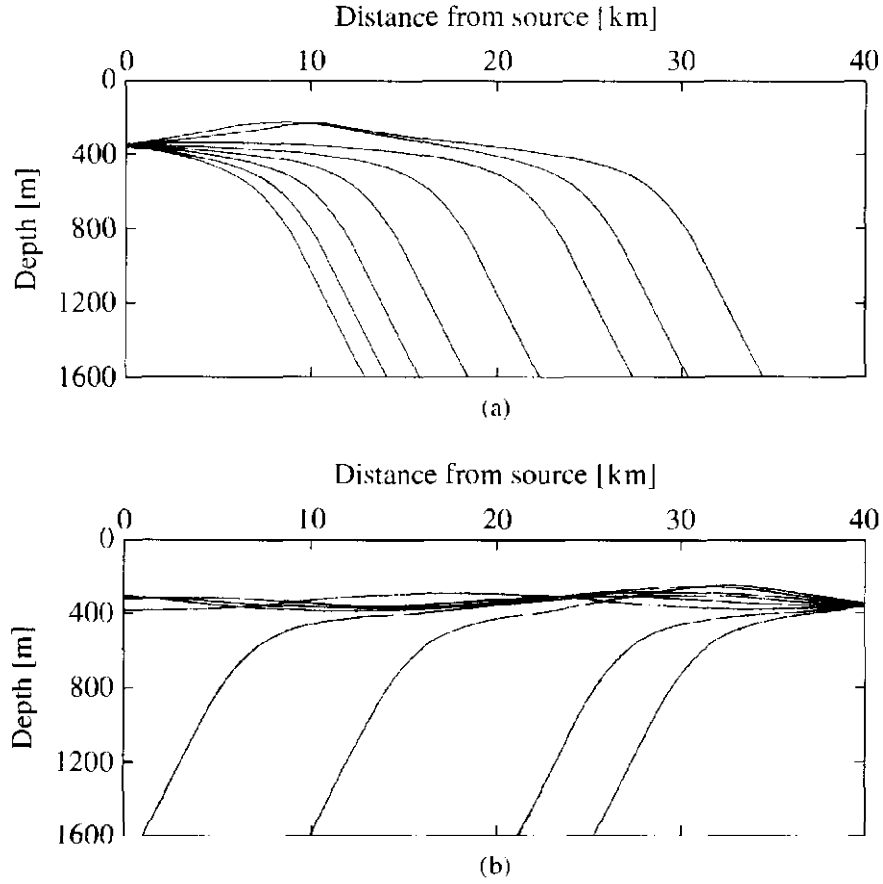


FIGURE 1.19. Ray path for (a) propagation in the direction of the current and (b) propagation against the current [1.19]

As experiments have shown [1.21] the fluctuations of the acoustical refractive index $n(\mathbf{r})$ in the upper mixed layer may be described by a structure function

$$D_n(\varrho) = \langle [n(\mathbf{r}_1) - n(\mathbf{r}_2)]^2 \rangle$$

(the brackets indicate ensemble averaging) obeying the Kolmogorov-Obukhov “2/3” law for local isotropic turbulence:

$$D_n(\varrho) = C_n^2 \varrho^{2/3}, \quad \varrho = |\mathbf{r}_2 - \mathbf{r}_1| \quad (1.4.1)$$

where C_n is the structure constant. The law (1.4.1) is valid for values $l_0 \leq \varrho \leq L_0$, l_0 and L_0 being the internal and external scales of turbulence, respectively. According to experimental estimates the value of l_0 does not exceed 1 cm, and L_0 is equal to a few metres.

In Fig. 1.20 the normalized structure function of the refractive index fluctuations is shown at a depth of 40 m for a 80-m-thick mixed layer. When $\varrho = L_0 \approx 1.8$ m, “saturation” of the structure function is observed.

Fluctuations of the sound velocity (the index of refraction) give rise to scattering of sound waves. The superposition of the primary and scattered waves leads to fluctuations of the amplitude and phase of the sound signal. Part of the scattered acoustic energy can leave the USC, resulting in additional attenuation of the sound

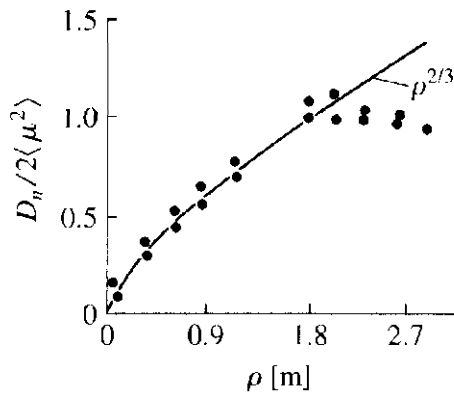


FIGURE 1.20. Normalized structure function $D_n(\rho)$ of fluctuations of the refractive index n [1.21]. $\langle\mu^2\rangle$ is the mean square of the fluctuations

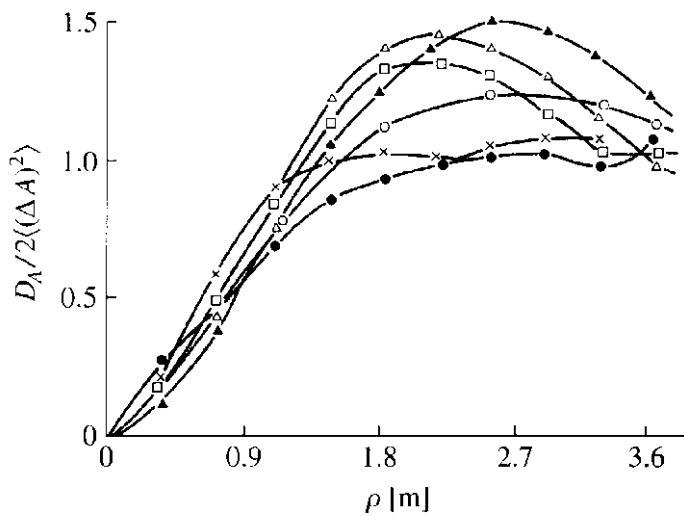


FIGURE 1.21. Normalized transverse structure function $D_A(\rho)$ of the amplitude fluctuations A of a sound signal for 6 different ranges r [1.21]. r in metres: (●) 180; (×) 340; (△) 580; (□) 710; (▲) 960; (○) 1100; $\langle(\Delta A)^2\rangle$ is the mean square of amplitude fluctuations

field. In Fig. 1.21 a series of normalized transverse structure functions of the sound signal amplitude A is presented. Fluctuations for 6 different distances from a source are shown as an example.

1.5 Ocean Surface

The ocean surface is rarely calm. Its most characteristic feature is a complex wave motion. Waves generated by turbulent wind have an extremely irregular, random character. As a result, the main experimentally observed characteristic of the wind-generated waves—the displacement $\zeta(\mathbf{r}, t)$ of the surface from the mean plane—is a random function of the horizontal radius vector \mathbf{r} and time t . According to experimental data obtained in the ocean, the statistical distribution of ζ at a fixed point is close to the normal (Gaussian) law, but has a small skewness and, furthermore, appears to be more peaked (Fig. 1.22). The two-dimensional distribution of the wave slopes has a similar character, but the deviation from the normal law is even greater (Fig. 1.23). However, for most of the problems relating to sound scattering from the ocean surface these deviations are not very significant,

FIGURE 1.22. Probability density of the surface displacements at a fixed point [1.22]. Dots represent 11,786 individual measurements, the solid curve the empirical distribution, the dashed curve the normal distribution with the same variance $\sigma^2 = \langle \zeta^2 \rangle$ [1.23]

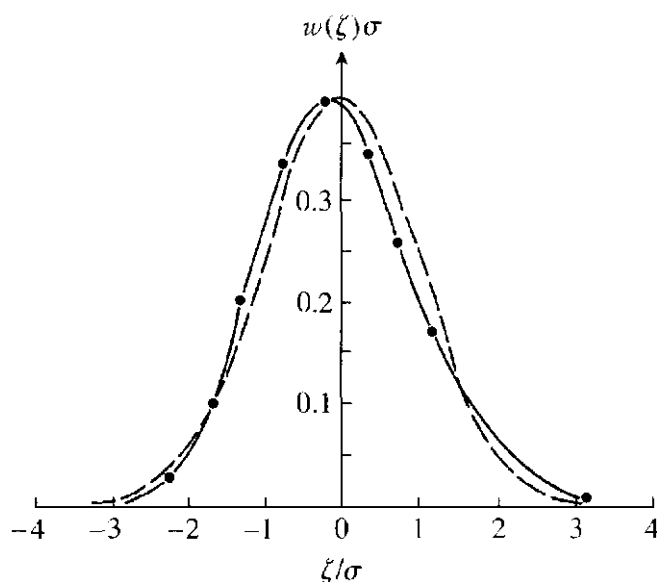
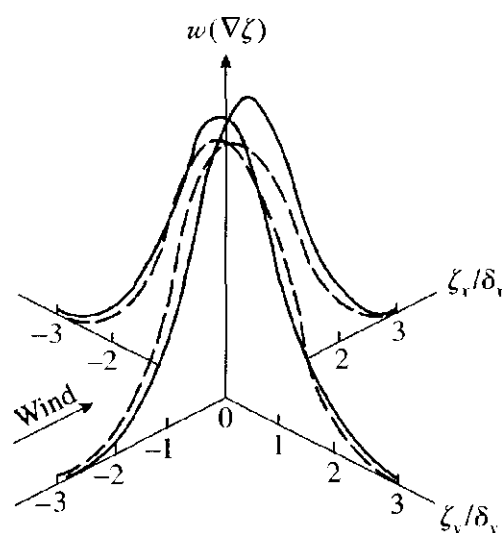


FIGURE 1.23. Probability density of the surface slopes [1.24]. The solid curves represent the measured distribution along two coordinate axes, the dashed curves the normal distribution with the same variances $\delta_x^2 = \langle \zeta_x^2 \rangle$, $\delta_y^2 = \langle \zeta_y^2 \rangle$ [1.23]



and the normal distribution for the wave displacement and slopes may be assumed as a first approximation.

The frequency spectra have been studied in some detail for fully developed roughness. Its parameters depend only on wind speed. In Fig. 1.24 are presented the results of the dimensional analysis of a great mass of experimental material carried out by *Pierson* and *Moskovitz* [1.25].

The angular distribution of the energy of wind-generated waves in the horizontal plane depends on the wave frequency. The low-frequency components of sea roughness have a narrow angular spectrum, but the high-frequency part of the spectrum is practically isotropic.

In the polar areas of the oceans the effect of the ice cover on sound propagation is significant; the relatively smooth areas of the ice cover are interrupted with rows of sea-ice ridges. An irregular underwater part of the ice ridges gives rise to strong

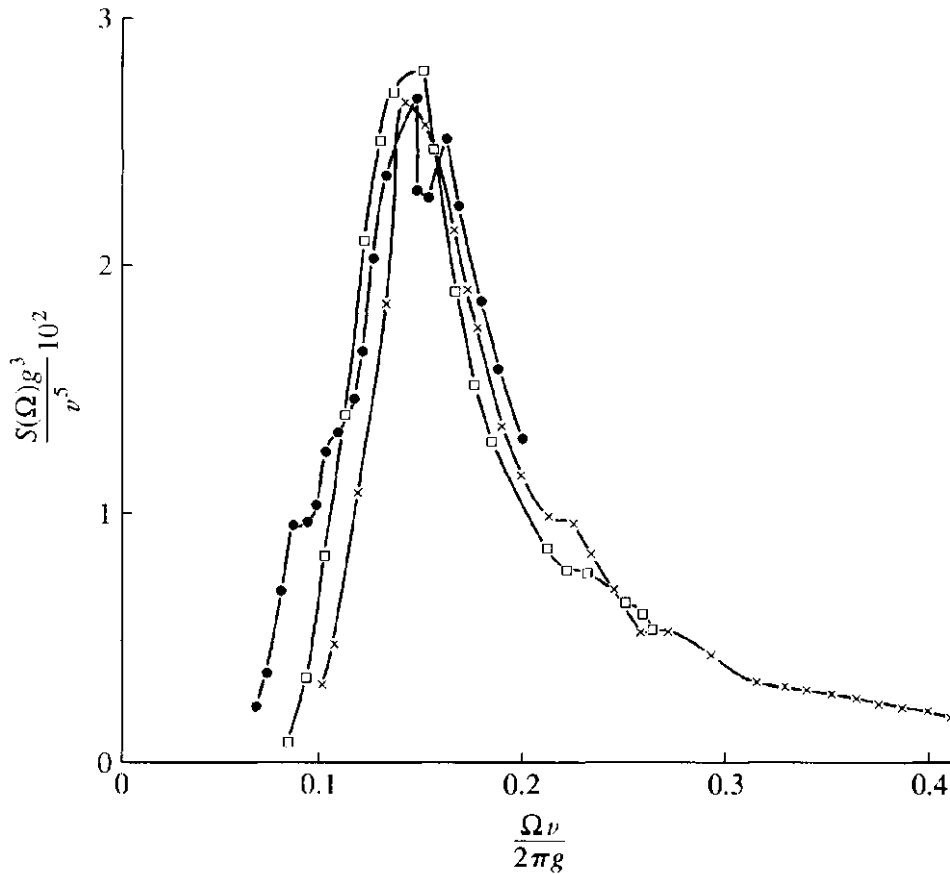


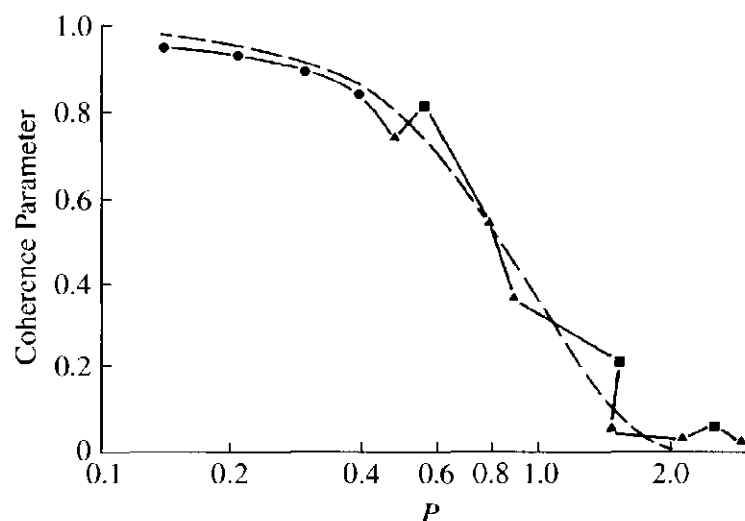
FIGURE 1.24. Pierson-Moscovitz frequency spectrum $S(\Omega)$ for a fully developed sea for different wind velocities v measured at a height of 19.5 m, (\bullet) 10 m/s; (\square) 16.3 m/s; (\times) 20.6 m/s [1.26]

scattering of the sound waves which have multiple contacts with the ice cover due to the positive gradient of the sound velocity in water.

1.6 Sound Scattering at the Ocean Surface

When a sound wave in water is incident on a rough ocean surface, scattered waves arise. There are coherent and incoherent components in the scattered sound field. The coherent component is a wave propagating in the direction of specular reflection and can be calculated by the statistical averaging of the scattered field on the ensemble of the functions ζ . The ratio of the amplitude of this wave to that of the incident wave defines the coherent (mean) reflection coefficient. If the surface is even, the reflection coefficient of sound from it is rather close to -1 , i.e., the ocean surface is practically perfectly reflecting. The acoustic energy incident on the rough sea surface also returns to water completely, but because of the dispersal of a part of it to the scattered field, the coherent reflection coefficient is always less than unity and decreases with increasing height of the surface waves (scaled to the sound wavelength). The useful quantity is the coherence parameter, that is, the ratio of the coherent intensity component to the total (coherent plus inco-

FIGURE 1.25.
Dependence of the
coherence parameter
on the Rayleigh parameter
for different values of
 σ : (●) 6 cm, (▲) 10 cm,
(■) 23 cm [1.27]



herent) intensity. Figure 1.25 gives experimental data for the dependence of the coherence parameter upon the Rayleigh parameter $P = 2k\sigma \sin \chi$, where k is the sound-wave number, σ is the root-mean-square displacement of the rough surface, χ is the grazing angle of a sound wave (relative to the horizontal plane). The data obtained for different σ are denoted by different symbols. The function $\exp(-P^2)$ (the dashed line) approximates the experimental dependence rather well. For large values of the Rayleigh parameter, $P \gg 1$, the coherent component is close to zero, and the scattered field is almost completely incoherent.

In underwater acoustics the back-scattered sound, i.e., that scattered in the direction of the sound source, is of great interest. The typical dependence of the back-scattering coefficient⁴ upon the grazing angle χ_0 is given in Fig. 1.26 [1.28]. The data were obtained in midocean conditions with fully developed wind waves (wind speed $v \approx 9.5$ m/s). At grazing angles $\chi_0 \geq 60^\circ$ the scattered field is mainly due to the specular reflections—"glitters"—from separate facets of the rough sea surface. At smaller grazing angles the "resonant" scattering of sound is more important (Chap. 9). At high frequencies (10–20 kHz) and small grazing angles the scattering coefficient depends only slightly on the grazing angle; in this case air bubbles in the upper ocean layer are the main contributors to the scattered field. The relative contribution of the air bubbles increases with an increase in sound frequency.

The frequency spectrum of the field scattered in the specular direction consists of a spectral line at the frequency of the incident wave f_0 , a coherent component of the field, and a continuous spectrum of the incoherent field in the form of two "wings" on the left- and right-hand sides of this line. Such spectra for incident wave frequencies of 110 and 312 Hz are shown in Fig. 1.27 [1.29]. The experiment was carried out in a deep ocean area with wind speed about 8.5 m/s and grazing angle $\chi_0 \approx 30^\circ$. The solid lines 1 and 2 are the wings of the scattered wave spectra

⁴The scattering coefficient m_s (a nondimensional quantity) is equal to the ratio of the acoustic power scattered by the unit surface per unit solid angle to the incident wave intensity.

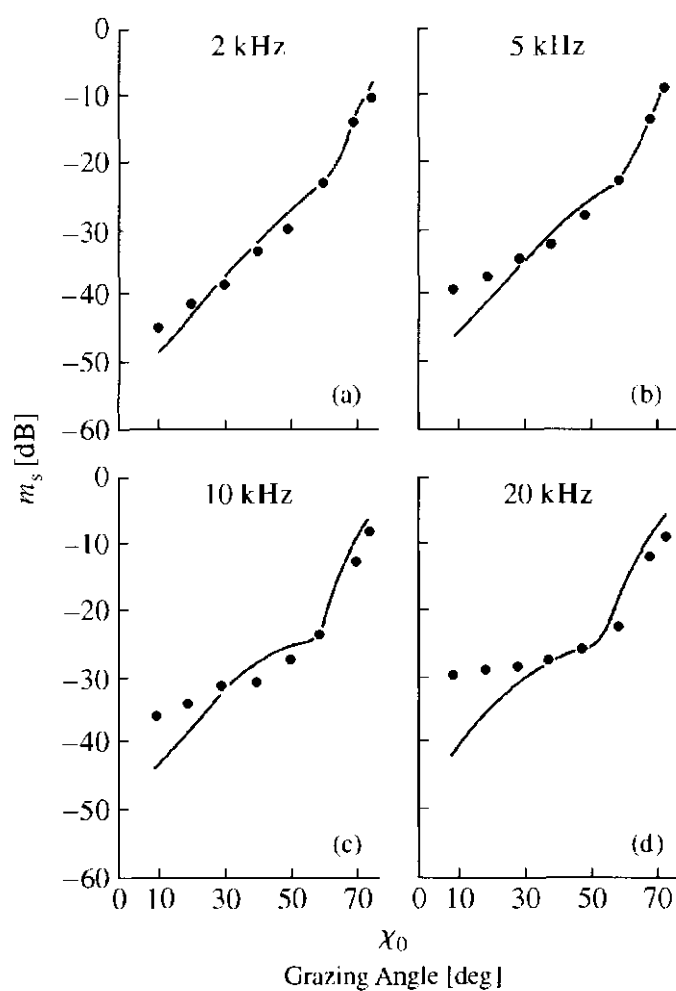


FIGURE 1.26. Back-scattering coefficient vs grazing angle for frequencies 2–20 kHz [1.28]. Solid lines are the theoretical values based on a two-scale model of sea roughness (Sect. 9.11)

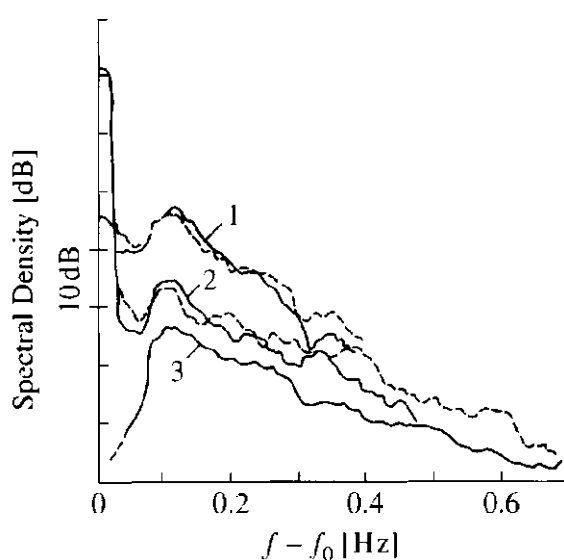


FIGURE 1.27. Experimental spectra of the scattered waves for the frequencies 110 Hz (curve 1) and 312 Hz (curve 2). Curve 3 represents the spectrum of the sea roughness [1.29]

for $f > f_0$. The wings, shown by the dashed lines, are supposed to be on the left-hand side relative to the central line, and are mirror images with respect to the central line in the figure for better comparison with the right-hand wings. It can

be seen that the right-hand and left-hand wings are similar to each other as well as to the rough surface wave spectrum (curve 3).

1.7 Sound Scattering by Air Bubbles

Air bubbles generated by wave breaking in a relatively thin surface layer contribute considerably to sound scattering and absorption. The effect is especially large when bubbles are “resonant,” i.e., when the eigenfrequency of their radial oscillations coincides with the sound-wave frequency. The resonant frequency of an air bubble in water at depth z in metres is approximately given by the formula (Chap. 11)

$$f_0 = (327/a)(1 + 0.1z)^{1/2} \text{ [Hz]} \quad (1.7.1)$$

where a is the bubble radius [cm].

Bubble radii distributions, especially their concentration as a function of depth and environmental conditions, have so far been hardly investigated; experimental data are scanty. The distributions at depths of 1.5, 4, and 8 metres are given in Fig. 1.28 [1.30]. The measurements were carried out in the midocean isotherm (14°C) layer of 25-metre thickness. The bubble concentration $n(a)$ —the number of bubbles per cubic metre with radii between a and $a + \Delta a$, $\Delta a = 1.5 \cdot 10^{-3}$ cm—is plotted along the vertical axis. It can be seen that bubbles with radii between $1.5 \cdot 10^{-3}$ and $3.5 \cdot 10^{-2}$ cm (resonance frequency band ~ 10 –235 kHz) are present at the depth of 1.5 m. The resonance frequency band becomes narrower

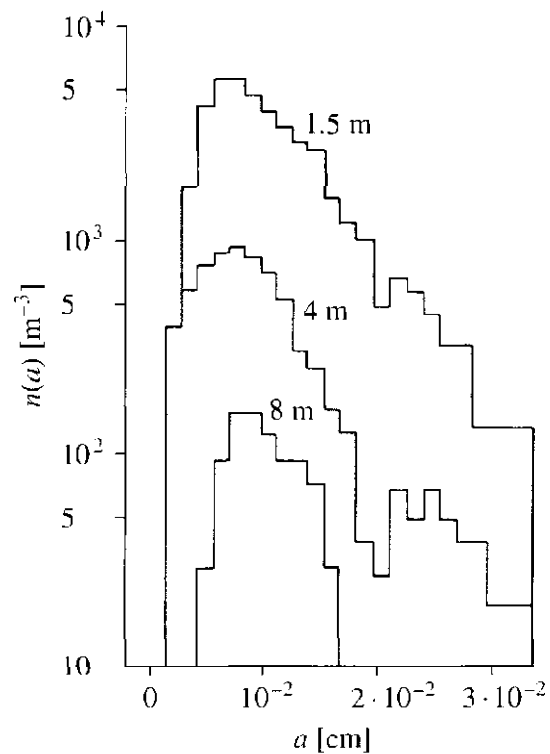


FIGURE 1.28. Distribution of bubble radii at depths of 1.5, 4, and 8 m for a wind velocity 11–13 m/s [1.30]

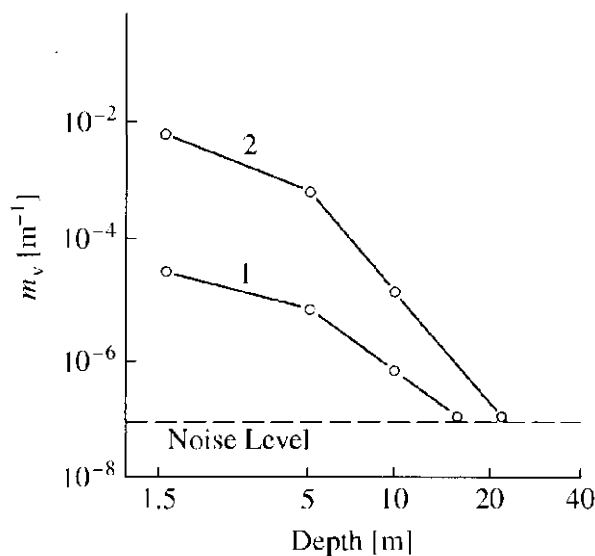


FIGURE 1.29. Depth dependence of the volume scattering coefficient for a sound frequency of 10 kHz and a wind velocity of 4–8 m/s (curve 1) and 11–12 m/s (curve 2) [1.31]

at greater depths, the maximum of the bubble distribution is displaced to larger radii, and its value decreases. At the depth of 8 m the resonance frequencies vary from 25 to 97 kHz.

The dependence of the volume scattering coefficient m_v ⁵ upon depth at frequency 10 kHz with two values for the wind speed is presented in Fig. 1.29. The scattering coefficient has a maximum value at a depth of 1.5 m (the smallest depth of the measurements), decreases monotonically with depth, and falls off down to the noise level ($\approx 10^{-7} \text{ m}^{-1}$) at a depth of about 20 m.

The propagation of sound through a medium containing bubbles is accompanied by fluctuations of the sound-wave phase due to the sound velocity fluctuations. The latter are the result of a change either of the distribution of bubble resonant frequencies due to a change in the height of wind waves with time and, therefore, in the hydrostatic pressure, or of the total volume of air contained in the bubbles.

1.8 Deep-Scattering Layers (DSL)

Another mechanism of sound scattering is related to the existence of deep sound-scattering layers in the ocean formed by assemblages of small marine animals—fish, siphonophores, crustaceans, small calmars, jellyfish, and so on. The DSL are of very large horizontal extent, often stretching from one continent to another. They can be observed in all deep-sea areas, except the polar ones, but sometimes they have been detected even there. The characteristic feature of DSL is their diurnal migration. At sunset the layers rise to a depth of 100–150 m, at sunrise they go down to depths of 300–600 m. It is this migration that suggested the idea of the biological nature of DSL after their discovery. Now the point of view is generally accepted that the sound scattering by the DSL is mainly due to the

⁵The coefficient m_v is determined in the same way as m_s above but in respect to unit volume.

resonant oscillations from the swimming bladders of small bathypelagic fish with a length between 2–3 and 10–12 cm. According to theoretical calculations, the presence of a few “resonant” fish per 1–10 thousand cubic metres of water is sufficient to produce the acoustic effect observed. The resonant frequency of the swimming bladders depends upon both their size and the depth of the DSL. The theoretical dependence of the resonant frequency upon the fish length for different depths is shown in Fig. 1.30 [1.32]. The largest fish (~7–20 cm) present in the DSL at a depth of 600 m (daytime) have resonant frequencies between 3 and 7 kHz. The resonant frequency of the smallest fish (2–3 cm) at this depth is about 20 kHz. With the rise of the DSL at night to smaller depths, the resonant frequencies decrease by a factor of about 1.5–2. These predictions of theory are in good agreement with numerous experimental data. The frequency dependence of the scattered-sound intensity obtained in the tropical Atlantic [1.32] is presented in Fig. 1.31. Every curve (for day and night) has two maxima corresponding to the resonant frequencies of two kinds of fish present in a layer. At nighttime when the layer was at a depth of 150–200 m, the resonant frequencies were 3.5 and 15 kHz. In the daytime (depths observed 400–500 m) the resonant frequencies were, indeed, much higher—5 and 20 kHz, respectively. With the help of Fig. 1.30 one can conclude that the length of the two kinds of fish present was 8 and 2 cm. Subsequent biological trawling confirmed these estimates.

Nonresonant scatterers, mainly animals with hard skeletons and testae, are responsible for sound scattering at frequencies above 30 kHz.

In the ocean, as a rule, regions with similar fauna stretch in the east-west direction, and sound scattering depends much more on latitude than longitude. As a result of extensive experimental studies over many years in the Atlantic and Pacific Oceans and adjacent seas [1.33] the following regularities have been established.

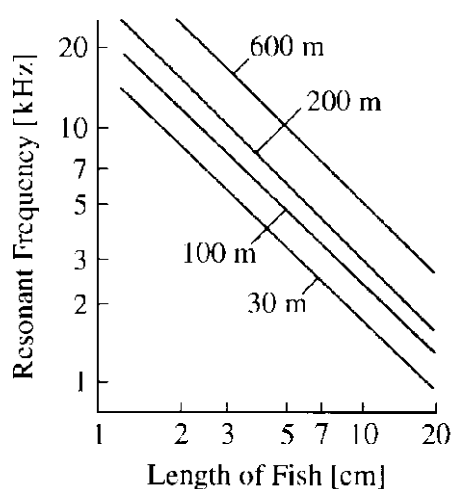


FIGURE 1.30. Theoretical dependence of the resonant frequency upon the length of fish for different depths [1.32]

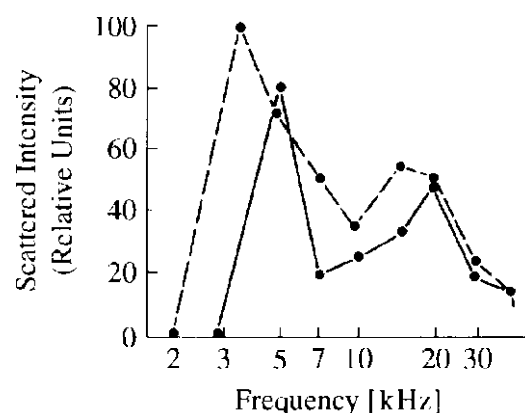


FIGURE 1.31. Frequency dependence of the sound intensity scattered by DSL (— day, --- night) [1.32]

The column strength⁶ reaches its greatest value at the equator in both the Atlantic and Pacific Oceans. At latitudes 5°–20° its general level decreases by a few decibels in both hemispheres. At higher latitudes, the scattering strength increases to values comparable to those at the equator. Very low values are observed in polar waters.

1.9 Ocean Bottom

If the ocean surface only scatters sound, the bottom of the ocean scatters and absorbs it, as well. A part of the acoustic energy incident on the bottom goes down into the ground. This is the main reason limiting the propagation range of low-frequency sound when the USC is absent. On the other hand, rays reflected from the bottom “insonify” the shadow zones where direct rays do not penetrate.

At present, the acoustical parameters of the very upper sediment layer down to a dozen metres have been investigated more or less completely. On the basis of the analysis of a great many specimens of deep-water sediments taken in different regions of the oceans some relations between the main acoustic parameters of the bottom have been established (Fig. 1.32). The sound velocity and the density of the sediment in Fig. 1.32 are related to those of the water. The reflection coefficient was calculated for normal incidence.

According to experimental data the sound absorption coefficient in a sediment is proportional to sound frequency. Its absolute value at the frequency 1 kHz equals 0.3–0.5 dB/m.

Regarding the reflection of sound by the ocean bottom, experimental studies in different regions of the oceans have shown that sound reflection is determined by the parameters of the sediment only at comparatively low frequencies. At frequencies above a few kilohertz, bottom relief plays a dominating role. Reflection from a very rough rocky bottom may appear to be less than that from a muddy sediment. In the case of a rather smooth bottom, the situation is reversed. Figure 1.33 shows the dependence of the reflection coefficient at normal incidence of a sound wave with a frequency of 9.6 kHz upon the general bottom relief. The data were obtained during the continuous passage of a research vessel. It can be seen that during the transition from a very rough bottom region to the abyssal plain the reflection coefficient undergoes a steep increase. Numerical values of the reflection coefficient for some regions in the Atlantic and Indian Oceans are given in Table 1.1 [1.36].

Within various geomorphologic zones (abyssal plains, basins; abyssal hills and oceanic rises; crests of underwater ridges) the angular and frequency dependence of the bottom sound-scattering coefficient are different. In Fig. 1.34 the dependence of the back-scattering strength ($10 \log m_s$, where m_s is the scattering coefficient) upon the angle of incidence at different frequencies is shown for the abyssal plain. One can see a rapid decrease of the scattering strength with an increase in the angle

⁶The scattering strength of the water column or, briefly, the column strength, equals the integral of the volume scattering coefficient over the depth between boundaries of the layer.

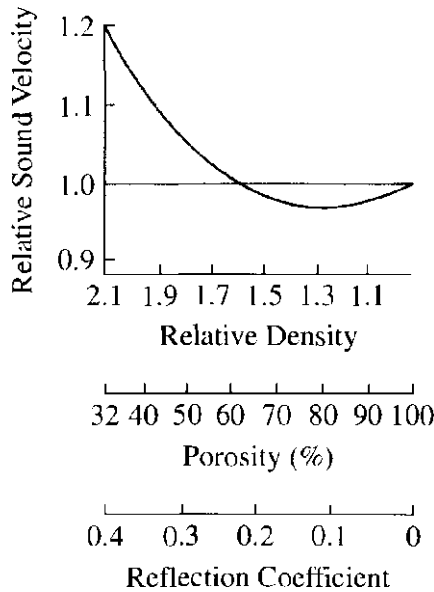


FIGURE 1.32. Relationship between the main characteristics of underwater sediments [1.34]. Cited after [1.35]

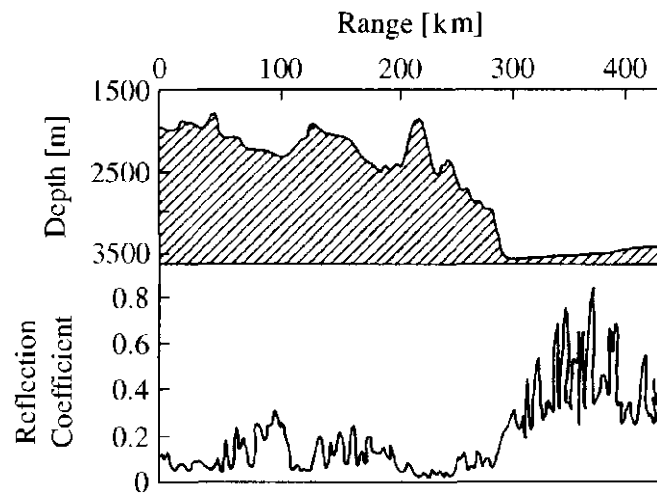


FIGURE 1.33. The bottom relief along a track of measurements (upper), reflection coefficient from the ocean floor (lower) [1.36]

TABLE 1.1. Average values of the reflection coefficient from the bottom for frequency 9.6 kHz and normal incidence of sound [1.36]

Ocean Area	Degree of Roughness	Reflection Coefficient
The Atlantic Ocean		
The crest of the Mid-Atlantic ridge	Maximal	0.6–0.09
Greater Antillean Arcs	Maximal	0.09
The Bermuda Rise	Mean	0.19–0.21
The region off the Cape Verde Islands	Mean	0.12–0.22
The abyssal plain Nares	Smooth relief	0.39–0.48
The abyssal plain Sohm	Smooth relief	0.41–0.45
The Indian Ocean		
The Maldives Ridge	Maximal	0.09
Rough part of the Andaman Sea	Maximal	0.06
Hill's zone of the Central Basin	Mean	0.31
The Bay of Bengal	Smooth relief	0.44
The plain of the Andaman Sea	Smooth relief	0.37
The plain of the Central Basin	Smooth relief	0.49

of incidence for small angles. When the angle of incidence $\theta > 15^\circ$ the angular dependence approximately corresponds to Lambert's law ($m_s \sim \cos^2 \theta$). Figure 1.35 represents the scattering strength at the same frequencies in the case of the very rough bottom near the southern boundary of the abyssal plain Sohm. Here the dependence upon the angle of incidence is weak for nearly the whole range of angles.

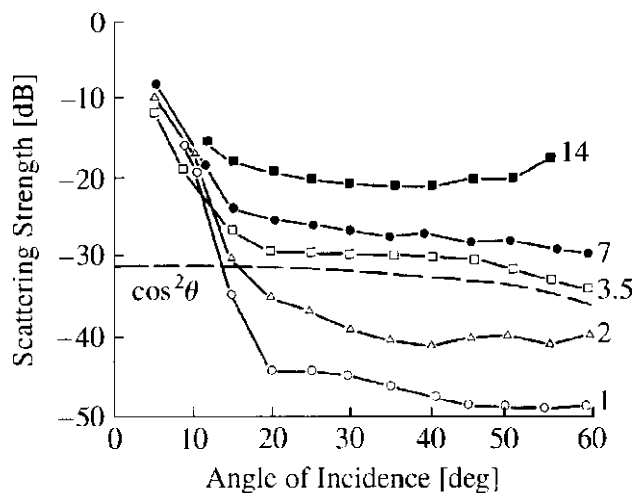


FIGURE 1.34. Angular dependence of the back-scattering coefficient from the bottom of an abyssal plain at different frequencies [1.36]. Numbers near curves indicate the sound frequency to kHz

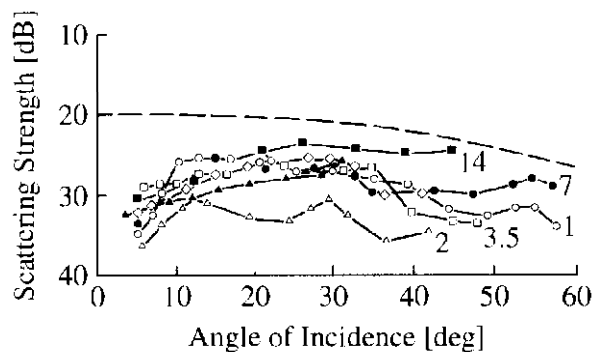


FIGURE 1.35. As in Fig. 1.34 for a very rough bottom [1.36]

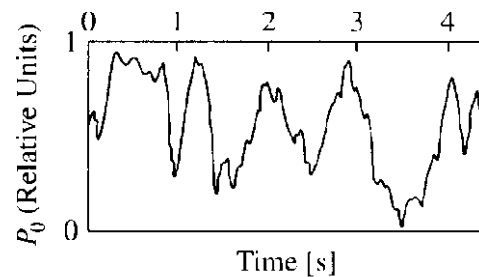


FIGURE 1.36. Fluctuations of the envelope of the scattered signal at normal incidence of 5 kHz sound, with the drift speed of the vessel 1.2 knots [1.36]

When a sound source or a receiver (or both) is in motion, fluctuations of the bottom-scattered signal are observed. Figure 1.36 is an example of a record of the scattered-signal envelope at a normal incidence of sound with the frequency 5 kHz when the speed of the drifting vessel with a sound source (and receiver) was about 1.2 knots. The spectral-correlation analysis of fluctuations of this kind allows us to obtain data on the bottom relief which cannot be obtained by using an echo sounder.

1.10 Ambient Noise

An important acoustic characteristic of the ocean is its underwater ambient noise. It contains a great bulk of information concerning the state of the ocean surface, the atmosphere over the ocean, tectonic processes in the earth's crust under the ocean, the behaviour of marine animals and so on.

At low frequencies (0.1–10 Hz) the main noise sources are earthquakes, underwater volcanic eruptions, distant storms, turbulence in the ocean and atmosphere, as well as some processes at the ocean surface (nonlinear interaction of surface waves).

In the frequency band 50–300 Hz underwater noise is mainly due to remote ship traffic. More than one thousand ships are under way simultaneously in the North Atlantic alone. Since the attenuation of sound at these frequencies in the deep ocean is small, a continuous noise background is generated.

In the frequency band 0.5–50 kHz underwater noise is directly associated with the state of the ocean surface and the wind in the area considered. There are many mechanisms responsible for noise generation in this frequency band, including the breaking of waves and the collapsing of air bubbles in the air-saturated surface layer (cavitation noise).

At frequencies above 100 kHz molecular thermal noise is dominant.

Biological noise produced by marine animals for communication with each other, the location of prey, frightening enemies and so on, is relatively intensive only in some regions of the ocean and at certain periods of time. This kind of noise is very important for studying the individual and group behaviour of many representatives of marine fauna.

The frequency spectra of underwater noise in the band from 1 Hz to 100 kHz are given in Fig. 1.37. These spectra were measured at various locations by many researchers, summarized by Wenz [1.37] and supplemented by Furduev at a later time [1.38]. On the average, noise levels decrease with frequency. For each given frequency the dynamic range can vary from 40 to 60 dB depending on hydrometeorological conditions. At low frequencies the noise levels usually decrease rather steeply—from 8 to 10 dB per octave. In the band 10–500 Hz, the noise spectrum is greatly variable—its smooth growth sometimes is changed by the steep decay. At frequencies of 0.5–500 Hz, the typical rate of the noise level decrease is 5–6 dB per octave.

The specific kind of ambient noise is observed under the ice in the polar regions of the ocean. This noise is mainly related to the dynamics of the ice cover—movements and oscillations of separate ice floes and whole ice fields, fracturing of the ice under compression, friction of the ice floes against each other, thermal cracking, sweeping of the snow or ice pellets by the wind along the ice surface, etc. To this kind of the noise, we can assign the noise of melting icebergs in their motion from polar regions to warmer ones. It is assumed that this noise is due to the explosion of tiny air bubbles residing in the ice under pressure and released when icebergs melt or by the collapse of the air cavities inside the ice under the force of water. The iceberg noise level depends on its size, sea depth, air content in the ice, the rate of melting, and so on. In one of the experiments carried out in the Northern Atlantic [1.39], the noise level of an isolated iceberg 25 m in height and 60 m in diameter was 82 dB re 1 Pa/Hz^{1/2} at a frequency of 10 kHz in the band of 1 Hz at a distance of 150–200 m (Fig. 1.38). Referring to Fig. 1.38, we can see the rise of the noise level in the range 5–50 kHz, which exceeds the background level by 15–40 dB at a depth of 10 m.

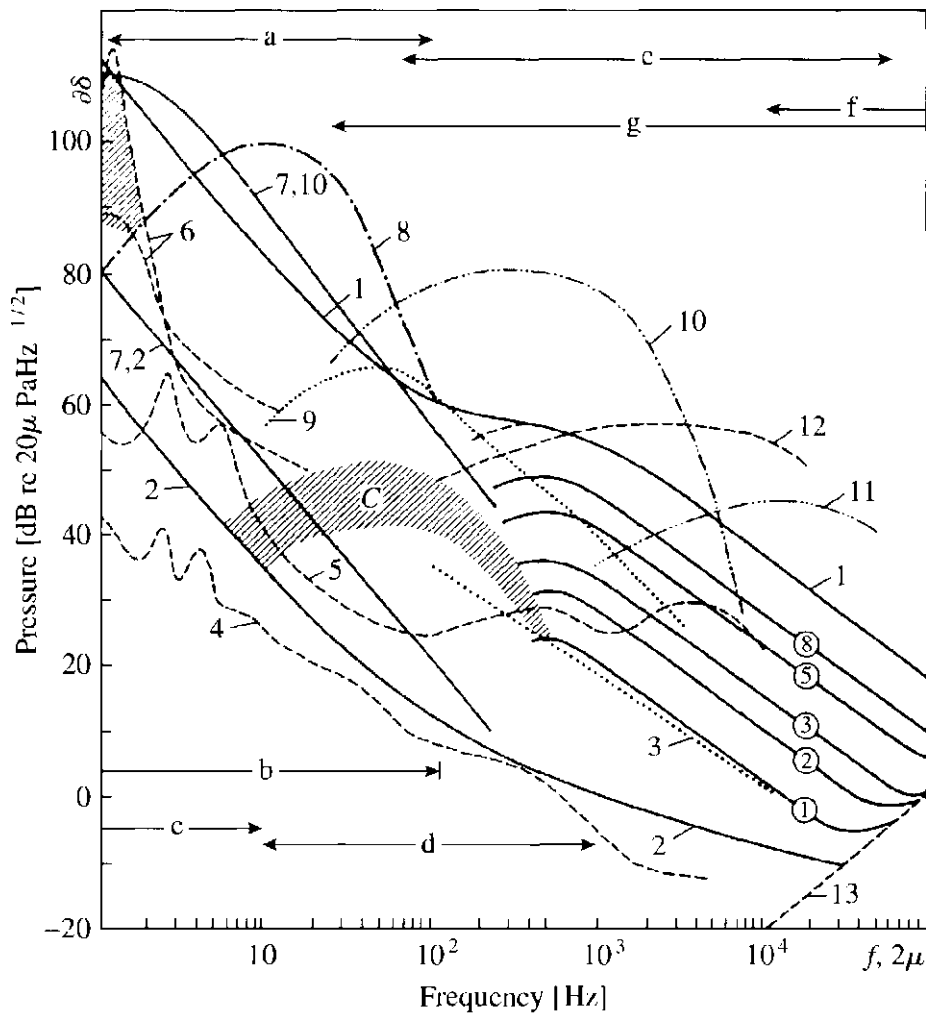


FIGURE 1.37. Averaged frequency spectra of ocean ambient noise [1.38] 1, 2—maximum and minimum levels of dynamic noise; 3—noise during a calm, the numbers in circles—wind speed force (Beaufort); 4, 5—under-ice noise; 6—seismic background noise; 7, 2 and 7, 10—pseudo-sound (numbers after comma denote the pulsation speed of turbulent vortex, m/s; 8—noise from earthquakes; 9—traffic noise (region C—noise of shipping lines); 10, 11—noise off fish from the drum and shrimp families; 12—very heavy rain at sea; 13—thermal noise. Horizontal arrows denote frequency ranges of main sources of noise: a—seismic background, explosions, earthquakes, and ice reefing; b—turbulence; c—surface waves; d—industrial activity; e—cavitation and rain; f—thermal noise; g—sea organisms

1.11 Intrathermocline Lenses

In the last two decades very intense meso-scale eddies of a specific kind, called *intrathermocline lenses*, have been discovered in the ocean. Contrary to the rings near the large-scale frontal currents and eddies of the open ocean (see Sects. 1.4.1 and 1.4.2), they have a deepened core which greatly differs in hydrological characteristics or their vertical distribution from surrounding waters. So for a lens found

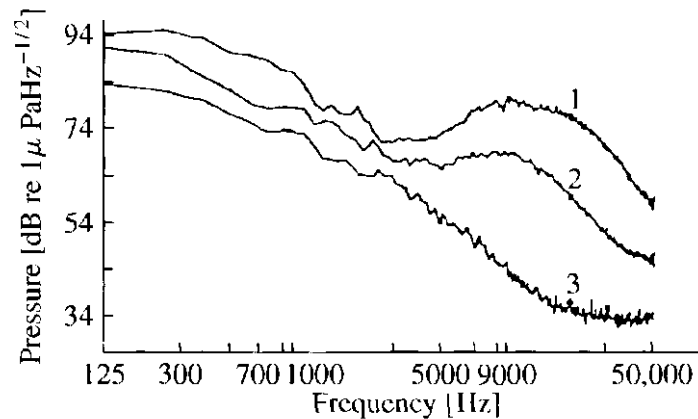


FIGURE 1.38. Frequency spectrum of an isolate iceberg. Depth of reception (1) 10 m; (2) 50 m; (3) oceanic ambient noise level at a distance of 20 km from the iceberg [1.39]

in the Canary Basin of the Atlantic Ocean in 1989, this difference makes up to 4.6°C in temperature, 1.1‰ in salinity, and 18.6 m/s in sound velocity at depths of 900–1000 m [1.40]. It seems to be the greatest anomalies of hydrological characteristics of all lenses described up to now. Now more than 300 lenses are found in very different geographic zones—from tropical zones to subpolar regions of the Arctic and Antarctic, at depths from 50 to 4000 m. The lens parameters vary in a rather wide range: a diameter from 1 to 100 km or even more; a vertical size from tens of metres to several kilometres; an eddy current speed up to several tens of cm/s ; and a lifetime of 1 to 10 years depending on the lens size and the other conditions (instrumental observations of one Mediterranean lens have been continued for two years) [1.41]. Figure 1.39 exhibits the vertical profiles of the density anomaly $\sigma_t(z)$, temperature $T(z)$, salinity $S(z)$, and sound velocity $c(z)$. The intrathermocline lenses were first recorded apparently at the drifting ice station “North Pole-1” [1.42]. However, at the time such high anomalies of the unsteady current speeds ($20\text{--}30\text{ cm/s}$), detected at depths of 50–100 m, did not receive the attention they deserve. Now these data are interpreted as the manifestation of the Arctic lenses.

The field observations show that the most pronounced lenses are generated at boundaries of different water masses. A typical example is the intrusion of the Mediterranean waters at intermediate depths into the Atlantic Ocean near the Gibraltar Strait. The lenses of this kind (“meddies”) have been studied the best.

The intrathermocline lenses perturb the sound velocity field, which results in the modification of the spatial-temporal structure of the sound field in the ocean—shadow zones are insonified, boundaries of convergence zones are displaced, new deep shadow zones are formed (in the absence of the zonal structure for background conditions), and a horizontal refraction of sound rays appear. The rotation of the lenses results in a phase change of sound waves transmitted through the lens. Figure 1.40 presents the ray pattern calculated for the sound velocity profile shown in Fig. 1.39 [1.39]. A sound source is located at a depth of 900 m at a 33-km distance from the lens center. The insonification of the first and second shadow zones is clearly seen; it is caused by the lens.

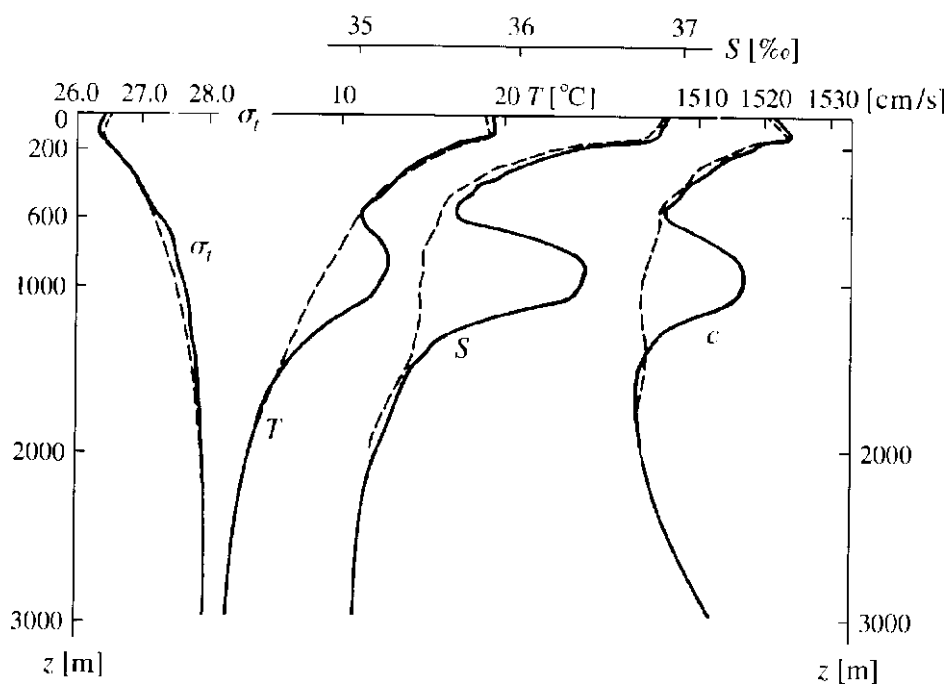


FIGURE 1.39. Profiles of density anomaly $\sigma_t(z)$, temperature $T(z)$, salinity $S(z)$, and sound velocity $c(z)$ in the core of a Mediterranean lens (solid lines), background conditions (dashed lines) [1.40]

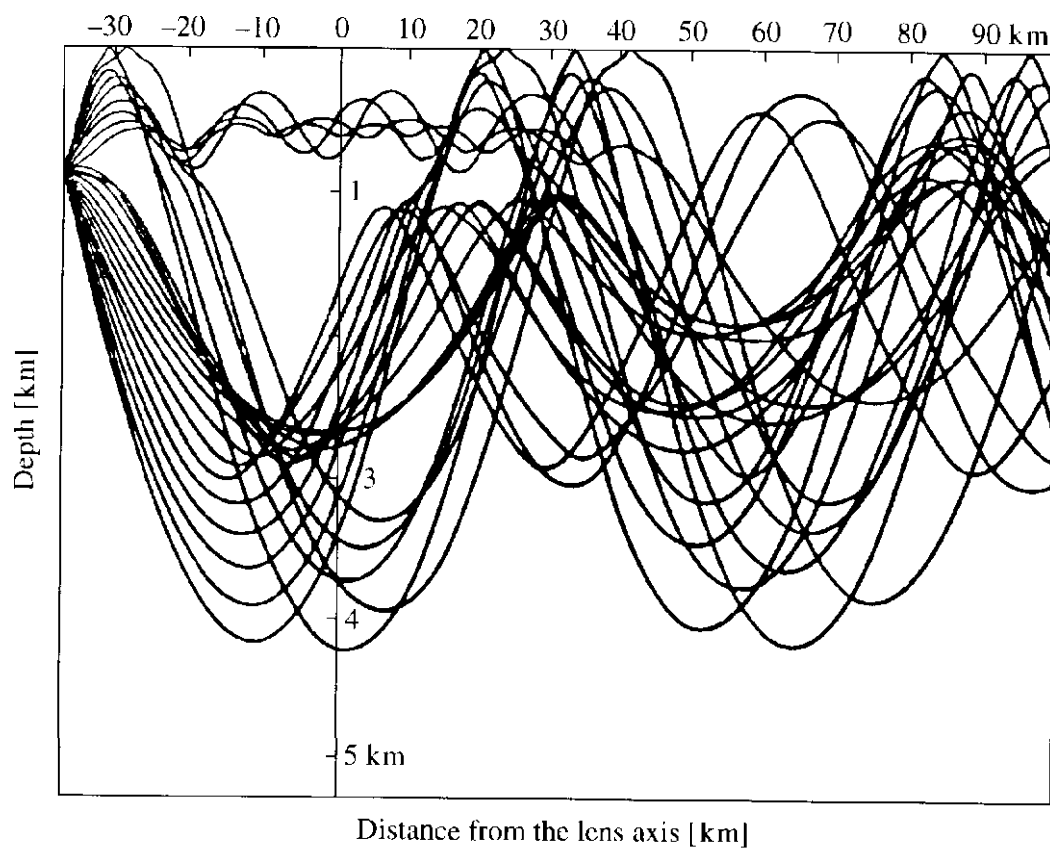


FIGURE 1.40. Ray pattern in the presence of a lens [1.40]

2

Ray Theory of the Sound Field in the Ocean

Ray theory, in spite of its approximate nature, is a very effective method for the study of sound propagation at sufficiently high frequencies in inhomogeneous media such as the ocean. In this chapter we derive the basic equations of ray acoustics and give their solutions for a stratified ocean. In later chapters the ray approach is applied to waveguide sound propagation, reflection of the sound from the sea surface, and some other problems.

2.1 Wave Equation for an Inhomogeneous Medium

The propagation of sound in inhomogeneous media (ocean, atmosphere) is described by the wave equation obtained by the linearization of the hydrodynamic equations of the ideal liquid. The initial equations appear here [2.1].

The Euler equation is

$$\frac{\partial \mathbf{v}}{\partial t} + (\mathbf{v} \nabla) \mathbf{v} = -\frac{1}{\rho} \nabla p, \quad (2.1.1)$$

where \mathbf{v} is the particle velocity, p is the sound pressure, ρ is the density of the medium, and t is time. The continuity equation is

$$\frac{\partial \rho}{\partial t} + \nabla(\rho \mathbf{v}) = 0. \quad (2.1.2)$$

By neglecting the thermal conductivity and diffusion of components, we may treat sound propagation as the adiabatic process. In this case, the state equation written as

$$\frac{dp}{dt} = c^2 \frac{d\rho}{dt}, \quad (2.1.3)$$

where $c = \sqrt{(dp/d\rho)_S}$, is the adiabatic sound velocity, S -entropy. In the general case, c and S can depend on spatial coordinates. For an inhomogeneous medium, Equation (2.1.3) should be written only in total derivatives because this equation

must be satisfied for a chosen particle rather than for the chosen point of the medium.

Under the effect of a sound wave, the pressure p and density ρ are disturbed; they take the following values:

$$p = p_0 + p', \quad \rho = \rho_0 + \rho', \quad (2.1.4)$$

where p_0 and ρ_0 are the values of p and ρ in the absence of sound wave; and p' and ρ' are disturbances of these quantities caused by the sound wave ($p' \ll p_0$, $\rho' \ll \rho_0$). Assuming p' and ρ' as quantities of the first order of smallness with respect to v/c , we neglect the terms of the second and higher orders in (2.1.1)–(2.1.3). As a result, we obtain

$$\frac{\partial \mathbf{v}}{\partial t} = -\frac{1}{\rho_0} \nabla p', \quad (2.1.5)$$

$$\frac{\partial \rho'}{\partial t} = \nabla(\rho_0 \mathbf{v}) = 0, \quad (2.1.6)$$

$$\frac{1}{c^2} \frac{\partial p'}{\partial t} = \frac{\partial \rho'}{\partial t} + (\mathbf{v} \nabla) \rho_0. \quad (2.1.7)$$

In the case of the homogeneous medium, the convection term $(\mathbf{v} \nabla) \rho_0$ vanishes in (2.1.7).

Differentiating (2.1.6) with respect to time, we obtain

$$\frac{\partial^2 \rho'}{\partial t^2} + \nabla \left(\rho_0 \frac{\partial \mathbf{v}}{\partial t} \right) = 0. \quad (2.1.8)$$

Substituting $\rho_0 \partial \mathbf{v} / \partial t$, according to (2.1.5), yields

$$\frac{\partial^2 \rho'}{\partial t^2} = \Delta p', \quad (2.1.9)$$

where Δ is the Laplace operator.

Differentiating (2.1.7) with respect to time, we rewrite it in the following form:

$$\frac{1}{c^2} \frac{\partial^2 p'}{\partial t^2} = \frac{\partial^2 \rho'}{\partial t^2} + \left(\frac{\partial \mathbf{v}}{\partial t} \nabla \right) \rho_0. \quad (2.1.10)$$

Having replaced the first term according to (2.1.9) and $\partial \mathbf{v} / \partial t$ according to (2.1.5) in the right-hand side of (2.1.10), we obtain (omitting indices)

$$\Delta p - \frac{1}{c^2} \frac{\partial^2 p}{\partial t^2} - \nabla \ln \rho \nabla p = 0. \quad (2.1.11)$$

In a homogeneous medium ($\rho = \text{const}$) the last term in (2.1.11) vanishes and (2.1.11) reduces to the wave equation

$$\Delta p - \frac{1}{c^2} \frac{\partial^2 p}{\partial t^2} = 0. \quad (2.1.12)$$

In this case, the sound field can be characterized by the acoustic velocity potential ψ determined by the expression

$$\mathbf{v} = \nabla \psi. \quad (2.1.13)$$

Substituting (2.1.13) in (2.1.5) yields the relation between the velocity potential and sound pressure:

$$p = -\rho \partial \psi / \partial t. \quad (2.1.14)$$

For harmonic waves $p \sim \exp(-i\omega t)$, the wave equation (2.1.12) reduces to the Helmholtz equation

$$\Delta p + k^2 p = 0, \quad (2.1.15)$$

where $k = \omega/c$ is the wave number of sound. The velocity potential ψ also satisfies (2.1.15).

Equation (2.1.11) can be converted to that of the Helmholtz equation type. Introducing a new function F instead of p :

$$F = p / \sqrt{\rho}, \quad (2.1.16)$$

we obtain

$$\Delta F + K^2 F = 0, \quad (2.1.17)$$

where

$$K^2 = k^2 + \frac{1}{2\rho} \Delta \rho - \frac{3}{4} \left(\frac{1}{\rho} \nabla \rho \right)^2. \quad (2.1.18)$$

Boundary Conditions. If the liquids are bounded or their parameters are discontinuous at some surfaces, then boundary conditions must be specified for these equations. At free water surface, the boundary condition consists of the equality of the sound pressure to zero:

$$p = 0. \quad (2.1.19)$$

At an interface of two liquid media, the boundary condition consists of the continuity of the sound pressure and the normal component of the particle velocity from both sides:

$$p = p_1, \quad v_n = v_{1n}, \quad \text{or} \quad \frac{1}{\rho} \frac{\partial p}{\partial t} = \frac{1}{\rho_1} \frac{\partial p_1}{\partial t}, \quad (2.1.20)$$

where \mathbf{n} is the unit vector of the normal to the interface. The index “1” refers to the second medium.

$$\frac{\partial p}{\partial n} = 0. \quad (2.1.21)$$

2.1.1 Simplest Solutions of the Helmholtz Equation

Now we consider two of the simplest solutions of (2.1.15) for an inhomogeneous medium (k is constant).

The first one is the spherical wave describing the field of an omnidirectional point source (a pulsating sphere of small radius)

$$p = \frac{-i\omega\rho V_0}{4\pi R} \exp(ikR), \quad (2.1.22)$$

where $R = (x^2 + y^2 + z^2)^{1/2}$, $V_0 = 4\pi a^2 v_0$ is the volume velocity of the source, a is the radius of the oscillating sphere, and v_0 is the amplitude of its surface velocity. The sound source is assumed to be at the origin of coordinates $x = y = z = 0$. One can easily verify that (2.1.22) satisfies (2.1.15) by direct differentiation, writing the Laplacian in the spherical system of coordinates

$$\Delta p = \frac{\partial^2 p}{\partial R^2} + \frac{2}{R} \frac{\partial p}{\partial R},$$

allowing p to depend in this case only on R .

Another simple and important solution of (2.1.15) is a plane wave

$$p = A \exp[i(k_x x + k_y y + k_z z)], \quad (2.1.23)$$

where A is the amplitude of the wave, and k_x , k_y , and k_z are three arbitrary constants (components of the wave vector along the coordinate axes) satisfying the relation

$$k_x^2 + k_y^2 + k_z^2 = k^2. \quad (2.1.24)$$

The surfaces of constant phase (wave fronts) of the spherical wave (2.1.22) are spheres ($R = \text{const}$), and the rays, which, by definition, are a family of lines orthogonal to the fronts, are straight lines starting from the point $R = 0$. In the case of the plane wave (2.1.23), the fronts are planes, $k_x x + k_y y + k_z z = \text{const}$, and the rays are the family of parallel straight lines orthogonal to these planes.

The solution of (2.1.5) in the form of a plane wave is of great importance. In many cases, especially at sufficiently large distances from the source, the sound wave can be represented as a plane wave or as a superposition of plane waves. This is obvious, for instance, for a spherical wave at large distances where the wave front curvature may be disregarded.

2.2 Refraction of Sound Rays

Consider first a horizontally stratified ocean where sound velocity only depends upon the depth [$c = c(z)$], and the surface and bottom of the ocean are horizontal planes. Even with these simplifying assumptions one can only succeed in finding exact solutions of (2.1.1) in exceptional cases. Therefore, the ray acoustics approximation is widely used. The necessary (but not sufficient) condition for its application is that the product of the relative gradient of the sound velocity and the wavelength must be small:

$$\frac{\lambda}{c} \left| \frac{dc}{dz} \right| \ll 1. \quad (2.2.1)$$

Furthermore, it is necessary that the reference point is not in the shadow zone or near its boundaries, and also not at the caustics (see below) or near them. If all the conditions of applicability of the ray theory are fulfilled, one can determine the sound intensity (and as a consequence the sound pressure) at any point, according to the law of expansion of a ray tube. In the ray theory approximation one can also define the sound-wave phase or the travel time of the sound pulse along a given ray.¹

Let us now show that in a horizontally stratified medium, at every z , a ray must satisfy the relation (Snell's law),

$$\frac{\cos \chi(z)}{c(z)} = \text{const} \quad (2.2.2)$$

where $\chi(z)$ is the grazing angle which a ray makes with planes $z = \text{const}$. For this purpose we imagine that the medium is divided by horizontal planes into a set of a great many thin homogeneous layers, and assume that the ray at the boundaries of these layers does not undergo reflection, just refraction. Let us denote the layers by $1, 2, \dots, n, n+1, \dots$. According to the refraction law (see below), at the boundary of layers n and $n+1$ with velocities c_n and c_{n+1} we have

$$\frac{\cos \chi_{n+1}}{c_{n+1}} = \frac{\cos \chi_n}{c_n}.$$

Similarly at the boundary of layers n and $(n-1)$:

$$\frac{\cos \chi_n}{c_n} = \frac{\cos \chi_{n-1}}{c_{n-1}},$$

and so on.

Let the number of layers tend to infinity and their thickness to zero, then we obtain the law (2.2.2) for the layered medium. This law, despite its simplicity, appears to be rather useful. So, all ray pictures in Sect. 1.2 have been plotted on the basis of this law.

With its help one can solve, for example, the problem of what angle χ a ray should leave a depth at which the sound velocity is c_1 in order to be horizontal at the depth where $c = c_2$ (Fig. 2.1). Since the grazing angle of this ray is zero (and its cosine is equal to unity) at the latter depth, then, using (2.2.2), for these two depths we have

$$\cos \chi = c_1/c_2$$

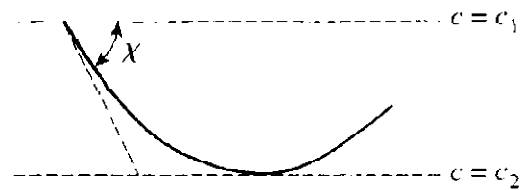


FIGURE 2.1. Relation between the grazing angle of a ray and the turning depth

¹ More detailed description of the transform of the Helmholtz equation to ray-theory equations is given in Sect. 2.6.

from which we define the angle χ . Usually c_2 is close to c_1 , and χ is small. Therefore, expanding the cosine in a series in χ , taking into account terms up to the second order, and denoting $c_2 - c_1 = \Delta c$, we find

$$\chi = (2\Delta c/c_1)^{1/2}. \quad (2.2.3)$$

This formula will be used often in the subsequent discussion.

Let us determine the relation between the ray curvature and the sound velocity gradient. For this purpose we shall write (2.2.2) in the form

$$c_0 \cos \chi = c \cos \chi_0,$$

where χ_0 and c_0 are the grazing angle and the sound velocity at some fixed depth. Differentiating this equality with respect to z gives

$$-c_0 \sin \chi \frac{d\chi}{dz} = \cos \chi_0 \frac{dc}{dz} \quad \text{or} \quad \frac{d\chi}{ds} = -q \frac{dc}{dz}, \quad (2.2.4)$$

where $ds = dz/\sin \chi$ is the element of the ray path length (Fig. 2.2) and

$$q = \frac{\cos \chi_0}{c_0} \quad (2.2.5)$$

is the constant parameter for each ray. We see that the derivative $d\chi/ds$, that is, the ray curvature at a given depth, is proportional to the sound velocity gradient at this depth. The minus sign in (2.2.4) shows that the grazing angle decreases with the increase in the sound velocity with depth, and vice versa.

The radius of curvature of the ray \mathcal{R} is

$$\mathcal{R}^{-1} = \left| \frac{d\chi}{ds} \right| = q \left| \frac{dc}{dz} \right|. \quad (2.2.6)$$

When the gradient $dc/dz = \text{const}$, $\mathcal{R} = \text{const}$, i.e., for the case of a constant sound velocity gradient, the ray is the arc of a circle.

Substituting (2.2.5) in (2.2.6) yields

$$\mathcal{R} = \frac{1}{a \cos \chi_0}$$

where $a = c_0^{-1} dc/dz$ is the vertical relative gradient of the sound velocity. The greater a and the less χ_0 , the stronger the ray refraction. On the contrary, if a ray comes out from the source vertically up or down ($\chi_0 = \pm\pi/2$) $\mathcal{R} = \infty$ and the refraction is absent.

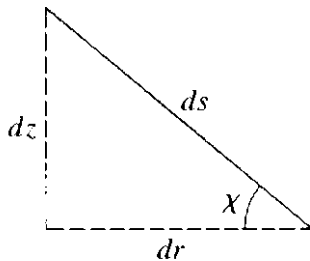


FIGURE 2.2. Ray element

2.3 Horizontal Distance Covered by a Ray

Let $r = 0$, $z = z_1$, and r, z be coordinates of a source and reference point, respectively. For an arbitrary infinitely small element of a ray (Fig. 2.2) one has $dr = |dz / \tan \chi|$. The total horizontal distance covered by the ray is

$$r = \left| \int_{z_1}^z \frac{dz}{\tan \chi} \right|. \quad (2.3.1)$$

According to (2.2.2) the grazing angle $\chi(z)$ can be expressed in terms of χ_1 , the angle at the source depth,

$$\cos \chi = (1/n) \cos \chi_1,$$

where $n = n(z) \equiv c_1/c(z)$, and c_1 is the sound velocity. Thus, (2.3.1) can be written as

$$r = \cos \chi_1 \left| \int_{z_1}^z [n^2(z) - \cos^2 \chi_1]^{-1/2} dz \right|. \quad (2.3.2)$$

We shall use this equation very frequently later on. Here r is assumed to be a single-valued function of z . If this is not the case (for instance, in the underwater sound channel where a ray repeatedly returns to some fixed depth), (2.3.2) is applied to those parts of the ray for which it is single valued. For instance, if a ray between the source and receiver has its turning point at depth z' , the equation for r consists of two parts:

$$r = \cos \chi_1 \left| \int_{z_1}^{z'} (n^2 - \cos^2 \chi_1)^{-1/2} dz \right| + \cos \chi_1 \left| \int_{z'}^z (n^2 - \cos^2 \chi_1)^{-1/2} dz \right|. \quad (2.3.3)$$

The travel time of the sound wave along the element of length ds is

$$dt = ds/c = |dz / (c \sin \chi)|.$$

Hence, the total travel time along the ray is

$$t = \left| \int_{z_1}^z \frac{dz}{c \sin \chi} \right|$$

or, expressing χ and c in terms of n and χ_1 ,

$$t = \frac{1}{c_1} \left| \int_{z_1}^z n^2 (n^2 - \cos^2 \chi_1)^{-1/2} dz \right| \quad (2.3.4)$$

where for the sake of simplicity we omit the argument z in $n(z)$. If a source radiates a harmonic wave of frequency $\omega = 2\pi f$, its phase at the reference point (r, z) is ωt ; the time t is given by the latter equation.

Differentiating r and t with respect to χ , we obtain

$$v \equiv \frac{\partial r / \partial \chi}{\partial t / \partial \chi} = \frac{c_1}{\cos \chi_1} = \text{const.}$$

Thus, $v = \partial r / \partial t$ —the horizontal component of the phase velocity of a wave propagating along the ray—is constant. Note also that $c_1 / \cos \chi_1$ is equal to the sound velocity at the turning depth z' and, therefore, $v = c(z')$.

2.4 Constant-Gradient Approximation of the Sound Velocity Profile

In order to plot rays for an arbitrary profile $c(z)$ one usually assumes a medium which consists of a certain number of layers with the simple law $c(z)$ and, as a consequence, with a simple rule for tracing the ray within each layer.

At the very outset of underwater acoustics the medium was divided into a set of homogeneous layers. The sound velocity changes by jumps at the layer boundaries. The rays in these layers are straight lines. Their direction changes upon refraction at the layer boundaries.

Later, division into layers where the dependence of velocity on depth is linear became widely used. In this case not the sound velocity but its gradient undergoes a discontinuity at the boundaries. As we already know, the rays in these layers are the arcs of circles. The direction of a ray, when it goes through a layer boundary, changes continuously, but its curvature changes discontinuously. A certain drawback of this method is that the discontinuity of the velocity gradient at the layer boundaries leads to pseudocaustics, as *Pedersen* [2.2] first showed. Approximations of $c(z)$ in some layers by polynomials of second and third orders (see, for example, [2.3, 4]) are used, as well.

Considering the simplicity and wide application of the constant-gradient approximation, we shall discuss it in detail. In Fig. 2.3 on the left-hand side, a profile $c(z)$ is shown according to this approximation, and on the right-hand side one of the

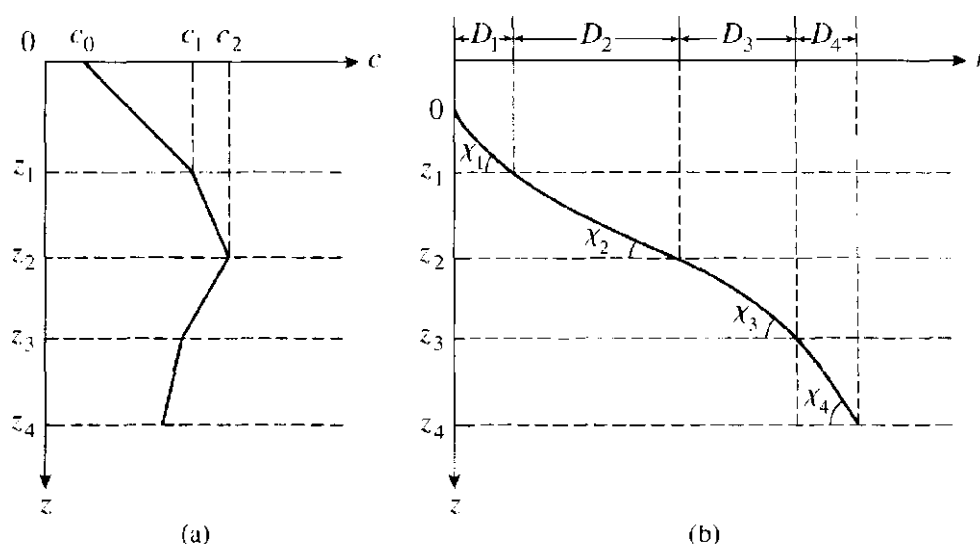


FIGURE 2.3. On the calculation of the ray diagram for the case of a constant-gradient approximation to the sound velocity

rays. We denote layer boundaries by z_1, z_2 etc. Let $h_i = z_i - z_{i-1}$ ($i = 1, 2, 3, 4$) be the thickness, and c_i and χ_i the sound velocity and the grazing angle at the lower boundary of each layer, respectively. They are related by Snell's law, $\cos \chi_i / c_i = \text{const}$, where the constant is determined by the grazing angle χ_1 of a ray at a source. The sound velocity gradient in the i th layers is $(c_i - c_{i-1})/h_i$. In Fig. 2.3 the gradient is positive in the two upper layers and negative in the two lower ones, and, correspondingly, the ray curvature has different signs in these layers.

Let us find the horizontal distance D_i covered by the ray in the i th layer. Setting $\chi_1 = \chi_{i-1}$ in (2.3.2), using the relation $\cos \chi = \cos \chi_1 / n(z)$ [where $n(z) = c_{i-1}/c(z)$], and passing to integration over χ , we obtain with (2.2.4)

$$D_i = \frac{1}{\cos \chi_{i-1}} \left| \frac{1}{a_i} \int_{\chi_{i-1}}^{\chi_i} \cos \chi \, d\chi \right| = \frac{1}{\cos \chi_{i-1}} \left| \frac{1}{a_i} (\sin \chi_i - \sin \chi_{i-1}) \right|, \quad (2.4.1)$$

where $a_i = (c_i - c_{i-1})/c_{i-1}h_i$ is the relative sound velocity gradient in the i th layer, and χ_{i-1}, χ_i are the grazing angles at its boundaries. For the total horizontal distance covered by the ray we have

$$r = \sum_i D_i.$$

2.5 Sound Intensity, Focusing Factor, and Caustics

It can be shown that the acoustical energy flux at any point in the medium is directed along a ray. Therefore, it is pertinent to imagine a ray tube formed by a set of rays leaving the source O and passing at some distance through an arbitrary small contour Γ (Fig. 2.4). In the ray theory approximation the acoustic energy is supposed to "flow" along the ray tube and not cross its walls. In what follows we will be interested in the sound intensity, that is, the energy flux per unit area of a cross-section of the ray tube per unit time. It is obvious that this quantity will decrease with distance from the source inversely proportional to the area of the ray tube cross-section.

In a homogeneous medium the area of the ray tube cross-section increases proportionally to the square of the distance from the source and, therefore, the

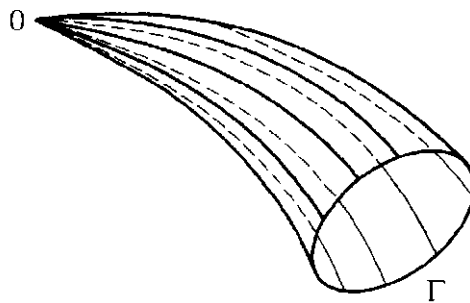


FIGURE 2.4. Ray tube

sound intensity decreases as the inverse distance squared. It is given by

$$I_0 = \frac{WN(\chi_1, \varphi_1)}{4\pi R^2}, \quad (2.5.1)$$

where W is the radiated acoustic power, R is the distance from the source, and $N(\chi_1, \varphi_1)$ is the factor (often called the pattern function) characterizing the directivity of the source. It depends upon the grazing angle χ_1 and the azimuth φ_1 of a ray at the source.

By definition, the mean value of the pattern function over all angles is equal to unity, that is

$$(4\pi)^{-1} \int_0^{2\pi} \int_{-\pi/2}^{\pi/2} N(\chi_1, \varphi_1) \cos \chi_1 d\chi_1 d\varphi_1 = 1.$$

In what follows we will omit the factor $N(\chi_1, \varphi_1)$ for the sake of simplicity. Therefore, our results will be valid, strictly speaking, only for omnidirectional sources. However, this factor can always be included in the final formulas for the sound intensity.

Now we obtain a formula for the sound intensity at an arbitrary point $A(r, z)$ (Fig. 2.5) for the horizontally stratified medium [$c = c(z)$] when sound refraction takes place. Let the source be located at the point $r = 0, z = z_1$. The horizontal distance r travelled by an arbitrary ray is a function of the initial angle χ_1 , i.e., $r = r(\chi_1)$. Let the ray leaving the source at the angle $\chi_1 + d\chi_1$ arrive at point C located at the same depth z as point A . Obviously $AC = |\partial r / \partial \chi_1| d\chi_1$. The ray tube cross-section in the r, z plane illustrated in the figure is

$$BC = AC \sin \chi = \left| \frac{\partial r}{\partial \chi_1} \right| \sin \chi d\chi_1,$$

where χ is the grazing angle at point A .

Since the source is supposed to be omnidirectional, the sound field has cylindrical symmetry with respect to the z axis. If we imagine that the diagram in Fig. 2.5 is rotated about the z axis, we obtain for the area of the wave front contained between these rays

$$dS = 2\pi r \left| \frac{\partial r}{\partial \chi_1} \right| \sin \chi d\chi_1.$$

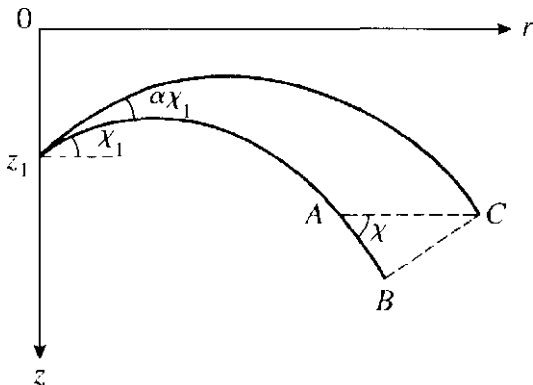


FIGURE 2.5. On the calculation of the focusing factor

The power W radiated by the source into the interval $d\chi_1$ flows through this area. Obviously, the power dW is related to the total power output of the source, as the solid angle $2\pi \cos \chi_1 d\chi_1$ corresponding to this area is related to 4π . Hence,

$$dW = (W/2) \cos \chi_1 d\chi_1.$$

Now, for the sound intensity, i.e., for the power flux per unit of the wave front surface, we obtain

$$I = \frac{dW}{dS} = \frac{W \cos \chi_1}{4\pi r \left| \frac{\partial r}{\partial \chi_1} \right| \sin \chi}. \quad (2.5.2)$$

In the case of a directional source, the factor $N(\chi_1, \varphi_1)$ must be introduced into this equation.

In the theoretical analysis of the sound field structure, the source power W is not essential (linear acoustics!) and, therefore, it is reasonable to normalize I to the value $I_0 = W/(4\pi r^2)$ —the sound intensity of the same source in the homogeneous medium at point (r, z) . We shall call the ratio

$$f = \frac{I}{I_0} = \frac{r \cos \chi_1}{\left| \frac{\partial r}{\partial \chi_1} \right| \sin \chi} \quad (2.5.3)$$

the focusing factor. The case $f \ll 1$ corresponds to a strong decrease of the field due to an anomalously large divergence of rays (as compared with the spherical wave). In contrast, the case $f \gg 1$ corresponds to an increase of the field due to the focusing of the rays.² Ray theory is not applicable, as a rule, in these two extreme cases.

Caustics is the term used to describe the loci at which the focusing factor is equal to infinity. These are the envelopes of the family of rays. In Fig. 2.6 the ray diagram with a caustic AA is shown.

The equation for each ray can be given in the form

$$r = r(\chi_1, z), \quad (2.5.4)$$

where χ_1 is a parameter of the family of rays leaving the source O . As is known, the envelope of such a family of rays can be found by elimination of χ_1 from (2.5.4) and

$$\frac{\partial r(\chi_1, z)}{\partial \chi_1} = 0. \quad (2.5.5)$$

²The exception is the case $r = 0$ ($z \neq z_1$), where f is equal to zero, not because of any peculiarity of the field, but just by virtue of our definition of f . Sometimes for the definition of f the quantity I in (2.5.2) is related to $I_0 = W/(4\pi R^2)$, where R is the total (inclined) distance from the source to receiver. However, the definition (2.5.3) is more convenient for practical purposes.

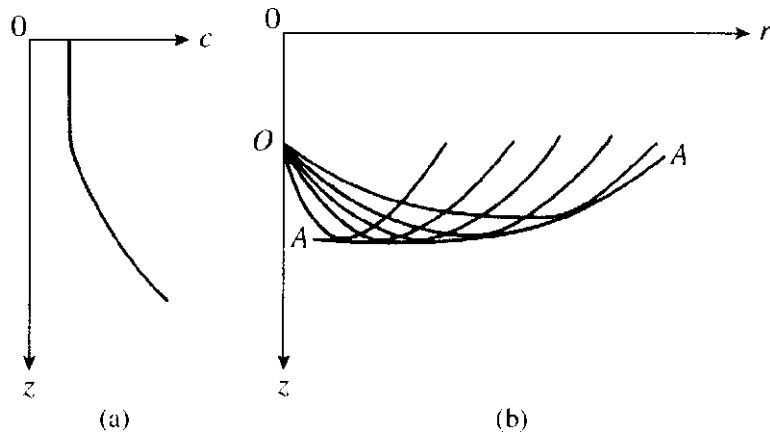
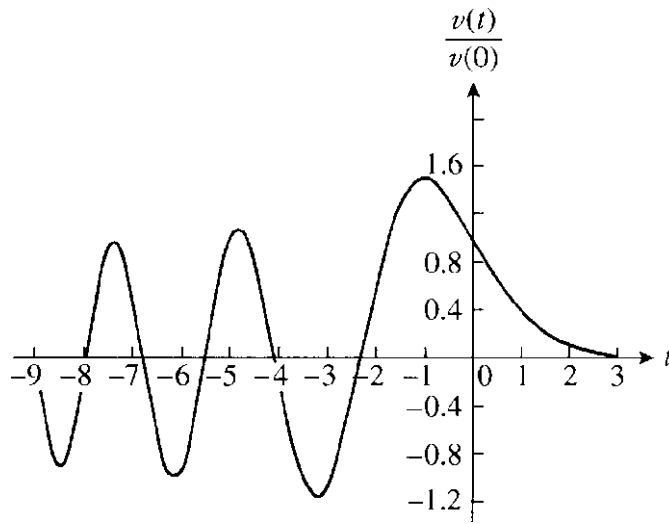
FIGURE 2.6. (a) Profile $c(z)$ and (b) ray diagram with a caustic

FIGURE 2.7. Plot of the Airy function

From (2.5.3) and (2.5.5) one can see that the focusing factor, indeed, goes to infinity on the envelope of the family of rays. For the calculation of the focusing factor on the caustic and near it, geometrical acoustics requires some modification. We cannot go into details here (see [Ref. 2.5, Sect. 45]) and only note that the focusing factor on and near the caustic is given by

$$f = 2^{5/3} \frac{\cos \chi_1 (k_1 \sin \chi_1)^{1/3}}{\sin \chi} r \left| \frac{\partial^2 r}{\partial \chi_1^2} \right|^{-2/3} v^2(t), \quad (2.5.6)$$

where $v(t)$ is the Airy function plotted in Fig. 2.7 with $v(0) = 0.6293$. The argument of the Airy function is given by

$$t = \pm 2^{1/3} \left| \frac{\partial^2 r}{\partial \chi_1^2} \right|^{-1/3} (k_1 \sin \chi_1)^{2/3} (r - r_0). \quad (2.5.7)$$

Here $r - r_0$ is the horizontal distance between the observation point and caustic. In (2.5.7) we must choose the plus sign when $\partial^2 r / \partial \chi_1^2 < 0$ and minus sign when

$\partial^2 r / \partial \chi_1^2 > 0$. At one side of the caustic (above the caustic in Fig. 2.6) two rays intersect at each point. The spatial oscillations of the field are due to the interference between these two rays ($t < 0$ in Fig. 2.7). At the other side of the caustic (below it in Fig. 2.6) none of the rays of this family arrive. This is a shadow zone corresponding to the rapid decrease of the field with distance from the caustic ($t > 0$ in Fig. 2.7).

2.6 "Three-Dimensional" Refraction

In a medium where the index of refraction $n = n(\mathbf{R})$ may be a function of all three coordinates, a ray will not be confined in one plane, i.e., we will have three-dimensional refraction. In ocean acoustics, we encounter such refraction, for example, when analyzing the effect of an internal wave on a sound field. The same problem arises when studying long-range sound propagation in a range-dependent ocean. Three-dimensional refraction is also observed near icebergs which form local regions of cooling and freshening and at well-defined boundaries of ocean currents.

In order to derive equations for ray acoustics in a three-dimensional case, we represent the sound pressure $p(\mathbf{R})$ in the form

$$p(\mathbf{R}) = A(\mathbf{R}) \exp[ik_0 W(\mathbf{R})], \quad \mathbf{R} = \{x, y, z\} \quad (2.6.1)$$

where A and $k_0 W$ are the amplitude and phase of a sound wave, the function W often being called the *eikonal*, $k_0 = \omega/c_0$, and c_0 is the sound velocity at some fixed point (usually at the point where the sound source is located). Substitution of (2.6.1) in the Helmholtz equation

$$\Delta p + k^2(\mathbf{R})p = 0, \quad k(\mathbf{R}) = k_0 n(\mathbf{R})$$

yields

$$\Delta A + ik_0(2\nabla A \cdot \nabla W + A\Delta W) + k_0^2 A[n^2 - (\nabla W)^2] = 0. \quad (2.6.2)$$

Equations for ray theory are obtained from (2.6.2) when k_0 tends to infinity $k_0 \rightarrow \infty$ (sound wavelength $\lambda = 2\pi/k_0 \rightarrow 0$). Neglecting the first term in (2.6.2) and then equating the real and imaginary parts in the remaining equation separately to zero, we obtain two equations:

the *eikonal equation*

$$(\nabla W)^2 = n^2 \quad (2.6.3)$$

and the *transport equation*

$$2\nabla A \cdot \nabla W + A\Delta W = 0. \quad (2.6.4)$$

The eikonal equation (2.6.3) defines the geometry of the rays, i.e., the lines orthogonal to the wave fronts, with $W = \text{const}$. If \mathbf{R} is a radius vector of a point on a ray, and s is the distance along the ray, then this orthogonality gives for

$d\mathbf{R}/ds \equiv \mathbf{e}$ the unit vector along the ray

$$n\mathbf{e} = \nabla W. \quad (2.6.5)$$

Differentiating (2.6.5) with respect to s and using (2.6.3) and (2.6.5), we obtain the ordinary differential equation for the ray's trajectories

$$\begin{aligned} \frac{d}{ds}(n\mathbf{e}) &= \frac{d}{ds}(\nabla W) = (\mathbf{e} \cdot \nabla)\nabla W = n^{-1}(\nabla W \cdot \nabla)\nabla W \\ &= (2n)^{-1}\nabla(\nabla W)^2 = (2n)^{-1}\nabla(n^2) = \nabla n. \end{aligned} \quad (2.6.6)$$

Thus,

$$\frac{d}{ds}(n\mathbf{e}) = \nabla n. \quad (2.6.7)$$

For the case of a homogeneous medium $n = 1$ and from (2.6.7) it follows that

$$\frac{d\mathbf{e}}{ds} = 0$$

and, therefore, $\mathbf{e} = \text{const}$ along the ray whose equation can now be written as

$$\mathbf{R} = s\mathbf{e} + \mathbf{R}_0$$

—the equation for a straight line—where \mathbf{R}_0 is a radius vector of the point at which the ray originates.

Multiplying vectors \mathbf{e} and ∇n in (2.6.7) by the horizontal component of the unit vector \mathbf{e}_r and taking into account that the scalar products $\mathbf{e}\mathbf{e}_r = \cos \chi$ and $\nabla n\mathbf{e}_r = 0$, we directly obtain Snell's law $n \cos \chi = \text{const}$. Multiplying the same vectors by the vertical component of the unit vector \mathbf{e}_z , we obtain

$$\frac{d}{ds}(n \sin \chi) = \frac{dn}{dz}$$

from whence expression (2.2.6) for the radius of ray curvature is easily obtained.

It is more convenient in numerical calculation to use, instead of (2.6.7), the equivalent system of two first-order equations:

$$\frac{d\mathbf{R}}{dt} = \frac{c^2}{\omega}\mathbf{k}, \quad \frac{d\mathbf{k}}{dt} = \frac{\omega}{n}\nabla n. \quad (2.6.8)$$

This equivalence can be easily proved if we take into account that $\mathbf{e} = d\mathbf{R}/ds = c^{-1}d\mathbf{R}/dt$, t is the travel time along the ray, $\mathbf{k} = k_0 n\mathbf{e}$ is the wave vector at point \mathbf{R} , and $k = \omega/c(\mathbf{R})$, $c(\mathbf{R}) = c_0/n(\mathbf{R})$. The frequency ω only enters (2.6.8) formally, because the wave vector was chosen as one of the ray coordinates. The ray geometry does not depend on ω .

Having found the ray trajectory $\mathbf{R} = \mathbf{R}(s)$ from (2.6.8), we can represent the function W as an integral along the ray. This becomes, by virtue of (2.6.5),

$$\frac{dW}{ds} = \mathbf{e} \cdot \nabla W = n$$

whence

$$W = \int_0^s n[\mathbf{R}(s)] ds.$$

The transport equation (2.6.4) determines the wave amplitude. Let us obtain an expression for it in explicit form. Application of the divergence operator to (2.6.5) yields

$$\Delta W = \mathbf{e} \cdot \nabla n + n \nabla \mathbf{e}. \quad (2.6.9)$$

The divergence of the unit vector along a ray is given by [Ref. 2.6, Sect. 150]

$$\nabla \mathbf{e} = \frac{\partial}{\partial s} \ln D \quad (2.6.10)$$

where

$$D = \frac{\partial(x, y, z)}{\partial(t, k_x^0, k_y^0)} = \frac{d\mathbf{R}}{dt} \cdot \left(\frac{\partial \mathbf{R}}{\partial k_x^0} \times \frac{\partial \mathbf{R}}{\partial k_y^0} \right) \quad (2.6.11)$$

is the Jacobian of the transform from Cartesian coordinates (x, y, z) to the ray coordinates (t, k_x^0, k_y^0) , where $k_x^0 = k_0 \sin \theta_0 \cos \varphi_0$, $k_y^0 = k_0 \sin \theta_0 \sin \varphi_0$, and θ_0, φ_0 are the angles of the ray at a sound source in the spherical coordinate system.

The expression for D , using (2.6.8), can be written

$$D = \frac{c^2}{\omega} \mathbf{k} \cdot \left(\frac{\partial \mathbf{R}}{\partial k_x^0} \times \frac{\partial \mathbf{R}}{\partial k_y^0} \right). \quad (2.6.12)$$

The quantities $\partial \mathbf{R} / \partial k_j^0$, ($j = x, y$) necessary for calculation of D are found by differentiating (2.6.8) with respect to k_j^0

$$\begin{aligned} \frac{d}{dt} \frac{\partial \mathbf{R}}{\partial k_j^0} &= \frac{1}{\omega} \frac{\partial}{\partial k_j^0} (c^2 \mathbf{k}) = \frac{c_0^2}{\omega} \frac{\partial}{\partial k_j^0} \left(\frac{\mathbf{k}}{n^2} \right) \\ &= \frac{c^2}{\omega} \left[\frac{\partial \mathbf{k}}{\partial k_j^0} - \frac{2\mathbf{k}}{n} \left(\nabla n \cdot \frac{\partial \mathbf{R}}{\partial k_j^0} \right) \right]. \end{aligned}$$

Here we have taken into account that

$$\frac{\partial n}{\partial k_j^0} = \frac{\partial n}{\partial x} \frac{\partial x}{\partial k_j^0} + \frac{\partial n}{\partial y} \frac{\partial y}{\partial k_j^0} + \frac{\partial n}{\partial z} \frac{\partial z}{\partial k_j^0} = \left(\nabla n \cdot \frac{\partial \mathbf{R}}{\partial k_j^0} \right).$$

Similarly, we find

$$\frac{d}{dt} \frac{\partial \mathbf{k}}{\partial k_j^0} = \frac{\omega}{n} \left[\left(\frac{\partial \mathbf{R}}{\partial k_j^0} \cdot \nabla \right) \nabla n - \frac{\nabla n}{n} \left(\nabla n \cdot \frac{\partial \mathbf{R}}{\partial k_j^0} \right) \right].$$

Let us now find the quantity $\nabla A \cdot \nabla W$ entering into the transport equation (2.6.4). Since

$$\nabla W = \frac{dW}{ds} \mathbf{e} \quad \text{and} \quad \frac{dW}{ds} = n, \quad (2.6.13)$$

then

$$\nabla A \cdot \nabla W = \frac{\partial A}{\partial s} \frac{dW}{ds} = n \frac{\partial A}{\partial s}. \quad (2.6.14)$$

Substituting (2.6.9) and (2.6.14) in (2.6.4), and taking into account that $\nabla n \cdot \mathbf{e} = \partial n / \partial s$, after some simple transformations we obtain

$$\frac{\partial}{\partial s}(A^2 n D) = 0.$$

Hence, the quantity $A^2 n D$ is constant along a ray and, therefore,

$$A = B(nD)^{-1/2}. \quad (2.6.15)$$

Here B is a constant determined from the conditions near the sound source where one can neglect the refraction and consider a medium as homogeneous ($n = 1$). For a point source in the homogeneous medium $A = 1/R$ and $B = (D_0)^{1/2}/R$, where D_0 is the value of D for $n = 1$. Thus,

$$A(\mathbf{R}) = \frac{1}{R} \left(\frac{D_0}{nD} \right)^{1/2}. \quad (2.6.16)$$

For the homogeneous medium

$$\mathbf{R} = R(\mathbf{k}_0/k_0), \quad \frac{d\mathbf{R}}{dt} = c_0(\mathbf{k}_0/k_0), \quad \mathbf{k}_0 = \{k_x^0, k_y^0, k_z^0\}$$

and

$$D_0 = \frac{c_0 R^2}{k_0^2 \cos \theta_0}. \quad (2.6.17)$$

Substitution of (2.6.17) in (2.6.16) yields

$$A(\mathbf{R}) = \frac{1}{k_0} \left(\frac{c}{D \cos \theta_0} \right)^{1/2}. \quad (2.6.18)$$

On caustics $D = 0$ and the amplitude of the sound wave becomes infinite. For this case the sound field can be calculated by use of asymptotical formulae contained, for example, in the work by *Kravtsov* [2.7].

2.7 Snell's Law for the Range-Dependent Ocean

Snell's law (2.2.2) is a fundamental relationship in ray theory. It relates the grazing angle χ of a ray at some depth to the sound velocity c at this depth as well as to the sound velocity c_0 and angle χ_0 at the source, and thereby determines the ray structure of the sound field. Using Snell's law we can determine an important characteristic of the USC: the maximum grazing angle χ_{\max} of rays trapped by the waveguide, which in turn determines the relative amount of the trapped acoustic power [see (6.1.3)].

If there is range dependence, the ray pattern of the sound field undergoes changes which result in the spatial redistribution of acoustic power. To examine these perturbations of the sound field it is necessary to obtain Snell's law for a range-dependent environment. If variations of the refraction index in the horizontal

direction are slow enough, we may use Snell's law in the form of (7.2.10), considering r as a parameter. Here we obtain, however, another form of Snell's law for this case, following the paper by *Henrich* and *Burkon* [2.8]. Let us start from (2.6.7) and assume that sound velocity variations in a horizontal plane across the propagation track can be neglected. Hence, the ray initially lying in the xz plane will remain in the same plane at any distance from the source. Then, assuming in (2.6.7)

$$\mathbf{e} = \{\cos \alpha, 0, \sin \alpha\},$$

we obtain

$$\frac{d}{ds} (n \cos \chi) = \frac{\partial n}{\partial x}, \quad \frac{d}{ds} (n \sin \chi) = \frac{\partial n}{\partial z}. \quad (2.7.1)$$

Integrating the first equation in (2.7.1) with respect to s over the ray path, we find

$$n \cos \chi|_0^s = n \cos \chi - \cos \chi_0 = \int_0^s \frac{\partial n}{\partial x} ds. \quad (2.7.2)$$

Taking into account that $n = c_0/c$ and setting $ds = dx/\cos \chi$, (2.7.2) can be rewritten as

$$\frac{\cos \chi}{c} = \frac{\cos \chi_0}{c_0} - \int_0^s \frac{\partial c}{\partial x} \frac{1}{\cos \chi} dx. \quad (2.7.3)$$

Further simplifications are based on the small fractional variation of the sound velocity that occurs in the ocean,

$$(c - c_0)/c_0 \equiv \varepsilon \ll 1.$$

The order of magnitude ε is 10^{-2} . It is evident also that

$$\cos \chi = \cos \chi_0 [1 + O(\varepsilon)].$$

Keeping in mind these approximations, we retain in (2.7.3) only the terms not higher than the first order of ε . As a result, we obtain Snell's law for a range-dependent environment:

$$\cos \chi = \cos \chi_0 \left(\frac{c}{c_0} - \int_0^s \frac{\partial c}{\partial x} \frac{dx}{c_0 \cos^2 \chi_0} \right). \quad (2.7.4)$$

This expression determines the angle χ for any z which belongs to the given ray path.

To demonstrate possible variations of the ray pattern of the sound field in the range-dependent ocean, it is useful to consider the sound velocity c' at the turning depth of a ray. Setting $\chi = 0$ in (2.7.4), we find

$$c' = \frac{c_0}{\cos \chi_0} + \int_0^s \frac{\partial c}{\partial x} \frac{dx}{\cos^2 \chi_0}. \quad (2.7.5)$$

The first term corresponds to the range-independent ocean, whereas the second term describes an effect of cumulative horizontal sound velocity variation along the ray path. From (2.7.5) it follows that c' varies along the ray path.

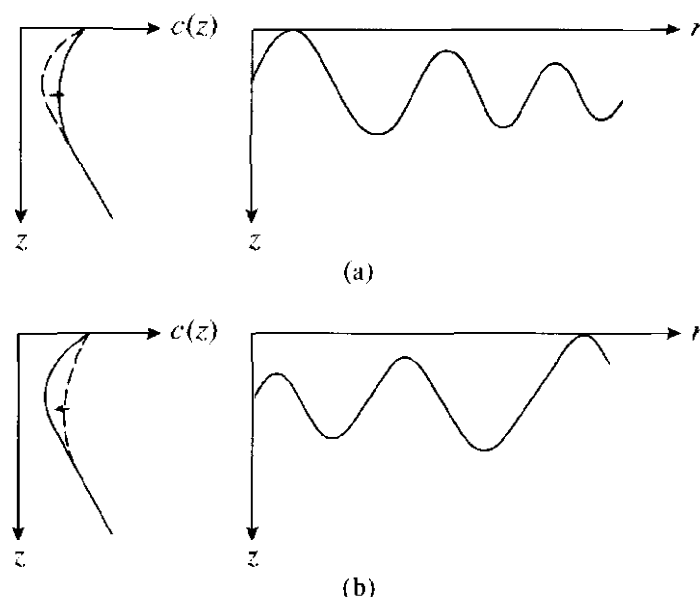


FIGURE 2.8. Effects of horizontal sound velocity gradients on the ray picture (a) $\partial c/\partial x > 0$; (b) $\partial c/\partial x < 0$

For positive sound velocity gradients ($\partial c/\partial x > 0$), $c' > c_0/\cos \chi_0$ and, therefore, the depth of the lower turning points in the USC increases, while that for the upper ones decreases as x increases (Fig. 2.8a). As a result, it can happen that beginning from some distance, c' will exceed c_b the sound velocity near the ocean bottom. In this case a ray will be reflected from the bottom. The sound field level in water due to this ray will be greatly reduced either in long-range sound propagation when multiple bottom reflections lead to large total losses of acoustic power, or in a case of a very lossy bottom.

For negative sound velocity gradients ($\partial c/\partial x < 0$), c' will be less than $c_0/\cos \chi_0$, and the depth of lower turning points decreases, while that for the upper ones increases (Fig. 2.8b). For this reason the ray arriving at a given depth at small ranges will not reach it at long ranges. As a result, the number of rays arriving at the receiver may appear to be less than in a range-independent ocean. The sound field level may also be reduced in this case.

Several examples of Snell's law used in the form of (2.7.4) for the numerical calculation of the reduction of the sound field level in convergence zones arising in sound propagation across a ring of the Gulf Stream are given in [2.8].

2.8 Ocean Acoustic Tomography

As noted in Sect. 1.4, the World Ocean is extremely variable—fronts, large-scale currents, eddies of different sizes disturb water masses over vast space. The ocean variability has a pronounced effect on the ocean climate and weather on the earth; it determines in many respects the biological productivity of the ocean and significantly changes the zonal structure of acoustic fields, causes sound signal fluctuations, and disturbs ray paths. Certainly, information on the behaviour

of water masses obtained from research vessels and satellites is very great, but, nevertheless, it is insufficient for practical purposes since it refers mainly to the surface and subsurface layers of the ocean.

The problematic acquisition of necessary information can be solved by the organization of monitoring over a long period of time (about a year) over the aquatorium of the area of 10^6 km^2 . Low-frequency acoustic waves are best suited for such monitoring because they can propagate to very long distances (Sect. 1.2) and they possess the high sensibility to inhomogeneities of the water column and boundary roughnesses of various kinds. The latter change acoustic signal characteristics such as travel times along rays, phase and group velocities of modes, and space-frequency interference patterns of the acoustic field. For the determination of hydrophysical parameters of the ocean medium, ocean acoustic tomography (OAT) uses variations of acoustic probing signals transmitted through a tested region between groups of sources and receivers. The existing methods of OAT differ by a technique of field measurements, type of signals used, inhomogeneities reconstructed, and methods of the inversion (reconstruction) of hydrophysical parameters. A typical scheme of ocean acoustic tomography is shown in Fig. 2.9. Here, S_1 – S_3 are the acoustic transmitters and R_1 – R_4 are the receivers. The concept of OAT was first advanced by *Munk* and *Wunsch* [2.9]. The scheme they suggested was destined for the reconstruction of the meso-scale inhomogeneities of the sound velocity field by measuring arrival times of impulse signals along different ray paths. The difference in the arrival times may also be used for the reconstruction the other characteristics of the sea medium such as temperature, speed of currents, and salinity. Acoustic thermometry of the ocean medium is already used for monitoring the global warming of the earth's climate [2.10, 11]. It is also shown that acoustic halinometry may be used for remote determination of the salinity in the under-ice layers in the Arctic Ocean [2.12].

We consider the basic relationships of ray tomography. The travel time t_m of an acoustic signal along a ray path Γ_m connecting some transmitter with one of the

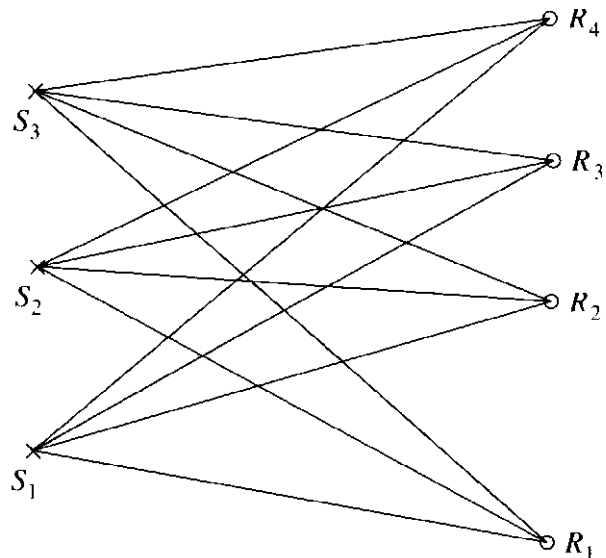


FIGURE 2.9. Typical scheme of ocean acoustic tomography

receivers is given by

$$t_m = \int_{\Gamma_m} \frac{ds}{c(\mathbf{r}, z)}, \quad (2.8.1)$$

where $c(\mathbf{r}, z)$ is the sound velocity in the medium and ds is the element of the ray path Γ_m . Represent $c(\mathbf{r}, z)$ as

$$c(\mathbf{r}, z) = c_0(\mathbf{r}, z) + \Delta c(\mathbf{r}, z), \quad (2.8.2)$$

where $c_0(\mathbf{r}, z)$ is the known (reference) value of the sound velocity field (for $\Delta c = 0$) and $\Delta c(\mathbf{r}, z)$ is the disturbance caused by the presence of inhomogeneities in the water column, which are subject to the determination. As c_0 , one may choose different distributions, for example, such as the mean-climate distribution of the sound velocity field averaged over the aquatorium. The specific choice of c_0 depends on the amount of the hydrophysical data and on the possibility of calculating ray trajectories in a given inhomogeneous medium. Therefore, the tomography problem reduces to that of finding t_m by a set of Δc . In the exact statement, this problem is very complicated. It is nonlinear since Δc appears in the denominator, and in addition the integration path Γ_m depends on Δc . However, the problem is greatly simplified due to the presence of a small parameter $\varepsilon = |\Delta c/c_0|$, which even for the most intense eddies—the rings of the Gulf Stream—is usually no larger than 0.02 [2.13, 14]. Taking into account the smallness of ε , we expand the right-hand side in (2.8.1) in powers of ε and retain only terms no higher than the first order of smallness:

$$t_m = t_m^{(0)} + t_m^{(1)} + \dots,$$

where

$$t_m^{(0)} = \int_{\Gamma_m^{(0)}} \frac{ds}{c_0(\mathbf{r}, z)}$$

is the time of signal transmission in the unperturbed medium along the ray $\Gamma_m^{(0)}$, and ds is the element of its length. A linear correction to $t_m^{(0)}$ is given by

$$t_m^{(1)} = - \int_{\Gamma_m^{(0)}} \frac{\Delta c}{c_0^2} ds. \quad (2.8.3)$$

It is precisely this equation that is the basis of the Munk–Wunsch tomography method. The replacement Γ_m by $\Gamma_m^{(0)}$ in (2.8.3) leads to an error that for rather small values of ε is not large and depends on spatial scales of inhomogeneities, path length transmitted by the l th ray within the inhomogeneous region, and the general extension of the acoustic track. It is assumed that the ray $\Gamma_m^{(0)}$ continuously passes to the ray Γ_m at $\Delta c \rightarrow 0$ [2.13]. The linearization of (2.8.1) is sometimes not true. The point is that even for small values of ε , the shape of the ray $\Gamma_m^{(0)}$ can significantly differ from that of ray Γ_m . In this case the reconstruction of inhomogeneities becomes impossible. The estimation of a quadratic correction to $t_m^{(0)}$ and the condition of the application of the linear approximation are given

in [2.14]. A value $t_m^{(1)}$ and measured time t_m of the signal arrival at the point of reception are related by the relation $t_m^{(1)} = t_m - t_m^{(0)}$.

Equation (2.8.3) is written for each of rays $m = 1, 2, 3, \dots, N$, connecting all transmitters and receivers. In the multimode propagation of sound in the underwater sound channel, the total number of rays is $N = srl$, where s is the number of sources, r is that of receivers, and l is the typical number of rays connecting every pair transmitter–receiver. The parameter l is determined by the properties of the medium and disposition of the corresponding points of transmission and reception. For a numerical solution of (2.8.3), we divide the test region into cells of arbitrary form. Their dimensions should be no larger than spatial scales of fluctuations Δc . Assume also that fluctuations Δc within each cell are constant and equal to Δc_n . Then (2.8.3) reduces to the linear system of algebraic equations [2.13–15]

$$t_m^{(1)} = \sum_{n=1}^N E_{mn} \Delta c_n, \quad (2.8.4)$$

where $E_{mn} = 0$ if a perturbed ray m does not pass through cell n , and $E_{mn} = \int_{\Gamma_{mn}^{(0)}} c^{-2} ds$ otherwise. Here $\Gamma_{mn}^{(0)}$ is the path of ray m in cell n . The system (2.8.4) can be solved by a standard method.

We consider now the question on tomography of the currents [2.14, 15]. Assume that the Mach number is small compared to unity, $M = v/c$, where v is the current speed. In this case the fluctuations of signal travel time in the first approximation in ε and M are given to be

$$t_m^{(1)} = - \int_{\Gamma_m^{(0)}} c_0^{-2} (\Delta c + \mathbf{v} \mathbf{e}_m) ds, \quad (2.8.5)$$

where \mathbf{e}_m is the unit vector along the ray $\Gamma_m^{(0)}$. In order to determine \mathbf{v} , it is necessary to measure $t_m^{(1)}$ when the signal propagates up- and downstream, i.e., to interchange positions of the transmitter and receiver. Let expression (2.8.5) describe the travel time downstream. Denoting the travel time fluctuations upstream through $\tilde{t}_m^{(1)}$, we have

$$\tilde{t}_m^{(1)} = - \int_{\Gamma_m^{(0)}} c_0^{-2} (\Delta c - \mathbf{v} \mathbf{e}_m) ds. \quad (2.8.6)$$

Subtracting (2.8.6) from (2.8.5) yields

$$\Delta t_m^{(1)} = - \int_{\Gamma_m^{(0)}} c_0^{-2} \mathbf{v} \mathbf{e}_m ds, \quad (2.8.7)$$

where

$$\Delta t_m^{(1)} = \frac{t_m^{(1)} - \tilde{t}_m^{(1)}}{2}.$$

The possibility of using (2.8.7) for the reconstruction of speed currents is based on the assumption that real ray trajectories are rather close to $\Gamma_m^{(0)}$ for sound propagation in opposite directions. Note also that (2.8.7) determines only the

projection of the vector \mathbf{v} on the direction \mathbf{e}_m rather than the true vector \mathbf{v} . Only for shallow grazing angles of rays in the vertical plane can the vector \mathbf{e}_m be replaced by the horizontal vector \mathbf{e} directed from the emission point to that of reception. Denoting $v_0 = \mathbf{v}\mathbf{e}$, we obtain

$$\Delta t_m^{(1)} = - \int_{\Gamma_m^{(0)}} c_0^{-2} v_0 ds. \quad (2.8.8)$$

The structure of (2.8.8) coincides with that of (2.8.3) and can also be reduced to a system of linear algebraic equations.

Note that for the successful realization of the considered tomography scheme, one needs severe monitoring for the exact disposition of transmitters and receivers at any time, synchronization of their operation, rather intense and well-separated signals, long-term observations, and appropriate choice of the reference sound velocity distribution close to the true one.

Except for ray tomography, other methods of OAT have received significant development: the mode method using perturbations of phase and group velocities of the acoustic modes of low numbers as initial data [2.9, 16]; the interference method based on the measurements of the phase difference of separated modes [2.13, 15]; and the diffraction method, where reconstructed parameters are perturbations of the sound velocity field and the density of the water column as well as statistical characteristics of the rough sea surface and the ocean bottom [2.17]. In spite of significant differences among these methods, they all refer in essence to a general group because of the identical setup measurements based on the use of broad-band pseudo-pulsed signals propagating between transmitters and receivers lying at anchor. This group is usually referred to as traditional tomography. A different approach uses transmitters and/or receivers lowered from aboard a moving ship (dynamic tomography) [2.18, 19]. Traditional tomography is convenient for long-term observations since it can be realized without any operator and yields oceanographic parameters of the meso-scale environmental inhomogeneities averaged over acoustic tracks, whereas dynamic tomography provides a greater number of propagation tracks and the rather high horizontal resolution. In addition, it allows us easily to change the region of investigations and the strategy of measurements in the course of investigations [2.19]. Dynamic tomography is most suitable for probing meso-scale inhomogeneities. A detailed classification of recent methods of ocean acoustic tomography is given in [2.13, 15]. The problems and methods of ocean acoustic tomography are comprehensively presented in the fundamental monography [2.20].

2.9 Weakly Divergent Bundles of Rays

The experiments on vertical sensing of an acoustic field in the deep ocean at long distances from a source have revealed intervals of depths with the increased level of radiated signals [2.21]. It appears that, under certain hydrological conditions, the acoustic energy can be focused at several depths instead of the uniform distribution

over the whole water column. In works [2.21, 22], a hypothesis is advanced that supposes anomalies of the acoustic intensity are due to weakly divergent bundles (WDB) of rays whose launch-grazing angles from the source are close to the points of smooth extrema of the dependence of the ray cycle length $D(\chi_0)$ on χ_0 . In other words, the weakly divergent bundles arise near specific rays for which $dD/d\chi_0 = 0$. Such bundles are localized in space and have a quasi-periodic structure.

We consider WDB of rays in an underwater sound channel with the sound velocity profile that is typical for the Northern Atlantic [2.23]:

$$c(z) = \begin{cases} c_0 - a_1 z, & -h \leq z \leq 0, \\ c_0 + a_2 z, & 0 \leq z \leq z_2, \\ c_2 + a_3(z - z_2), & z_2 \leq z \leq H, \end{cases} \quad (2.9.1)$$

where c_0 is the sound velocity at the channel axis $z = 0$, $z = -h$ is the sea surface, $z = H$ is the ocean bottom, and a_1 , a_2 , and a_3 are the sound velocity gradients in the layers (Fig. 2.10).

The ray cycle length is determined by (2.3.1), where integration limits extend from z' (the upper turning point) to z'' (the lower turning point):

$$D(\chi_0) = 2 \int_{z'}^{z''} \frac{dz}{\tan \chi(z)}.$$

It is expedient to express $\tan \chi(z)$ in terms of the horizontal component of the phase velocity of a wave propagating along the ray, $v = c_0 / \cos \chi_0 = c(z) / \cos \chi(z)$, with $c(z') = c(z'') = v$. In this case,

$$D(v) = 2 \int_{z'}^{z''} \left[\frac{v^2}{c^2(z)} - 1 \right]^{-1/2} dz. \quad (2.9.2)$$

Substituting (2.9.1) in (2.9.2) yields

$$D(v) = \eta [(v^2 - c_0^2)^{1/2} - \mu (v^2 - c_2^2)^{1/2}], \quad (2.9.3)$$

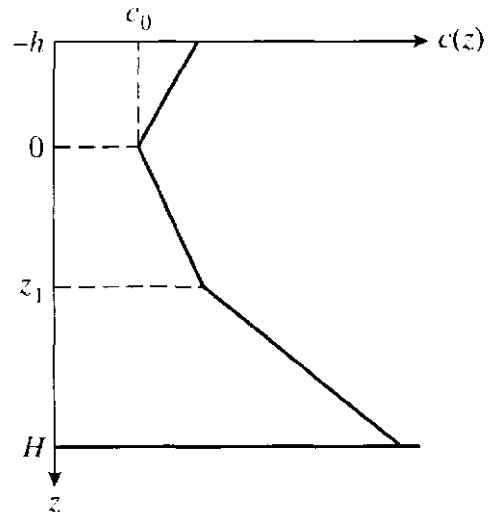


FIGURE 2.10. Sound velocity profile typical for the Northern Atlantic [2.23]

where

$$\eta = 2(a_1^{-1} + a_2^{-1}),$$

$$\mu = \begin{cases} 0, & v < c_2, \\ \frac{1 - a_2/a_3}{1 + a_2/a_1}, & v > c_2. \end{cases}$$

Differentiating (2.9.3) with respect to χ_0 , we obtain

$$\frac{dD}{d\chi_0} = \frac{dD}{dv} \frac{dv}{d\chi_0} = \frac{dD}{dv} v \tan \chi_0. \quad (2.9.4)$$

An extreme value $\chi_0 = 0$ corresponds to a ray launching from the source under the zero grazing angle. When the source is located close to the channel axis, this bundle corresponds to the near-axis rays over which the main part of the acoustic energy propagates. The other extreme points, corresponding to steeper rays, are determined from the equation $dD/dv = 0$. Differentiating (2.9.3) with respect to v , we obtain

$$\frac{dD}{dv} = \eta \left[\left(1 - \frac{c_0^2}{v^2}\right)^{-1/2} - \mu \left(1 - \frac{c_2^2}{v^2}\right)^{-1/2} \right]. \quad (2.9.5)$$

From (2.9.5) it follows that at $a_2 = a_3$ (bilinear profile) or at $a_3 < a_2$ (the gradient of the lower layer is less than that of the middle layer), $\mu < 0$ and therefore $dD/dv \neq 0$, i.e., additional WDB are absent. At $a_3 > a_2$, $\mu > 0$, and $dD/dv = 0$, the extreme value of the phase velocity is

$$v_{\text{ext}} = \frac{c_2 \left(1 - \frac{\mu^2 c_0^2}{c_2^2}\right)^{1/2}}{1 - \mu^2}. \quad (2.9.6)$$

Let us estimate the launch angle of the extreme ray from the source located at $z = 0$ (the channel axis). Assuming that $c_0 = 1490$ m/s, $c_2 = 1499$ m/s, $a_1 = a_2 = 0.015$ l/s, we find $v_{\text{ext}} = 1500.5$ m/s, which corresponds to $\chi_0 = 6.8^\circ$.

Figure 2.11 [2.21] exhibits two families of rays: (a) weakly divergent bundles and (b) conventional rays. Both types of rays are computed for hydrological conditions specific for the Canary Basin at distances 900–1200 km from the source. The discreteness of the launch angles of these rays is 0.1° in the range -11° – 9° for (a) and -8° – 6° for (b). In the first case, due to the lesser divergence of the rays, the greater angular density is reached, which testifies to the higher sound intensity. The experiments carried out in this region have shown that the high-intensity zones are observed up to distances of 3400 km. Such a pattern is observed even in the case when the sound source and receiver are displaced from the channel axis by the significant distance, and hydrological characteristics vary strongly along the sound propagation track. The ray pattern for conventional rays has a quite different form although a weaker concentration of rays nevertheless takes place for separate groups of rays.

In the case of the bilinear sound channel, the WDB are absent only among pure water rays, but they can exist among rays reflected from the ocean surface. The

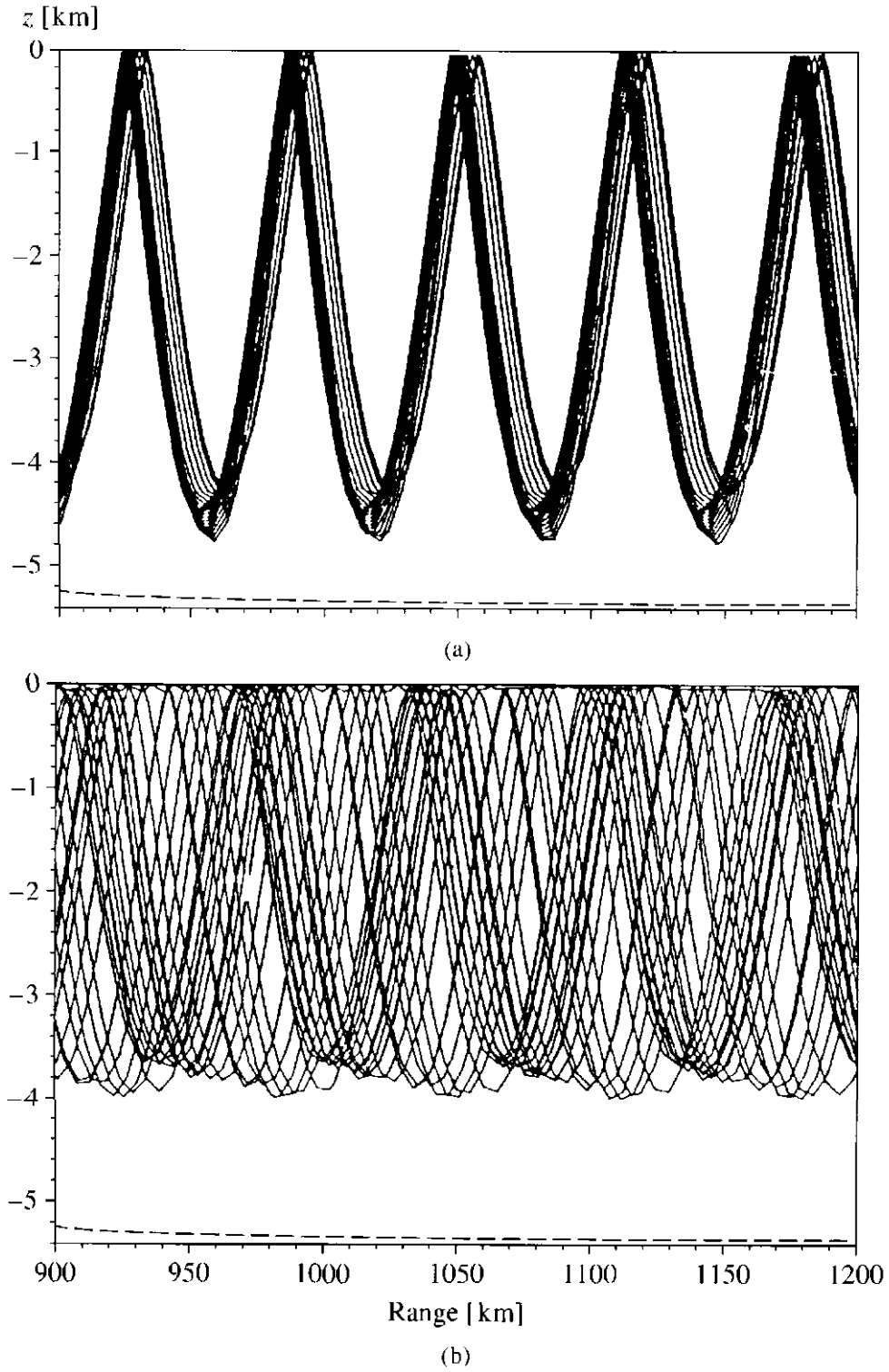


FIGURE 2.11. Comparison of two families of rays: (a) weakly convergent bundles of rays in the angular range of -11° – 9° ; (b) conventional rays in the angular range of -8° – 6° . Discreteness of launch angles is 0.1° [2.21]

cycle length of a ray reflected from the ocean surface is given by

$$D(v) = 2 \int_{-h}^{z''} \left(\frac{v^2}{c^2(z)} - 1 \right)^{-1/2} dz. \quad (2.9.7)$$

Substituting (2.9.1) in (2.9.7) and taking into account that $a_2 = a_3$, we find

$$D(v) = \frac{2}{a}(v^2 - c_0^2)^{1/2} - \frac{2}{a_1}(v^2 - c_s^2)^{1/2}, \quad (2.9.8)$$

where c_s is the sound velocity at the ocean surface and $a^{-1} = (a_1^{-1} + a_2^{-1})$. Now the equation for the determination v_{ext} takes the form

$$\frac{dD}{dv} = \left(1 - \frac{c_0^2}{v^2}\right)^{-1/2} - \frac{a}{a_1} \left(1 - \frac{c_s^2}{v^2}\right)^{-1/2} = 0, \quad (2.9.9)$$

from which we obtain

$$v_{\text{ext}} = \frac{c_s \left(1 - \frac{\gamma^2 c_0^2}{c_s^2}\right)^{1/2}}{(1 - \gamma^2)^{1/2}}, \quad (2.9.10)$$

where $\gamma = a/a_1$. Setting $h = 600$ m and $a_2 = 0.06$ 1/s, we find $v_{\text{ext}} = 1515$ m/s and $\chi_0 = 10.4^\circ$. It is worth noting that weakly divergent bundles of rays can be destroyed under reflection from the rough ocean surface.

It is possible to give a very simple explanation of the independence of the cycle length of an extreme ray on its launch angle. The point is that the decrease of the horizontal range passed by such a ray in the upper layer, as the grazing angle increases, is totally compensated for by its increase in the lower layer. The same situation takes place for pure water rays—decrease of the horizontal range with grazing angle in some layers is compensated for by its increase in other layers. The conditions of the existence of weakly divergent bundles of rays in the stratified ocean with the power dependence of the squared refractive index have been analysed in [2.24].

Reflection of Sound from the Surface and Bottom of the Ocean: Plane Waves

The surface and bottom of the ocean are highly complex boundaries. They are usually rough, and underwater ground is an essentially inhomogeneous medium. However, even regarding the boundaries as plane and the media as homogeneous, it is still possible to obtain useful results. This case will be considered in this chapter. In addition, we shall limit ourselves to the simplest case of plane waves. At the initial stage of the theory presented below, media are assumed to be liquid. This theory is completely applicable to the air-water interface and approximately (but not badly) to the water-ground boundary.

3.1 Reflection and Transmission Coefficients at an Interface Separating Two Liquids

We shall assume that the interface between the media is horizontal. The densities of the upper and lower media will be denoted by ϱ and ϱ_1 , respectively, the sound velocity by c and c_1 , and the angle of incidence by θ (Fig. 3.1). Omitting the factor $\exp(-i\omega t)$, we shall write the acoustic pressure¹ for the incident wave

$$p_i = \exp[ik(x \sin \theta + z \cos \theta)], \quad k \equiv \omega/c. \quad (3.1.1)$$

The amplitude of this wave is assumed to be as unity, and the plane xz is chosen as the plane of incidence. The reflected wave can be written in the form

$$p_r = V \exp[ik(x \sin \theta - z \cos \theta)], \quad (3.1.2)$$

where V is the reflection coefficient. The total field in the upper medium will be

$$p = p_i + p_r = [\exp(ikz \cos \theta) + V \exp(-ikz \cos \theta)] \exp(ikx \sin \theta). \quad (3.1.3)$$

The refracted wave in the lower medium can be written in the form

$$p_1 = W \exp[ik_1(x \sin \theta_1 + z \cos \theta_1)], \quad k_1 \equiv \omega/c_1 \quad (3.1.4)$$

¹As is seen from (2.1.2) the acoustic pressure p and the velocity potential ψ for a harmonic wave differ from each other by a constant factor only, and therefore, it is immaterial which of these quantities is used.

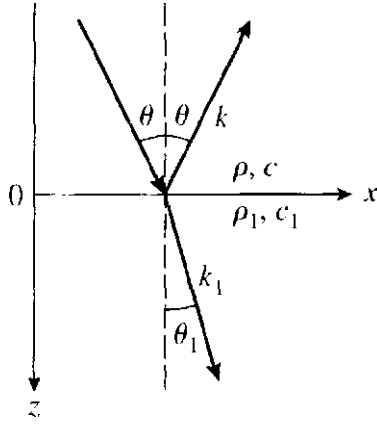


FIGURE 3.1. Parameters for the derivation of expressions for the reflection and transmission coefficients

where W is the transmission coefficient and θ_1 is the angle of refraction. The quantities V , W , and θ_1 are determined from the continuity conditions for the acoustic pressure and the normal component of the particle velocity at the interface

$$p = p_1, \quad v_z = v_{1z} \quad (3.1.5)$$

at $z = 0$ or [see (2.1.2)]

$$p = p_1, \quad \frac{1}{\varrho} \frac{\partial p}{\partial z} = \frac{1}{\varrho_1} \frac{\partial p_1}{\partial z}. \quad (3.1.6)$$

Substituting (3.1.3, 4) into the first equation of (3.1.6), we obtain

$$1 + V = W \exp[i(k_1 \sin \theta_1 - k \sin \theta)x]. \quad (3.1.7)$$

Since the left-hand side is independent of x , the right-hand side must also be independent of x , from which we obtain the well-known refraction law

$$k \sin \theta = k_1 \sin \theta_1. \quad (3.1.8)$$

This relation expresses the equality of the phase velocities of the waves propagating along the interface in the upper and lower media. It can also be written in the form

$$\sin \theta = n \sin \theta_1, \quad (3.1.9)$$

where $n = k_1/k = c/c_1$; i.e., the refraction index of the boundary. Now (3.1.7) takes the form

$$1 + V = W. \quad (3.1.10)$$

Furthermore, substitution of (3.1.3, 4) into the second equation of (3.1.6) gives

$$\varrho_1(1 - V) \cos \theta = n \varrho W \cos \theta_1. \quad (3.1.11)$$

Defining $m = \varrho_1/\varrho$ and using (3.1.9), we find from (3.1.10, 11)

$$\begin{aligned} V &= \frac{m \cos \theta - n \cos \theta_1}{m \cos \theta + n \cos \theta_1} = \frac{m \cos \theta - \sqrt{n^2 - \sin^2 \theta}}{m \cos \theta + \sqrt{n^2 - \sin^2 \theta}}, \\ W &= \frac{2m \cos \theta}{m \cos \theta + \sqrt{n^2 - \sin^2 \theta}}. \end{aligned} \quad (3.1.12)$$

Note the following interesting features of the reflection and transmission coefficients:

1. As $\theta \rightarrow \pi/2$ we have $V \rightarrow -1$, $W \rightarrow 0$ independent of the parameters of the media.
2. At the angle of incidence θ satisfying the equation

$$m \cos \theta - \sqrt{n^2 - \sin^2 \theta} = 0, \quad \text{i.e.,} \quad \sin \theta = \sqrt{\frac{m^2 - n^2}{m^2 - 1}}, \quad (3.1.13)$$

the reflection coefficient becomes zero and the boundary will be completely transparent.

3. Let n be real, $n < 1$, and $\sin \theta > n$. In this case (3.1.12) may be written

$$V = \frac{m \cos \theta - i\sqrt{\sin^2 \theta - n^2}}{m \cos \theta + i\sqrt{\sin^2 \theta - n^2}}. \quad (3.1.14)$$

This expression may also be written as

$$V = \exp(i\varphi), \quad \varphi = -2 \arctan \frac{\sqrt{\sin^2 \theta - n^2}}{m \cos \theta}. \quad (3.1.15)$$

For the modulus of the reflection coefficient we have $|V| = 1$, i.e., in this case total reflection occurs. The phase difference between the reflected and incident waves at the interface is given by φ . The upper curve in Fig. 3.2a and the lower one in Fig. 3.2b are the modulus and phase of the reflection coefficient, respectively, for a sandy bottom ($m = 1.95$, $n = 0.86$) as a function of the grazing angle ($\chi = \pi/2 - \theta$) when attenuation in the bottom is absent [3.1].

When absorption is present in a medium, n will be complex, $n = n_0(1 + i\alpha)$, $\alpha > 0$. Now separating the modulus and phase of the reflection coefficient, we have

$$V = |V| \exp(i\varphi), \quad |V| < 1.$$

In Fig. 3.2 the modulus and phase of the reflection coefficient for different α are plotted.

For the case $n > 1$ (the sound velocity in the bottom is less than that in water) total reflection does not occur. Figure 3.3 illustrates the curves for the modulus and phase of the reflection coefficient for $m = 1.56$, $n = 1.008$ (clayed mud), and various values of α [3.1].

Equation (3.1.2) for the reflection coefficient may also be written in the form

$$V = \frac{Z_1 - Z}{Z_1 + Z}, \quad (3.1.16)$$

where $Z = \rho c / \cos \theta$ and $Z_1 = \rho_1 c_1 / \cos \theta_1$ are the impedances of the upper and lower media for plane waves propagating in directions forming angles θ and θ_1 with the normal to the interface.

For the perfectly rigid bottom ($\rho_1 \rightarrow \infty$) we have $Z_1 \rightarrow \infty$, $V = 1$. In this case, according to (3.1.6), $\partial p / \partial z = 0$ at the boundary. If the wave is incident from

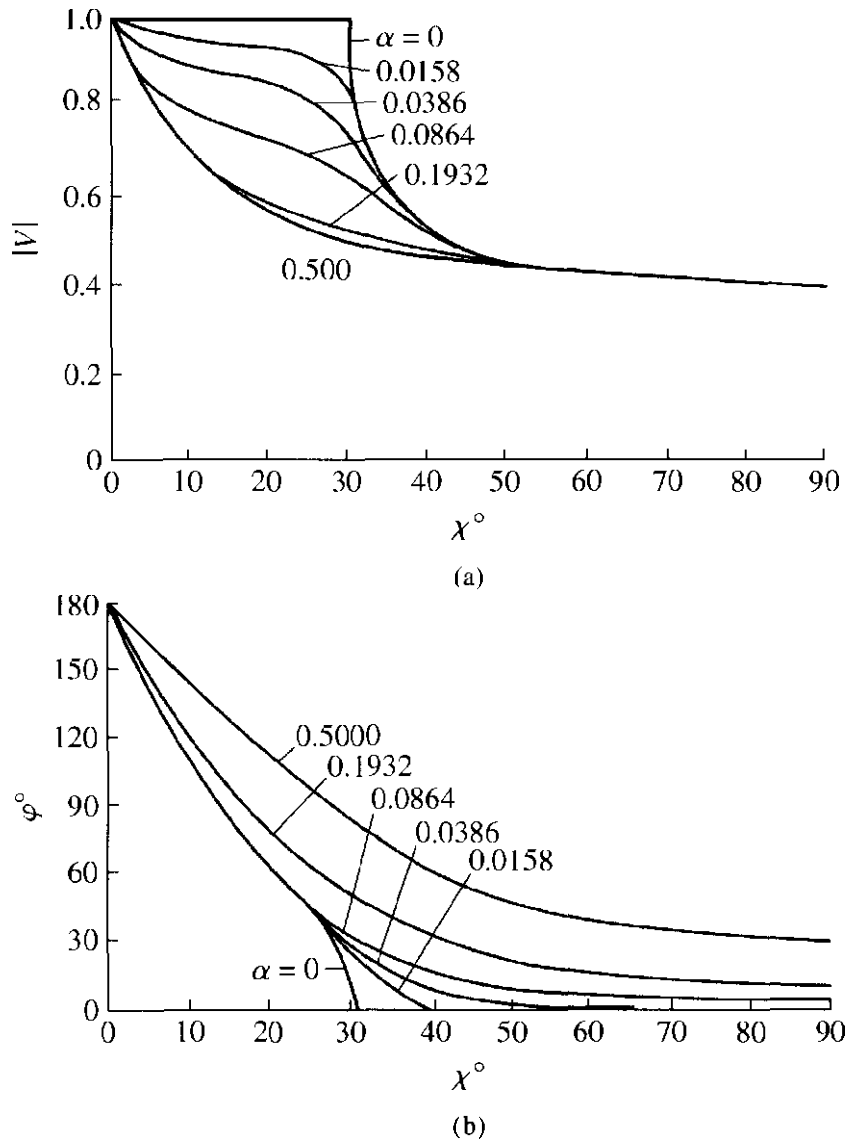


FIGURE 3.2. Modulus (a) and phase (b) of the reflection coefficient for $\rho_1/\rho = 1.95$, $c/c_1 = 0.86$ with different absorption (α) in the sandy bottom

water on the free sea surface, then $\rho_1 \rightarrow 0$, $Z_1 \rightarrow 0$, and $V = -1$. The acoustic pressure, according to (3.1.3), becomes zero at the free surface.

Equation (3.1.16) for V also remains valid in the case where the lower half-space ($z > 0$) is a solid or even a stratified inhomogeneous medium. In this case, Z_{in} , the “input impedance” of the lower half-space, should be used instead of Z_1 . The value of Z remains unchanged (Sec. 3.4).

We also note that Z_1 sometimes has a value which is independent of the angle of incidence, the so-called normal impedance (for example, see [3.1]). This concept, useful in room acoustics, is probably of no use in underwater acoustics. Actually, as can be easily shown [3.2], this concept is applicable for the ocean only in the case where the sound velocity in the bottom is much less than that in water, and consequently waves in the bottom propagate almost normal to the boundary. In fact, this never takes place.

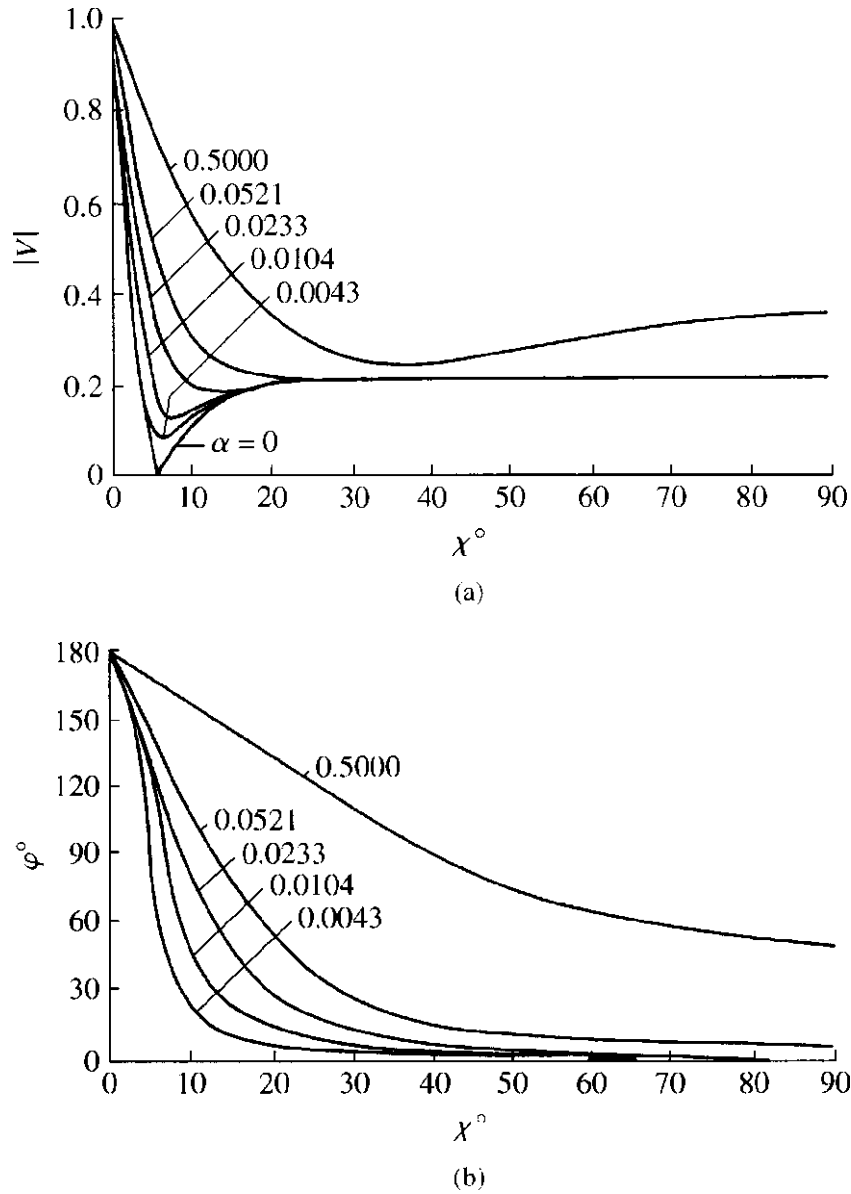


FIGURE 3.3. Modulus (a) and phase (b) of the reflection coefficient for $\rho_1/\rho = 1.56$, $c/c_1 = 1.008$ with different absorption in the bottom

3.2 Transmission of a Sound Wave from Water into Air and Vice Versa

For the case when a sound wave is incident from water on the boundary with air we have in (3.1.12) $m = \rho_a/\rho_w = 0.0013$, $n^2 = c_w^2/c_a^2 = 20.6$. Then, (3.1.12) for the transmission coefficient can be written with good accuracy in the form

$$W = (2m/n) \cos \theta. \quad (3.2.1)$$

The transmission will be maximal at normal incidence ($\theta = 0$). In this case

$$W = 2m/n \approx 5.7 \cdot 10^{-4},$$

a very small quantity.

According to (3.1.10), the reflection coefficient V will differ from -1 by the same quantity. Therefore, the frequently used assumption $V = -1$ is very good for this case.

Let us consider now the inverse case when the wave is incident from the air on the water surface. The results obtained may, at first glance, appear surprising. Let us again use the equations (3.1.12) for the reflection and transmission coefficients. However, now index "1" should be ascribed to water. As a result, we obtain

$$m = \rho_w / \rho_a = 770, \quad n = c_a / c_w = 0.22.$$

Since m is very great, we have $m \cos \theta \gg 1$ for all θ except $\theta \approx \pi/2$ and, consequently, in accordance with (3.1.12), $V \approx 1$ and $W \approx 2$. This means that almost total transmission occurs, the acoustic pressure in the transmitted wave (in water) being two times greater than that in the incident wave.

No matter how surprising this result is, it could have been easily predicted beforehand. Indeed, the acoustic pressure in the air near the surface is twice the acoustic pressure in the incident wave due to the summation of the acoustic pressure in the incident and reflected waves. Since the acoustic pressure is continuous across the boundary, it should also be the same in water.

Thus, while the acoustic pressure decreases approximately 2000 times for the wave transmitted from water into air, it increases by a factor of two for the wave transmitted from air into water. As a consequence, fish can perceive air noise well, while we cannot hear the sound of fish.

The question arises as to whether the doubling of the acoustic pressure in water simultaneous with the almost total reflection of a wave from the water surface does not contradict the energy conservation law. Another question is how may we explain the presence of such asymmetry in the transmission of sound from one medium into another through the water surface. We will show now that the energy conservation law is satisfied and that symmetry is present if we consider the reflection and transmission of energy (rather than the acoustic pressure). For simplicity we consider a case of normal incidence and accept the amplitude of acoustic pressure in the incident wave again as unity. Then the amplitudes of the acoustic pressure in the reflected and transmitted waves will be V and W , respectively. For the power flux density we have, respectively,

$$I_i = (2\rho c)^{-1}, \quad I_r = V^2(2\rho c)^{-1}, \quad I_t = W^2(2\rho_1 c_1)^{-1}. \quad (3.2.2)$$

Here index "1" refers to the medium from which reflection occurs regardless of whether it is water or air. The law of energy conservation is expressed in our case by the equality

$$I_i = I_r + I_t \quad (3.2.3)$$

or substituting (3.2.2)

$$1 - V^2 = (n/m)W^2. \quad (3.2.4)$$

On the other hand, from (3.1.12) for normal incidence ($\theta = 0$) we have

$$V = (m - n)/(m + n), \quad W = 2m/(m + n). \quad (3.2.5)$$

It is easy to verify that after substituting these expressions into (3.2.4), the latter becomes an identity.

Also of interest is the expression for the energy transparency of the boundary, i.e., the ratio

$$I_t/I_i = (n/m)W^2.$$

Taking into account the second formula in (3.2.5), we obtain

$$I_t/I_i = 4mn/(m+n)^2. \quad (3.2.6)$$

For the water-air interface ($m = 770$, $n = 0.22$) we have

$$I_t = 10^{-3} I_i,$$

i.e., only one-thousandth part of the energy passes across the boundary. Formula (3.2.6) remains unchanged if we change the ordering of the media, i.e., if we interchange $\varrho \leftrightarrow \varrho_1$, $c \leftrightarrow c_1$, $m \rightarrow 1/m$, and $n \rightarrow 1/n$. Thus, the energy transparency of the boundary does not depend on the supporting medium of the incident wave.

Let us now consider the oblique incidence of the sound wave on the water surface from air. This case is interesting since total internal reflection occurs at $\sin \theta > n = 0.22$, i.e., $\theta > 12^\circ 43'$. In (3.1.4) for the acoustic pressure in water we obtain, using (3.1.8),

$$k_1 \cos \theta_1 = ik \sqrt{\sin^2 \theta - n^2}, \quad (3.2.7)$$

where k is the wave number in air. Taking into account that $W \approx 2$ (see above), we obtain for the amplitude of the acoustic pressure in water

$$|p_1| \approx 2 \exp(-\delta z), \quad \delta = k(\sin^2 \theta - n^2)^{1/2}. \quad (3.2.8)$$

Thus, the amplitude of the acoustic pressure decreases exponentially with depth. In Fig. 3.4 the quantity δ is shown as a function of the angle of incidence θ for various frequencies. In addition to the frequency f , the corresponding wavelength in water λ_1 is indicated for each curve. For example, at a frequency of 100 Hz ($\lambda_1 = 15$ m) and an angle of incidence $\theta = 45^\circ$, we obtain $\delta = 1.3 \text{ m}^{-1}$, i.e., the amplitude of the wave diminishes by a factor of 2.7 at a depth of 77 cm.

3.3 Sound Wave Reflection from an Ocean Bottom Consisting of Liquid Layers

Complicating the model of the ocean bottom further, we will assume that it consists of one or several homogeneous liquid layers lying on the homogeneous liquid half-space.

3.3.1 Reflection from a Homogeneous Layer

The basis of this discussion will be the solution of the simplest problem concerning reflection of the sound wave incident from half-space 3 (Fig. 3.5) on layer 2 which lies on half-space 1. The media 1, 2, and 3 are assumed to be homogeneous.

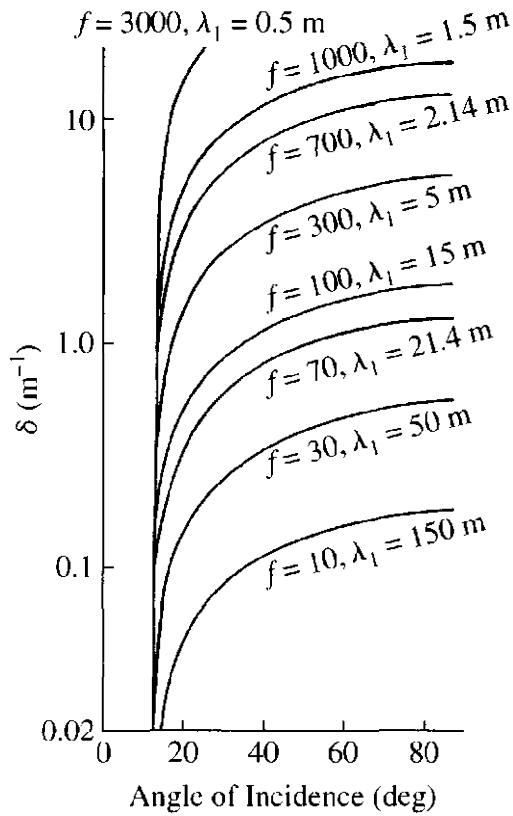


FIGURE 3.4. Attenuation coefficient of acoustic pressure in water at total reflection of a plane sound wave incident from air

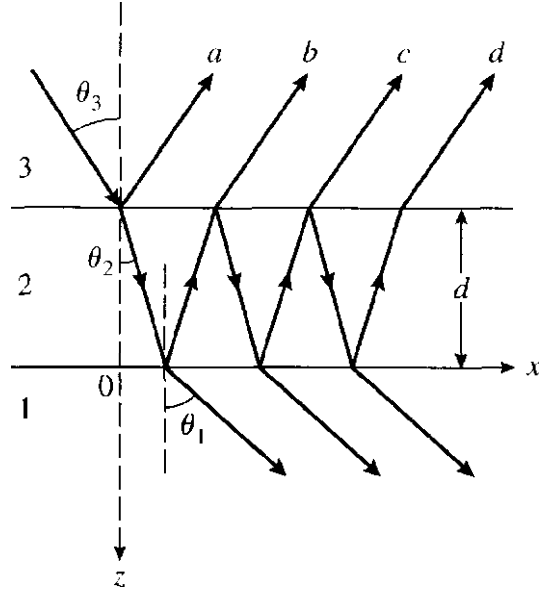


FIGURE 3.5. System of waves upon reflection from a layer

The reflection coefficient V from a layer can be written in terms on the “partial” reflection coefficients V_{23} and V_{12} at the boundaries 2, 3 and 1, 2, respectively. According to the results of Sect. 3.1, we have

$$V_{23} = \frac{Z_2 - Z_3}{Z_2 + Z_3};$$

V_{12} is similar, with a corresponding replacement of indices. Here,

$$Z_j = \rho_j c_j / \cos \theta_j, \quad j = 1, 2, 3. \quad (3.3.1)$$

As before, we assume that the amplitude of the wave incident on the layer is equal to unity. The resultant wave reflected from the layer may be regarded as a superposition of the following waves (Fig. 3.5):

- the wave reflected from the front boundary of the layer (interface between media 2 and 3); the amplitude of this wave is V_{23} ;
- the wave which penetrates the front boundary of the layer, passes through the layer, reflects from its rear boundary, passes through the layer again, and finally exits the layer through its front boundary; its (complex) amplitude is

$$W_{32} V_{12} W_{23} \exp(2i\alpha d), \quad \alpha \equiv k_2 \cos \theta_2.$$

In the last expression the phase change of the wave during its double passage through the layer was taken into account; the quantities W_{32} and W_{23} are the transmission coefficients of the boundary between media 2, 3 when a wave passes between them in the forward and backward directions. According to (3.1.10)

$$W_{32} = 1 + V_{32}, \quad W_{23} = 1 + V_{23}, \quad (3.3.2)$$

- c) the wave which penetrates the layer, reflects twice from the rear boundary and once from the front boundary, passes through the layer four times, and then exits the layer through its front boundary; obviously its amplitude is

$$W_{32} V_{12} V_{32} V_{12} W_{23} \exp(4i\alpha d),$$

and so on.

As a result, summing up all the waves which form the total field of the reflected wave, we find for its amplitude (which will also be the reflection coefficient since the amplitude of the incident wave was taken as unity)

$$\begin{aligned} V &= V_{23} + W_{32} V_{12} W_{23} \exp(2i\alpha d) + W_{32} V_{32} V_{12}^2 W_{23} \exp(4i\alpha d) \\ &+ W_{23} V_{32}^2 V_{12}^3 W_{23} \exp(6i\alpha d) + \dots = V_{23} + W_{32} W_{23} V_{12} \exp(2i\alpha d) \\ &\times \sum_{n=0}^{\infty} [V_{32} V_{12} \exp(2i\alpha d)]^n. \end{aligned}$$

Using the sum for the infinite geometric series, we obtain

$$V = V_{23} + W_{32} W_{23} V_{12} \frac{\exp(2i\alpha d)}{1 - V_{32} V_{12} \exp(2i\alpha d)}.$$

Then, applying (3.3.2) and the relationship $V_{32} = -V_{23}$ and after some transformations, we find

$$V = \frac{V_{23} + V_{12} \exp(2i\alpha d)}{1 + V_{23} V_{12} \exp(2i\alpha d)}. \quad (3.3.3)$$

This formula solves the problem stated at the beginning of this section.

Another convenient approach to the problem of wave reflection from a layer is to determine the input impedance of the layer. As a result of multiple reflections at the boundaries of the layer, a system of waves is formed which propagate in both positive and negative z directions and have the same phase velocity in the x direction. Omitting the factor $\exp(ik_2 x \sin \theta_2 - i\omega t)$ for simplicity, the acoustic pressure in the layer can be written in the form

$$p_2 = A \exp(i\alpha z) + B \exp(-i\alpha z), \quad (3.3.4)$$

where A and B are constants. The normal component of the velocity is

$$v_z = \frac{1}{i\omega \rho_2} \frac{\partial p_2}{\partial z} = \frac{\alpha}{\omega \rho_2} [A \exp(i\alpha z) - B \exp(-i\alpha z)]. \quad (3.3.5)$$

In general, the ration $Z(z) = p/v_z$ which may be determined for an arbitrary z is called the impedance. The latter changes continuously when crossing the

boundary, since p and v_z are continuous. The useful quantity $Z(0) \equiv Z_{\text{in}}^{(1)}$ is the input impedance for medium 1. Dividing (3.3.4) by (3.3.5), setting $z = 0$, taking the value α into account, and using (3.3.1), we obtain

$$Z_{\text{in}}^{(1)} = Z_2 \frac{A + B}{A - B}, \quad \text{whence} \quad B = \frac{Z_{\text{in}}^{(1)} - Z_2}{Z_{\text{in}}^{(1)} + Z_2} A. \quad (3.3.6)$$

Further, the quantity $Z_{\text{in}}^{(2)} \equiv Z(-d)$ will be the input impedance for the upper boundary of the layer $z = -d$. Once again, from (3.3.4, 5) we find

$$Z_{\text{in}}^{(2)} = Z_2 \frac{A \exp(-i\alpha d) + B \exp(i\alpha d)}{A \exp(-i\alpha d) - B \exp(i\alpha d)}. \quad (3.3.7)$$

Taking into account the relationship between A and B according to (3.3.6), we obtain

$$Z_{\text{in}}^{(2)} = Z_2 \frac{Z_{\text{in}}^{(1)} - iZ_2 \tan \alpha d}{Z_2 - iZ_{\text{in}}^{(1)} \tan \alpha d}, \quad (3.3.8)$$

which is an important equation, making it possible to recalculate the input impedance from one layer boundary to another.

Let us show that in the simplest case considered, when medium 1 is a homogeneous half-space, $Z_{\text{in}}^{(1)} = Z_1$, where Z_1 is given by (3.3.1) for $j = 1$. Indeed, since the impedance $Z(z)$ is continuous at the boundary $z = 0$, $Z_{\text{in}}^{(1)}$ can be calculated using the values of the acoustic pressure and the normal velocity in medium 1.

For arbitrary z in medium 1 (omitting the same factor as above)

$$p_1 = W_1 \exp(ik_1 z \cos \theta_1),$$

$$v_{1z} = \frac{1}{i\omega \rho_1} \frac{\partial p_1}{\partial z} = \frac{k_1 W_1 \cos \theta_1}{\omega \rho_1} \exp(ik_1 z \cos \theta_1).$$

Thus,

$$Z_{\text{in}}^{(1)} = \left(\frac{p_1}{v_{1z}} \right)_{z=0} = \frac{\omega \rho_1}{k_1 \cos \theta_1} = Z_1.$$

Now the input impedance of the layer according to (3.3.8) is

$$Z_{\text{in}}^{(2)} = \frac{Z_1 - iZ_2 \tan \alpha d}{Z_2 - iZ_1 \tan \alpha d} Z_2. \quad (3.3.9)$$

Having found $Z_{\text{in}}^{(2)}$, we may express the reflection coefficient by the simple formula

$$V = \frac{Z_{\text{in}}^{(2)} - Z_3}{Z_{\text{in}}^{(2)} + Z_3}. \quad (3.3.10)$$

In fact, the total field of the incident and reflected waves in medium 3 may be written in the form

$$p_3 = \exp[ik_3(z + d) \cos \theta_3] + V \exp[-ik_3(z + d) \cos \theta_3]. \quad (3.3.11)$$

Using the last equation we can determine v_{3z} , and requiring that the relationship $Z(-d) \equiv (p_3/v_{3z})_{z=-d} = Z_{\text{in}}^{(2)}$ be fulfilled, we obtain formula (3.3.10). This formula and (3.3.3) give an expression for V in two different forms; in other respects they are identical and can be transformed into one another.

Let us consider some special cases.

- a) Let $\alpha d = N\pi$, $N = 1, 2, 3, \dots$, or taking in account the value of α , $d = N\lambda_2/(2 \cos \theta_2)$, that is the layer thickness is equal to an integral number of $\lambda_2/(2 \cos \theta_2)$, where λ_2 is the sound wavelength in medium 2. At normal incidence and $N = 1$, this is the case of the half-wave layer. Since $\tan \alpha d = 0$ in this case, we obtain from (3.3.9) that $Z_{\text{in}}^{(2)} = Z_1$.

Thus, the half-wave layer has no effect on the incident wave (as if the layer were absent), and reflection takes place just as if media 3 and 1 were in direct contact with one another.

- b) Let $\alpha d = (2N - 1)(\pi/2)$ or $d = \lambda_2(2N - 1)/(4 \cos \theta_2)$, i.e., the layer thickness is equal to an odd number of $\lambda_2/(4 \cos \theta_2)$. At normal incidence and $N = 1$ this is the case of a quarter-wave layer. Since $\tan \alpha d = \infty$ in this case, we obtain from (3.3.9) that $Z_{\text{in}}^{(2)} = Z_2^2/Z_1$. Now it is clear from (3.3.10) that if the condition $Z_2^2 = Z_1 Z_3$ is also fulfilled, we have $V = 0$, i.e., reflection is absent and a wave will completely transmit into the lower half-space.

In the particular examples considered, absorption was supposed to be absent in all media. In order to take account of absorption, it is sufficient, as always, to assume that wave numbers k_1 , k_2 , and k_3 are complex. In this case, impedances Z_1 , Z_2 , and Z_3 will be complex, as well.

3.3.2 Reflection from an Arbitrary Number of Layers

Let us suppose that between two semi-infinite media which we denote by 1 and $n + 1$ there are $n - 1$ layers denoted by 2, 3, \dots , n (Fig. 3.6). Let a plane wave be incident on the last layer at an angle of incidence θ_{n+1} . Our problem is to determine the reflection coefficient.

It is clear from the above presentation that for this purpose it is sufficient to find the input impedance of the entire system of layers $Z_{\text{in}}^{(n)}$. Obviously, the latter can be determined by the $(n - 1)$ -fold application of (3.3.8). Indeed, setting $Z_{\text{in}}^{(1)} = Z_1$, $d = d_2$, and $\alpha = \alpha_2 - k_2 \cos \theta_2$, we obtain the input impedance $Z_{\text{in}}^{(2)}$ at the upper boundary of the lowest layer. Further, carrying out in the right-hand side of (3.3.8) the replacements $Z_{\text{in}}^{(1)} \rightarrow Z_{\text{in}}^{(2)}$, $Z_2 \rightarrow Z_3$, $\alpha \rightarrow \alpha_3$, and $d \rightarrow d_3$, we obtain for the left-hand side $Z_{\text{in}}^{(3)}$, the input impedance of the second layer from the bottom and so forth. Finally, having found $Z_{\text{in}}^{(n-1)}$, from the relationship

$$Z_{\text{in}}^{(n)} = \frac{Z_{\text{in}}^{(n-1)} - iZ_n \tan \alpha_n d_n}{Z_n - iZ_{\text{in}}^{(n-1)} \tan \alpha_n d_n} Z_n \quad (3.3.12)$$

we determine the required input impedance of the system of layers. The reflection

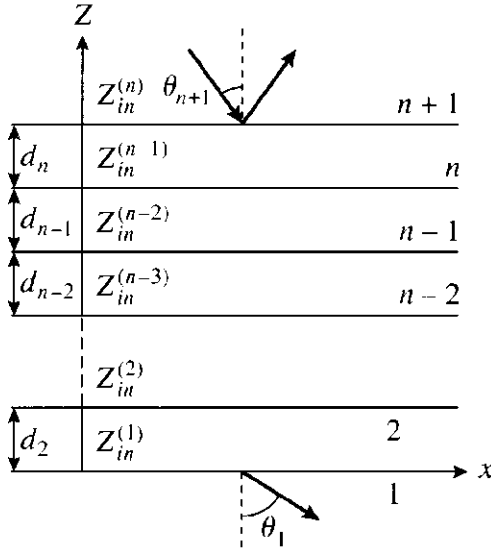


FIGURE 3.6. Parameters for the calculation of the reflection and transmission coefficients for a system of layers

coefficient will now be

$$V = \frac{Z_{in}^{(n)} - Z_{n+1}}{Z_{in}^{(n)} + Z_{n+1}}. \quad (3.3.13)$$

As before, the quantities Z_1, Z_2, \dots, Z_{n+1} are given by (3.3.1).

Let us write, for example, the input impedance for a system of two layers ($n = 3$) in the explicit form

$$Z_{in}^{(3)} = \frac{Z_1 Z_2 - Z_1 Z_3 \delta_2 \delta_3 - i(Z_2^2 \delta_2 + Z_2 Z_3 \delta_3)}{Z_2 Z_3 - Z_2^2 \delta_2 \delta_3 - i(Z_1 Z_3 \delta_2 + Z_2 Z_1 \delta_3)} \quad (3.3.14)$$

where $\delta_j \equiv \tan \alpha_j d_j$ and $j = 1, 2, 3$.

Obviously, the reflection coefficient for a system of layers can also be found by the successive application of formula such as (3.3.3); we will not, however, dwell on this.

The distinctive feature of the reflection coefficient for one or many layers is the oscillating character of its dependence upon the wave frequency and the angle of incidence due to the interference of waves undergoing multiple reflections from the layer boundaries.

3.4 Sound Reflection from a Solid

In a number of cases, it is necessary to take into account the shear elasticity of the bottom. This will be done in this section. We shall assume that the bottom is an infinite homogeneous half-space $z > 0$ with the density ρ_1 and the Lámé elastic parameters λ_1 and μ_1 . The half-space $z < 0$ from which the plane sound wave impinges on the boundary $z = 0$ is supposed to be a liquid of density ρ and sound velocity c (the Lámé parameter $\lambda = \rho c^2$).

The velocities of longitudinal and transverse waves in the solid are expressed in terms of ρ_1, λ_1 , and μ_1 , as follows:

$$c_1 = \left(\frac{\lambda_1 + 2\mu_1}{\rho_1} \right)^{1/2}, \quad b_1 = \left(\frac{\mu_1}{\rho_1} \right)^{1/2}. \quad (3.4.1)$$

The particle velocity at each point of the solid can be expressed in terms of the scalar φ_1 and vector ψ_1 potentials [3.3]

$$\mathbf{v}_1 = \text{grad } \varphi_1 + \text{rot } \psi_1. \quad (3.4.2)$$

In the case of a two-dimensional problem, assuming that all quantities only depend upon the coordinates x and z , and the vector \mathbf{v}_1 also lies in the xz plane, the potential ψ_1 can be chosen such that only its y component, which we shall denote ψ_1 , differs from zero. Then, according to (3.4.2) \mathbf{v}_1 will be a vector with components

$$v_{1x} = \frac{\partial \varphi_1}{\partial x} - \frac{\partial \psi_1}{\partial z}, \quad v_{1y} = 0, \quad v_{1z} = \frac{\partial \varphi_1}{\partial z} + \frac{\partial \psi_1}{\partial x}, \quad (3.4.3)$$

and φ_1 and ψ_1 can be called the potentials of longitudinal and transverse (shear) waves. It can be shown that these potentials satisfy the wave equations

$$\Delta \varphi_1 = \frac{1}{c_1^2} \frac{\partial^2 \varphi_1}{\partial t^2} \quad \text{and} \quad \Delta \psi_1 = \frac{1}{b_1^2} \frac{\partial^2 \psi_1}{\partial t^2}. \quad (3.4.4)$$

The normal components of the velocity, v_z , and of the stress tensor, Z_z , must be continuous across the boundary, between the liquid and solid. Since the tangential stresses in the liquid vanish, the component Z_x must be zero at the boundary.

In the two-dimensional case we have the following expressions for the components of stress tensor of interest to us [3.3]:

$$\begin{aligned} Z_z &= \lambda_1 \left(\frac{\partial u_x}{\partial x} + \frac{\partial u_z}{\partial z} \right) + 2\mu_1 \frac{\partial u_z}{\partial z}, \\ Z_x &= \mu_1 \left(\frac{\partial u_x}{\partial z} + \frac{\partial u_z}{\partial x} \right), \quad Z_y = 0, \end{aligned} \quad (3.4.5)$$

where u_x and u_z are the displacements along the x and z axes, respectively, obtained for a harmonic wave by dividing the velocity components v_{1x} and v_{1z} by $-i\omega$.

We specify the sound field in the liquid by the potential φ . The particle velocity is then $\mathbf{v} = \text{grad } \varphi$.

Now the boundary conditions at the bottom $z = 0$ are written for the continuity of Z_z :

$$\lambda \Delta \varphi = \lambda_1 \Delta \varphi_1 + 2\mu_1 \left(\frac{\partial^2 \varphi_1}{\partial z^2} + \frac{\partial^2 \psi_1}{\partial x \partial z} \right), \quad (3.4.6)$$

for Z_x equal to zero:

$$2 \frac{\partial^2 \varphi_1}{\partial x \partial z} + \frac{\partial^2 \psi_1}{\partial x^2} - \frac{\partial^2 \psi_1}{\partial z^2} = 0, \quad (3.4.7)$$

and for the continuity of v_z :

$$\frac{\partial \varphi}{\partial z} = \frac{\partial \varphi_1}{\partial z} + \frac{\partial \psi_1}{\partial x}. \quad (3.4.8)$$

Let a plane sound wave

$$\varphi_i = \exp[ik(x \sin \theta + z \cos \theta)] \quad (3.4.9)$$

be incident from a liquid on a liquid-solid surface. The potential of the reflected wave can be written in the form

$$\varphi_r = V \exp[ik(x \cos \theta - z \cos \theta)]. \quad (3.4.10)$$

Thus, the total sound field in the liquid will be

$$\varphi = [\exp(ikz \cos \theta) + V \exp(-ikz \cos \theta)] \exp(ikx \sin \theta). \quad (3.4.11)$$

The potentials of the longitudinal and transverse waves in the solid can be written in the form

$$\varphi_1 = W \exp[ik_1(x \sin \theta_1 + z \cos \theta_1)], \quad (3.4.12)$$

$$\psi_1 = P \exp[i\kappa_1(x \sin \gamma_1 + z \cos \gamma_1)], \quad (3.4.13)$$

where k , k_1 , and κ_1 are wave numbers

$$k = \omega/c, \quad k_1 = \omega/c_1, \quad \kappa_1 = \omega/b_1, \quad (3.4.14)$$

and θ_1 and γ_1 are the angles between the z axis and the normals to the wave fronts of longitudinal and transverse waves in the solid, respectively.

Substituting (3.4.11–13) into (3.4.6–8) and setting $z = 0$, we obtain three equations from which the coefficients V , W , and P and the angles θ_1 and γ_1 can be found. Thus, (3.4.8) gives

$$k(1 - V) \cos \theta = k_1 W \cos \theta_1 \exp[i(k_1 \sin \theta_1 - k \sin \theta)x] \\ - \kappa_1 \sin \gamma_1 P \exp[i(\kappa_1 \sin \gamma_1 - k \sin \theta)x]. \quad (3.4.15)$$

Since the left-hand side is independent of x here, the right-hand side must also be independent of x . This is possible only if the equations

$$k \sin \theta = k_1 \sin \theta_1 = \kappa_1 \sin \gamma_1 \quad (3.4.16)$$

are satisfied. The latter determine the directions of waves in the solid.

Now (3.4.15) can be written as

$$k(1 - V) \cos \theta = k_1 W \cos \theta_1 - \kappa_1 P \sin \gamma_1. \quad (3.4.17)$$

Similarly, from (3.4.7) we obtain

$$k_1^2 W \sin 2\theta_1 + \kappa_1^2 P \cos 2\gamma_1 = 0. \quad (3.4.18)$$

Furthermore, we add and subtract $2\mu_1 \partial^2 \varphi_1 / \partial x^2$ on the right-hand side of (3.4.6) and take into account that the sum of the second derivatives of φ_1 with respect to x and z is $\Delta \varphi_1$. Then this equation can be rewritten in the form

$$\lambda \Delta \varphi = (\lambda_1 + 2\mu_1) \Delta \varphi_1 + 2\mu_1 \left(\frac{\partial^2 \psi_1}{\partial x \partial z} - \frac{\partial^2 \varphi_1}{\partial x^2} \right), \quad z = 0. \quad (3.4.19)$$

Noting that $\Delta \varphi = -k^2 \varphi$ and $\Delta \varphi_1 = -k_1^2 \varphi_1$, taking into account (3.4.1, 14), and using, as usual, the notation $m = \varrho_1 / \varrho$, the last equation can be written in the

simpler form

$$\frac{\varphi}{m} = \varphi_1 - \frac{2}{\kappa_1^2} \left(\frac{\partial^2 \psi_1}{\partial x \partial z} - \frac{\partial^2 \varphi_1}{\partial x^2} \right), \quad z = 0. \quad (3.4.20)$$

Substituting the values of φ , φ_1 , and ψ_1 into this equation, we obtain the third equation for the determination of the coefficients V , W , and P :

$$\frac{1+V}{m} = \left[1 - 2 \left(\frac{k_1}{\kappa_1} \right)^2 \sin^2 \theta_1 \right] W - P \sin 2\gamma_1. \quad (3.4.21)$$

Solving the system of equations (3.4.17, 18, 21), and making some transformations in which (3.4.14) is used, we find

$$V = \frac{Z_{\text{in}} - Z}{Z_{\text{in}} + Z}, \quad Z_{\text{in}} \equiv Z_1 \cos^2 2\gamma_1 + Z_t \sin^2 2\gamma_1. \quad (3.4.22)$$

Here Z and Z_1 have the same meaning as in Sect. 3.1, and $Z_t = \rho_1 b_1 / \cos \gamma_1$. The quantity Z_{in} in accordance with Sect. 3.1 may be called the input impedance for the solid half-space. Furthermore

$$mW = \frac{2Z_1 \cos 2\gamma_1}{Z_{\text{in}} + Z}, \quad -mP = \frac{2Z_t \sin 2\gamma_1}{Z_{\text{in}} + Z}. \quad (3.4.23)$$

3.4.1 Analysis of the Reflection Coefficient

Note some interesting facts about V given by (3.4.22).

- a) At normal incidence of the sound wave on the boundary ($\theta = \theta_1 = \gamma_1 = 0$) we have $Z_{\text{in}} = Z_1$, $P = 0$, i.e., the shear waves are not generated.
- b) For $\theta \neq 0$ we have from (3.4.16) for the angles of refraction of the longitudinal and transverse waves

$$\sin \theta_1 = (c_1/c) \sin \theta, \quad \sin \gamma_1 = (b_1/c) \sin \theta. \quad (3.4.24)$$

If $\theta = \arcsin(c/\sqrt{2}b_1)$, then $\gamma_1 = 45^\circ$, $Z_{\text{in}} = Z_t$, and $W = 0$, i.e., only transverse waves are generated in the solid in this case.

- c) Let the velocity of the longitudinal waves in the bottom be less than that in water, i.e., $c_1 < c$. Of course, in this case also $b_1 < c$. The quantity Z_{in} is real, i.e., the boundary is resistive. The reflection coefficient is also real and always less than unity (except for the case $\theta = \pi/2$). The energy is carried away from the boundary into the solid half-space by the longitudinal as well as by transverse waves.

Expression (3.4.22) for Z_{in} can be transformed into

$$\frac{Z_{\text{in}}}{Z_1} = 1 - \left(1 - \frac{\tan \gamma_1}{\tan \theta_1} \right) \sin^2 2\gamma_1.$$

Since $b_1 < c_1$ always and, consequently [by virtue of (3.4.24)] $\gamma_1 < \theta_1$, then $(Z_{\text{in}}/Z_1) < 1$. Thus, the total impedance of the solid boundary is less than the impedance of the liquid with the same values of ρ_1 and c_1 , i.e., the excitation

of the transverse waves leads to some “softening” of the boundary, and, as a consequence, to a decrease of the reflection coefficient.

It should also be noted that, as has been shown by *Tartakovskii* [3.4], the impedance Z_{in} varies with the angle of incidence θ less than the impedance Z_1 of the liquid with the same ρ_1 and c_1 .

- d) Let us now consider the case $c_1 > c$, $b_1 < c$, as is frequently the case for the bottom. If $\sin \theta < c/c_1$, that is $\sin \theta_1 < 1$, there is nothing new as compared with case c). However, at $\sin \theta = c/c_1$, there is already an interesting phenomenon. From (3.4.24) we obtain $\theta_1 = \pi/2$ and consequently $Z_1 = \infty$, $Z_{in} = \infty$, and $V = 1$, that is, total reflection occurs. With a further increase in θ , partial reflection will once again take place. Indeed, it is clear from (3.4.24) that $\cos \theta_1 = (1 - \sin^2 \theta_1)^{1/2} = \pm i |\cos \theta_1|$, when $\sin \theta > c/c_1$. By requiring that (3.4.12) be bounded as $z \rightarrow \infty$, one has to choose the upper sign. Consequently, we have $Z_1 = -i|Z_1|$. Now the longitudinal wave in the solid is an “inhomogeneous” one propagating along the boundary and exponentially attenuating with distance from it. The transverse wave will be an ordinary plane wave leaving the boundary at the angle γ_1 . The input impedance Z_{in} according to (3.4.22) can be rewritten as

$$Z_{in} = Z_t \sin^2 2\gamma_1 - i|Z_1| \cos^2 2\gamma_1, \quad (3.4.25)$$

i.e., the input impedance is complex. Its resistive part is due to the transverse waves, and its reactive part due to the longitudinal waves.

Substituting (3.4.25) into the first formula of (3.4.22), we obtain the reflection coefficient. The square of its modulus is

$$|V|^2 = \frac{(Z_t \sin^2 2\gamma_1 - Z)^2 + |Z_1|^2 \cos^4 2\gamma_1}{(Z_t \sin^2 2\gamma_1 + Z)^2 + |Z_1|^2 \cos^4 2\gamma_1}. \quad (3.4.26)$$

This quantity is less than unity since a certain part of the acoustic energy is carried away from the boundary by a transverse wave.

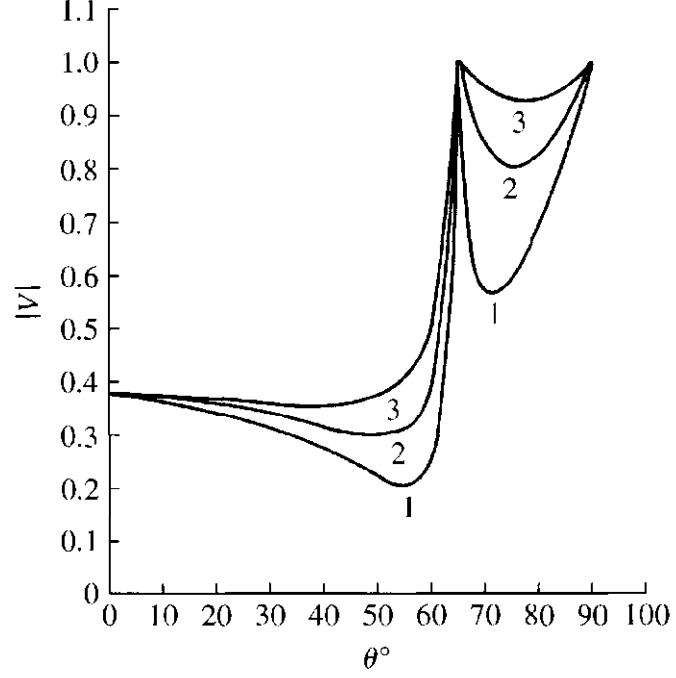
We will not go into detailed consideration of the case, rare for underwater acoustics, when the velocity of the transverse waves in the bottom is higher than that in water ($b_1 > c$). Of course, in this case $c_1 > c$. The reader can easily understand that at $\sin \theta > c/c_1$ there is the usual partial reflection, but that part of the input impedance which is due to the longitudinal waves is reactive, i.e., (3.4.26) is valid. Finally, when $\sin \theta > c/b_1$ the input impedance is purely imaginary and reflection is total. More detailed consideration of the reflection of sound waves from the water-solid boundary is given by *Brekhovskikh* [Ref. 3.2, Sect. 7].

Figure 3.7 illustrates the modulus of the reflection coefficient from the underwater bottom as a function of the angle of incidence θ for $\rho_1/\rho = 2$, $c/c_1 = 0.9$, and $b_1/c = 0.3 - 0.5$.

3.4.2 Surface Rayleigh and Stonely Waves

A surface wave can propagate along the interface of solid and liquid half-spaces. Its velocity is independent of frequency and less than both that in the solid and that

FIGURE 3.7. Modulus of the reflection coefficient from the underwater bottom for $\varrho_1/\varrho = 2$, $c/c_1 = 0.9$, $b_1/c = 0.5$ (curve 1), 0.4 (curve 2), and 0.3 (curve 3)



in the liquid. Therefore, its amplitude decreases exponentially in both media with distance from the interface, and along the interface the wave propagates without attenuation. Such a wave at the interface of two solid media was discovered by Stonley and is called the Stonley wave. By analogy, a wave at the interface of a solid and a liquid has also been called a Stonley wave. A wave at the interface of a solid half-space and a vacuum was discovered by Rayleigh and is called the Rayleigh wave.

Since the surface wave can exist alone without an incident wave, the conditions of its existence can be obtained from previous results if we require that the amplitude of an incident wave approach zero and the amplitudes of the other waves remain finite. This means that we shall have $V \rightarrow \infty$, $W \rightarrow \infty$, $P \rightarrow \infty$, i.e., according to (3.4.22) and (3.4.23),

$$Z_{\text{in}} + Z = 0. \quad (3.4.27)$$

Now taking the equality (3.4.16) into account and denoting $\xi = k \sin \theta = \omega/v$, where v is the velocity of the surface wave, we have $k \cos \theta = i(\xi^2 - k^2)^{1/2}$, $k_1 \cos \theta_1 = i(\xi^2 - k_1^2)^{1/2}$, $\kappa_1 \cos \gamma_1 = i(\xi^2 - \kappa_1^2)^{1/2}$. Substituting Z_{in} from (3.4.22) in (3.4.27), keeping in mind that $Z = \varrho c / \cos \theta$, $Z_1 = \varrho_1 c_1 / \cos \theta_1$, and $Z_t = \varrho_1 b_1 / \cos \gamma_1$, and denoting

$$s = (\kappa_1/\xi)^2 = (v/b_1)^2, \quad q = (b_1/c_1)^2, \quad r = (b_1/c)^2, \quad (3.4.28)$$

we obtain the equation for s , the velocity of the Stonley wave,

$$(\varrho/\varrho_1)s^2(1-sq)^{1/2}(1-sr)^{-1/2} = 4(1-s)^{1/2}(1-sq)^{1/2} - (2-s)^2, \quad (3.4.29)$$

which always has one real root $s < 1$, $sr < 1$. In the particular case $\varrho/\varrho_1 = 0$, (3.4.29) reduces to the equation for the velocity of the Rayleigh wave.

3.5 Reflection from a Continuously Layered Medium

In this section we again assume the bottom to be liquid, but take into account that the sound velocity increases with depth as is usually the case in practice.

For the model adopted in this section, Fig. 3.8 illustrates the sound velocity profile on the left and one of rays incident from water onto the bottom on the right. This ray turns at the depth $z = z_m$, then returns into the upper half-space.

We suppose that the sound velocity at the water-bottom interface (the plane $z = 0$) is continuous. The vertical sound velocity gradient in the bottom is assumed to be sufficiently small (variation of the sound velocity per wave-length is small) and reflection in the region $z_m < z < 0$ may be neglected.

Let us assume that a plane sound wave from above is incident at the angle θ_0 on the boundary $z = 0$. For this case the expression for its reflection coefficient can be written easily (see this in more detail [Ref. 3.4, Sect. 25]). The wave propagating downwards in the half-space $z > 0$ in each elementary layer dz experiences the phase shift $k_z dz$, where

$$k_z = [k^2(z) - \xi^2]^{1/2}, \quad k(z) = \omega/c(z), \quad \xi = k_0 \sin \theta_0, \quad k(z_m) = \xi. \quad (3.5.1)$$

The integral phase shift due to wave propagation from the boundary $z = 0$ to depth z_m is

$$- \int_0^{z_m} k_z dz$$

and has the same value when the wave propagates in the backward direction. All this can be easily visualized. However, the fact that cannot be visualized, but which can be explained on the basis of the more exact theory of this process, is that the wave loses the phase $\pi/2$ upon reflection from the depth $z = z_m$. As a result, the wave returns into the upper homogeneous medium with the same amplitude as an

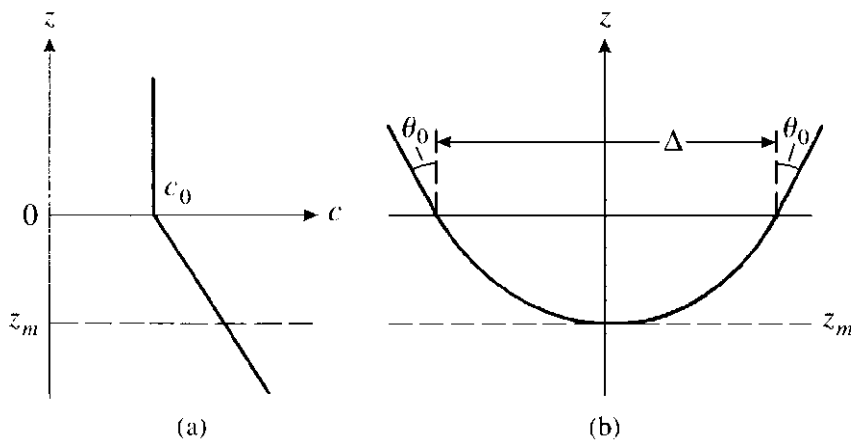


FIGURE 3.8. Reflection from a continuously layered medium. (a) profile $c(z)$, (b) one of the rays

incident wave but with an additional phase

$$\varphi = 2 \int_{z_m}^0 k_z dz - \frac{\pi}{2} = 2 \int_{z_m}^0 |k^2(z) - \xi^2|^{1/2} dz - \frac{\pi}{2}. \quad (3.5.2)$$

The approximation used to obtain this expression (the variation of properties of a medium per wavelength is small) is called the WKB (Wentzel-Kramers-Brillouin) approximation.

Reflection of Sound from the Surface and Bottom of the Ocean: Point Source

In Chap. 3 we have considered the reflection of plane waves from the surface and bottom of the ocean. But in real situations, a sound source is usually located at a finite distance from boundaries of the medium. In acoustics the simplest source is a pulsating sphere of small radius (a “point” source). We are thus led to the problem of a field of a point omnidirectional source located at a finite distance from a plane interface between two media, i.e., to the problem of reflection of a spherical wave—the topic of this chapter.

4.1 Sound Field of an Underwater Source Located Near the Water Surface

4.1.1 Wave Representations

The acoustic pressure of a point (omnidirectional) sound source in free space is given using (2.1.3) by the formula

$$p = -i\omega_0 V_0 (4\pi R)^{-1} \exp[i(kR - \omega t)]. \quad (4.1.1)$$

For simplicity we shall omit the factor $-(i\omega_0 V_0/4\pi) \exp(-i\omega t)$ so that

$$p = R^{-1} \exp(ikR). \quad (4.1.2)$$

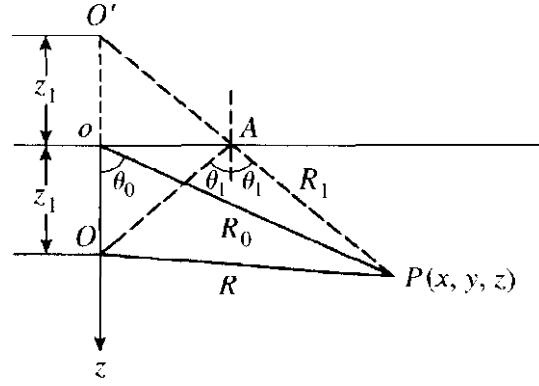
The omitted factor can be included in the final formulae.

Now let this source 0 be at a distance z_1 from the water surface $z = 0$ (Fig. 4.1). The acoustic pressure must also satisfy the Helmholtz equation (Sect. 2.1)

$$\Delta p + k^2 p = 0 \quad (4.1.3)$$

and the boundary condition [see the remark after (3.1.16)]

$$p = 0 \quad \text{at} \quad z = 0. \quad (4.1.4)$$

FIGURE 4.1. Source O and the “image” source O' 

It can easily be seen that this condition is satisfied by the sum of the spherical wave (4.1.2) and the spherical wave radiated by an “image” source at point $O'(0, -z_1)$ which is obtained by specular reflection of the source O at the water surface (see Fig. 4.1). As a result, we obtain for the sound pressure

$$p = R^{-1} \exp(ikR) - R_1^{-1} \exp(ikR_1) \quad (4.1.5)$$

where

$$R = [r^2 + (z - z_1)^2]^{1/2} \quad \text{and} \quad R_1 = [r^2 + (z + z_1)^2]^{1/2}. \quad (4.1.6)$$

In fact, at $z = 0$ we have $R = R_1$ and, consequently, $p = 0$. The expression (4.1.5) for p satisfies (4.1.3) as well as the other necessary conditions, it, namely, represents an outgoing wave at $r, z \rightarrow \infty$ and behaves as $1/R$ when a reference point approaches the source ($R \rightarrow 0$).

4.1.2 Ray Representation

In ray theory formula (4.1.5) is obtained as follows. A sound field at point P (Fig. 4.1) will be a sum of the field of the direct ray OP and that of the reflected ray OAP . The intensity of sound along the direct ray decreases with increasing R as R^{-2} , and this means that the acoustic pressure decreases as R^{-1} . The phase of a wave at distance R is kR . As a result, we obtain the first term in (4.1.5), i.e., the acoustic pressure for the direct ray.

The acoustic intensity and phase along the reflected ray OAP behave in an analogous way. The reflected ray can be considered as beginning at the image source O' since $OAP = O'AP = R_1$. The reflection coefficient from the water surface is equal to -1 [see (3.1.12) for $m = \rho_1/\rho = 0$]. Therefore, the image source must be 180° out of phase with the principal source. As a result, we obtain the second term in (4.1.5) with the minus sign.

4.1.3 Directional Pattern

The summation of both terms in (4.1.5) yields a comparatively complex interference pattern for the sound field. For the sake of simplicity, we shall consider the sound field at a distance R which is much greater than the depth of the source z_1 .

In this case, R and R_1 in the denominators of both terms in (4.1.5) can be replaced by $R_0 = (r^2 + z^2)^{1/2}$ (Fig. 4.1). As a result, the expression for p can be written

$$p = R_0^{-1} \exp(ikR_0) [\exp ik(R - R_0) - \exp ik(R_1 - R_0)], \quad (4.1.7)$$

where

$$\begin{aligned} R - R_0 &= [r^2 + (z - z_1)^2]^{1/2} - R_0 = [R_0^2 + (z - z_1)^2 - z^2]^{1/2} - R_0 \\ &= R_0 \{ [1 + (z_1^2 - 2zz_1)R_0^{-2}]^{1/2} - 1 \}. \end{aligned} \quad (4.1.8)$$

The second term under the square root is small compared with unity; therefore

$$R - R_0 = (z_1^2 + 2zz_1)(2R_0)^{-1}. \quad (4.1.9)$$

The expression for $R_1 - R_0$ is obtained when z_1 is replaced by $-z_1$. Thus

$$R_1 - R_0 = (z_1^2 + 2zz_1)(2R_0)^{-1}. \quad (4.1.10)$$

Furthermore, we have (Fig. 4.1) $z/R_0 = \cos \theta_0$. As a result, (4.1.7) can be written as

$$\begin{aligned} p &= R_0^{-1} \exp(ikR_0) [\exp(-ikz_1 \cos \theta_0) - \exp(ikz_1 \cos \theta_0)] \\ &\quad \times \exp[ikz_1^2/(2R_0)]. \end{aligned} \quad (4.1.11)$$

Let R_0 be large enough to satisfy the condition¹

$$kz_1^2/R_0 \ll 1 \quad \text{or} \quad \exp[ikz_1^2/(2R_0)] \approx 1. \quad (4.1.12)$$

Then (4.1.11) becomes

$$p = -(2i/R_0) \sin(kz_1 \cos \theta_0) \exp(ikR_0). \quad (4.1.13)$$

For the amplitude of the acoustic pressure $|p|$ we obtain

$$|p| = (2/R_0) |\sin(kz_1 \cos \theta_0)|. \quad (4.1.14)$$

For a point source in free space we would have $|p| = 1/R_0$. Thus, a system of the point source plus the water surface or, what is the same, a system of the source plus its image is equivalent to the point source with the directional pattern

$$F(\theta_0) = 2 |\sin(kz_1 \cos \theta_0)|. \quad (4.1.15)$$

In the directions satisfying the condition

$$kz_1 \cos \theta_0 = \pi(N + 1/2), \quad N = 0, 1, 2, \dots, \quad (4.1.16)$$

the acoustical pressure is maximal and equal to the doubled acoustic pressure of the single source. In the directions for which

$$kz_1 \cos \theta_0 = N\pi \quad (4.1.17)$$

the acoustic pressure is zero.

¹This means that the reference point is in the Fraunhofer zone, that is, far enough to consider in Fig. 4.1 the lines OP , $O'P$, and OP to be parallel and to use the approximate expressions

$$R - R_0 = -z_1 \cos \theta_0 \quad \text{and} \quad R_1 - R_0 = z_1 \cos \theta_0.$$

If the depth of a source is small as compared with the wavelength, i.e.,

$$kz_1 \ll 1, \quad (4.1.18)$$

then

$$F(\theta_0) = 2kz_1 \cos \theta_0, \quad (4.1.19)$$

that is, we obtain a cosinusoidal directional pattern as for dipole. This is natural since a source at small depth forms an acoustic dipole with its image.

In underwater acoustics the dependence of sound pressure on distance at a fixed depth is of great importance. In the case considered, this dependence reveals intermittent maxima and minima of the sound pressure. However, at large distances (or small z_1, z) $kz_1 \cos \theta_0 = kzz_1/R_0 \ll 1$, the acoustic pressure decreases with distance monotonically

$$|p| \simeq 2kzz_1/r^2. \quad (4.1.20)$$

Consequently, the sound intensity decreases with distance as r^{-4} .

Up to now a medium where sound propagates was assumed to be homogeneous. However, the main features of this phenomenon also remain valid in the presence of ray refraction.

Figure 4.2 gives, for example, the profile $c(z)$ and the ray diagram for a real case (tropical Atlantic) at a source depth of $z_1 = 20$ m. At depths $z > 50$ m and distances $r > 3$ km there is a shadow zone. At smaller distances two rays, direct and reflected from the surface, interfere at each point. Variation of the acoustic pressure with distance for $z_1 = 20$ m, $z = 400$ m, and sound frequency $f = 400$ Hz is shown in Fig. 4.3 for this case. We see that the sound field really has a well-pronounced interference character in the insonified zone and rapidly decreases in the shadow zone. At distances $r > 6$ km the sound field is mainly due to the sound waves reflected from the ocean bottom.

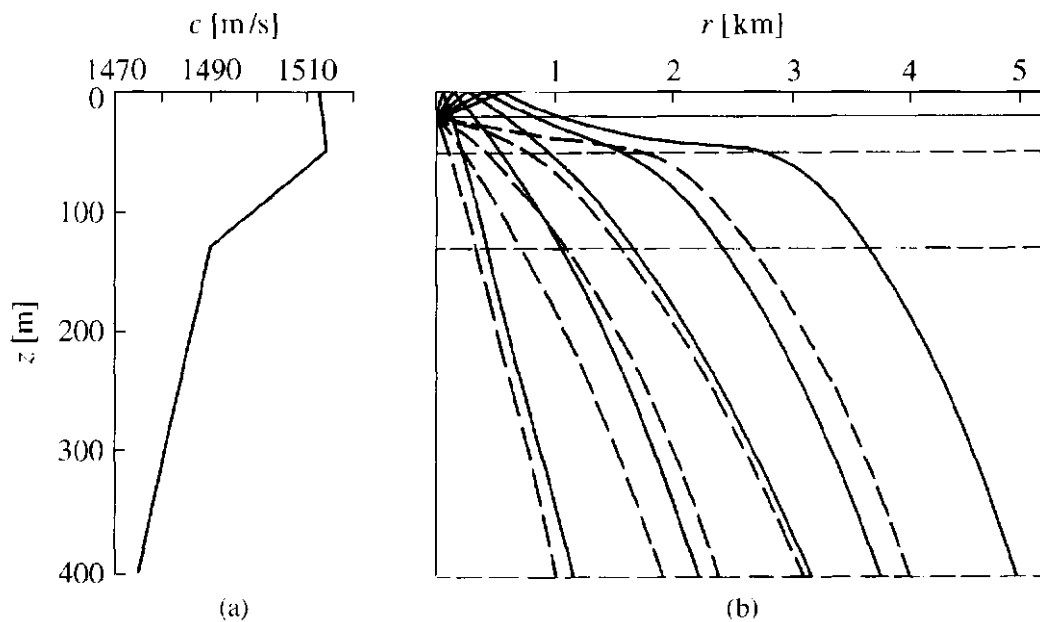


FIGURE 4.2. (a) Profile $c(z)$ and (b) ray diagram

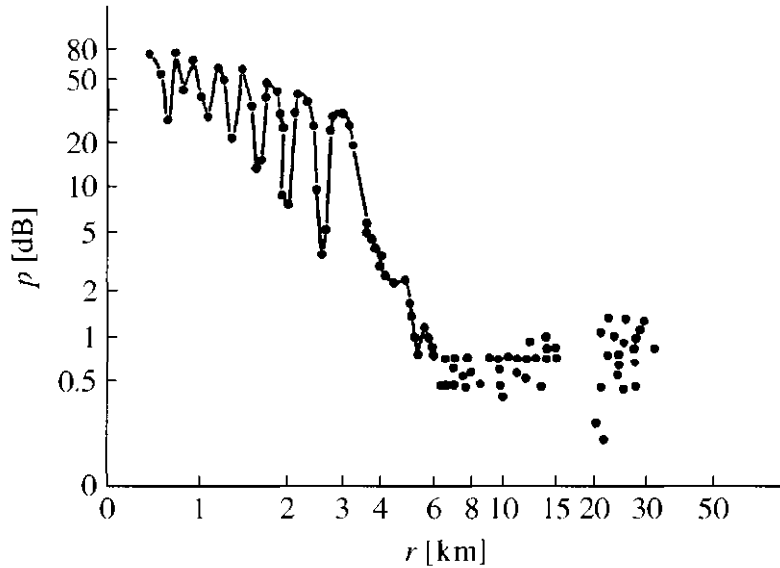


FIGURE 4.3. Acoustic pressure variation with distance for the case shown in Fig. 4.2

4.1.4 Radiated Power

We have seen above that at small z_1 the sound field in water can be considered as that of a dipole, the amplitude of the acoustic pressure at any point decreasing with decreasing z_1 . Quite naturally the radiated acoustical power also decreases. We can also foresee it according to rather simple physical considerations. Indeed, when a pulsating sphere (which approximates our source) is located near the water surface, its periodic expansions and contradictions only cause small local changes of the water level, without producing essential compression-rarefaction waves in the water. Using the assumption about the image source, it is sometimes said that at small depth z_1 an “acoustical short circuit” takes place on the image working in the antiphase of this source.

Thus, the total radiated power increases with an increase in z_1 when z_1 is small. When the source is very far from the surface its radiation will obviously be the same as in free space. Let us obtain a formula for the radiation power with arbitrary z_1 , assuming that the volume velocity V_0 of the source does not change with its depth. In free space, if the acoustic pressure is given by (4.1.2) we have for the radiated power

$$W_0 = 4\pi R_0^2 |p|^2 (2\rho c)^{-1} = 2\pi (\rho c)^{-1} \quad (4.1.21)$$

where R_0 is the distance from the source and p is the acoustic pressure at this distance.

Taking into account the water surface, we have for the amplitude of the acoustic pressure (4.1.14) and, consequently, for the specific sound power flux at distance R_0 in the direction given by the angle θ_0

$$|p|^2 (2\rho c)^{-1} = 2(\rho c R_0^2)^{-1} \sin^2(kz_1 \cos \theta_0). \quad (4.1.22)$$

To find the total radiated power, the last expression must be multiplied by the area of the band lying on the semisphere with radius R_0 and restricted by the angles θ_0

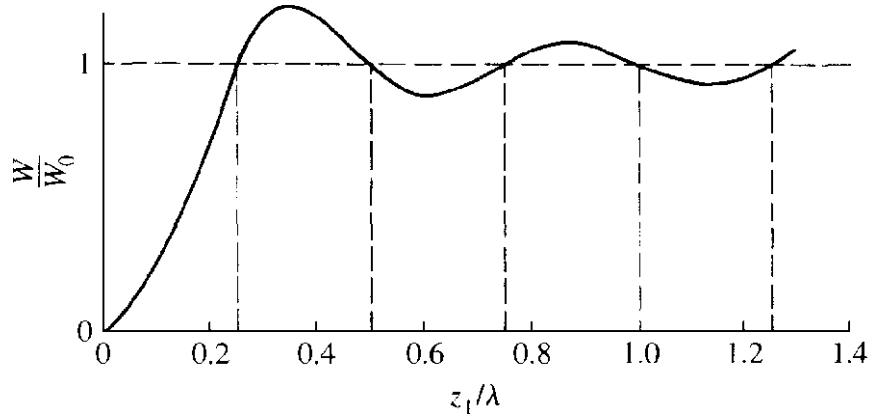


FIGURE 4.4. Power output of a source as a function of source depth

and $\theta_0 + d\theta_0$, which is equal to $2\pi R_0^2 \sin \theta_0 d\theta_0$, and then integrated in respect to θ_0 from 0 to $\pi/2$. We have then

$$W = 4\pi(\rho c)^{-1} \int_0^{\pi/2} \sin^2(kz_1 \cos \theta_0) \sin \theta_0 d\theta_0.$$

Having introduced a new variable $kz_1 \cos \theta_0 = x$ and performed an elementary integration, we find

$$W = 2\pi(\rho c)^{-1} [1 - (2kz_1)^{-1} \sin 2kz_1]. \quad (4.1.23)$$

Taking (4.1.21) also into account, the ratio of powers in the presence of the water surface and in free space is written in the form

$$W/W_0 = 1 - (2kz_1)^{-1} \sin 2kz_1. \quad (4.1.24)$$

In Fig. 4.4 the ratio W/W_0 is plotted as a function of $kz_1/2\pi = z_1/\lambda$. If $kz_1 \rightarrow \infty$, then $W/W_0 \rightarrow 1$ as expected for a source in free space. The source power output will be maximal at $z_1/\lambda = 3/8$. In this case $W \approx 1.2W_0$.

Sometimes the radiated power is written in the form $W = Z_1 V_0^2$, where Z_1 is the radiation impedance of a source. For this case, the plot in Fig. 4.4 also gives the depth dependence of the radiation impedance.

4.2 Expansion of a Spherical Wave into Plane Waves

The difficulty of the problem of the reflection and refraction of a spherical wave at a plane interface between two media is due to the difference between the symmetry of the wave and that of the boundary. Whereas the wave has a spherical symmetry, the boundary is a plane. It is therefore natural to approach the problem by expanding the spherical wave into plane waves, especially since the theory of the reflection and refraction of plane waves is well developed.

We assume that the source is at the origin, so that in (4.1.2) we have $R = (x^2 + y^2 + z^2)^{1/2}$. In the plane $z = 0$, the field of the spherical wave is $\exp(ikr)/r$, where $r = (x^2 + y^2)^{1/2}$. We expand this field in a double Fourier integral in the

variables x and y

$$\exp(ikr)/r = \iint_{-\infty}^{\infty} A(k_x, k_y) \exp[i(k_x x + k_y y)] dk_x dk_y. \quad (4.2.1)$$

$A(k_x, k_y)$ is given by the inverse Fourier transform

$$(2\pi)^2 A(k_x, k_y) = \iint_{-\infty}^{\infty} r^{-1} \exp(ikr) \exp[-i(k_x x + k_y y)] dx dy. \quad (4.2.2)$$

Next, transform to polar coordinates and use the notation

$$\begin{aligned} k_x &= \xi \cos \psi, & k_y &= \xi \sin \psi, & \xi &= (k_x^2 + k_y^2)^{1/2}, \\ x &= r \cos \varphi, & y &= r \sin \varphi, & dx dy &= r dr d\varphi. \end{aligned} \quad (4.2.3)$$

We then obtain

$$(2\pi)^2 A(k_x, k_y) = \int_0^{2\pi} d\varphi \int_0^{\infty} \exp\{ir[k - \xi \cos(\psi - \varphi)]\} dr.$$

The integral over r is elementary. Moreover, assuming that k has a small positive imaginary part (small absorption in the medium), substitution of the upper limit yields zero, and we obtain

$$(2\pi)^2 A(k_x, k_y) = i \int_0^{2\pi} \frac{d\varphi}{k - \xi \cos(\psi - \varphi)} = ik^{-1} \int_0^{2\pi} \frac{d\alpha}{1 - (\xi/k) \cos \alpha}.$$

Here the integral is elementary, hence

$$A(k_x, k_y) = i(2\pi)^{-1} (k^2 - \xi^2)^{-1/2} = i(2\pi)^{-1} (k^2 - k_x^2 - k_y^2)^{-1/2}. \quad (4.2.4)$$

Thus,

$$\exp(ikr)/r = i(2\pi)^{-1} \iint_{-\infty}^{\infty} (k^2 - k_x^2 - k_y^2)^{-1/2} \exp[i(k_x x + k_y y)] dk_x dk_y. \quad (4.2.5)$$

This expression, describing the field in the xy plane, can be easily “continued” into space. As is well known, each Fourier component will then correspond to a plane wave in space. Formally, for this “continuation” it is sufficient to add the term $\pm ik_z z$ in the exponent in the integrand, where

$$k_z = (k^2 - k_x^2 - k_y^2)^{1/2} = (k^2 - \xi^2)^{1/2}. \quad (4.2.6)$$

The plus (minus) sign corresponds to waves propagating in the positive (negative)

z direction in the half-space $z > 0$ ($z < 0$). Thus,

$$\begin{aligned}
 z &\geq 0 \\
 \exp(ikR)/R &= i(2\pi)^{-1} \iint_{-\infty}^{\infty} k_z^{-1} \exp[i(k_x x + k_y y + k_z z)] dk_x dk_y, \\
 z &\leq 0 \\
 \exp(ikR)/R &= i(2\pi)^{-1} \iint_{-\infty}^{\infty} k_z^{-1} \exp[i(k_x x + k_y y + k_z z)] dx_x dx_y.
 \end{aligned} \tag{4.2.7}$$

The validity of such a “continuation” is proved by the fact that the right-hand sides of the last expressions satisfy the Helmholtz equation (since it is satisfied by the integrands) and give the correct value for the field at $z = 0$.

Equations (4.2.7) represent the expansion of a spherical wave into plane waves. The exponent in the integrand is a plane wave propagating in the direction given by the components k_x , k_y , and k_z of the wave vector.

4.3 Reflected Wave

Now we shall assume that a source is at the point $r = 0$, $z = z_0$ (Fig. 4.5). The plane $z = 0$ is the boundary between two liquids as in Sect. 3.1.

Each plane wave in the integrand in (4.2.7) propagating from the source to the boundary and via reflection to the receiver at point (r, z) builds up the phase $k_x x + k_y y + k_z(z + z_0)$. Its amplitude must be multiplied by the reflection coefficient $V(k_z)$, $k_z = k \cos \theta$, where θ is the angle of incidence. As a result, we obtain for the reflected wave

$$p_r = i(2\pi)^{-1} \iint_{-\infty}^{\infty} k_z^{-1} V(k_z) \exp[i(k_x x + k_y y + k_z(z + z_0))] dk_x dk_y \tag{4.3.1}$$

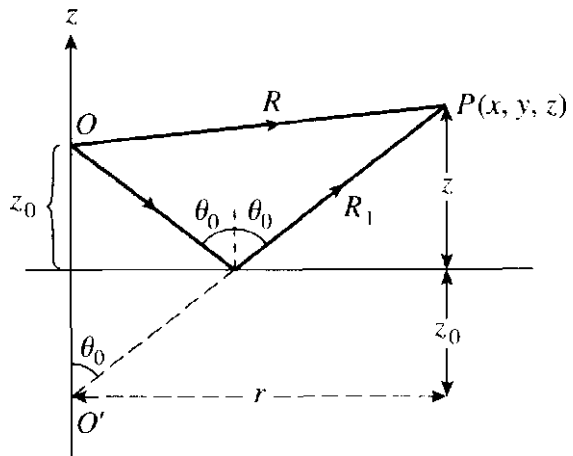


FIGURE 4.5. Positions of the source O and the reference point P with respect to the interface

or in polar coordinates, using (4.2.3),

$$p_r = i(2\pi)^{-1} \int_0^\infty k_z^{-1} V(k_z) \exp[ik_z(z + z_0)] \xi d\xi \int_0^{2\pi} \exp[i\xi \cos(\varphi - \psi)] d\psi.$$

The integral over ψ is equal to $2\pi J_0(\xi r)$, where $J_0(\xi r)$ is a Bessel function of zero order. Let us use the well-known relation in the theory of cylindrical functions

$$J_0(\xi r) = 2^{-1} [H_0^{(1)}(\xi r) + H_0^{(2)}(\xi r)],$$

where $H_0^{(1)}$ and $H_0^{(2)}$ are the Hankel functions of the first and the second kind. Hence

$$p_r = i2^{-1} \left[\int_0^\infty H_0^{(1)}(\xi r) + \int_0^\infty H_0^{(2)}(\xi r) \right] k_z^{-1} V(k_z) \exp[ik_z(z + z_0)] \xi d\xi.$$

In the second integral we replace ξ by $-\xi$ and make use of the relation [Ref. 4.1, p. 89] $H_0^{(2)}[\xi r \exp(-\pi i)] = -H_0^{(1)}(\xi r)$. We obtain then in this integral exactly the same integrand as in the first one, the limits of integration being 0, $-\infty$. Combining both integrals into one, we have

$$p_r = i2^{-1} \int_{-\infty}^\infty k_z^{-1} V(k_z) H_0^{(1)}(\xi r) \exp[ik_z(z + z_0)] \xi d\xi. \quad (4.3.2)$$

If the reflection coefficient V is not a function of the angle of incidence, it can be taken outside the integral sign. Then the remaining integral is [Ref. 4.2, Chap. 4]

$$\begin{aligned} \int_{-\infty}^\infty H_0^{(1)}(\xi r) k_z^{-1} \exp[ik_z(z + z_0)] \xi d\xi &= -2i R_1^{-1} \exp(ik R_1), \\ R_1 &= [r^2 + (z + z_0)^2]^{1/2}. \end{aligned} \quad (4.3.3)$$

As a result, the reflected wave is

$$p_r = V R_1^{-1} \exp(ik R_1), \quad (4.3.4)$$

i.e., the outgoing spherical wave centred at the image source O' (Fig. 4.5).

Let us turn to a general case. The field at distances which are large compared to the wavelength is of interest to us. Under these conditions it is convenient to use an asymptotic representation of the Hankel function

$$H_0^{(1)}(\xi r) \approx [2/(\pi \xi r)]^{1/2} \exp[i(\xi r - \pi/4)] [1 + (8i \xi r)^{-1} + \dots]. \quad (4.3.5)$$

Having restricted ourselves to the first term in this expansion, we obtain from (4.3.2)

$$p_r = (2\pi r)^{-1/2} \exp(\pi i/4) \int_{-\infty}^\infty (\sqrt{\xi}/k_z) V(k_z) \exp[iw(\xi)] d\xi \quad (4.3.6)$$

where

$$w(\xi) \equiv \xi r + k_z(z + z_0). \quad (4.3.7)$$

Note that

$$r = R_1 \sin \theta_0, \quad z + z_0 = R_1 \cos \theta_0 \quad (4.3.8)$$

where R_1 is the distance from the receiving point P to the image source O' , and θ_0 is the angle between the line OP and the z axis (Fig. 4.5). Then,

$$w(\xi) = R_1(\xi \sin \theta_0 + k_z \cos \theta_0). \quad (4.3.9)$$

Since, according to our assumption, R_1 is large compared with the wavelength, the exponential in the integrand (4.3.6) will be a rapidly varying function, and the value of the integral can be estimated by using the method of stationary phase.² The main contribution to the integral is given by the vicinity of the point of the stationary phase ξ_0 which can be found from the equation $(dw/d\xi)_{\xi_0} = 0$. Taking into account (4.3.7) and the value of k_z (4.2.6), we obtain

$$\xi_0 = k \sin \theta_0. \quad (4.3.10)$$

Thus, the point of stationary phase corresponds to rays $O'P$ in Fig. 4.5 for which the horizontal component of the wave vector is given by (4.3.10). All factors in the integrand (4.3.6), except the exponential, can be taken outside the integral sign (as a slowly varying function) at $\xi = \xi_0$, and for the evaluation of the remaining integral $w(\xi)$ can be expanded into a power series of ξ_0

$$w(\xi) = w(\xi_0) + 2^{-1}w''(\xi_0)(\xi - \xi_0)^2. \quad (4.3.11)$$

As a result, we obtain from (4.3.6)

$$\begin{aligned} p_r &= V(\theta_0)(2\pi k R_1 \cos^2 \theta_0)^{1/2} \exp \left[i w(\xi_0) + \frac{\pi i}{4} \right] \\ &\times \int_{-\infty}^{\infty} \exp[iw''(\xi_0)(\xi - \xi_0)^2/2] d\xi \end{aligned} \quad (4.3.12)$$

where $V(\theta_0) \equiv V(k_z)|_{\xi=\xi_0}$. Let us change the integration variable from ξ to s ,

$$w''(\xi_0)(\xi - \xi_0)^2/2 = is^2$$

or

$$\begin{aligned} \xi - \xi_0 &= [2/w''(\xi_0)]^{1/2} \exp(i\pi/4)s \quad \text{for } w''(\xi_0) > 0, \\ \xi - \xi_0 &= [-2/w''(\xi_0)]^{1/2} \exp(-i\pi/4)s \quad \text{for } w''(\xi_0) < 0. \end{aligned}$$

The path of integration over s goes from $-\infty \exp(\pm i\pi/4)$ to $\infty \exp(\pm i\pi/4)$, but it can be deformed so that it will go along the real axis. As a result, using the value of the integral

$$\int_{-\infty}^{\infty} \exp(-s^2) ds = \sqrt{\pi},$$

we obtain

$$\int_{-\infty}^{\infty} \exp[iw''(\xi_0)(\xi - \xi_0)^2/2] d\xi = [2\pi/|w''(\xi_0)|]^{1/2} \exp(\pm i\pi/4) \quad (4.3.13)$$

the sign in the exponential being coincident with the sign of $w''(\xi_0)$.

²The method of stationary phase is a particular case of the steepest descent method considered, for example, in the book by *Brekhovskikh* [Ref. 4.3, Sect. 27].

Substituting (4.3.10) into (4.3.9) yields $w(\xi_0) = kR_1$. Then, differentiating (4.3.9) twice with respect to ξ , taking into account k_z from (4.2.6), and again substituting ξ_0 from (4.3.10), we have

$$w''(\xi_0) = -R_1/(k \cos^2 \theta_0).$$

Now, taking into account (4.3.13), we obtain from (4.3.12)

$$p_r = V(\theta_0)R_1^{-1} \exp(ikR_1). \quad (4.3.14)$$

Thus, in this approximation the result is quite simple. The field of the reflected wave is equal to that of the image source O' (Fig. 4.5) multiplied by the reflection coefficient $V(\theta_0)$.

As will be shown below, this approximation is not always sufficient in practice. To calculate p_r in the next approximation we have to do the following:

1. take into account the next term in the expansion of the Hankel function (4.3.5);
2. expand the function $w(\xi)$ in (4.3.6) up to the term $(\xi - \xi_0)^4$; and
3. expand the integrand except the exponential in (4.3.6) up to the term $(\xi - \xi_0)^2$.

We shall not deal here with these in principle simple, yet rather cumbersome calculations, but just give the final result³

$$p_r = R_1^{-1} \exp(ikR_1) [V(\theta_0) - iN/kR_1], \quad (4.3.15)$$

where

$$N = 2^{-1} [V''(\theta_0) + V'(\theta_0) \cot \theta_0]. \quad (4.3.16)$$

Here a prime stands for the derivative with respect to θ .

Using (3.1.12) for the reflection coefficient of a sound wave from the interface of two liquids, we obtain after differentiating

$$N = \frac{m(1 - n^2)}{q_0^3(m\gamma_0 + q_0)^3} [2m(n^2 - 1) + 3m\gamma_0^2 + q_0\gamma_0(2n^2 - \gamma_0^2 + 1) - m\gamma_0^4], \quad (4.3.17)$$

where

$$\gamma_0 = \cos \theta_0, \quad q_0 = (n^2 - \sin^2 \theta_0)^{1/2}. \quad (4.3.18)$$

Approximation of Geometrical Acoustics. The second term in the square brackets in (4.3.15) vanishes as $k \rightarrow \infty$, and therefore, (4.3.14) is called the approximation of geometrical acoustics. Analysing the limits of the validity of this approximation is of interest here.

First of all we note that $N = 0$ if V is constant, i.e., when the reflection coefficient is independent of the angle of incidence. This occurs, in particular, for a perfectly reflecting surface ($V = \pm 1$). The applicability of geometrical acoustics in this case is well known (Sect. 4.1). The reflection coefficient is also independent of angle when the sound velocity is the same in both media. In fact, setting $n = 1$ in (3.1.12), we obtain $V = (m - 1)/(m + 1)$.

³For the complete derivation of formula (4.3.15) with integration in the complex plane θ where $\xi = k \sin \theta$ see Brekhovskikh [Ref. 4.3, Sect. 28].

Now we will derive a criterion to indicate when the correction term in (4.3.15) can be neglected if V is not constant. For simplicity, consider the case in which the source is located at the interface ($R = R_1$, see Fig. 4.5). The correction term in (4.3.15) is small compared with the sum of the direct wave $\exp(ikR)/R$ and the reflected wave $V(\theta_0) \exp(ikR)/R$ if

$$kR|1 + V(\theta_0)| \gg |N| \quad (4.3.19)$$

or using (3.1.12) for $V(\theta_0)$ if

$$\frac{2mkR \sin \theta_0}{m \cos \theta_0 + \sqrt{n^2 - \cos^2 \theta_0}} \gg |N|. \quad (4.3.20)$$

Since kR is assumed to be large, this condition is automatically fulfilled, except in the case when $\cos \theta_0 \ll 1$ and $\theta_0 \simeq \pi/2$. In the latter case, taking into account that in (4.3.17) $\gamma_0 = \cos \theta_0 \ll 1$ and $R \cos \theta_0 = z$, condition (4.3.20) can be rewritten as

$$kz \gg \left| \frac{m\sqrt{n^2 - 1}}{(m \cos \theta_0 + \sqrt{n^2 - 1})^2} \right|. \quad (4.3.21)$$

If $m \cos \theta_0 \ll (n^2 - 1)^{1/2}$, the last condition can be also written as

$$kz \gg m/\sqrt{n^2 - 1}. \quad (4.3.22)$$

Thus, the elevation of the receiver above the interface must be large compared to the wavelength for geometrical acoustics to be applicable.⁴ It should be noted that geometrical acoustics is also not applicable if $q_0 \rightarrow 0$ and $\sin \theta_0 \rightarrow n$ (the case of total internal reflection).

At $m \rightarrow \infty$ we have the transition to a perfectly reflecting boundary since $V \rightarrow 1$ (3.1.12). Accordingly, the right-hand side of (4.3.21) tends to zero, and geometrical acoustics is valid for any z .

4.4 Lateral Wave

Some interesting phenomena arise when a spherical wave undergoes total internal reflection ($n < 1$, $\sin \theta_0 > n$). Using (3.1.15) for V in this case, we rewrite (4.3.6) for the reflected wave in the form

$$p_r = (2\pi r)^{-1} \exp(i\pi/4) \int_{-\infty}^{\infty} \exp[iw(\xi)](k^2 - \xi^2)^{-1/2} \xi^{1/2} d\xi, \quad (4.4.1)$$

where

$$w(\xi) = \xi r + k_z(z + z_0) + \varphi(\xi). \quad (4.4.2)$$

Expression (3.1.15) for the phase φ of the reflection coefficient in terms of ξ is

$$\varphi = -2 \arctan[(\xi^2 - k_1^2)^{1/2}/m(k^2 - \xi^2)^{1/2}]. \quad (4.4.3)$$

⁴The same result occurs if the receiver is at the interface and the elevation of the source above the interface is large.

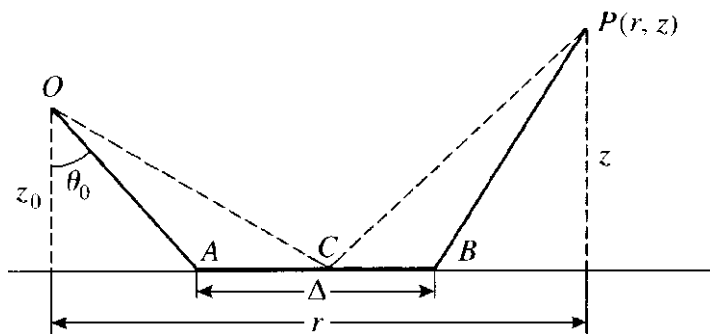


FIGURE 4.6. Lateral wave as a result of ray displacement on reflection

A point of stationary phase $\xi = \xi_0$ is found from the equation $w'(\xi_0) = 0$. Taking into account the value of $k_z = (k^2 - \xi^2)^{1/2}$, the latter can be written

$$r = -\varphi'(\xi_0) + \xi_0(z + z_0)(k^2 - \xi_0^2)^{-1/2} = \Delta + (z + z_0) \tan \theta_0 \quad (4.4.4)$$

where

$$\Delta = -\varphi'(\xi_0) \quad (4.4.5)$$

and the angle θ_0 is introduced according to the relation $\xi_0 = k \sin \theta_0$. Expression (4.4.4) allows a simple geometrical interpretation (Fig. 4.6). The horizontal distance r covered by the ray $OABP$ consists of the segments $z_0 \tan \theta_0$ and $z \tan \theta_0$ and the displacement Δ of the ray along the boundary.

Here for the first time we encounter the interesting phenomenon of ray displacement along the boundary at total internal reflection. Formula (4.4.5) obtained for ray displacement is applicable for any case of total reflection (Sect. 4.5) when the reflection coefficient is represented in the form $V = \exp(i\varphi)^5$ and φ is real. For the case when φ is given by (4.4.3), we find

$$\varphi'(\xi) = \frac{2m\xi(k^2 - k_1^2)}{[m^2(k^2 - \xi^2) + \xi^2 - k_1^2](\xi^2 - k_1^2)^{1/2}(k^2 - \xi^2)^{1/2}}. \quad (4.4.6)$$

Note that the displacement $\Delta = -\varphi'(\xi_0)$, generally of the order of $1/k$, increases significantly when $\xi_0 \rightarrow k_1$, i.e., when θ_0 approaches the angle of total internal reflection. As will be seen below, this case is of the utmost interest. Therefore, setting $\xi = \xi_0 = k_1$ everywhere in (4.4.6) except in the difference $\xi^2 - k_1^2$, we obtain for the ray displacement

$$\Delta \simeq \frac{2n}{m(1 - n^2)^{1/2}(\xi_0^2 - k_1^2)^{1/2}} = \frac{2n}{km(1 - n^2)^{1/2}(\sin^2 \theta_0 - n^2)^{1/2}}. \quad (4.4.7)$$

Now, let us again return to the ray equation (4.4.4) and consider the case of sufficiently large r . One can easily see that two rays arrive at the point $P(r, z)$. One of them is the ray just considered. It is incident on the boundary at an angle close to that of total internal reflection ($\sin \theta_0 \simeq n$) and has a relatively large displacement Δ . Rays of this kind comprise the so-called lateral wave. Another ray, OCP , is incident on the boundary at a substantially greater angle and has a very small displacement (in Fig. 4.6 it is equal to zero). This ray belongs to the family of

⁵The most complete research on this phenomenon is reported in the paper by Lotsch [4.4].

rays corresponding to the reflected wave studied above. Consider the lateral wave in more detail by turning to the integral (4.4.1) and estimating its value given by that part of the integration path which includes the point of stationary phase close to $\xi_0 = k_1$. To do this, everything except the exponential can be taken outside the integral at $\xi = k_1$, and the phase in the exponential, i.e., the function $w(\xi)$ given by (4.4.2), can be represented in the form given in (4.3.11).

Assuming further that $w(\xi_0) = w(k_1)$, we obtain from (4.4.1)

$$p_r = (2\pi kr)^{-1/2} [n/(1-n^2)]^{1/2} \exp(i\pi/4) \exp\{i[k_1 r + k(1-n^2)^{1/2}(z+z_0)]\} \\ \times \int_{-\infty}^{\infty} \exp[iw''(\xi_0)(\xi - \xi_0)^2/2] d\xi. \quad (4.4.8)$$

Differentiating (4.4.2) twice with respect to ξ , retaining only the terms which contain the difference $(\xi^2 - k_1^2)$ to the highest negative power for the derivative of $\varphi(\xi)$, and setting $\xi_0 = k_1$, everywhere except in this difference, we obtain

$$w''(\xi_0) = \frac{2nk_1}{m(1-n^2)^{1/2}(\xi_0^2 - k_1^2)^{3/2}} - \frac{k^2(z+z_0)}{(k^2 - k_1^2)^{3/2}}. \quad (4.4.9)$$

Since $\xi_0^2 - k_1^2$ is small, we assume that the second term can be neglected. Then, taking into account (4.4.7) for the displacement Δ , we have

$$w''(\xi_0) = km^2(1-n^2)(4n)^{-1}\Delta^3. \quad (4.4.10)$$

Finally, taking into account (4.3.13) [at $w''(\xi_0) > 0$], we obtain from (4.4.8)

$$p_r = \frac{2in}{km(1-n^2)r^{1/2}\Delta^{3/2}} \exp\{i[k_1 r + k(1-n^2)^{1/2}(z+z_0)]\}. \quad (4.4.11)$$

For small $z+z_0$ and large r we have $\Delta \sim r$ from (4.4.4). In this case the amplitude of the lateral wave will decrease with distance as $1/r^2$.

One can understand the origin of the lateral wave using simple physical reasoning. A spherical wave from the source O incident at point A on the boundary at an angle of total internal reflection δ ($\sin \delta = n$) generates a wave which propagates along the boundary in the lower medium (Fig. 4.7). During propagation this wave continuously reradiates a part of its energy into the upper medium, giving rise to a lateral wave. In accordance with the law of refraction, the rays corresponding to the lateral wave (one of them, BP , is shown in Fig. 4.7 by a solid line, the others by dashed lines) leave the boundary at an angle δ with respect to the normal to the boundary. The front $P'P''$ of the lateral wave is a straight line in the plane of the figure, but in space it is a conic considering the symmetry with respect to the vertical axis including O .

Now, let us show that the phase of the lateral wave (4.4.11) corresponds to the phase change along the ray $OABP$. This ray consists of the segments $L_0 = OA$ and $L = BP$ along which the wave propagates with a velocity $c = \omega/k$ and the segment $\Delta = AB$ with a velocity $c_1 = \omega/k_1 = \omega/kn$. In fact, we have for the phase of the lateral wave [the brackets in the exponent in (4.4.11)] if we set $\theta_0 = \delta$

3. The lateral wave plays a predominant role in the oceanic waveguide at frequencies below that of the first mode.
4. The source and receiver are located very close to the ocean bottom when the incident and specularly reflected waves almost cancel each other.
5. The lateral wave characteristics can be used to extract unique information about the medium where the wave propagates. This property of the lateral wave is the basis for method of refracted waves in seismic prospecting.

The theory of lateral waves is given in [4.5–7].

Concluding this section, we note that all our considerations were related to the case of large r and Δ when the families of rays corresponding to the usual reflected and lateral waves were well separated. At moderate and small values of Δ these two families approach each other, forming the caustic—the case not considered here [4.3].

4.5 Reflection from the Layered Inhomogeneous Half-Space: Caustics

The calculations in Sect. 4.4 which led to the expression for the lateral wave are easily generalized for the case of total reflection from an arbitrary layered half-space with the reflection coefficient given in the form

$$V = \exp[i\varphi(\xi)], \quad \xi = k \sin \theta, \quad (4.5.1)$$

where k is the wave number in the homogeneous half-space and θ is the angle of incidence. The integral expression (4.4.1) for p_r , (4.4.4) for a ray, and expression (4.4.5) for the ray displacement still hold.

Let us suppose that the parameters of an inhomogeneous half-space change slowly with respect to z so that φ is given by formula (3.5.2). Then, Δ can be obtained by ray approximations if we trace the rays in the lower half-space (Fig. 3.8). In fact, differentiating the phase (3.5.2) we obtain

$$\Delta = - \left(\frac{\partial \varphi}{\partial \xi} \right)_{\xi_0} = 2 \left| \int_0^{z_m} [k^2(z) - \xi_0^2]^{-1/2} \xi_0 dz \right|, \quad (4.5.2)$$

which coincides with (2.3.2) since $\xi_0 = k_0 \cos \chi_1$, $z_1 = 0$, and $z = z_m$. The point of the stationary phase $\xi = \xi_0$ for the integral (4.4.1) can again be found from the equation $w'(\xi_0) = 0$. Taking everything except the exponential outside the integral for $\xi = \xi_0$ and replacing the expression in the exponent by the expansion

$$w(\xi) = w(\xi_0) + w''(\xi_0)(\xi - \xi_0)^2/2, \quad (4.5.3)$$

we obtain

$$\begin{aligned} p_r &= \xi_0^{1/2} [2\pi r(k^2 - \xi_0^2)]^{-1/2} \exp[i\pi/4 + iw(\xi_0)] \\ &\times \int_{-\infty}^{\infty} \exp[iw''(\xi_0)(\xi - \xi_0)^2/2] d\xi, \end{aligned} \quad (4.5.4)$$

$$w(\xi_0) = \xi_0 r + (z + z_0)(k^2 - \xi_0^2)^{1/2} + \varphi(\xi_0). \quad (4.5.5)$$

Taking into account $\xi_0 = k \sin \theta_0$ and (4.3.13), expression (4.5.4) yields

$$p_r = [kr \cot \theta_0 \cos \theta_0 |w''(\xi_0)|]^{-1/2} \exp[iw(\xi_0) + i\varepsilon], \quad (4.5.6)$$

where $\varepsilon = \pi/2$ for $w''(\xi_0) > 0$ and $\varepsilon = 0$ for $w''(\xi_0) < 0$.

Expression (4.5.6) is identical with that obtained using methods from geometrical acoustics. Indeed, we have [see (4.4.2) for $w(\xi)$]

$$\begin{aligned} w''(\xi_0) &= \frac{\partial^2}{\partial \xi_0^2} [(z + z_0)(k^2 - \xi_0^2)^{1/2} + \varphi(\xi_0)] \\ &= -\frac{\partial}{\partial \xi_0} [\xi_0(z + z_0)(k^2 - \xi_0^2)^{-1/2} - \varphi'(\xi_0)] \end{aligned} \quad (4.5.7)$$

or, taking into account the equations for the ray (4.4.4, 5)

$$w''(\xi_0) = -\frac{\partial r}{\partial \xi_0}. \quad (4.5.8)$$

Since

$$\frac{\partial}{\partial \xi_0} = (k \cos \theta_0)^{-1} \frac{\partial}{\partial \theta_0}, \quad w''(\xi_0) = -(k \cos \theta_0)^{-1} \frac{\partial r}{\partial \theta_0}. \quad (4.5.9)$$

Now (4.5.6) yields for the sound intensity

$$|p_r|^2 = [kr \cot \theta_0 \cos \theta_0 |w''(\xi_0)|]^{-1} = \tan \theta_0 \left(r \left| \frac{\partial r}{\partial \theta_0} \right| \right)^{-1}. \quad (4.5.10)$$

On the other hand, we have in accordance with the definition of the focusing factor f (Sect. 2.5)

$$|p_r|^2 = fr^{-2}. \quad (4.5.11)$$

Comparison of (4.5.10) and (4.5.11) yields

$$f = r \tan \theta_0 \left| \frac{\partial r}{\partial \theta_0} \right|^{-1}, \quad (4.5.12)$$

which coincides with (2.5.3) if $\chi = \chi_1 = \pi/2 - \theta_0$ is taken into consideration.

We leave it to the reader to prove that the phase in (4.5.6) can also be obtained in the framework of ray theory.

Formula (4.5.6) for the reflected wave can be used everywhere except in the regions where $w''(\xi_0)$ (as well as $\partial r / \partial \theta_0$) equals zero or is small. Excluding θ_0 from the equation $\delta r / \delta \theta_0 = 0$ and the equation of a family of rays $r = r(z, \theta_0)$, we obtain the envelope of this family, or the caustic. The field on this caustic and near it must be calculated in a special way.

As an example let us consider the case when the sound velocity in the half-space $z < 0$ increases linearly with the distance from the boundary

$$c = c_0(1 - az), \quad k(z) = k_0/(1 - az), \quad k_0 = \omega/c_0 \quad (4.5.13)$$

where c_0 is the sound velocity in the upper homogeneous half-space. Substituting $k(z)$ into (4.5.2), carrying out the simple integration [substituting $\xi_0(1 - az) =$

$k_0 \sin \theta]$, and remembering that $\xi_0 = k_0 \sin \theta_0$, we obtain

$$\Delta = (2/a) \cot \theta_0. \quad (4.5.14)$$

Substitution of Δ into (4.4.4) gives the ray equation

$$z > 0, \quad r = (z + z_0) \tan \theta_0 + (2/a) \cot \theta_0. \quad (4.5.15)$$

As we have seen, $\partial r / \partial \theta_0 = 0$ on the caustic, i.e.,

$$\frac{\partial r}{\partial \theta_0} = (z + z_0) \cos^{-2} \theta_0 - 2(a \sin^2 \theta_0)^{-1} = 0. \quad (4.5.16)$$

Excluding θ_0 from (4.5.15, 16), we obtain the equation for the caustic

$$z + z_0 = ar^2/8. \quad (4.5.17)$$

In Fig. 4.8 the ray pattern and the caustic for $az_0 = 1/8$ are given in non-dimensional coordinates az and ar . The paths of rays in the lower medium (which are arcs of circles) are not shown in this figure (Sect. 2.2).

Now, let us analyze the field on and near the caustic. Let us introduce the auxiliary function $g(\xi)$ by the identity

$$g(\xi) = r - w'(\xi). \quad (4.5.18)$$

We have seen that rays are defined by the equation $w'(\xi) = 0$, i.e., $r = g(\xi)$. To each point (r_0, z_0) of the caustic there corresponds a certain ξ_0 —the parameter of a ray tangent to the caustic at this point whence $g'(\xi) = 0$. Figure 4.9 illustrates

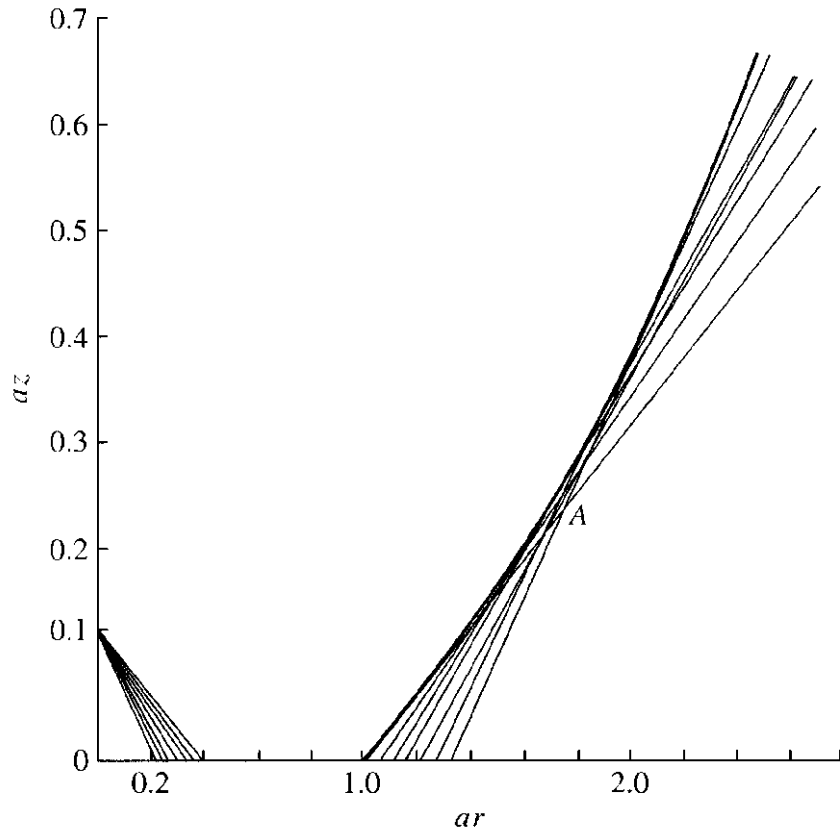


FIGURE 4.8.
Caustic formed on
reflection from an
inhomogeneous
half-space

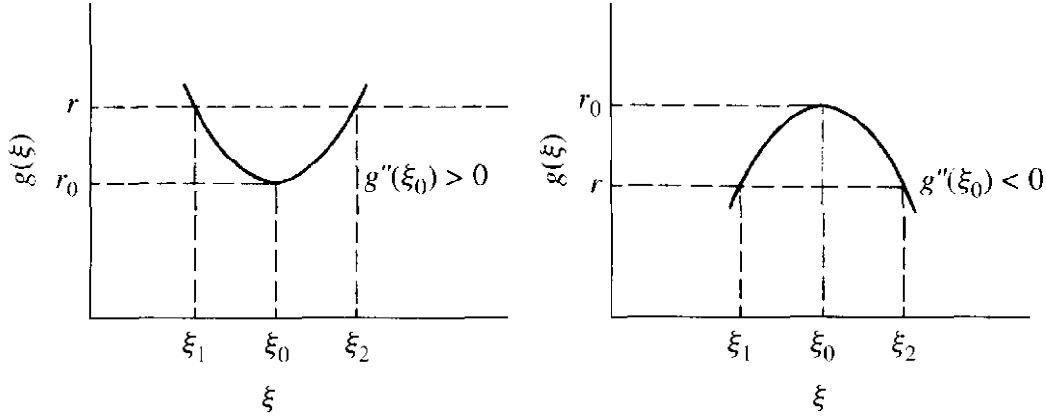


FIGURE 4.9. Parameters for the calculation of a sound field in the vicinity of a caustic

the function $g(\xi)$ for values ξ close to ξ_0 for the two possible cases $g''(\xi_0) > 0$ and $g''(\xi_0) < 0$. As can be seen from the figure, in the first case (realized in Fig. 4.8) two rays arrive at each point $r = g(\xi_1) = g(\xi_2) > r_0$. In the second case a similar situation occurs at $r < r_0$. The general rule is that the caustic of a given family of rays always separates the region where the rays of this family do not arrive and the region where two rays arrive at each point (e.g., at point A in Fig. 4.8—one of them has already touched the caustic and the other is still approaching it). Figure 4.9 suggests that near ξ_0 corresponding to the caustic, it is reasonable to use the expansion of the function $g(\xi)$ in a power series of $\xi - \xi_0$

$$g(\xi) = g(\xi_0) + g''(\xi_0)(\xi - \xi_0)^2/2 + \dots$$

Taking into account (4.5.18), we find $w(\xi)$ by integration. The integration constant is defined from the condition $w = w_0$ at $\xi = \xi_0$. As a result, taking into account that $g(\xi) = r$ and $g(\xi_0) = r_0$, we obtain

$$w = w_0 + (r - r_0)(\xi - \xi_0) - g''(\xi_0)(\xi - \xi_0)^3/6 + \dots \quad (4.5.19)$$

Taking all the terms in (4.4.1) except the variable part of the exponential outside the integral at the value $\xi = \xi_0 = k \sin \theta_0$ and limiting ourselves to the terms written in (4.5.19), we obtain for the reflected wave

$$p_r = [\sin \theta_0 / (2\pi k r \cos^2 \theta_0)]^{1/2} \exp[i(w_0 + \pi/4)] \\ \times \int_{-\infty}^{\infty} \exp[i(r - r_0)(\xi - \xi_0) - ig''(\xi_0)(\xi - \xi_0)^3/6] d\xi. \quad (4.5.20)$$

We replace ξ by the new variable s and $r - r_0$ by the nondimensional distance t from the caustic according to the relations

$$s = \pm[g''(\xi_0)/2]^{1/3}(\xi - \xi_0), \quad t = \pm[g''(\xi_0)/2]^{-1/3}(r - r_0), \quad (4.5.21)$$

where the signs are chosen opposite to the sign of $g''(\xi_0)$. Then, the exponent in the integrand can be written as $\exp i(st + s^3/3)$. We split the integral over s into two integrals, one from $-\infty$ to 0 and the other from 0 to ∞ , and replace s by $-s$ in the first of these integrals; as a result, the two integrals can be combined into

one integral from 0 to ∞ , and in the integrand of the combined integral a sum of exponents will be transformed into a cosine. Then, the expression (4.5.20) can be rewritten as

$$p_r = 2^{1/3} [2 \sin \theta_0 / (k r \cos^2 \theta_0)]^{1/2} |g''(\xi_0)|^{-1/3} \exp[i(w_0 + \pi/4)] v(t), \quad (4.5.22)$$

where

$$v(t) = \frac{1}{\sqrt{\pi}} \int_0^\infty \cos \left(st + \frac{1}{3} s^3 \right) ds \quad (4.5.23)$$

is the Airy function.

A plot of the function $v(t)/v_0$, where $v(0) = 0.6293$, is given in Fig. 2.7. At $t < 0$ the function $v(t)$ has an oscillatory character. It has maximum value at negative t , namely, $v(-1) = 0.949$. At $t > 0$ the function $v(t)$ decreases monotonically with increasing t . Oscillations at $t < 0$ are due to the interference between two rays crossing at each point on this side of the caustic. On its other side ($t > 0$) there is the shadow zone in which the sound field decreases monotonically with distance from the caustic.

It is reasonable in the derivative $r''(\xi_0) = g''(\xi_0)$ to transfer from ξ to an angular variable θ , according to the relations $\xi = k \sin \theta$ and $\xi_0 = k \sin \theta_0$. Then,

$$\frac{\partial r}{\partial \xi} = (k \cos \theta)^{-1} \frac{\partial r}{\partial \theta}$$

and, since $(\delta r / \delta \theta)_{\theta_0} = 0$ on the caustic, we have

$$\left(\frac{\partial^2 r}{\partial \xi^2} \right)_{\xi_0} = (k \cos \theta_0)^{-2} \frac{\partial^2 r}{\partial \theta_0^2}. \quad (4.5.24)$$

It is reasonable, as usual, to characterize the intensity of the wave (4.5.22) by the focusing factor

$$f = r^2 |p_r|^2 = 2^{5/3} k_0^{1/3} \sin \theta_0 \cos^{-2/3} \theta_0 r(\theta_0) \left| \frac{\partial^2 r}{\partial \theta_0^2} \right|^{-2/3} v^2(t). \quad (4.5.25)$$

The latter formula is the important particular case of the general formula (2.5.6) when $\chi = \chi_1 = \pi/2 - \theta_0$.

One should keep in mind that (4.5.22) has only been obtained for a limited distance from the caustic, so that we can limit ourselves to the terms in the expansion of the phase written in (4.5.19). The corresponding criterion can be obtained if we require that the first omitted term $g'''(\xi_0)(\xi - \xi_0)^4$ in (4.5.19) be small as compared with unity, i.e., distortion of the phase is negligible.⁶ Since $g(\xi) = r$

⁶In the book by *Brekhovskikh* [Ref. 4.3, Sect. 45] it is incorrectly assumed that this term must be small compared with the last retained term, and, as a result, the criterion obtained there is weaker.

and $g(\xi_0) = r_0$, we have

$$r_0''' \left(\frac{r - r_0}{r_0''} \right)^2 \ll 1. \quad (4.5.26)$$

Let L be some spatial scale of the ray pattern (e.g., the radius of curvature of the caustic); then $r_0'' \sim L/k^2$ and $r_0''' \sim L/k^3$, and our criterion will be

$$k(r - r_0)^2/L \ll 1. \quad (4.5.27)$$

Propagation of Sound in Shallow Water

In shallow-water propagation any ray (except a direct one in the case of a homogeneous medium) undergoes one or more reflections from the bottom. At relatively long ranges the sound field is mainly due to the multiple reflections of the rays from the bottom. The theory of sound propagation in shallow water will be presented below, assuming constant water depth.

5.1 Ray Representation of the Sound Field in a Layer: Image Sources

Let us suppose that a homogeneous layer is bounded by the free surface $z = 0$ above and by the bottom $z = h$ below (Fig. 5.1). The point sound source O_{01} is assumed to be at the point $r = 0, z = z_1$.

The sound field will be specified by the acoustic pressure $p(r, z)$ normalized in a way that near the source

$$p = R_{01}^{-1} \exp(ikR_{01}), \quad R_{01} = [r^2 + (z_1 - z)^2]^{1/2}. \quad (5.1.1)$$

The acoustic pressure $p(r, z)$ satisfies the Helmholtz equation

$$\Delta p + k^2 p = 0, \quad k = \omega/c. \quad (5.1.2)$$

The condition

$$p = 0, \quad z = 0 \quad (5.1.3)$$

must be fulfilled at the surface (pressure release boundary, Sect. 3.1). The case of the perfectly rigid bottom will be considered first, the boundary conditions being $(\partial p / \partial z)_{z=h} = 0$.

Equation (5.1.1) is the solution of (5.1.2), but it does not satisfy the condition at the boundaries $z = 0, z = h$. To satisfy these conditions, we should take account of the reflections of the wave from the boundaries. Adding to (5.1.1) the wave reflected from the lower boundary, we obtain for the acoustic pressure

$$p = p_{01} + p_{02} = \frac{\exp(ikR_{01})}{R_{01}} + \frac{\exp(ikR_{02})}{R_{02}}, \quad (5.1.4)$$

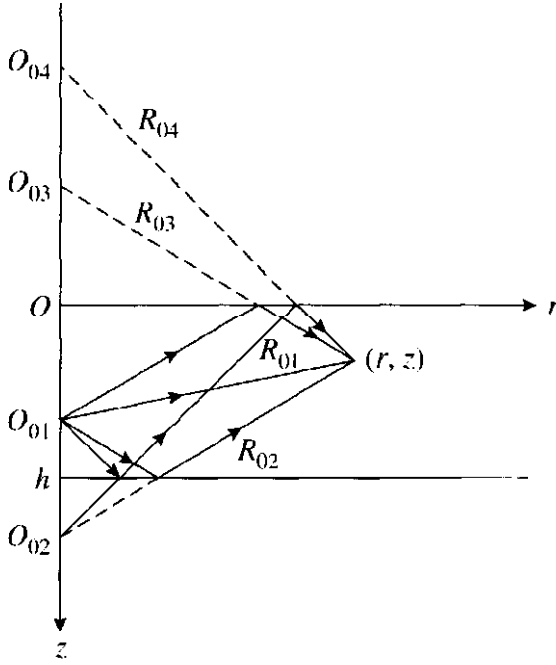


FIGURE 5.1. Reflections of a wave from the boundaries of a layer, and the image sources

where

$$R_{02} = [r^2 + (2h - z - z_1)^2]^{1/2}.$$

The reflected wave may be considered as emitted from the image source O_{02} obtained by specular reflection of the source O_{01} at the lower boundary of the layer.

Equation (5.1.4) satisfies (5.1.2). It also satisfies the boundary condition at the bottom because O_{01} and O_{02} are symmetrical with respect to the boundary $z = h$; it follows from this symmetry that $(\partial p / \partial z)_{z=h} = 0$. This can also be proved by direct differentiation of (5.1.4) over z . However, (5.1.4) does not satisfy the condition at the boundary $z = 0$. Therefore, we add to the sources O_{01} and O_{02} the pair of image sources O_{03} and O_{04} which are obtained by specular reflection of the first two sources at the water surface and by changing their phases by π . The total field of four sources will be

$$p = \frac{\exp(ikR_{01})}{R_{01}} + \frac{\exp(ikR_{02})}{R_{02}} - \frac{\exp(ikR_{03})}{R_{03}} - \frac{\exp(ikR_{04})}{R_{04}} \quad (5.1.5)$$

where

$$R_{03} = [r^2 + (z + z_1)^2]^{1/2}, \quad R_{04} = [r^2 + (2h + z - z_1)^2]^{1/2}.$$

Equation (5.1.5) satisfies (5.1.2) and the boundary condition $(p)_{z=0} = 0$ since $R_{01} = R_{03}$ and $R_{02} = R_{04}$ at $z = 0$.

However, now the symmetry with respect to the lower boundary is distorted and, as a result, the boundary condition at $z = h$ is not satisfied. This symmetry can be restored by the addition of two image sources O_{11} and O_{12} , obtained by the specular reflection of O_{03} and O_{04} at the lower boundary. Now, the boundary conditions are satisfied at the lower boundary but are not satisfied at the upper boundary. Continuing this construction of the succession of image sources further,

we alternately satisfy the conditions at one or the other boundary. However, since each additional pair of sources is farther away, the contribution to the sound field will be less each time, and in the limit of an infinite number of image sources the boundary conditions will be fulfilled at both boundaries.

As a result, the total field can be written in the form

$$p = \sum_{l=0}^{\infty} (-1)^l \left[\frac{\exp(ikR_{l1})}{R_{l1}} + \frac{\exp(ikR_{l2})}{R_{l2}} - \frac{\exp(ikR_{l3})}{R_{l3}} - \frac{\exp(ikR_{l4})}{R_{l4}} \right], \quad (5.1.6)$$

where

$$\left. \begin{aligned} R_{lj} &= (r^2 + z_{lj}^2)^{1/2}, & l &= 0, 1, 2, \dots, \infty, & j &= 1, 2, 3, 4 \\ z_{l1} &= 2hl + z_1 - z, & z_{l2} &= 2h(l+1) - z_1 - z, \\ z_{l3} &= 2hl + z_1 + z, & z_{l4} &= 2h(l+1) - z_1 + z \end{aligned} \right\}. \quad (5.1.7)$$

Generalizing (5.1.6) for the case of a partially reflecting bottom is very simple if the reflection coefficient is not dependent on the angle of incidence. Then, instead of (5.1.6) we have

$$p = \sum_{l=0}^{\infty} (-V)^l \left[\frac{\exp(ikR_{l1})}{R_{l1}} + V \frac{\exp(ikR_{l2})}{R_{l2}} - \frac{\exp(ikR_{l3})}{R_{l3}} - V \frac{\exp(ikR_{l4})}{R_{l4}} \right]. \quad (5.1.8)$$

In a number of cases (5.1.8) is approximately valid even when V depends on the angle of incidence $V = V(\theta)$. Naturally, there are specific θ_{lj} and $V(\theta_{lj})$ for each of the image sources in these cases.

In the case of pulse radiation, the sound pressure in the direct wave is given by $R^{-1} f(t - R/c)$. The total field in a layer at point (r, z) at time t is (for the case of a rigid bottom)

$$p = \sum_{l=0}^{\infty} (-1)^l \left[\frac{f(t - R_{l1}/c)}{R_{l1}} + \frac{f(t - R_{l2}/c)}{R_{l2}} - \frac{f(t - R_{l3}/c)}{R_{l3}} - \frac{f(t - R_{l4}/c)}{R_{l4}} \right]. \quad (5.1.9)$$

If the duration of the pulse radiated is π , the pulses overlap at the receiving point at time t when the condition

$$0 \leq t - R_{lj}/c \leq \tau$$

is fulfilled.

5.2 Integral Representation of the Field in the Layer

Starting from the representation of a spherical wave as a superposition of plane waves, we can obtain another expression for the field of the point source in a layer valid for arbitrary parameters of the bottom.

In free space, only a direct spherical wave can be observed at point (r, z) . According to (4.2.7), this wave can be represented as a superposition of plane waves of the type $\exp[i(k_x x + k_y y + k_z(z_1 - z))]$. If there is a lower boundary $z = h$, a reflected wave will be also observed which can be represented as a superposition of plane waves of the kind $V \exp[i(k_x x + k_y y + k_z(2h - z - z_1))]$. The reflection coefficient V can be an arbitrary function of the angle of incidence. The wave reflected from the upper boundary can be similarly represented as a superposition of plane waves $-\exp[i(k_x x + k_y y + k_z(z + z_1))]$. The minus sign arises because $V = -1$ for a free surface.

Continuing these considerations, we have an infinite series of waves having different numbers of reflections at the boundaries of a layer. The phase of each wave is $k_x x + k_y y + k_z z_{lj}$, where z_{lj} (z is the projection of the wave's path) is given by (5.1.7). Thus, for the direct wave ($l = 0, j = 1$) $z_{01} = z_1 - z$; for the wave reflected from the lower boundary ($l = 0, j = 2$) $z_{02} = 2h - z - z_1$; for the wave reflected from the upper boundary ($l = 0, j = 3$) $z_{03} = z + z_1$; for the wave reflected first from the lower and then from the upper boundary ($l = 0, j = 4$) $z_{04} = 2h + z - z_1$, etc.

We obtain the total field by first summing all the plane waves with the same k_x and k_y but with a different number of reflections from the boundaries, and then integrating over k_x and k_y . Taking into account the expansion of a spherical wave (4.2.7) into plane waves, and also remembering that at each reflection from the lower boundary the amplitude of the wave is multiplied by the reflection coefficient V , and at reflection from the upper boundary by a factor of -1 , we obtain in a way analogous to Sect. 5.1 for the total field in a layer (for $z < z_1$)

$$p(r, z) = \frac{i}{2\pi} \iint_{-\infty}^{\infty} \exp[i(k_x x + k_y y)] \{ \exp[ik_z(z_1 - z)] + V \exp[ik_z(2h - z - z_1)] - \exp[ik_z(z_1 + z)] - V \exp[ik_z(2h + z - z_1)] \} \sum_{l=0}^{\infty} (-V)^l \exp(2ik_z h l) \frac{dk_x dk_y}{kz}. \quad (5.2.1)$$

By interchanging z and z_1 we obtain the analogous expression for $z > z_1$.

We will transform (5.2.1) further, taking into account the identity

$$\begin{aligned} & \{ \exp[ik_z(z_1 - z)] + V \exp[ik_z(2h - z - z_1)] - \exp[ik_z(z_1 + z)] - V \exp[ik_z(2h + z - z_1)] \} \\ &= -2i \sin k_z z \{ \exp(ik_z z_1) + V \exp[ik_z(2h - z_1)] \} \end{aligned} \quad (5.2.2)$$

and the infinite geometric progression formula¹

$$\sum_{l=0}^{\infty} (-V)^l \exp(2ik_z h l) = [1 + V \exp(2ik_z h)]^{-1}. \quad (5.2.3)$$

¹The series on the left-hand side of (5.2.3) converges if $|V| < 1$ or if the wave number k has a small imaginary part (absorption in the medium).

Let us introduce in (5.2.1) the new integration variables ξ and φ according to the relations $k_x = \xi \cos \varphi$ and $k_y = \xi \sin \varphi$ (ξ is the modulus of the horizontal wave number, φ is the heading of a wave). We have $k_z = (k^2 - \xi^2)^{1/2} \equiv \alpha$ and $dk_x dk_y = \xi d\xi d\varphi$. The integral over φ in (5.2.1) gives $2\pi J_0(\xi r)$ (4.3.1). Replacing the zero-order Bessel function by half of the sum of the Hankel functions of the first and second kind, and carrying out the same transformations as for the derivation of (4.3.2), one obtains

$$p(r, z) = \int_{-\infty}^{\infty} \frac{\sin \alpha z \{ \exp[-i\alpha(h - z_1)] + V \exp[i\alpha(h - z_1)] \}}{\alpha \exp(-i\alpha h) [1 + V \exp(2i\alpha h)]} H_0^{(1)}(\xi r) \xi d\xi. \quad (5.2.4)$$

Interchanging z and z_1 in (5.2.4) for integrand yields for $z_1 < z$

$$p(r, z) = \int_{-\infty}^{\infty} \frac{\sin \alpha z_1 \{ \exp[-i\alpha(h - z)] + V \exp[i\alpha(h - z)] \}}{\alpha \exp(-i\alpha h) [1 + V \exp(2i\alpha h)]} H_0^{(1)}(\xi r) \xi d\xi. \quad (5.2.5)$$

Formulae (5.2.4, 5) give an integral representation of the field of the point source in a layer. The bottom is specified by the reflection coefficient $V = V(\xi)$, and can be arbitrarily layered.

5.3 Normal Modes in the Ocean with a Perfectly Reflecting Bottom

For the simplest case of a layer with a perfectly rigid bottom when $V = 1$ (Sect. 3.1) we obtain from (5.2.4, 5) for $z < z_1$

$$p(r, z) = \int_{-\infty}^{\infty} \frac{\sin \alpha z \cos \alpha(h - z_1)}{\alpha \cos \alpha h} H_0^{(1)}(\xi r) \xi d\xi, \quad (5.3.1)$$

and for $z > z_1$

$$p(r, z) = \int_{-\infty}^{\infty} \frac{\sin \alpha z_1 \cos \alpha(h - z)}{\alpha \cos \alpha h} H_0^{(1)}(\xi r) \xi d\xi. \quad (5.3.2)$$

These integrals can be reduced to the sum of the residues at the poles of the integrand. The poles are determined by the roots of the equation

$$\cos \alpha h = 0, \quad (5.3.3)$$

that is

$$\alpha_l = (\pi/h)(l + 1/2), \quad l = 0, 1, 2, \dots \quad (5.3.4)$$

Taking into account the relation $\alpha = (k^2 - \xi^2)^{1/2}$, we obtain

$$\xi_l = \pm [k^2 - (\pi/h)^2(l + 1/2)^2]^{1/2}. \quad (5.3.5)$$

The roots ξ_l are on the real axis in the ξ plane if $\pi(l + 1/2) < kh$, and on the imaginary axis if $\pi(l + 1/2) > kh$. It is convenient to assume that k has a small positive imaginary part (small absorption in the medium). Then, the roots are displaced from the positive half-axis to the first quadrant, and from the negative

half-axis to the third quadrant. We now move the path of integration in (5.3.1) away from the real axis to infinity in the upper half-plane ξ . It can be shown that the contributions due to the infinite part of the integration path are zero. As a result, the integral reduces to the sum of the residues at the poles in the first quadrant,

$$p(r, z) = 2\pi i \sum_{l=0}^{\infty} \left[\frac{\sin \alpha_l z \cos \alpha_l (h - z_1)}{\alpha_l d(\cos \alpha_l h)/d\xi} \right]_{\xi_l} H_0^{(1)}(\xi_l r) \xi_l \quad (5.3.6)$$

or, taking into account (5.3.5),

$$p(r, z) = \sum_{l=0}^{\infty} p_l = \frac{2\pi i}{h} \sum_l = 0 \sin \alpha_l z \sin \alpha_l z_1 H_0^{(1)}(\xi_l r). \quad (5.3.7)$$

The last expression for p does not change when z is replaced by z_1 and vice versa, and, consequently, is valid for any z ($0 \leq z \leq h$). Each term p_l in (5.3.7) satisfies the Helmholtz equation (5.1.2) and the boundary conditions, and is called a normal mode.

We will consider the basic features of the normal modes. At large (compared with the wavelength) distances from the source ($|\xi_l r| \gg 1$), the Hankel function can be replaced by the first term of its asymptotic representation (4.3.5) which yields

$$p_l(r, z) \simeq \frac{2}{h} \left(\frac{2\pi}{\xi_l r} \right)^{1/2} \sin \alpha_l z_1 \sin \alpha_l z \exp[i(\xi_l r - \pi/4)]. \quad (5.3.8)$$

We see that each normal mode is a travelling wave in the horizontal direction and a standing one in the z direction. From this it follows that each normal mode can be represented as the superposition of two travelling quasi-plane wave

$$p_l(r, z) \sim r^{-1/2} \{ \exp[i(\xi_l r + \alpha_l z)] - \exp[i(\xi_l r - \alpha_l z)] \} \quad (5.3.9)$$

propagating at an angle

$$\chi_l = \pm \arcsin(\alpha_l/k) \quad (5.3.10)$$

with respect to the horizontal plane. χ_l increases when l increases. The amplitude of each normal mode decreases along the layer as $r^{-1/2}$. Depending on whether the quantity

$$(\pi/kh)(l + 1/2)$$

is less or more than unity, the normal mode will propagate in the layer without attenuation² or decrease exponentially with distance, respectively. The lowest frequency f_l at which the wave still propagates without attenuation is called the critical or "cutoff" frequency of this normal mode. It is determined from the equation

$$(\pi/kh)(l + 1/2) = 1 \quad \text{or} \quad f_l = (c/2h)(l + 1/2). \quad (5.3.11)$$

²A case of real k is considered.

The lower l is, the lower the critical frequency. At frequencies

$$f < c/4h \equiv f_0$$

all normal modes attenuate. In this case, only the “near” field in the vicinity of the source is observed.

The phase velocity of the normal mode along the layer

$$v_l = \omega/\xi_l = c[1 - (f_l/f)^2]^{-1/2} \quad (5.3.12)$$

depends upon the sound frequency f . As $f \rightarrow \infty$, the phase velocity approaches the sound velocity in free space; at the critical frequency, v_l becomes infinitely large and for $f < f_l$ it is purely imaginary. Equation (5.3.12) describes the *waveguide* or *geometric* dispersion which is the cause of the pulse deformation when propagating in the layer. The group velocity of the normal mode is

$$u_l = \frac{d\omega}{d\xi_l} = c[1 - (f_l/f)^2]^{1/2}. \quad (5.3.13)$$

Taking into account (5.3.4, 10), we find $u_l = c \cos \chi_l$. Note that the group velocity u_l is equal to the ratio of the ray's cycle length D_l to the travel time t_l of the sound wave over the cycle. Indeed, since

$$D_l = 2h \cot \chi_l, \quad t_l = (2h/c) \sin \chi_l,$$

we have

$$D_l/t_l = c \cos \chi_l = u_l.$$

An analogous relationship is valid for the stratified ocean.

The frequency dependence of the phase and group velocities is shown in Fig. 5.2. At the critical frequency the normal mode is transformed into a standing one in the z direction and, consequently, $u_l = 0$. As $f \rightarrow \infty$, the group velocity trends to

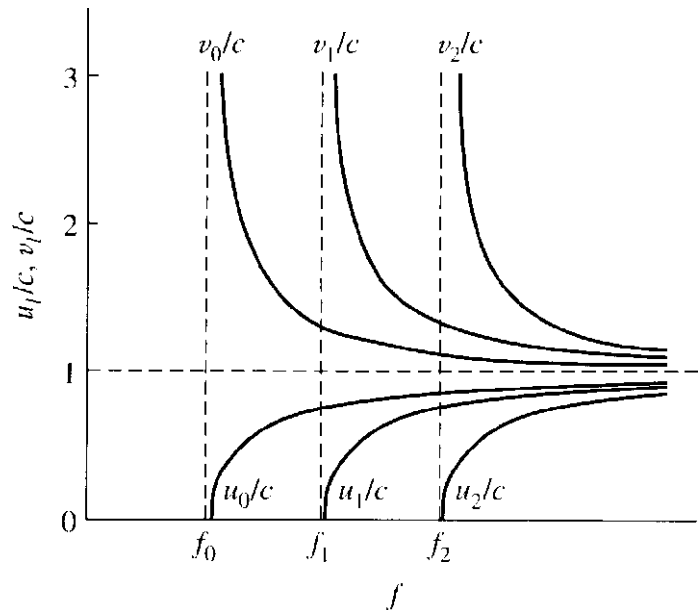


FIGURE 5.2. Dependence of the phase v_l and group u_l velocities of normal modes on the sound frequency

c —the sound velocity in free space. The phase and group velocities of the normal modes obey a simple relation

$$v_l u_l = c^2. \quad (5.3.14)$$

The z dependence of the amplitude of the normal modes is due to the factor $\sin \alpha_l z$. This dependence for $l = 0, \dots, 3$ is shown in Fig. 5.3. One sees that l is the number of depths in a layer (except $z = 0$) where the acoustic pressure is zero.

The quantity

$$(2\pi i/h) \sin \alpha_l z_1 \quad (5.3.15)$$

can be called the excitation function of the l th mode in the case considered. It becomes zero for every l if a source is at the free surface ($z_1 = 0$). If the source is near the surface (small z_1) the excitation functions differ from zero, but are small. This is due to the “dipole effect” (Sect. 4.1).

For calculation of the sound intensity or $|p|^2$ we must multiply the sum of expressions (5.3.8) by the complex-conjugate expression. In this case we obtain terms having the form $\exp[i(\xi_l - \xi_{l'})r]$ where l and l' include all the assumed values. Each such term oscillates with changing r with the period $\Lambda_{l,l'} = 2\pi/|\xi_l - \xi_{l'}|$. The horizontal period of interference of two neighbouring modes will be the largest period

$$\Lambda_{l,l+1} = 2\pi/(\xi_l - \xi_{l+1}). \quad (5.3.16)$$

If $kh \gg 1$, the value of ξ_l will be close to ξ_{l+1} . From (5.3.5) we have approximately

$$(\xi_l - \xi_{l+1})/k \simeq \pi \alpha_l / (kh \xi_l) \ll 1.$$

Then,

$$\Lambda_{l,l+1} = 2h \cot \chi_l = D(\chi_l) \quad (5.3.17)$$

where $D(\chi_l)$ is the length of the ray cycle, i.e., the horizontal distance between two successive reflections of the ray from the water surface or from the bottom (Fig. 5.4). The angle χ_l is determined by (5.3.10). The relationship (5.3.17) indicates the connection between the normal modes and the rays. For a more general case this relationship will be demonstrated in Sect. 6.6.

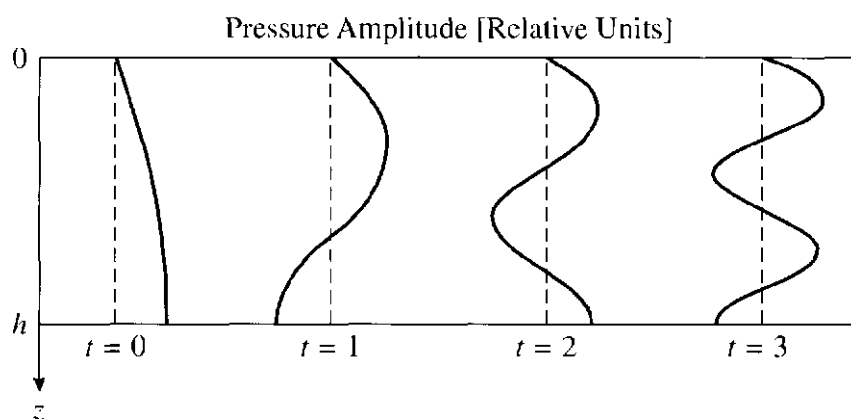
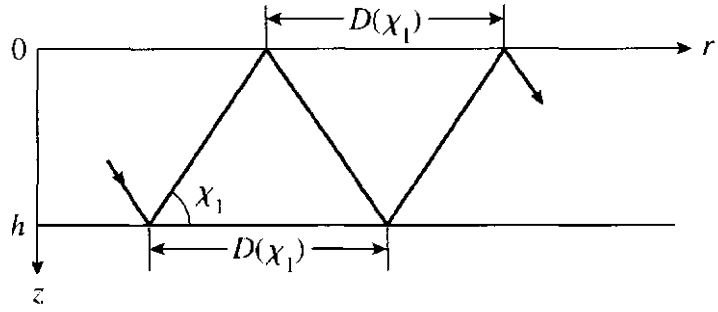


FIGURE 5.3. Amplitude variations of the first four normal modes over the layer

FIGURE 5.4. Cycle distance D of a ray

5.4 Relation Between the Different Representations of the Field

In Sects. 5.1–3 three different representations of the field of the point harmonic source in a layer with a perfectly reflecting bottom have been obtained. The mode representation is usually used when the thickness of layer h is small and the field is determined by only a few propagating modes. At large h and relatively small r it is convenient to use the ray representation of the field. A direct ray and only a few reflecting rays are important in this case. The integral representation is sometimes used for numerical calculations.

Since all three of these representations describe the same field, they can be transformed one into another. The relation between the integral representation and the normal modes has been established in Sect. 5.3. Let us now transform the sum of the normal modes into rays. We shall use the Poisson summation formula [Ref. 5.1, Sect. 2.13] for this purpose:

$$\sum_{l=-\infty}^{\infty} F(l) = \sum_{l=-\infty}^{\infty} f(2\pi l), \quad (5.4.1)$$

where

$$f(x) = \int_{-\infty}^{\infty} F(l) \exp(-ixl) dl. \quad (5.4.2)$$

We identify the left-hand side of (5.4.1) with a sum of the normal modes, transforming for this purpose (5.3.7) into the sum from $l = -\infty$ to $l = \infty$. The identity

$$\begin{aligned} & \sum_{l=0}^{\infty} \sin \alpha_l z \sin \alpha_l z_1 H_0^{(1)}(\xi_l r) \\ &= \frac{1}{4} \sum_{l=-\infty}^{\infty} \{ \exp[-i\alpha_l(z_1 - z)] - \exp[-i\alpha_l(z_1 + z)] \} H_0^{(1)}(\xi_l r) \end{aligned}$$

can be easily proved, taking into account that $\alpha_{-l} = -\alpha_{l-1}$. Now, we have

$$F(l) = \frac{\pi i}{2h} \{ \exp[-i\alpha_l(z_l - z)] - \exp[-i\alpha_l(z_l + z)] \} H_0^{(1)}(\xi_l r). \quad (5.4.3)$$

Substituting (5.4.3) into (5.4.2) and using the relation [5.2]

$$\int_{-\infty}^{\infty} H_0^{(1)}(r\sqrt{k^2 - u^2}) \exp(iuz) du = -2iR^{-1} \exp(ikR),$$

$$R = (r^2 + z^2)^{1/2}, \quad (5.4.4)$$

we find

$$f(2\pi l) = (-1)^l \left[\frac{\exp(ikR_{l1})}{R_{l1}} - \frac{\exp(ikR_{l3})}{R_{l3}} \right], \quad (5.4.5)$$

where R_{l1} and R_{l3} are given by (5.1.7). Substituting (5.4.5) into the right-hand side of (5.4.1) and transforming it into a series over l from 0 to ∞ , we obtain expression (5.1.5).

Now we shall transform the integral representation into the rays. To do this, we replace the trigonometrical functions in (5.3.1) by the exponential ones and represent $1/\cos \alpha h$ as a geometric progression

$$\frac{1}{\cos \alpha h} = \frac{2 \exp(i\alpha h)}{1 + \exp(2i\alpha h)} = 2 \sum_{l=0}^{\infty} (-1)^l \exp[i\alpha h(2l + 1)]. \quad (5.4.6)$$

This yields

$$p(r, z) = \frac{i}{2} \sum_{l=0}^{\infty} (-1)^l \int_{-\infty}^{\infty} [\exp(i\alpha z_{l1}) + \exp(i\alpha z_{l2}) - \exp(i\alpha z_{l3}) - \exp(i\alpha z_{l4})] H_0^{(1)}(\xi r) \frac{\xi d\xi}{\sqrt{k^2 - \xi^2}}, \quad (5.4.7)$$

where z_{lj} is given by (5.1.7).

Using the identity (4.3.3), one can write the integrals in (5.4.7) as

$$\int_{-\infty}^{\infty} \exp(i\alpha z_{lj}) H_0^{(1)}(\xi r) \frac{\xi d\xi}{\sqrt{k^2 - \xi^2}} = -2i \frac{\exp(ikR_{lj})}{R_{lj}}. \quad (5.4.8)$$

Substituting (5.4.8) into (5.4.7), we obtain immediately the expression (5.1.6).

5.5 Normal Modes in a Two-Layered Liquid

Now we apply expressions (5.2.4, 5) to the more complicated case of a layer lying on a liquid homogeneous half-space. The reflection coefficient V from the lower boundary of the layer is given by (3.1.12),

$$V = \frac{m \cos \theta - \sqrt{n^2 - \sin^2 \theta}}{m \cos \theta + \sqrt{n^2 - \sin^2 \theta}}, \quad m = \frac{\varrho_1}{\varrho}, \quad n = \frac{c}{c_1}, \quad (5.5.1)$$

where ϱ , c and ϱ_1 , c_1 are the density and sound velocity in the layer and in the lower half-space, respectively.

One can see from (5.5.1) that V is now a two-valued function of θ due to the radial $(n^2 - \sin^2 \theta)^{1/2}$. It is reasonable to introduce a Riemann surface with two sheets; on each of them V will be single valued. The branch point of these sheets is $\theta = \arcsin n$. The integrals (5.2.4, 5) now can be reduced to the sum of residues at the poles (discrete spectrum) and the integral along the sides of a properly drawn branch line from the branch point (continuous spectrum). The reader can find a detailed study of the continuous spectrum in other places ([Ref. 5.3, Sect. 37.3], and [Ref. 5.4, Sect. 2.21]). Here we will discuss the discrete spectrum (normal modes). This is the main part of the field at sufficiently large ranges from a source if $c_1 > c$ and the frequency of the source is not too close to the cutoff frequency of either of the normal modes.

According to (5.2.4, 5), the equation for poles is

$$1 + V \exp(2i\alpha h) = 0. \quad (5.5.2)$$

Taking (5.5.1) into account and introducing the notation

$$x = \alpha h = h(k^2 - \xi^2)^{1/2}, \quad v = kh(1 - n^2)^{1/2}, \quad n = k_1/k < 1, \quad \xi = k \sin \theta, \quad (5.5.3)$$

it can be rewritten as

$$\cot x = -(mx)^{-1}(v^2 - x^2)^{1/2}. \quad (5.5.4)$$

In the case considered ($v^2 > 0$), this equation has real roots $x_l < v$, $l = 1, 2, \dots$. The horizontal wave numbers of normal modes will be

$$\xi_l = (1/h)[(kh)^2 - x_l^2]^{1/2}. \quad (5.5.5)$$

Considering only such modes, we will calculate the residues in (5.2.4). Using the equation for poles, we can show that

$$\begin{aligned} \{\exp[-i\alpha(h - z_1)] + V \exp[i\alpha(h - z_1)]\}_{\alpha_l} &= 2i \exp(-ix_l) \sin(x_l z_1/h), \\ \left[\frac{d}{d\xi} V \exp(2i\alpha h) \right]_{\alpha_l} &= \frac{\xi_l h}{\alpha_l} \left(2i + \frac{1}{V} \frac{dV}{dx} \right)_{x_l}. \end{aligned} \quad (5.5.6)$$

In terms of x (5.5.1) is

$$V = (mx - \sqrt{x^2 - v^2})(mx + \sqrt{x^2 - v^2})^{-1}.$$

Now, using (5.5.4), we find

$$\left(\frac{1}{V} \frac{dV}{dx} \right)_{x_l} = -2i(v/mx_l)^2 (1/x_l) \sin^2 x_l \tan x_l. \quad (5.5.7)$$

As a result, we obtain the following expression for the modes in the layer

$$p(r, z) = \frac{2\pi i}{h} \sum_l \frac{\sin(x_l z/h) \sin(x_l z_1/h)}{1 - (v/mx_l)^2 (1/x_l) \sin^2 x_l \tan x_l} H_0^{(1)}(\xi_l r). \quad (5.5.8)$$

Expression (5.5.8) is invariant under the interchange of z and z_1 and, therefore, is valid for any z within the region $0 \leq z \leq h$.

Let us determine the cutoff frequencies of the normal modes. It follows from (5.5.4) that the largest real x_l determining the cutoff frequency f_l of mode l is obtained when equations $x_l = \pi(l + 1/2)$ and $x_l = v$ are simultaneously satisfied. Then f_l can be found from the equation $v = \pi(l + 1/2)$ or in the explicit form

$$f_l = \frac{c(l + 1/2)}{2h\sqrt{1 - n^2}}. \quad (5.5.9)$$

Expression (5.5.9) is an important relation between the layer thickness h , the refraction index n , and the cutoff frequency f_l . Thus, knowing h and f_l , we can find n and, consequently, the sound velocity in the lower medium.

The condition $x_l < v$ for unattenuating modes has a simple physical meaning. Using (5.5.3), it can be written as $\xi_l > kn$ or $\sin \theta_l > n$. Since θ_l is the angle of incidence for corresponding plane waves, this condition means that the plane waves composing an unattenuating mode undergo total internal reflection at the boundary $z = h$.

In Fig. 5.5 x_l for $l = 0, 1, 2$ and $m = 2$ are given as a function of the parameter v . At $v \rightarrow \infty$ we have $x_l \rightarrow \pi(l + 1)$. As the sound frequency increases, the number of real roots and, consequently, the number of propagating modes become greater.

Figure 5.6 [5.5] shows the depth dependence of the amplitude of the first ($l = 0$) normal mode for five different frequencies from 118 to 13,160 Hz for the case $h = 90$ m, $c = 1500$ m/s, $c_1 = 1501.5$ m/s, $\rho_1 = 2\rho$ (the depth dependence of the sound velocity is shown at the left in the figure). The amplitude decreases exponentially with depth in the lower medium, and the greater the frequency, the more rapid the decrease. At high frequencies, practically all the energy of the wave is contained within the layer. The cutoff frequency for this case is 93.3 Hz. The phase velocity of the first mode is also shown in this figure for various frequencies. It is always greater than the sound velocity in the layer and approaches it as the frequency increases.

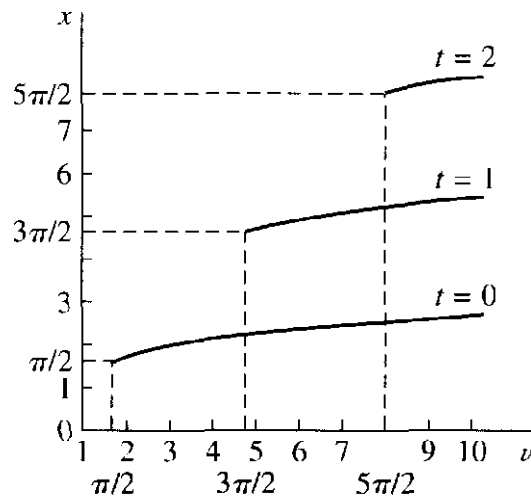
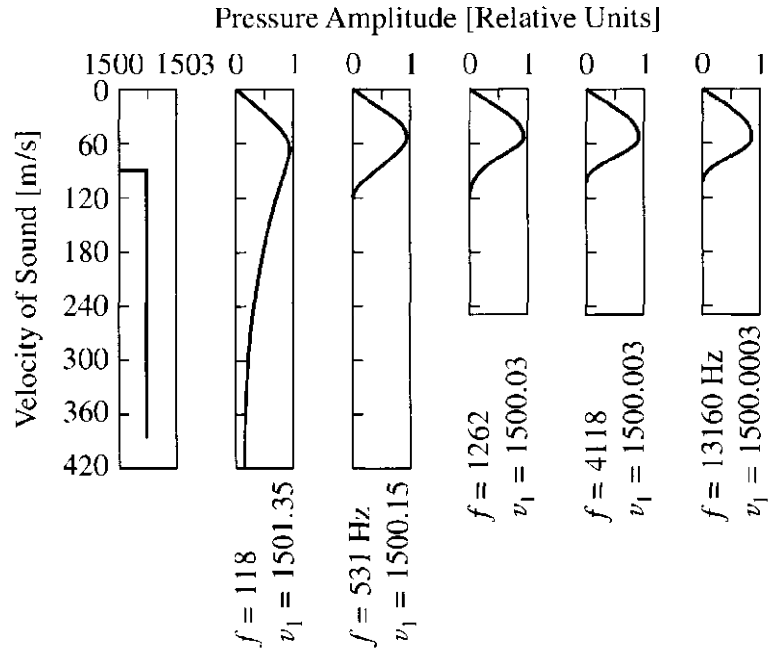


FIGURE 5.5. Roots of the dispersion equation vs the layer thickness and sound frequency

FIGURE 5.6.
 z -dependence of the
 amplitude of the first
 normal mode for various
 frequencies; v_1 is the
 phase velocity of the
 normal mode [5.5]



5.6 Averaged Decay Law

The methods presented above allow us to carry out an exact calculation of the sound field. However, such a calculation often appears to be rather complicated. Meanwhile, many details of the sound field, e.g., the fine interference structure, are sometimes of no use at all. For practical applications an estimate of the sound intensity is sometimes quite sufficient.

In this section we shall give a simple analytic formula for calculation of an “averaged” law for squared sound pressure versus range in shallow water when ray refraction and multiple reflections from the bottom occur. The derivation of this formula is based on the assumption of the applicability of ray theory and the incoherent summation of rays. We assume that the depth of the sea is constant and the water surface is smooth (the effect of a rough sea is considered below, in Sect. ??).

Let us consider a narrow beam of rays with angular width $d\chi_1$ leaving a source located at depth $z = z_1$ at angle χ_1 and having the cycle range $D(\chi_1)$. The square of the modulus of acoustic pressure in this beam, according to Sect. 2.5, is $|p|^2 = fE/r^2$, where f is the focusing factor (2.5.3), $E = E(\chi_1)$ is the decay factor due to absorption in the medium and bottom reflection losses. The power output of the source is assumed to be normalized so that in a homogenous medium $|p|^2 = 1/r^2$. We assume that r is large compared with D and find $\langle |p|^2 \rangle$ due to the chosen beam and the symmetrical beam leaving the source at angle $-\chi_1$. The operation $\langle \dots \rangle$ represents averaging over cycle range. To fulfill such an averaging, the expression $|p|^2 = fE/r^2$ has to be multiplied by the probability that the points at the receiving horizon z will be insonified by these beams. This probability is equal to the fourfold ratio of the beam’s width in the r direction, i.e., the quantity

$4(\partial r / \partial \chi_1) d\chi_1$, to the cycle range $D(\chi_1)$. The factor 4 arises because we have two beams (leaving the source at the angles $\pm\chi_1$), each crossing the receiving depth twice over the total cycle (if they arrive at this depth at all). All the points at depth z within the cycle are assigned the same weight. Thus, we obtain

$$\langle |p|^2 \rangle = \frac{4fE}{r^2 D} \frac{\partial r}{\partial \chi_1} d\chi_1$$

or, using the value f from (2.5.3) and integrating over all χ_1 —the angles of rays arriving at depth z —we obtain for the total field

$$\langle |p|^2 \rangle = \frac{4}{r} \int E(D \sin \chi)^{-1} \cos \chi_1 d\chi_1. \quad (5.6.1)$$

The decay factor E can be written as

$$E = |V(\chi_h)|^{2N} \exp(-\beta r), \quad (5.6.2)$$

where β is the volume absorption coefficient in water, $V(\chi_h)$ is the amplitude reflection coefficient at the bottom, and $N = N(\chi_h)$ is the number of reflections. Assuming that β is the same for rays with different χ_1 , taking $\exp(-\beta r)$ outside the integral, and setting $N \approx r/D(\chi_h)$ for large N , we obtain from (5.6.1)

$$\langle |p|^2 \rangle = \left(\frac{4}{r} \right) \exp(-\beta r) \int (D \sin \chi)^{-1} \exp \left[\left(\frac{2r}{D} \right) \ln |V(\chi_h)| \right] \cos \chi_1 d\chi_1. \quad (5.6.3)$$

Here χ_h and χ are expressed in terms of χ_1 by the relation

$$\frac{\cos \chi}{c} = \frac{\cos \chi_1}{c_1} = \frac{\cos \chi_h}{c_h} \quad (5.6.4)$$

where c_h , c_1 , c are the sound velocities at the bottom and at the source and receiver horizons, respectively.

Another way of deriving the expression (5.6.3) can be found in the book by *Brekhovskikh* [Ref. 5.6; Sect. 18]. Its generalization for the case of range-dependent conditions of propagation is in the paper by *Smith* [5.7].

Let us consider some particular cases using formula (5.6.3).

5.6.1 Homogeneous Layer ($c = c_1 = c_h$)

In this case

$$D = 2h \cot \chi_1, \quad 0 \leq \chi_1 \leq \pi/2, \quad \chi = \chi_1 = \chi_h \quad (5.6.5)$$

where h is the depth of the sea.

In the idealized case of a perfectly reflecting bottom ($|V| = 1$), the exponent in the integrand in (5.6.3) becomes unity. Then substitution of (5.6.5) into (5.6.3) gives

$$\langle |p|^2 \rangle = \frac{2}{rh} \exp(-\beta r) \int_0^{\pi/2} d\chi = \frac{\pi}{rh} \exp(-\beta r). \quad (5.6.6)$$

As a result, we have the well-known cylindrical propagation law with attenuation.

In the case of an absorbing bottom, small χ_h are most important in the integral (5.6.3). When χ_h increases, the exponent in the integrand decreases rapidly due to the increase of $1/D(\chi_h)$ as well as of $\ln |V(\chi_h)|$. Let us denote

$$s \equiv - \left[\frac{\partial}{\partial \chi} \ln |V(\chi)| \right]_{\chi=0}. \quad (5.6.7)$$

Then, with accuracy to χ^2 we have

$$[2r/D(\chi)] \ln |V(\chi)| \simeq -sr\chi^2/h.$$

Expanding the slowly varying part of the integrand in a series in χ , only the first term may be kept, yielding

$$\langle |p|^2 \rangle = \frac{2}{rh} \exp(-\beta r) \int_0^\infty \exp\left(-\frac{sr\chi^2}{h}\right) d\chi = \left(\frac{\pi}{sh}\right)^{1/2} \exp(-\beta r) \cdot r^{-3/2}. \quad (5.6.8)$$

Here ∞ is taken as the upper integration limit, but this does not affect the result since only small values of χ are significant for $sr/h \gg 1$ (the fulfillment of this condition is assumed). Thus, we obtain for $\langle |p|^2 \rangle$ the law of “3/2” which is intermediate between the cylindrical law for the layer with a perfectly reflecting bottom and the spherical law for free space.

The quantity s can be obtained from the experimental data for the reflection coefficient, or theoretically using certain assumptions about the structure of the bottom. In the simplest case where the bottom is a liquid homogeneous half-space, the reflection coefficient is defined by (3.1.12), where $\theta = \pi/2 - \chi$, and for s we obtain

$$s = 2 \operatorname{Re}\{m/\sqrt{n^2 - 1}\}, \quad (5.6.9)$$

where the symbol Re denotes the real part ($m = \varrho_1/\varrho$ as well as $n = c/c_1$ can be complex).

The 3/2 law (5.6.8) also has some limitations for large r . This is due to the fact that ray theory and the assumptions which are used for deriving (5.6.3, 8) are valid only when the number of significant modes is large [5.3]. As r increases, this number decreases, and at a sufficiently large range only one mode (which has the least attenuation) remains. In this case (5.6.8) becomes inapplicable.

A maximal range $r = r_m$ for which (5.6.8) is still valid can be estimated in the following way. In the integral of (5.6.8) the maximal significant value of χ is of the order $\chi_m \sim (h/sr)^{1/2}$. On the other hand, each normal mode corresponds to a family of rays with the same χ . The total number of propagating normal modes is approximately $2h/\lambda$, where λ is the length of the sound wave. The angles within the interval $0, \pi/2$ correspond to these modes. Within the interval of $0, \chi_m$ the

number of normal modes is equal to $(2\chi_m/\pi)(2h/\lambda)$. From the condition that this number is much greater than unity, we obtain

$$r_m \ll 16h^3/(\pi^2 s \lambda^2). \quad (5.6.10)$$

For $r \gg r_m$ only one mode can be taken into account and we have [5.8]

$$|p|^2 = \frac{4 \exp(-\beta r)}{k h^2 r} \exp \left[- \left(\frac{\pi}{k h} \right)^2 \frac{s r}{h} \right] \quad (5.6.11)$$

which is the cylindrical law with an additional attenuation. Assuming that the expression in the square brackets is small, we obtain from (5.6.11) the criterion (5.6.10) again.

5.6.2 Layer with Negative Refraction

Let the sound velocity decrease with depth. Then all sound rays refract downwards and sound propagates via successive reflections from the bottom (as in Fig. 5.7).

We shall again start from (5.6.3) and use the notation $\chi_m \equiv (\chi_h)_{\min} = \arccos(c_h/c_1)$, the grazing angle at the bottom of the ray leaving a source horizontally ($\chi_1 = 0$). At sufficiently large r the integral (5.6.3) can be easily estimated provided the expression in the exponent is negative and its absolute value increases with increasing χ_1 .

In this case, the slowly varying part of the integrand can be taken outside the integral, setting $\chi_1 = 0$, $\chi_h = \chi_m$, and the expression in the exponent can be represented as a power series of χ_1 up to χ_1^2 . Denoting

$$f(\chi_1) \equiv -D^{-1}(\chi_h) \ln |V(\chi_h)|, \quad (5.6.12)$$

we have

$$f(\chi_1) = f(0) + \frac{1}{2} f''(0) \chi_1^2 \quad (5.6.13)$$

where

$$f(0) = -D^{-1}(\chi_m) \ln |V(\chi_m)|. \quad (5.6.14)$$

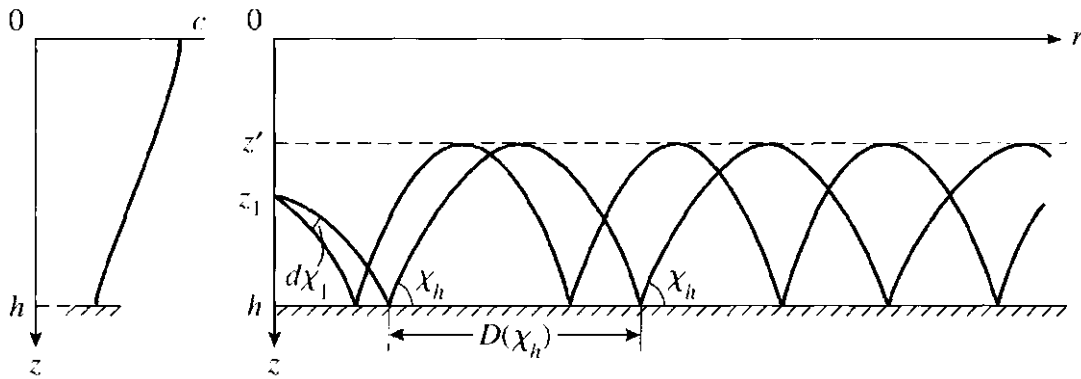


FIGURE 5.7. Spreading of a sound beam in shallow-water propagation

Here, $f''(0)$ is the second derivative with respect to χ_1 . Using (5.6.4), we find

$$\begin{aligned} f'(\chi_1) &= \frac{\partial}{\partial \chi_h} \left[\frac{\ln |V(\chi_h)|}{D(\chi_h)} \right] \frac{c_h \sin \chi_1}{c_1 \sin \chi_h}, \quad f'(0) = 0 \\ f''(0) &= \left\{ \frac{\partial}{\partial \chi_h} \left[\frac{\ln |V(\chi_h)|}{D(\chi_h)} \right] \cot \chi_h \right\}_{\chi_m}. \end{aligned} \quad (5.6.15)$$

Substituting (5.6.12–15) into (5.6.3) and taking the upper limit as infinity, we obtain

$$\langle |p|^2 \rangle = 2\pi^{1/2} [r^3 f''(0)]^{-1/2} (D \sin \chi)_{\chi_1=0}^{-1} \exp\{-r[\beta + 2f(0)]\}. \quad (5.6.16)$$

The decay law becomes $r^{-3/2}$ again but with an additional attenuation due to absorption in the bottom.

Formula (5.6.16) is invalid for such a large r where only one or a few modes remain. The estimate of the maximum permissible $r = r_m$ is made just as in the case of the homogeneous layer. The interval of significant values of χ_1 in the evaluation of the integral (5.6.3) is of the order $[r f''(0)]^{-1/2}$. The total number of modes is approximately $2h/\lambda$. In the interval of significant values there will be $[r f''(0)]^{-1/2} (4h/\pi\lambda)$ of them. The requirement that this number is much greater than unity determines the condition.

$$r_m \ll (4h/\pi\lambda)^2 [f''(0)]^{-1}. \quad (5.6.17)$$

We have to note that (5.6.16) is also invalid if the source and receiver are at the same depth. Then, $1/\sin \chi \rightarrow \infty$ when $\chi_1 \rightarrow 0$. A detailed study of averaged decay laws has been carried out by *Weston* [5.9].

Underwater Sound Channel

The underwater sound channel (USC) is a typical natural waveguide. The types of ocean stratification leading to the formation of a USC have been given in Sect. 1.2. The theory of sound propagation in the USC is presented here.

6.1 Simple Ray Theory of the USC: Trapping Coefficient of the USC

We begin by obtaining the expression for the trapping coefficient of the acoustic energy of a point omnidirectional source—an important characteristic of the USC.

Let the sound velocity at the boundaries of the USC be c_b (for example, $c_b = c_h$ in the case shown in Fig. 1.2) and c_1 at the source's depth. All rays leaving the source at grazing angles in the interval $(-\chi_m, \chi_m)$ will be trapped by the USC. Here χ_m is the maximum grazing angle defined by Snell's law

$$\cos \chi_m = c_1/c_b. \quad (6.1.1)$$

The acoustic energy trapped by the USC relates to the total radiated energy as the solid angle

$$\int_{-\chi_m}^{\chi_m} \int_0^{2\pi} \cos \chi \, d\chi \, d\varphi = 4\pi \sin \chi_m$$

relates to the total solid angle 4π . Thus, the trapping coefficient is

$$K = \sin \chi_m. \quad (6.1.2)$$

Since χ_m is always small,

$$K \approx \chi_m \approx [2(c_b - c_1)/c_b]^{1/2}. \quad (6.1.3)$$

The lower c_1 is, i.e., the closer a source is to the channel axis, the greater the trapping coefficient K . On the contrary, when the source approaches boundaries of the channel ($c_1 \rightarrow c_b$) K tends to zero. In real cases K is small, usually $(c_b - c_1)/c_b \lesssim 0.03$, and, therefore, $\chi_m \lesssim 15^\circ$, $K \lesssim 1/4$. Nevertheless, sound waves propagating in the USC can be registered at distances of many thousands of kilometres from sources.

6.1.1 “Linear” Model of the USC

Characteristics of the USC are determined by the sound velocity profile $c(z)$. There is a great variety of such profiles. However, many features of sound propagation in the USC can be obtained on the basis of simple “model” profiles $c(z)$. Ray pictures for a number of such profiles were thoroughly analyzed in the paper by *Pedersen and White* [6.1]. Here we will consider the simplest model, assuming that the sound velocity increases linearly with depth from the surface down to the bottom. Such a model allows a qualitative description of the main features of sound propagation in the USC since the sound velocity, in fact, increases linearly with depth in the deep ocean at great depths (in the Atlantic at depths of more than 1.5 km, for example). The linear model was first proposed [6.2] to describe the USC in the Sea of Japan where it had been discovered by Soviet scientists in 1946 [6.3], independently of American scientists who had previously discovered the USC in the Atlantic. In the Sea of Japan a linear dependence $c(z)$ is observed from depths of 200–300 m to the bottom (about 2 km in the deep-sea parts). Analogous stratification takes place in the Black Sea. The linear model is also useful in the theory of the surface sound channel.

Let the ocean depth be h and

$$c(z) = c_0(1 + az), \quad 0 \leq z \leq h. \quad (6.1.4)$$

As usual, z_1 is the depth of the source, and $c_1 = c_0(1 + az_1)$ and $c_h = c_0(1 + ah)$ are the sound velocities at the source’s depth and at the bottom, respectively (Fig. 6.1a). We denote by χ_0 , χ_1 , and χ the grazing angles of a ray at the surface, source, and receiver levels (Fig. 6.1b). According to Snell’s law, they are related by the equations

$$\cos \chi_0 / c_0 = \cos \chi_1 / c_1 = \cos \chi / c. \quad (6.1.5)$$

Let us determine z_m , the maximum penetration depth of a ray, by replacing χ and c in (6.1.5) by their values at $z = z_m$, i.e., $\chi = 0$ and $c = c_0(1 + az_m)$, which yields

$$(1 + az_1)^{-1} \cos \chi_1 = (1 + az_m)^{-1}.$$

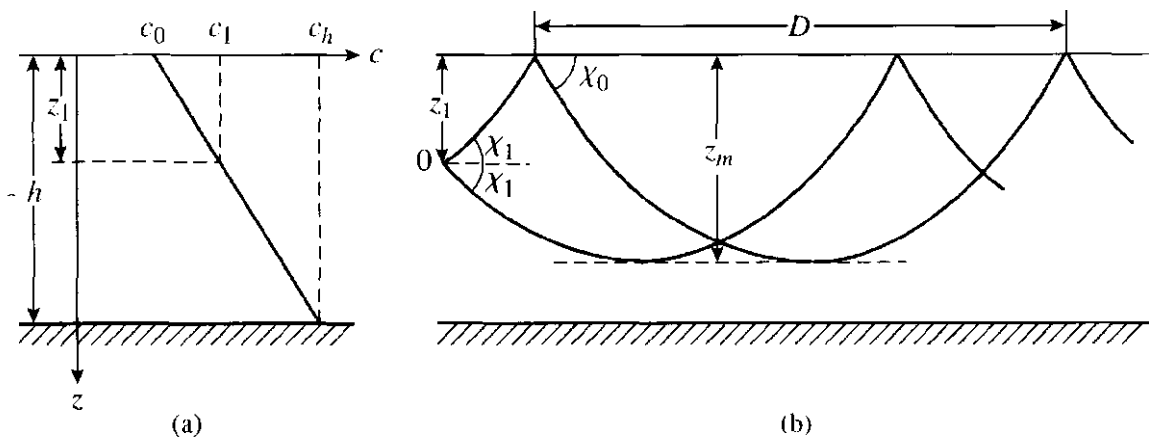


FIGURE 6.1. Parameters for the calculation of rays for a linear sound velocity profile

We thus obtain

$$az_m = (1 + az_1 - \cos \chi_1) \cos^{-1} \chi_1 = [az_1 + 2 \sin^2(\chi_1/2)] \cos^{-1} \chi_1. \quad (6.1.6)$$

Sometimes it is useful to express z_m in terms of χ_0 . Setting $z_1 = 0$ and $\chi_1 = \chi_0$ in the last formula, we obtain

$$z_m = [2/(a \cos \chi_0)] \sin^2(\chi_0/2). \quad (6.1.7)$$

Since χ_1 is usually small so the $\cos \chi_1 \approx 1$ and $\sin \chi_1/2 \approx \chi_1/2$, we have, approximately

$$z_m - z_1 = \chi_1^2/(2a). \quad (6.1.8)$$

Those rays for which $z_m \leq h$ are trapped by the waveguide; we shall call them the “channel rays.” The untrapped rays, propagating via bottom reflections, strongly attenuate and at great ranges can be ignored. From (6.1.8) the maximum angle χ_1 for the channel rays is

$$\chi_m = [2a(h - z_1)]^{1/2}. \quad (6.1.9)$$

As we have seen, this is also the expression for the trapping coefficient K .

Each ray propagates via reflections from the water surface. The distance D between two successive reflections, called the cycle length, is obtained from formula (2.4.1); if we set

$$\chi_i = 0, \quad \chi_{i-1} = \chi_0, \quad D = 2D_i, \quad (6.1.10)$$

then

$$D = (2/a) \tan \chi_0. \quad (6.1.11)$$

We omit the subscript i for a_i . The greater the grazing angle χ_0 , the greater is the cycle length. The maximum cycle length is

$$D_{\max} = (2/a) \tan(\chi_0)_{\max} \simeq 2(2h/a)^{1/2}. \quad (6.1.12)$$

For $h = 5$ km (deep ocean) and $a = 1.2 \cdot 10^{-5} \text{m}^{-1}$ (the hydrostatic velocity gradient) $D_{\max} = 57.6$ km.

A lot of rays differing from each other by the number of cycles can arrive at the receiving point. Thus, if the source and receiver are located near the water surface at range r from each other, they will be connected by rays which leave the source at an angle satisfying the obvious equation

$$r = (2N/a) \tan \chi_{0N}, \quad N = 1, 2, \dots, \infty, \quad (6.1.13)$$

whence

$$\chi_{0N} = \arctan(ar/2N). \quad (6.1.14)$$

The larger the number of cycles N , the closer the ray is to the surface, and in the limit of $N \rightarrow \infty$ the ray propagates along the surface. An increased concentration of rays and acoustic energy density is then observed near the surface. In fact, according to (6.1.7), all the rays leaving the source at grazing angles between 0 and χ_0 remain in the layer of the thickness $z_m \simeq \chi_0^2/(2a)$. The acoustic energy

within this layer decreases as χ_0 does, that is, more slowly than z_m . The ratio of the energy radiated into the layer to the thickness increases with decreasing χ_0 as $1/\chi_0$. Such a concentration of energy near the boundary is completely analogous to the “whispering galleries” effect probably observed for the first time in St. Paul’s Cathedral in London. This effect was explained by Rayleigh, and consists of an increase in the density of acoustic energy near a curved surface. The only difference is that in the phenomenon of the whispering galleries the boundary is curved and the rays are straight, whereas in the present case the opposite is true. However, it is possible to show that only the relative curvature of the rays and boundary matters.

If a source is not near the surface ($z_1 \neq 0$), then, setting $\chi_1 = 0$ in (6.1.5) and taking into account that $c_1 = c_0(1 + az_1)$, we obtain for the minimum grazing angle near the surface

$$(\chi_0)_{\min} \simeq (2az_1)^{1/2} \quad (6.1.15)$$

and from (6.1.11) for the minimum cycle length

$$D_{\min} \simeq 2(2z_1/a)^{1/2}. \quad (6.1.16)$$

Despite the simplicity of the linear law for $c(z)$, the total ray pattern will be rather complex. It is shown in Fig. 6.2 for the case $az_1 = 0.012$. Nondimensional quantities az and ar are plotted along the axes. Thick lines show the envelopes of the ray families (caustics).

6.1.2 Travel Time

Impulse radiation, for example, is often used while exploring the USC. When a single pulse is radiated a number of pulses arrive at the reference point, traveling along different rays and having different propagation times. We first determine the travel time along a ray between arbitrary depths z_1 and z_2 . Travel time along the ray’s element $ds = |dz/\sin \chi|$ is $dt = ds/c(z) = |dz/[c(z)\sin \chi]|$. Using the relation $c(z) = c_0(1 + az)$ and expressing dz in terms of $d\chi$ by

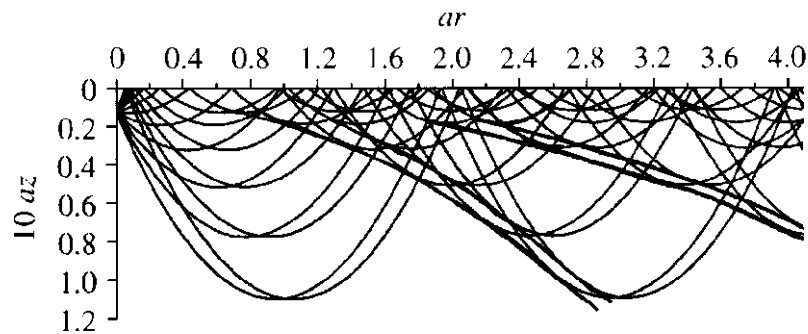


FIGURE 6.2. System of rays and caustics in the sound channel with the sound velocity linearly dependent on depth. Dimensionless values of ar and $10 az$ are plotted along the axes

differentiating (2.2.2), we find for the travel time

$$t = \frac{1}{ac_0} \left| \int_{\chi_1}^{\chi_2} \frac{d\chi}{\cos \chi} \right|,$$

where $\chi_1 \equiv \chi(z_1)$ and $\chi_2 \equiv \chi(z_2)$. This is a well-known integral so that we have

$$t = \frac{1}{2ac_0} \left(\ln \frac{1 + \sin \chi_1}{1 - \sin \chi_1} - \ln \frac{1 + \sin \chi_2}{1 - \sin \chi_2} \right). \quad (6.1.17)$$

Setting here $\chi_1 = \chi_0$, $\chi_2 = 0$, we obtain the travel time from the water surface to the turning point of a ray (we denote it by $\Delta t/2$)

$$\frac{\Delta t}{2} = \frac{1}{2ac_0} \ln \frac{1 + \sin \chi_0}{1 - \sin \chi_0}.$$

The travel time for the complete cycle is

$$\Delta t = \frac{1}{ac_0} \ln \frac{1 + \sin \chi_0}{1 - \sin \chi_0} \simeq \frac{2\chi_0}{ac_0} \left(1 + \frac{1}{6}\chi_0^2 + \frac{1}{24}\chi_0^4 + \cdots \right). \quad (6.1.18)$$

For the sake of simplicity, we assume that the source and receiver are located near the water surface. Then, the total travel time from source to receiver along the ray having N cycles will be approximately (neglecting terms χ_0^4 , etc.)

$$t_N = \frac{2N\chi_0}{ac_0} \left(1 + \frac{1}{6}\chi_0^2 \right). \quad (6.1.19)$$

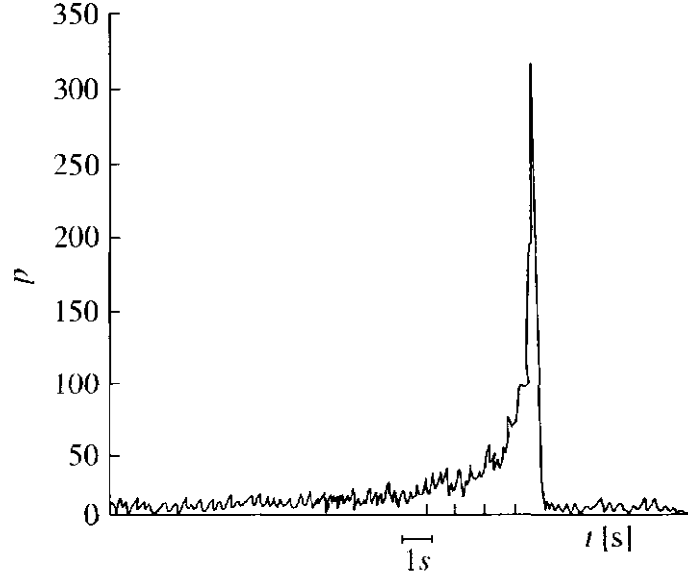
According to (6.1.14), $\chi_0 = \arctan(ar/2N)$. Expanding the right-hand side in a powers series of $ar/2N$, substituting the result in (6.1.19) for χ_0 , and neglecting the fourth and higher powers of $(ar/2N)$, we obtain

$$t_N = \frac{r}{c_0} \left(1 - \frac{a^2 r^2}{24N^2} \right). \quad (6.1.20)$$

Thus, a pulse travelling along a ray comprising the least number of cycles and most closely approaching the bottom will have the shortest travel time. The more often a ray is reflected from the surface, the later the pulse travelling along it will arrive. The pulse propagating along the horizontal arrives the latest. The time intervals between adjacent arrivals decrease continuously as N increases. On the recording an increase in sound intensity is observed towards the end because of the concentration of arrivals. The typical experimental pattern for source and receiver at a great distance and near the channel's axis is the same: an increase in sound intensity from the beginning to the end of the recording and a sharp cutoff at the end. This cutoff takes place after the arrival of the last ray, the one nearest to the channel axis. Only the bottom bounding rays arrive later, having low intensity at long ranges.

Figure 6.3 is the record of the sound signal at a distance of 1880 km from the source in the central Atlantic. The radiation (the explosion of 25 kg of TNT) was at a depth of 700 m, and the hydrophone was at a depth of 1200 m. The acoustic pressure is plotted on the vertical axis in a linear scale in some arbitrary units. The

FIGURE 6.3. Shape of a sound signal in the central Atlantic at a range of 1880 km



slow increase of the intensity of signal at the beginning and its sharp drop at the end of the signal are quite evident.

Now, we shall determine the total duration T of a signal, taking into account channel rays only. According to (6.1.20),

$$T = \frac{a^2 r^3}{24c_0} (N_{\min}^{-2} - N_{\max}^{-2}), \quad (6.1.21)$$

where N_{\min} and N_{\max} are the minimum and the maximum number of cycles for the rays arriving at the receiving point. At great ranges $N_{\max} \gg N_{\min}$ and the second term in the parentheses can be neglected. According to (6.1.13), $N_{\min} = ar/[2 \tan(\chi_0)_{\max}] = ar(2ah)^{-1/2}/2$. As a result, from (6.1.21), we obtain

$$T = \frac{ah}{3c_0} r. \quad (6.1.22)$$

Sometimes T is called the signal spreading time which, as we can see, increases proportionally to the range.

6.2 Canonical Underwater Sound Channel

Munk [6.4] suggested for the $c(z)$ profile

$$[c(z) - c_0]/c_0 = \varepsilon(c^\eta - \eta - 1) \quad (6.2.1)$$

which resembles the real features of the USC very closely; c_0 is the sound velocity at the channel axis $z = z_0$, $\eta = 2(z - z_0)/B$ (the z axis is directed upwards), B is the effective width of the sound channel, $\varepsilon = (B/2)1.14 \cdot 10^{-2}$ is the fractional adiabatic velocity increase over a scale depth.

For large upward deviations of z from the channel axis ($\eta \gg 1$), we have $c(z) - c_0 \simeq \varepsilon c_0 e^\eta$, i.e., the sound velocity increases exponentially. For large downward deviations ($-\eta \gg 1$), $c(z) - c_0 \simeq -\varepsilon c_0 \eta$, i.e., the sound velocity increases with

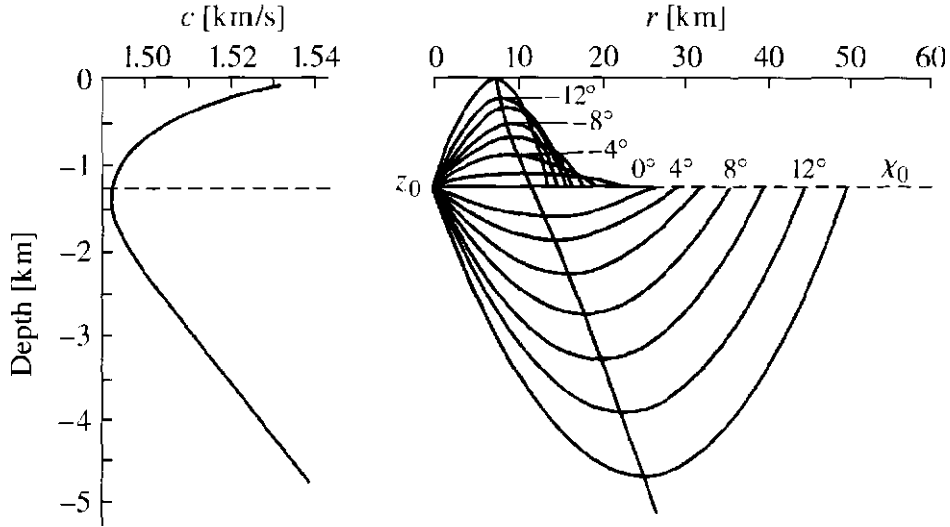


FIGURE 6.4. Profile $c(z)$ for the canonical sound channel according to Munk (on the left). Upper and lower semicycles of rays (on the right) leaving a source at the grazing angles $\chi_0 = -14^\circ, -12^\circ, \dots, 12^\circ, 14^\circ$. The curve through the ray apexes is nearly linear for this model [6.4]

depth linearly. Figure 6.4 (which is a slight modification of [Ref. 6.4, Fig. 2]) gives the profile $c(z)$ (left) for $z_0 = B = -1.3$ km, $c_0 = 1492$ m/s. *Munk* called this form of the USC the canonical sound channel. On the right the first semicycles of rays are shown when the source is at the channel axis. The rays leaving the source at the angle $\chi_0 = -14^\circ, -12^\circ, \dots, 12^\circ, 14^\circ$ are plotted. Note that the curve connecting the ray apexes is nearly a straight line.

As can be shown [6.4], the length of the upward (D^+) and downward (D^-) semicycles is

$$D^\pm = D_0 \left(1 \mp \frac{2\sqrt{2}}{3\pi} \hat{\phi} + \frac{1}{12} \hat{\phi}^2 + \dots \right), \quad (6.2.2)$$

where $D_0 = B\pi\epsilon^{1/2}/2$ is the half-cycle length of an axial ray (in Fig. 6.4, $D_0 = 23.7$ km); $\hat{\phi} = (\hat{c} - c_0)/(\epsilon c_0)$, where \hat{c} is the sound velocity at the turning point of the ray. Thus, the length of the upper semicycle is less and the length of the lower one is larger than the length of the axial ray's semicycle.

The travel time along the upper (t^+) and the lower (t^-) semicycles is

$$t^\pm = \tau^\pm + D_0/c_0, \quad (6.2.3)$$

where

$$\tau^\pm = \tau_0 \left(\pm \frac{2\sqrt{2}}{9\pi} \hat{\phi}^3 - \frac{1}{24} \hat{\phi}^4 + \dots \right), \quad (6.2.4)$$

$\tau_0 = B\pi\epsilon^{1/2}/(2c_0)$, and $\tau_0 = 0.137$ s for the profile example shown in Fig. 6.4. The travel time over the total cycle is

$$t = t^+ + t^- = \frac{D}{c_0} - \frac{\tau_0}{12} \hat{\phi}^4 + \dots, \quad (6.2.5)$$

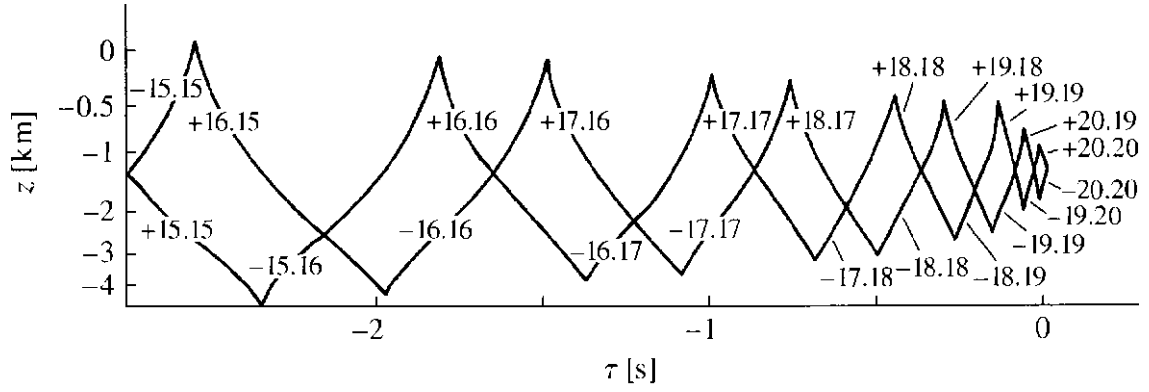


FIGURE 6.5. τ, z diagram for the canonical sound channel for a source located on the channel axis ($z_0 = -1.3$ km) [6.5]

where $D = 2D_0$ is the cycle length of an axial ray ($D \simeq 50$ km for the example in Fig. 6.4), or the distance between the convergence zones, as we shall see below. From (6.2.5) it follows that the axial ray ($\hat{\phi} = 0$) arrives last.

The τ, z diagram for the determination of the arrival time of rays at different depths at a range of 1000 km in the canonical sound channel is shown in Fig. 6.5 [6.5]. The depth z is plotted on the vertical axis. The source is at the channel axis ($z_0 = -1.3$ km). The quantity $\tau = t - t_0$ [t and t_0 being the arrival times of the given and axial (last) rays, respectively, $\tau < 0$] is plotted on the horizontal axis. Each branch of the plot is marked by a sign and two numbers. The plus (minus) sign refers to the ray leaving the source upward (downward). The first number indicates the number of a ray's turning points above the channel axis, and the second one the number below it. In order to find the arrival times of rays at a receiver located at depth $z = -2.5$ km, for example, we cut the plot at the horizontal line $z = -2.5$ km, and obtain that the ray +15.15 arrives first ($\tau = -2.52$ s), followed by the ray -15.16 ($\tau = -2.15$ s), and so on. The rays +18.18 ($\tau = -0.26$ s) and -18.19 ($\tau = -0.25$ s) arrive last. The same pattern will obviously be observed when the receiver is at the channel axis and the source is at a depth of 2.5 km. This plot demonstrates the decrease in the interval between adjacent arrivals at the end of the signal. The number of cycles is maximum if the source and receiver are at the channel axis, and equals 20 for the case considered.

6.3 Convergence Zones

Sound propagation in the deep ocean from a shallow source is accompanied by an interesting phenomenon, the formation of convergence zones.

We shall consider the schematic profile $c(z)$ shown on the left-hand side of Fig. 6.6. Let us assume that (as is shown in this figure) $c_1 < c_h$, i.e., the sound velocity is less at the depth of the source than near the bottom. The sound channel traps the rays leaving the source at the grazing angles satisfying the condition $|\chi_1| \leq \arccos(c_1/c_h)$. These rays form a beam (the right-hand side of Fig. 6.6) insonifying the space except for the shadow zones $A, A' \dots$ and $B, B' \dots$. Only

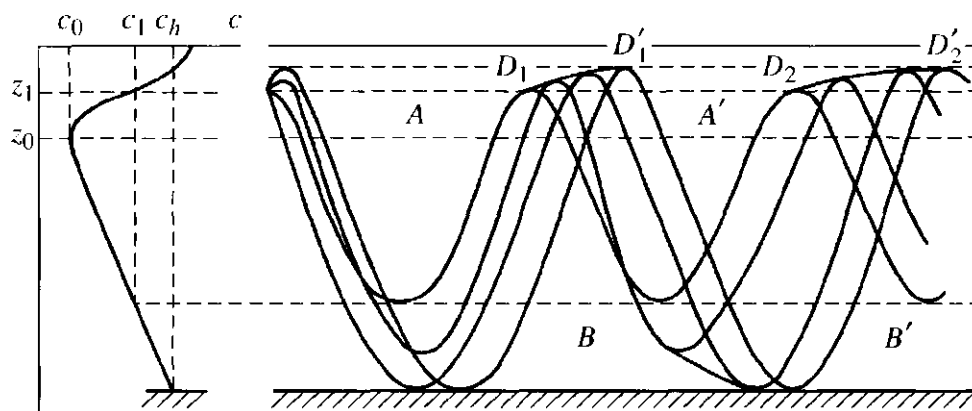


FIGURE 6.6. Scheme of the formation of convergence zones

the rays reflected from the bottom (not indicated in the figure) arrive at these zones. Thus, if we go away from the source but remain at a constant depth, for example, $z = z_1$, then after the comparatively weak sound field in zones A, A' etc. a considerable increase of the field is observed in the zones $D_1 D'_1, D_2 D'_2$ etc. These zones usually begin with the caustics (sections of which are shown by thick lines in the ray picture in Fig. 6.6) and are characterized by the high value of the focusing factor. Due just to this fact, they are called "convergence zones." The width of the convergence zones (at the level $z = z_1$ which is the length of sections $D_1 D'_1, D_2 D'_2$) increases with distance, while the width of the shadow zones between them decreases.

The farther a source is from the channel axis, the smaller the width of the convergence zones. If $c_1 \geq c_h$ there are no such zones. If the sound velocity at the surface is less than that at the bottom, the convergence zones will reach the surface and partially include the rays reflected from the surface.

Figure 6.7 shows the profile $c(z)$ (left) and the ray pattern (right) typical for the tropical Atlantic. For convenience, the scale of depths for $z > 1$ km has been compressed. The solid lines show the rays leaving the source in an upward direction and dashed lines in a downward direction. The formation of the convergence zones can be clearly seen. At a depth $z = 150$ m, for example, they extend over ranges 55–70 and 110–140 km.

In Fig. 6.8 the solid line shows the experimental dependence of the sound intensity anomaly A (excess over the spherical law $1/r^2$) on range in the first convergence zone for hydrology similar to that in Fig. 6.7 [6.6]. The sound frequency is 1.2 kHz. The depths of the source and receiver are the same, $z = z_1 = 150$ m. The dashed line gives the theoretical value of the same quantity obtained on the basis of ray theory and the incoherent summation of rays. It can be seen that there is some agreement between the theoretical and experimental curves. The mean levels of curves and their general dependence on range are similar. However, many features of the curves differ. In particular, the experimental convergence zone is about 1 km closer to the source compared to the theoretical one. The reasons for this can be the inaccuracy of the ray approximation, insufficient accuracy of the measurement of the profile $c(z)$ at great depths, or an unsatisfactory approximation of the profile assumed in the calculations.

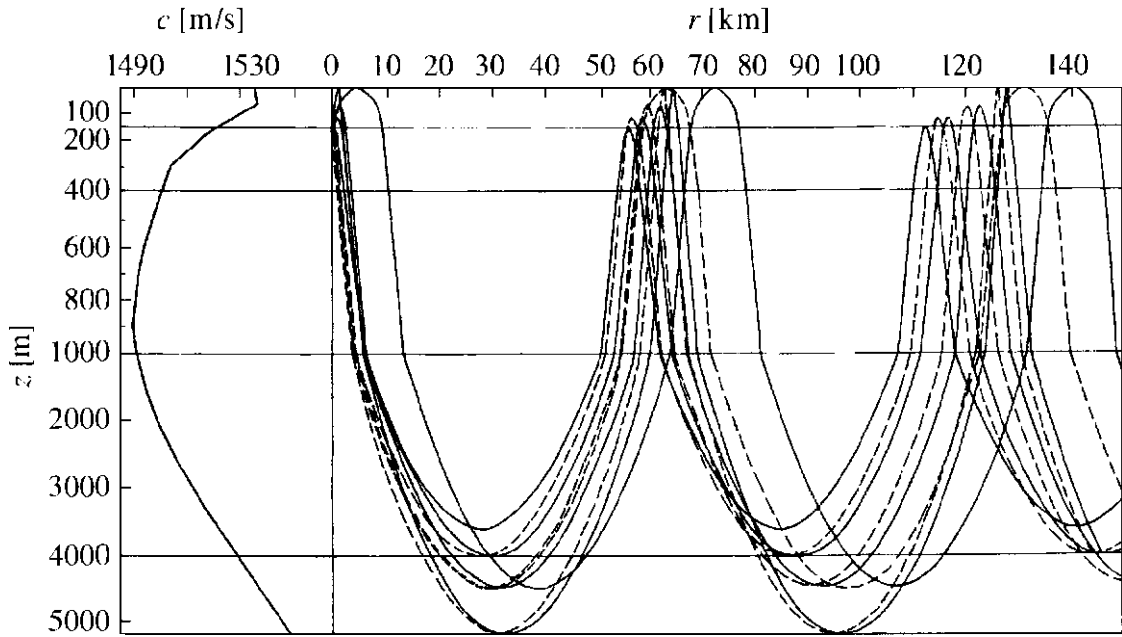
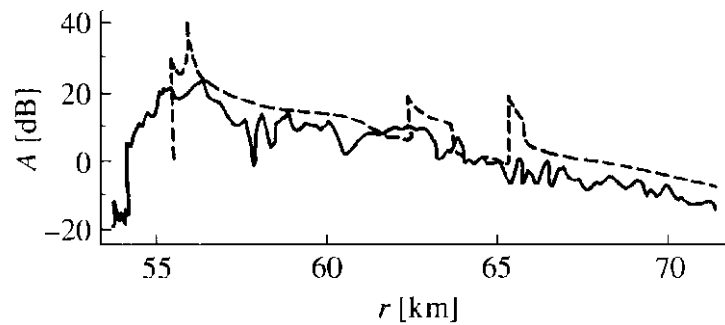


FIGURE 6.7. Ray pattern in the real USC illustrating the formation of convergence zones

FIGURE 6.8. Theoretical (dashed line) and experimental (solid line) distribution of the sound intensity in the first convergence zone for the velocity profile similar to that in Fig. 6.7, with the depth of the source and receiver $z_1 = z_2 = 150$ m

Sometimes a simple way of estimating the average sound intensity over an entire convergence zone can be useful [6.7]. Let $-\chi_m$ to χ_m be the interval of the grazing angles of the rays at the source forming the convergence zones. The acoustic power radiated into this interval will be $W\chi_m$ (Sect. 6.1), where W is the power output of the omnidirectional source, and it is assumed that $\chi_m \ll 1$. We denote the width of a convergence zone in the r direction by δ and the mean range from it to the source by r . Then, this power will be distributed over a ring with an area $2\pi r\delta$. The mean sound intensity (specific) in this zone is equal to the ratio of the transported power to the area of the projection of this ring on the direction normal to the rays. Let some mean grazing angle in the zone at the depth of the receiver be χ_r ($\chi_r \ll 1$). Then the area of the zone normal to the rays is $2\pi r\chi_r\delta$. The mean sound intensity in the zone is $I = W\chi_m/(2\pi\chi_r\delta)$. For the focusing

factor $f = I/I_0$ where $I_0 = W/(4\pi r^2)$ we obtain

$$f = 2r\chi_m/(\chi_r\delta). \quad (6.3.1)$$

We apply this formula to the case in Fig. 6.8. Here the receiver and the source are at the same depth; hence the grazing angles are the same at the source and receiver. Therefore, $\chi_r \approx \chi_m/2$ and we obtain from (6.3.1) $f = 4r/\delta$. As can be seen from Fig. 6.8, the convergence zone (the zone where $f > 1$) extends approximately from 55 to 65 km, i.e., $\delta = 10$ km and $r = 60$ km. Thus, $f \approx 24$ and the sound intensity anomaly $A = 10 \log f = 14$ dB. Comparison with Fig. 6.8 shows that this value is slightly too large, but the order of magnitude is correct, nevertheless.

6.4 Field of a Point Source in the Underwater Sound Channel as a Sum of Normal Waves (Modes)

Ray theory has limited applications. It is inapplicable in the shadow zones and near caustics. Since caustics get wider with increasing range, they limit the applicability of ray theory at large distances. Ray theory also cannot be used for low frequencies, when the wavelength of sound becomes comparable with the vertical scale of the sound velocity variation. Therefore, in practice one ultimately has to resort to the wave solution of the problem.

In this section we present the results of *Ahluwalia* and *Keller* [6.8] and obtain an expression for the sound field as a sum of normal waves (modes). This expression will be limited to the case of an ocean with a perfectly reflecting bottom. However, if we are interested in the field at large ranges from a source, then the most significant modes will be those which do not interact with the bottom (otherwise they rapidly attenuate with range), and, therefore, the boundary conditions at the bottom are not essential at all.

We consider the horizontally stratified ocean with the sound velocity profile $c(z)$ (where $0 < z < h$) bounded by the free surface from above and by the horizontal plane formed by an absolutely rigid bottom from below. The acoustic pressure $p = p(r, z)$ of the point source located at the point $r = 0, z = z_1$ with a singularity $p = 1/R, R = [r^2 + (z - z_1)^2]^{1/2}$ at $R \rightarrow 0$ is described by the Helmholtz equation

$$\frac{\partial^2 p}{\partial r^2} + \frac{1}{r} \frac{\partial p}{\partial r} + \frac{\partial^2 p}{\partial z^2} + k^2(z)p = -\frac{2}{r} \delta(z - z_1) \delta(r) \quad (6.4.1)$$

with the boundary conditions

$$p(r, 0) = 0, \quad \left(\frac{\partial p}{\partial z} \right)_{z=h} = 0. \quad (6.4.2)$$

The solution of the homogeneous form of (6.4.1) can be found by separation of variables. The solution describing a wave outgoing from the source has the form

$$p(r, z) = H_0^{(1)}(\xi r) \psi(z, \xi), \quad (6.4.3)$$

where $H_0^{(1)}(\xi r)$ is a Hankel function of the first kind of zero order, and the function $\psi(z, \xi)$ satisfies the equation

$$\frac{d^2\psi}{dz^2} + [k^2(z) - \xi^2]\psi = 0 \quad (6.4.4)$$

and the boundary conditions

$$\psi(0, \xi) = 0, \quad \psi'(h, \xi) = 0, \quad \psi' \equiv \frac{d\psi}{dz}. \quad (6.4.5)$$

Let two linearly independent solutions of (6.4.4) be $\Psi_1(z, \xi)$ and $\Psi_2(z, \xi)$. Then

$$\psi(z, \xi) = B_1 \Psi_1(z, \xi) + B_2 \Psi_2(z, \xi), \quad (6.4.6)$$

where B_1, B_2 are constants.

Substituting (6.4.6) into (6.4.5), we obtain the characteristic equation for the eigenvalues ξ_l

$$\Psi_1(0, \xi) \Psi_2'(h, \xi) - \Psi_2(0, \xi) \Psi_1'(h, \xi) = 0, \quad (6.4.7)$$

and the relation between B_1 and B_2 for an arbitrary ξ_l

$$B_1 = -B_2 \Psi_2(0, \xi_l) / \Psi_1(0, \xi_l).$$

Now we represent the solution of the inhomogeneous equation (6.4.1) as the sum of normal modes

$$p(r, z) = \sum_l A_l H_0^{(1)}(\xi_l r) \psi_l(z), \quad \psi_l(z) \equiv \psi(z, \xi_l). \quad (6.4.8)$$

To find the excitation coefficients A_l of the normal modes we substitute (6.4.8) into (6.4.1) and use the known equation for the Hankel function

$$\left(\frac{d^2}{dr^2} + \frac{1}{r} \frac{d}{dr} + \xi_l^2 \right) H_0^{(1)}(\xi_l r) = \frac{2i}{\pi r} \delta(r).$$

As a result we obtain

$$\sum_l A_l \psi_l(z) = i\pi \delta(z - z_1). \quad (6.4.9)$$

Multiplying (6.4.9) by $\psi_m(z)$, integrating over z from 0 to h , and using the orthogonality of the normal modes

$$\int_0^h \psi_l(z) \psi_m(z) dz = 0, \quad l \neq m,$$

we obtain

$$A_l = i\pi \psi_l(z_1) / \int_0^h \psi_l^2(z) dz. \quad (6.4.10)$$

In (6.4.8) we can use normalized function $\psi_l(z)$ so that the integral in the denominator (6.4.10) will be equal to unity. As a result, we obtain

$$p(r, z) = \pi i \sum_l \psi_l(z_1) \psi_l(z) H_0^{(1)}(\xi_l r). \quad (6.4.11)$$

6.5 Integral Representation of the Sound Field in the USC

Now we obtain the integral representations of the field in the underwater sound channel valid for arbitrary bottom characteristics.

The solution of (6.4.1) can be expressed as the Fourier-Bessel integral

$$p(r, z) = \int_0^\infty \tilde{p}(z, \xi) J_0(\xi r) \xi d\xi. \quad (6.5.1)$$

A function $\tilde{p}(z, \xi)$ is determined by the inverse transformation

$$\tilde{p}(z, \xi) = \int_0^\infty p(r, z) J_0(\xi r) r dr. \quad (6.5.2)$$

Multiplying (6.4.1) by $J_0(\xi r) r dr$ and integrating over r from 0 to ∞ , we obtain (see for details [Ref. 6.8, Appendix 3.3A])

$$\tilde{p}'' + [k^2(z) - \xi^2] \tilde{p} = -2\delta(z - z_1) \quad (6.5.3)$$

where the prime indicates differentiation with respect to z .

The function \tilde{p} satisfies the homogeneous equation

$$\tilde{p}'' + [k^2(z) - \xi^2] \tilde{p} = 0 \quad (6.5.4)$$

for all z except z_1 . To find conditions which must be satisfied by \tilde{p} at $z = z_1$, we integrate (6.5.3) over z from $z_1 - \Delta$ to $z_1 + \Delta$ and set $\Delta \rightarrow 0$, obtaining

$$(\tilde{p}')_{z_1+0} - (\tilde{p}')_{z_1-0} = -2. \quad (6.5.5)$$

Thus, \tilde{p}' has a discontinuity at $z = z_1$. The function \tilde{p} itself, as can be easily shown, is continuous:

$$(\tilde{p})_{z_1+0} = (\tilde{p})_{z_1-0}. \quad (6.5.6)$$

We denote by $\tilde{p}_1(z)$ and $\tilde{p}_2(z)$ ¹ two solutions of (6.5.4), choosing them so that $\tilde{p}_1(z)$ satisfies the condition at the free ocean surface

$$\tilde{p}_1 = 0, \quad z = 0 \quad (6.5.7)$$

and $\tilde{p}_2(z)$ satisfies the boundary conditions at the bottom.

The solution of (6.5.3) satisfying all the necessary conditions is

$$\begin{aligned} \tilde{p}(z) &= \frac{2\tilde{p}_2(z_1)\tilde{p}_1(z)}{w}, \quad 0 \leq z \leq z_1 \\ &= \frac{2\tilde{p}_2(z)\tilde{p}_1(z_1)}{w}, \quad z \geq z_1 \end{aligned} \quad (6.5.8)$$

where

$$w = w(\xi) = \tilde{p}_1'(z)\tilde{p}_2(z) - \tilde{p}_1(z)\tilde{p}_2'(z) \quad (6.5.9)$$

is the Wronskian.

¹The parameter ξ in the argument of functions $\tilde{p}_1(z)$ and $\tilde{p}_2(z)$ is omitted for brevity.

Substituting (6.5.8) into (6.5.1) and transforming the integral with the Bessel function $J_0(\xi r)$ into an integral with the Hankel function $H_0^{(1)}(\xi r)$ where the limits are from $-\infty$ to ∞ (as in Sect. 4.3), we obtain

$$\begin{aligned} p(r, z) &= \int_{-\infty}^{\infty} \frac{\tilde{p}_2(z_1) \tilde{p}_1(z)}{w} H_0^{(1)}(\xi r) \xi d\xi, & 0 \leq z \leq z_1 \\ p(r, z) &= \int_{-\infty}^{\infty} \frac{\tilde{p}_2(z) \tilde{p}_1(z_1)}{w} H_0^{(1)}(\xi r) \xi d\xi, & z > z_1. \end{aligned} \quad (6.5.10)$$

Formulae (6.5.10) give the integral representation of the sound field of a point source in the underwater sound channel. The latter integrals can be calculated by different methods including a direct numerical calculation. It is usually possible to separate the main part of these integrals, the nonattenuating or weakly attenuating normal modes. This part $p(r, z)$, also called the discrete spectrum, essentially determines the sound field at large ranges. The other part (the continuous spectrum) can, if necessary, also be estimated by one or another method.

6.6 Transformation of the Integral Representation into the Sum of Normal Modes

We will show that in the case of the absolutely rigid bottom when

$$\tilde{p}_2'(h) = 0 \quad (6.6.1)$$

expression (6.4.11) for the normal modes follows from the integrals (6.5.10).

Let us displace the integration path in (6.5.10) in the complex ξ plane from the real axis to the infinite semicircle in the upper half-plane. The integral over this semicircle is equal to zero and, as a result, the integrals in (6.5.10) are reduced to the sum of the residues at simple poles ξ_l of the integrand. The poles are the roots of the equation

$$w(\xi_l) = 0. \quad (6.6.2)$$

Thus, for example, for the field in the region $0 \leq z \leq z_1$ from (6.5.10) we have

$$p(r, z) = 2\pi i \sum_l \tilde{p}_2(z_1, \xi_l) \tilde{p}_1(z, \xi_l) \left(\frac{\partial w}{\partial \xi} \right)_{\xi_l}^{-1} H_0^{(1)}(\xi_l r) \xi_l. \quad (6.6.3)$$

Because the Wronskian is equal to zero at $\xi = \xi_l$, there is a linear dependence between \tilde{p}_2 and \tilde{p}_1 , i.e., $\tilde{p}_2(z, \xi_l) = A_l \tilde{p}_1(z, \xi_l)$, A_l being a constant. Therefore, $\tilde{p}_1(z, \xi_l)$ and $\tilde{p}_2(z, \xi_l)$ each satisfy both equation (6.4.4) and the boundary conditions (6.4.5), that is, each of them is proportional to $\psi_l(z)$. Therefore, we can set

$$\tilde{p}_1(z, \xi_l) = \psi_l(z), \quad \tilde{p}_2(z, \xi_l) = A_l \psi_l(z). \quad (6.6.4)$$

Since the Wronskian (6.5.9) does not depend on z , we may determine it at some z , say $z = 0$. Keeping in mind that $\tilde{p}_1(0) = 0$ and restoring ξ in the argument, we

have from (6.5.9)

$$w(\xi) = \tilde{p}'_1(0, \xi) \tilde{p}_2(0, \xi),$$

$$\frac{\partial w}{\partial \xi} = \frac{\partial \tilde{p}_1(0, \xi)}{\partial z} \frac{\partial \tilde{p}_2(0, \xi)}{\partial \xi} + \frac{\partial^2 \tilde{p}_1(0, \xi)}{\partial z \partial \xi} \tilde{p}_2(0, \xi). \quad (6.6.5)$$

The second term becomes zero if $\xi \rightarrow \xi_l$ since $\tilde{p}_2(0, \xi_l) = A_l \psi_l(0) = 0$ and, as a result, from (6.6.4) we obtain

$$p(r, z) = 2\pi i \sum_l \psi_l(z_1) \psi_l(z) \left[\frac{\partial \psi_l(0)}{\partial z} \right]^{-1} \left[\frac{\partial \psi_l(0)}{\partial \xi} \right]^{-1} \xi_l H_0^{(1)}(\xi_l r). \quad (6.6.6)$$

In differentiating with respect to ξ , $\psi_l(0)$ is assumed to be determined as a function of ξ according to the relation $\psi_l(0) = \tilde{p}_2(0, \xi)/A_l$ (see the example with the linear waveguide below). Expression (6.6.6) for p does not change when z is replaced by z_1 and vice versa, and is appropriate for any z ($0 \leq z \leq h$). However, this expression is not always convenient to use. In particular, if the waveguide axis is deep, there are some normal modes with exponentially small amplitude $\psi_l(0)$ at the surface. In this case, it is more convenient to use expression (6.4.11) which can be also obtained from (6.6.3). For this purpose let us consider (6.4.4) for ψ_l and analogously (6.5.4) for $\tilde{p}_2(z, \xi)$. Multiply the first by \tilde{p}_2 and the second by ψ_l , subtract one result from the other, and integrate over z from 0 to h , taking into account that $\psi_l'' \tilde{p}_2 - \psi_l \tilde{p}_2'' = (\psi_l' \tilde{p}_2 - \psi_l \tilde{p}_2')'$. As a result we obtain

$$[\psi_l' \tilde{p}_2 - \psi_l \tilde{p}_2']_0^h = -(\xi^2 - \xi_l^2) \int_0^h \psi_l \tilde{p}_2 dz.$$

Here $\psi_l'(h) = \tilde{p}_2'(h) = 0$, $\psi_l(0) = 0$. Using (6.6.5) for $w(\xi)$, we find

$$\frac{\psi_l'(0)}{\tilde{p}_1'(0)} \frac{w(\xi)}{(\xi - \xi_l)} = (\xi + \xi_l) \int_0^h \psi_l \tilde{p}_2 dz.$$

Assuming $\xi \rightarrow \xi_l$, we have $w(\xi) = (\partial w / \partial \xi)_{\xi_l} (\xi - \xi_l)$, since $w(\xi_l) = 0$. In addition, as has been shown above, we have $\tilde{p}_1(z) \rightarrow \psi_l(z)$, $\tilde{p}_2(z) \rightarrow A_l \psi_l(z)$, and consequently

$$\left(\frac{\partial w}{\partial \xi} \right)_{\xi_l} = 2A_l \xi_l \int_0^h \psi_l^2 dz. \quad (6.6.7)$$

Here the integral is equal to unity if the functions ψ_l are normalized. Then (6.4.11) follows from (6.6.3).

6.6.1 Linear Waveguide

Let us apply the general theory developed above to the case of the surface waveguide with the linear dependence $n^2(z)$:

$$n^2(z) = 1 - 2az, \quad 0 \leq z \leq 1/(2a). \quad (6.6.8)$$

For the sound velocity we have

$$c(z) = c_0(1 - 2az)^{-1/2}, \quad c_0 \equiv c(0), \quad c(z) = c_0/n(z). \quad (6.6.9)$$

We are mainly interested in the normal modes of low orders l whose energy is concentrated near the boundary $z = 0$. In this connection we notice that for $2az \ll 1$, (6.6.9) is rather close to the linear law (6.1.4) for the sound velocity.

Equation (6.5.4) in the case considered is written

$$\tilde{p}'' + [k_0^2(1 - 2az) - \xi^2]\tilde{p} = 0, \quad k_0 = \omega/c_0. \quad (6.6.10)$$

We introduce a new variable instead of z ,

$$t = t_0 + z/H, \quad H = (2ak_0^2)^{-1/3}, \quad t_0 = H^2(\xi^2 - k_0^2). \quad (6.6.11)$$

Then (6.6.10) becomes

$$\frac{d^2 \tilde{p}(t)}{dt^2} = t \tilde{p}(t). \quad (6.6.12)$$

The solutions of this equation are the Airy functions. Since these functions are frequently used in the theory of sound and electromagnetic wave propagation, and have previously been used in Sect. 4.5, and will be used below in Chap. 8, we list some relevant data mainly following *Fock* [6.9]. A good presentation of this matter can be found in the work by *Jeffreys* and *Swirles* [6.10].

Let us consider the integral

$$Z(t) = \frac{1}{\sqrt{\pi}} \int_{\Gamma} \exp\left(tz - \frac{1}{3}z^3\right) dz, \quad (6.6.13)$$

where the integration path Γ in the complex z plane follows along a ray arc $z = -2\pi/3$ from infinity to zero and then along the real axis from $z = 0$ to infinity. This integral converges for all complex values of t and satisfies (6.6.12). In fact, we have

$$\begin{aligned} \frac{d^2}{dt^2} Z(t) - tZ(t) &= \frac{1}{\sqrt{\pi}} \int_{\Gamma} (z^2 - t) \exp\left(tz - \frac{1}{3}z^3\right) dz \\ &= \frac{-1}{\sqrt{\pi}} \int_{\Gamma} \exp\left(tz - \frac{1}{3}z^3\right) d\left(tz - \frac{1}{3}z^3\right) = 0 \end{aligned}$$

as $\exp(tz - \frac{1}{3}z^3) \rightarrow 0$ at both limits.

Assuming that t is real, we separate the real and imaginary parts in $Z(t)$, setting

$$Z(t) = u(t) + iv(t), \quad (6.6.14)$$

$u(t)$ and $v(t)$ being the linearly independent solutions of (6.6.12) that are referred to as the Airy function.²

In the above-mentioned references it has been shown that $v(t)$ is given by the integral (4.5.23), and asymptotic expansions for $u(t)$ and $v(t)$ at large t are also obtained. Let us write the asymptotic expansions, retaining two main terms. For

²The functions $\text{Ai}(t) \equiv (1/\sqrt{\pi})v(t)$ and $\text{Bi}(t) \equiv (1/\sqrt{\pi})u(t)$ are often referred to as the Airy functions [6.10].

$t > 0$, setting $v \equiv \frac{2}{3}t^{3/2}$, we have

$$\begin{aligned} u(t) &= t^{-1/4} \exp(v) \left(1 + \frac{5}{72v} + \dots \right), \\ v(t) &= \frac{1}{2} t^{-1/4} \exp(-v) \left(1 - \frac{5}{72v} + \dots \right). \end{aligned} \quad (6.6.15)$$

For $t < 0$, setting $v \equiv \frac{2}{3}(-t)^{3/2}$ we get

$$\begin{aligned} u(t) &= (-t)^{-1/4} \left[\cos(v + \pi/4) + \frac{5}{72v} \sin(v + \pi/4) + \dots \right], \\ v(t) &= (-t)^{-1/4} \left[\sin(v + \pi/4) - \frac{5}{72v} \cos(v + \pi/4) + \dots \right]. \end{aligned} \quad (6.6.16)$$

The function $v(t)$ is plotted in Fig. 2.7. Its zeros t_1, t_2, t_3, \dots are negative and equal to $t_l = -y_l, l = 1, 2, \dots$, where $y_1 = 2.33811, y_2 = 4.08795$, and $y_3 = 5.52056$. If one denotes $v_l = (2/3)(-t_l)^{3/2}, l = 1, 2, \dots$, then

$$v_l = \pi \left(l - \frac{1}{4} \right) + \frac{0.088419}{4l-1} - \frac{0.08328}{(4l-1)^3} + \dots \quad (6.6.17)$$

As the number l increases, this formula becomes more accurate.

To find zeros of the function $Z(t)$, we transform the integral (6.6.13). We replace t by $t \exp(i\pi/3)$ and split the integral over the path Γ into two integrals, one from $\infty \exp(-2\pi i/3)$ to 0, and the other from 0 to ∞ . Let us introduce a new integration variable $s = z \exp(\pm i\pi/6)$ where the plus sign is taken for the first integral and the minus for the second one. Then we obtain

$$\begin{aligned} Z[t \exp(i\pi/3)] &= \pi^{-1/2} \exp(i\pi/6) \left\{ \int_0^{(-i\pi/6)\infty} \exp \left[i \left(ts - \frac{1}{3}s^3 \right) \right] ds \right. \\ &\quad \left. + \int_0^{(i\pi/6)\infty} \exp \left[-i \left(ts - \frac{1}{3}s^3 \right) \right] ds \right\}. \end{aligned}$$

Here the integration path in both integrals can be displaced on the real axis and, as a result, we obtain for $v(t)$, taking into account the integrand (4.5.23),

$$Z[t \exp(i\pi/3)] = 2v(-t) \exp(i\pi/6). \quad (6.6.18)$$

Hence the zeros of the function Z lie on the ray arc $t = \pi/3$ at points $y_l \exp(i\pi/3)$.

Now we turn to the expression for normal modes (6.6.6), taking the function $v(z, \xi_l)$ vanishing at $z \rightarrow \infty$ for $\psi_l(z)$. The eigenvalues are found from the equation

$$v(0, \xi_l) \quad \text{or} \quad v(t_0) = 0.$$

The solution of the latter, as we have seen, is $t_0 = -y_l$. Then from (6.6.11) we find

$$\xi_l^2 = k_0^2 - y_l/H^2. \quad (6.6.19)$$

At $y_l/H^2 < k_0^2$, ξ_l are real, i.e., the modes do not attenuate.

Let us denote

$$t_l = z/H - y_l, \quad t_{ll} = z_l/H - y_l \quad (6.6.20)$$

where z_l , as above, is the coordinate of a source. Furthermore, we take into account that, according to (6.6.11),

$$\frac{\partial}{\partial z} = (1/H) \frac{\partial}{\partial t}, \quad \frac{\partial}{\partial \xi} = 2H^2 \xi \frac{\partial}{\partial t}.$$

Equation (6.6.6) in the case considered can be written as

$$p(r, z) = \frac{\pi i}{H} \sum_l \frac{v(t_l) v(t_{ll}) H_0^{(1)}(\xi_l r)}{[v'(-y_l)]^2}. \quad (6.6.21)$$

Figure 6.9 shows the dependence of the amplitude of the first three normal modes upon z . The nondimensional coordinate z/H is plotted along the vertical axis. We see that the quantity H determines the width of the waveguide to an order of magnitude.

The phase velocity v_l of the normal modes is

$$v_l = \omega/\xi_l = c_0[1 - y_l/(k_0 H)^2]^{-1/2}. \quad (6.6.22)$$

The group velocity is

$$u_l = \frac{\partial \omega}{\partial \xi_l} = c_0 \left(\frac{\partial k_0}{\partial \xi_l} \right). \quad (6.6.23)$$

Taking into account the relation (6.6.11) between k_0 and ξ_l (the parameter H also depends on k_0), we obtain

$$u_l = c_0[1 - y_l/(k_0 H)^2]^{1/2}[1 - 2y_l/(3k_0^2 H^2)]^{-1}. \quad (6.6.24)$$

In the oceanic surface channel the linear law (6.6.8) is observed down to a certain depth z , below which $n(z)$ first decreases more slowly with depth and then

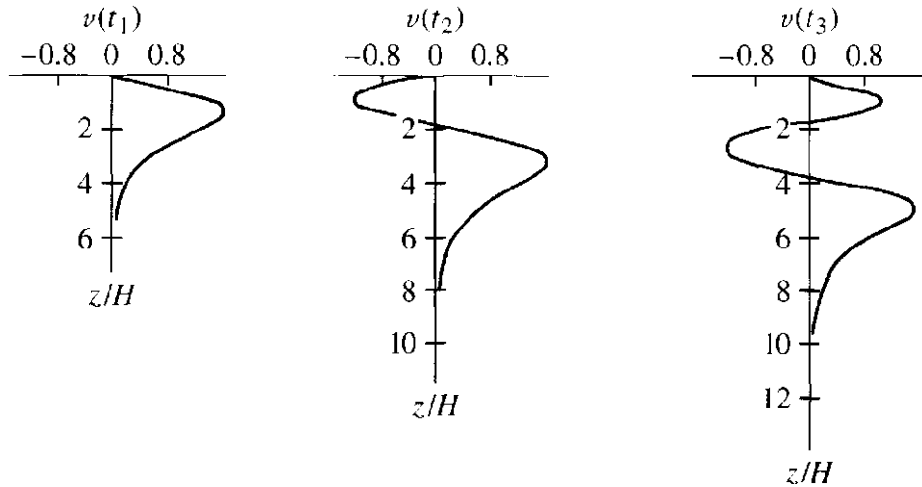


FIGURE 6.9. Dependence of the amplitude of the first three normal modes upon the nondimensional coordinate z/H for the case of the linear subsurface sound channel

begins to increase. Calculation of the characteristics of sound propagation for the bilinear profile $n^2(z)$ when the linear decrease of $n^2(z)$ turns into a linear increase at some depth has been performed by *Kibblewhite* and *Denham* [6.11].

6.7 Normal Modes in the WKB Approximation: Phase Integral

Let us put $k(z) = k_0 n(z)$, where k_0 is a wave number at some fixed depth $z = z_0$ (usually, at the channel axis). Equation (6.5.4) is now written

$$\tilde{p}'' + k_0^2 \gamma^2(z) \tilde{p} = 0, \quad \gamma = [n^2(z) - (\xi/k_0)^2]^{1/2}. \quad (6.7.1)$$

We shall consider the case of high frequencies and, consequently, of large k_0 . Then an approximate solution of (6.7.1) can be found on the basis of the following idea. We denote by Z the characteristic vertical scale of variation of $n(z)$. For $\lambda_0 = 2\pi/k_0 \ll Z$ the medium can be regarded as locally homogeneous. If the medium were real and homogeneous ($\gamma = \text{const}$), the solutions of (6.7.1) would be the exponents $\exp(\pm i k_0 \gamma z)$. For our case of the locally homogeneous medium one may hope to obtain a reasonable solution in the form

$$\tilde{p}(z) = \exp[i k_0 M(z)], \quad (6.7.2)$$

where $M(z)$ is represented as a power series in $1/k_0$, beginning with the zero power. It is convenient to assume

$$M(z) = \int_{z_0}^z \sum_{v=0}^{\infty} \frac{y_v(z)}{k_0^v} dz, \quad (6.7.3)$$

where $y_v(z)$ are new unknown functions.

Now, we substitute (6.7.2) into (6.7.1). We have

$$\begin{aligned} \tilde{p}'' &= [i k_0 M'' - k_0^2 (M')^2] \exp(i k_0 M), \\ M' &= \sum_{v=0}^{\infty} y_v / k_0^v, \quad M'' = \sum_{v=0}^{\infty} y'_v / k_0^v. \end{aligned}$$

Equating the coefficient of powers k_0^2 , k_0 , and k_0^0 to zero yields a sequence of equations

$$y_0^2 = \gamma^2(z), \quad -2y_0 y_1 + i y'_0 = 0, \quad -2y_0 y_2 - y_1^2 + i y'_1 = 0.$$

Whence we have

$$y_0 = \pm \gamma(z), \quad y_1 = i(\ln \gamma^{1/2})', \quad y_2 = \pm \frac{1}{2} \gamma^{-1/2} (\gamma^{-1/2})''.$$

Limiting ourselves to the first two terms of the series in (6.7.3), we find from (6.7.2)

$$\tilde{p}(z) = \left[\frac{\gamma(z_0)}{\gamma(z)} \right]^{1/2} \exp \left(\pm i k_0 \int_{z_0}^z \gamma dz \right). \quad (6.7.4)$$

The last expression is called the WKB (Wentzel-Kramers-Brillouin) approximation for the solution of (6.7.1).

If we take into account the term with y_2 in the expansion (6.7.3), an additional factor

$$\exp \left\{ \pm i \int_{z_0}^z \left[\frac{(\gamma^{-1/2})''}{2k_0 \gamma^{1/2}} \right] dz \right\} \quad (6.7.5)$$

appears. For the validity of the WKB approximation it is necessary (but not sufficient at all) that the expression in the braces be much less than unity, imposing restrictions on the value of the derivatives of $\gamma(z)$ with respect to z .

Expression (6.7.4) represents a superposition of two waves propagating without interaction in opposite directions. There is no reflection in an inhomogeneous medium in this approximation, which is not surprising since the WKB approximation is a form of geometrical acoustics (see below). The integral in the exponent in (6.7.4) gives the phase change as the wave propagates between depths z_0 and z . The factor in front of the exponent ensures that the energy conservation law for each wave (the energy flux in the z direction is constant) is fulfilled. The WKB approximation has already been used in Sect. 3.5.

Formula (6.7.4) obviously fails at z equal or close to certain z' where $\gamma(z') = 0$, that is at the so-called turning depth and near it.

We will not use the WKB approximation for analysis of the sound field in the waveguide. In this case, it must be kept in mind that there can be four types of normal modes depending on the region of depths wherein a given normal mode is concentrated [depths where $\gamma_l = \gamma(\xi_l)$ is real]:

1. $0 < z < z'_l$. The region is bounded by the water surface from above and the turning depth z'_l , at which $\gamma_l(z'_l) = 0$, from below.
2. $z''_l < z < z'_l$. The region is bounded by two turning depths $\gamma_l(z'_l) = \gamma_l(z''_l) = 0$. On the bottom and at the water surface the field of a normal mode is exponentially small.
3. $z''_l < z < h$. The region is bounded by the turning depth z''_l from above and by the bottom from below.
4. $0 < z < h$. The region is extended from the surface to the ocean bottom. As has been said above, only the first two types of modes, which do not interact with the bottom, will be of interest to us.

The general solution for the second type of mode in the insonified regions $z'' < z < z'$ (γ is real) and $z > z'$ (γ is imaginary) can be written, using (6.7.4), in the form

$$\tilde{p}(z) = \gamma^{-1/2} \left[C_1 \exp \left(ik_0 \int_{z'}^z \gamma dz \right) + C_2 \exp \left(-ik_0 \int_{z'}^z \gamma dz \right) \right], \quad z'' < z < z' \quad (6.7.6)$$

$$\tilde{p}(z) = |\gamma|^{-1/2} C_3 \exp \left(-k_0 \int_{z'}^z |\gamma| dz \right), \quad z > z'. \quad (6.7.7)$$

One can take any other fixed value of z as a lower limit in the integrals instead

of z' , since only the arbitrary constants C_1 , C_2 , and C_3 change in value. If we set $z'' = 0$, (6.7.6) also becomes applicable for the first type of mode.

Two terms in (6.7.6) correspond to waves propagating in the positive or negative z directions. Expression (6.7.7) describes a wave attenuating exponentially with increasing z . The constants C_1 and C_2 can be expressed in terms of C_3 using the continuity condition for the fields given by (6.7.6, 7) at $z = z'$. It can be done, for example, by describing a field in the region close to z' by means of the Airy functions. However, we shall not do this here but write the result immediately (see [Ref. 6.12, Sect. 24] where C_4 stands for C_3),

$$C_1 = C_3 \exp(i\pi/4), \quad C_2 = C_3 \exp(-i\pi/4). \quad (6.7.8)$$

Equation (6.7.7) is not of no interest to us, and (6.7.6) can be written as

$$\tilde{p}(z) = 2C_3 \gamma^{-1/2} \cos \left(k_0 \int_z^{z'} \gamma dz - \pi/4 \right), \quad (6.7.9)$$

where C_3 still remains undefined.

To obtain the normal modes $\psi_l(z)$ from the last expression for $\tilde{p}(z)$ the boundary conditions must be satisfied at $z = 0$ for the first type of mode, and at $z = z''$ for the second type. In the first case we must require $\tilde{p}(0) = 0$ yielding

$$k_0 \int_0^{z'_l} \gamma_l dz = \pi(l - 1/4), \quad l = 1, 2, 3, \dots \quad (6.7.10)$$

where, according to (6.7.1),

$$\gamma_l = [n^2(z) - \xi_l^2/k_0^2]^{1/2}. \quad (6.7.11)$$

The expression on the left-hand side of (6.7.10) is called the phase integral, by means of which, therefore, the equation for poles is written in the WKB approximation.

To obtain a similar equation for the second type of mode, we assume $k_0 z'' \gg 1$, i.e., the turning depth is sufficiently far from the surface so that the normal modes do not interact with the latter at all. The boundary condition at $z = z''$ can be stated as follows (Sect. 3.5): a wave reflected at this depth lags in phase by $\pi/2$ behind an incident one. We represent in (6.7.9) the cosine as a sum of two exponents

$$\begin{aligned} \cos \left(k_0 \int_z^{z'} \gamma dz - \frac{\pi}{4} \right) &= \frac{1}{2} \exp \left(ik_0 \int_z^{z'} \gamma dz - \frac{\pi i}{4} \right) \\ &+ \frac{1}{2} \exp \left(-ik_0 \int_z^{z'} \gamma dz + \frac{\pi i}{4} \right). \end{aligned}$$

Here the first exponent is a wave propagating in the direction of negative z , i.e., a wave incident from below on the depth $z = z'$. The second exponent describes a wave propagating in the positive z direction (the reflected wave). The requirement that the ratio of the first exponent to the second one at $z = z''$ equals $\exp(i\pi/2)$

multiplied by $1 = \exp(2\pi il)$ (l is an integer or zero) gives the equation

$$k_0 \int_{z_l''}^{z_l'} \gamma_l(z) dz = \pi(l + 1/2), \quad l = 0, 1, 2, \dots \quad (6.7.12)$$

Now from (6.7.9) we obtain the expression for eigenfunctions (normal modes)

$$\psi_l(z) = 2C_3 \gamma_l^{-1/2} \cos \left(k_0 \int_z^{z_l'} \gamma_l dz - \frac{\pi}{4} \right), \quad (6.7.13)$$

where $\gamma_l = \gamma_l(z)$ is determined in terms of ξ_l from (6.7.11), and ξ_l is found from (6.7.10, 12) for the first and second types of wave, respectively.

The constant C_3 is determined from the normalization condition, $\int_0^h \psi_l^2 dz = 1$. Regarding our assumptions above we can perform the integration here, approximately limiting it by the interval $0, z_l'$ for the first type of mode. Therefore

$$4C_3^2 \int_0^{z_l'} [\gamma_l(z)]^{-1} \cos^2 \left(k_0 \int_z^{z_l'} \gamma_l dz - \frac{\pi}{4} \right) dz = 1.$$

Assuming that within one period of the cosine $\gamma_l(z)$ can be regarded as a constant (the higher the order l of a wave, the better this assumption holds), we can replace the square of the cosine by $1/2$ —its mean value over the period. Taking into account the value $\gamma_l(z)$ from (6.7.11), we obtain

$$2C_3^2 \int_0^{z_l'} \left[n^2(z) - \frac{\xi_l^2}{k_0^2} \right]^{-1/2} dz = 1. \quad (6.7.14)$$

This integral has a simple physical meaning if we refer to the ray representations. Expressing θ in terms of the grazing angle $\chi_l = \pi/2 - \theta$, we obtain from (2.3.2)

$$D_l = 2 \cos \chi_l \int_0^{z_l'} (n^2 - \cos^2 \chi_l)^{-1/2} dz, \quad (6.7.15)$$

the cycle length of the ray leaving the depth $z = 0$ at angle $\chi_l = \arccos(\xi_l/k_0)$ (see Fig. 3.8). Comparing (6.7.14) and (6.7.15) yields $C_3^2 = \cos \chi_l / D_l$.

Substituting (6.7.13) into (6.4.11) and taking into account the value of C_3 , we obtain

$$p(r, z) = 4\pi i \sum_l \frac{\xi_l H_0^{(1)}(\xi_l r)}{k_0 D_l [\gamma_l(z) \gamma_l(z_1)]^{1/2}} \cos \left(k_0 \int_z^{z_l'} \gamma_l dz - \frac{\pi}{4} \right) \times \cos \left(k_0 \int_{z_1}^{z_l'} \gamma_l dz - \frac{\pi}{4} \right). \quad (6.7.16)$$

This expression is also valid for the second type of mode, but z_l'' must be taken instead of $z = 0$ as a lower limit in the integrals in (6.7.14, 15). All normal modes giving an essential contribution to the value of $p(r, z)$ in (6.7.16) must be taken into account. For modes of the first type, these are normal modes for which $z, z_1 < z_l'$. For the second type of mode an analogous condition is $z_l'' < z < z_l', z_l'' < z_1 < z_l'$.

We again refer to the linear waveguide given by law (6.6.8). Substituting the latter into the equation for poles (6.7.10), setting $\xi_l = k_0 \cos \chi_l$ and taking into account that $k(z) = k_0 n(z)$, we obtain after the elementary integration

$$\sin^3 \chi_l = (3a\pi/k_0)(l - 1/4). \quad (6.7.17)$$

On the other hand, in the exact theory of the linear sound channel we have from (6.6.19), again expressing ξ_l in terms of χ_l ,

$$\sin^3 \chi_l = (2a/k_0)y_l^{3/2}. \quad (6.7.18)$$

Equation (6.7.17) is in agreement with (6.7.18) if in (6.6.17) for $v_1 = (2/3)y_l^{3/2}$ only the first term of a series is retained.

We see from (6.6.17) that the WKB approximation gives the more exact values of the poles ξ_l for larger l . Even for $l = 1$ this approximate value is reasonably good. On the other hand, for sufficiently large r even a small error in ξ_l results in an error in the phase of a wave $\xi_l r$. Therefore, for a normal mode of any large number l there is a range r at which the WKB approximation breaks down. A more complete analysis of this problem is given in [Ref. 6.12, Sect. 48.5].

Similarly we can show that (6.6.21) for the normal modes in the linear waveguide is in agreement with (6.7.16) if in (6.6.21) we use an asymptotic representation of the function $v(t)$ at $t < 0$ (6.6.16)

$$\begin{aligned} v(t) &= (-t)^{-1/4} \sin \left[\frac{2}{3}(-t)^{3/2} + \frac{\pi}{4} \right], \\ -v'(t) &= (-t)^{1/4} \cos \left[\frac{2}{3}(-t)^{3/2} + \frac{\pi}{4} \right], \end{aligned} \quad (6.7.19)$$

and note that in (6.7.16), according to (2.3.2), in the case considered we have

$$D_l = (1/a) \sin \chi_l. \quad (6.7.20)$$

6.7.1 Normal Modes and Rays

The WKB approximation is in essence another form of geometrical acoustics. To illustrate this statement we show that each normal mode in (6.7.16) corresponds to a system of rays. In fact, if the cosines in (6.7.16) are replaced by a sum of exponents, and the Hankel function by its asymptotic representation, an expression for each normal mode will consist of four terms. The phase of each term is (omitting some additive constants)

$$\varphi_l(r, z, z_1) = \xi_l r \pm k_0 \int_z^{z'} \gamma_l dz \pm k_0 \int_{z_1}^{z'} \gamma_l dz. \quad (6.7.21)$$

The rays are, by definition, the lines orthogonal to the wave fronts, i.e., to the surfaces where $\varphi_l = \text{const}$. In other words, the unit vector \mathbf{e} tangent to a ray has the same direction as $\nabla \varphi_l$

$$\mathbf{e} = \frac{\nabla \varphi_l}{|\nabla \varphi_l|}.$$

But from (6.7.21) we have

$$\begin{aligned}\nabla_r \varphi_l &= \xi_l = k_0 \cos \chi_l, & \nabla_z \varphi_l &= \mp k_0 \gamma_l \mp k_0 [n^2(z) - \cos^2 \chi_l]^{1/2} \\ |\nabla \varphi| &= k_0 n(z), & e_r &= \cos \chi_l / n(z).\end{aligned}\quad (6.7.22)$$

Let us denote by $\chi_l(z)$ the angle between a ray and depth z (the grazing angle). It is obvious that $\cos \chi_l(z) = e_r$ or, taking into account (6.7.22),

$$n(z) \cos \chi_l(z) = \cos \chi_l. \quad (6.7.23)$$

As a result we have the well-known Snell's law for a ray. Figure 6.10 shows a system of rays corresponding to the l th normal mode.

One may consider the question of the equivalence of rays and normal modes from the other point of view and show that a ray can be represented as a superposition of normal modes of neighbouring orders. In fact, let us suppose that at some point (r, z) the l th mode and neighbouring modes are in phase giving rise to the local maximum of the sound field ("constructive interference"). If we shift away from this point remaining at the same depth z , the normal modes become dephased due to their different phase velocities, and the sound level will be lower. However, if we also change z , we can arrive at the point where the modes are in phase again. Let us show, following the work of *Tindle* and *Guthrie* [6.13], that a locus at which the modes are in phase is a ray. If the number of modes is large, which is the case when the WKB approximation is valid, the change of phase $\varphi_l(r, z, z_1)$ with l can be estimated by the derivative $\partial \varphi_l / \partial l$. The modes interfere constructively if the phase difference between modes l and $l + 1$ is equal to $-2\pi m$, m being an integer, i.e., $\partial \varphi_l / \partial l = -2\pi m$.

Using φ_l from (6.7.21) and γ_l from (6.7.11), we obtain by differentiating

$$\begin{aligned}\frac{d\xi_l}{dl} \left\{ r \pm \cos \chi_l \int_z^{z'} [n^2(z) - \cos^2 \chi_l]^{-1/2} dz \right. \\ \left. \pm \cos \chi_l \int_{z_1}^{z'} [n^2(z) - \cos^2 \chi_l]^{-1/2} dz \right\} = -2\pi m,\end{aligned}\quad (6.7.24)$$

where, as above, the notation $\cos \chi_l = \xi_l / k_0$ is used.

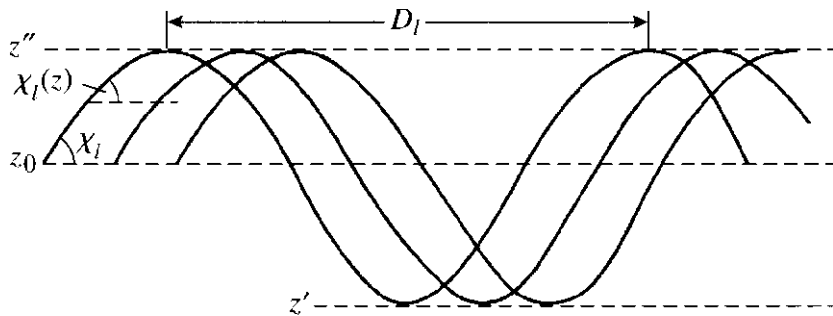


FIGURE 6.10. System of rays corresponding to the normal mode of order l

On the other hand, differentiating the equation for poles (6.7.12) with respect to l (we consider the modes of the second type, for definiteness), we obtain

$$\frac{d\xi_l}{dl} \cos \chi_l \int_{z''}^{z'} [n^2(z) - \cos^2 \chi_l]^{-1/2} dz = -\pi. \quad (6.7.25)$$

The integrals in (6.7.24, 25), as is seen from comparison with (2.3.2), give the horizontal length of different sections covered by a ray, namely (Fig. 6.11)

$$\begin{aligned} \cos \chi_l \int_z^{z'} [n^2 - \cos^2 \chi_l]^{-1/2} dz &= r_{DE} = r_{EF}, \\ \cos \chi_l \int_{z_1}^{z'} [n^2 - \cos^2 \chi_l]^{-1/2} dz &= r_{AB} = r_{BC}, \\ \cos \chi_l \int_{z''}^{z'} [n^2 - \cos^2 \chi_l]^{-1/2} dz &= D_l/2, \end{aligned} \quad (6.7.26)$$

where D_l is the length of the ray cycle, r_{AB} is the horizontal range AB, etc. We have now from (6.7.25, 26) an important formula

$$\frac{d\xi_l}{dl} = -\frac{2\pi}{D_l}. \quad (6.7.27)$$

The physical meaning of this result will be explained later. Equation (6.7.24) can be rewritten now as

$$r = m D_l \pm r_{AB} \pm r_{DE}. \quad (6.7.28)$$

An analytic expression for the ray is shown in Fig. 6.11 for the case $m = 1$. The combination of signs in this case will be:

- ++, if the source is at point (r_A, z_1) , the receiver at point (r_F, z)
- +−, if the source is at point (r_A, z_1) , the receiver at point (r_D, z)
- −+, if the source is at point (r_C, z_1) , the receiver at point (r_F, z)
- −−, if the source is at point (r_C, z_1) , the receiver at point (r_D, z) .

Ray- or normal-mode methods are widely used for the description of waveguide sound propagation in the ocean. But if the wavelength of sound is small compared to the ocean depth, the number of significant modes becomes very large, which introduces computational difficulties. At great distances from the source the number of rays arriving at the receiver is also large. The efficiency of these methods

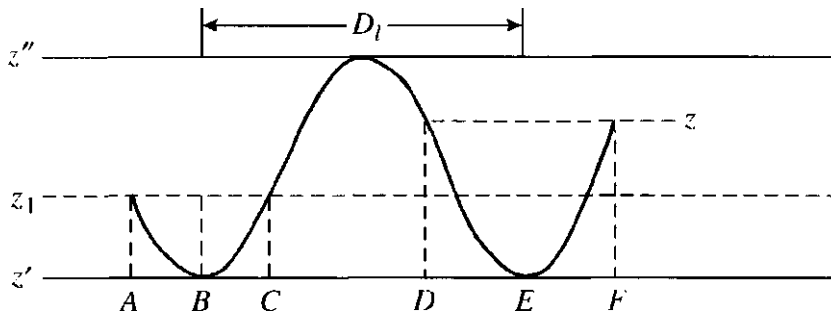


FIGURE 6.11.
Representation of
a ray as a
superposition of
normal modes

can be increased if they are used in combination rather than separately. The basic idea of such “hybrid” ray-mode method is that the angular density of rays arriving at the receiver and the eigenvalues of modes are not identical in different angular domains. The number of modes that propagate in the vicinity of the axis of the USC (small grazing angles) is small, while the number of rays is large. Far from the axis, the reverse is true. So, for the eigenvalue difference of two adjacent modes l and $l + 1$ we obtain from (6.7.27), taking into account that $\xi_l = k \cos \chi_l$,

$$\Delta \chi_{l,l+1} = 2\pi / (k D_l \sin \chi_l), \quad (6.7.29)$$

i.e., the less the cycle length D_l and the grazing angle χ_l , the greater $\Delta \chi_{l,l+1}$ and, therefore, the less the angular density of the modes.

Similarly, from (6.1.14) for the angle difference of two rays arriving at the receiver at a range r and comprising N and $N + 1$ cycles, respectively, we find (at $N \gg 1$) that

$$\Delta \chi = ar \cos^2 \chi / 2N^2$$

or, taking into account that $N \sim r/D$,

$$\Delta \chi = (a \cos^2 \chi / 2r) D^2, \quad (6.7.30)$$

i.e., $\Delta \chi$ rapidly increases as the cycle length D increases (the angular density of rays decreases). This takes place for turning points located at greater distances from the axis of the USC.

Thus, the field of waves whose turning points lie in the vicinity of the axis of the USC can be calculated by the mode method, and the ray method should be used if the turning points are far from the axis of the USC. The total number of modes and rays in the hybrid method is usually less than in cases when modes and rays are used separately.

There is another advantage of the hybrid method. As is known the ray method fails in the vicinity of caustics or if the grazing angles at the depths of the source and receiver are very small. In these cases it is useful to replace a group of rays by modes. In contrast, the calculation of eigenvalues for a group of modes that forms the acoustic field at some range may be much simpler than determination of the total mode spectrum. Then, the remaining part of the acoustic field is calculated by the ray method.

Some examples of practical applications of the hybrid ray-mode method for acoustic field calculations in the ocean are presented in [6.16, 17].

6.7.2 *Spatial Periods of Interference*

The important characteristics of the sound field in the ocean are the horizontal and vertical scales of its variability.

The horizontal variability is mainly due to the mutual interference of different normal modes. The largest horizontal scale of variability (the distance between the neighbouring convergence zones or, what is the same, the length of the ray cycle) is due to the interference of the modes of neighbouring orders. In fact, to

determine the sound intensity $|p^2|$ we have to square the sum (6.7.16). As a result and using the asymptotic representation of the Hankel function, we obtain terms containing factors of the type $\exp[i(\xi_l - \xi_{l'})r]$. Each of these terms oscillates along r with periods $\Lambda_{l,l'} = 2\pi/|\xi_l - \xi_{l'}|$. The largest period corresponds to the least difference $\xi_l - \xi_{l'}$, that is when $l' = l + 1$. In this case, $\xi_l - \xi_{l'} = \partial\xi_l/\partial l$, and taking into account (6.7.27), we find $\Lambda_{l,l+1} = D_l$, i.e., this interference period coincides with the length of the complete ray cycle.

In the sound field there are also other shorter interference periods. The shortest period corresponds to the maximum difference $\xi_l - \xi_{l'} = k_0(\cos \chi_l - \cos \chi_{l'})$, which occurs for the minimum χ_l ($\chi_l \simeq 0$ if a source is located at the channel axis), and maximum $\chi_{l'}$ corresponding to the limiting ray trapped by a sound channel. In other words, the wider the angular range of the waves trapped by the sound channel, the shorter is the minimum period of interference.

The vertical periods of variability of the sound intensity are considerably shorter and are due to the interference of waves propagating in the directions of positive and negative z , composing the mode of order l . Since for this mode the quantity $k_0\gamma_l(z)$ is the vertical wave number, the interference period will be

$$\frac{\pi}{k_0\gamma_l} = \frac{\pi}{k_0}[n^2(z) - \cos^2 \chi_l]^{-1/2}.$$

The larger χ_l is, that is, the larger the grazing angle of a ray is with respect to the horizon, the smaller the vertical period of interference. However, it is usually equal to the length of the sound wave up to an order of magnitude.

The interference pattern in the coordinates of range and frequency is of considerable importance. It has been observed in experiments and appeared to be fairly steady [6.18]

According to (6.4.11), the sound intensity at large distances from the source ($|\xi_l r| \gg 1$) may be represented as

$$I(\omega, r, z) = |p(\omega, r, z)|^2 = \sum_{l,m} B_l B_m^* \cos(\kappa_{lm} r), \quad (6.7.31)$$

where $\kappa_{lm} \equiv \xi_l - \xi_m$ and the dependence of I upon z is included into the amplitudes of modes.

Following [6.19], consider first the interference of just two modes. If we ignore (usually a weak) dependence of the coefficients $B_{l,m}$ on the sound frequency, the condition for the maximum sound intensity for interference of modes l and m is

$$\kappa_{lm} r = 2\pi N, \quad N = 1, 2, \dots \quad (6.7.32)$$

This is a functional relation between the frequency ω and range r along the lines of maximum intensity. It is evident that the distance between two successive maxima along the axis r is equal to the interference period $\Lambda_{lm} = 2\pi/\kappa_{lm}$. Between maxima the sound intensity $I(\omega, z, z)$ varies along the axis r according to the sine law, but along the axis ω its variations are determined by the function $\kappa_{lm}(\omega)$, and due to waveguide dispersion are not periodical.

The important parameter for our discussion—the slope of maximum intensity lines in the plane (ω, r) —is obtained by differentiating (6.7.32) with respect to ω

$$\frac{d\omega}{dr} = -\frac{\varkappa_{lm}}{r d\varkappa_{lm}/d\omega}. \quad (6.7.33)$$

The value of the derivative $d\omega/dr$ decreases as the distance r from the sound source increases, whereas its sign is determined by the sign of the derivative $d\varkappa_{lm}/d\omega = 1/u_l - 1/u_m$, where $u_l = d\omega/d\xi_l$ is the horizontal component of the group velocity of the mode l .

Consider, for example, a homogeneous ocean with a perfectly reflecting bottom. For some first modes that satisfy the condition $[(\pi/kh)(l + 1/2)]^2 \ll 1$ (small grazing angles), we obtain approximately from (5.3.5)

$$\varkappa_{lm} = (\pi^2 c/2h^2)[(m + 1/2)^2 - (l + 1/2)^2](1/\omega). \quad (6.7.34)$$

Now, setting (6.7.32) in (6.7.30), we obtain

$$\omega = (\pi c/4h^2 N)[(m + 1/2)^2 - (l + 1/2)^2]r,$$

i.e., in this approximation the lines of maximum intensity are straight and their slope in the ω - r plane is equal

$$d\omega/dr = \omega r. \quad (6.7.35)$$

Using the results of *Chuprov* [6.18], we now consider the interference pattern for a group of modes. Increments of frequency $d\omega$ and range dr which do not change the level of the sound intensity $I(\omega, r, z) = \text{const}$, are found from the equation

$$\frac{d\omega}{dr} = -\frac{\partial I/\partial r}{\partial I/\partial \omega}. \quad (6.7.36)$$

Let us express $\partial I/\partial r$ and $\partial I/\partial \omega$ in the vicinity of the range r and frequency ω . Ignoring again a weak dependence of mode amplitudes upon r and ω , we obtain from (6.7.31)

$$\begin{aligned} \frac{\partial I}{\partial r} &= -\omega \sum_{l,m} B_l B_m^* (1/v_l - 1/v_m) \sin \varkappa_{lm} r, \\ \frac{\partial I}{\partial \omega} &= -r \sum_{l,m} B_l B_m^* (1/u_l - 1/u_m) \sin \varkappa_{lm} r, \end{aligned} \quad (6.7.37)$$

where $v_l = \omega/\xi_l$ is the horizontal component of the phase velocity of the mode l . Now, take into consideration that the sound field at a fixed range in the stratified ocean is essentially formed by a group of modes with close numbers [Ref. 5.4, Sect. 2]. Within such a group the phase velocity v_l and group velocity u_l are close to some average values which we designate as v and u , respectively. Moreover, the phase and group velocities are related by a functional dependence, $u = u(v)$. In the WKB approximation and sometimes in the exact solution also, this relationship depends neither on the mode number, nor on the sound frequency. Taking into

account these considerations, we may expand $1/u_l$ in the vicinity $1/u$ into a power series of $(1/v_l - 1/v)$, and retain only the two first terms

$$1/u_l = 1/u + \frac{d(1/u)}{d(1/v)}(1/v_l - 1/v). \quad (6.7.38)$$

Then, using (6.7.36–38), we find that the quantity

$$\beta \equiv \frac{r}{\omega} \frac{d\omega}{dr} = -\frac{d(1/v)}{d(1/u)} = -\left(\frac{u}{v}\right)^2 \frac{dv}{du} \quad (6.7.39)$$

is some invariant of an interference pattern within a group of modes determining the sound intensity at the point (r, z) and frequency ω . As follows from (6.7.39), β is related only to the average value of the derivative $d(1/u)/d(1/v)$ for a given group of modes. The invariant β was first introduced in [6.20].

In the particular case of the homogeneous ocean with perfectly reflecting bottom the phase and group velocities of modes are related by (5.3.14). Then, for a mode of any number we obtain (omitting index l)

$$\frac{dv}{du} = -\frac{v}{u}.$$

Taking into account the relationships

$$v = c/\cos \chi, \quad u = c \cos \chi,$$

which hold for the waveguide considered, we find

$$\beta = u/v = \cos^2 \chi,$$

where χ is the grazing angle of the mode l . At small grazing angles $\beta \approx 1$. The same result can be immediately obtained from (6.7.35).

For the surface sound channel with linear dependence in $n^2(z)$ (6.6.8), the phase and group velocities of modes are given by (6.6.22) and (6.6.23). It is evident that for a mode of any number we have

$$u = \frac{3v}{2 + (v/c_0)^2}. \quad (6.7.40)$$

Then from (6.7.39) we find

$$\beta = -\frac{3}{2(v/c_0)^2}. \quad (6.7.41)$$

At frequencies far from the cutoff frequency we have $v \sim c_0$ and therefore $\beta \approx -3$. The minus sign means that if at the range r there is an interference maximum at the frequency ω , then an increase of the frequency by $d\omega$ will displace this maximum by dr towards the sound source.

Results of numerical calculations of the sound field in shallow sea (depth 30 m) are plotted in Fig. 6.12. Each curve shows the r dependence (in the 10- to 11-km interval) of the sound intensity at a fixed frequency. For convenience, adjacent curves are displaced relative to one another by 2 dB. The lower curve corresponds to 300 Hz, the upper one to 307.5 Hz. The total number of curves is 26 (frequency

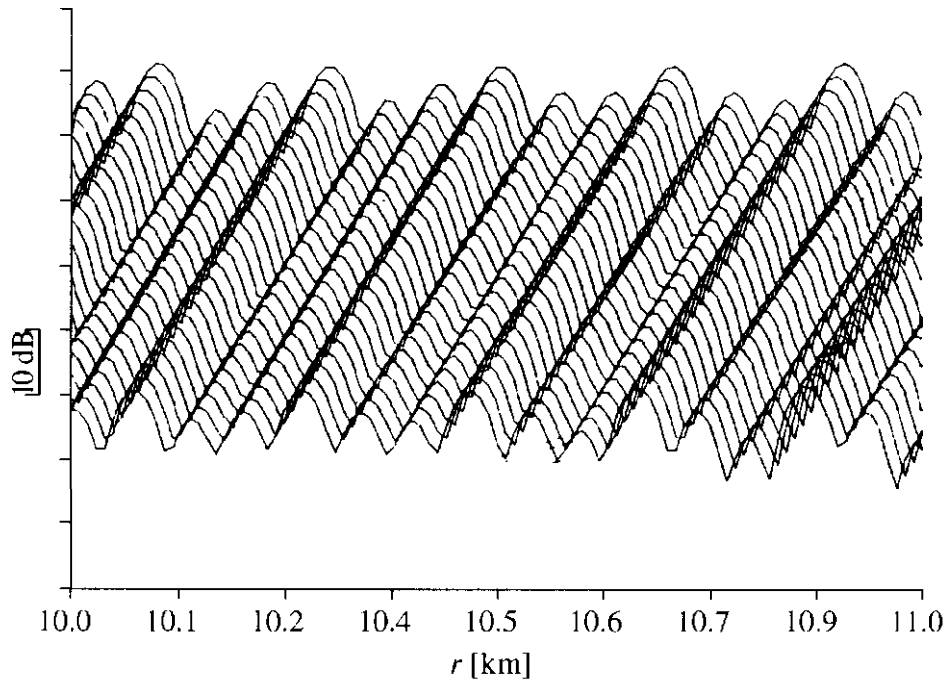


FIGURE 6.12. Interference structure of the sound field in a shallow sea (Figures 6.12, 13 were obtained by V.N. Kulakov)

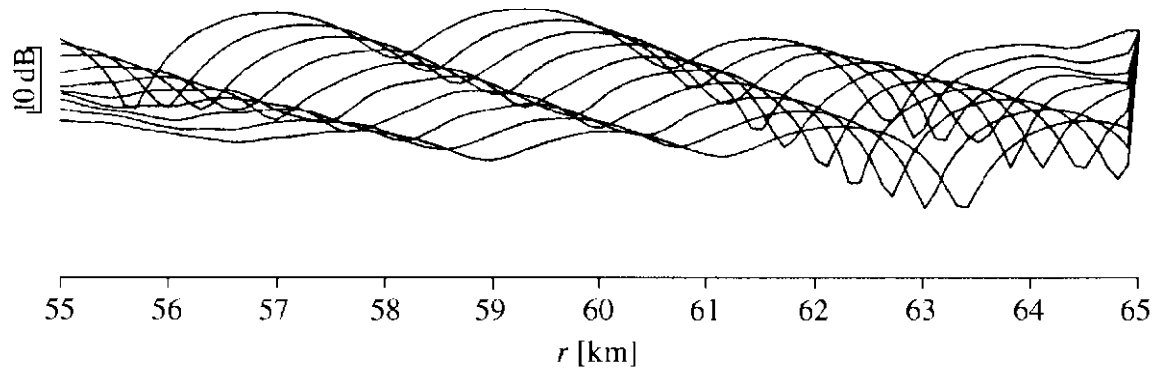


FIGURE 6.13. As in Fig. 6.12, for a surface sound channel with a constant sound velocity gradient

spacing is 0.3 Hz). The sound velocity in the water layer is assumed to be 1.5 km/s, and the bottom is a liquid half-space with a sound velocity of 1.8 km/s and a density of 1.6g/cm^3 . The source and receiver are located at a depth of 15 m. Only those modes that propagate without attenuation have been taken into account in computations. With these parameter values their number is 3. Having found the values of $\Delta r/r$ and $\Delta\omega/\omega$ from the plot, we obtain from (6.7.39) that $\beta \approx 1$.

The interference pattern of the sound field calculated for conditions of the Mediterranean Sea (Sect. 1.2), where a surface sound channel with a constant gradient of the sound velocity from the surface to the very bottom exists, is shown in Fig. 6.13. Some modes that attenuate have been taken into account as well. In this case the value of β is -3 , which is in agreement with a theoretical

estimation obtained for a linear waveguide. Note that having found β for a group of modes and using (6.7.39), we may determine the distance between the source and observation point.

It should be noted that (6.7.39) is approximate in two respects. In deriving it we have neglected the dependence of mode amplitudes upon frequency, and have used the expansion (6.7.38) valid only for a bounded group of modes essential for given r and ω . If r and ω change, the sound field will be determined by another group of modes for which the function $u_l(v_l)$ may have a different form. This results in a change of β . But if the function $u_l(v_l)$ is the same for all modes, as for example in the case of the surface sound channel, β will not change by changing r and ω .

Some other calculations and experiments show that β being invariant is rather useful for analysis of the general character of the interference pattern of the sound field in the ocean [6.18]. Results of comprehensive investigations of the interference structure of broad-band sound in the ocean are presented in the book [6.21].

In a weakly range-dependent oceanic waveguide where the transfer of the acoustic energy between modes is absent (adiabatic approximation), the phase of the l th mode is

$$\int_0^r \xi_l(r) dr,$$

where $\xi_l(r)$ is a local eigenvalue. In this case the invariant β is given by [6.18]

$$\beta = -\frac{d[1/v(r)]}{d[\langle 1/u \rangle]}, \quad (6.7.42)$$

where $v(r)$ is the average phase velocity of a group of modes received at the distance r from the source and $\langle 1/u \rangle$ is the value of $1/u$ averaged over the track:

$$\langle 1/u \rangle = (1/r) \int_0^r [1/u(r)] dr,$$

where $u(r)$ is a local value of the group velocity of a mode whose phase velocity is v at the distance r .

Recently the expression for the invariant β was extended to a more complicated case of shallow-water environments where the bottom bathymetry varies with range r and azimuth φ [6.22]. In this case the invariant β depends on range r and azimuth φ , $\beta = \beta(r, \varphi)$. As properties of the environment and the range between the source and receiver vary, the direction of the line of constant spectral level is given by

$$\frac{d\bar{\omega}}{\bar{\omega}} = \beta(r, \varphi) \frac{dr}{r} - \frac{\beta(r_0)}{\beta(r, \varphi)} \frac{\partial}{\partial \varphi} (\beta(r, \varphi)) d\varphi, \quad (6.7.43)$$

where $\beta(r_0)$ is the value β at the point of reception. It is evident that for a range- and azimuth-independent waveguide, this expression reduces to (6.7.39).

Range-Dependent Waveguide

In the previous chapters we have considered the propagation of sound in the ocean where the depth, the acoustical characteristics of the sea bottom, and the sound velocity profile $c(z)$ in water do not vary along the propagation path. Very often this is a rather good approximation to a real situation and, therefore, the theory developed above has a wide variety of practical applications. Sometimes, however, we need the generalization of this theory to the case when the characteristics of the ocean acoustic waveguide vary with a horizontal range. It is necessary, in particular,

- a) when sound propagates in the coastal wedge, where variation of sea depth is significant;
- b) when sound waves cross frontal zones in the ocean, for example, such currents as the Gulf Stream, Kuroshio, etc.; and
- c) when sound propagates over large ranges of the order of thousands of kilometres. Variation of the $c(z)$ profile is essential in this case, especially when the propagation path lies in the meridional direction.

The sound propagation theory for a general case of a medium whose characteristics vary along all three coordinates has not yet been sufficiently developed. But there is a circumstance which makes the matter easier in our case, namely, variations of the characteristics of ocean waveguide in the horizontal direction are slow. It is possible to introduce corresponding small parameters: a small slope of the bottom or a small ratio of the horizontal gradient of the sound velocity to the vertical one for the case of a range-dependent profile $c(z, r)$. The presence of such small parameters simplifies the theory considerably.

At present, three methods of analyzing wave propagation in such media are rather well developed—the reference waveguide method, the parabolic equation method, and the ray method.

7.1 Normal Modes in an Almost Stratified Medium: Reference Waveguide Method

Now let us consider the oceanic acoustic waveguide for which the sound velocity $c(z, \mathbf{r})$ varies not only with depth but also with horizontal range $\mathbf{r} = \{x, y\}$, though

much slower. The problem is to find the solution of the Helmholtz equation for the acoustic pressure $p(z, \mathbf{r})$

$$\Delta p + k^2(z, \mathbf{r})p = 0, \quad k(z, \mathbf{r}) = \omega/c(z, \mathbf{r}) \quad (7.1.1)$$

with the appropriate conditions near the source, at the boundaries, and at infinity. For the present we assume that the bottom and surface of the ocean are perfectly reflecting. We will use the term *reference waveguide* at fixed $\mathbf{r} = \mathbf{r}_1$ for the homogeneous r -independent waveguide for which the vertical sound velocity profile is given by the function $c(z, \mathbf{r}_1)$. In general, the depth depends on \mathbf{r} , $h = h(\mathbf{r})$. But the reference waveguide corresponding to the point \mathbf{r}_1 has a horizontal bottom at depth $h = h(\mathbf{r}_1)$.

We will assume that for the reference waveguide corresponding to an arbitrary \mathbf{r} there is a total system of orthogonal eigenfunctions $\psi_l(z, \mathbf{r})$, $l = 1, 2, \dots$ depending on z (\mathbf{r} is taken as a parameter) satisfying the equation

$$\frac{d^2 \psi_l}{dz^2} + [k^2(z, \mathbf{r}) - \xi_l^2] \psi_l = 0 \quad (7.1.2)$$

and boundary conditions at the bottom and surface. Here $\xi_l = \xi_l(\mathbf{r})$ are the eigenvalues of the reference waveguide at \mathbf{r} .

In principle, any field depending on z for given \mathbf{r} can be represented as an expansion in terms of the functions ψ_l . Therefore, we represent the solution of (7.1.1) in the form

$$p(z, \mathbf{r}) = \sum_l \Psi_l(\mathbf{r}) \psi_l(z, \mathbf{r}). \quad (7.1.3)$$

The expansion coefficients are given by $\Psi_l = B_l H_0^{(1)}(\xi_l r)$, where B_l are constants for a range-independent stratified waveguide. It should be expected that in our case B_l are slowly varying functions of \mathbf{r} .

Substituting (7.1.3) into (7.1.1) and omitting for brevity the functional arguments, we obtain

$$\begin{aligned} \frac{\partial^2 p}{\partial z^2} &= \sum_l \Psi_l \frac{\partial^2 \psi_l}{\partial z^2}, \\ \frac{\partial^2 p}{\partial x^2} + \frac{\partial^2 p}{\partial y^2} &\equiv \nabla_r^2 p = \sum_l (\Psi_l \nabla_r^2 \psi_l + 2 \nabla_r \Psi_l \nabla_r \psi_l + \psi_l \nabla_r^2 \Psi_l), \\ \nabla_r &= \left\{ \frac{\partial}{\partial x}, \frac{\partial}{\partial y} \right\}. \end{aligned} \quad (7.1.4)$$

It is assumed that functions ψ_l are orthogonal, i.e.,

$$\int_0^h \psi_l \psi_m dz = \delta_{lm}.$$

Then, insertion of (7.1.4) into (7.1.1) and subsequent multiplication by $\psi_m(z, \mathbf{r})$ followed by integration over z from 0 to h yield the following set of coupled

differential equations:

$$(\nabla_r^2 + \xi_m^2)\Psi_m = -2 \sum_l \nabla_r \Psi_l \int \psi_m \nabla_r \psi_l dz - \sum_l \Psi_l \int \psi_m \nabla_r^2 \psi_l dz. \quad (7.1.5)$$

It is this equation that provides the basis of the reference waveguide method. The similar equation for the electromagnetic case seems to have been first obtained by *Katzenelenbaum* [7.1]. In the acoustical case it was obtained by *Pierce* [7.2] and later by *Milder* [7.3], and has been applied many times by investigators. For the case of the parabolic vertical sound velocity profile it was considered in detail by *Chwieroth et al.* [7.4].

The right-hand side of (7.1.5) is small if the properties of the waveguide vary sufficiently slowly with horizontal range. If we assume that the right-hand side is zero, the equations for the normal modes are uncoupled. Each normal mode propagates in the waveguide independently of the others, adjusting to the varying conditions in the waveguide. The approximation in which the interaction between normal modes is neglected is usually called *adiabatic*.

It is to be noted that coupling between modes can result from boundary conditions, as in the case of a sloping bottom.

7.2 Adiabatic Approximation: Ray Invariant

For the sake of simplicity we consider a problem that has cylindrical symmetry, i.e., the sound velocity $c = c(r, z)$ depends on z and the range r . Then we have in the adiabatic approximation

$$\frac{1}{r} \frac{\partial}{\partial r} \left(r \frac{\partial \Psi_m}{\partial r} \right) + \xi_m^2(r) \Psi_m = 0. \quad (7.2.1)$$

Let us introduce a new function $F_m(r) = r^{1/2} \Psi_m(r)$ which satisfies the equation

$$F_m'' = - \left(\xi_m^2 + \frac{1}{4r^2} \right) F_m. \quad (7.2.2)$$

We are interested in a solution of the latter for $\xi_m r \gg 1$. Then, neglecting the second term in parentheses, we obtain the equation for F_m ,

$$F_m'' = -\xi_m^2(r) F_m. \quad (7.2.3)$$

The solution of this equation in the WKB approximation, as can be seen from comparison with (6.7.1), is

$$F_m(r) = A_m \xi_m^{-1/2}(r) \exp \left[i \int_0^r \xi_m(r) dr \right] \quad (7.2.4)$$

where A_m is an arbitrary constant.

Taking into account all normal modes, we obtain for the acoustic pressure (7.1.3)

$$p(z, r) = \sum_l A_l \psi_l(z, r) (\xi_l r)^{-1/2} \exp \left(i \int_0^r \xi_l dr \right). \quad (7.2.5)$$

For the case of a horizontally homogeneous waveguide, $p(z, r)$ is given by (6.4.11). Under the assumption that $\xi_l r \gg 1$ when the asymptotic form for the Hankel function can be used, (6.4.11) becomes

$$p(z, r) = (2/\pi)^{1/2} \exp(-i\pi/4) \sum_l \psi_l(z) \psi_l(z_1) (\xi_l r)^{-1/2} \exp(i\xi_l r). \quad (7.2.6)$$

At relatively small ranges r from the source (but large compared with the sound wavelength) the variation of properties of the medium in the horizontal direction does not affect the sound field, and ξ_l can be considered a constant. Therefore, for these ranges (7.2.5) and (7.2.6) must be identical. Since for constant ξ_l ,

$$\int_0^r \xi_l dr = \xi_l r,$$

we obtain

$$A_l = (2/\pi)^{1/2} \exp(-i\pi/4) \psi_l(z_1, 0), \quad (7.2.7)$$

where $\psi_l(z_1, 0) = \psi_l(z_1)$ is a vertical eigenfunction in the region close to the source ($r = 0$). Now (7.2.5) for the acoustic pressure is written

$$p(z, r) = (2/\pi)^{1/2} \exp(-i\pi/4) \sum_l \psi_l(z_1, 0) \psi_l(z, r) (\xi_l r)^{-1/2} \exp\left(i \int_0^r \xi_l dr\right). \quad (7.2.8)$$

We recall that $\xi_l = \xi_l(r)$ are the eigenvalues of the depth equation (7.2.1) for the reference waveguide corresponding to a given r .

7.2.1 Ray Invariant

In obtaining (7.2.8) we used the WKB approximation for the solution of the range equation (7.2.3). Our postulation that properties of the medium in the horizontal direction vary slowly can, as a rule, be considered quite justified.¹ For the cases when the waveguide is sufficiently wide in the vertical direction and the number of propagating modes is sufficiently large, the WKB approximation can also be used to solve the depth equation, i.e., the procedure described in Sect. 6.6 can be applied. The eigenvalues ξ_l can be found by using the phase integral in this case. For an internal waveguide, for example, it becomes by virtue of (6.7.12)

$$k_0 \int_{z'_l}^{z''_l} [n^2(z, r) - \xi_l^2/k_0^2]^{1/2} dz = \pi(l + 1/2), \quad (7.2.9)$$

where the turning points z'_l and z''_l (at which the expression under the radical becomes zero) as well as k_0 and ξ_l depend upon r .

It has been shown in Sect. 6.7 that there is a system of rays corresponding to each normal mode taken in the WKB approximation. In the horizontally homogeneous

¹ We recall that we are considering a cylindrically symmetric problem with a fairly simple ray picture in the horizontal plane. In more complex cases when the rays in the horizontal plane can form caustics (Sect. 7.3), the WKB approximation should be modified.

waveguide the angle that these rays make with the channel axis ($z = z_0$, $c = c_0$) is $\chi_l \equiv \chi_l(z_0) = \arccos(\xi_l/k_0)$. For other depths a similar angle $\chi_l(z)$ is defined in terms of χ_l by Snell's law (6.7.23). The same is the case with a waveguide whose properties vary slowly with horizontal range, but where χ_l and $\chi_l(z)$ also depend on r . However, they are still related by (6.7.23), that is

$$n(z, r) \cos \chi_l(z, r) = \cos \chi_l(r), \quad (7.2.10)$$

where r is considered a parameter.

On the basis of ray representations one can imagine just how slowly a medium must vary with horizontal range so that the adiabatic approximation is valid. Obviously it is necessary that variation of the waveguide characteristics is small over the ray cycle length. In other words, a subsequent cycle must differ only a little from the preceding one. These qualitative considerations will be specified later, but now we write (7.2.9) in terms of rays. Substituting $\xi_l/k_0 = \cos \chi_l(r)$ in (7.2.9) and also using (7.2.10), we obtain

$$\int_{z'_l}^{z''_l} \frac{\sin \chi_l(z, r)}{c(z, r)} dz = (\pi/\omega)(l + 1/2). \quad (7.2.11)$$

Since the right-hand side of this equation does not depend on r , the integral in the left-hand side is also constant. This is an important result which expresses one of the "conservation laws" for the adiabatic approximation.

Angles $\chi_l(r)$ and $\chi_l(z, r)$ change discretely with l . However, if the number of normal modes is large, this change can be considered continuous. In this case the index l is unnecessary, and (7.2.11) can be written in the form

$$l = \oint \frac{\sin \chi(z, r)}{c(z, r)} dz = \text{const.} \quad (7.2.12)$$

The integral is taken over the total cycle of a ray. The quantity l is called a ray invariant. It can be related to the travel time T of a sound wave over the cycle and the cycle range D . Omitting, for brevity, arguments in $\chi(z, r)$ and $c(z, r)$, we have (2.3.1, 4)

$$T = \oint \frac{dz}{c \sin \chi}, \quad D = \oint \frac{dz}{\tan \chi}. \quad (7.2.13)$$

According to Snell's law we have $\cos \chi/c = \cos \chi_0/c_0$, where c_0 and χ_0 are the sound velocity and grazing angle of a ray on the waveguide axis. Using this law, we have the evident identity

$$\frac{\sin \chi}{c} = \frac{1}{c \sin \chi} - \frac{\cos \chi_0}{c_0} \cdot \frac{1}{\tan \chi}.$$

Integrating the latter over a ray cycle and using (7.2.13), we obtain

$$l = T - qD, \quad (7.2.14)$$

where $q = (1/c_0) \cos \chi_0 = 1/v$, and v is the horizontal component of the phase velocity of a wave travelling along a ray path, which is equal to the sound velocity at the turning depths $z = z'$ or $z = z''$, where $\chi = 0$.

Let us represent T and D as

$$T = \oint c^{-2}(c^{-2} - q^2)^{-1/2} dz, \quad D = q \oint (c^{-2} - q^2)^{-1/2} dz$$

and after taking into account the evident relationship

$$\frac{dT}{dq} = q \frac{dD}{dq},$$

we obtain

$$\frac{dI}{dq} = -D.$$

We show now that the ratio D/T is equal to the horizontal component of the group velocity $u = d\omega/d\xi$. Equation (7.2.11) may be rewritten as

$$\omega I = \text{const.}$$

Differentiating it with respect to ξ and taking into account that $q = \xi/\omega$ and $dq/d\xi = (1 - qu)/\omega$, we find

$$u = - \left(\frac{dI}{dq} \right) / \left(I - q \frac{dI}{dq} \right) = \frac{D}{T}.$$

Now the ray invariant may be represented as

$$I = D \left(\frac{1}{u} - \frac{1}{v} \right).$$

The concept of the ray invariant is useful in many respects. Using it, for example, one can obtain $\chi_0(r)$, the grazing angle of a ray at the channel axis as a function of r . The concept of the ray invariant in underwater acoustics was first formulated by *Weston* [7.5].

We have proved rigorously the constancy of I for a problem with cylindrical symmetry. But it is obvious that assuming cylindrical symmetry is not necessary at all, and the result can be applied to any case provided it is possible to choose the plane r, z so that a ray propagating in this plane does not leave it, i.e., the horizontal refraction of the ray can be neglected.

7.2.2 An Example of Using the Ray Invariant

Consider sound propagation in the sea where the depth $h = h(r)$ monotonically increases along the propagation path (a coastal wedge, for instance), and the sound velocity for any r linearly decreases from the surface $z = 0$ to the bottom $z = h$,

$$c = c_s(1 - az), \quad 0 \leq z \leq h(r). \quad (7.2.15)$$

The sound velocity c_s at the surface and the gradient a can be arbitrary continuous functions of r .

Figure 7.1 shows the ray diagram for the case when c_s and a are constant, and h increases linearly with r : the coastal wedge with a slope angle $\phi = 30'$. We

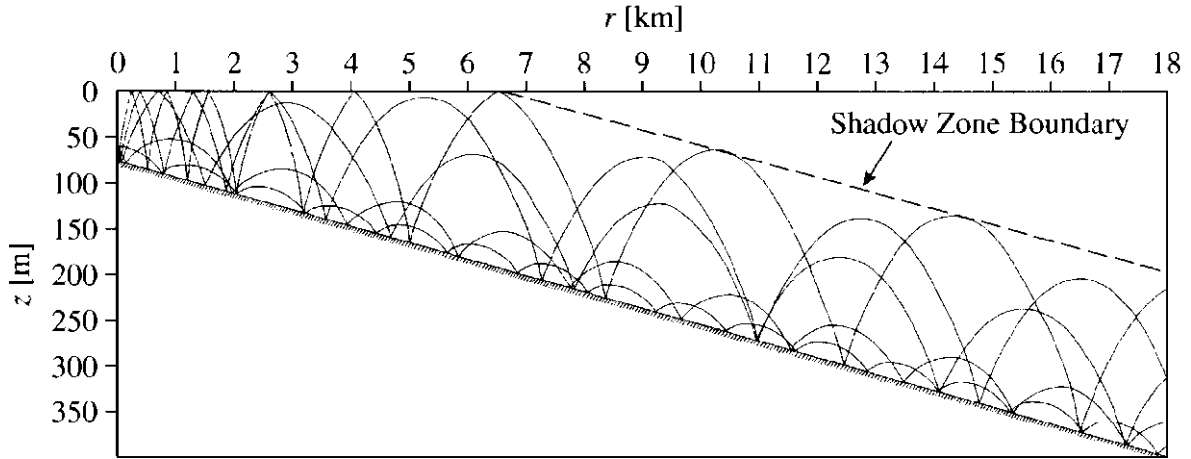


FIGURE 7.1. Ray diagram of sound propagation in an ocean with a sloped bottom and a negative sound velocity gradient. Depth of the source is $z_1 = 75$ m, $\phi = 30^\circ$, $a = 1.2 \cdot 10^{-4} \text{ m}^{-1}$ [7.6]

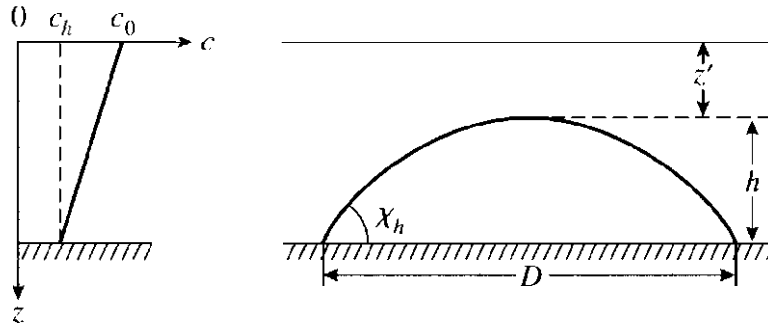


FIGURE 7.2. Complete cycle of a downward refracted ray

see that beginning from a certain r the zone of the acoustic shadow starts near the surface. The zone's width increases with distance. Let us determine using the ray invariant the conditions for the shadow zone formation and the law for its expansion.

The reference waveguide for any fixed r is a plane layer at a depth according to (7.2.15) with a constant. Let us evaluate the ray invariant for the ray shown in Fig. 7.2. We have

$$I = 2 \int_{z'}^h (\sin \chi / c) dz. \quad (7.2.16)$$

We will use χ as an integration variable instead of z . According to Snell's law we have

$$\cos \chi(z) / c(z) = \cos \chi_h / c_h. \quad (7.2.17)$$

where χ_h and c_h are the grazing angle and sound velocity, respectively, at the

bottom. Differentiating (7.2.17) we obtain, omitting the arguments in $\chi(z)$ and $c(z)$,

$$\sin \chi d\chi = -(\cos \chi_h/c_h) \frac{dc}{dz} dz = (\cos \chi_h/c_h) a c_s dz. \quad (7.2.18)$$

By virtue of (7.2.17, 18), (7.2.16) becomes

$$I = (2/ac_s) \int_0^{\chi_h} \tan \chi \sin \chi d\chi.$$

In real cases χ_h is usually small. Therefore, setting $\tan \chi \sim \sin \chi \sim \chi$ and integrating, we obtain

$$I = 2(3ac_s)^{-1} \chi_h^3 = \text{const.} \quad (7.2.19)$$

An interesting conclusion results from this relationship. If a and c_s do not depend on r , the angle χ_h which the ray makes with the horizontal at the bottom is constant for any kind of variation of $h(r)$.

From (7.2.17), taking into account that $\chi(z') = 0$, $c(z') = c_s(1 - az')$, $c_h = c_s(1 - ah)$, and χ_h , az' , and ah are small, we also find

$$\chi_h^2 = 2a(h - z'), \quad (7.2.20)$$

where z' is the turning depth of a ray (Fig. 7.2). Approaching a smaller h (as well as r), we eventually reach the depth $h = h_0$ (at $r = r_0$) where the turning depth coincides with the surface ($z' = 0$). The grazing angle of the ray at the bottom at such r_0 will be, as can be seen from (7.2.19), $\chi_{h_0} = (2a_0h_0)^{1/2}$, where $a_0 \equiv a(r_0)$. Now we can rewrite (7.2.19) in the form

$$(ac_s)^{-1} \chi_h^3 = (a_0c_{s0})^{-1} \chi_{h_0}^3 = (a_0c_{s0})^{-1} (2a_0h_0)^{3/2}.$$

Hence, we find $\chi_h = (2a_0h_0)^{1/2} (ac_s/a_0c_{s0})^{1/3}$ and, substituting this into (7.2.20), obtain for z' the depth of the shadow zone for the rays under consideration

$$z' = h - h_0(a_0/a)^{1/3} (c_s/c_{s0})^{2/3}. \quad (7.2.21)$$

If a and c_s are constant, we obtain another interesting result,

$$z'(r) = h(r) - h_0. \quad (7.2.22)$$

i.e., the lower boundary of the shadow zone repeats the bottom relief being a constant distance h_0 from it (see Fig. 7.1 for the particular case of a flat sloping bottom).

The depth h_0 can be easily determined if we consider the ray invariant for depths $h < h_0$ (i.e., $r < r_0$) where a ray is reflected from both the bottom and the water surface. In this case the source's depth and the aperture angle of its directivity pattern must be specified. A ray leaving the source at the maximum grazing angle will determine the shadow zone whose boundary has just been found. For application of the ray invariant to more complex cases see the paper by Harrison [7.7].

7.2.3 Conditions for the Validity of the Adiabatic Approximation and Ray Invariant²

Let us now obtain the conditions required to neglect the right-hand side of (7.1.5). We do not change its order of magnitude by retaining only the first sum and keeping a single term $l = m + 1$ in it because the interaction of adjacent modes is the most effective. In addition, replacing ∇_r by $\partial/\partial x$, where x is the coordinate in the direction of wave propagation, we obtain for Ψ_m an equation

$$\frac{\partial^2 \Psi_m}{\partial x^2} + \xi_m^2 \Psi_m = -2S_{ml} \frac{\partial \Psi_l}{\partial x}, \quad l = m + 1 \quad (7.2.23)$$

where

$$S_{ml} = \int \psi_m \frac{\partial \psi_l}{\partial x} dz. \quad (7.2.24)$$

To estimate an order of magnitude of the right-hand side of (7.2.23), Ψ_l can be evaluated in the WKB approximation (up to the accuracy of a constant factor)

$$\Psi_l = \xi_l^{-1/2} \exp\left(i \int \xi_l dx\right).$$

Once again within an order-of-magnitude accuracy

$$\frac{\partial \Psi_l}{\partial x} \sim \xi_l^{1/2} \exp\left(i \int \xi_l dx\right) \sim \xi_l^{1/2} \exp(i\xi_l x). \quad (7.2.25)$$

Substituting (7.2.25) into (7.2.23), we obtain the known equation for forced oscillations of the harmonic oscillator, the solution of which, as can be easily verified, is

$$\Psi_m \sim \frac{2S_{ml}\xi_l^{1/2}}{\xi_m^2 - \xi_l^2} \exp(i\xi_l x);$$

Ψ_m is the correction to the m th normal mode due to its interaction with the l th one. The adiabatic approximation is valid if this correction is small compared with $\xi_m^{-1/2}$, the amplitude of the m th normal mode, that is

$$\frac{2S_{ml}\xi_l^{1/2}\xi_m^{1/2}}{\xi_m^2 - \xi_l^2} \ll 1. \quad (7.2.26)$$

Here $\xi_l \sim \xi_m \sim k_0$. Remembering that $l = m + 1$, we find from (6.7.27) $\xi_m - \xi_l = 2\pi/D$, where D is the cycle range of a corresponding ray. As a result, condition (7.2.26) of the applicability of the adiabatic approximation may be written as

$$S_{ml}D \ll 1. \quad (7.2.27)$$

Estimating S_{ml} and D in each particular case is not difficult. However, at least for normal modes of low numbers S_{ml} can also be generally estimated. In fact, in

²Authors thank A.G. Voronovich for very valuable advice while writing this paragraph.

(7.2.24) we have $\partial\psi_l/\partial x \sim \psi_l/M$, where M is a scale of the horizontal variation of the medium. The quantity $\int \psi_m \psi_l dz$ does not exceed a norm of the functions ψ_m and ψ_l , i.e., unity. Therefore, (7.2.27) may be rewritten as

$$D/M \ll 1, \quad (7.2.27')$$

i.e., the cycle range of the ray must be small compared with the scale of the horizontal variation of the medium—the condition mentioned above. Let us consider this condition for some particular cases, estimating D using the approximate expression

$$D = 2\pi/(\xi_l - \xi_{l+1}) \sim 4\pi k_0/(\xi_l^2 - \xi_{l+1}^2). \quad (7.2.28)$$

1. Homogeneous ocean of variable depth with absolutely rigid bottom. The quantity ξ_l is given by (5.3.5). Taking into account that $l = O(1)$, we obtain from (7.2.28) that $D = O(k_0 h^2)$, and condition (7.2.27') is written as

$$k_0 h^2/M \ll 1, \quad (7.2.29)$$

that is, the lower the frequency (the smaller k_0), the better is the adiabatic approximation.

2. Surface linear waveguide. This case has been considered in Sect. 6.6 when a is constant. Now we can remove this restriction and set $a = a(r)$. The quantity ξ_l^2 is given by (6.6.19). Taking into account that $y_l = O(1)$, we find $D = O(k_0 H^2)$, and the criterion (7.2.27') is written as

$$k_0 H^2/M \ll 1 \quad (7.2.30)$$

which coincides with the formula in the book by *Brekhovskikh* [Ref. 7.8, Eq. (52.36)] obtained by a different method. By virtue of (6.6.11), the last condition reduces to

$$M(k_0 a^2)^{1/3} \gg 1. \quad (7.2.30')$$

As we see, in this case the adiabatic approximation is more exact, the higher the frequency.

3. Internal waveguide with a range-dependent parabolic profile

$$k^2(x, z) = k_0^2 \left[1 - \frac{1}{4} \left(\frac{z}{h} \right)^2 \right], \quad h = h(x). \quad (7.2.31)$$

For this case the ψ_l are parabolic cylinder functions and, according to the book by *Brekhovskikh* [Ref. 7.8, Eq. (52.45)] we have

$$\xi_l^2 = k_0^2 - (k_0/h)(l + 1/2). \quad (7.2.32)$$

Now we have $D = O(h)$ and the criterion (7.2.27') is

$$h/M \ll 1 \quad (7.2.33)$$

where the frequency is not included at all.

7.2.4 Coupled Modes

Now we obtain the solution of equation (7.1.5) allowing for the interaction of modes, and we limit our consideration to the problem with cylindrical symmetry. For the previously obtained function $F_n(r)$ at $\xi_n r \gg l$, (7.1.5) takes the form

$$\left(\frac{d^2}{dr^2} + \xi_n^2\right) F_n(r) = - \sum_{n \neq m} \left(T_{mn} + S_{mn} \frac{d}{dr}\right) F_m(r), \quad (7.2.34)$$

where the coupling coefficients T_{mn} and S_{mn} are given by

$$T_{mn} = \int \psi_n \nabla_r^2 \psi_m dz, \quad S_{mn} = 2 \int \psi_n \nabla_r \psi_m dz$$

(the coefficient S_{mn} differs from its determination in the one-dimensional case by the factor 2).

Following *McDaniel* [A.7.1], we represent each mode as a sum of a forward propagating component and a backscattered component:

$$F_n(r) = u_n \exp(i\bar{\xi}_n r) + v_n \exp(-i\bar{\xi}_n r), \quad (7.2.35)$$

where

$$\bar{\xi}_n r = \int_0^r \xi_n(r') dr'.$$

Introducing two new functions u_n and v_n (instead of a single function F_n), we subject them to the condition

$$\frac{du_n}{dr} \exp(i\bar{\xi}_n r) + \frac{dv_n}{dr} \exp(-i\bar{\xi}_n r) = 0. \quad (7.2.36)$$

Substituting (7.2.35) in (7.2.34) and taking into account (7.2.36), we obtain

$$\begin{aligned} & \frac{du_n}{dr} \exp(i\bar{\xi}_n r) - \frac{dv_n}{dr} \exp(-i\bar{\xi}_n r) \\ &= -\xi_n^{-1} \frac{d\xi_n}{dr} [u_n \exp(i\bar{\xi}_n r) - v_n \exp(-i\bar{\xi}_n r)] \\ & \quad + i\xi_n^{-2} \sum_{m \neq n} S_{mn} [u_m \exp(i\bar{\xi}_m r) + v_m \exp(-i\bar{\xi}_m r)] \\ & \quad - \sum_{m \neq n} \frac{\xi_m}{\xi_n} T_{mn} [u_m \exp(i\bar{\xi}_m r) - v_m \exp(-i\bar{\xi}_m r)]. \end{aligned} \quad (7.2.37)$$

Simultaneous solving of these equations yields

$$\frac{du_n}{dr} = \sum_{m \neq n} \frac{1}{2} \exp(-i\bar{\xi}_n r) [C_{nm}^{(1)} u_m \exp(i\bar{\xi}_m r) + C_{nm}^{(2)} v_m \exp(-i\bar{\xi}_m r)] \quad (7.2.38)$$

and

$$\frac{dv_n}{dr} = - \sum_{m \neq n} \frac{1}{2} \exp(i\bar{\xi}_n r) [C_{nm}^{(1)} u_m \exp(i\bar{\xi}_m r) + C_{nm}^{(2)} v_m \exp(-i\bar{\xi}_m r)], \quad (7.2.39)$$

where the matrices $C_{mn}^{(1)}$ and $C_{mn}^{(2)}$ are given by

$$C_{mn}^{(1,2)} = \mp \xi_n^{-1} \frac{d\xi_n}{dr} \delta_{nm} + i\xi_n^{-1} S_{nm} \mp (\xi_m/\xi_n) T_{mn}, \quad \delta_{nm} = \begin{cases} 1, & n = m, \\ 0, & n \neq m. \end{cases}$$

Here, upper signs refer to $C_{mn}^{(1)}$ and the lower signs to $C_{mn}^{(2)}$.

Neglecting backscattered waves, we obtain a relatively simple equation for $u_n(r)$:

$$\frac{du_n}{dr} = \frac{1}{2} \sum_{m \neq n} C_{nm}^{(1)} u_m \exp[i(\bar{\xi}_m - \bar{\xi}_n)r]. \quad (7.2.40)$$

Having found the solution of this equation and substituted it in (7.2.39), we obtain the equation for the backscattered waves.

As an example, we consider the propagation of sound in the ocean with smooth varying depth [A.7.1]. For small bottom slopes, which is characteristic for shelf regions, the interaction between modes is weak and the coupling coefficient and modal wave numbers may be considered invariant with distance. Assume that only one mode (the first) is initially excited. The propagation of the first mode will be accompanied by the excitement of higher modes; the coupling of the first mode and the n th mode ($n \neq 0$) is described by the equation

$$\frac{du_n}{dr} = \frac{1}{2} C_{n1}^{(1)} u_1 \exp[i(\bar{\xi}_1 - \bar{\xi}_n)r]. \quad (7.2.41)$$

For above-mentioned assumptions about parameters of the problem, its solution with the initial condition $u_n(0) = 0$ ($n \neq 1$) has the form (u_n may be considered constant for the weak coupling)

$$u_n(r) = C_{n1}^{(1)} u_1 \kappa_{n1}^{-1} \exp(i\kappa_{n1}r) \sin(\kappa_{n1}r/2), \quad (7.2.42)$$

where $\kappa_{n1} = \bar{\xi}_1 - \bar{\xi}_n$. From (7.2.42) it follows that the higher-order mode amplitude periodically varies with the distance r , and the period of oscillations $L = 4\pi/\kappa_{n1}$ will be independent of distance. The function $u_n(r)$ reaches its first maximum at the distance termed the conversion length $r_{n1} = \pi/\kappa_{n1}$. The ratio of the peak amplitude of a higher-order mode to the initial amplitude of the first mode $|u_n(\pi/\kappa_{n1})/u_1(0)|$ characterizes the magnitude of exchange energy between these modes.

Let us substitute (7.2.42) in (7.2.39) and reject in the right-hand side terms describing the backscattered modes because their amplitudes with smooth depth variation are significantly less than those propagating in the forwards direction. Assume again that only the first mode is initially excited. Equation (7.2.39) then takes the form

$$\frac{dv_n}{dr} = -\frac{1}{2} C_{n1}^{(1)} u_1 \exp[i(\bar{\xi}_1 + \bar{\xi}_n)r]. \quad (7.2.43)$$

Subject to the boundary condition $v_n(R) = 0$, the solution of this equation is

$$v_n(r) = C_{n1}^{(1)} u_1(\kappa'_{n1})^{-1} \exp[i\kappa'_{n1}(R+r)/2] \sin[\kappa'_{n1}(R-r)/2], \quad (7.2.44)$$

where $\kappa'_{n1} = \bar{\xi}_1 + \bar{\xi}_2$.

Results of numerical calculations of the various characteristics of the first- and higher-order modes are presented in [A.7.1].

7.3 Rays in a Horizontal Plane

A parameter ξ_l frequently encountered above is the horizontal wave number of the l th normal mode. The phase velocity of the latter in the horizontal plane is $v_l = \omega/\xi_l$. In Chaps. 5 and 6 ξ_l and, consequently, v_l were constants. In this chapter ξ_l depends on \mathbf{r} and, consequently, the plane $\mathbf{r} = \{x, y\}$ represents for a normal mode a two-dimensional space with propagation velocity depending on \mathbf{r} .

For this medium we can define the refraction index $n(\mathbf{r}) = \xi_l(\mathbf{r})/\xi_l(0) = v_l(0)/v_l(\mathbf{r})$ and develop ray theory for wave propagation in such a medium. Suppose, for example, that a point source is located at point $\mathbf{r} = 0$. For the case with cylindrical symmetry considered above, when $n = n(r)$ this theory will be extremely simple. All the rays will be directed along radii vectors \mathbf{r} . The change of phase over each ray is $\int_0^r \xi_l dr$. The wave amplitude decreases with r as $r^{-1/2}$ (energy decreases as r^{-1}) according to the law of ray spreading. For the general case $n = n(\mathbf{r})$ we can develop a ray theory using the results of Sect. 2.6 in their two-dimensional version. In particular, the ray trajectory can be found as solutions to the eikonal equation (2.6.3), subsequently using (2.6.5) or the solutions of equation (2.6.7). The phase difference between points \mathbf{r}_1 and \mathbf{r}_2 along the ray is given by

$$\int_{r_1}^{r_2} \xi_l(\mathbf{r}) \mathbf{e}(\mathbf{r}) d\mathbf{r},$$

\mathbf{e} being the unit vector of a line tangent to the ray, and the amplitude determined from the law of spreading of the rays. The rigorous formulation of ray theory for normal modes in the horizontal plane was given by *Burridge and Weinberg* [7.9].

7.3.1 The Case of a Coastal Wedge

As an example consider the horizontal refraction of normal modes in a coastal wedge. Let the edge of the wedge (a line of zero depth) coincide with the x axis and the depth of sea increase proportionally to the y coordinate, i.e., to a distance from the edge $h = \varepsilon y$, $\varepsilon \ll 1$. It is assumed that the bottom is absolutely rigid and the sound velocity c in water is constant. According to (5.3.5), one has for $\xi_l(y)$

$$\xi_l(y) = \left[k^2 - \left(\frac{\pi}{\varepsilon y} \right)^2 (l + 1/2)^2 \right]^{1/2}, \quad k = \omega/c. \quad (7.3.1)$$

Let the source be at point $x = 0$, $y = y_0$, where the depth of the sea is $h_0 = \varepsilon y_0$. Then the square of the refraction index in respect to this point will be

$$n^2(y) = \xi_l^2(y)/\xi_l^2(y_0) = \left[k^2 - \left(\frac{\pi}{\varepsilon y} \right)^2 (l + 1/2)^2 \right] \left[k^2 - \left(\frac{\pi}{\varepsilon y_0} \right)^2 (l + 1/2)^2 \right]^{-1}. \quad (7.3.2)$$

It is more convenient to express (7.3.2) in terms of the angle χ_l^0 which a ray corresponding to the l th mode makes with the horizontal plane near the source. According to (5.3.4, 10), we have

$$\sin \chi_l^0 = \pi (k \varepsilon y_0)^{-1} (l + 1/2). \quad (7.3.3)$$

Now (7.3.2) may be written as

$$n^2(y) = [1 - (y_0/y)^2 \sin^2 \chi_l^0] \cos^{-2} \chi_l^0. \quad (7.3.4)$$

Since the refraction index only depends on one Cartesian coordinate, a ray picture in the horizontal plane can be easily calculated using the results of Sect. 2.3 and replacing r by x , and z by y . Since $n(y)$ decreases when y decreases, ray $OBCD$ (Fig. 7.3) becomes parallel to the x axis at a certain $y = y_m$ and then propagates away from the coastal line.

Denoting by ϕ_0 the angle which the ray makes with the y axis at point O , we can find y_m by virtue of Snell's law from the relationship $n(y_m) = \sin \phi_0$, $\phi_0 > \pi/2$. Using (7.3.4) we obtain

$$y_m = y_0 \sin \chi_l^0 (1 - \sin^2 \phi_0 \cos^2 \chi_l^0)^{-1/2}. \quad (7.3.5)$$

A ray launched to the coast along the y axis ($\phi_0 = \pi$) turns back at point $y_m = y_0 \sin \chi_l^0$ for which $n(y_m) = 0$. The first normal mode (the smallest value of χ_l^0) approaches the coast closer than any other mode.

The horizontal refraction of normal modes is natural in virtue of the coordinate dependence of the refraction index $n(\mathbf{r})$ determined above. However, this effect can also be easily understood if one considers rays equivalent to normal modes (in the WKB approximation). A ray at each reflection from the sloping bottom

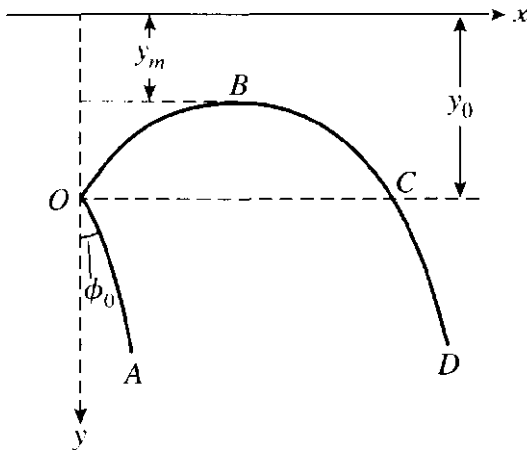


FIGURE 7.3. Rays in the horizontal plane (for a separate normal mode) for the coastal wedge example. The x axis coincides with the coastal line

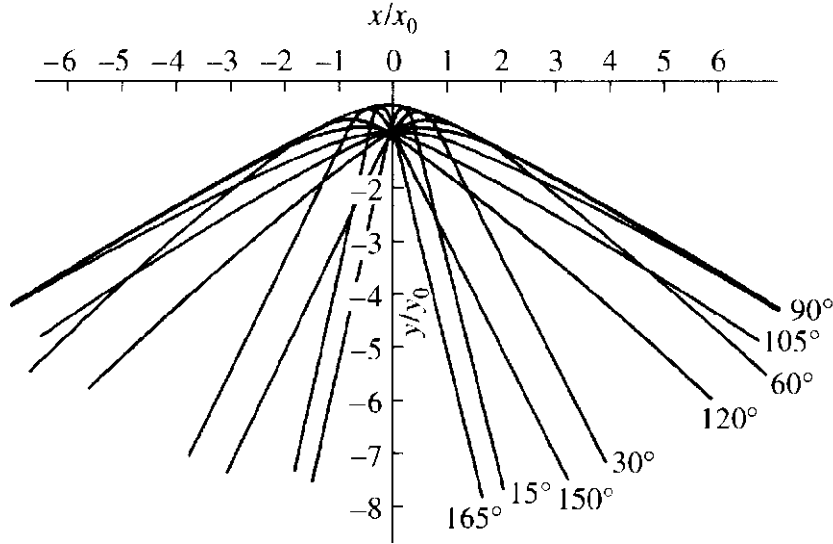


FIGURE 7.4. Rays and their envelope for $l = 0$ in the case of a coastal wedge; the wavelength is equal to the doubled sea depth near a source

changes its inclination angle in the vertical plane and its heading in the horizontal one. A more detailed description can be found in the works of *Harrison* [7.7, 10].

Now we find the ray equation in the horizontal plane for a sloped bottom in the ocean. For those segments which do not include a turning point (segments OA and OB in Fig. 7.3) formula (2.3.2) is written in the case under consideration as

$$x = \sin \phi_0 \int_{y_0}^y [n^2(y) - \sin^2 \phi_0]^{-1/2} dy. \quad (7.3.6)$$

Substituting $n^2(y)$ from (7.3.4), we obtain by elementary integration the ray equation as a hyperbola,

$$y^2(1 - \cos^2 \chi_l^0 \sin^2 \phi_0) = y_0^2 \sin^2 \chi_l^0 + [x(1 - \cos^2 \chi_l^0 \sin^2 \phi_0) \times (\sin \phi_0 \cos \chi_l^0)^{-1} - y_0 \cos \chi_l^0 \cos \phi_0]^2. \quad (7.3.7)$$

The envelope of this family of rays is also a hyperbola which is given by [7.10]

$$y^2 = x^2 \tan^2 \chi_l^0 + y_0^2 \sin^2 \chi_l^0. \quad (7.3.8)$$

It passes between the source and coastal line and has an asymptote $y = x \tan \chi_l^0$ which makes the same angle χ_l^0 with the x axis as a ray corresponding to a given normal mode makes with the horizontal. The exterior region of this hyperbola is a shadow zone not penetrated by rays.

A number of rays and their envelope for the fundamental mode $l = 0$ for $\sin \chi_l^0 = \pi/(2kh_0) = 1/2$, $\lambda = 2h_0$ are shown in Fig. 7.4.

7.4 Parabolic Equation Method

Recently another approximate method has received widespread use in underwater acoustics—the parabolic equation method first suggested by *Leontovich* and *Fock* [7.11] in the theory of radio wave propagation in the atmosphere. Application of

this method became possible due to the small grazing angles which are characteristic of long-range sound propagation in the ocean. As a rule, these angles are not greater than 10° .

We will again proceed from the Helmholtz equation

$$\Delta p + k_0^2 n^2(r, \varphi, z) p = 0. \quad (7.4.1)$$

Here $k_0 = \omega/c_0$, c_0 being the sound velocity at some reference depth, for example, at the axis of the sound channel. In a cylindrical coordinate system r, φ, z one has

$$\Delta p = \frac{1}{r} \frac{\partial}{\partial r} \left(r \frac{\partial p}{\partial r} \right) + \frac{1}{r^2} \frac{\partial^2 p}{\partial \varphi^2} + \frac{\partial^2 p}{\partial z^2}. \quad (7.4.2)$$

The solution of (7.4.1) for waves propagating in the directions close to the horizontal may be attempted in the form³

$$p(r, \varphi, z) = F(r, \varphi, z) H_0^{(1)}(k_0 r). \quad (7.4.3)$$

Here the Hankel function $H_0^{(1)}(k_0 r)$ describes the part of the solution rapidly varying in the r direction, and $F(r, \varphi, z)$ is a slowly varying function in all three coordinates.

Substituting (7.4.3) into (7.4.1) and considering the sound field in the wave zone ($k_0 r \gg 1$) where

$$H_0^{(1)}(k_0 r) \sim [2/(\pi k_0 r)]^{1/2} \exp(ik_0 r), \quad (7.4.4)$$

we obtain an equation for F

$$\frac{\partial^2 F}{\partial r^2} + 2ik_0 \frac{\partial F}{\partial r} + \frac{1}{r^2} \frac{\partial^2 F}{\partial \varphi^2} + \frac{\partial^2 F}{\partial z^2} + k_0^2 (n^2 - 1) F = 0. \quad (7.4.5)$$

In virtue of the small variations of F over a distance of the order of the wavelength, we have $\partial F / \partial r \ll k_0 F$. Taking this into account, we neglect the first term in (7.4.5) which is small, at least compared with the second one, and then we obtain our main equation of the parabolic type

$$2ik_0 \frac{\partial F}{\partial r} + \frac{1}{r^2} \frac{\partial^2 F}{\partial \varphi^2} + \frac{\partial^2 F}{\partial z^2} + k_0^2 (n^2 - 1) F = 0. \quad (7.4.6)$$

The subsequent simplifications of this equation are the following. At great ranges from a source we may neglect the curvature of the wave front and set $r d\varphi = dy$. As a result, we obtain

$$2ik_0 \frac{\partial F}{\partial r} + \frac{\partial^2 F}{\partial y^2} + \frac{\partial^2 F}{\partial z^2} + k_0^2 (n^2 - 1) F = 0. \quad (7.4.7)$$

If variations of the sound field with azimuth can be neglected, we have a simpler equation

$$2ik_0 \frac{\partial F}{\partial r} + \frac{\partial^2 F}{\partial z^2} + k_0^2 [n^2(r, z) - 1] F = 0. \quad (7.4.8)$$

³In this presentation of the parabolic equation method we follow mainly *Tappert* [7.12].

Taking an imaginary part of $n(r, z)$ into account also allows us to describe the absorption of waves.

The procedure of working with equations (7.4.6–8) is the following. At first, one chooses some range $r = r_0$ sufficiently small that the field could be evaluated by some other methods (method of geometrical acoustics, for example), but sufficiently large so that the parabolic equation method would be applicable. Then, by means of (7.4.8) and using computers, one continues the field $F(r_0, z)$ for larger values of r step by step up to a desirable limit. One of the methods of fitting parabolic equation solutions to a field near the source can be found in *Tappert's* lecture [7.12]. The boundary conditions for $F(r, z)$ at the water surface and bottom are the same, as in the other methods.

The main advantage of the parabolic equation method consists in the possibility of evaluating sound fields in the ocean with a sound velocity that depends upon all three coordinates. Moreover, as a slowly changing envelope F of the sound field is of interest in this case, then computations can be carried out over spatial scales greatly exceeding the sound wavelength. This greatly reduces the necessary computer time. But the parabolic equation method has some limitations—it neglects backscattering and the phase of waves travelling in the forward direction is determined with an error that grows as the distance from the sound source increases.

Following *McDaniel* [7.13] we apply the parabolic equation method to the case of horizontally stratified medium [$n = n(z)$]. Comparing results obtained in this way with those following from the exact normal mode method we can evaluate the limits of validity of the parabolic equation method.

At sufficiently large range the m th normal mode is given by

$$p_m = A_m r^{-1/2} u_m(z) \exp(i\xi_m r), \quad (7.4.9)$$

where $u_m(z)$ and ξ_m are the eigenfunctions and eigenvalues of the depth equation

$$\frac{d^2 u_m}{dz^2} + [k_0^2 n^2(z) - \xi_m^2] u_m = 0, \quad (7.4.10)$$

and A_m is a constant.

The parabolic equation (7.4.8) for $n = n(z)$ also has a solution in the form of normal modes. Hence, we set

$$F_m = u_m(z) R_m(r) \quad (7.4.11)$$

and separate the variables in (7.4.8), denoting a separation constant as ξ_m^2 . As a result, the equation for $u_m(z)$ coincides with (7.4.10), and the equation for $R_m(r)$ is

$$\frac{dR_m}{dr} = \frac{i}{2k_0} (\xi_m^2 - k_0^2) R_m. \quad (7.4.12)$$

The solution of the latter is

$$R_m = A_m \exp \left[\frac{i}{2k_0} (\xi_m^2 - k_0^2) r \right]. \quad (7.4.13)$$

In order to obtain p_m we need, according to (7.4.3, 4), to multiply F_m in (7.4.11) by $r^{-1/2} \exp(ik_0 r)$. As a result we obtain an expression of the same form as (7.4.9), in which the exponent will be $\xi'_m r$ instead of $\xi_m r$ where $\xi'_m = (k_0^2 + \xi_m^2)/2k_0$.

Thus, the parabolic approximation gives a somewhat distorted value of the phase velocity (and the group velocity, too) of normal modes. This gives rise to the distortion of the normal-mode phase which increases with range. In turn, the phase distortion of each mode leads to the distortion of the interference pattern of the sound field. The closer ξ_m to k_0 is, i.e., the closer the direction of propagation is to the horizontal, the smaller all these distortions.

For estimating the error in the phase of a normal mode we consider the case of the homogeneous ocean ($c = c_0 = \text{const.}$) of constant depth h , bounded by the absolutely rigid bottom from below and the flat surface above. According to (5.3.5) we have for this case

$$\xi_m^2 = k_0^2 - (\pi/h)^2(m + 1/2)^2. \quad (7.4.14)$$

Rays may correspond to the normal mode of a number m and have the grazing angle χ_m found from the relation $\xi_m = k_0 \cos \chi_m$ which, by virtue of (7.4.14), becomes

$$\sin \chi_m = (\pi/k_0 h)(m + 1/2). \quad (7.4.15)$$

Since we bear in mind the small-angles approximation, we suppose that $(\pi/k_0 h)(m + 1/2) \ll 1$.

The error in the phase of a normal mode can be found by expanding (7.4.14) in a power series of $\pi(m + 1/2)/k_0 h$. Then

$$(\xi'_m - \xi_m)r = \left(\frac{k_0^2 + \xi_m^2}{2k_0} - \xi_m \right) r \approx \frac{k_0 r}{8} \left(\frac{\pi(m + 1/2)}{k_0 h} \right)^4 = \frac{1}{8} k_0 r \sin^4 \chi_m. \quad (7.4.16)$$

We may expect that wave phases, and, consequently, the interference pattern will be correctly given if this value is small compared with unity, i.e.,

$$k_0 r \sin^4 \chi_m < 1. \quad (7.4.17)$$

There is reason to suppose that this condition is also valid for the stratified ocean [$n = n(z)$]. For more complete analysis of the errors of the parabolic equation method we refer the reader to the work by *DeSanto* [7.14]. This author, together with *Baer* [7.15], has proposed some modification of the parabolic equation method which reduces its error substantially. Accordingly, we use the following expression for p in terms of F instead of (7.4.3)⁴

$$p(r, z) = \left[F(r, z) + \frac{i r}{2k} \frac{\partial^2 F}{\partial r^2} \right] (k_0 r)^{-1/2} \exp(ik_0 r). \quad (7.4.18)$$

The second term in the square brackets is new. If it is neglected, (7.4.18) reduces to (7.4.3) (at $k_0 r \gg 1$).

⁴It is convenient here to denote by F the quantity which in [7.15] is denoted by p .

Equation (7.4.18), called the corrected parabolic approximation (CPA), was compared with an exact normal mode example [7.16] and resulted in an improvement in the amplitude over the parabolic approximation, and a considerable improvement in the phase (see also [5.4]).

On the basis of a parabolic equation solution it is possible to introduce a functional which is the exact solution of the Helmholtz equation (7.4.1). Such a functional was first introduced by *Polyanskii* [7.17] for a two-dimensional horizontally stratified waveguide. For a three-dimensional case including a range-dependent waveguide an analogous integral transform has been obtained by *DeSanto* [7.14, 18] which we will follow in the discussion below.

For the case of a stratified medium which is homogeneous in the horizontal plane, this functional has the form

$$p(r, z) = C \int_0^\infty F(t, z) t^{-1} \exp(i\varphi) dt, \quad (7.4.19)$$

where

$$\varphi \equiv k_0(t + r^2 t^{-1})/2 \quad (7.4.20)$$

and C is a constant.

The validity of (7.4.19) can be proved either by a direct substitution into (7.4.1), or using an expression for F as a sum of modes. We follow the latter way.

Taking into account (7.4.11, 13) we obtain

$$F(t, z) = \sum_m A_m u_m(z) \exp[i(\xi_m^2 - k_0^2)r/2k_0]. \quad (7.4.21)$$

Now, we substitute (7.4.21) into (7.4.19). This yields

$$p(r, z) = C \sum_m A_m u_m(z) \int_0^\infty \exp\left[i\left(\alpha_m^2 t + \frac{\beta^2}{4t}\right)\right] t^{-1} dt, \quad (7.4.22)$$

where

$$\alpha_m \equiv \xi_m (2k_0)^{-1/2}, \quad \beta \equiv r (2k_0)^{1/2}.$$

The integral in (7.4.22) is equal to $\pi i H_0^{(1)}(\xi_m r)$ [7.19]. As a result, we obtain for $p(r, z)$ the expression which is identical to the Helmholtz equation solution (6.4.8) if we assume $C = 1/\pi i$ and $u_m(z) \equiv \psi_m(z)$.

Calculating the integral in (7.4.19) by the method of stationary phase (stationary point $t = r$), we obtain an approximate solution

$$p(r, z) \sim C (2/\pi k_0)^{1/2} r^{-1/2} \exp(ik_0 r) F(r, z),$$

which is identical to (7.4.3) at $k_0 r \gg 1$ and $C = 1/\pi i$. Thus, the approximate solution obtained by the parabolic equation method coincides with the asymptotics of the exact solution to the Helmholtz equation.

For a range-dependent waveguide with cylindrical symmetry, the corresponding functional has the form

$$p(r, z) = C \int_0^\infty F(t, z) V(t, r, z) t^{-1} \exp(i\varphi) dt, \quad (7.4.23)$$

where $V(t, r, z)$ satisfies the equation

$$\begin{aligned} & \frac{\partial^2 V}{\partial r^2} + \left(\frac{1}{r} + \frac{2ik_0 r}{t} \right) \frac{\partial V}{\partial r} + \frac{\partial^2 V}{\partial z^2} + 2ik_0 \frac{\partial V}{\partial t} + 2 \frac{\partial V}{\partial z} \frac{\partial}{\partial z} \ln F \\ & = k_0^2 [n^2(z, t) - n^2(z, r)] F. \end{aligned} \quad (7.4.24)$$

Equation (7.4.24) is rather complicated since the coefficient before $\partial V / \partial z$ is a solution to (7.4.8) in its turn. However, the presence of the stationary point $t = r$ allows us to obtain a simple approximate solution. Indeed, at $t = r$ the right-hand side of (7.4.24) becomes zero and the solution to this particular equation is a constant. Since C is arbitrary, this constant may be chosen to be unity. Note that for a horizontally stratified medium $n = n(z)$ we have $V = 1$ at any t .

If the refraction index has the form

$$n^2(z, r) = n_0^2(z) + \mu(z, r),$$

the right-hand side of (7.4.24) is proportional to μ . For typical oceanic conditions, μ is a small quantity ($\sim 10^{-2}$) and, therefore, the function V is very close to unity.

Now expanding the functions $V(t, r, z)$, $F(t, z)$, and $n^2(z, t)$ in the vicinity of $t = r$ in a power series of $(t - r)$ and equating separately the terms of the same orders, we obtain a recursive system for the coefficients $V^{(m)}(r, z)$ of the expansion of $V(t, r, z)$. The first four coefficients (omitting their arguments) [7.14] are:

$$\begin{aligned} V^{(0)} &= 1, & V^{(1)} &= -1/2r, & V^{(3)} &= 1/2r^2, \\ V^{(3)} &= -r^{-3} + k_0 \partial n^2 / \partial r. \end{aligned} \quad (7.4.25)$$

We see that the correction related to the variation of the refraction index occurs in the third-order term.

Antiwaveguide Sound Propagation

In contrast to waveguide propagation, antiwaveguide propagation of sound occurs when a ray leaving a source never returns to the depth of its source. An example of antiwaveguide propagation is given in Fig. 1.8. Here we shall consider this kind of propagation for two different cases, i.e., depending on whether the velocity gradient dc/dz at an antiwaveguide axis is nonzero (Sect. 8.1) or equals zero (Sects. 8.2, 3).

8.1 Linear Antiwaveguide Adjacent to Water Surface

Let us assume that in the half-space $z > 0$ bounded by a free water surface at $z = 0$, the square of the refractive index is given by the linear law

$$n^2(z) = 1 + az. \quad (8.1.1)$$

At small az it approximately corresponds to the linear law for sound velocity $c(z)$ (Sect. 6.6). Equation (6.5.4) with $k(z) = k_0 n(z)$ is reduced to (6.6.12) if we set

$$t = t_0 - z/H,$$

where

$$t_0 = H^2(\xi^2 - k_0^2), \quad H = (ak_0^2)^{-1/3}. \quad (8.1.2)$$

The sound field at an arbitrary point is again described by (6.6.6) with the properly chosen eigenfunctions $\psi_l(z)$.

For the antiwaveguide conditions these functions at $z \rightarrow \infty$ must represent outgoing waves. This condition is satisfied by the Airy function $Z(t)$ (Sect. 6.6) whose asymptotic representation as $z \rightarrow \infty$ is, by virtue of (6.6.14, 16),

$$Z(t) \sim (-t)^{-1/4} \exp[i(\nu + \pi/4)], \quad \nu = \frac{2}{3} \left(\frac{z}{H} - t_0 \right)^{3/2}. \quad (8.1.3)$$

The boundary condition requires that this function be zero at $z = 0$ (free water surface),

$$Z(t)_{z=0} = 0 \quad \text{or} \quad Z(t_0) = 0, \quad (8.1.4)$$

which gives the equation for eigenvalues ξ_l .

Taking into account the results obtained in Sect. 6.6, the solution of (8.1.4) may also be written as

$$t_0 \equiv t_{0l} = y_l \exp(i\pi/3). \quad (8.1.5)$$

Using the relation between t_0 and ξ (8.1.2), we obtain

$$\xi_l^2 = k_0^2 + (y_l/H^2) \exp(i\pi/3). \quad (8.1.6)$$

Thus, all ξ_l are complex and, therefore, all waves¹ are attenuated. Attenuation increases with the mode number l .

If we take into account that

$$\frac{\partial}{\partial z} = -\frac{1}{H} \frac{\partial}{\partial t}, \quad \frac{\partial}{\partial \xi} = 2\xi H^2 \frac{\partial}{\partial t},$$

the acoustic pressure at point (r, z) can be written using (6.6.6) as

$$p(r, z) = \frac{-i\pi}{H} \sum_l Z(t_l) Z(t_{1l}) \left[\frac{\partial Z}{\partial t} \right]_{t_{0l}}^{-2} H_0^{(1)}(\xi_l r) \quad (8.1.7)$$

where

$$t_{0l} = y_l \exp(i\pi/3), \quad t_l = t_{0l} - z/H, \quad t_{1l} = t_{0l} - z_1/H.$$

As usual, the sound source is assumed to be at point $(0, z)$.

It is of interest to consider the asymptotic behaviour of (8.1.7) for $z_1, z \gg H$, $\xi_l r \gg 1$. In this case t_l and t_{1l} are negative, and their moduli are large. Then, using asymptotic representations of the Hankel function and of the function $Z(t)$ (8.1.3), we have

$$Z(t_l) Z(t_{1l}) H_0^{(1)}(\xi_l r) = 2^{1/2} (\pi \xi_l r)^{-1/2} (t_l t_{1l})^{-1/4} \times \exp[i(v_l + v_{1l} + \xi_l r + \pi/4)], \quad (8.1.8)$$

where

$$\begin{aligned} v_l &= (2/3)(z/H)^{3/2} (1 - t_{0l} H/z)^{3/2} \approx (2/3)(z/H)^{3/2} - (z/H)^{1/2} t_{0l}, \\ v_{1l} &\approx (2/3)(z_1/H)^{3/2} - (z_1/H)^{1/2} t_{0l}, \\ \xi_l &= (k_0^2 + t_{0l}/H^2)^{1/2} \approx k_0 + t_{0l}(2k_0 H^2)^{-1}. \end{aligned} \quad (8.1.9)$$

Now the exponential in (8.1.8) is

$$\begin{aligned} v_l + v_{1l} + \xi_l r &= k_0 r + (2/3)[(z/H)^{3/2} + (z_1/H)^{3/2}] \\ &\quad + t_{0l}(2k_0 H^2)^{-1}(r - r_m), \end{aligned} \quad (8.1.10)$$

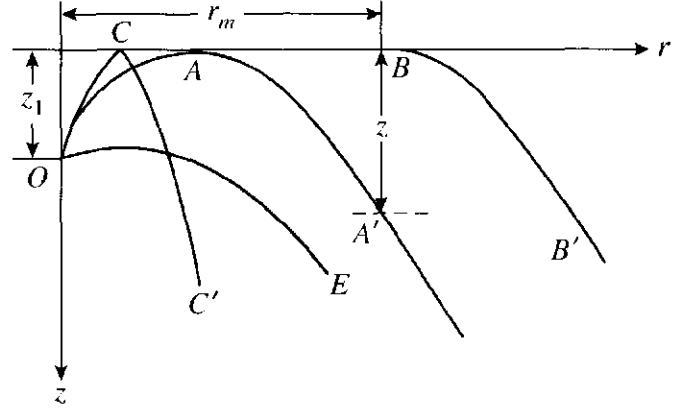
where

$$r_m = 2(\sqrt{z} + \sqrt{z_1})/\sqrt{a}. \quad (8.1.11)$$

In Fig. 8.1 OAA' is the limiting ray tangent to the water surface ($z = 0$). On the left of the line AA' there is a zone insonified by the direct rays and rays reflected from

¹For reasons which will be clear in Sect. 8.2 these waves are called quasi-modes.

FIGURE 8.1. Formation of a geometrical shadow zone, and diffraction rays



the water surface (rays OE and OCC'). On the right of AA' there is a geometric shadow zone where neither direct rays nor rays reflected from the surface arrive, and the acoustic pressure in the geometric approximation equals zero.

It can be easily shown that r_m is the horizontal distance covered by the limiting ray OAA' for fixed z and z_1 (Fig. 8.1). In fact, $r_m = r_{OA} + r_{AA'}$ where r_{OA} and $r_{AA'}$ are the horizontal projections of OA and AA'. r_{OA} can be found from (2.4.1) if we take into account that, for $az \ll 1$, (8.1.1) corresponds to the linear law for $c(z)$, $c(z) \approx c_0(1 - az/2)$. Therefore, (2.4.1) should be set so that $D_i = r_{OA}$, $\chi_{i-1} = 0$, $\chi_i = \chi_1$, $a_i = a/2$, and we obtain $r_{OA} = (2/a) \sin \chi_1$. Now, keeping in mind that χ_1 is small, and using formula (2.2.3) which in our case gives $\chi_1 = (az_1)^{1/2}$, we obtain $r_{OA} = 2(z_1/a)^{1/2}$. The range $r_{AA'}$ is obtained from r_{OA} by replacing z_1 by z , and we get expression (8.1.11) for r_m .

Now, using the value of H from (8.1.2), we write the asymptotic representation of (8.1.7) in the form

$$\begin{aligned}
 p(r, z) \approx & (2\pi/r)^{1/2} (a/k_0)^{1/6} (zz_1)^{-1/4} \\
 & \times \exp\{i[k_0 r + (2/3)k_0 a^{1/2}(z^{3/2} + z_1^{3/2}) + \pi/4]\} \sum_l \left(\frac{\partial Z}{\partial t}\right)_{t_{0l}}^{-2} \\
 & \times \exp[(y_l/4)(i - \sqrt{3}) \times (k_0 a^2)^{1/3}(r - r_m)]. \quad (8.1.12)
 \end{aligned}$$

It can be seen that beginning at the boundary of the geometrical shadow each wave decays with the distance, according to the law $\exp[-\beta_l(r - r_m)]$, where

$$\beta_l = (\sqrt{3}/4)(k_0 a^2)^{1/3} y_l = 3^{1/2} \cdot 2^{-2} y_l / (H^2 k_0). \quad (8.1.13)$$

For $(r - r_m) \gg H$, only the first wave in (8.1.12) may be considered for which $y_l = 2.2338$. For $|r - r_m| \lesssim H$, i.e., in the transition zone of width H encompassing section AA' of the limiting ray, many waves should be taken into account. It should also be mentioned that the asymptotic representation (8.1.12) is not valid in the layer having a width of order H adjacent to the water surface.

The sound field in the geometric shadow zone can be described on the basis of ray representations if we introduce the concept of diffraction rays, following Keller and collaborators (see, for example, [8.1]), and Brekhovskikh [Ref. 8.2, Sect. 54]. To obtain diffraction rays one should imagine that the limiting ray OAA' in Fig. 8.1

is split at point A into the rays AA' and AB, the latter passing along the boundary and at each point giving rise to diffraction rays (one of them, BB', is shown in the figure) propagating in the medium according to ordinary ray laws. In the limit $k_0 \rightarrow \infty$ the amplitude of the diffraction rays becomes zero.

8.2 Symmetric Antiwaveguide: Quasi-Modes²

The main features of the case considered in the previous section is that the vertical gradient of the refraction index has a finite value at the antiwaveguide axis (coinciding with the water surface $z = 0$). The character of propagation is considerably different when this gradient equals zero (Fig. 8.2a). In particular, a limiting ray and a shadow zone are absent in this case (Fig. 8.2b). The ray with zero grazing angle at the axis approaches this axis asymptotically (at $r \rightarrow \infty$), as can be seen, for example, from (2.3.2) if one sets $\cos \chi_1 = n(0)$ there and expands $n^2(z) - n^2(0)$ in a series in z (beginning with z^2). In this case, we obtain $z \rightarrow 0$ and $r \rightarrow \infty$ as $\ln z$.

Let us consider a case when the wave number squared is described by a symmetric function with respect to the plane $z = 0$,

$$k^2(z) = k_1^2(1 - A/\cosh^2 bz). \quad (8.2.1)$$

As $z \rightarrow \pm\infty$, we have $k(z) \rightarrow k_1$. The quantity b is inverse to the width of the antiwaveguide.

We shall start from the general formulae (6.5.10) for the sound pressure of a point source. The functions $\tilde{p}_1(z)$ and $\tilde{p}_2(z)$ as $z \rightarrow \pm\infty$ must correspond to outgoing waves at infinity. Denoting

$$\mu = (k_1^2 - \xi^2)^{1/2}/b \quad (8.2.2)$$

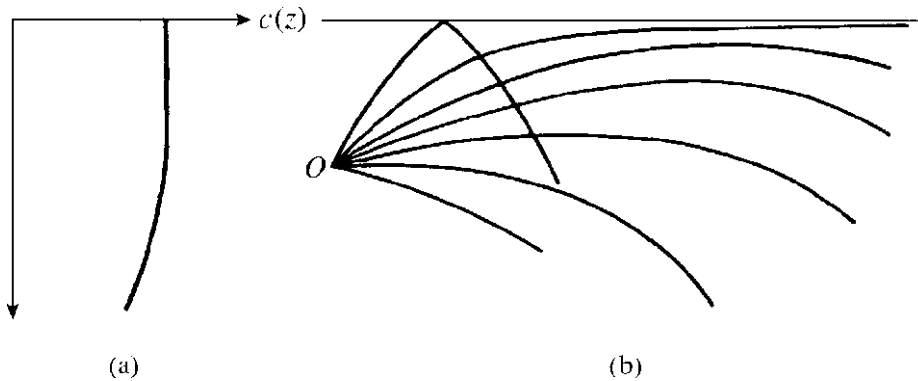


FIGURE 8.2. Profile $c(z)$ of the antiwaveguide for $c'(0) = 0$ and (b) schematic ray diagram

²The authors acknowledge A.G. Voronovich for his help in development of the present section and the next one.

we have

$$\begin{aligned}\tilde{p}_1(z) &\rightarrow \exp(-i\mu bz), & z &\rightarrow -\infty, \\ \tilde{p}_2(z) &\rightarrow \exp(i\mu bz), & z &\rightarrow +\infty.\end{aligned}\quad (8.2.3)$$

The radical in (8.2.2) is chosen so that

$$\text{Im}\{\mu\} \geq 0. \quad (8.2.4)$$

This assures finite values of \tilde{p}_1 and \tilde{p}_2 as $z \rightarrow \pm\infty$. The functions $\tilde{p}_1(z)$ and $\tilde{p}_2(z)$ must satisfy (6.5.4). Denoting

$$M = Ak_1^2/b^2 \quad (8.2.5)$$

this equation can be written as

$$\tilde{p}'' + b^2 \left(\mu^2 - \frac{M}{\cosh^2 bz} \right) \tilde{p} = 0. \quad (8.2.6)$$

It can be shown by direct substitution that the solution of (8.2.6) is

$$\tilde{p}_1(z) = \exp(-i\mu bz) F(1+s, -s, 1-i\mu; \zeta_1), \quad \zeta_1 = (1 + \tanh bz)/2 \quad (8.2.7)$$

where $F(a, b, c; \zeta)$ is the hypergeometric function satisfying the equation [8.3]

$$\frac{d^2 F}{d\zeta^2} - \frac{(1+a+b)\zeta - c}{\zeta(1-\zeta)} \frac{dF}{d\zeta} - \frac{ab}{\zeta(1-\zeta)} F = 0. \quad (8.2.8)$$

The function F is represented by a series

$$F(a, b, c; \zeta) = 1 + \frac{a \cdot b}{1 \cdot c} \zeta + \frac{a(a+1)(b+1)}{1 \cdot 2 \cdot c(c+1)} \zeta^2 + \dots \quad (8.2.8')$$

The parameter s in (8.2.7) is any root of the equation $s(s+1) + M = 0$. We shall take

$$s = -\frac{1}{2} - \left(\frac{1}{4} - M \right)^{1/2}, \quad (8.2.9)$$

setting for $M > 1/4$, $(1/4 - M)^{1/2} = i(M - 1/4)^{1/2}$. The fulfillment of the first condition of (8.2.3) is obvious since $\tanh bz \rightarrow -1$, $\zeta_1 \rightarrow 0$, $F \rightarrow 1$ as $z \rightarrow -\infty$. As the second independent solution of (8.2.6) we take

$$\begin{aligned}\tilde{p}_2(z) &= \tilde{p}_1(-z) = \exp(i\mu bz) F(1+s, -s, 1-i\mu; \zeta_2), \\ \zeta_2 &= (1 - \tanh bz)/2.\end{aligned}\quad (8.2.10)$$

The latter satisfies the second condition in (8.2.3). As is seen from formulac (6.5.10), it is necessary to know the Wronskian w . Since it does not depend on z , we calculate it for $z \rightarrow -\infty$, taking (8.2.3) for \tilde{p}_1 . To find $\tilde{p}_2(-\infty)$ we use the

known formula for hypergeometric functions [$\Gamma(x)$ is the gamma function]

$$\begin{aligned} F(a, b, c; \zeta) &= \frac{\Gamma(c)\Gamma(c-a-b)}{\Gamma(c-a)\Gamma(c-b)} F(a, b, a+b-c+1; 1-\zeta) \\ &+ \zeta^{1-c}(1-\zeta)^{c-a-b} \frac{\Gamma(c)\Gamma(a+b-c)}{\Gamma(a)\Gamma(b)} \\ &\times F(1-a, 1-b, c-a-b+1; 1-\zeta). \end{aligned} \quad (8.2.11)$$

As $z \rightarrow -\infty$ we have $\zeta_2 \rightarrow 1$, and from (8.2.11), using (8.2.9) and the formula $\Gamma(x)\Gamma(1-x) = \pi/\sin \pi x$ [8.3], we find as $z \rightarrow -\infty$

$$\tilde{p}_2 \rightarrow \frac{\Gamma(1-i\mu)\Gamma(-i\mu)}{\Gamma(-i\mu-s)\Gamma(1-i\mu+s)} \exp(i\mu bz) + i \frac{\sin \pi s}{\text{sh } \pi \mu} \exp(-i\mu bz). \quad (8.2.12)$$

Now, taking into account the relationship $\Gamma(1-i\mu) = -i\mu\Gamma(-i\mu)$, we obtain for the Wronskian

$$w = \tilde{p}'_1 \tilde{p}_2 - \tilde{p}'_2 \tilde{p}_1 = \frac{2b\Gamma^2(1-i\mu)}{\Gamma(-i\mu-s)\Gamma(1-i\mu+s)}. \quad (8.2.13)$$

Let us note, by the way, that considering the first term in (8.2.12) as a plane wave incident on the layer defined by (8.2.1), the second term as a wave reflected from it, and \tilde{p}_2 given by (8.2.3) as a wave transmitting through the layer, we can obtain expressions for the reflection V and transmission W coefficients for the layer

$$V = \frac{2\mu b \sin \pi s}{w \text{sh } \pi \mu}, \quad W = \frac{-2i\mu b}{w}. \quad (8.2.14)$$

Using the value of w from (8.2.13), we obtain from (6.5.10) for the sound pressure

$$p(r, z) = (2b)^{-1} \int_{-\infty}^{\infty} \Gamma(-i\mu-s)\Gamma(-i\mu+1+s) \frac{\tilde{p}_1(\xi z) \tilde{p}_2(\xi, z_1)}{\Gamma^2(1-i\mu)} H_0^{(1)}(\xi r) \xi d\xi. \quad (8.2.15)$$

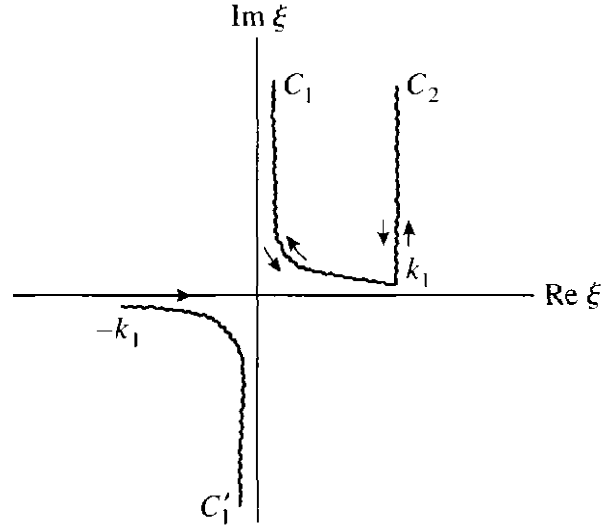
We calculate the integral by deforming the original integration path into an infinite semicircle in the upper half-plane over which the integral (as can be easily shown) is zero. The integrand is a double-valued function of ξ due to the radical $\mu = (k_1^2 - \xi^2)^{1/2}/b$. The integration path in (8.2.15) passes over the "upper" sheet where the condition (8.2.4) is satisfied. To distinguish "upper" ($\text{Im}\{\mu\} > 0$) and "lower" ($\text{Im}\{\mu\} < 0$) sheets, we make the cuts from the points $\xi = \pm k_1$ along the lines $\text{Im}\{\mu\} = 0$. Assuming that k_1 has a small imaginary part, these cuts are shown by the wavy lines C_1 and C'_1 in Fig. 8.3.

Let us now investigate the singularities of the integrand in (8.2.15). Since the functions

$$\frac{\tilde{p}_1(z)}{\Gamma(1-i\mu)} = \exp(-i\mu bz) F(1+s, -s, 1-i\mu; \zeta_1) / \Gamma(1-i\mu)$$

and $\tilde{p}_2(z) / \Gamma(1-i\mu)$

FIGURE 8.3. Cuts in the complex plane ξ going out from points $\xi = \pm k_1$



have no singularities in the ξ plane,³ the only singular points may be the poles determined by the equations

$$-i\mu - s = -l, \quad -i\mu + 1 + s = -l, \quad l = 0, 1, 2, \dots \quad (8.2.16)$$

where one or another Γ function in the numerator in the integrand (8.2.15) is infinite. The solution of the first equation is

$$\mu = \mu_l = i(s - l) = i \left[-\frac{1}{2} - \left(\frac{1}{4} - M \right)^{1/2} - l \right]. \quad (8.2.17)$$

For $M < 1/4$ when μ is purely imaginary, as well as for $M > 1/4$ when $(1/4 - M)^{1/2} = i(M - 1/4)^{1/2}$, we have $\text{Im}\{\mu_l\} < 0$, i.e., the poles lie on the lower sheet. In the same way this may be proved for the second family of poles for which

$$\mu = \mu_1 = -i(1 + s + l) = -i \left[\frac{1}{2} - \left(\frac{1}{4} - M \right)^{1/2} + l \right]. \quad (8.2.18)$$

Thus, the integrand in (8.2.15) has no poles on the upper sheet. Therefore, the solution of our problem only has a continuous spectrum (the branch-line integral) and does not include normal modes. However, for calculation of the branch-line integral it appears reasonable to displace the integration path from cut C_1 to cut C_2 (Fig. 8.3) since, as we shall see below, the integral over the sides of the latter is easily calculated by the steepest descent method. In this case the integration path passes from the right side of C_1 (where an arrow indicates the upward path direction) over an upper sheet to C_2 without any consequences. On the contrary, the integration path from the left side of C_1 passes in the process of deformation to C_2 over the lower sheet (where $\text{Im}\{\mu\} < 0$), and we must add to the solution the residues at the poles lying on the lower sheet between C_1 and C_2 . This enables

³It can easily be shown, using a series (8.2.8'), that the function $F(a, b, c; \xi)/\Gamma(c)$ is analytic everywhere with respect to the parameter c

us to separate some waves in the solution analogous to normal modes, which are called quasi-modes or leaky (or virtual or improper) modes.

Continuing the analysis of the poles, it can easily be seen that for $M < 1/4$ no poles lie between C_1 and C_2 . In fact, in this case μ_l in (8.2.17, 18) is purely imaginary; hence $\xi_l^2 = k_1^2 - \mu_l^2 b^2 > k_1^2$.

For $M > 1/4$ (8.2.17) is written as

$$\mu_l = -i(l + 1/2) + (M - 1/4)^{1/2}. \quad (8.2.19)$$

We shall show that in this case a finite number of poles can lie between C_1 and C_2 . For this purpose, let us turn to Fig. 8.4a in the ξ plane. This figure shows the quantities μb , $(\mu b)^2$ (both in the fourth quadrant), $\xi^2 = k_1^2 - (\mu b)^2$, and ξ as vectors (the index l is omitted). In this case, $\text{Re}\{\xi\} < k_1$ and, therefore, a pole lies between C_1 and C_2 . However, this is true if condition

$$\text{Re}\{\mu\} > -\text{Im}\{\mu\}, \quad \text{i.e.,} \quad (M - 1/4)^{1/2} > (l + 1/2) \quad (8.2.20)$$

is fulfilled.

The opposite case ($|\arg\{\mu\}| > 45^\circ$) is shown in Fig. 8.4b. Here, $\mu^2 b^2$ is in the third quadrant, which results in the inequality $\text{Re}\{\xi\} > k_1$, and a pole is on the right of C_2 and is thus not interesting to us.

In this way it can be shown that all the poles of the family (8.2.18) lie on the right of C_2 . As a result, we see that quasi-modes will be given by residues at the poles (8.2.19) provided that (8.2.20) is fulfilled. The latter determines the maximum number of quasi-modes l_m

$$l_m = \{(M - 1/4)^{1/2} - 1/2\}, \quad (8.2.21)$$

where the curly brackets $\{\dots\}$ mean the nearest smallest integer. Thus, it is clear that the following conditions are needed for the existence of one quasi-mode ($l = 0$):

$$M > 1/2 \quad \text{or} \quad 2Ak_1^2/b^2 > 1, \quad (8.2.22)$$

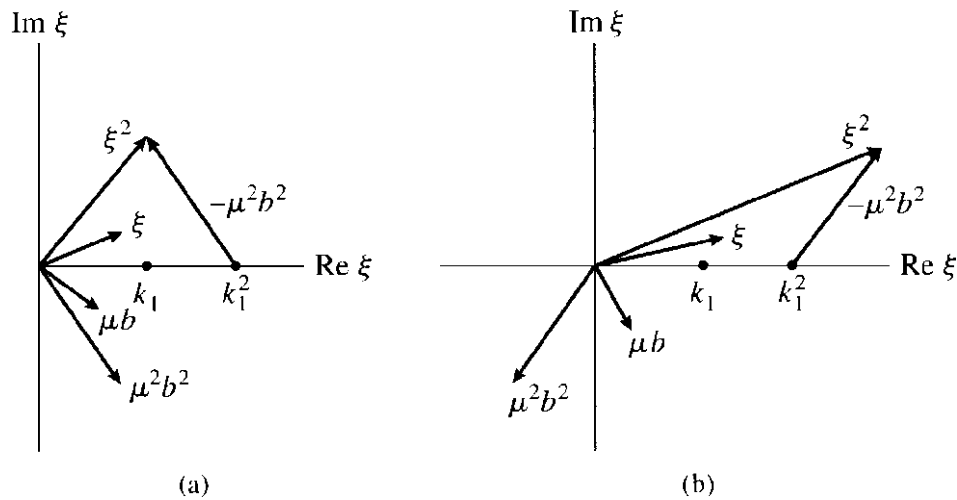


FIGURE 8.4. Analysis of poles in the complex ξ plane

that is, A cannot be too small, and the width of the antichannel $1/b$ cannot be very small compared with the wavelength.

Calculating the residues at the poles by successively using the basic relation for Γ functions

$$\Gamma(z) = (1/z)\Gamma(z+1),$$

one can obtain

$$\Gamma(x-l) \approx \frac{\Gamma(x+1)}{(x-l)(x-l+1)\cdots(x-1)x} = \frac{(-1)^l}{l!} \frac{1}{x}, \quad x \rightarrow 0.$$

Applying this result to $\Gamma(-i\mu-s) = \Gamma[-i(\mu-\mu_l)-l]$ in (8.2.15) in the vicinity of the pole μ_l and setting $x = -i(\mu-\mu_l)$, we obtain in this vicinity

$$\Gamma(-i\mu-s) \approx i \frac{(-1)^l}{l!} \frac{1}{\mu-\mu_l}. \quad (8.2.23)$$

Outside it one can set $\mu = \mu_l + i(s-l)$ in (8.2.15). When estimating the residues we integrate over a variable μ using the relation $d\xi = (d\xi_l/d\mu_l)d\mu = -b^2(\mu_l/\xi_l)d\mu$. Having denoted

$$A_l \equiv \frac{1}{l!} \frac{\Gamma(2s-l+1)}{\Gamma(s-l+1)\Gamma(s-l)}, \quad (8.2.24)$$

$$\begin{aligned} \Psi_l(z) &\equiv \tilde{p}_1(\xi_l, z) = \exp[(s-l)bz] F\left(1+s, -s, 1+s-l; \frac{1+\tanh bz}{2}\right), \\ \tilde{p}_2(\xi_l, z) &= \tilde{p}_1(\xi_l, -z) = \Psi_l(-z), \end{aligned} \quad (8.2.25)$$

we obtain from (8.2.15) for the field determined by a sum of residues

$$p(r, z) = i\pi b \sum_l (-1)^l A_l \Psi_l(z) \Psi_l(-z_1) H_0^{(1)}(\xi_l r). \quad (8.2.26)$$

Using (8.2.11) with $\zeta = \zeta_1$ given by (8.2.7), it can be shown that $\Psi_l(z)$ is an even function with respect to z for even l and an odd for odd l . Then (8.2.26) for the sum of quasi-modes can be written as

$$p(r, z) = i\pi b \sum_l A_l \Psi_l(z) \Psi_l(z_1) H_0^{(1)}(\xi_l r). \quad (8.2.27)$$

It is symmetric with respect to z and z_1 and, therefore, is valid for $z < z_1$ and $z > z_1$ as well. The form of this expression is quite analogous to (6.4.11) for the sum of normal modes in the waveguide. But each quasi-mode in (8.2.27) is a fairly peculiar formation. So according to (8.2.3) we have

$$z \rightarrow -\infty, \quad \Psi_l(z) \rightarrow \exp(-i\mu_l bz)$$

but, as we have seen, $\text{Im}\{\mu_l\} < 0$ and, therefore, Ψ_l grow exponentially as $z \rightarrow -\infty$. It can be easily shown that Ψ_l behaves in the same way as $z \rightarrow +\infty$. Thus, the energy contained in each mode is infinite. In spite of that, they often appear convenient to use [8.4–6].

The quasi-modes always arise if leakage of energy from a channel occurs. In particular, the waves considered in Sect. 8.1 are quasi-modes.

If we use the asymptotic representation of the Hankel function in (8.2.26), we will see that the amplitude of each quasi-mode decreases with distance r according to the law $\exp(-r\text{Im}\{\xi_l\})$. Taking into account that $\xi_l^2 = k_1^2 - \mu_l^2 b^2$, we obtain for small l ($l \ll M^{1/2}$), using the value of μ_l from (8.2.19),

$$\text{Im}\{\xi_l\} = [\Lambda/(1 - A)]^{1/2}(l + 1/2). \quad (8.2.28)$$

The attenuation coefficient does not depend on frequency and increases when l increases. It is shown in [Ref. 8.2, Sect. 55] for an arbitrary $n(z)$ that, when the antichannel axis coincides with the water surface, in the WKB approximation the attenuation coefficient for the lowest quasi-mode ($l = 1$ in our numeration) is equal to $(3/2)[n''(0)]^{1/2}$.⁴ The index of refraction $n(z) = c(0)/c(z)$ is scaled here with respect to the antichannel axis $z = 0$, and it is assumed that $n'(0) = 0$. It is easy to show that the latter expression coincides with (8.2.28) for $l = 1$ and for $n(z)$ under consideration here.

For sufficiently high frequencies the field in the antichannel can be calculated by the ray method. Figures 8.5 and 8.6 show the ray diagrams in the coordinates br and bz for the cases $z_1 = 0$, $bz_1 = 2$, and $A = 0.04$. It can be most easily shown for

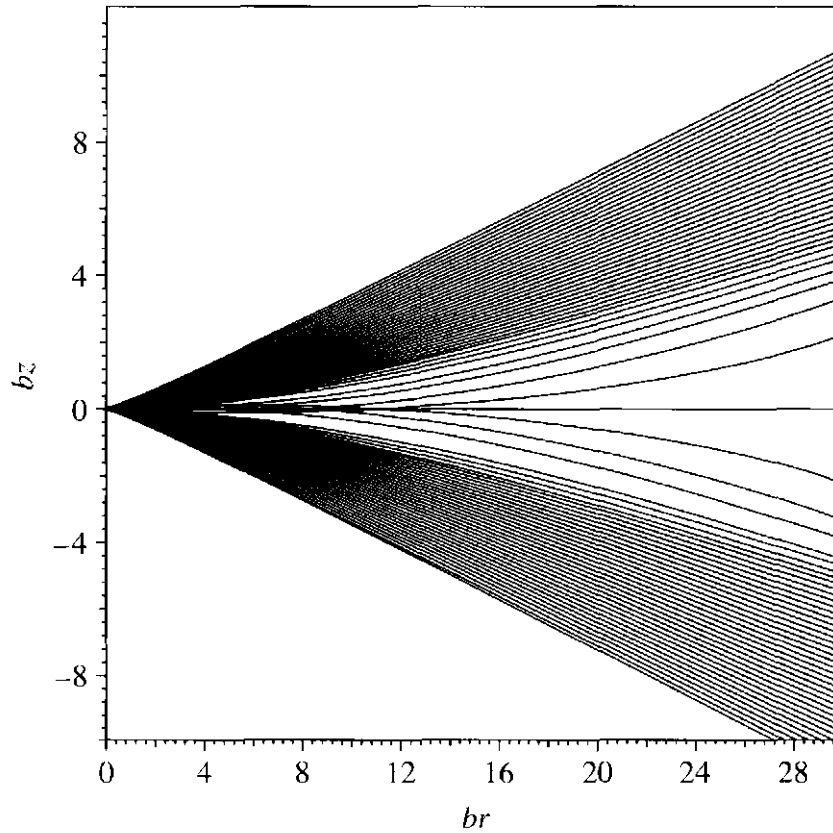
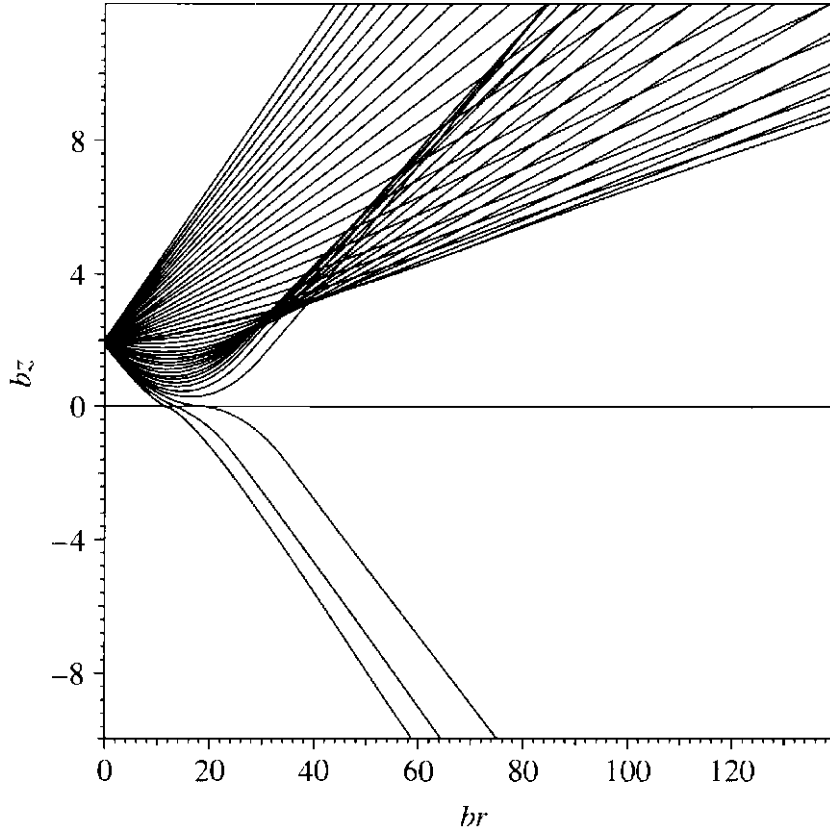


FIGURE 8.5. Ray diagram for $z_1 = 0$, $A = 0.04$

⁴In determining a [Ref. 8.2; Eq. (55.17)] $1/2$ mistakenly stands for unity.

FIGURE 8.6. As in Fig. 8.5 for $b_{z_1} = 2$

the case $z = z_1 = 0$ that the field obtained as a sum of quasi-modes completely coincides with the field in the ray approximation in the region where the latter is valid. The branch-line integral over C_1 can be neglected. Moreover, the sum of quasi-modes will describe the field in some cases when ray theory is invalid, for example, at the caustics. This result seems to be more generally valid than for the case considered here. Thus, for instance, in the case of sound propagation in a liquid layer over a liquid half-space, the quasi-modes will correspond to the rays having partial reflection at the interface with the half-space [8.7].

Summarising this section we note that expressions (8.2.25, 26) for the quasi-modes can also be used when a perfectly rigid or free surface is located at $z = 0$. In the first case, the field will be a sum of (8.2.26) and the field of an image source located symmetrically on the other side of the plane $z = 0$. As a result, the field will be given by a doubled sum of even quasi-modes (8.2.26). In the second case, the field will be a doubled sum of uneven quasi-modes.

8.3 Symmetric Antiwaveguide: Lateral Wave

The result of integration in (8.2.15) along the branch-line C_2 (Fig. 8.2) is called the lateral wave. In order to avoid cumbersome mathematics we consider the lateral wave for a case when a source and receiver are on the antiwaveguide's axis ($z = z_1 = 0$) and assume that $M \gg 1$. These simplifications do not interfere

with understanding the nature of the lateral wave and estimating the scope of its significance.

According to definitions (8.2.7, 10) and the formula for the hypergeometric function [8.3]

$$F\left(a, 1-a, c; \frac{1}{2}\right) = 2^{1-c} \pi^{1/2} \Gamma(c) \left[\Gamma\left(\frac{a+c}{2}\right) \Gamma\left(\frac{1+c-a}{2}\right) \right]^{-1} \\ (c \neq 0, -1, -2, \dots),$$

we have

$$\tilde{p}_1(0) = \tilde{p}_2(0) = F(1+s, -s, 1-i\mu; 1/2) \\ = 2^{i\mu} \pi^{1/2} \Gamma(1-i\mu) \left[\Gamma\left(\frac{2+s-i\mu}{2}\right) \Gamma\left(\frac{1-s-i\mu}{2}\right) \right]^{-1}. \quad (8.3.1)$$

Now, using the known “doubling formula” for Γ -functions

$$\Gamma(2z) = \pi^{-1/2} 2^{2z-1} \Gamma(z) \Gamma(z+1/2)$$

we obtain from (8.2.15) the expression for the lateral wave ($z = z_1 = 0$)

$$p_{\text{lat}} = (4b)^{-1} \int \phi(\mu) H_0^{(1)}(\xi r) \xi d\xi, \quad (8.3.2)$$

where

$$\phi(\mu) = \frac{\Gamma\left(\frac{-s-i\mu}{2}\right) \Gamma\left(\frac{1+s-i\mu}{2}\right)}{\Gamma\left(\frac{1-s-i\mu}{2}\right) \Gamma\left(\frac{2+s-i\mu}{2}\right)} \quad (8.3.3)$$

and the integral is taken along the branch-line sides of C_2 (Fig. 8.3). Since the value of the integrand at the same point but on different sheets only differs by the sign of μ , the integral (8.3.2) can be written as

$$p_{\text{lat}} = (4b)^{-1} \int_{k_1}^{k_1+i\infty} [\phi(\mu) - \phi(-\mu)] H_0^{(1)}(\xi r) \xi d\xi \quad (8.3.4)$$

where $\text{Im}\{\mu\} > 0$.

Expanding the function $\phi(\mu)$ in a series and using the known properties of the Γ function give

$$\phi(\mu) - \phi(-\mu) = 4iB\mu + O(\mu^3), \quad (8.3.5)$$

where

$$B = -\frac{\pi}{2 \sin \pi s} \frac{\Gamma\left(-\frac{s}{2}\right) \Gamma\left(\frac{1+s}{2}\right)}{\Gamma\left(\frac{1-s}{2}\right) \Gamma\left(\frac{2+s}{2}\right)}. \quad (8.3.6)$$

Let us introduce into (8.3.4) a new integration variable s , so that $\xi = k_1 + is^2$,

$0 < s < \infty$. For small s we have

$$\mu \approx -(1/b)(2k_1)^{1/2}s \exp(-i\pi/4).$$

Using an asymptotic representation for the Hankel function, we obtain in (8.3.4) the integral

$$\int_0^\infty \exp(-rs^2)s^2 ds = \left(\frac{1}{4}\right) \pi^{1/2} r^{-3/2}. \quad (8.3.7)$$

Now we see that the cut C_2 in Fig. 8.3 is indeed a path of steepest descent. In the integral (8.3.4), small μ and s are significant at large r . As a result, we obtain

$$z_1 = z = 0: \quad p_{\text{lat}} = -ik_1 B(br)^{-2} \exp(ik_1 r); \quad (8.3.8)$$

p_{lat} has the same typical features as a lateral wave in the case of a waveguide, namely, it propagates with the velocity $c_1 = \omega/k_1$ equal to the sound velocity outside the antiwaveguide and its amplitude decreases as $1/r^2$ at long ranges.

At short ranges from a source quasi-modes supply a large contribution to the field. But since all of them decrease exponentially with range, the field of the lateral wave prevails at $r > r_t$, where r_t is some "transition" range. We will estimate this range for the case $z_1 = z = 0$, $M = A(k_1/b)^2 \gg 1$, i.e., when the antiwaveguide is wide compared to the wavelength. To evaluate B in (8.3.6), we use the asymptotic representation of the Γ function given by

$$x \rightarrow \infty, \quad \Gamma(x+a)/\Gamma(x+b) \rightarrow x^{a-b}. \quad (8.3.9)$$

Then, since $s \approx -1/2 - iM^{-1/2}$, $|s| \gg 1$, we obtain

$$B \approx -2\pi i M^{-1/2} \exp(-\pi M^{1/2}). \quad (8.3.10)$$

Estimating the field of quasi-modes can be done with the least attenuating wave ($l = 0$). Using the asymptotic representation of the Γ -function $\Gamma(x) \rightarrow (2\pi)^{1/2} \exp(-x)x^{x-1/2}$, $x \rightarrow \infty$, we obtain from (8.2.24) the order of magnitude

$$|A_0| \sim (2s)^{1/2} \sim M^{1/4}.$$

Taking into account that $\Psi_l(0)$ is of the order of unity, and an asymptotic representation of the Hankel function and (8.2.27) for $l = 0$, we obtain the order-of-magnitude estimate for the field of quasi-modes

$$\pi^{3/2} b(k_1 r)^{-1/2} M^{1/4} \exp(-bA^{1/2}r/2). \quad (8.3.11)$$

A comparison of (8.3.11) and (8.3.8) using (8.3.10) shows that a range can be taken as a rough estimate for r_t , at which the expressions in the exponents are equal,

$$\frac{1}{2} bA^{1/2} r_t \simeq \pi M^{1/2}$$

or, taking into account that $M^{1/2} \simeq A^{1/2}(k_1 b)$,

$$r_t = 2\pi k_1 / b^2. \quad (8.3.12)$$

Thus, r_t is equal to the range at which the width of the antiwaveguide coincides with that of the Fresnel zone.

Figure 8.7 shows for $\Lambda = 0.04$, $k_1/b = 10$ the range dependence of the amplitude of the first (and single for these conditions) quasi-mode (curve 1), the lateral wave (curve 2), and their sum (curve 3). The oscillations on curve 3 are caused by interference of the quasi-mode and lateral wave. The range at which their amplitudes become equal is $R \equiv k_1 r = 725$. An estimation according to (8.3.12) gives $k_1 r_t = 628$, that should be regarded as satisfactory agreement.

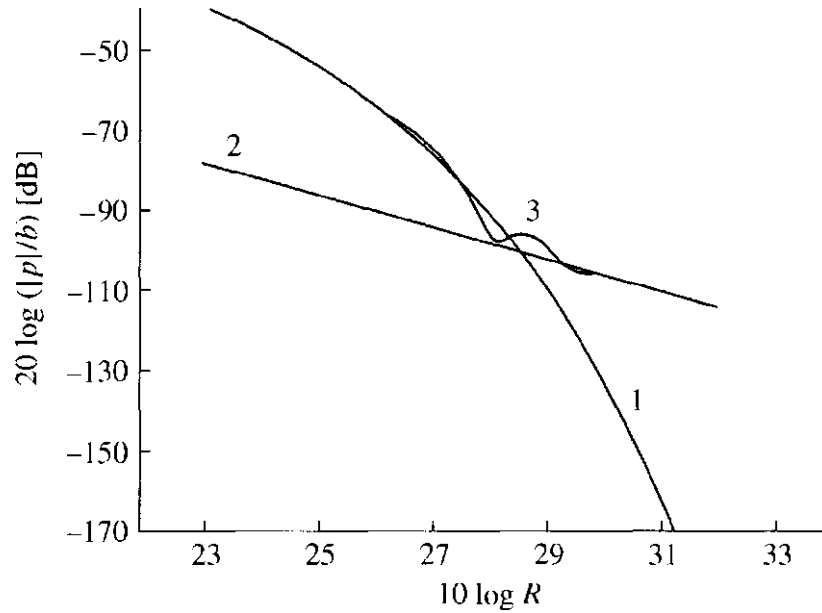


FIGURE 8.7. Range dependence of the amplitude of the first quasi-mode (curve 1), the lateral wave (curve 2), and their sum (curve 3)

Scattering of Sound at Rough Surfaces

As has already been pointed out in Chapter 1, the ocean surface and bottom are random rough surfaces. The exact theory of wave scattering for surfaces of this kind is absent. However, effective approximate methods have been developed for some important particular cases such as roughness with small heights and slopes and large smooth roughness.

9.1 Rayleigh Parameter

The roughness of the sea surface has a continuous spatial spectrum with wavelengths from a few millimetres to hundreds of metres and with amplitude ranging from millimetres to metres. The spectrum of the bottom relief is also very wide—from small “ripple marks” formed by currents on sand to the great mid-oceanic ridges extending over a thousand kilometres with a height of a few kilometres.

In the wave-scattering theory the vertical scale of roughness is usually specified by the *Rayleigh parameter*¹ $P \equiv 2k\sigma \cos \theta_0$ where k is the wave number of sound, θ_0 is the angle of incidence of the sound wave, and σ is the root-mean-square displacement of the rough surface from its mean level. At $P \ll 1$ the roughness of the surface is *small*, and the surface scatters sound slightly—the main part of the sound energy propagates in the specular direction as a coherent wave. The value $P \gg 1$ corresponds to *large* roughness which causes considerable sound scattering in a relatively wide angular interval. To reveal the physical meaning of P let us consider the reflections of sound from the rough surface $z = \zeta(\mathbf{r})$, $\mathbf{r} = \{x, y\}$ and find an additional phase change along the ray ACD relative to the mean plane $z = 0$ (Fig. 9.1). It can be seen from Fig. 9.1 that the phase difference is equal to

$$\Delta\varphi = k(BC + CD) = k(2CD - AB).$$

But since

$$CD = \zeta / \cos \theta_0, \quad AB = 2\zeta \tan \theta_0 \sin \theta_0,$$

¹In Sect. 1.6 the Rayleigh parameter was defined in terms of the grazing angle $\chi = \pi/2 - \theta_0$.

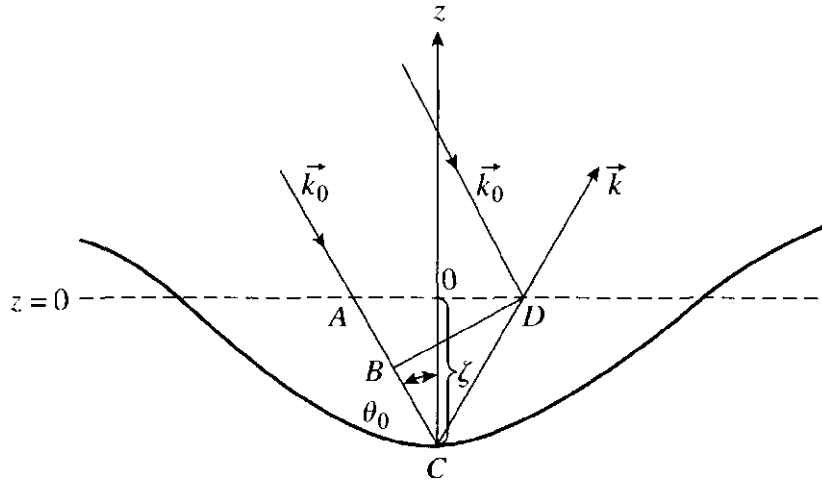


FIGURE 9.1. On the derivation of the Rayleigh parameter

then

$$\Delta\varphi = 2k\zeta \cos \theta_0.$$

Hence, the root-mean-square value of $\Delta\varphi$ is exactly equal to P ,

$$[\langle(\Delta\varphi)^2\rangle]^{1/2} = 2k\sigma \cos \theta_0 = P, \quad \sigma = (\langle\zeta^2\rangle)^{1/2}. \quad (9.1.1)$$

We also see that $P \rightarrow 0$ if $\sigma/\lambda \rightarrow 0$ or $\theta_0 \rightarrow \pi/2$. In this case scattering does not occur and reflection becomes specular.

9.2 Method of Small Perturbation (MSP)

If a rough surface deviates only slightly from a certain mean surface (usually a plane) and has sufficiently small slopes, then the field scattered by this surface can be approximately calculated by the MSP. The basic idea of this method is that the boundary conditions at a rough surface $z = \zeta(\mathbf{r})$ can be transferred to the mean surface by expanding them into a power series of ζ . The sound field in a half-space $z > \zeta$ can also be expanded in powers of ζ , and the conditions which must be satisfied by the first, second and further approximations at the mean surface are found. As a result, the problem of wave scattering at a rough surface is reduced to the problem of radiation by the distribution of “virtual” sound sources.

Rayleigh was the first who used the MSP in his works on the scattering of sound at periodically irregular surfaces [9.1, 2]. Considerable contributions to the development of the MSP were made by *Feinberg* [9.3], and *Bass* and *Fuks* [9.4]

Let us consider the simplest case of a perfectly reflecting rough surface and assume that the xy plane coincides with the mean surface, i.e., $\langle\zeta\rangle = 0$. For the pressure-release surface the boundary condition has a form

$$\text{a) } p[\mathbf{r}, \zeta(\mathbf{r})] = 0 \quad (9.2.1)$$

and for an absolutely rigid surface

$$\text{b)} \quad \left(\frac{\partial p}{\partial n} \right)_{z=\zeta} = (\nabla p \cdot \mathbf{n})_{z=\zeta} = 0 \quad (9.2.2)$$

where $\mathbf{n} = \{\mathbf{n}_\perp, \mathbf{n}_z\}$ is the unit vector of the inner normal to a rough surface, and

$$\frac{\mathbf{n}_\perp}{\mathbf{n}_z} = -\nabla_\perp \zeta, \quad \nabla_\perp = \left\{ \frac{\partial}{\partial x}, \frac{\partial}{\partial y} \right\}. \quad (9.2.3)$$

Now we expand the boundary conditions (9.2.1, 2) in a power series of ζ retaining only the terms not higher than ζ ,

$$\begin{aligned} \text{a)} \quad & p + \zeta \frac{\partial p}{\partial z} = 0, \\ \text{b)} \quad & \frac{\partial p}{\partial z} + \zeta \frac{\partial^2 p}{\partial z^2} - \nabla_\perp p \cdot \nabla_\perp \zeta = 0 \end{aligned} \quad (9.2.4)$$

at $z = 0$.

Analogously we assume for the total sound field in the half-space $z > 0$,

$$p(\mathbf{r}, z) = p_0(\mathbf{r}, z) + p_s(\mathbf{r}, z) \quad (9.2.5)$$

where p_0 is the sound field in the absence of roughness and p_s is the first-order scattered field.

Substituting (9.2.5) into (9.2.4) and equating separately the terms of the order of ζ^0 and ζ , we obtain the boundary conditions at the plane $z = 0$,

$$\text{a)} \quad p_0 = 0, \quad (9.2.6)$$

$$p_s = -\zeta \frac{\partial p_0}{\partial z}, \quad (9.2.7)$$

$$\text{b)} \quad \frac{\partial p_0}{\partial z} = 0, \quad (9.2.8)$$

$$\frac{\partial p_s}{\partial z} = -\zeta \frac{\partial^2 p_0}{\partial z^2} + \nabla_\perp p_0 \cdot \nabla_\perp \zeta. \quad (9.2.9)$$

One can see that in case b) the scattered field depends not only upon ζ but also upon the slope of the rough surface $\nabla_\perp \zeta$.

The solution of the Helmholtz equation

$$\Delta p + k^2 p = 0 \quad (9.2.10)$$

with the boundary conditions (9.2.6, 8) for p_0 is well known (Chap. 3). For a plane incident wave it is

$$p_0(\mathbf{r}, z) = \exp(i\xi_0 \cdot \mathbf{r}) [\exp(-i\gamma_0 z) \pm \exp(i\gamma_0 z)] \quad (9.2.11)$$

where the first term is the incident wave and the second the specularly reflected wave, the minus sign refers to the pressure-release surface, and the plus sign to the rigid surface; ξ_0 and $-\gamma_0$ are the horizontal and vertical components of the wave vector \mathbf{k}_0 of the incident wave satisfying the condition

$$\xi_0^2 + \gamma_0^2 = k_0^2 \quad (k_0 \equiv k).$$

Substituting (9.2.11) into (9.2.7) and (9.2.9), we obtain

$$a) \quad p_s(\mathbf{r}, 0) = 2i\gamma_0 \zeta(\mathbf{r}) \exp(i\xi_0 \cdot \mathbf{r}), \quad (9.2.12)$$

$$b) \quad \frac{\partial p_s(\mathbf{r}, 0)}{\partial z} = 2[\gamma_0^2 \zeta(\mathbf{r}) + i\xi_0 \cdot \nabla_{\perp} \zeta(\mathbf{r})] \exp(i\xi_0 \cdot \mathbf{r}). \quad (9.2.13)$$

We represent $\zeta(\mathbf{r})$ as a Fourier integral,

$$\zeta(\mathbf{r}) = \int_{-\infty}^{\infty} A(\boldsymbol{\kappa}) \exp(i\boldsymbol{\kappa} \cdot \mathbf{r}) d\boldsymbol{\kappa}. \quad (9.2.14)$$

Then, in case a) we have at $z = 0$

$$p_s(\mathbf{r}, 0) = 2i\gamma_0 \int_{-\infty}^{\infty} A(\boldsymbol{\kappa}) \exp[i(\xi_0 + \boldsymbol{\kappa}) \cdot \mathbf{r}] d\boldsymbol{\kappa}. \quad (9.2.15)$$

To obtain an expression for the sound field at $z > 0$ it is sufficient to introduce in (9.2.15) the factor $\exp(i\gamma z)$ where $\gamma = [k^2 - (\xi_0 + \boldsymbol{\kappa})^2]^{1/2}$ and $\text{Im}\{\gamma\} > 0$,

$$p_s(\mathbf{r}, z) = 2i\gamma_0 \int_{-\infty}^{\infty} A(\boldsymbol{\kappa}) \exp[i(\xi_0 + \boldsymbol{\kappa}) \cdot \mathbf{r} + i\gamma z] d\boldsymbol{\kappa}. \quad (9.2.16)$$

This expression satisfies both the boundary condition (9.2.15) and the Helmholtz equation (9.2.10) since the latter is satisfied by the plane wave in the integrand.

Thus, in the first approximation of the MSP each Fourier component of roughness gives rise to its own scattered plane wave propagating in the direction (ξ, γ) which obeys Bragg's law

$$\xi = \xi_0 + \boldsymbol{\kappa}. \quad (9.2.17)$$

Similarly, for a rigid surface we obtain, using (9.2.13),

$$p_s(\mathbf{r}, z) = -2i \int_{-\infty}^{\infty} A(\boldsymbol{\kappa}) (\gamma_0^2 - \boldsymbol{\kappa} \cdot \xi_0) \exp[i(\xi_0 + \boldsymbol{\kappa}) \cdot \mathbf{r} + i\gamma z] \gamma^{-1} d\boldsymbol{\kappa}. \quad (9.2.18)$$

9.3 Average Intensity

The statistical characteristics of the scattered field $p_s(\mathbf{r}, z)$ averaged over an ensemble of random surfaces $\zeta(\mathbf{r})$ are of the most interest. According to (9.2.16), the mean value of a scattered field, i.e., $\langle p_s \rangle$, is zero, since we have assumed that $\langle \zeta \rangle = 0$ and, consequently, $\langle A(\boldsymbol{\kappa}) \rangle = 0$. But the mean value of the sound intensity (mean square of the modulus of acoustic pressure) $I_s = \langle |p_s|^2 \rangle$ is not zero.

9.3.1 An Infinite Surface

First we consider the case when a rough surface is infinite and the reference point is far from the surface as compared with the sound wavelength. In this case only nonattenuating waves for which γ is real are significant in the integral (9.2.16).

The corresponding range of $\boldsymbol{\kappa}$ is denoted by Γ_1 . Then, for I_s we obtain

$$I_s = 4\gamma_0^2 \int_{\Gamma_1} \int_{\Gamma_1} \langle A(\boldsymbol{\kappa}) A^*(\boldsymbol{\kappa}') \rangle \exp[i(\boldsymbol{\kappa} - \boldsymbol{\kappa}') \cdot \mathbf{r} + i(\gamma - \gamma')z] d\boldsymbol{\kappa} d\boldsymbol{\kappa}', \quad (9.3.1)$$

where the asterisk denotes the complex conjugate quantity, and

$$\gamma' = [k^2 - (\xi_0 + \boldsymbol{\kappa}')^2]^{1/2}.$$

Let us assume that the statistics of the rough surface are stationary in space, i.e., the correlation function of the displacement $\zeta(\mathbf{r})$

$$B(\boldsymbol{\varrho}) = \langle \zeta(\mathbf{r}_1) \zeta(\mathbf{r}_2) \rangle, \quad \boldsymbol{\varrho} = \mathbf{r}_2 - \mathbf{r}_1 \quad (9.3.2)$$

depends only on $\boldsymbol{\varrho}$. The spectral amplitudes $A(\boldsymbol{\kappa})$ and $A^*(\boldsymbol{\kappa}')$, as can be easily shown, are delta correlated [9.5]

$$\langle A(\boldsymbol{\kappa}) A^*(\boldsymbol{\kappa}') \rangle = G(\boldsymbol{\kappa}) \delta(\boldsymbol{\kappa} - \boldsymbol{\kappa}') \quad (9.3.3)$$

where

$$G(\boldsymbol{\kappa}) = (2\pi)^{-2} \int_{-\infty}^{\infty} B(\boldsymbol{\varrho}) \exp(-i\boldsymbol{\kappa} \cdot \boldsymbol{\varrho}) d\boldsymbol{\varrho} \quad (9.3.4)$$

is the spatial spectrum of roughness.

Substituting (9.3.3) into (9.3.1) and integrating over $\boldsymbol{\kappa}'$ yield

$$I_s = 4\gamma_0^2 \int_{\Gamma_1} G(\boldsymbol{\kappa}) d\boldsymbol{\kappa}. \quad (9.3.5)$$

9.3.2 Bounded Scattering Surface: Far Zone

For real cases only a certain part of the rough surface is insonified due to the directivity of the sound sources and/or receiver or to the finite duration of the sound pulse. We will assume that the scattered field at the insonified section of the surface is given by (9.2.12), and is zero beyond it. Of course, the discontinuity of the field at the boundaries of the insonified section gives rise to a diffracted wave, the so-called edge effect. But it is negligible if the linear dimension l of the section is large as compared with both the wavelength of sound λ and the correlation radius ϱ_0 of the rough surface.

We will consider a scattered field in the far zone (a Fraunhofer zone). The criteria for the far zone for a slightly rough random surface are [9.6]

$$l \ll R, \quad \varrho_0 l / \lambda \ll R, \quad (9.3.6)$$

where R is the distance from the scattering surface to the reference point. For *small-scale* roughness ($\varrho_0 / \lambda \ll 1$) the first condition is sufficient, and for *large-scale* roughness ($\varrho_0 / \lambda \gg 1$) the second one.

The scattered field in the far zone can be characterized by the *scattering coefficient* m_s which is determined from the relation

$$I_s = SR^{-2} I_i m_s(\theta, \varphi), \quad (9.3.7)$$

where I_s is the intensity of the scattered field in the far zone, I_i is the intensity of the incident wave, and S is the area of the scattering surface. The scattering coefficient m_s does not depend on the distance R and is only a function of θ (the angle between the z axis and direction of the scattered wave), $\gamma = k \cos \theta$, and φ (the azimuth characterising the direction in the plane xy) as in $\xi_y/\xi_x = \tan \varphi$. To find m_s we assume that an infinite rough surface may be divided into sections which satisfy two conditions: 1) the linear dimension of each section is large in comparison with the wavelength of sound and the correlation radius of the rough surface; 2) the point of observation is in the far zone relative to each separate section. The intensity of the scattered field for a single section is described by (9.3.7). Since the scattered fields from such sections are incoherent, the total intensity of the field scattered by the entire surface will be the sum of the intensities from all sections. As sound intensity varies little from one section to another and the number of sections is infinite, summation may be replaced by integration. As a result, setting $I_i = 1$ we obtain

$$I_s = \int m_s(\theta, \varphi) R^{-2} dS \quad (9.3.8)$$

where the integration is carried out over the infinite surface.

Let P be the reference point where the waves scattered by various sections of the boundary OB (Fig. 9.2) are considered. Each point of the boundary can be characterised by the angles θ and φ introduced above. We will use these angles as new integration variables in (9.3.8). Thus, we have $dS = AB \cdot OA \cdot d\varphi$ where $OA d\varphi$ is the linear dimension of the surface in the direction normal to the plane shown in the figure.

But $OA = R \sin \theta$ and $AB = CA / \cos \theta = R d\theta / \cos \theta$. As a result, $dS = R^2 \tan \theta d\theta d\varphi$ and

$$I_s = \int_0^{2\pi} \int_0^{\pi/2} m_s(\theta, \varphi) \tan \theta d\varphi d\theta. \quad (9.3.9)$$

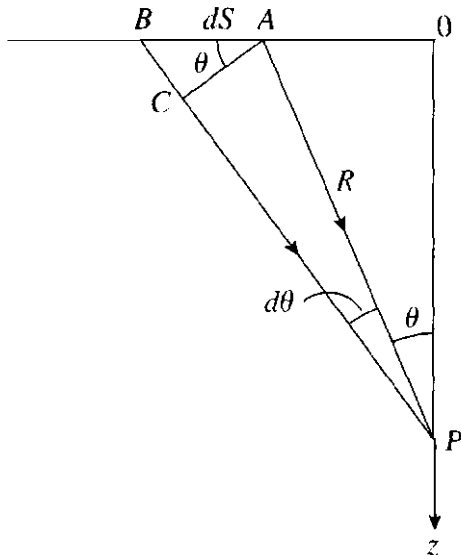


FIGURE 9.2. Parameters for the calculation of the sound field in the far zone in the MSP approximation

Changing the integration in (9.3.5) to θ and φ ($d\boldsymbol{\kappa} = d\xi = \xi d\xi d\varphi$, $\xi = k \sin \theta$), we obtain

$$I_s = 4\gamma_0^2 k^2 \int_0^{2\pi} \int_0^{\pi/2} G(\boldsymbol{\kappa}) \sin \theta \cos \theta d\varphi d\theta. \quad (9.3.10)$$

From the comparison of (9.3.9) and (9.3.10) we find

$$m_s(\theta, \varphi) = 4k^4 \cos^2 \theta_0 \cos^2 \theta G(\boldsymbol{\kappa}), \quad (9.3.11)$$

where $\gamma_0 = k \cos \theta_0$, and θ_0 is the angle of incidence of the sound wave.

It follows from (9.3.11) that in the first approximation of the MSP the scattering coefficient is determined by a single component of the spatial spectrum of roughness with wave vector $\boldsymbol{\kappa}$ which satisfies Bragg's law (9.2.17). Scattering of this kind is called *resonance* or *selective* scattering. For given directions of the incident wave (θ_0, φ_0) and scattered wave (θ, φ) the components of the resonance value of $\boldsymbol{\kappa}$ are

$$\kappa_x = \xi_x - \xi_{0x} = k(\sin \theta \cos \varphi - \sin \theta_0 \cos \varphi_0), \quad (9.3.12)$$

$$\kappa_y = \xi_y - \xi_{0y} = k(\sin \theta \sin \varphi - \sin \theta_0 \sin \varphi_0). \quad (9.3.13)$$

For backscattering ($\theta = \theta_0$, $\varphi = \varphi_0 + \pi$) we obtain

$$\kappa = (\kappa_x^2 + \kappa_y^2)^{1/2} = 2k \sin \theta_0, \quad \alpha \equiv \arctan(\kappa_y/\kappa_x) = \varphi_0. \quad (9.3.14)$$

Thus, the scattered field in the backwards direction is due to the component of rough sea surface which has the same azimuth angle α as the incident sound wave and the wavelength

$$\Lambda = 2\pi/\kappa = \lambda/(2 \sin \theta_0).$$

The scattered field in the specular direction is due to the component with infinitely large wavelength. In fact, assuming in (9.3.12, 13) $\theta = \theta_0$ and $\varphi = \varphi_0$, we obtain $\kappa = 0$.

Relation (9.3.11) gives a direct connection between the scattering coefficient m_s and the spatial spectrum of the roughness $G(\boldsymbol{\kappa})$. Having measured m_s for a sufficiently wide interval of sound frequencies or angles θ , φ and θ_0 , we can estimate the spectrum $G(\boldsymbol{\kappa})$. This method can be useful because the direct measurement of the spatial spectrum of the wind waves in the open ocean meets some technical difficulties.

9.3.3 Correlation Function of the Scattered Field

An important characteristic of a scattered sound field is the spatial correlation function. In some cases this function allows us to obtain the solution of an inverse problem, i.e., to find the correlation function of roughness. As in Sect. 9.3.1, we assume that the rough surface is infinite, the incident wave is plane, and the distance of the reference point from the rough surface is much longer than the sound-wave length. For the spatial correlation function of the field scattered by a

pressure-release surface we have according to (9.2.16, 17) and (9.3.3):

$$B_s(\boldsymbol{\varrho}, \eta) = \langle p_s(\mathbf{r}_1, z_1) p_s^*(\mathbf{r}_2, z_2) \rangle = 4\gamma_0^2 \int_{\Gamma} G(\boldsymbol{\varkappa}) \exp[-i(\boldsymbol{\xi} \cdot \boldsymbol{\varrho} + \gamma\eta)] d\boldsymbol{\xi}, \quad (9.3.15)$$

where $\boldsymbol{\varrho} = \mathbf{r}_2 - \mathbf{r}_1$, $\eta = z_2 - z_1$, $\gamma = (k^2 - \xi^2)^{1/2}$, and Γ is a domain of ξ corresponding to real values of γ .

Sometimes it is reasonable to express the correlation function in terms of the energy flux density. Changing the integration in (9.3.15) to the variables θ and φ , we obtain

$$B_s(\boldsymbol{\varrho}, \eta) = (2k\gamma_0)^2 \int_0^{2\pi} \int_0^{\pi/2} G(\theta, \varphi) \exp[ikF(\boldsymbol{\varrho}, \eta; \theta, \varphi)] \sin \theta \cos \theta d\theta d\varphi, \quad (9.3.16)$$

where

$$F(\boldsymbol{\varrho}, \eta; \theta, \varphi) \equiv \sin \theta (\varrho_x \cos \varphi + \varrho_y \sin \varphi) + \eta \cos \theta,$$

and ϱ_x, ϱ_y are components of the vector $\boldsymbol{\varrho}$ along the axes x and y , respectively.

Now setting $\varrho_x = \varrho_y = \eta = 0$ in (9.3.16), we obtain for the scattered field intensity

$$I_s = (2k\gamma_0)^2 \int_0^{2\pi} \int_0^{\pi/2} G(\theta, \varphi) \cos \theta d\Omega, \quad (9.3.17)$$

where $d\Omega = \sin \theta d\theta d\varphi$ is a solid angle under which a section ds of the rough surface is seen from the reference point in the direction θ, φ .

The angular density of the energy flux or the ray intensity will be

$$J_s \equiv \frac{dI_s}{d\Omega} = (2k\gamma_0)^2 G(\theta, \varphi) \cos \theta. \quad (9.3.18)$$

Substituting (9.3.18) into (9.3.16), we find

$$B_s(\boldsymbol{\varrho}, \eta) = \int_0^{2\pi} \int_0^{\pi/2} J_s \exp[ikF(\boldsymbol{\varrho}, \eta; \theta, \varphi)] \sin \theta d\theta d\varphi. \quad (9.3.19)$$

Relation (9.3.19) appears to be a rather general one. It relates the correlation function of any sound field to the ray intensity. The latter need not be evaluated due to the MSP. It is only necessary that the scattered field be stationary in space, i.e., the correlation function should depend only on $\boldsymbol{\varrho}$ and η . Thus we may use (9.3.19) to calculate the correlation function of a field scattered by a rough surface with large smooth roughness.

It is possible also to obtain a useful expression for $B_s(\boldsymbol{\varrho}, \eta)$ in terms of the scattering coefficient (9.3.9). Having found from (9.3.9) the ray intensity

$$J_s = m_s(\theta, \varphi) / \cos \theta$$

and substituting it into (9.3.19), we obtain

$$B_s(\boldsymbol{\varrho}, \eta) = \int_0^{2\pi} \int_0^{\pi/2} m_s(\theta, \varphi) \exp[ikF(\boldsymbol{\varrho}, \eta; \theta, \varphi)] \tan \theta d\theta d\varphi. \quad (9.3.20)$$

Proceeding to the integration over the mean plane of the rough surface, and taking into account that $ds = R^2 \tan \theta d\theta d\varphi$, we obtain

$$B_s(\boldsymbol{\varrho}, \eta) = \int_S m_s(\theta, \varphi) R^{-2} \exp[ik F(\boldsymbol{\varrho}, \eta; \theta, \varphi)] ds. \quad (9.3.21)$$

Equations (9.3.15, 19–21) allow us to evaluate the correlation function of the scattered field, if the spatial spectrum of roughness, or the ray intensity of the scattered field, or the scattering coefficient are known.

For the sea surface roughness described by empirical spectra, such calculations can be carried out only numerically. For that reason we consider below some models of the rough sea spectrum and obtain some results concerning correlation characteristics of the scattered field.

I. *Large-scale roughness* ($k\varrho_0 \gg 1$, ϱ_0 is the correlation radius of roughness)

- (a) Horizontal correlation function ($\eta = 0$). From (9.3.15) we obtain for this case

$$B_s(\boldsymbol{\varrho}) = 4\gamma_0^2 \int_{\Gamma} G(\boldsymbol{\kappa}) \exp(i\boldsymbol{\xi} \cdot \boldsymbol{\varrho}) d\boldsymbol{\xi}. \quad (9.3.22)$$

With large-scale roughness the function $G(\boldsymbol{\kappa})$ is not zero only at small values $\kappa \leq 1/\varrho_0$, and falls off very rapidly as κ increases. By virtue of this, we may proceed in (9.3.22) to integration over $\boldsymbol{\kappa}$ and extend the integration limits to $\pm\infty$. As a result, we obtain

$$B_s(\boldsymbol{\varrho}) = 4\gamma_0^2 \exp(i\boldsymbol{\xi}_0 \cdot \boldsymbol{\varrho}) \int_{-\infty}^{\infty} G(\boldsymbol{\kappa}) \exp(i\boldsymbol{\kappa} \cdot \boldsymbol{\varrho}) d\boldsymbol{\kappa} = 4\gamma_0^2 \exp(i\boldsymbol{\xi}_0 \cdot \boldsymbol{\varrho}) B(\boldsymbol{\varrho}), \quad (9.3.23)$$

where $B(\boldsymbol{\varrho})$ is the correlation function of roughness (9.3.2). Hence the envelope of the correlation function of the scattered field appears to be proportional to that of roughness, i.e., the correlation function is “transported” without distortion to any plane $z = \text{const}$ [Ref. 9.5, Sect. 10]. Evidently the field’s horizontal correlation radius is equal to that of roughness.

- (b) Vertical correlation function ($\boldsymbol{\varrho} = 0$). In this case it is convenient to use (9.3.20). Let us assume that the correlation function of roughness has the Gaussian form

$$B(\boldsymbol{\varrho}) = \sigma^2 \exp(-\boldsymbol{\varrho}^2/\varrho_0^2).$$

The scattering coefficient will be

$$m_s(\theta, \varphi) = A \cos^2 \theta \exp[-(\kappa\varrho_0/2)^2], \quad (9.3.24)$$

where $A = (1/\pi)(k\sigma)^2(k\varrho_0)^2 \cos^2 \theta_0$.

Substituting (9.3.24) into (9.3.20), we obtain at $\varrho_x = \varrho_y = 0$:

$$B_s(\eta) = A \int_0^{2\pi} \int_0^{\pi/2} \exp[-(\kappa\varrho_0/2)^2 + ik\eta \cos \theta] \sin \theta \cos \theta d\theta d\varphi. \quad (9.3.25)$$

For the sake of simplicity, below we assume $\theta_0 = 0$. Taking into account that $\kappa = k \sin \theta$ in this case, the integration with respect to φ yields 2π . Since only small values of $\sin \theta \sim 2/k\varrho_0$ are significant in (9.3.25), we may approximately set $\cos \theta \approx 1 - (1/2) \sin^2 \theta$. Having integrated

in (9.3.25) over θ , we find for the correlation coefficient (normalized correlation function):

$$N_s(\eta) = B_s(\eta)/B_s(0) = [1 + (2\eta/k\varrho_0^2)^2]^{-1} \exp(ik\eta - i\alpha), \quad (9.3.26)$$

where $\alpha = \arctan(2\eta/k\varrho_0^2)$.

As follows from (9.3.26), the radius of the vertical correlation is of the order $\eta_0 \sim k\varrho_0^2$, i.e., it is $k\varrho_0$ times larger than that of horizontal one.

II. Small-scale roughness ($k\varrho_0 \ll 1$)

- (a) Horizontal correlation function ($\eta = 0$). On the basis of (9.3.20, 24) we find

$$B_s(\varrho) = A \int_0^{2\pi} \int_0^{\pi/2} \exp[ikF(\varrho; \theta, \varphi)] \sin \theta \cos \theta d\theta d\varphi.$$

The integral over φ gives $2\pi J_0(k\varrho \sin \theta)$. The resulting integral can be found in standard tables. As a result, we obtain for the correlation coefficient

$$N_s(\varrho) = 2J_1(k\varrho)/k\varrho, \quad (9.3.27)$$

where $J_1(k\varrho)$ is the first-order Bessel function. The correlation radius of the scattered field is of the order of the sound-wave length.

- (b) Vertical correlation function ($\varrho = 0$). The function is given by the integral

$$B_s(\eta) = A \int_0^{2\pi} \int_0^{\pi/2} \exp(ik\eta \cos \theta) \sin \theta \cos \theta d\theta d\varphi,$$

which is easily evaluated. The correlation coefficient is an oscillating function, and its envelope is determined by the expression

$$|N_s(\eta)| = 2\sqrt{2}(k\eta)^{-2} [1 + \cos k\eta + k\eta \sin k\eta + (k\eta)^2/2]. \quad (9.3.28)$$

It can be shown that the vertical correlation radius is of the order of the sound-wave length also. Results (9.3.26–28) were previously obtained in [Ref. 9.5, Sect. 10] by considering plane wave diffraction at a random screen.

9.4 Scattering Coefficient for the Ocean Surface

Unfortunately, few experimental data on the spatial spectrum of wind waves $G(\kappa)$ have been reported, and no data at all are available for the open ocean. Most of the available data refer to the frequency spectra. We use this data keeping in mind that the dispersion relation for deep-ocean gravity waves has the form

$$\Omega^2 = g\kappa \quad (9.4.1)$$

where Ω is the frequency of surface waves, κ is the wave number, and g is the gravitational acceleration. For this case we have [9.7]

$$G(\kappa) = 2^{-1} g^{1/2} \kappa^{-3/2} S(\sqrt{g\kappa}) K(\kappa, \alpha). \quad (9.4.2)$$

Here, $S(\sqrt{g\kappa}) = S(\Omega)$ is the frequency spectrum, $K(\kappa, \alpha)$ is a function of the angular distribution of sea wave energy normalized so that

$$\int_{-\pi}^{\pi} K(\kappa, \alpha) d\alpha = 1$$

where α is the angle between the average direction of the wind and the direction of propagation of a surface wave with wave number κ . The experimental data are satisfactorily described by the function [9.8]

$$K(\kappa, \alpha) = \begin{cases} b \cos^{\nu(\kappa)} \alpha, & |\alpha| \leq \pi/2 \\ 0, & |\alpha| > \pi/2 \end{cases} \quad (9.4.3)$$

where $\nu(\kappa)$ varies from 10 at low frequencies to 2 at high frequencies. The factor b has to be determined from the normalization condition. Sometimes values of $\nu = 2$ or $\nu = 4$ are used for all κ .

Substituting (9.4.2) into (9.3.11) gives

$$m_s = 2k^4 g^{1/2} \kappa^{-3/2} \cos^2 \theta_0 \cos^2 \theta S(\sqrt{g\kappa}) K(\kappa, \alpha) \quad (9.4.4)$$

where $\kappa = (\kappa_x^2 + \kappa_y^2)^{1/2}$ and $\tan \alpha = \kappa_y / \kappa_x$. For the fully developed wind waves described by the Pierson-Neuman frequency spectrum [9.9]

$$S(\Omega) = C \Omega^{-6} \exp \left[-2 \left(\frac{g}{\Omega v} \right)^2 \right] \quad (9.4.5)$$

where $C = 2.4 \text{ m}^2/\text{s}^5$ and v is the wind speed in m/s, we obtain

$$m_s = (2^{1/2} C / g^3) (k / \kappa)^4 v \cos^2 \theta_0 \cos^2 \theta a^{-1/2} \exp(-1/a) K(\nu, \alpha) \quad (9.4.6)$$

where

$$a \equiv (2g)^{-1} \kappa v^2.$$

We shall also give an expression for the scattering coefficient for fully developed wind waves described by the *Pierson-Moscovitz* frequency spectrum [9.10]:

$$S(\Omega) = 8.1 \cdot 10^{-3} g^2 \Omega^{-5} \exp[-0.74(g/\Omega v)^4] \quad (9.4.7)$$

which has recently been extensively applied. Substitution of (9.4.7) into (9.4.4) yields

$$m_s(\theta, \varphi) = 1.62 \cdot 10^{-2} (k / \kappa)^4 \cos^2 \theta_0 \cos^2 \theta \exp(-\kappa_0^2 / \kappa^2) K(\kappa, \alpha), \quad (9.4.8)$$

where $\kappa_0 \equiv 0.86g/v^2$.

As follows from (9.4.8), the scattering coefficient is equal to zero at $\kappa = 0$, i.e., in the specular direction. Note that the same result can be obtained from (9.4.6) also, assuming $\kappa = 0$, and hence $a = 0$. The scattering coefficient is zero in the specular direction for any spectrum of wind waves (at small values of the Rayleigh parameter). This is just a consequence of the fact that the mean value of a rough surface displacement is zero, in other words, the component with infinite wavelength responsible for scattering in the specular direction is absent.

The directions of the scattering pattern maxima and their angular width are of primary interest because they are the data that are necessary for the solution of other problems such as waveguide sound propagation in an ocean with a rough surface, long-range reverberation and so on.

Consider first the section of the scattering pattern with a conical surface $\theta = \theta_0$ for an isotropic rough sea ($K = 1/2\pi$) and find the extrema φ_m of the scattered field intensity. Differentiating $m_s(\theta_0, \varphi)$ with respect to φ and setting the result to zero, one obtains

$$[(\kappa_0/\kappa_m)^2 - 2] \cos[(\varphi_m - \varphi_0)/2] = 0, \quad (9.4.9)$$

where $\kappa_m = 2k \sin \theta_0 |\sin[(\varphi_m - \varphi_0)/2]|$. Assuming the first factor in (9.4.9) to be zero, we find

$$\kappa_m = \kappa_0/\sqrt{2},$$

$$\text{or} \quad \varphi_m = \varphi_0 \pm 2 \arcsin \varepsilon, \quad (9.4.10)$$

where $\varepsilon \equiv (\kappa_0/k)/(2\sqrt{2} \sin \theta_0)$. Since $\partial^2 m_s(\theta_0, \varphi)/\partial \varphi^2 < 0$ at $\varphi = \varphi_m$, φ_m determines the azimuths of two maxima symmetric relative to $\varphi = \varphi_0$. It is evident that such solutions occur only if $\varepsilon < 1$.

Assuming the second factor in (9.4.9) to be zero, we obtain one more extremum $\varphi_m = \varphi_0 + \pi$ in the backscattering direction. It is a minimum [$\partial m_s(\theta_0, \varphi)/\partial \varphi^2 > 0$ at $\varphi = \varphi_m$] if $\varepsilon < 1$ and maximum [$\partial^2 m_s(\theta_0, \varphi)/\partial \varphi^2 < 0$ at $\varphi = \varphi_m$] if $\varepsilon > 1$.

In the vertical plane $\varphi = \varphi_0$ the scattering pattern also has two maxima at $\theta = \theta_m$ [$\partial^2 m_s(\theta, \varphi_0)/\partial \theta^2 < 0$ at $\theta = \theta_m$], which can be found from the equation

$$(\kappa_0/\kappa_m)^2 - 2 = (\kappa_m/k) \sin \theta_m / \cos^2 \theta_m, \quad (9.4.11)$$

where $\kappa_m = k |\sin \theta_m - \sin \theta_0|$.

The solution of (9.4.11), provided that

$$|\theta_c| \ll 1, \quad \frac{1}{2} |\theta_c| \tan \theta_0 \ll 1, \quad (\theta_c \equiv \theta_m - \theta_0),$$

has the form

$$\sin \theta_m = \sin \theta_0 \pm \kappa_0/k\sqrt{2}. \quad (9.4.12)$$

Note that (9.4.12) is the well-known Bragg's law for diffraction spectra of order ± 1 for a sound wave scattered by a surface wave with wave number $\kappa_0/\sqrt{2}$ (the wavelength is $\Lambda_m = 2\sqrt{2}\pi/\kappa_0$) that corresponds to the spectral maximum of the rough sea surface. From (9.4.12) we may estimate the angle θ_c , i.e., the angular displacement of the scattering pattern maxima from the specular direction

$$\theta_c = \pm(\kappa_0/k)/(\sqrt{2} \cos \theta_0).$$

There exists one more solution of (9.4.11) provided that $(\kappa_0/\kappa)^2 \gg 1$. Taking into account that $\kappa_0 \sim 1/\varrho_0$, where ϱ_0 is the correlation radius of the rough surface, this condition can be rewritten as

$$k\varrho_0 |\sin \theta - \sin \theta_0| \ll 1.$$

This is valid either for small-scale roughness ($k\varrho_0 \ll 1$) and any θ , θ_0 or for large-scale roughness ($k\varrho_0 \gg 1$) and θ close to θ_0 .

From (9.4.11) we obtain

$$\begin{aligned}\theta_m &= \arccos[(k/\kappa_0)(1 - \sin \theta_0)^{3/2}], & \theta_m > 0, \\ \theta_m &= -\arccos[(k/\kappa_0)(1 + \sin \theta_0)^{3/2}], & \theta_m < 0.\end{aligned}\quad (9.4.13)$$

Assuming, for example, $\theta_m = 80^\circ$, $f = 50$ Hz ($k = 0.2 \text{ m}^{-1}$) and $v = 3$ m/s, we find that a significant value has only one maximum for which $\theta_m = -51.2^\circ$. The effective angular half-width $\Delta\theta$ of this maximum is given by the relation [9.11]

$$\Delta\theta = \arccos(\cos \theta_m / \sqrt{e}), \quad (9.4.14)$$

where $e = 2.718 \dots$. In the case considered, $\Delta\theta = 16.4^\circ$. The second maximum ($\theta_m > 0$), for which $\theta_m \sim \pi/2$, has a negligible value because of the factor $\cos^2 \theta$ in (9.4.8). A detailed analysis of the angular location of the scattering pattern maxima, their angular width, and some results of computation of the scattering pattern for different conditions is given in [9.11].

Now we consider the frequency dependence of the scattering coefficient. It seems obvious that, for the small Rayleigh parameters, the scattering coefficient always follows the law $m_s(\theta, \varphi) \sim f^4$, where f is the sound frequency. However, the analysis shows that this is not the case. This scattering law is obeyed only in the directions of its maxima and significantly differs from this law in other directions, particularly in the backscatter direction. Therefore, the frequency dependence of the scattering coefficient exhibits angular anisotropy. We illustrate this feature of the scattering coefficient from a rough sea surface described by the Pierson-Moscovitz frequency spectrum. Anisotropy of the frequency dependence of the scattering coefficient is of most interest in the vertical plane. We consider this frequency dependence first in the directions of scattering maxima. As follows from (9.4.12), the wave number of the resonance harmonics of sea roughness in the direction of maxima of the scattering pattern at $\varphi = \varphi_0$ is

$$\kappa_m = \kappa_0 / \sqrt{2} \quad (9.4.15)$$

Substituting (9.4.15) in (9.4.8), we obtain a well-known frequency dependence of the scattering coefficient for weak sea roughness

$$m_s(\theta_m, \varphi_0) \sim f^4. \quad (9.4.16)$$

Quite a different frequency dependence arises when sound is scattered in the back direction ($\theta = \theta_0$, $\varphi = \varphi_0 + \pi$). In this case the wave number of resonance surface harmonics is

$$\kappa = 2k \sin \theta_0. \quad (9.4.17)$$

Now, the ratio $(k/\kappa)^4$ in (9.4.8) no longer depends on sound frequency, and the scattering frequency dependence $m_s(\theta_0, \varphi_0 + \pi)$ is only determined by the exponential factor in (9.4.8). Substituting (9.4.17) in (9.4.8), we obtain

$$m_s(\theta_0, \varphi_0 + \pi) = A \exp[-0.185/(k\rho_0 \sin \theta_0)^2], \quad (9.4.18)$$

where A is a constant independent of the sound frequency, and the parameter $\rho_0 = v^2/g$ denotes the radius of spatial correlation of wind-induced waves. The

dimensionless parameter $k\rho_0 \sin \theta_0$ is the acoustic scale of roughness in the horizontal plane. As this parameter increases, the scattering coefficient tends towards saturation, i.e., it ceases to depend on frequency. The frequency dependence has the same character in all other directions different from maxima of the scattering pattern. Thus, the scattering coefficient of low-frequency sound (the Rayleigh parameter is small compared to unity) does not depend on frequency for $k\rho_0 \sin \theta_0 \gg 1$.

The frequency dependence of the scattering coefficient described by expression (9.4.6) in the direction of the scattering pattern maxima also follows the law f^4 . In the backscatter direction it takes the form

$$m_s(\theta_0, \varphi_0 + \pi) \sim k^{-1/2} \exp(-1/k\rho_0 \sin \theta_0). \quad (9.4.19)$$

The scattering coefficient reaches the maximum for $k = 2/\rho_0 \sin \theta_0$ and then decreases as the wave number k (frequency) increases.

9.5 Frequency Spectrum of the Scattered Field

In the previous sections we have neglected the temporal oscillations of the ocean surface because they have not changed the energetics of the scattered sound field considered until now. However, there exist phenomena which are due exclusively to the temporal oscillations of the surface. Displacement in the frequency of the scattered signal relative to that in the incident one is an example of such a phenomenon.

The frequency spectrum of the scattered field is determined by the Fourier transformation

$$F(\nu) = (2\pi)^{-1} \int_{-\infty}^{\infty} B_s(\tau) \exp(-i\nu\tau) d\tau \quad (9.5.1)$$

of the temporal correlation function of the scattered field

$$B_s(\tau) = \langle p_s(\mathbf{R}, t) p_s^*(\mathbf{R}, t + \tau) \rangle. \quad (9.5.2)$$

As follows from (9.5.1), the spectrum $F(\nu)$ is normalized to the mean intensity of the scattered field, i.e.,

$$\int_{-\infty}^{\infty} F(\nu) d\nu = B_s(0) = I_s. \quad (9.5.3)$$

Let us consider the scattering of a plane monochromatic wave with frequency ω_0 . To find $p_s(\mathbf{R}, t)$ we can use the boundary value (9.2.12) for p_s again in which the displacement ζ should be assumed to be a function not only of \mathbf{r} but also of t , and the omitted factor $\exp(-i\omega_0 t)$ should be restored. It is convenient to represent $\zeta(\mathbf{r}, t)$ as a superposition of progressive surface waves,

$$\zeta(\mathbf{r}, t) = \text{Re} \left\{ \int_{-\infty}^{\infty} A_0(\boldsymbol{\kappa}) \exp(\boldsymbol{\kappa} \cdot \mathbf{r} - \Omega t) d\boldsymbol{\kappa} \right\} \quad (9.5.4)$$

where $\Omega = \Omega(\boldsymbol{\kappa})$ and $A_0(\boldsymbol{\kappa})$ are the frequency and random amplitude of the surface wave with the wave number $\boldsymbol{\kappa}$.

Using (9.5.4) we obtain for the space-time correlation function of the rough sea surface [Ref. 9.4, Sect. 12]

$$\begin{aligned} B(\boldsymbol{\varrho}, \tau) &= \langle \zeta(\mathbf{r}, t) \zeta(\mathbf{r} + \boldsymbol{\varrho}, t + \tau) \rangle \\ &= \int_{-\infty}^{\infty} G_0(\boldsymbol{\kappa}) \cos[\boldsymbol{\kappa} \cdot \boldsymbol{\varrho} - \Omega(\boldsymbol{\kappa})\tau] d\boldsymbol{\kappa}, \end{aligned} \quad (9.5.5)$$

where $G_0(\boldsymbol{\kappa})$ is the spatial spectrum of the surface waves propagating in direction $\boldsymbol{\kappa}$. It is expressed in terms of the amplitudes $A_0(\boldsymbol{\kappa})$ and $A_0^*(\boldsymbol{\kappa})$ by the following relationships:

$$\begin{aligned} \langle A_0(\pm\boldsymbol{\kappa}) A_0^*(\pm\boldsymbol{\kappa}') \rangle &= 2G_0(\pm\boldsymbol{\kappa}) \delta(\boldsymbol{\kappa} - \boldsymbol{\kappa}'), \\ \langle A_0(\boldsymbol{\kappa}) A_0(-\boldsymbol{\kappa}') \rangle &= \langle A_0^*(-\boldsymbol{\kappa}) A_0^*(\boldsymbol{\kappa}') \rangle \equiv 0. \end{aligned}$$

For the scattered field at the point $\mathbf{R} = \{\mathbf{r}, z\}$, $z > 0$, we obtain

$$\begin{aligned} p_s(\mathbf{R}, t) &= i\gamma_0 \int_{-\infty}^{\infty} A_0(\boldsymbol{\kappa}) \exp\{i[(\boldsymbol{\xi}_0 + \boldsymbol{\kappa}) \cdot \mathbf{r} + \gamma_+ z - (\omega_0 + \Omega)t']\} d\boldsymbol{\kappa} \\ &\quad + i\gamma_0 \int_{-\infty}^{\infty} A_0(\boldsymbol{\kappa}) \exp\{i[(\boldsymbol{\xi}_0 - \boldsymbol{\kappa}) \cdot \mathbf{r} + \gamma_- z - (\omega_0 - \Omega)t]\} d\boldsymbol{\kappa}, \end{aligned} \quad (9.5.6)$$

where

$$\begin{aligned} \gamma_0 &= k \cos \theta_0, \\ \gamma_{\pm} &= \left[\left(\frac{\omega_0 \pm \Omega}{c} \right)^2 - (\boldsymbol{\xi}_0 \pm \boldsymbol{\kappa})^2 \right]^{1/2}, \quad \text{Im}\{\gamma_{\pm}\} > 0 \end{aligned}$$

or, since $\Omega \ll \omega_0$,

$$\gamma_{\pm} \simeq [k^2 - (\boldsymbol{\xi}_0 \pm \boldsymbol{\kappa})^2]^{1/2}, \quad k = \frac{\omega_0}{c}.$$

Having replaced $\boldsymbol{\kappa}$ by $-\boldsymbol{\kappa}$ in the second integral in (9.5.6), we obtain

$$\begin{aligned} p_s(\mathbf{R}, t) &= i\gamma_0 \int_{-\infty}^{\infty} \{A_0(\boldsymbol{\kappa}) \exp[-i(\omega_0 + \Omega)t] \\ &\quad + A_0(-\boldsymbol{\kappa}) \exp[-i(\omega_0 - \Omega)t]\} \exp[i(\boldsymbol{\xi}_0 + \boldsymbol{\kappa}) \cdot \mathbf{r} + i\gamma_+ z] d\boldsymbol{\kappa} \end{aligned} \quad (9.5.7)$$

where $\gamma_+ \equiv \gamma = k \cos \theta$.

One can see that the surface waves propagating in the direction $\pm\boldsymbol{\kappa}$ change the frequency of the scattered field by a value $\pm\Omega(\boldsymbol{\kappa})$. The physical nature of this phenomenon is similar to that of the combination scattering of waves [9.12].

According to (9.5.7), for the temporal correlation function of the scattered field at distances from the plane $z = 0$ which are large compared to the sound wavelength we obtain

$$\begin{aligned} B_s(\tau) &= 2\gamma_0^2 \int_{\Gamma_1} \{G_0(\boldsymbol{\kappa}) \exp[i(\omega_0 + \Omega)\tau] \\ &\quad + G_0(-\boldsymbol{\kappa}) \exp[i(\omega_0 - \Omega)\tau]\} d\boldsymbol{\kappa}. \end{aligned} \quad (9.5.8)$$

Equation (9.5.8) determines the function $B_s(\tau)$ for an infinite rough surface. If the rough surface is bounded, and the reference point is in the far zone, the function $B_s(\tau)$ will differ from (9.5.8) just as the expressions for scattered intensities differ from each other in these two cases [see (9.3.5, 7, 11)]. Thus, the function $B_s(\tau)$ in the far zone will have the form

$$B_s(\tau) = 2S(\gamma\gamma_0/R)^2 \{G_0(\boldsymbol{\kappa}) \exp[i(\omega_0 + \Omega)\tau] + G_0(-\boldsymbol{\kappa}) \exp[i(\omega_0 - \Omega)\tau]\}. \quad (9.5.9)$$

Inserting (9.5.9) in (9.5.1), we obtain for the frequency spectrum in the far zone

$$F(\nu) = 2S(\gamma\gamma_0/R)^2 \{G_0(\boldsymbol{\kappa}) \delta[\nu - \omega_0 - \Omega(\boldsymbol{\kappa})] + G_0(-\boldsymbol{\kappa}) \delta[\nu - \omega_0 + \Omega(\boldsymbol{\kappa})]\}. \quad (9.5.10)$$

It consists of only two spectral lines shifted relative to ω_0 by the value $\pm\Omega(\boldsymbol{\kappa})$, $\boldsymbol{\kappa} = |\xi - \xi_0|$ being the resonance wave number.

In the specular direction, $\boldsymbol{\kappa} = 0$ and, consequently, $\Omega(\boldsymbol{\kappa}) = 0$, i.e., there are no lateral lines in the spectrum. For deep-water gravity waves we have $\Omega = (g\boldsymbol{\kappa})^{1/2}$. Hence, the shift of lateral lines for the backscattering of sound in this case will be, taking account of (9.3.14),

$$\Omega = (2kg \sin \theta_0)^{1/2}. \quad (9.5.11)$$

The maximum frequency shift in the spectrum of the scattered field is observed at grazing incidence of sound ($\theta_0 \rightarrow \pi/2$),

$$\Omega_{\max} = (2kg)^{1/2}.$$

This result has been confirmed by numerous experimental data obtained with radio waves [9.4]. Setting, for example, $f = 0.5$ kHz ($k = 2.1 \text{ m}^{-1}$), we obtain $\Omega_{\max}/2\pi \simeq 1$ Hz.

Having integrated (9.5.10) over ν from $-\infty$ to ∞ , we find

$$I_s = 2S(\gamma\gamma_0/R)^2 [G_0(\boldsymbol{\kappa}) + G_0(-\boldsymbol{\kappa})] \quad (9.5.12)$$

where the first and second terms give the intensity of spectral lines shifted in frequency relative to ω_0 by $\Omega(\boldsymbol{\kappa})$ and $-\Omega(\boldsymbol{\kappa})$, respectively.

Let us show that (9.5.12) is identical to (9.3.7). In fact, setting $\tau = 0$ in (9.5.5), we obtain

$$B(\boldsymbol{\varrho}, 0) = \frac{1}{2} \int_{-\infty}^{\infty} [G_0(\boldsymbol{\kappa}) + G_0(-\boldsymbol{\kappa})] \exp(i\boldsymbol{\kappa} \cdot \boldsymbol{\varrho}) d\boldsymbol{\kappa}. \quad (9.5.13)$$

From a comparison of (9.5.13) and (9.3.4) one obtains

$$G(\boldsymbol{\kappa}) = [G_0(\boldsymbol{\kappa}) + G_0(-\boldsymbol{\kappa})]/2 \quad (9.5.14)$$

where $G(\boldsymbol{\kappa})$ is the spatial spectrum of the motionless sea surface. Substituting (9.5.14) into (9.5.12) yields

$$I_s = 4S(\gamma\gamma_0/R)^2 G(\boldsymbol{\kappa}) = SR^{-2} m_s(\theta, \varphi)$$

which agrees with (9.3.7) for $I_i = 1$.

If a source and a receiver are in the near zone, there is a finite range of angles θ_0 and θ of incident and scattered waves which corresponds to an interval of allowable values of \varkappa and, consequently, $\Omega(\varkappa)$. As a result, a spectral band of finite width appears instead of a spectral line. The spectral components close to the central line, i.e., the coherent component of the field, are due to the sections of surface adjacent to the specular reflection point (Fig. 1.27).

Using the measured frequency spectrum of a scattered field it is possible to estimate the spectrum of wind waves.

9.6 Reflection Coefficient in the Specular Direction

The reflection coefficient of underwater sound from a flat ocean surface is very close to -1 (Chap. 3). When the surface is rough, the modulus of the reflection coefficient is less than unity because some acoustic energy goes into the scattered field. To find the mean reflection coefficient in the specular direction from the rough surface in the second approximation of the MSP, one can use the energy conservation law; the vertical energy flux through a unit surface in the incident wave must be equal to the sum of the flux in the reflected and scattered waves. Assuming, as before, the pressure amplitude in the incident wave equal to unity and taking (9.3.5) into account, we can write this law in the form

$$\cos \theta_0 = |V_c|^2 \cos \theta_0 + 4\gamma_0^2 \int_{\Gamma_1} G(\varkappa)(\gamma/k) d\varkappa, \quad (9.6.1)$$

where $\gamma/k = \cos \theta = (1/k)[k^2 - (\xi_0 + \varkappa)^2]^{1/2}$, and V_c is a reflection coefficient to be determined. From (9.6.1) we have, taking into account that the second term in the right-hand side is small compared to unity

$$|V_c| = 1 - 2k \cos \theta_0 \int_{\Gamma_1} G(\varkappa)[k^2 - (\xi_0 + \varkappa)^2]^{1/2} d\varkappa. \quad (9.6.2)$$

Setting $\varkappa = \{\varkappa \cos \alpha, \varkappa \sin \alpha\}$ we pass to the integration in (9.6.2) over the wave number \varkappa and the azimuth angle α , taking (9.3.12, 13) into account,

$$|V_c| = 1 - 2k^2 \cos \theta_0 \iint G(\varkappa, \alpha)[\cos^2 \theta_0 + 2(\varkappa/k) \sin \theta_0 \cos(\alpha - \varphi_0) - (\varkappa/k)^2]^{1/2} \varkappa d\varkappa d\alpha. \quad (9.6.3)$$

The ranges of integration over \varkappa and α correspond to the real values of the radical in the integrand.

The quantity V_c is called the coherent or mean reflection coefficient. While averaging over an ensemble of surfaces ζ , the scattered waves vanish because of their random phases and only the specular reflected wave remains because of its definite phase difference relative to the incident wave.

Let us consider some particular cases of (9.6.3).

1. Large-scale roughness of the sea surface, $\theta_0 \pm \pi/2$. Since $G(\varkappa, \alpha)$ is the Fourier transform of the correlation function, it only has significant values at $\varkappa \leq 1/\varrho_0$

and rapidly falls off at $\varkappa > 1/\varrho_0$, where ϱ_0 is the spatial correlation radius of the rough surface. We assume that the condition $k\varrho_0 \cos^2 \theta_0 \gg 1$ is fulfilled. Then, it is sufficient to retain only the first term under the radical and integrate over \varkappa from 0 to ∞ , and over α from $-\pi$ to π . Hence, we have

$$|V_c| = 1 - 2(k \cos \theta_0)^2 \int_0^\infty \int_{-\pi}^\pi G(\varkappa, \alpha) \varkappa d\varkappa d\alpha. \quad (9.6.4)$$

But

$$\int_0^\infty \int_{-\pi}^\pi G(\varkappa, \alpha) \varkappa d\varkappa d\alpha = \sigma^2,$$

so

$$|V_c| = 1 - 2(k\sigma \cos \theta_0)^2 = 1 - P^2/2, \quad (9.6.5)$$

where P is the Rayleigh parameter.

2. Large-scale roughness, grazing incidence of sound ($k\varrho_0 \gg 1$, $k\varrho_0 \cos^2 \theta_0 \ll 1$, $\sin \theta_0 \simeq 1$). In this case we can retain only the second term. The integration over \varkappa can be carried out again from 0 to ∞ , and over α from $-\pi/2 + \varphi_0$ to $\pi/2 + \varphi_0$. In addition, we assume

$$G(\varkappa, \alpha) = 2\pi G(\varkappa)K(\alpha),$$

where $G(\varkappa)$ is the spectrum of the isotropic rough surface and $K(\alpha)$ is the function determining the angular distribution of wind wave energy (9.4.2). As a result we obtain

$$|V_c| = 1 - 4\pi \sqrt{2} k^{3/2} \cos \theta_0 E(\varphi_0) \int_0^\infty G(\varkappa) \varkappa^{3/2} d\varkappa, \quad (9.6.6)$$

where the function

$$E(\varphi_0) = \int_{-\pi/2}^{\pi/2} K(\alpha + \varphi_0) \sqrt{\cos \alpha} d\alpha$$

describes the influence of roughness anisotropy on the mean reflection coefficient. For the isotropic roughness $K = (2\pi)^{-1}$ and

$$E = \Gamma\left(\frac{3}{4}\right) \left[2\sqrt{\pi} \Gamma\left(\frac{5}{4}\right) \right]^{-1}$$

where Γ is the Euler gamma function.

For the isotropic sea surface described by the Pierson-Neumann frequency spectrum (9.4.5), taking (9.4.2) into account, we obtain

$$|V_c| = 1 - C \Gamma\left(\frac{3}{4}\right) \left[4g^4 \sqrt{2\pi} g \Gamma\left(\frac{5}{4}\right) \right]^{-1} k^{3/2} v^4 \cos \theta_0, \quad (9.6.7)$$

where v is the wind speed in m/s.

9.7 Method of Tangent Plane: Basic Concept

The perturbation method presented in the preceding sections is only applicable for the case of a small Rayleigh parameter. However, the waves on the ocean surface and roughness of the bottom are frequently much greater than the sound wavelength and do not satisfy this condition. Another method should be used in these cases. If the roughness is sufficiently smooth (though large), one can assume that sound reflection takes place at each point of the surface according to geometrical acoustics law, i.e., in the same manner as reflection at an infinite plane tangent to a rough surface at the point considered (Fig. 9.3). The acoustic properties of this plane are the same as those of the rough surface under consideration at the tangent point.

In this case the values of p_s and $\partial p_s / \partial n$ are determined in terms of p_i on the boundary according to the relations

$$p_s(\mathbf{R}) = V p_i(\mathbf{R}), \quad \frac{\partial}{\partial n} p_s(\mathbf{R}) = -V \frac{\partial}{\partial n} p_i(\mathbf{R}), \quad (9.7.1)$$

where V is a local reflection coefficient, and \mathbf{n} is the unit vector of the normal to the rough surface at the point $\mathbf{R} = \{\mathbf{r}, \zeta(\mathbf{r})\}$ where, as always, $\mathbf{r} = \{x, y\}$.

This assumption is analogous to the well-known Kirchhoff principle in diffraction theory. Therefore, the tangent plane method is often also called the Kirchhoff approximation.

The tangent plane method yields good results only for those directions of scattering which are close to the directions of specular reflection at various points of a rough surface. Moreover, this approximation will be good only if one can separate out in the tangent plane around the tangent point some area large in linear dimension compared to the sound wavelength which is not much deflected at its boundary from the rough surface. This results in the following condition

$$2k\mathcal{R} \sin \chi \gg 1, \quad (9.7.2)$$

where \mathcal{R} is the lesser of two major radii of curvature at the given point and χ is the local grazing angle. In Fig. 9.4a the grazing angle χ is zero at point A: hence condition (9.7.2) is not fulfilled. Near this point the scattered and incident waves are not connected by simple relations (9.7.1).

In Fig. 9.4b section AB is in the shadow relative to the incident wave, and the method is again inapplicable in its usual form. But it can be modified assuming

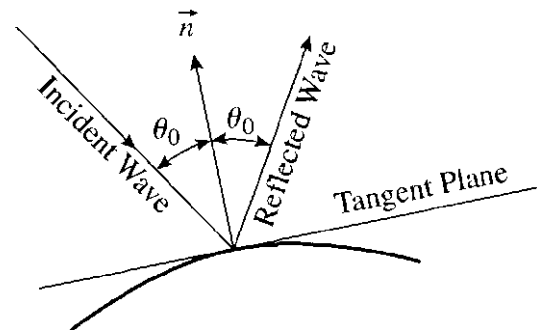


FIGURE 9.3. "Local" scattering geometry. θ_0 is the local angle of incidence with respect to the normal at the point considered

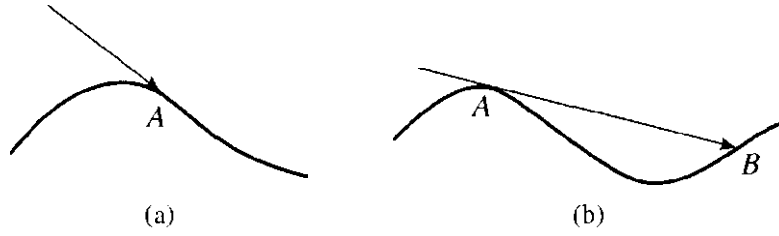


FIGURE 9.4. (a) Grazing angle χ of an incident wave at point A becomes zero; (b) the section of rough surface AB is in the "shadow" with respect to an incident wave

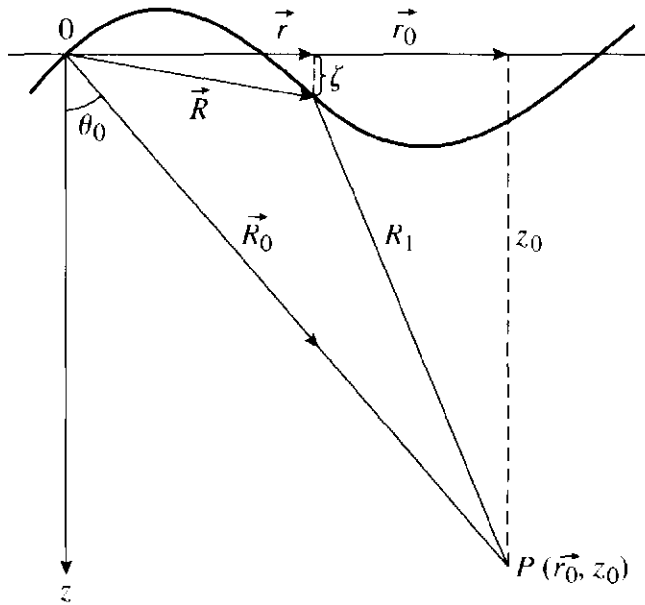


FIGURE 9.5. Parameter for the calculation of the scattered field in the far zone in the tangent plane approximation

that the field in the insonified sections of the rough surface is determined as before and exactly equals zero in shadow.²

When the values of p_s and $\partial p_s / \partial n$ have been determined at the rough surface in this way, the scattered field at any point $\mathbf{R}_0 = \{\mathbf{r}_0 z_0\}$, $z_0 > \zeta$, can be calculated without further approximations by Green's formula [Ref. 9.14; Chap. 7],

$$p_s(\mathbf{R}_0) = (4\pi)^{-1} \int \left[p_s(\mathbf{R}) \frac{\partial}{\partial n} \frac{\exp(ikR_1)}{R_1} - \frac{\exp(ikR_1)}{R_1} \frac{\partial}{\partial n} p_s(\mathbf{R}) \right] dS \quad (9.7.3)$$

where $R_1 = |\mathbf{R}_0 - \mathbf{R}|$ is the distance between the reference point and the point at a rough surface (Fig. 9.5).

Substituting the boundary values (9.7.1) in (9.7.3) we obtain

$$p_s(\mathbf{R}_0) = (4\pi)^{-1} \int V \left[p_i(\mathbf{R}) \frac{\partial}{\partial n} \frac{\exp(ikR_1)}{R_1} + \frac{\exp(ikR_1)}{R_1} \frac{\partial}{\partial n} p_i(\mathbf{R}) \right] dS. \quad (9.7.4)$$

²Here we will not discuss in more detail the conditions for the validity of the tangent plane method [9.13]; we just note that as in diffraction theory this method works well in regions close to those illuminated in the geometrical approximation.

As follows from formula (9.7.4) the fields scattered at the free (pressure-release) surface ($V = -1$) and the absolutely rigid surface ($V = 1$) differ from one another only by the sign (a phase shift π) in this approximation.

There exist other cases when the reflection coefficient is independent of the angle of incidence. This is the case, for example, for some underwater sediments if the sound velocities in water and in these sediments are equal (Sect. 3.1). In all these cases the reflection coefficient V in (9.7.4) may be taken outside the integral.

The tangent plane method for solving the problems of acoustic and electromagnetic waves scattering was first proposed by *Brekhovskikh* [9.13, 15, 16] for periodically rough surfaces and then extended by *Issakovich* [9.17] for random surfaces.

9.8 Average Field

To obtain the mean value of the scattered field, expression (9.7.4) must be statistically averaged over the ensemble of random surfaces $\zeta(\mathbf{r})$. First, however, we have to transform (9.7.4). By analogy with (4.2.7), we have

$$\left(\frac{\exp(ikR_1)}{R_1} \right)_{z=\zeta} = i(2\pi)^{-1} \int_{-\infty}^{\infty} \gamma^{-1} \exp[i\boldsymbol{\xi} \cdot (\mathbf{r}_0 - \mathbf{r}) + i\gamma(z_0 - \zeta)] d\boldsymbol{\xi},$$

$$\gamma = (k^2 - \xi^2)^{1/2}.$$

Differentiating and taking into account that

$$\frac{\partial}{\partial n}(\mathbf{r} \cdot \boldsymbol{\xi}) = \nabla(\mathbf{r} \cdot \boldsymbol{\xi}) \mathbf{n} = \boldsymbol{\xi} \cdot \mathbf{n} = -n_z(\boldsymbol{\xi} \cdot \nabla_{\perp} \zeta),$$

we find

$$\left(\frac{\partial}{\partial n} \frac{\exp(ikR_1)}{R_1} \right)_{z=\zeta} = n_z(2\pi)^{-1} \int_{-\infty}^{\infty} \gamma^{-1} (\gamma - \boldsymbol{\xi} \cdot \nabla_{\perp} \zeta) \times \exp[i\boldsymbol{\xi} \cdot (\mathbf{r}_0 - \mathbf{r}) + i\gamma(z_0 - \zeta)] d\boldsymbol{\xi}. \quad (9.8.1)$$

Similarly, for a plane incident wave

$$p_i = \exp[i(\boldsymbol{\xi}_0 \cdot \mathbf{r} - \gamma_0 z)] \quad (9.8.2)$$

we have

$$\left(\frac{\partial p_i}{\partial n} \right)_{z=\zeta} = -in_z(\gamma_0 + \boldsymbol{\xi}_0 \cdot \nabla_{\perp} \zeta) \exp[i(\boldsymbol{\xi}_0 \cdot \mathbf{r} - \gamma_0 \zeta)]. \quad (9.8.3)$$

Substituting (9.8.1–3) into (9.7.4) and keeping in mind that $dS = dx dy / n_z$, we obtain

$$p_s(\mathbf{R}_0) = V(8\pi^2)^{-1} \iint_{-\infty}^{\infty} \gamma^{-1} (q - \boldsymbol{\kappa} \cdot \nabla_{\perp} \zeta) \times \exp[-i(\boldsymbol{\kappa} \cdot \mathbf{r} + q\zeta) + i(\boldsymbol{\xi} \cdot \mathbf{r}_0 + \gamma z_0)] d\mathbf{r} d\boldsymbol{\xi} \quad (9.8.4)$$

where $q \equiv \gamma + \gamma_0$, $\boldsymbol{\kappa} \equiv \boldsymbol{\xi} - \boldsymbol{\xi}_0$, $\mathbf{r} = \{x, y\}$, and $d\mathbf{r} = dx dy$.

Now, we average (9.8.4) and take into account that

$$\langle \exp(-iq\zeta) \rangle \equiv f_1(-q) = \int_{-\infty}^{\infty} \exp(-iq\zeta) w(\zeta) d\zeta \quad (9.8.5)$$

is the characteristic function of a random quantity ζ , $w(\zeta)$ being, by definition, the probability density of ζ . Since the one-dimensional characteristic function does not depend on coordinates,

$$\langle \nabla_{\perp} \zeta \exp(-iq\zeta) \rangle = (i/q) \nabla_{\perp} \langle \exp(-iq\zeta) \rangle = (i/q) \nabla_{\perp} f_1(-q) = 0. \quad (9.8.6)$$

The integration over \mathbf{r} in (9.8.4) gives the delta function $\delta(\boldsymbol{\kappa})$, and then the integral over ξ can be calculated. As a result we obtain

$$\langle p_s \rangle = V_c p_0, \quad V_c \equiv V f_1(-2\gamma_0) \quad (9.8.7)$$

where $p_0 = \exp[i(\xi_0 \mathbf{r}_0 + \gamma_0 z_0)]$ is a plane sound wave reflected from an infinite flat surface, and V_c is the mean (coherent) reflection coefficient, i.e., the reflection coefficient in the specular direction.

A generalization of (9.8.7) to multiple scattering has recently been made by *DeSanto* [9.18].

Now we consider the case when the scattering surface has finite dimensions (Sect. 9.3) and the point of observation is in the far zone. When we analyze the mean scattered field the criterion for the far zone is the same as for a flat surface, i.e., $R \gg l^2/\lambda$ where l is a linear dimension of the surface. Using the assumption we have (Fig. 9.5)

$$R_1 \simeq R_0 - \mathbf{R} \cdot \mathbf{R}_0 / R_0.$$

We denote by $\mathbf{k} = \{\xi, \gamma\}$ a wave vector of a scattered wave, where $\xi = k\mathbf{r}_0/R_0$ and $\gamma = kz_0/R_0$. Then, setting $\mathbf{R} = \{\mathbf{r}, \zeta\}$, \mathbf{r} being the radius vector in the plane $z = 0$, we obtain

$$\begin{aligned} \frac{\exp(ikR_1)}{R_1} &\simeq (1/R_0) \exp[i(kR_0 - \xi \cdot \mathbf{r} - \gamma\zeta)], \\ \frac{\partial}{\partial n} \frac{\exp(ikR_1)}{R_1} &\simeq -in_z (1/R_0) (\gamma - \xi \cdot \nabla_{\perp} \zeta) \exp[i(kR_0 - \xi \cdot \mathbf{r} - \gamma\zeta)]. \end{aligned} \quad (9.8.8)$$

Substituting (9.8.2, 3, 8) into (9.7.4) yields

$$p_s(\mathbf{R}_0) = \frac{-iV \exp(ikR_0)}{4\pi R_0} \int_S (q - \boldsymbol{\kappa} \cdot \nabla_{\perp} \zeta) \exp[-i(\boldsymbol{\kappa} \cdot \mathbf{r} + q\zeta)] d\mathbf{r}. \quad (9.8.9)$$

Averaging (9.8.9) and using (9.8.5, 6), we obtain

$$\langle p_s \rangle = \frac{-iqV \exp(ikR_0)}{4\pi R_0} f_1(-q) \int_S \exp(-i\boldsymbol{\kappa} \cdot \mathbf{r}) d\mathbf{r}. \quad (9.8.10)$$

For $kl \gg 1$, which is assumed, the integral in (9.8.10) is approximately zero for all directions except $\boldsymbol{\kappa} = 0$. For $\boldsymbol{\kappa} = 0$, i.e., for scattering in the specular direction, it is equal to S . In this case (9.8.7) still holds for $\langle p_s \rangle$ with

$$p_0 = -ikS \cos \theta_0 \exp(ikR_0)/(2\pi R_0) \quad (9.8.11)$$

and the same V_c .

Formula (9.8.7) also holds for a spherical incident wave if we introduce in (9.8.11) the additional factor $\exp(ikR_0^1)/R_0^1$ where R_0^1 is the distance between the origin of coordinates located within the scattering area and the source. It is also assumed that the source is in the far zone relative to S .

Let us discuss now the expression (9.8.7) for the mean reflection coefficient V_c . Let ζ be distributed normally with mean value $\langle \zeta \rangle = 0$,

$$w(\zeta) = (\sigma\sqrt{2\pi})^{-1} \exp(-\zeta^2/2\sigma^2). \quad (9.8.12)$$

Then,

$$V_c = V \int_{-\infty}^{\infty} \exp(-2i\gamma_0\zeta) w(\zeta) d\zeta = V \exp(-P^2/2) \quad (9.8.13)$$

where P is the Rayleigh parameter. For $P^2 \ll 1$ we have

$$V_c = V(1 - P^2/2),$$

that coincides with (9.6.5) when $|V| = 1$.

The mean reflection coefficient V_c rapidly falls off when the Rayleigh parameter increases, $V_c/V \simeq 10^{-2}$ for $P = 3$, because the phases of waves scattered from different samples of a rough surface are random for large P . Consequently, the scattered field is incoherent in this case, and its mean value tends to zero. In contrast, for $P \rightarrow 0$ the scattered waves have the same phase, and the field appears to be coherent. Thus, V_c is a measure of the scattered field coherence.

Having measured the mean reflection coefficient V_c over a sufficiently wide range of values $\gamma_0 = k \cos \theta_0$ [that is, frequency of sound and (or) the angle of incidence] and using (9.8.5, 7), one can obtain an estimate of the probability density $w(\zeta)$ (for a known value of V),

$$w(\zeta) = (\pi V)^{-1} \int_{-\infty}^{\infty} V_c(\gamma_0) \exp(2i\gamma_0\zeta) d\gamma_0.$$

9.9 Scattering Coefficient of High-Frequency Sound

To estimate the scattering coefficient of high-frequency sound in the far zone, formula (9.8.9) can be used. One can expect that the main contribution to the integral over \mathbf{r} is given by stationary phase points determined by the equation

$$\nabla_{\perp}(\boldsymbol{\kappa} \cdot \mathbf{r} + q\zeta) = 0 \quad \text{or} \quad \nabla_{\perp}\zeta = -\boldsymbol{\kappa}/q \quad (9.9.1)$$

and their vicinities. Let us note that the slope of a rough surface, $\nabla_{\perp}\zeta$, given by (9.9.1) provides local specular reflection of an incident wave in the direction $\{\xi, \gamma\}$, i.e., to the reference point. In fact, for such a reflection from a small area of a rough surface with normal \mathbf{n} , an equality $\mathbf{k} \cdot \mathbf{n} = -\mathbf{k}_0 \cdot \mathbf{n}$ or $(\mathbf{k} + \mathbf{k}_0) \cdot \mathbf{n} = 0$ must be satisfied. Keeping in mind that $\mathbf{k} = \{\xi, \gamma\}$ and $\mathbf{k}_0 = \{\xi_0, -\gamma_0\}$, the latter can be written in the form

$$(\gamma - \gamma_0) - (\xi - \xi_0) \cdot \nabla_{\perp}\zeta = 0.$$

Now a simple substitution of (9.9.1) in the last equation transforms it into an identity. The value $\nabla_{\perp}\zeta$ in (9.8.9) can be replaced by (9.9.1). Denoting

$$F = \frac{\kappa^2 + q^2}{2kq}, \quad (9.9.2)$$

we obtain from (9.8.9)

$$P_s(\mathbf{R}_0) = \frac{-ikFV \exp(ikR_0)}{2\pi R_0} \int_S \exp[-i(\boldsymbol{\kappa} \cdot \mathbf{r} + q\zeta)] d\mathbf{r}. \quad (9.9.3)$$

Multiplying (9.9.3) by the complex conjugate quantity and averaging, we obtain for the mean square pressure

$$I_s \equiv \langle |p_s(\mathbf{R}_0)|^2 \rangle = \left(\frac{kFV}{2\pi R_0} \right)^2 \iint_S \exp[-i\boldsymbol{\kappa} \cdot (\mathbf{r}_1 - \mathbf{r}_2)] f_2(-q, q) d\mathbf{r}_1 d\mathbf{r}_2 \quad (9.9.4)$$

where

$$\begin{aligned} f_2(-q, q) &\equiv \langle \exp[-iq(\zeta_1 - \zeta_2)] \rangle \\ &= \iint_{-\infty}^{\infty} \exp[-iq(\zeta_1 - \zeta_2)] w(\zeta_1, \zeta_2) d\zeta_1 d\zeta_2 \end{aligned} \quad (9.9.5)$$

is the two-dimensional characteristic function of the random quantity $\{\zeta_1, \zeta_2\}$ specified in terms of the probability density $w(\zeta_1, \zeta_2)$, $\zeta_i = \zeta(\mathbf{r}_i)$ and $i = 1, 2$. For a smooth rough surface the difference $\zeta_1 - \zeta_2$ can be expanded in a power series of $\boldsymbol{\varrho} = \mathbf{r}_2 - \mathbf{r}_1$. Retaining only the first nonvanishing term, we obtain

$$\zeta_1 - \zeta_2 = -\boldsymbol{\varrho} \cdot \nabla_{\perp}\zeta. \quad (9.9.6)$$

Substitution of (9.9.6) into (9.9.5) yields

$$f_2(-q, q) = \langle \exp(iq\boldsymbol{\varrho} \cdot \nabla_{\perp}\zeta) \rangle = \int_{-\infty}^{\infty} \exp(iq\mathbf{a} \cdot \boldsymbol{\varrho}) w(\mathbf{a}) d\mathbf{a} \quad (9.9.7)$$

where $w(\mathbf{a})$ is the two-dimensional probability density of slopes, $\mathbf{a} \equiv \nabla_{\perp}\zeta = \{\zeta_x, \zeta_y\}$.

We substitute (9.9.7) into (9.9.4) and introduce a new variable of integration $\boldsymbol{\varrho}$, extending the integration limits to $\pm\infty$. Then,

$$\int_{-\infty}^{\infty} \exp[i(q\mathbf{a} + \boldsymbol{\kappa})\boldsymbol{\varrho}] d\boldsymbol{\varrho} = (2\pi)^2 \delta(q\mathbf{a} + \boldsymbol{\kappa}).$$

The integral over \mathbf{r}_1 gives the scattering area S . As a result, we have

$$I_s = S(kFV/R_0)^2 \int_{-\infty}^{\infty} w(\mathbf{a}) \delta(q\mathbf{a} + \boldsymbol{\kappa}) d\mathbf{a} = S(kFV/qR_0)^2 w(-\boldsymbol{\kappa}/q). \quad (9.9.8)$$

From (9.9.8) and (9.3.7) we obtain the scattering coefficient

$$m_s = (V\tilde{F})^2 w(-\boldsymbol{\kappa}/q) \quad (9.9.9)$$

where

$$\tilde{F} \equiv kF/q = \frac{1}{2}(1 + \kappa^2/q^2). \quad (9.9.10)$$

It follows from (9.9.9) that the scattering coefficient in this case is independent of both the sound frequency f and σ , and is determined only by the mean-square slopes of the surface. This again shows that the scattered field in the tangent plane approximation is formed by the specular reflection—"glitters"—from those parts of the rough surface which have slopes satisfying condition (9.9.1).

Using the values of the scattering coefficient measured in a sufficiently wide range of angles of incidence and scattering, it is possible to determine the two-dimensional distribution of the rough surface slopes on the basis of the formula (9.9.9).

For normally distributed slopes

$$w(\zeta_x, \zeta_y) = (2\pi\delta_x\delta_y)^{-1} \exp \left[-\frac{1}{2} \left(\frac{\zeta_x^2}{\delta_x^2} + \frac{\zeta_y^2}{\delta_y^2} \right) \right] \quad (9.9.11)$$

where δ_x^2 and δ_y^2 are the mean-square surface slopes along x and y , we obtain from (9.9.9)

$$m_s = (V\tilde{F})^2 (2\pi\delta_x\delta_y)^{-1} \exp \left[-\frac{1}{2q^2} \left(\frac{\kappa_x^2}{\delta_x^2} + \frac{\kappa_y^2}{\delta_y^2} \right) \right]. \quad (9.9.12)$$

In the case of an isotropic rough surface $\delta_x = \delta_y \equiv \delta$ we have

$$m_s = (V\tilde{F})^2 (2\pi\delta^2)^{-1} \exp \left(-\frac{\kappa^2}{2q^2\delta^2} \right). \quad (9.9.13)$$

To estimate the reverberation the value of the backscattering coefficient must be used. In this case $\xi = -\xi_0$, $\kappa = 2\xi_0 = 2k \sin \theta_0$, $q = 2k \cos \theta_0$, and, therefore,

$$m_s(\theta_0) = V^2 (8\pi\delta^2 \cos^4 \theta_0)^{-1} \exp \left(-\frac{\tan^2 \theta_0}{2\delta^2} \right). \quad (9.9.14)$$

9.9.1 Scattering Pattern

It is convenient to describe the angular dependence of the scattering coefficient in terms of a scattering pattern determined by the relation

$$D(\theta, \varphi) \equiv m_s(\theta, \varphi)/m_0$$

where m_0 is the scattering coefficient in the specular direction ($\kappa = 0$).

For isotropic roughness with normally distributed slopes, using (9.9.13), we obtain

$$D(\theta, \varphi) = 4\tilde{F}^2 \exp \left(-\frac{\kappa^2}{2q^2\delta^2} \right). \quad (9.9.15)$$

According to (9.3.12, 13), we have

$$\kappa^2 = \kappa_x^2 + \kappa_y^2 = k^2 [\sin^2 \theta + \sin^2 \theta_0 - 2 \sin \theta \sin \theta_0 \cos(\varphi - \varphi_0)]. \quad (9.9.16)$$

Thus, $D(\theta, \varphi)$ only depends on φ and φ_0 in terms of the difference $\varphi - \varphi_0$. This is trivial for the isotropic roughness. It is less trivial, however, that for $\varphi = \varphi_0$ the function $D(\theta, \varphi_0)$ can be represented in the form

$$D(\theta, \varphi_0) = \cos^{-4}(\Delta\theta/2) \exp \left[-\frac{\tan^2(\Delta\theta/2)}{2\delta^2} \right] \quad (9.9.17)$$

where we used the trigonometrical identity

$$\frac{\sin \theta - \sin \theta_0}{\cos \theta + \cos \theta_0} = \tan(\Delta\theta/2)$$

with $\Delta\theta = \theta - \theta_0$. Thus, the scattering pattern in the vertical plane only depends on the difference $\theta - \theta_0$. Hence, when the angle θ_0 changes, the pattern turns at the same angle without changing its form.

For small slopes ($\delta \ll 1$) the scattered field is concentrated near the specular direction and rapidly falls off with distance from it. According to (9.9.17), the effective angular half-width of the scattering pattern $\Delta\theta$, defined by the function $D(\theta, \varphi_0)$ reaching e^{-1} of its maximum value, is found from the equation

$$\tan(\Delta\theta/2) = \sqrt{2}\delta,$$

or for small values of δ

$$\Delta\theta = \sqrt{2}\delta. \quad (9.9.18)$$

Figure 9.6 shows the dependence of $\Delta\theta$ on the wind speed for scattering from the rough sea surface. For calculations, (9.9.18) has been used where δ was determined by the relation [9.19]

$$\delta^2 = (3 + 5.12 v) \cdot 10^{-3},$$

where v is the wind speed, in m/s.

As follows from (9.9.15, 16), the dependence of $D(\theta, \varphi)$ on the azimuthal angle φ is weaker. There is no such dependence at all for $\theta = \theta_0 = 0$ (normal incidence). For $\theta = \theta_0 \neq 0$ we have $\kappa^2/q^2 = \tan^2 \theta \sin^2[(\varphi - \varphi_0)/2]$. Hence, the effective angular half-width $\Delta\varphi = \varphi - \varphi_0$ of the scattering pattern in the horizontal plane

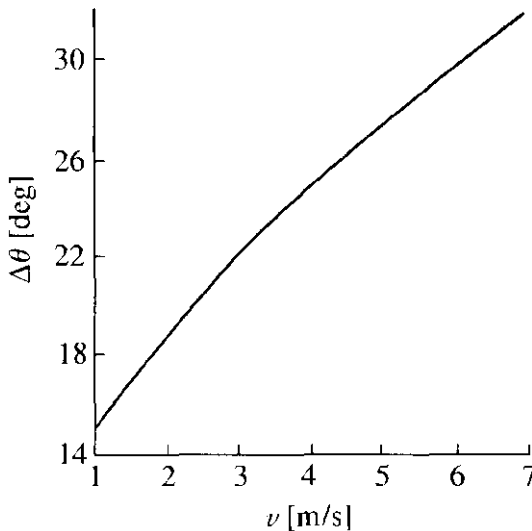


FIGURE 9.6. Dependence of the effective angular half-width of the scattering pattern of the rough sea surface on the wind speed for the case when the tangent plane approximation applies

is determined from the relation

$$\sin(\Delta\varphi/2) = \sqrt{2\delta}/\tan\theta_0.$$

For $\tan\theta_0 < \sqrt{2\delta}$ the last equation is meaningless. The function $D(\theta, \varphi)$ changes less than a factor of e^{-1} times its maximum value when φ changes by 2π . At small values of $\Delta\varphi$ we have

$$\Delta\varphi = 2\sqrt{2\delta}/\tan\theta_0. \quad (9.9.19)$$

With increasing angle θ_0 the directivity of the scattered field in the horizontal plane increases ($\Delta\varphi$ decreases).

When deriving expression (9.9.8) for the intensity of the scattered field in the far zone we started from expression (9.8.9) which is valid for $R \gg l^2/\lambda$. But it can be shown that the validity of the expression is, in fact, restricted to a considerably weaker condition. To prove this statement it is necessary at first to find an expression for the intensity of the scattered field using the general expression (9.7.4) and only then to make approximation corresponding to the far zone. In this case, the criterion of the far zone for a very rough surface ($k\sigma \gg 1$) has the form [9.6]

$$R \gg \frac{\varrho_0 l}{2\pi\sigma} = \frac{l^2}{\lambda} \left(\frac{\varrho_0}{lk\sigma} \right), \quad (9.9.20)$$

i.e., the distance to the far zone is $k\sigma(l/\varrho_0)$ times less than that given by the criterion presented above and, moreover, is independent of the wavelength of sound.

It is easy to give a simple physical interpretation of the condition (9.9.20). Let us denote by $\Delta\theta_c \equiv l/R$ an angle at which the scattering area is visible from the reference point, and by $\Delta\theta_p \equiv 2\Delta\theta = 4\sqrt{2\delta}$ the effective width of the scattering pattern. Then, keeping in mind that $\Delta \sim \sigma/\varrho_0$, (9.9.20) can be written as

$$\Delta\theta_c/\Delta\theta_p \ll 1. \quad (9.9.21)$$

Condition (9.3.6) can also be written in the form (9.9.21). The location of the reference point in the far and near zones is illustrated in Fig. 9.7. The ratio $\Delta\theta_c/\Delta\theta_p$ is one of the most important parameters in scattering theory.

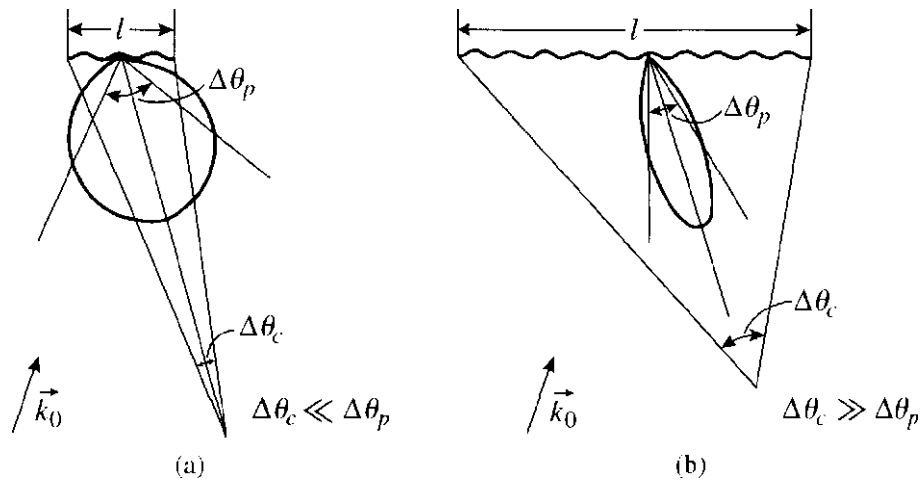


FIGURE 9.7. Position of the point of observation in the (a) far and (b) near zones with respect to the scattering section l . Thick curves show the scattering pattern

9.10 Frequency Spectrum

Now, we use the tangent plane approximation for evaluating the frequency spectrum of the sound field scattered at the rough sea surface. The temporal correlation function of the scattered field

$$B_s(\tau) = \langle p_s(t) p_s^*(t + \tau) \rangle, \quad B_s(0) = I_s$$

can be obtained by multiplying (9.9.4) by $\exp(i\omega_0\tau)$ and taking into account that now in (9.9.5) $\zeta_1 = \zeta(\mathbf{r}_1, t)$ and $\zeta_2 = \zeta(\mathbf{r}_2, t + \tau)$. For the case of normal distribution of ζ (which we assume) we have in (9.9.5) [Ref. 9.4; Sect. 3]

$$f_2(-\mathbf{q}, \mathbf{q}) = \exp\{-(q\sigma)^2[1 - N(\mathbf{q}, \tau)]\}, \quad \mathbf{q} = \mathbf{r}_2 - \mathbf{r}_1 \quad (9.10.1)$$

where $N(\mathbf{q}, \tau) = (1/\sigma^2)B(\mathbf{q}, \tau)$ is the correlation coefficient (normalized correlation function) of roughness.

If we change the variable \mathbf{r}_2 in (9.9.4) by \mathbf{q} , then the remaining integral over \mathbf{r}_1 gives an area of scattering section S . As a result we obtain (setting also $V = -1$)

$$B_s(\tau) = S \left(\frac{kF}{2\pi R_0} \right)^2 \exp(i\omega_0\tau) \int \exp\{i\boldsymbol{\kappa} \cdot \mathbf{q} - (q\sigma)^2[1 - N(\mathbf{q}, \tau)]\} d\mathbf{q}. \quad (9.10.2)$$

For a very rough surface $[(q\sigma)^2 \gg 1]$ the integrand in (9.10.2) rapidly falls off with increases in \mathbf{q} and τ , and the main contribution is given by small \mathbf{q} and τ . Therefore, $N(\mathbf{q}, \tau)$ can be expanded in a power series of $\mathbf{q} = \{x, y\}$ and τ . Retaining the terms not higher than second order, we obtain

$$N(x, y, \tau) = 1 - (1/\sigma^2)(a_1x^2 + a_2y^2 + a_3\tau^2 - a_4x\tau) \quad (9.10.3)$$

where

$$a_1 = -\frac{1}{2} \frac{\partial^2 B}{\partial x^2}, \quad a_2 = -\frac{1}{2} \frac{\partial^2 B}{\partial y^2}, \quad a_3 = -\frac{1}{2} \frac{\partial^2 B}{\partial \tau^2}, \quad a_4 = \frac{\partial^2 B}{\partial x \partial \tau} \quad (9.10.4)$$

at $x = y = \tau = 0$. The terms $\partial^2 B / \partial x \partial \tau$ and $\partial^2 B / \partial y \partial \tau$ are equal to zero due to symmetry considerations since the spatial spectrum of surface waves is symmetrical with respect to the mean wind direction (x axis).

Due to the dispersion of the surface waves the function $B(\mathbf{q}, \tau)$ can be represented in the form

$$B(\mathbf{q}, \tau) = \int_{-\infty}^{\infty} G_0(\boldsymbol{\kappa}) \cos(\boldsymbol{\kappa} \cdot \mathbf{q} - \Omega\tau) d\boldsymbol{\kappa}. \quad (9.10.5)$$

Then, using (9.4.2), we obtain for the case of the Pierson-Neumann spectrum (9.4.5), with $K = (2/\pi) \cos^2 \alpha$ for $|\alpha| \leq \pi/2$, and $K = 0$ for $|\alpha| > \pi/2$,

$$a_1 = \frac{3C\sqrt{\pi}}{16\sqrt{2}g^3} v, \quad a_2 = \frac{\sigma_1}{3}, \quad a_3 = \frac{C\sqrt{\pi}}{16\sqrt{2}g^3} v^3, \quad a_4 = \frac{2C}{3\pi g^3} v^2. \quad (9.10.6)$$

Substituting (9.10.3) into (9.10.2) and integrating over x and y from $-\infty$ to ∞ , we find

$$B_s(\tau) = A \exp[-q^2 E \tau^2 + i(\omega_0 + \kappa_x T) \tau], \quad (9.10.7)$$

where

$$A = \frac{\sqrt{3}\pi S}{a_1 q^2} \left(\frac{kF}{2\pi R_0} \right)^2 \exp \left(-\frac{\kappa_x^2 + 3\kappa_y^2}{4a_1 q^2} \right),$$

$$E = a_3 - \frac{a_4^2}{4a_1}, \quad T = \frac{a_4}{2a_1}. \quad (9.10.8)$$

Finally, substituting (9.10.7) into (9.5.1) yields

$$F(\nu) = \frac{A}{\sqrt{\pi} \Delta \nu} \exp \left[-\frac{(\nu - \nu_m)^2}{(\Delta \nu)^2} \right], \quad (9.10.9)$$

where

$$\nu_m = \omega_0 + \kappa_x T, \quad \Delta \nu = 2qE^{1/2}$$

are the frequency of the spectrum maximum and the half-width of the latter defined by that point when the function $F(\nu)$ reaches e^{-1} of its maximum value.

In general the central frequency of the scattered field is displaced relative to the frequency of the incident wave by the value

$$\nu_c = \nu_m - \omega_0 = \kappa_x T = 0.45 \kappa_x \nu. \quad (9.10.10)$$

In the specular direction only, $\kappa_x = 0$ and $\nu_m = \omega_0$, i.e., this frequency coincides with that of the incident wave. In the backwards direction $\kappa_x = -2k \sin \theta_0 \cos \varphi_0$ (9.3.12). For $|\varphi_0| < \pi/2$ (the x component of the vector \mathbf{k}_0 is directed downwind), $\kappa_x < 0$ and the spectral maximum is displaced toward low frequencies. In contrast, for $|\varphi_0| > \pi/2$ (the x component of the vector \mathbf{k}_0 is directed upwind), $\kappa_x > 0$ and the spectral maximum is displaced towards high frequencies. This displacement is due to the Doppler effect. In the first case a surface wave is moving away from the observer, whereas in the second towards the observer.

Using (9.10.6, 8) we obtain

$$\Delta \nu = 1.75 \cdot 10^{-2} q \nu^{3/2}. \quad (9.10.11)$$

The wind speed ν is expressed in m/s, $q = k(\cos \theta + \cos \theta_0)$ in m^{-1} . It can be seen that the width of the frequency spectrum $\Delta \nu$ increases with the wind speed and sound frequency and decreases with angles θ_0 and θ . Let us assume $\theta = \theta_0 = 45^\circ$, $\varphi = 0$, $f = 3$ kHz, and $\nu = 10$ m/s. Then $\nu_c = -13$ Hz and $\Delta \nu = 2$ Hz. It is interesting to note that the frequency corresponding to the maximum of the rough sea surface spectrum for $\nu = 10$ m/s is about 0.1 Hz.

9.11 Sound Scattering from a Surface with Two Scales of Roughness

In the previous sections the scattering of sound by small and large irregularities has been considered separately. However, the rough sea surface and ocean bottom usually have a relatively broad spatial spectrum (Sects. 1.5, 9). For a theoretical description of the wave scattering from such surfaces we use a method which is a combination of the MSP and the tangent plane approximation. It is based on the assumption that surface roughness can be divided into two components—a small-scale component and a large-scale one. We obtain such a “two-scale” model of the rough surface superimposing the surface with a small displacement $\zeta(\mathbf{r})$ upon another, smooth, large-scale surface $\eta(\mathbf{r})$ (Fig. 9.8). The rough surfaces $\zeta(\mathbf{r})$ and $\eta(\mathbf{r})$ must satisfy the conditions

$$2k\sigma_1 \sin \chi \ll 1, \quad \langle (\nabla_\eta \zeta)^2 \rangle \ll 1, \quad \sigma_1^2 \equiv \langle \zeta^2 \rangle \quad (9.11.1)$$

$$2k\mathcal{R} \sin \chi \gg 1 \quad (9.11.2)$$

where \mathcal{R} is the mean radius of curvature of the large-scale surface, χ is the local grazing angle measured from the tangent plane to the large-scale surface, and ∇_η is the gradient operator in the tangent plane.

Now the scattering coefficient m_s can be represented in the form

$$m_s = m_1 + m_2 \quad (9.11.3)$$

where m_2 is the scattering coefficient (9.9.14) for the surface $\eta(\mathbf{r})$ calculated by using the tangent plane method and m_1 is the scattering coefficient for $\zeta(\mathbf{r})$ overlapping the large-scale rough surface $\eta(\mathbf{r})$.

To obtain m_1 we use the following simple considerations. The effect of the large-scale underlying surface $\eta(\mathbf{r})$ consists in changing local angles at which small-scale roughness is insonified. We shall assume that an insonified region of $\eta(\mathbf{r})$ has linear dimensions which are small in comparison with its radius of curvature and large in comparison with the correlation radius of the small-scale roughness. Within this region the direction of the normal \mathbf{n} to the surface $\eta(\mathbf{r})$ can be assumed constant. Then the local scattering coefficient due to the small-scale roughness in this region can be calculated as if this region were a plane (Sect. 9.3). We shall denote this coefficient by $m_{\text{loc}}(\boldsymbol{\kappa}_\eta)$ where $\boldsymbol{\kappa}_\eta$ is the projection of the vector $\mathbf{k} - \mathbf{k}_0$ on the plane tangent to the surface $\eta(\mathbf{r})$, \mathbf{k}_0 and \mathbf{k} being the wave vectors of the incident and scattered waves, respectively. To find m_1 , the quantity

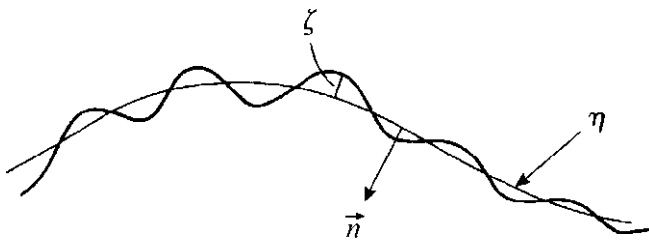


FIGURE 9.8. Decomposition of a rough surface into small- and large-scale components

$m_{\text{loc}}(\boldsymbol{\kappa}_\eta)$ should be averaged over all possible large-scale surface slopes

$$m_1 = \int m_{\text{loc}}(\boldsymbol{\kappa}_\eta) w(\mathbf{a}) d\mathbf{a}, \quad (9.11.4)$$

where $w(\mathbf{a}) = w(\nabla_\perp \eta)$ is the two-dimensional distribution of these slopes.

Let us apply this theory to scattering caused by a ripple on a large wind wave or swell. The local scattering coefficient due to the ripple, using (9.3.11), can be written in the form

$$m_{\text{loc}}(\boldsymbol{\kappa}_\eta) = (4/n_z)(\mathbf{k} \cdot \mathbf{n})^2 (\mathbf{k}_0 \cdot \mathbf{n})^2 G(\boldsymbol{\kappa}_\eta), \quad (9.11.5)$$

where

$$G(\boldsymbol{\kappa}_\eta) = (2\pi)^{-2} \int_{-\infty}^{\infty} B(\boldsymbol{\varrho}) \exp(-i\boldsymbol{\kappa}_\eta \cdot \boldsymbol{\varrho}) d\boldsymbol{\varrho} \quad (9.11.6)$$

is the spatial spectrum of the ripple, and $B(\boldsymbol{\varrho})$ is its correlation function. The factor $1/n_z$ in (9.11.5) is due to the slope of the surface η .

Substituting (9.11.5) into (9.11.4), we obtain

$$m_1 = 4 \int (1/n_z)(\mathbf{k} \cdot \mathbf{n})^2 (\mathbf{k}_0 \cdot \mathbf{n})^2 G(\boldsymbol{\kappa}_\eta) w(\mathbf{a}) d\mathbf{a}, \quad (9.11.7)$$

which is a generalization of (9.3.11) for the case that the mean surface is not a plane. If $\eta = 0$, the quantities

$$n_z = 1, \quad \mathbf{k} \cdot \mathbf{n} = \gamma = k \cos \theta, \quad \mathbf{k}_0 \cdot \mathbf{n} = \gamma_0 = k \cos \theta_0, \quad G(\boldsymbol{\kappa}_\eta) = G(\boldsymbol{\kappa})$$

are independent of the integration variable $\mathbf{a} = \nabla_\perp \eta$ and can be taken outside the integral sign. Then, the integral over \mathbf{a} will be equal to unity and (9.3.11) immediately follows from (9.11.7).

Let us consider the simplest case of the isotropic ripple characterised by the correlation function

$$B(\boldsymbol{\varrho}) = 2\sigma_1^2 J_1(\boldsymbol{\varrho}/\varrho_1)(\boldsymbol{\varrho}/\varrho_1)^{-1}, \quad (9.11.8)$$

where J_1 is the Bessel function of first order, and ϱ_1 is the correlation radius of the ripple. In this case

$$G(\boldsymbol{\kappa}_\eta) = \begin{cases} (1/\pi)(\sigma_1 \cdot \varrho_1)^2, & \kappa_\eta \varrho_1 < 1 \\ 0, & \kappa_\eta \varrho_1 > 1. \end{cases} \quad (9.11.9)$$

Since κ_η is always less than or equal to $2k$, the condition $\kappa_\eta \varrho_1 < 1$ reduces to $k\varrho_1 \leq 0.5$.

We also assume that the slopes of the large waves are isotropic and normally distributed,

$$w(\mathbf{a}) = (2\pi\delta^2)^{-1} \exp(-a^2/2\delta^2). \quad (9.11.10)$$

Under these assumptions the integral in (9.11.7) is reduced by simple transformations to the probability integral [9.20]. Figure 9.9 shows the ratio $Q = m_1/\tilde{m}_1$ for backscattering as a function of the angle of incidence θ_0 , where \tilde{m}_1 is the scattering coefficient from the ripple located on the plane ($\eta = 0$). Different curves

correspond to the different root-mean-square slopes values δ of the large-scale roughness. Figure 9.9 illustrates that with an increase of the angle of incidence θ_0 and δ the role played by large waves in the backscattering of sound at a ripple becomes more important. This effect is due to the fact that for scattering in the backwards direction a relative decrease of the local angle of incidence is most significant at large angles of incidence.

The backscattering coefficient m_2 due to the large-scale part of the roughness spectrum for a normal distribution (9.11.10) is given by (9.9.14) where $V = -1$.

Figure 9.10 illustrates the dependence of the total scattering coefficient $m_s = m_1 + m_2$ on the angle of incidence θ_0 . As can be seen, the scattering coefficient m_1 is considerably less than m_2 for small values of θ_0 but with an increase of θ_0 it decreases more slowly than m_2 , and at an angle $\theta_0 \geq 25^\circ$ it is greater than m_2 . Such a dependence of the scattering coefficient m_s on the angle of incidence θ_0 is typical for a two-scale model. The results of numerical calculation of the backscattering coefficient for the real sea surface (solid curves) are given in Fig. 1.26. The calculations have been carried out on the basis of the two-scale model and with use of the empirical spectra for ripple and large waves. As may be seen, the theoretical results are in satisfactory agreement with experimental data except that at small angles of incidence the measured values systematically exceed the computed ones. This disagreement increases with increasing sound frequency. A possible reason for such a disagreement is the occurrence of air bubbles under the rough sea surface which has not been taken into account in the theory discussed above.

The two-scale model of a scattering surface was first proposed by *Kur'yanov* [9.20]. *Fuks* [9.21] has formulated the conditions of its applicability to the case of the rough surface with continuous spatial spectrum.

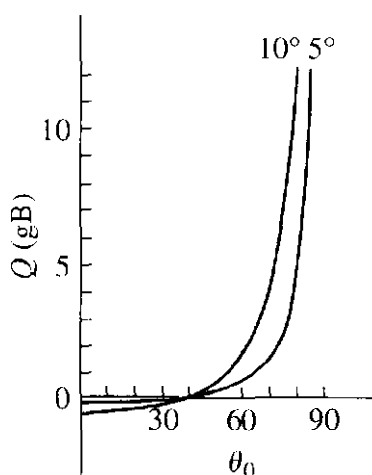


FIGURE 9.9. Factor Q vs the angle of incidence θ_0 for various mean-square slopes of large-scale irregularities

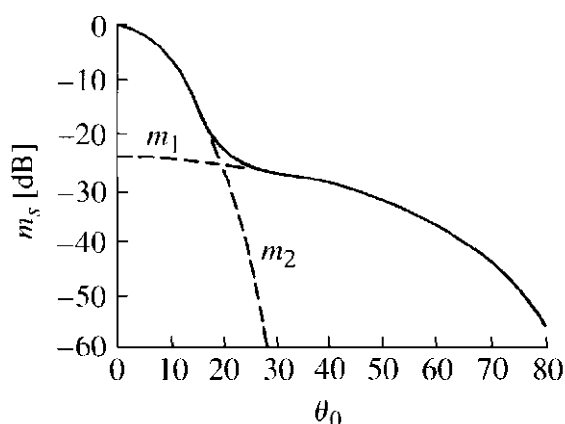


FIGURE 9.10. Backscattering coefficient m_s as a function of the angle of incidence θ_0 . $(k\sigma_1)^2 = 0.05$, $(k\sigma_2)^2 = 0.1$, $\delta = 0.1$

9.12 Surface Channel with a Rough Boundary

The roughness of the sea surface has an especially intense effect on the propagation of sound in a surface sound channel since sound waves have multiple contacts with the surface in this case. At each contact the coherent component of the sound field (specularly reflected waves) decreases due to scattering caused by the sea roughness. Simultaneously, this scattering increases the fluctuating (incoherent) field component which is of a random nature. As sound waves propagate in the channel, the acoustic energy is continuously “pumped over” from the coherent component to the incoherent one. As a result, the intensity of the coherent component decreases with distance more quickly than for the case of the smooth upper boundary. In addition to the decay due to the spreading of the wave front and absorption in water, the exponential decay appears due to scattering. As the reference point moves away from the source, the total sound field becomes more and more randomized.

The rate of decay of the incoherent component depends greatly on the properties of the rough sea surface: the wider its scattering pattern, the more quickly the incoherent component decreases. This is due to the fact that part of the acoustical energy of this component is carried away from the channel by waves scattered at angles exceeding the critical angle.³ As a result of this energy leakage from the channel, the sound intensity level in the region below the channel increases.

In this section a decay law for the coherent component is obtained in the ray approximation (it is assumed that the sound wavelength is small compared to the thickness of the channel). The calculation of the incoherent component is a significantly more complicated problem which is not considered here. Some results have been obtained by *Meecham* [9.22], *Kryazhev et al.* [9.23], and *Beilis and Tappert* [9.24].

9.12.1 Attenuation Along a Single Ray

If the sea surface is ideally smooth, the sound intensity along a ray at horizontal distance r and at depth z is given by (2.5.2),

$$I(r, z) = I_0 \cos \chi_1 \left(r \left| \frac{\partial r}{\partial \chi_1} \right| \sin \chi \right)^{-1}, \quad (9.12.1)$$

where $I_0 = W/4\pi$ is the sound intensity at a unit distance from the source, W the power output of the source, and χ_1 and χ are the grazing angles at the depths of the source z_1 and receiver z , respectively. However, if the sea surface is rough, the intensity of a specularly reflected ray decreases by a factor $|V_c|^{2N}$ where V_c is the coherent reflection coefficient (Sects. 9.6, 8), and N is the number of reflections of the given ray from the sea surface. For $N \gg 1$ (large r), $N \simeq r/D(\chi_0)$ where $D(\chi_0)$ is the cycle length of a ray the grazing angle of which is equal to χ_0 near the surface.

³The grazing angle near the sea surface of a ray turning at the lower boundary of the surface channel.

Consider just the small values of the Rayleigh parameter for which the modulus of V_c differs only slightly from unity, $1 - |V_c|^2 \equiv \varepsilon \ll 1$, $|V_c|^2 \simeq \exp(-\varepsilon)$. Then we have approximately

$$|V_c|^{2N} = \exp(-\beta r), \quad (9.12.2)$$

where

$$\beta \equiv [1 - |V_c(\chi_0)|^2]/D(\chi_0) \quad (9.12.3)$$

is the attenuation coefficient due to scattering at the rough surface. Now, using (9.12.1), we obtain

$$I(r, z) = I_0 \cos \chi_1 \left(r \left| \frac{\partial r}{\partial \chi_1} \right| \sin \chi \right)^{-1} \exp(-\beta r). \quad (9.12.4)$$

Let us suppose that the surface channel is formed by a linear increase in the sound velocity from the surface to a depth h ; below this depth the sound velocity remains constant or decreases with depth. In this case (6.1.11)

$$D(\chi_0) = (2/a) \tan \chi_0, \quad (9.12.5)$$

where a is the relative sound velocity gradient. Substitution of (9.12.5) in (9.12.3) yields

$$\beta = a[1 - |V_c(\chi_0)|^2]/2 \tan \chi_0. \quad (9.12.6)$$

For small values of the Rayleigh parameters, the reflection coefficient V_c is determined for different cases by (9.6.5–7). If we use expression (9.6.5), taking into account that $\chi_0 = \pi/2 - \theta_0$, we find from (9.12.6)

$$\beta = a(k\sigma)^2 \sin 2\chi_0. \quad (9.12.7)$$

The smaller the grazing angle χ_0 (if $\chi_0 < \pi/4$), the less the attenuation is. Since the root mean square of the sea surface displacement σ depends on the wind speed v , β also depends on v . The explicit forms of the functions $\sigma(v)$ and $\beta(v)$ are determined by the spectrum of the sea roughness. In particular, for the Pierson-Neumann frequency spectrum (9.4.5), we have

$$\sigma \simeq 0.18 \cdot 10^{-2} v^{2.5} \text{ m} \quad (9.12.8)$$

where v is the wind speed in m/s.

Substitution of (9.12.8) yields

$$\beta \simeq 2.4 \cdot 10^{-1} a f^2 v^5 \sin 2\chi_0 \text{ [dB/km]} \quad (9.12.9)$$

where f is the sound frequency [kHz], and a is the relative gradient of the sound velocity [m^{-1}].

Expression (9.6.5) for V_c holds when $k\rho_0 \sin^2 \chi_0 \gg 1$ (ρ_0 is the correlation radius of the roughness). In contrast, when $k\rho_0 \gg 1$ but $k\rho_0 \sin^2 \chi_0 \ll 1$, V_c is given by (9.6.6). For the case of isotropic sea roughness described by the spectrum (9.4.5), we obtain

$$\beta \simeq 4.3 \cdot 10^{-1} a f^{3/2} v^4 \text{ [dB/km]}. \quad (9.12.10)$$

All parameters are expressed in the same units, as above.

In this case the attenuation coefficient is proportional to the frequency to the 3/2 power which corresponds to the known empirical law obtained for the USC [9.25]. At small grazing angles the attenuation coefficient is the same for all rays.

It should be noted that (9.12.9, 10) are only valid for small values of the Rayleigh parameter ($P^2 \ll 1$).

9.12.2 Averaged Decay Law for a Coherent Field

To approximately estimate the mean square of the sound pressure of the coherent field due to all specularly reflected rays arriving at a reference point, it is advisable to use (5.6.3). This defines the average decay law with distance for the sound pressure squared in a shallow sea when rays undergo multiple reflections from a smooth bottom. These two problems will be quite similar if V is replaced by V_c in (5.6.3).

Equation (5.6.3), using (9.12.2), can also be written as

$$|p(r, z)|^2 = 2r^{-1}(c_1/c_0)^2 \exp(-\beta_0 r) \int_{q_1}^q \frac{\exp(-\beta r) \sin 2\chi_0}{\sin \chi_1 \sin \chi D(\chi_0)} d\chi_0, \quad (9.12.11)$$

where χ_1 , χ , and χ_0 are related by Snell's law

$$\cos \chi_1/c_1 = \cos \chi/c = \cos \chi_0/c_0,$$

c_1 , c , c_0 being values of the sound velocity at the source, receiver, and surface ($z = 0$). In (9.12.11), in contrast to (5.6.3), the absorption coefficient in water is denoted as β_0 . The quantities q , q_1 , and q_2 are given by

$$q = [2(c_h - c_0)/c_0]^{1/2}, \quad q_1 = [2(c_{\max} - c_0)/c_0]^{1/2}, \\ q_2 = [2(c_{\min} - c_0)/c_0]^{1/2},$$

where c_h is the sound velocity at the lower boundary of the surface channel $z = h$, and c_{\max} and c_{\min} are the sound velocities at $z_{\max} = \max\{z, z_1\}$ and $z_{\min} = \min\{z, z_1\}$, respectively.

If the attenuation coefficient β is not a function of the grazing angle χ_0 , then $\exp(-\beta r)$ in (9.12.11) can be taken outside the integral,

$$|p(r, z)|^2 = 2r^{-1}(c_1/c_0)^2 \exp[-(\beta_0 + \beta)r] \int_{q_1}^q \frac{\sin 2\chi_0 d\chi_0}{\sin \chi_1 \sin \chi D(\chi_0)}. \quad (9.12.12)$$

Thus, for $|p(r, z)|^2$ we have the cylindrical law of decay with an additional attenuation.

Consider in more detail the case of the linear surface channel. Now $D(\chi_0)$ is given by (9.12.5). Taking into account further, that the grazing angles are small, we obtain

$$|p(r, z)|^2 = 4ar^{-1}(c_1/c_0)^2 \exp[-(\beta_0 + \beta)r] \int_{q_1}^q \frac{d\chi_0}{[(\chi_0^2 - q_1^2)(\chi_0^2 - q_2^2)]^{1/2}}. \quad (9.12.13)$$

The integral in (9.12.13) is reduced by substituting $\sin \alpha = (\chi_0^2 - q_1^2)^{1/2} / (\chi_0^2 - q_2^2)^{1/2}$ to the elliptic integral of the first kind,

$$F(\mu, t) = \int_0^\mu (1 - t^2 \sin^2 \alpha)^{-1/2} d\alpha,$$

where

$$\mu = \arcsin[(q - q_1)/(q - q_2)]^{1/2}, \quad t = (q_2/q_1)^{1/2}.$$

As a result, we have

$$|p(r, z)|^2 = 4a(rq_1)^{-1}(c_1/c_0)^2 F(\mu, t) \exp[-(\beta_0 + \beta)r]. \quad (9.12.14)$$

If the attenuation coefficient β is a function of χ_0 , the value of the integral in (9.12.11) can be found either numerically, or asymptotically under some additional assumptions concerning the parameters of the problem being considered.

9.13 Fore-reverberation of Sound in the Ocean

According to ray theory, the spatial-temporal structure of the sound field in the USC at large distances from the sound source represents a discrete set of pulses arriving to a receiving point along different ray paths. The number of pulses and their arrival times are a functional of a sound velocity profile $c(z)$ and depend upon the distance from the sound source.

This picture turned out to be far from complete. In experiments with explosive sources in a surface sound channel in deep ocean it has been observed that before arrival of pulses which correspond to the profile $c(z)$, a prolonged continuous signal appeared [9.26]. Later it was called *fore-reverberation*.⁴ Further investigations have shown that the fore-reverberation is observed in the SOFAR channel also.

Figure 9.11 is the record of the sound signal at a distance of ~ 290 km from an explosive source in the surface sound channel. The source and receiver are located at depths of 300 and 200 m, respectively, in a 5000-m-deep ocean. A sound pulse has propagated along the ray that has made 6 cycles. The fore-reverberation (A), the main part of signal (B), and reverberation (C) are clearly discerned.

The fore-reverberation is observed only when a sound pulse propagates along a ray that has made not less than one whole cycle near the axis of the USC, or has had not less than one reflection from the rough sea surface. The fore-reverberation is absent for a pulse travelling along the limiting ray tangent to the bottom or the lower boundary of the USC.

The fore-reverberation intensity increases towards the moment of the arrival of the main signal and is usually higher than that of the reverberation. Its relative intensity grows also as the distance from the source increases and, at distances of some hundreds of kilometres attains 0.2–0.3 of the maximum value of main peak.

⁴In contrast to reverberation which is a signal which is observed after the arrival of the main pulses.

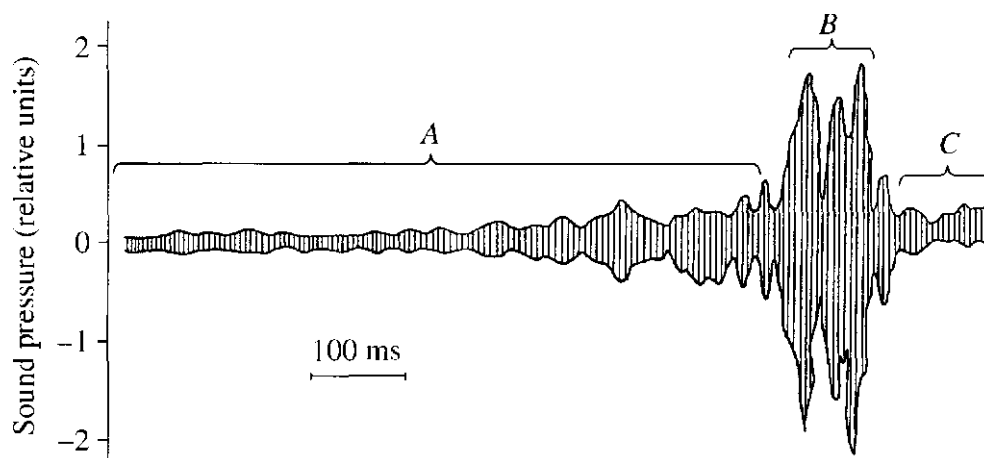


FIGURE 9.11. Shape of a sound signal in deep ocean at a range of 290 km. A—fore-reverberation, B—main part of the signal, C—reverberation

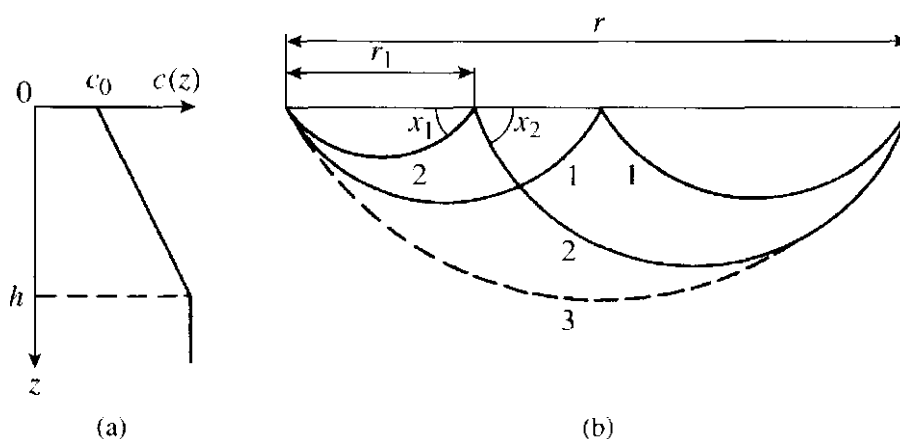


FIGURE 9.12. Fore-reverberation: (a) profile $c(z)$, (b) ray diagram

The duration of the fore-reverberation at a range of about 300 km exceeds 300 ms and grows as the distance increases.

The fore-reverberation is due to sound scattering from volume inhomogeneities in water or from the roughness of ocean boundaries. Below we consider a model of the fore-reverberation related to the sound scattering from a rough sea surface [9.26]. Figure 9.12 shows the profile $c(z)$ for the surface sound channel (a) and a corresponding ray diagram (b). Let the sound velocity in a layer $0 \leq z \leq h$ vary according to $c(z) = c_0(1 + az)$, where a is the relative gradient of the sound velocity. The source and receiver are assumed to be located near the surface. Consider a ray 1 (Fig. 9.12) which experiences specular reflection at a point located at a distance $r/2$ from the source, and makes two cycles. If the ocean surface is smooth, the next pulse will arrive at the receiving point along a ray that has made three cycles. But in the case of a rough surface some pulses will come along scattered rays which have also made two cycles. It can be shown that the pulse along ray 2 arrives earlier than the pulse along ray 1. Using (2.3.4) and taking into account that grazing angles of rays in the USC are small, we obtain for the difference between

arrival times of pulses along rays 1 and 2 (duration of fore-reverberation):

$$\Delta t_2 = T_0[1 - 4(r_1/r) + 4(r_1/r)^2], \quad (9.13.1)$$

where the index 2 indicates the number of cycles and $T_0 = a^2 r^3 / 32 c_0$. The meaning of r and r_1 is clear from Fig. 9.12. The plot of the function $\Delta t_2 / T_0$ is shown in Fig. 9.13. The interval Δt_2 attains a maximum value at $r_1 \rightarrow 0$ or $r_1 \rightarrow r$, i.e., in the cases when a pulse before or after scattering propagates along a ray close to the limiting ray 3. For the pulse travelling along the limiting ray the fore-reverberation is absent, since the arrival time along it is at a minimum.

If a ray has made $2N$ cycles, the duration of the fore-reverberation is

$$\Delta t_{2N} = N \Delta t_2. \quad (9.13.2)$$

Quite similarly we can estimate the duration of the fore-reverberation for an uneven number of cycles.

Using (9.13.1, 2), we can calculate the maximum duration of the fore-reverberation for the case of a surface sound channel that simulates experimental conditions in which the record of a sound signal (Fig. 9.11) has been obtained. For simplicity we assume that a constant gradient of the sound velocity ($a = 1.1 \cdot 10^{-5} \text{ m}^{-1}$) is observed from the sea surface to the very bottom of a 4650-m-deep ocean. The cycle length of a ray that has made 6 cycles over a range $r = 290 \text{ km}$ is 48.9 km. According to (6.1.12) the length of the limiting ray is 58 km. Thus, in this case the maximum duration is obtained at $r_1/r = 0.4$, and a scattered pulse propagates along the limiting ray. Setting $c_0 = 1.5 \cdot 10^3 \text{ m/s}$, we find $\Delta t_6 \approx 300 \text{ ms}$, which is in agreement with experimental data.

A measured duration sometimes can be less than the calculated one, if the angular width of the scattering pattern of the rough sea surface is not wide enough to include the grazing angle of the limiting ray. If the duration of the fore-reverberation is known, we can determine the effective angular width of the scattering pattern. Having measured a value Δt_2 , we find r_1 and $r - r_1$ (r is known) that are related to the grazing angles χ_1 and χ_2 (Fig. 9.12):

$$\chi_1 = \arctan(ar_1/2), \quad \chi_2 = \arctan[a(r - r_1)/2].$$

Then the difference $\Delta\chi = \chi_2 - \chi_1$ gives an estimation of the scattering pattern width for the case when a wave is incident upon the rough surface at the grazing angle χ_1 .

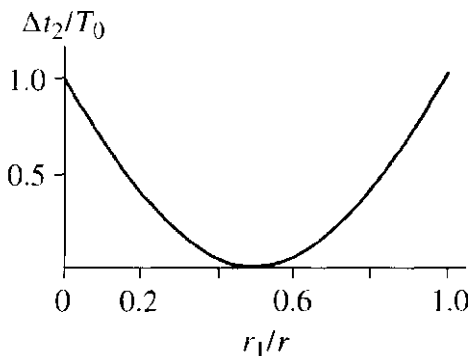


FIGURE 9.13. Dependence of fore-reverberation duration upon the ratio r_1/r

Moreover, from measured values of the fore-reverberation intensity $I(t)$, where $t \in \Delta t_2$, it is possible to determine an angular dependence of the scattering coefficient $m_s(\chi_1, \chi_2)$. At small grazing angles the focusing factor is close to unity and, therefore, $I(t) \sim I_0 m_s(\chi_1, \chi_2)$, where I_0 is the sound intensity in a homogeneous medium at the same distance r . The focusing factor can be also introduced, if necessary.

Using the model developed above, the increase in sound intensity towards the moment of the main signal arrival can be understood. The main signal propagates along the specularly reflected ray ($\chi_1 = \chi_2$) that corresponds to the maximum sound intensity. In contrast, scattered pulses propagate along rays deflected from the specular direction. The larger the ray deflection, the less the intensity of the scattered signal as well as arrival time of a pulse which propagates along this ray.

9.14 Small-Slope Approximation in Wave Scattering by Rough Surfaces

A small-slope method (SSM) is based on two tenets: first, the *Rayleigh* hypothesis on the feasibility to represent a scattered sound field as a superposition of plane waves propagating in the direction from a rough surface; second, the expansion of the scattering amplitude in a series in a small parameter $|\nabla \zeta|$ which is the rough surface slope [9.27–30]. In contrast to other parameters used in classic methods of wave scattering by rough surfaces, this parameter does not depend on the wavelength of incident radiation. This is a very important fact because the surface slope is really small in many cases. So, for the rough sea surface it is no larger than 0.1.

Below we will give the fundamentals of the small-slope method. We use the coordinate system shown in Fig. 9.1 and notations accepted in Sect. 9.2. Let a plane monochromatic wave $p_i(\mathbf{r}, z) = \exp(i\xi_0 \mathbf{r} + i\gamma_0 z)$ be incident from below on the rough surface $z = \zeta(\mathbf{r})$. The boundary condition at the rough surface is given by expression (9.2.1). According to the *Rayleigh* hypothesis, the total sound field in a half-space $z \leq \min \zeta(\mathbf{r})$ may be represented as

$$\begin{aligned} p(\mathbf{r}, z) &= p_i(\mathbf{r}, z) + p_s(\mathbf{r}, z) \\ &= \exp(i\xi_0 \mathbf{r} + i\gamma_0 z) + \int S(\xi, \xi_0) \exp(i\xi \mathbf{r} - i\gamma z) d\xi, \end{aligned} \quad (9.14.1)$$

where $S(\xi, \xi_0)$ is the scattering amplitude, $\gamma = (k^2 - \xi^2)^{1/2}$, and $\text{Im } \gamma \geq 0$. When integration limits are not denoted, the integral is assumed to be taken in infinite limits.

The *Rayleigh* hypothesis often was subjected to serious criticism. The point is that expression (9.14.1), correctly describing a sound field in the half-space $z \leq \min \zeta(\mathbf{r})$, is not the total solution to the Helmholtz equation in the region $\min \zeta(\mathbf{r}) \leq z \leq \max \zeta(\mathbf{r})$. In this region the total scattered field must be a sum of waves propagating from the rough surface and those propagating to the rough surface (in positive direction of the z axis). *Deryugin* [9.31] was the first to call

attention to this fact. However, for rather sloping surfaces, the Rayleigh hypothesis appeared valid. So *Millar* [9.32] has shown that this hypothesis is applicable for a particular case of the sinusoidal surface $\zeta(x) = a \cos px$ for $ap < 0.448$. According to the *Voronovich* estimation [9.33], the Rayleigh hypothesis, somewhat after its modification, will be valid even for a surface whose slope at each point is less than unity.

The knowledge of the scattering amplitude $S(\xi, \xi_0)$ allows one to find various characteristics of a scattered field, such as the mean (coherent) reflection coefficient V_c and the scattering coefficient m_s . The scattering amplitude is determined by the Rayleigh equation obtained in substituting expression (9.14.1) in the boundary condition (9.2.1):

$$\int S(\xi_1, \xi_0) \exp(i\xi_1 \mathbf{r} - i\gamma_1 \zeta) d\xi_1 = -\exp(i\xi_0 \mathbf{r} + i\gamma_0 \zeta), \quad (9.14.2)$$

where $\zeta \equiv \zeta(\mathbf{r})$ and $\gamma_1 = (k^2 - \xi_1^2)^{1/2}$.

Multiplying both sides of this equation by $\exp(-i\xi \mathbf{r} + i\gamma \zeta)$ and integrating with respect to \mathbf{r} , we find

$$\int S(\xi_1, \xi_0) \exp[-i(\xi - \xi_1)\mathbf{r} + i(\gamma - \gamma_1)\zeta] d\xi_1 d\mathbf{r} = -\int \exp(-i\kappa \mathbf{r} + iq\zeta) d\mathbf{r}, \quad (9.14.3)$$

where $\kappa = \xi - \xi_0$ and $q = \gamma + \gamma_0$.

Let us set $\exp[i(\gamma - \gamma_1)\zeta] = \{\exp[i(\gamma - \gamma_1)\zeta] - 1\} + 1$ and use the identity

$$\begin{aligned} & \int \exp[i(\xi - \xi_1)\mathbf{r}] \{\exp[i(\gamma - \gamma_1)\zeta] - 1\} d\mathbf{r} \\ &= -\left(\frac{\xi + \xi_1}{\gamma + \gamma_1}\right) \int \exp[-i(\xi - \xi_1)\mathbf{r} + i(\gamma - \gamma_1)\zeta] \nabla \zeta d\mathbf{r}, \end{aligned} \quad (9.14.4)$$

that is obtained with integrating by parts under the assumption that $\zeta(\mathbf{r}) \rightarrow 0$ for $\mathbf{r} \rightarrow \pm\infty$.

Take into account also that

$$\int S(\xi_1, \xi_0) \exp[-i(\xi - \xi_1)\mathbf{r}] d\mathbf{r} d\xi_1 = (2\pi)^2 S(\xi, \xi_0). \quad (9.14.5)$$

Substituting (9.14.4) and (9.14.5) in (9.14.3), we obtain

$$\begin{aligned} S(\xi, \xi_0) &= -(2\pi)^{-2} \int \exp(-i\kappa \mathbf{r} + iq\zeta) d\mathbf{r} + (2\pi)^{-2} \int \left(\frac{\xi + \xi_1}{\gamma + \gamma_1}\right) S(\xi_1, \xi_0) \\ &\quad \times \exp[-i(\xi - \xi_1)\mathbf{r}_1 + i(\gamma - \gamma_1)\zeta_1] d\mathbf{r}_1 d\xi_1, \end{aligned} \quad (9.14.6)$$

where $\zeta_1 \equiv \zeta(\mathbf{r}_1)$.

Now equation (9.14.6) contains the necessary small parameter $\nabla \zeta$, which allows one to seek the solution by the method of iterations. In zero order in $\nabla \zeta$ we obtain

$$S_0(\xi, \xi_0) = -(2\pi)^{-2} \int \exp(-i\kappa \mathbf{r} + iq\zeta) d\mathbf{r}. \quad (9.14.7)$$

The first approximation yields

$$\begin{aligned} S_1(\xi, \xi_0) = S_0(\xi, \xi_0) - (2\pi)^{-4} \int \left(\frac{\xi + \xi_1}{\gamma + \gamma_1} \right) \nabla \zeta_1 \\ \times \exp[-i(\xi_1 - \xi_0)\mathbf{r} - i(\xi - \xi_1)\mathbf{r}_1 + i(\gamma + \gamma_0)\zeta \\ + i(\gamma - \gamma_1)(\zeta_1 - \zeta)] d\mathbf{r} d\mathbf{r}_1 d\xi_1. \end{aligned} \quad (9.14.8)$$

Expression (9.14.8) can be significantly simplified. To do this, we replace the factor $\exp[i(\gamma - \gamma_1)(\zeta_1 - \zeta)]$ by unity in the second integral because in the expansion

$$\exp[i(\gamma - \gamma_1)(\zeta_1 - \zeta)] = 1 + i(\gamma - \gamma_1)(\zeta_1 - \zeta) + \dots \quad (9.14.9)$$

the second and following terms of the series introduce in $S_1(\xi, \xi_0)$ the contributions of the higher orders in $\nabla \zeta$. Introducing $\zeta(\mathbf{r}_1) = \int \zeta(\mathbf{u}) \exp(i\mathbf{u}\mathbf{r}_1) d\mathbf{u}$ and taking into account that the integral with respect to \mathbf{r}_1 yields the delta function $(2\pi)^2 \delta(\xi - \xi_1 - \mathbf{u})$, we write $S_1(\xi, \xi_0)$ as

$$\begin{aligned} S_1(\xi, \xi_0) = S_0(\xi, \xi_0) - (2\pi)^{-2} \int \left(\frac{2\xi - \mathbf{u}}{\gamma + \tilde{\gamma}} \right) i\mathbf{u} \tilde{\zeta}(\mathbf{u}) \\ \times \exp[-i(\xi - \xi_0 - \mathbf{u})\mathbf{r} + i(\gamma + \gamma_0)\zeta] d\mathbf{r} d\mathbf{u}, \end{aligned} \quad (9.14.10)$$

where $\tilde{\gamma} = [k^2 - (\xi - \mathbf{u})^2]^{1/2}$.

When integrating with respect to \mathbf{u} , the main contribution is given by values $\mathbf{u} \sim k(\xi - \xi_0)$. In view of this, we can expand a pre-exponential factor in (9.14.10), dependent on \mathbf{u} , in a series in powers of $(\xi - \xi_0 - \mathbf{u})$ and retain only the first term since following terms introduce a higher order of smallness in $\nabla \zeta$ [9.34].

Setting $\mathbf{u} = \xi - \xi_0$ in the expression standing in the parentheses, we obtain

$$\begin{aligned} S_1(\xi, \xi_0) = S_0(\xi, \xi_0) - (2\pi)^{-2} \int \left(\frac{\xi + \xi_0}{\gamma + \gamma_0} \right) i\mathbf{u} \tilde{\zeta}(\mathbf{u}) \\ \times \exp[-i(\xi - \xi_0 - \mathbf{u})\mathbf{r} + i(\gamma + \gamma_0)\zeta] d\mathbf{r} d\mathbf{u}. \end{aligned} \quad (9.14.11)$$

Now, taking into account that

$$i \int \mathbf{u} \tilde{\zeta}(\mathbf{u}) \exp(i\mathbf{u}\mathbf{r}) d\mathbf{u} = \nabla \zeta,$$

we write expression (9.14.11) as

$$\begin{aligned} S_1(\xi, \xi_0) = S_0(\xi, \xi_0) - (2\pi)^{-2} \int \left(\frac{\xi + \xi_0}{\gamma + \gamma_0} \right) \nabla \zeta \\ \times \exp[-i(\xi - \xi_0)\mathbf{r} + i(\gamma + \gamma_0)\zeta] d\mathbf{r}. \end{aligned} \quad (9.14.12)$$

Using the identity

$$\nabla \zeta \exp[i(\gamma + \gamma_0)\zeta] = -i(\gamma + \gamma_0)^{-1} \nabla \{\exp[i(\gamma + \gamma_0)\zeta] - 1\},$$

integrating by parts in (9.14.12), and uniting $S_0(\xi, \xi_0)$ and $S_1(\xi, \xi_0)$ in the single integral, we obtain for the scattering amplitude in the first approximation of the SSM the following expression:

$$S(\xi, \xi_0) = -(2\pi)^{-2} \left(\frac{2\gamma_0}{\gamma + \gamma_0} \right) \int \exp(-i\kappa \mathbf{r} + iq\zeta) d\mathbf{r}. \quad (9.14.13)$$

In what follows the index "1" for $S(\xi, \xi_0)$ is omitted. In the higher approximation, the scattering amplitude is given in [9.28].

The mean value of the scattered field in the first approximation of the SSM is given by

$$\langle p_s(\mathbf{r}, z) \rangle = \int \langle S(\xi, \xi_0) \rangle \exp(i\xi \mathbf{r} - i\gamma z) d\xi. \quad (9.14.14)$$

According to (9.14.13)

$$\langle S(\xi, \xi_0) \rangle = -V_c \delta(\xi - \xi_0), \quad (9.14.15)$$

where $V_c = f_1(q) = \langle \exp(iq\zeta) \rangle$ is the one-dimensional characteristic function of a random quantity $\zeta(\mathbf{r})$, which is defined by expression (9.8.5). For the normal distribution of $\zeta(\mathbf{r})$, we have $f_1(q) = \exp(-2\gamma_0^2 \sigma^2)$, where $\sigma^2 = \langle \zeta^2(\mathbf{r}) \rangle$ is the mean square of the rough surface displacement. Substituting (9.14.15) in (9.14.14) yields

$$\langle p_s(\mathbf{r}, z) \rangle = -V_c \exp(i\xi_0 \mathbf{r} - i\gamma_0 z), \quad (9.14.16)$$

where $V_c = \exp(-2\gamma_0^2 \sigma^2)$ is the mean (coherent) reflection coefficient, which coincides with the result given by the tangent plane approximation (9.8.7).

Now we determine the scattering coefficient m_s . Let us write the scattering amplitude as a sum of mean and fluctuation components

$$S(\xi, \xi_0) = \langle S(\xi, \xi_0) \rangle + \Delta S(\xi, \xi_0),$$

where $\langle S(\xi, \xi_0) \rangle = -V_c \delta(\xi - \xi_0)$, $\langle \Delta S(\xi, \xi_0) \rangle = 0$.

The intensity of the fluctuation component of the scattered field ΔI_s is connected with the scattering coefficient m_s by relationship (9.3.9) (in the latter the intensity of the fluctuation component is denoted as I_s). On the other hand, ΔI_s can be represented as the difference between the total intensity of the scattered field I_s and the intensity of the mean field, I_c : $\Delta I_s = I_s - I_c$.

Using expression (9.14.13), we easily find for the total scattered intensity I_s

$$I_s = \int_{\Gamma_1} \left\{ (2\pi)^{-2} \left(\frac{2\gamma_0}{\gamma + \gamma_0} \right) \int f_2(q, -q; \boldsymbol{\rho}) \exp(i\kappa \boldsymbol{\rho}) d\boldsymbol{\rho} \right\} d\xi, \quad (9.14.17)$$

where Γ_1 is the integration interval that corresponds to real values γ and $f_2(q, -q; \boldsymbol{\rho}) = \langle \exp(iq\zeta - iq\zeta_1) \rangle$ is the two-dimensional characteristic function of a random quantity $\zeta(\mathbf{r})$, $\boldsymbol{\rho} = \mathbf{r}_1 - \mathbf{r}$. For the normal distribution, the function $f_2(q, -q; \boldsymbol{\rho}) = \exp[-q^2 \sigma^2 + q^2 B(\boldsymbol{\rho})]$, where the correlation function of the surface displacement $B(\boldsymbol{\rho})$ is defined by expression (9.3.2). Taking into account that

$I_c = V_c^2$, we write the difference $I_s - I_c$ in the form

$$\Delta I_s = I_s - I_c = \int_{\Gamma_1} \Pi(\xi, \xi_0) d\xi, \quad (9.14.18)$$

where

$$\Pi(\xi, \xi_0) = (2\pi)^{-2} \int \left(\frac{2\gamma_0}{\gamma + \gamma_0} \right)^2 [f_2(q, -q; \rho) - V_c^2] \exp(i\kappa\rho) d\rho. \quad (9.14.19)$$

Changing the integration in (9.14.18) to θ and φ ($d\xi = \xi d\xi d\varphi$, $\xi = k \sin \theta$), we obtain

$$\Delta I_s = k^2 \int_0^{2\pi} \int_0^{\pi/2} \Pi(\xi, \xi_0) \sin \theta \cos \theta d\theta d\varphi. \quad (9.14.20)$$

From comparison between (9.14.20) and (9.3.9), we find the scattering coefficient

$$m_s = \gamma^2 \Pi(\xi, \xi_0) \quad (9.14.21)$$

or, in the explicit form,

$$m_s = (2\pi)^{-2} \int \left(\frac{2\gamma\gamma_0}{\gamma + \gamma_0} \right)^2 \exp(-q^2\sigma^2) \{ \exp[q^2 B(\rho)] - 1 \} \exp(i\kappa\rho) d\rho. \quad (9.14.22)$$

This is the basic formula for calculation m_s in the first-approximation SSM.

The applicability conditions of the SSM are determined by the following relationships [9.28]. If grazing angles of the incident and scattered waves are of the order of unity, it is sufficient then that $|\nabla\zeta| \ll 1$. At shallow grazing incidence (scattering), the condition of the applicability is more severe: $|\nabla\zeta| \ll \chi_{\min}$, where $\chi_{\min} = \min(\chi_0, \chi)$, which is necessary to avoid geometrical shadowing.

Figure 9.14 exhibits the cross section of the scattering pattern (in the vertical plane) of sound scattered by fully developed wind waves described by the *Pierson-Moscovitz* frequency spectrum (Sect. 9.4) (numerical calculations from formula (9.14.22) [9.35]). At low frequencies and directions far from the specular direction (curves 1 and 2), the angular dependence of the scattering coefficient in the approximation SSM coincides rather well with results of the MSP. In the specular direction, the scattering pattern exhibits a dip, which, however, does not reach zero level as in the scattering pattern in the approximation MSP. At frequencies 1–2 kHz, the scattering pattern near the specular direction corresponds to the tangent plane approximation. However, as the scattering direction deviates from the specular one, the intensity of the scattered field does not decay exponentially as in the case of the tangent plane approximation. At high frequencies (6 and 10 kHz), the SSM scattering pattern is similar to that in the tangent plane approximation but its maximum displaced from the specular direction, this displacement being increased with frequency. So, at a frequency of 10 kHz, this displacement reaches 10° . As frequency increases, one can observe the transition of the two-peak MSP scattering pattern to one-peak scattering pattern in the tangent plane approximation. The dip

in the specular direction gradually decreases to total disappearance and turns into a maximum. In this case, the width of scattering pattern lobes increases, but the magnitude of the maximum decreases. The last fact can be related to scattering of the acoustic energy in the specular direction, which is taken into account in the framework of the SSM.

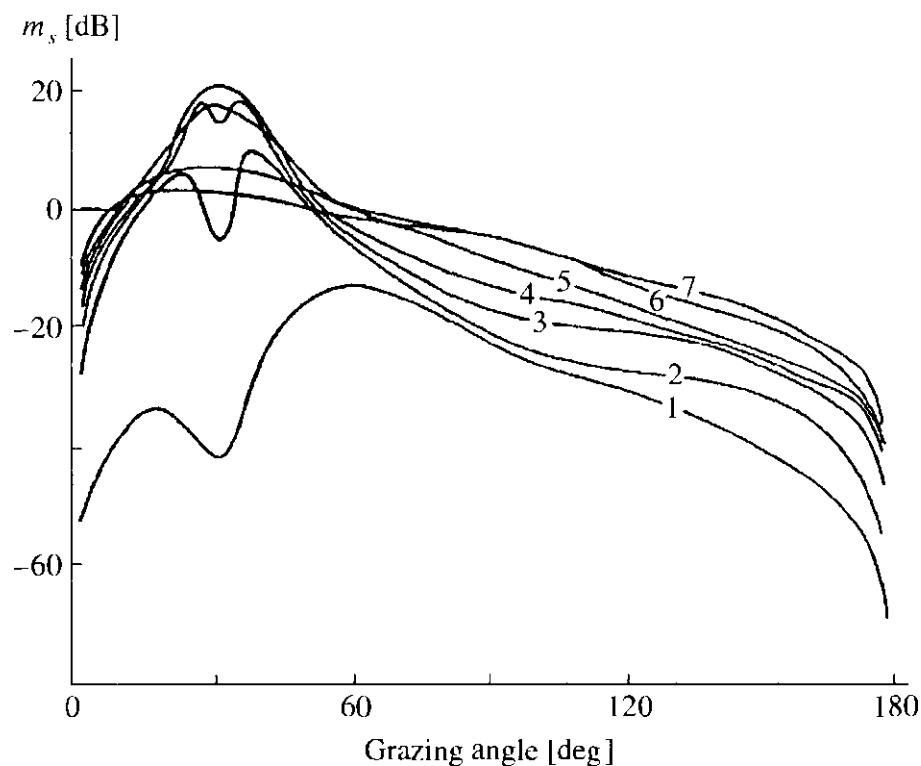


FIGURE 9.14. Cross section of the scattering pattern in the vertical plane by fully developed wind-driven waves ($v = 10$ m/s, angle of incidence $\chi_0 = 31^\circ$, sound frequencies (1) 80, (2) 200, (3) 500 Hz, (4) 1.0, (5) 2.0, (6) 6.0, (7) 10 kHz [9.35])

Sound Propagation in the Random Ocean

There are two types of inhomogeneities in the ocean, regular and random. The latter are produced by turbulence, internal waves, mesoscale eddies, etc. They cause the scattering of sound and fluctuations of its intensity, reduce coherence of sound waves and change their frequency spectrum.

Propagation of sound in a random inhomogeneous medium is described by a wave equation in which the sound velocity is a random function of coordinates and sometimes of time. The solution of this complicated statistical problem can only be obtained by means of approximate methods. At present the most developed of them are the method of small perturbations, the smooth perturbations method (Rytov's method), and the parabolic equation method.

Wave propagation theory in random inhomogeneous media is systematically presented in the books by *Tatarskii* [10.1], *Chernov* [10.2], and *Rytov et al.* [10.3], as well as some multiauthor books edited by *Flatte* [10.4], *Keller and Papadakis* [10.5], and *Strohbein* [10.6]. In the present chapter only some elements of the theory in application to the ocean are considered.

10.1 Amplitude and Phase Fluctuations

Let us suppose that a spatial scale a of random inhomogeneities is large compared with the sound wavelength λ ($a^{1/2} \gg \lambda^{1/2}$). In this case the ray acoustics approximation can be used. Numerical estimations show that the sound velocity (the refraction index) fluctuations in the ocean exceed density fluctuations by an order of magnitude [Ref. 10.2; Sect. 11]. Therefore, in what follows we will neglect the density fluctuations. The relative sound velocity fluctuations are not large either; in one typical example the root-mean-square quantity $\Delta c/c$ is equal to $\sim 5 \cdot 10^{-4}$ in the upper layers and $\sim 3 \cdot 10^{-6}$ at great depths [10.7]. Nevertheless for long-range sound propagation the effect can be rather marked.

10.1.1 Phase Fluctuations

We start from the eikonal equation (2.6.3), where the index of refraction $n(\mathbf{R})$ is now given as a sum of an average $n_0(z)$ (over the ensemble of realizations of the medium) and a random component $\mu(\mathbf{R})$,

$$n(\mathbf{R}) = n_0(z) + \mu(\mathbf{R}), \quad \langle \mu \rangle = 0, \quad \mathbf{R} = \{x, y, z\}. \quad (10.1.1)$$

We suppose that μ is small, $(\langle \mu^2 \rangle)^{1/2} \ll n_0$. Let us present the eikonal W as a series

$$W = W_0 + W_1 + W_2 + \dots \quad (10.1.2)$$

where W_0 satisfies the unperturbed eikonal equation

$$(\nabla W_0)^2 = n_0^2, \quad (10.1.3)$$

and W_1, W_2, \dots are the correction terms of first, second, etc. orders with respect to μ . Substituting (10.1.1) into (2.6.3), and taking (10.1.3) into account, we obtain in the next approximation in μ

$$\nabla W_0 \cdot \nabla W_1 = \mu n_0. \quad (10.1.4)$$

Since, according to (2.6.5),

$$\nabla W_0 = n_0 \mathbf{e} \quad (10.1.5)$$

where \mathbf{e} is a unit vector along an unperturbed ray, we find from (10.1.4)

$$\nabla W_0 \cdot \nabla W_1 = n_0(\mathbf{e} \cdot \nabla W_1) = n_0 \frac{dW_1}{ds} = \mu n_0, \quad (10.1.6)$$

where ds is an element of the ray. Hence, we obtain

$$W_1 = \int_0^s \mu ds, \quad (10.1.7)$$

where integration is carried out along the unperturbed ray.

The correlation function for fluctuations of the sound-wave phase $\varphi_1 = k_0 W_1$, where k_0 is the wave number at some fixed point in the medium, is, according to (10.1.7),

$$\begin{aligned} B_\varphi(\mathbf{R}_1, \mathbf{R}_2) &= k_0^2 \langle W_1(\mathbf{R}_1) W_1(\mathbf{R}_2) \rangle \\ &= k_0^2 \int_0^{s_1} ds' \int_0^{s_2} B_\mu(\mathbf{R}', \mathbf{R}'') ds'' \end{aligned} \quad (10.1.8)$$

where $B_\mu = \langle \mu(\mathbf{R}') \mu(\mathbf{R}'') \rangle$ is the correlation function for the refraction index fluctuations: $\mathbf{R}' = \mathbf{R}(s')$ and $\mathbf{R}'' = \mathbf{R}(s'')$ are the radii vectors of successive points on the rays; and s_1 and s_2 are the ray lengths between a source and the points \mathbf{R}_1 and \mathbf{R}_2 , respectively. Let us assume that in the absence of background regular inhomogeneities ($n_0 = 1$) the refraction index fluctuations are statistically homogeneous and the correlation function B_μ only depends on the separation $\mathbf{R}'' - \mathbf{R}'$. In our case, however, it also depends on the mean depth $z = (z' + z'')/2$ because of the horizontal stratification of the medium [$n_0 = n_0(z)$].

On the basis of the above assumptions we obtain

$$B_\varphi(\mathbf{R}_1, \mathbf{R}_2) = k_0^2 \int_0^{s_1} ds' \int_0^{s_2} B_\mu(\mathbf{R}'' - \mathbf{R}'; z) ds''. \quad (10.1.9)$$

Consider the rays arriving at the points \mathbf{R}_1 and \mathbf{R}_2 (Fig. 10.1), denoting by $\xi = s'' - s'$ a distance between the successive points along the upper ray, and by $\varrho(s')$ a transverse distance between the rays. Since a spatial scale of random fluctuations μ in the ocean is much less than a scale of variation of n_0 and, therefore, much less than the radius of curvature of rays, it is admissible to set, in the region of significant values of B_μ ,

$$\mathbf{R}'' - \mathbf{R}' \simeq \varrho(s') + \xi \mathbf{e}(s'),$$

where \mathbf{e} is a unit vector along the ray at point s' . We proceed now in (10.1.9) to the integration over ξ ,

$$B_\varphi(\mathbf{R}_1, \mathbf{R}_2) = k_0^2 \int_0^{s_1} ds \int_{-s}^{s_2-s} B_\mu[\xi, \varrho(s); z(s)] d\xi. \quad (10.1.10)$$

Since the function B_μ rapidly tends to zero for $|\xi| \geq \xi_0$, where ξ_0 is the correlation radius, the integration limits over ξ for $s_2 > s_1 \gg \xi_0$ can be extended from $-\infty$ to ∞ ,

$$B_\varphi(\mathbf{R}_1, \mathbf{R}_2) = k_0^2 \int_0^{s_1} ds \int_{-\infty}^{\infty} B_\mu[\xi, \varrho(s); z(s)] d\xi. \quad (10.1.11)$$

It can be shown that in the case $s_1 > s_2 \gg \xi_0$ the same expression for B_φ is obtained by replacing s_1 by s_2 . In both cases we have

$$B_\varphi(\mathbf{R}_1, \mathbf{R}_2) = k_0^2 \int_0^{s_m} ds \int_{-\infty}^{\infty} B_\mu[\xi, \varrho(s); z(s)] d\xi. \quad (10.1.12)$$

where $s_m = \min\{s_1, s_2\}$,

We now apply (10.1.12) to the case of a medium with $n_0 = 1$. Let a plane sound wave propagate along the x axis. The rays are parallel straight lines; the quantity ϱ does not depend on x and is equal to the transverse distance between the reference points \mathbf{R}_1 and \mathbf{R}_2 .

From (10.1.12) we obtain

$$B_\varphi(\mathbf{R}_1, \mathbf{R}_2) = k_0^2 x_m \int_{-\infty}^{\infty} B_\mu(\xi, \varrho) d\xi. \quad (10.1.13)$$

where $x_m = \min\{x_1, x_2\}$.

Let us consider the longitudinal autocorrelation of the phase fluctuations when the reference points are located along the same ray ($\varrho = 0$). In this case, taking

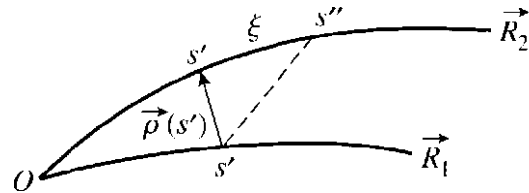


FIGURE 10.1. Parameters for the determination of the correlation function of the phase fluctuations

into account that $B_\mu(\xi, 0)$ is an even function of ξ , we have

$$B_\varphi(x_1, x_2) = 2k_0^2 x_m \int_0^\infty B_\mu(\xi, 0) d\xi. \quad (10.1.14)$$

We define the integral scale of inhomogeneities as

$$L_0 \equiv (\langle \mu^2 \rangle)^{-1} \int_0^\infty B_\mu(\xi, 0) d\xi = \int_0^\infty N_\mu(\xi, 0) d\xi,$$

where $\langle \mu^2 \rangle$ and $N_\mu(\xi, 0)$ are the mean square and the correlation coefficient (normalized autocorrelation function) of the refraction index fluctuations. Then

$$B_\varphi(x_1, x_2) = 2k_0^2 \langle \mu^2 \rangle L_0 x_m. \quad (10.1.15)$$

The transverse correlation function of the phase fluctuations ($x_1 = x_2 \equiv x$), according to (10.1.13), is

$$B_\varphi(x, \varrho) = k_0^2 x \int_{-\infty}^\infty B_\mu(\xi, \varrho) d\xi. \quad (10.1.16)$$

for example, assuming

$$B_\mu(\xi, \varrho) = \langle \mu^2 \rangle \exp[-(\xi^2 + \varrho^2)/a^2], \quad (10.1.17)$$

we obtain

$$B_\varphi(x, \varrho) = \sqrt{\pi} a k_0^2 \langle \mu^2 \rangle x \exp(-\varrho^2/a^2).$$

Hence, we have $\varrho_\perp \sim a$ for the radius of transverse correlation of the phase fluctuations.

The mean square (variance) of the phase fluctuations is found from (10.1.16), setting $\varrho = 0$,

$$\langle \varphi_1^2 \rangle \equiv B_\varphi(x, 0) = k_0^2 x \int_{-\infty}^\infty B_\mu(\xi, 0) d\xi = 2k_0^2 \langle \mu^2 \rangle L_0 x. \quad (10.1.18)$$

Thus, the mean square of the phase fluctuations linearly grows with an increase in distance x . This result has a simple physical interpretation. At $x \gg a$ there is a great number ($\sim x/a$) of noncorrelated inhomogeneities along the ray path. The mean square of the phase fluctuations is proportional to the number of inhomogeneities and, consequently, to x .

Setting $N_\mu(\xi) = \exp(-\xi^2/a^2)$, we find $L_0 = a\sqrt{\pi}/2$ and

$$\langle \varphi_1^2 \rangle = \sqrt{\pi} a k_0^2 \langle \mu^2 \rangle x. \quad (10.1.19)$$

The correlation coefficient is determined as the ratio of the correlation function of the fluctuations to their root-mean-square values. Thus, for example, the longitudinal correlation coefficient $N_\varphi(x_1, x_2)$ of the phase fluctuations has the form

$$N_\varphi(x_1, x_2) = B_\varphi(x_1, x_2) [\langle \varphi_1^2(x_1) \rangle \cdot \langle \varphi_1^2(x_2) \rangle]^{-1/2}.$$

This becomes by virtue of (10.1.15, 18)

$$N_\varphi(x_1, x_2) = x_m(x_1, x_2)^{-1/2}$$

or, setting $x_1 = x_m$ and denoting $x_2 \equiv x$,

$$N_\varphi(x_m, x) = (x_m/x)^{1/2}, \quad x \geq x_m.$$

The phase difference at two points is defined by the structure function

$$D_\varphi = \langle [\varphi_1(\mathbf{R}_1) - \varphi_1(\mathbf{R}_2)]^2 \rangle.$$

If the reference points are separated by distance ϱ in the transverse direction, then

$$D_\varphi(\varrho) = 2[B_\varphi(x, 0) - B_\varphi(x, \varrho)]$$

or, using (10.1.16, 18),

$$D_\varphi(\varrho) = 2k_0^2 x \int_{-\infty}^{\infty} [B_\mu(\xi, 0) - B_\mu(\xi, \varrho)] d\xi. \quad (10.1.20)$$

At $\varrho \rightarrow \infty$, $B_\mu(\xi, \varrho) \rightarrow 0$ and D_φ reaches "saturation" at the value $4k_0^2 \langle \mu^2 \rangle L_0 x$.

Using the well-known relationship between correlation and structure functions [Ref. 10.2; Sect. 1]

$$B_\mu(\xi, \varrho) = \frac{1}{2} [D_\mu(\xi, \infty) - D_\mu(\xi, \varrho)],$$

we write (10.1.20) in the form

$$D_\varphi(\varrho) = k_0^2 x \int_{-\infty}^{\infty} [D_\mu(\xi, \varrho) - D_\mu(\xi, 0)] d\xi. \quad (10.1.21)$$

The last expression is valid even in the case when a random field μ is only locally homogeneous.

The structure function of phase fluctuations allows us to calculate the mean square of the arrival angle fluctuations of a ray at a receiving antenna. Let a wave front of an incident wave be, on the average, parallel to a linear antenna. Then deflection of a ray from the normal to the element of length dl of the antenna gives rise to a phase difference $d\varphi$ between ends of the element. At small deflections there exists the obvious relationship

$$\chi = k_0^{-1} d\varphi/dl.$$

Deflection of the normal to the wave front from its mean (normal to antenna) direction, averaged over the whole length of the antenna, will be

$$\chi = (k_0 l)^{-1} \int_0^l \frac{d\varphi}{dl} dl = (k_0 l)^{-1} [\varphi(l) - \varphi(0)].$$

Now, squaring this expression and statistically averaging, we obtain

$$\langle \chi^2 \rangle = D_\varphi(l)/(k_0 l)^2,$$

where $D_\varphi(l)$ is the structure function of phase fluctuations. Taking into account (10.1.17, 20), we find

$$\langle \chi^2 \rangle = 2\sqrt{\pi} \langle \mu^2 \rangle (x/a)(a/l)^2 [1 - \exp(-l^2/a^2)].$$

Hence

$$\langle \chi^2 \rangle = \begin{cases} 2\sqrt{\pi} \langle \mu^2 \rangle (x/a), & l \ll a \\ 2\sqrt{\pi} \langle \mu^2 \rangle (x/a) [1 - \exp(-1)], & l = a \\ 2\sqrt{\pi} \langle \mu^2 \rangle (x/a) (a^2/l^2), & l \gg a. \end{cases}$$

We see that in the case when $l \gg a$, the arrival angle fluctuations decrease as the length of the antenna increases. This fact demonstrates the averaging effect of the antenna.

10.1.2 Amplitude Fluctuations

Now we obtain an expression for fluctuations of the amplitude level $\eta = \ln(A/A_0)$ where A_0 is some reference value of the amplitude. The quantity 2η determines the sound intensity level. An equation for η follows from the transport equation (2.6.4),

$$2\nabla\eta \cdot \nabla W + \Delta W = 0. \quad (10.1.22)$$

We represent η as a power series

$$\eta = \eta_0 + \eta_1 + \eta_2 + \dots, \quad \eta_m \sim \mu^m \quad (10.1.23)$$

where η_0 is the unperturbed value of the amplitude level. Substituting the series (10.1.23) and an analogous one for W (10.1.2) into (10.1.22), and equating separately the terms of the same order of μ , we obtain two equations:

$$2\nabla\eta_0 \cdot \nabla W_0 + \Delta W_0 = 0 \quad (10.1.24)$$

and

$$2\nabla\eta_1 \cdot \nabla W_0 + \Delta W_1 + 2\nabla\eta_0 \cdot \nabla W_1 = 0. \quad (10.1.25)$$

At large distances from a source ($x \gg a$), ∇W_1 and ΔW_1 can be approximately replaced by $\nabla_{\perp} W_1$ and $\Delta_{\perp} W_1$, where $\nabla_{\perp} = \nabla - \mathbf{e}(\mathbf{e} \cdot \nabla)$ and $\Delta_{\perp} = \nabla_{\perp}^2$ are operators of transverse (with respect to a ray) differentiation. Such a replacement is allowable provided that $|\nabla_{\parallel} W_1| \ll |\nabla_{\perp} W_1|$, ∇_{\parallel} being an operator of longitudinal differentiation. For estimating an order of magnitude, we assume

$$|\nabla_{\perp} W_1| \sim (\langle W_1^2 \rangle)^{1/2}/a = (\langle \varphi_1^2 \rangle)^{1/2}/(k_0 a)$$

or, using (10.1.19),

$$|\nabla_{\perp} W_1| \sim [\langle \mu^2 \rangle x/a]^{1/2}.$$

On the other hand, by virtue of (10.1.6),

$$|\nabla_{\parallel} W_1| = \left| \frac{dW_1}{ds} \right| \sim |\mu| \sim (\langle \mu^2 \rangle)^{1/2}.$$

Hence,

$$|\nabla_{\parallel} W_1|/|\nabla_{\perp} W_1| \sim (a/x)^{1/2} \ll 1.$$

Now (10.1.25) can be written as

$$2\nabla\eta_1 \cdot \nabla W_0 + \Delta_\perp W_1 + 2\nabla_\perp \eta_0 \cdot \nabla_\perp W_1 = 0. \quad (10.1.26)$$

Here the term with $\nabla_\perp \eta_0$ describing the variation of the wave amplitude along the wave surface ($\varphi_0 = \text{const}$) may be neglected in all those regions where geometrical acoustics is valid. In the homogeneous medium for plane and spherical waves it is identically equal to zero.

Then, using (10.1.5), we obtain from (10.1.26),

$$\frac{d\eta_1}{ds} = -(2n_0)^{-1} \Delta_\perp W_1$$

from which

$$\eta_1 = -\frac{1}{2} \int_0^s n_0^{-1} \Delta_\perp W_1 ds \quad (10.1.27)$$

where the integration is carried out along an unperturbed ray.

Let us consider the correlation of the amplitude level fluctuations in a statistically homogeneous medium with $n_0 = 1$. For the transverse correlation function of a plane wave propagating along the x axis, we obtain (10.1.27)

$$\begin{aligned} B_\eta(x, \boldsymbol{\varrho}) &= \langle \eta_1(x, \boldsymbol{\varrho}_1) \eta_1(x, \boldsymbol{\varrho}_2) \rangle \\ &= (2k_0)^{-2} \int_0^x \int_0^x \Delta'_\perp \Delta''_\perp B_\varphi(\mathbf{R}', \mathbf{R}'') dx' dx'', \end{aligned} \quad (10.1.28)$$

where $B_\varphi(\mathbf{R}', \mathbf{R}'')$ is the correlation function of the phase fluctuations (10.1.13); $\mathbf{R}' = \{x', \boldsymbol{\varrho}'\}$ and $\mathbf{R}'' = \{x'', \boldsymbol{\varrho}''\}$ are the radii vectors of successive points on the rays; $\boldsymbol{\varrho} = \boldsymbol{\varrho}_2 - \boldsymbol{\varrho}_1$ is the transverse distance between two parallel rays; and Δ'_\perp , Δ''_\perp are the transverse Laplacian operators over the variables $\boldsymbol{\varrho}'$ and $\boldsymbol{\varrho}''$. Substituting (10.1.13) into (10.1.28), and taking into account that $\Delta'_\perp B_\varphi = \Delta''_\perp B_\varphi$ since $\boldsymbol{\varrho}'$ and $\boldsymbol{\varrho}''$ only enter in the argument of the function B_φ as the difference $\boldsymbol{\varrho}'' - \boldsymbol{\varrho}'$, we obtain

$$B_\eta(x, \boldsymbol{\varrho}) = \frac{1}{4} \int_0^x \int_0^x x_m dx' dx'' \int_{-\infty}^{\infty} \Delta_\perp^2 B_\mu(\xi, \boldsymbol{\varrho}) d\xi \quad (10.1.29)$$

where $x_m = \min\{x', x''\}$.

Integration over x' and x'' gives

$$\int_0^x \int_0^x x_m dx' dx'' = \int_0^x dx' \left(\int_0^{x'} x'' dx'' + \int_{x'}^x x' dx'' \right) = \frac{1}{3} x^3.$$

The result is

$$B_\eta(x, \boldsymbol{\varrho}) = \frac{x^3}{12} \int_{-\infty}^{\infty} \Delta_\perp^2 B_\mu(\xi, \boldsymbol{\varrho}) d\xi. \quad (10.1.30)$$

Thus, the amplitude level fluctuations grow proportional to the cubed of the range

covered by a sound wave. It follows from the comparison of (10.1.16, 30) that

$$B_\eta(x, \boldsymbol{\varrho}) = \frac{x^2}{12k_0^2} \Delta_\perp^2 B_\varphi(x, \boldsymbol{\varrho}). \quad (10.1.31)$$

Setting $\boldsymbol{\varrho} = 0$ in (10.1.30), we obtain for the mean square (variance) of the amplitude level fluctuations

$$\langle \eta_1^2 \rangle \equiv B_\eta(x, 0) = \frac{x^3}{6} \int_0^\infty [\Delta_\perp^2 B_\mu(\xi, \boldsymbol{\varrho})]_{\boldsymbol{\varrho}=0} d\xi. \quad (10.1.32)$$

If the correlation function B_μ is given, for example by (10.1.17), then

$$\langle \eta_1^2 \rangle = (8/3) \sqrt{x} \langle \mu^2 \rangle (x/a)^3. \quad (10.1.33)$$

To evaluate the ratio of the mean squares of the phase and amplitude level fluctuations, we assume that $B_\eta \sim \langle \eta_1^2 \rangle$, $\Delta_\perp^2 B_\varphi \sim \langle \varphi_1^2 \rangle / a^4$, and substitute into (10.1.31). We get

$$\langle \varphi_1^2 \rangle / \langle \eta_1^2 \rangle \sim (k_0 a^2 / x)^2 \sim (a^2 / \lambda x)^2 \gg 1 \quad (10.1.34)$$

since the ray theory can be used if the condition $a^2 \gg \lambda x$ is satisfied [Ref. 10.2; Chap. 2]. Thus, in the ray theory approximation fluctuations of the amplitude level are small compared with the phase fluctuations. The latter can be large enough since they increase with acoustic frequency (10.1.18).

A rather detailed analysis of the phase and amplitude level fluctuations including the case of a spherical wave in the ray approximation was given by *Rytov et al.* [10.3]. The generalization to strong amplitude level fluctuations is given in the works by *Tatarskii* [10.1] and *Chernov* [10.2].

10.2 Scattering of Sound by Random Inhomogeneities

Propagation of sound in a random inhomogeneous medium is accompanied not only by the amplitude and phase fluctuations of a sound wave but by its scattering, too. We consider the wave scattering under the assumption that the sound velocity in a medium deviates only slightly from its mean value. In this case the method of small perturbations (MSP) can be used.

As usual, we start from the Helmholtz equation

$$\Delta p(\mathbf{R}) + k_0^2 n^2(\mathbf{R}) p(\mathbf{R}) = 0, \quad (10.2.1)$$

where k_0 is the wave number at some fixed point and $n(\mathbf{R})$ is given by (10.1.1). Taking into account that μ is small, we represent p as a sum

$$p = p_0 + p_s \quad (10.2.2)$$

where p_0 is an unperturbed sound field satisfying (10.2.1) with $\mu = 0$, and p_s is a scattered field of the first order with respect to μ . Substituting (10.2.2) into (10.2.1) and using (10.1.1) yield an equation for the scattered field

$$\Delta p_s(\mathbf{R}) + k_0^2 n_0^2(z) p_s(\mathbf{R}) = -2k_0^2 n_0(z) \mu(\mathbf{R}) p_0(\mathbf{R}). \quad (10.2.3)$$

The solution of the inhomogeneous equation (10.2.3) can be represented in the form [Ref. 10.8; Sect. 7.2]

$$p_s(\mathbf{R}) = \frac{k_0^2}{2\pi} \int_V n_0(z_1) \mu(\mathbf{R}_1) p_0(\mathbf{R}_1) G(\mathbf{R}, \mathbf{R}_1) d\mathbf{R}_1, \quad (10.2.4)$$

where the integration is carried out over the scattering volume V . Here $G(\mathbf{R}, \mathbf{R}_1)$ is the Green's function satisfying the Helmholtz equation

$$\Delta G(\mathbf{R}, \mathbf{R}_1) + k_0^2 n_0^2(z) G(\mathbf{R}, \mathbf{R}_1) = -4\pi \delta(\mathbf{R} - \mathbf{R}_1), \quad (10.2.5)$$

$\mathbf{R}_1 = \{x_1, y_1, z_1\}$ being the radius vector of the source point within the scattering volume.

Equation (10.2.4) forms the basis for the calculation of various statistical properties of the scattered field in the first MSP approximation.

10.2.1 Average Intensity of a Scattered Field

We assume that the medium is homogeneous on the average, i.e., $n_0 = 1$ ($k_0 \equiv k$), and fluctuations of the refraction index μ are statistically homogeneous in space. Let the unperturbed sound field $p_0(\mathbf{R})$ be given as a spherical wave

$$p_0(\mathbf{R}) = \frac{\exp(ikR'_0)}{R'_0}, \quad R'_0 = |\mathbf{R} - \mathbf{R}_0| \quad (10.2.6)$$

where \mathbf{R}_0 is the radius vector of a sound source.

The Green's function G describing the field of a point source in the homogeneous medium is

$$G(\mathbf{R}, \mathbf{R}_1) = \frac{\exp(ikR')}{R'}, \quad R' = |\mathbf{R} - \mathbf{R}_1| \quad (10.2.7)$$

where \mathbf{R} is the radius vector of the reference point.

From (10.2.6, 7) we obtain

$$p_s(\mathbf{R}) = \frac{k^2}{2\pi} \int_V \mu(\mathbf{R}_1) \frac{\exp[ik(R' + R'_0)]}{R'_0 R'} d\mathbf{R}_1. \quad (10.2.8)$$

Multiplying (10.2.8) by its complex conjugate, averaging statistically over the ensemble of realizations of the medium, and introducing the correlation function for the refraction index fluctuations

$$B_\mu(\mathbf{q}) = \langle \mu(\mathbf{R}_1) \mu(\mathbf{R}_2) \rangle, \quad \mathbf{q} = \mathbf{R}_2 - \mathbf{R}_1 \quad (10.2.9)$$

we obtain for the mean sound intensity of the scattered field

$$I_s \equiv \langle |p_s|^2 \rangle = \left(\frac{k^2}{2\pi} \right)^2 \iint_{VV} \frac{\exp(ikW)}{R' R'_0 R'' R''_0} B_\mu(\mathbf{q}) d\mathbf{R}_1 d\mathbf{R}_2 \quad (10.2.10)$$

where

$$W \equiv (R' - R'') + (R'_0 R''_0), \quad R'' = |\mathbf{R} - \mathbf{R}_2|, \quad R''_0 = |\mathbf{R}_2 - \mathbf{R}_0|.$$

We assume that the characteristic linear dimensions l of the scattering volume are large compared to the spatial scale (the correlation radius) of inhomogeneities and small compared to the distances of the source R_0 and receiver R from the origin of coordinates O located within the scattering volume (Fig. 10.2). Under this assumption R' , R'' , and R'_0 , R''_0 can be expanded in a series up to squares $\mathbf{R}_{1,2}/R$ and $\mathbf{R}_{1,2}/R_0$ which are small quantities.

Keeping up to square terms we get

$$\begin{aligned} R' &\simeq R - \mathbf{e} \cdot \mathbf{R}_1 + \frac{1}{2R} [R_1^2 - (\mathbf{e} \cdot \mathbf{R}_1)^2], \\ R'_0 &\simeq R_0 + \mathbf{e}_0 \cdot \mathbf{R}_1 + \frac{1}{2R_0} [R_1^2 - (\mathbf{e}_0 \cdot \mathbf{R}_1)^2], \end{aligned} \quad (10.2.11)$$

where $\mathbf{e}_0 \equiv -\mathbf{R}_0/R_0$ and $\mathbf{e} \equiv \mathbf{R}/R$ are unit vectors directed from the origin of coordinates. Expansions for R'' and R''_0 are obtained from (10.2.11) by substituting \mathbf{R}_2 for \mathbf{R}_1 . Now we obtain for the function W

$$\begin{aligned} W &= (\mathbf{e} - \mathbf{e}_0) \cdot \mathbf{q} - \left(\frac{1}{R} + \frac{1}{R_0} \right) \mathbf{u} \cdot \mathbf{q} + \frac{1}{R} (\mathbf{e} \cdot \mathbf{u})(\mathbf{e} \cdot \mathbf{q}) \\ &\quad + \frac{1}{R_0} (\mathbf{e}_0 \cdot \mathbf{u})(\mathbf{e}_0 \cdot \mathbf{q}), \end{aligned} \quad (10.2.12)$$

where $\mathbf{u} = (\mathbf{R}_1 + \mathbf{R}_2)/2$.

Let us consider (10.2.10) in the far (the Fraunhofer) zone with respect to the scattering volume. In this case, the denominator of the integrand can be limited to the first terms of expansions (10.2.11) and the quadratic terms in the exponent neglected. Then

$$I_s = \left(\frac{k^2}{2\pi R R_0} \right)^2 \iint_{V V} B_\mu(\mathbf{q}) \exp(i\mathbf{q} \cdot \mathbf{q}) d\mathbf{R}_1 d\mathbf{R}_2 \quad (10.2.13)$$

where $\mathbf{q} = \mathbf{k} - \mathbf{k}_0$, $\mathbf{k}_0 = k\mathbf{e}_0$, and $\mathbf{k} = k\mathbf{e}$ are the wave vectors of the incident and

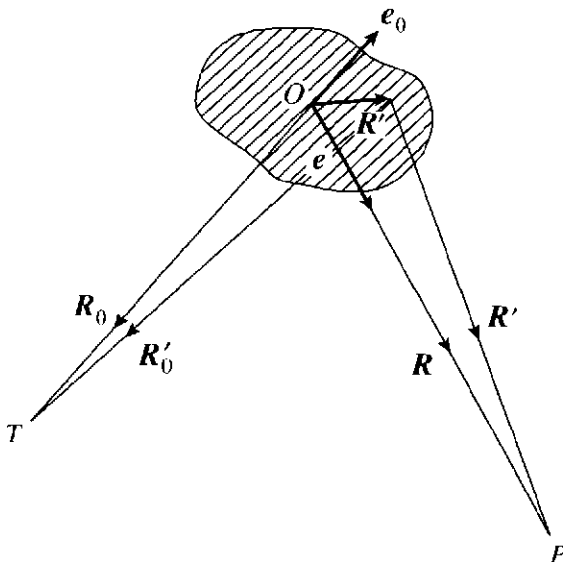


FIGURE 10.2. Parameters for the derivation of the expression for the scattering coefficient

scattered waves. The double integral over the scattering volume V in (10.2.13) can be evaluated, integrating first over the variable \mathbf{u} (the center-of-mass coordinate), and then over \mathbf{q} . As the integrand is independent of \mathbf{u} , the first integration gives the scattering volume V . Since the function $B_\mu(\mathbf{q})$ rapidly tends to zero at $q \geq a$, a being the spatial scale of inhomogeneities, the limits of integration over \mathbf{q} can be taken as $-\infty$ and ∞ . The integral over \mathbf{q} determines a power spectrum of inhomogeneities with an accuracy of the factor $(2\pi)^{-3}$,

$$G_\mu(\mathbf{q}) = (2\pi)^{-3} \int_{-\infty}^{\infty} B_\mu(\mathbf{q}) \exp(i\mathbf{q} \cdot \mathbf{q}) d\mathbf{q}. \quad (10.2.14)$$

As a result we obtain

$$I_s = 2\pi k^4 V (RR_0)^{-2} G_\mu(\mathbf{q}). \quad (10.2.15)$$

The conditions that the approximations used in deriving (10.2.15) are valid can be written as

$$l/R \ll 1, \quad (k/R)|\mathbf{u} \cdot \mathbf{q} - (\mathbf{e} \cdot \mathbf{u})(\mathbf{e} \cdot \mathbf{q})| \ll \pi \quad (10.2.16)$$

and similar for R_0 . Since the significant values of \mathbf{q} are of the order of a , and the maximum value of u is of the order of l , conditions (10.2.16) can be written

$$l/R \ll 1, \quad al/\lambda \ll R, \quad (10.2.17)$$

where λ is the sound wavelength. These conditions (10.2.17) coincide with (9.3.6) obtained for sound scattering from a surface with small random roughness.

Equation (10.2.15) can also be used for a plane incident wave if $1/R_0^2$, the intensity of the incident spherical wave, is replaced by that of the plane incident wave I_i . Then instead of (10.2.15) we obtain

$$I_s = 2\pi k^4 V R^{-2} I_i G_\mu(\mathbf{q}). \quad (10.2.18)$$

10.2.2 Volume Scattering Coefficient

The coefficient m_v is defined as a ratio of acoustical power W_s scattered by a unit volume into a unit solid angle in the direction \mathbf{k} , to the intensity of the incident wave, i.e.,

$$m_v = W_s/I_i. \quad (10.2.19)$$

Taking into account that $W_s = (I_s/V)R^2$, where I_s is determined by (10.2.18), yields

$$m_v = 2\pi k^4 G_\mu(\mathbf{q}). \quad (10.2.20)$$

It follows from (10.2.18, 20) that sound scattering by volume inhomogeneities has a resonance character. In fact, the intensity of the scattered field I_s and the scattering coefficient m_v in the far zone are determined by a single spatial component with the wave vector $\mathbf{q} = \mathbf{k} - \mathbf{k}_0$ of the continuous spectrum of refraction index fluctuations. The wavelength of this component is $\Lambda = 2\pi/q$. If we denote by θ

the angle between the wave vectors \mathbf{k} and \mathbf{k}_0 , then

$$q = |\mathbf{k} - \mathbf{k}_0| = 2k \sin(\theta/2) \quad (10.2.21)$$

and, consequently,

$$\Lambda = \frac{\lambda}{2 \sin(\theta/2)}. \quad (10.2.22)$$

The smaller θ , the larger is the scale of “resonant” inhomogeneities. In contrast, for backscattering ($\theta = \pi$) the smallest scale $\Lambda = \lambda/2$ is important.

Having measured the angular dependence of the scattering coefficient m_v , the spatial spectrum of the refraction index fluctuations can be estimated according to (10.2.20). This method has found practical application in the study of atmospheric turbulence. In the ocean its realization is more difficult since it requires well-stabilized, highly directional receiving-transmitting systems.

Now we shall consider some particular cases of (10.2.20).

1) *Isotropic Inhomogeneities*. In this case the function B_μ depends only on the modulus ϱ . It is expedient to introduce in (10.2.14) a spherical coordinate system $(\varrho, \alpha, \varphi)$, the polar axis of which coincides with vector \mathbf{q} , and to carry out the angular integration. Then

$$G_\mu(q) = (2\pi^2 q)^{-1} \int_0^\infty B_\mu(\varrho) \sin(q\varrho) \varrho d\varrho. \quad (10.2.23)$$

Setting

$$B_\mu(\varrho) = \langle \mu^2 \rangle \exp(-\varrho^2/a^2)$$

we obtain the tabulated integral in (10.2.23) and, using (10.2.20), find

$$m_v = (4\sqrt{\pi})^{-1} k^4 a^3 \langle \mu \rangle^2 \exp[ika \sin(\theta/2)]^2. \quad (10.2.24)$$

It follows from (10.2.24) that in the case of small-scale inhomogeneities ($ka \ll 1$) the scattered field is isotropic, and its frequency dependence follows the known Rayleigh law $m_v \sim k^4$. For large-scale inhomogeneities ($ka \gg 1$) the scattering coefficient has a sharp maximum in the direction of propagation of the incident wave ($\theta = 0$). Its effective width is $\sim 1/(ka)$. Differentiating (10.2.24) with respect to k , one can show that the frequency dependence also has a maximum at $k = \sqrt{2}[ka \sin(\theta/2)]^{-1}$. As θ decreases, the maximum displaces to higher frequencies.

2) *Turbulent Fluctuations*. If in the inertial range of scales ($1/L_0 < q < 1/l_0$), l_0 and L_0 being the internal and external scales (Sect. 1.4), fluctuations of the refraction index in the ocean are described by the Kolomogorov-Obukhov “2/3 law” [10.9, 10], then

$$G_\mu(q) = 0.033 C_n^2 q^{-11/3}, \quad (10.2.25)$$

where C_n is the structure constant equal to $6.6 \cdot 10^{-5} \text{ m}^{-1/3}$.

Substitution of (10.2.28) into (10.2.20) yields

$$m_v = 0.03 C_n^2 (f/c)^{1/3} [\sin(\theta/2)]^{-11/3}. \quad (10.2.26)$$

Here f is the sound frequency in Hz, and c is the sound velocity in m/s.

10.2.3 Sound Scattering by Highly Anisotropic Inhomogeneities with a Fractal Spectrum

According to recent views, random volume inhomogeneities of a sea medium (refractive index fluctuations) in a certain range of scales are highly anisotropic: their horizontal scales exceed by 10^2 – 10^3 times vertical ones [A.10.1]. In fact, they represent themselves as thin lenses. In addition, we assume that these inhomogeneities are large-scale (on the scale of the wavelength of sound) in the horizontal plane and small-scale in depth.

Taking this fact into account, we represent the correlation function of the refractive index fluctuations in the ocean in the form [A.10.1]

$$B_\mu(\rho) = \langle \mu^2 \rangle N_1(\xi/\xi_0) N_2(\eta/\eta_0), \quad \rho = \{\xi, \eta\} \quad (10.2.27)$$

where $\langle \mu^2 \rangle$ is the mean-square fluctuation, $N_1(\xi/\xi_0)$ and $N_2(\eta/\eta_0)$ are the correlation coefficients in the horizontal plane and in depth, respectively. According to our assumption, $k\xi_0 \gg 1$ and $k\eta_0 \gg 1$, where ξ_0 and η_0 are horizontal and vertical radii of correlation, respectively.

A key step in constructing a model of random inhomogeneities is the choice of the correlation coefficient of large-scale fluctuations. We take it in the form

$$N_1(\xi/\xi_0) = [2^{v-1} \Gamma(v)]^{-1} (\xi/\xi_0)^v K_v(\xi/\xi_0), \quad (10.2.28)$$

where $K_v(\xi/\xi_0)$ is the McDonald function of the order v , $\Gamma(v)$ is the gamma function, and v is a free parameter of the problem, which is chosen for physical reasons (see below). The function of such a type was suggested by *Karman* for approximating correlation functions in the theory of turbulence (see [I0.1]). According to (10.2.28), inhomogeneities in the horizontal plane are assumed to be isotropic. Their spatial spectrum is given by

$$G_1(q_\perp) = (2\pi)^{-2} \int_{-\infty}^{\infty} N_1(\xi/\xi_0) \exp(i\mathbf{q}_\perp \cdot \boldsymbol{\xi}) d\boldsymbol{\xi} = v\xi_0^2 [\pi(1 + q_\perp^2 \xi_0^2)^{v+1}]^{-1}, \quad (10.2.29)$$

where

$$q_\perp = k[\cos^2 \chi_0 + \cos^2 \chi - 2 \cos \chi_0 \cos \chi \cos(\varphi - \varphi_0)]^{1/2}$$

is the horizontal wave number of the resonance harmonics in the spectrum of fluctuations, which is expressed in terms of the angles characterizing the propagation directions of the incident (χ_0, φ_0) and scattered (χ, φ) waves.

Under the condition $(q_\perp \xi_0)^2 \gg 1$, the spectrum has the power form $G_1(q_\perp) \sim q_\perp^{2(v+1)}$, its exponent being nonintegral at some values v (for example, for $v = 0.25$). This property of the large-scale inhomogeneities is witnessed about their fractal nature [A.10.2–4]. The surface fractal dimension D of these inhomogeneities is given by the formula

$$D = \gamma + 2d, \quad (10.2.30)$$

where γ is the exponent in the expression for a spectrum and d is the dimension of the embedding space [A.10.4]. Taking into account that in this case the

dimension of the embedding space is $d = 2$, from (10.2.30) for $\nu = 0.25$, we obtain $D = 1.5$. Note that many natural media and objects have the inhomogeneous, unordered structure and possess fractal properties in a wide range of scales. A rough sea surface, the ocean bottom [A.10.4, 5], as well as atmospheric clouds are fractals [A.10.6]. *Hentschel* and *Procaccia* [A.10.6] have calculated the fractal dimension of cloud boundaries in the atmosphere in the framework of relative turbulent diffusion theory. According to these calculations, the dimension of cloud boundaries is within the range $1.37 < D < 1.41$. The inhomogeneities in the form of thin lenses in the ocean are essentially a kind of clouds in the water medium. For $\nu = 0.25$ the fractal dimensions of the boundaries of clouds in the ocean and atmosphere are very close. Note that the concept of fractals was first advanced by *Mandelbrot* [A.10.7].

As for the correlation coefficient of small-scale inhomogeneities, its specific form is of no concern. In fact, for $q_z \eta_0 \ll 1$, where $q_z = k|\sin \chi_0 + \sin \chi|$ is the vertical wave number of the resonance harmonics, the energy spectrum of small-scale inhomogeneities is approximately constant:

$$G_2(q_z) = (2\pi)^{-1} \int_{-\infty}^{\infty} N_2(\eta/\eta_0) \exp(iq_z \eta) d\eta \simeq \eta_0/\pi \quad (10.2.31)$$

Substituting (10.2.29) and (10.2.31) in (10.2.20) and taking into account that $G_\mu(q) = \langle \mu^2 \rangle G_1(q_\perp) G_2(q_z)$, we find

$$m_\nu = (2/\pi) \langle \mu^2 \rangle \xi_0^2 \eta_0 \nu k^4 (1 + q_\perp^2 \xi_0^2)^{-(\nu+1)} \quad (10.2.32)$$

In the vertical plane ($\varphi = \varphi_0$) the scattering coefficient m_ν has two maxima at $q_\perp = 0$: one maximum corresponds to the specular direction ($\chi = \chi_0$) and the second maximum is in the forwards direction ($\chi = -\chi_0$). The effective angular half-width of these peaks, determined by decreasing the coefficient m_ν by a factor of 2, is $\Delta\chi = \varepsilon^{1/2} (k\xi_0 \sin \chi_0)^{-1}$ at $k\xi_0 \sin \chi_0 \gg 1$ and $\Delta\chi = 4(\varepsilon)^{1/4} (k\xi_0)^{-1/2}$ at $\chi_0 = 0$. Here, $\varepsilon = 2^{1/(\nu+1)} - 1$; at $\nu = 0.25$, $\varepsilon \simeq 1$. In the direction of the maxima, the frequency dependence of the scattering coefficient follows the law $m_\nu \sim f^4$ for any value ν . In other directions under the condition $(q_\perp \xi_0)^2 \gg 1$, the scattering coefficient takes the form

$$m_\nu \simeq (2/\pi) \langle \mu^2 \rangle \xi_0^{-2\nu} \eta_0 \nu (q_\perp/k)^{-2(\nu+1)} k^{2(1-\nu)}, \quad (10.2.33)$$

and its frequency dependence follows the law $f^{2(1-\nu)}$. At $\nu = 0.25$ it has the form $f^{3/2}$. Note that three-dimensional isotropic inhomogeneities described by the Karman function would lead to a weaker frequency dependence that does not exceed the first power of frequency for any ν .

10.2.4 Attenuation of Low-Frequency Sound in an Underwater Sound Channel

Sound scattering by random volume inhomogeneities and the leakage of scattered waves from the USC lead to attenuation of a low-frequency sound field in the USC. In this case the frequency dependence of the attenuation coefficient is of

most interest. According to experimental data obtained in various regions of the World Ocean, the frequency dependence of the attenuation coefficient β of low-frequency sound follows the law $\beta \sim f^{3/2}$, where f is the sound frequency. All measurements were carried out in the conditions of the USC because sound attenuation at low frequencies is very weak and can be detected only at rather long acoustic tracks. At present, several different empirical relationships are known, which approximate the results of field measurements [A.10.8]. In particular, the *Sheehy-Halley* formula is well known [A.10.9]:

$$\beta = 0.036 f^{3/2} \text{ [dB/km]} \quad (10.2.34)$$

where f is the sound frequency in kHz. Averaged over a large body of field data, the frequency dependence of the attenuation coefficient β is also close to the law “3/2” in the range 0.1–5.0 kHz [A.10.8].

The law “3/2” has been theoretically interpreted first only for the case when attenuation is due to the transfer of the acoustic energy from the coherent component into the incoherent component because of multiple scattering of sound from the rough sea surface at shallow grazing angles in the subsurface channel (see Sect. 9.12). In the deep ocean, attenuation of sound can be caused by the leakage of acoustic energy from the USC due to scattering of sound wave by random volume inhomogeneities of the sea medium. The attenuation coefficient β is then determined by the integral of the volume scattering coefficient m_v over the solid angle Ω_m corresponding to scattered waves leaking out of the USC [A.10.1]:

$$\beta = \int_{\Omega_m} m_v d\Omega \quad (10.2.35)$$

Such an approach was previously used, but the frequency dependence of the attenuation coefficient always was either stronger than $f^{3/2}$ [10.2] or weaker than $f^{3/2}$ [A.10.10]. A possible reason for such a deviation is that inhomogeneities in all cases were assumed to be isotropic or locally isotropic. Here we use a model of highly anisotropic inhomogeneities considered in the previous section. It is evident that by substitution of (10.2.33) in (10.2.20) and subsequent integration with respect to angular variables, the frequency dependence of the attenuation coefficient will be the same as the scattering coefficient since the angular variables and frequency are separated now.

Let us calculate β . Substituting (10.2.32) in (10.2.35) and setting $\nu = 0.25$, we obtain

$$\beta = (1/2\pi) \langle \mu^2 \rangle \xi_0^{-1/2} \eta_0 k^{3/2} \int_{\Omega_m} \frac{\cos \chi d\chi d\varphi}{[(k\xi_0)^{-2} + (q_{\perp}/k)^2]^{5/4}}. \quad (10.2.36)$$

Here, integration with respect to χ is carried out over the regions $(-\chi_m, -\pi/2)$ and $(\chi_m, \pi/2)$, where χ_m is the boundary grazing angle for the USC; integration with respect to φ is carried out over the period of the integrand, for example, from $-\pi + \varphi_0$ to $\pi + \varphi_0$. Introducing a new variable $\varphi' = \varphi - \varphi_0$, the integral will not depend on the angle φ_0 , which is natural since the large-scale inhomogeneities are assumed to be isotropic in the horizontal plane. Let us also take into account that the angle χ_m in real sound channels is usually 5–15°. The value of the integral

in (10.2.36) is then determined mainly by integrating over a small vicinity near $\chi = \chi_m$ and $\varphi' = 0$. Rather simple calculations for $k\xi_0 \rightarrow \infty$ and $\chi_0 \ll \chi_m$ yield [A.10.1]

$$\beta \simeq 1.1 \langle \mu^2 \rangle \xi_0^{-1/2} \eta_0 k^{3/2} \chi_m^{-2}. \quad (10.2.37)$$

It is seen that the attenuation coefficient follows the law $\beta \sim f^{3/2}$. Thus, the exponent in the frequency dependence of the attenuation coefficient coincides with the fractal dimension of the large-scale inhomogeneities, which points to the fractal nature of attenuation of low-frequency sound in the USC.

The validity of expression (10.2.37) is limited from above by the condition $k\eta_0(\sin \chi_0 + \sin \chi) \leq 0.5$, which for $\eta_0 = 1$ m, $\chi_m = 7^\circ$, and $\chi_0 = 0$ corresponds to the frequency $f = 1$ kHz. From below, formula (10.2.37) is limited by the condition $k\xi_0 \geq \chi_m^{-2}$ which is confirmed by direct numerical calculations [A.10.1]. For $\xi_0 = 150$ m and the same grazing angles, we obtain $f = 0.1$ kHz.

Formula (10.2.37) predicts a rather strong dependence β on the angle χ_m . Physically this result is obvious: the smaller the angle χ_m , the greater the leakage of the acoustic energy of the USC, and hence the greater the attenuation coefficient.

We estimate β for the frequency $f = 1$ kHz ($k = 4.2$ 1/m) and $\langle \mu^2 \rangle = 8.4 \cdot 10^{-8}$; the rest of the parameters have the same values as above. As a result, we obtain $\beta = 2.4 \cdot 10^{-2}$ dB/km, which is rather close to the value given by formula (10.2.34). The attenuation coefficient increases with allowance for multiple scattering of sound by inhomogeneities. Note that at the present time the amount of experimental data of inhomogeneities of considered scales is very small. In the case considered, the value $\langle \mu^2 \rangle$ was determined from the empirical vertical spectrum of sound velocity fluctuations, which was measured at several regions of the Pacific Ocean [A.10.11]. Thus, the numerical estimates of the attenuation coefficient from formula (10.2.37) confirm the present-day notion of the lens structure of ocean waters.

Because the frequency dependence of the attenuation coefficient in the ocean ($\beta \sim f^{3/2}$) is confirmed by multiple field experiments, this dependence can be used for the remote determination of the spectrum of large-scale inhomogeneities, particularly for estimation of the parameter $M = \langle \mu^2 \rangle \xi_0^{-1/2} \eta_0$. Two parameters $\langle \mu^2 \rangle$ and η_0 can be estimated rather easily from field measurements. The parameter ξ_0 , which is difficult to measure, can then be estimated from the parameter M [A.10.1].

10.3 Phase Fluctuations due to Internal Waves

We will now consider sound propagation in the underwater sound channel (USC) when random fluctuations of the refraction index are present due to internal waves. In the USC many rays arrive at any reference point (Chap. 6). The statistical characteristics of the sound field under conditions of multipath propagation are mainly determined by the phase fluctuations of waves propagating along single rays. Thus, we will first consider the single-path phase fluctuations and then take into account the multipath effect (Sect. 10.4).

According to (10.1.11) the mean square of the single-path phase fluctuations is

$$\langle \varphi_1^2 \rangle = k_0^2 \int_0^s ds \int_{-\infty}^{\infty} B_\mu(\xi, 0, z) d\xi. \quad (10.3.1)$$

Here the zero in the argument of the function B_μ means that this function should be taken at $\mathbf{q} = 0$, where \mathbf{q} is the radius vector in the plane perpendicular to a ray.

We represent the correlation function B_μ in terms of the spatial spectrum $G_\mu(\gamma, \boldsymbol{\kappa}; z)$ for random fluctuations μ ,

$$B_\mu(\xi, \mathbf{q}; z) = \iint_{-\infty}^{\infty} G_\mu(\gamma, \boldsymbol{\kappa}; z) \exp[i(\gamma\xi + \boldsymbol{\kappa} \cdot \mathbf{q})] d\gamma d\boldsymbol{\kappa}, \quad (10.3.2)$$

where γ and $\boldsymbol{\kappa} = \boldsymbol{\kappa}(s)$ are the components of the wave vector of an internal wave along a ray and in the plane perpendicular to this ray at point s . Substituting (10.3.2) into (10.3.1) and carrying out the integration over ξ and γ , we get

$$\langle \varphi_1^2 \rangle = 2\pi k_0^2 \int_0^s ds \int_{-\infty}^{\infty} G_\mu(0, \boldsymbol{\kappa}; z) d\boldsymbol{\kappa}. \quad (10.3.3)$$

We assume that the unperturbed ray of interest lies in the xz plane, the z axis is the vertical with z positive upwards, and the source and receiver are at the USC axis. The element of path length along the ray is then given by

$$ds = dx / \cos \chi$$

where $\chi = \chi(s)$ is the grazing angle at point s . The wave vector $\boldsymbol{\kappa}$ has x , y , and z components $-\kappa_z \tan \chi$, κ_y , κ_z , respectively. Keeping in mind that $d\boldsymbol{\kappa} = d\kappa_y d\kappa_z / \cos \chi$, (10.3.3) can be written

$$\langle \varphi_1^2 \rangle = 2\pi k_0^2 \int_0^r \frac{dx}{\cos^2 \chi} \iint_{-\infty}^{\infty} G_\mu[-\kappa_z \tan \chi, \kappa_y, \kappa_z; z(x)] d\kappa_y d\kappa_z, \quad (10.3.4)$$

where r is the horizontal range between the source and receiver. Since the grazing angles in the USC are small, we shall set $\cos \chi = 1$ in the following formulae.

Now transform the spatial spectrum into the frequency one.¹ To do this we first choose as the new integration variables horizontal κ_H and vertical κ_V wave numbers

$$\kappa_H = (\kappa_z^2 \tan^2 \chi + \kappa_y^2)^{1/2}, \quad \kappa_V = \kappa_z. \quad (10.3.5)$$

Then we assume that the Brunt-Väisälä frequency $N(z) = (-g\rho^{-1}\partial\rho/\partial z)^{1/2}$, where ρ is the water density, varies with depth as

$$N(z) = N_0 \exp(z/B). \quad (10.3.6)$$

Such a distribution of $N(z)$ describes the real variations of $N(z)$ in the ocean sufficiently well, except for the upper mixed layer. For frequencies of the internal waves ω not very close to $N(z)$, κ_H and κ_V obey the approximate dispersion

¹In the following we will mainly follow the paper by *Munk and Zachariasen* [10.7].

relations

$$\begin{aligned}\kappa_H &= j\pi B^{-1}(\omega^2 - f^2)^{1/2}/N_0, \\ \kappa_V &= j\pi B^{-1}N(z)/N_0,\end{aligned}\quad (10.3.7)$$

where j is the mode number of the internal waves, $f = 2\Omega \sin \varphi$ is the inertial frequency (Coriolis parameter), $\Omega = 7.3 \cdot 10^{-5}$ rad/s is the angular speed of the earth's rotation, φ is geographical latitude, and B is a stratification scale. As has been shown by *Munk* [10.12] there is a certain relationship between the profiles of sound velocity $c(z)$ and density $\varrho(z)$ or the Brunt-Väisälä frequency $N(z)$ in a horizontally stratified ocean. The reason is that $c(z)$ and $\varrho(z)$ are functions of the same oceanographic factors, namely, temperature, salinity, and hydrostatic pressure. The profile $N(z)$ given by (10.3.6) corresponds to the profile $c(z)$ at which the so-called canonical USC is formed (Fig. 6.4).

For isotropic fluctuations in the horizontal plane the spatial and frequency spectra are related by

$$\begin{aligned}\langle \mu^2(z) \rangle &= 2\pi \iint G_\mu(\kappa_H, \kappa_V; z) \kappa_H d\kappa_H d\kappa_V \\ &= \sum_j \int_{\omega_L}^N F_\mu(\omega, j; z) d\omega,\end{aligned}\quad (10.3.8)$$

where $F_\mu(\omega, j; z)$ is the frequency spectrum of the refraction index fluctuations, and ω_L is the smallest frequency of internal waves corresponding to the smallest possible value of $\kappa_H = \kappa_V \tan \chi$ [see (10.3.5)]. Then it follows from (10.3.7) that $\omega_L^2 = f^2 + N^2 \tan^2 \chi$. It should be noted that although (10.3.7) is valid for ω not very close to N , the upper limit in the integral over ω in (10.3.8) can be taken as N . This is justified by the fact that the internal wave spectrum rapidly falls off with frequency as $\omega \rightarrow N$, and the value of the integral does not depend on an exact value of the upper limit.

On the basis of (10.3.6–8) we obtain

$$\langle \varphi_1^2 \rangle = 2\pi^{-1} k_0^2 B N_0 \int_0^r dx \sum_j j^{-1} \int_{\omega_L}^N F_\mu(\omega, j; z) (\omega^2 - \omega_L^2)^{-1/2} d\omega. \quad (10.3.9)$$

Here z and N are functions of x .

The spectrum $F_\mu(\omega, j; z)$ can be expressed in terms of the spectrum $F_\zeta(\omega, j; z)$ of the vertical displacements $\zeta(z)$ in the internal waves. Taking into account that $\mu(z) \approx -c^{-1}(\partial c / \partial z)\zeta(z)$, where $c = c(z)$ is the average profile of sound velocity in water, we have

$$F_\mu(\omega, j; z) = c^{-2}(\partial c / \partial z)^2 F_\zeta(\omega, j; z). \quad (10.3.10)$$

According to the model of the internal wave spectrum suggested by *Garrett* and *Munk* [10.13],

$$F_\zeta(\omega, j; z) = \langle \zeta^2(z) \rangle S(\omega) H(j) \quad (10.3.11)$$

with $S(\omega) = 4\pi^{-1} f(\omega^2 - f^2)^{1/2}/\omega^3$ for $f \leq \omega \leq N(z)$, $N(z) \gg f$; $S(\omega) = 0$ if ω is outside this interval. The function $S(\omega)$ satisfies the condition

$$\int_f^{N(z)} S(\omega) d\omega \simeq 1.$$

The weight function

$$H(j) = (j^2 + j_*^2)^{-1} \left/ \sum_{j=1}^{\infty} (j^2 + j_*^2)^{-1} \right.$$

characterizes the energy distribution over internal wave modes; j_* is a fixed number. On the basis of experimental data, *Munk* and *Zachariasen* take $j_* = 3$.

From (10.3.10, 11) one has

$$F_\mu(\omega, j; z) = \langle \mu^2(z) \rangle S(\omega) H(j).$$

When the fluctuations of the index of refraction are due to the internal waves, we have [10.7]

$$\langle \mu^2(z) \rangle = \langle \mu_0^2 \rangle (N/N_0)^3, \quad \mu_0 \equiv \mu(0)$$

and

$$F_\mu(\omega, j; z) = \langle \mu_0^2 \rangle (N/N_0)^3 S(\omega) H(j). \quad (10.3.12)$$

Substituting (10.3.12) into (10.3.9) yields

$$\langle \varphi_1^2 \rangle = \langle \mu_0^2 \rangle \langle j^{-1} \rangle k_0^2 B D_0 F_1(r)$$

where

$$F_1(r) = (8/\pi^2) (f/N_0^2) D_0^{-1} \int_0^r N^3 dx \int_{\omega_L}^N \left(\frac{\omega^2 - f^2}{\omega^2 - \omega_L^2} \right)^{1/2} \frac{d\omega}{\omega^3}, \quad (10.3.13)$$

and D_0 is an arbitrary factor having the dimension of length which is introduced in order to make F_1 dimensionless. It is convenient to choose D_0 as half of the axial ray range (Sect. 6.2). The integral over ω is reduced to the tabulated one by substituting $f^2 \omega^{-2} = t$. Taking into consideration that $f \ll N$, the upper limit of integration over t , equal to $(f/N)^2$, can be approximately replaced by zero. The result is

$$F_1(r) = 4(\pi^2 N_0^2 f D_0)^{-1} \int_0^r N^3 f_1(\delta) dx, \quad (10.3.14)$$

where

$$f_1(\delta) = (\delta^2 + 1)^{-1} + \frac{1}{2} \delta^2 (\delta^2 + 1)^{-3/2} \ln \frac{(\delta^2 + 1)^{1/2} + 1}{(\delta^2 + 1)^{1/2} - 1} \quad (10.3.15)$$

and

$$\delta = (N/f) \tan \chi.$$

The quantity $\langle j^{-1} \rangle$ is the average of j^{-1} weighted by the internal wave spectrum $H(j)$,

$$\begin{aligned} \langle j^{-1} \rangle &= \sum_j j^{-1} H(j) = \left[\sum_j j^{-1} (j^2 + j_*^2)^{-1} \right] / \sum_j (j^2 + j_*^2)^{-1} \\ &= 0.647, 0.519, 0.435, 0.379, 0.340 \quad \text{for } j_* = 1, 2, 3, 4, 5. \end{aligned}$$

For axial rays $\chi = \delta = 0$, $f_1(0) = 1$, and $N = N_m = \text{const}$, where N_m is a value of N on the USC axis. Thus, from (10.3.14) we obtain

$$F_1(r) = 4N_m^3(\pi^2 N_0^2 f)^{-1} (r/D_0). \quad (10.3.16)$$

Substituting specific values for the parameters in (10.3.16), $f = 7.3 \cdot 10^{-5}$ rad/s (30° latitude), $N_0 = 5.2 \cdot 10^{-3}$ rad/s, $N_m = 1.9 \cdot 10^{-3}$ rad/s, gives

$$F_1(r) = 1.436(r/D_0). \quad (10.3.17)$$

We consider now an upwards ray turning at the point (\hat{x}, \hat{z}) . Near the apex the equation of the ray may be approximately written as

$$z(x) \simeq \hat{z} - (2\mathcal{R})^{-1}(x - \hat{x})^2$$

where $\mathcal{R}^{-1} = |d^2z/dx^2|$ is the radius of the ray curvature at the apex. Then

$$\delta = (\hat{N}/f)(x - \hat{x})/\mathcal{R}, \quad \hat{N} = N(\hat{z}).$$

The function $f_1(\delta)$ cuts off rapidly with increasing δ and, therefore, only the vicinity of the ray apex gives the major contribution to the integral in (10.3.14). The integration limits can be extended to $\pm\infty$. As a result we obtain

$$F_1(r) \simeq 4\hat{N}^3(\pi^2 N_0^2 f D_0)^{-1} \int_{-\infty}^{\infty} f_1(\delta) dx = \frac{2\mathcal{R}}{D_0} \left(\frac{\hat{N}}{N_0} \right)^2. \quad (10.3.18)$$

It can be seen that $F_1(r)$ has the largest value for rays turning near the surface where N is maximum, and rapidly decreases with increasing turning point depth. Formula (10.3.18) can also be used for rays turning below the USC axis. It is obvious that their contribution will be much less than those turning near the surface. Therefore, if a ray at range r has M turning points near the surface, then

$$F_1(r) = \frac{2\mathcal{R}}{D_0} \left(\frac{\hat{N}}{N_0} \right)^2 M. \quad (10.3.19)$$

The variance of $d\varphi_1/dt$ can be obtained in a similar way, by inserting ω^2 in (10.3.9) in the integrand. The result is

$$\left\langle \left| \frac{d\varphi_1}{dt} \right|^2 \right\rangle = f N_0 \langle \mu_0^2 \rangle \langle j^{-1} \rangle k_0^2 B D_0 F_2, \quad (10.3.20)$$

where

$$F_2 = 8(\pi^2 N_0^3 D_0)^{-1} \int_0^r N^3 \ln(N/f) f_2(\delta) dx \quad (10.3.21)$$

and

$$f_2(\delta) = \left[\ln \frac{N}{f} - \frac{1}{2} \ln \frac{\delta^2}{4} - \frac{1}{2} (\delta^2 + 1)^{-1/2} \ln \frac{(\delta^2 + 1)^{1/2} + 1}{(\delta^2 + 1)^{1/2} - 1} \right] / \ln \left(\frac{N}{f} \right). \quad (10.3.22)$$

For axial rays ($f_2 = 1$) and near surface rays we have, respectively,

$$F_2 = (8/\pi^2)(N_m/N_0)^3 \ln(N_m/f)(r/D_0) = 0.132(r/D_0) \quad (10.3.23)$$

and

$$F_2 = (8/\pi^2)(2\pi/3)^{1/2}(B|\mathcal{R}|)^{1/2}D_0^{-1}(\hat{N}/N_0)^3 \ln(\hat{N}/f). \quad (10.3.24)$$

In the work by *Munk* and *Zachariasen* [10.7] cited above, the results of the numerical evaluation of F_1 and F_2 are also given for different rays in the canonical USC.

10.4 Fluctuations in Multipath Propagation

When two types of inhomogeneities—regular and random—are present in the ocean, the sound field at any point is a superposition of waves propagating along different rays and having random amplitudes and phases. It is convenient to present the theoretical analysis of the statistical properties of the sound field for the Cartesian pressure components. The acoustical signal arriving at a reference point along the i th ray can be written

$$p_i(t) = E_i(t) \cos[\omega t - \varphi_i(t)] = X_i \cos \omega t + Y_i \sin \omega t, \quad (10.4.1)$$

where $E_i(t)$ and $\varphi_i(t)$ are the amplitude and phase of the sound signal, and

$$X_i(t) = E_i(t) \cos \varphi_i(t), \quad Y_i(t) = E_i(t) \sin \varphi_i(t)$$

are the Cartesian components (conjugate random processes) which are slowly varying functions as compared with $\cos \omega t$ and $\sin \omega t$. An experimental method of detecting the Cartesian components is given, for example, in the paper by *Gulin* [10.14].

For n rays arriving at the reference point we have the Cartesian components for the total signal,

$$X(t) = \sum_{i=1}^N X_i(t) = E(t) \cos \varphi(t), \quad Y(t) = \sum_{i=1}^N Y_i(t) = E(t) \sin \varphi(t).$$

At large distances signals arriving along different rays may be assumed to be uncorrelated. In this case a correlation function for the X component is

$$B_X(\tau) = \sum_i \langle X_i(t) X_i(t + \tau) \rangle, \quad (10.4.2)$$

and similarly for $B_Y(\tau)$. In the model considered, the amplitudes E_i and phases φ_i of the single-path components are independent random variables [10.15]. Therefore,

$$B_X(\tau) = \sum_i \langle E_i(t) E_i(t + \tau) \rangle \langle \cos \varphi_i(t) \cos \varphi_i(t + \tau) \rangle. \quad (10.4.3)$$

Let us suppose that the scale of the temporal phase fluctuations is much less than that of the relative amplitude variations, i.e.,

$$\langle (dE_i/dt)^2 \rangle \ll \langle E_i^2 \rangle \langle (d\varphi_i/dt)^2 \rangle. \quad (10.4.4)$$

Then (10.4.3) may be approximated as

$$B_X(\tau) = \sum_i \langle E_i^2 \rangle \langle \cos \varphi_i(t) \cos \varphi_i(t + \tau) \rangle. \quad (10.4.5)$$

We also assume that the single-path phases $\varphi_i(t)$ are Gaussian random variables, their root-mean-square values for each ray exceed 2π , i.e., $(\langle \varphi_i^2 \rangle)^{1/2} \gg 2\pi$, and the structure function of phases can be represented as

$$\langle [\varphi_i(t + \tau) - \varphi_i(t)]^2 \rangle \simeq \nu^2 \tau^2, \quad (10.4.6)$$

where

$$\nu = [\langle (d\varphi_i/dt)^2 \rangle]^{1/2} \quad (10.4.7)$$

is the root-mean-square value of the frequency which in this model is assumed to be the same for every single-path signal. The approximation (10.4.6) is valid provided that

$$\langle (d^2\varphi_i/dt^2)^2 \rangle \ll \langle (d\varphi_i/dt)^4 \rangle.$$

Expressing the cosines in terms of the exponents and keeping in mind the assumptions made above, we find in (10.4.5)

$$\langle \cos \varphi_i(t) \cos \varphi_i(t + \tau) \rangle = \frac{1}{2} \exp(-\nu^2 \tau^2 / 2). \quad (10.4.8)$$

Denoting the mean square of the multipath signal amplitude as

$$A^2 \equiv \sum_i \langle E_i^2 \rangle, \quad (10.4.9)$$

we obtain from (10.4.5)

$$B_X(\tau) = \frac{1}{2} A^2 \exp(-\nu^2 \tau^2 / 2). \quad (10.4.10)$$

The frequency spectrum of the $X(t)$ component is defined as the Fourier transform of the function $B_X(\tau)$,

$$\begin{aligned} F_X(\omega) &= (2\pi)^{-1} \int_{-\infty}^{\infty} B_X(\tau) \exp(-i\omega\tau) d\tau \\ &= (8\pi)^{-1/2} (A^2/\nu) \exp(-\omega^2/2\nu^2). \end{aligned} \quad (10.4.11)$$

A similar result holds for $F_Y(\omega)$.

Thus, under the assumptions made, the frequency spectrum of the multipath Cartesian components is determined by the parameter ν , the root-mean-square frequency of the signal propagating along a typical ray.

The results presented in this section have been obtained by *Dyson* et al. [10.15]. The spectra of the intensity level and phase change were also evaluated there. The authors have observed good agreement between the calculated and experimentally measured spectra (Sect. 1.4).

To summarize this section, we note that a very detailed analysis of the joint effects of stratification and random inhomogeneities including internal waves on sound propagation in the ocean is [10.16].

Scattering and Absorption of Sound by Gas Bubbles in Water

Gas bubbles in sea water are most efficient sound scatterers. This is due to the fact that in a wide frequency range this scattering is of a resonance nature. The resonance scattering cross section of an air bubble near the water surface, for example, is approximately 10^3 times its geometrical cross section. The resonance bubbles not only scatter but absorb the acoustic energy, as well. Furthermore, at sufficiently high concentrations they markedly change the compressibility of water and, consequently, the sound velocity which appears to depend on the sound frequency.

Gas bubbles in sea water are very different in origin. In the first few metres near the surface air bubbles are due to waves breaking when the wind is strong (Sect. 1.7). The concentration of air bubbles is also high in a ship's wake. In deeper layers gas bubbles appear as a result of the vital functions of various microorganisms. Finally, the gas-filled swimming-bladders surrounded by soft tissues in fish also behave similarly to gas bubbles.

The theory of sound scattering and absorption by air bubbles in sea water will be presented below. All the main results can be directly referred to the case of gas bubbles and swimming-bladders of fish.

11.1 Sound Scattering by a Single Ideal Bubble

Let an air bubble of radius a , small compared with the wavelength λ , be insonified by a wave, the sound pressure of which at the bubble is

$$p_i = A \exp(-i\omega t). \quad (11.1.1)$$

This incident wave gives rise to pulsations of the bubble which generate, in turn, a spherical scattered wave in a medium. The acoustic pressure and radial component of the particle velocity in the scattered wave can be written in the form

$$\begin{aligned} p_s &= (B/R) \exp[i(kR - \omega t)], \\ v_s &= \frac{1}{i\omega\varrho} \frac{\partial p_s}{\partial R} = B \frac{(ikR - 1)}{i\omega\varrho R^2} \exp[i(kR - \omega t)], \end{aligned} \quad (11.1.2)$$

where ϱ is the water density, and R is the distance from the centre of the bubble to an arbitrary point in the medium. The unknown amplitude B is determined from the boundary conditions at the bubble surface.

Initially let us assume adiabatic oscillations of the bubble (heat exchange between the bubble and the environment is absent). Then, for the air in a bubble we have the adiabatic law

$$P V^\gamma = \text{const}, \quad (11.1.3)$$

where V is the bubble's volume, P is the pressure within the bubble, and $\gamma = c_p/c_v$ is the ratio of specific heats ($\gamma = 1.4$ for air).

Let the static pressure within the bubble in the absence of the sound wave be P_0 , and its corresponding volume $V_0 = (4/3)\pi a^3$. In the process of oscillating the bubble's volume changes by dV and the pressure by $dP = p$, the acoustic pressure ($|p| \ll P_0$, $|dV| \ll V_0$). Differentiating (11.1.3) with respect to time, one obtains

$$\frac{1}{P_0} \frac{dp}{dt} = -\frac{\gamma}{V_0} \frac{dV}{dt}. \quad (11.1.4)$$

Here

$$\frac{dV}{dt} = 4\pi a^2 \frac{d\xi}{dt} = 4\pi a^2 v_R, \quad (11.1.5)$$

where $\xi = \xi(t)$ is the displacement of the bubble's surface, and v_R is the radial component of the velocity at the surface.

Substituting (11.1.5) into (11.1.4) and taking into account that $dp/dt = -i\omega p$, we obtain

$$p = \frac{3\gamma P_0}{i\omega a} v_R. \quad (11.1.6)$$

Neglecting for the present the shear viscous stress and surface capillary tension, we write the boundary conditions at the bubble surface as

$$p_i + p_s = p, \quad (11.1.7)$$

$$v_i + v_s = v_R, \quad (11.1.8)$$

where v_i and v_s are the radial components of the particle velocity in the incident and scattered waves, respectively.

Since the sound wavelength is much greater than the bubble radius, the acoustic pressure in the incident wave is practically constant over the surface of the bubble. By virtue of this fact, v_i (proportional to $\partial p_i / \partial R$) will be very small and can be neglected in (11.1.8). Then, $v_s = v_R$ and, using (11.1.6), we can write the boundary conditions (11.1.7, 8) in the form of an equation

$$p_i + p_s = \frac{3\gamma P_0}{i\omega a} v_s. \quad (11.1.9)$$

Substitution of (11.1.1, 2) into (11.1.9) yields

$$A + (B/a) \exp(ika) = -\frac{3\gamma P_0}{\varrho \omega^2 a^3} B(ika - 1) \exp(ika). \quad (11.1.10)$$

Since $ka \ll 1$, we have approximately $\exp(ika) \simeq 1 + ika$ to find

$$B = aA[f_0/f]^2 - 1 - ika)^{-1}, \quad (11.1.11)$$

where

$$f_0 = (2\pi a)^{-1}(3\gamma P_0/\varrho)^{1/2}. \quad (11.1.12)$$

Equation (11.1.11) together with (11.1.2) determines the field of the scattered wave. Its amplitude reaches a maximum at $f = f_0$, the resonant frequency of the bubble. The term ika in (11.1.11) is due to the radiation losses during the bubble's oscillations.

Substituting $P_0 = 10^5(1 + 0.1z)Pa$, $\varrho = 1 \text{ g/cm}^3$, and $\gamma = 1.4$ into (11.1.12) for an air bubble in water at depth z metres, we obtain

$$f_0 = (327/a)(1 + 0.1z)^{1/2} \text{ [Hz]} \quad (11.1.13)$$

where the radius a of the bubble is expressed in cm. Thus, for example, for a bubble with $a = 0.01 \text{ cm}$ near the surface ($z = 0$) the resonant frequency $f = 32.7 \text{ kHz}$.

The efficiency of scatterers is usually characterized by the *scattering cross section* σ_s defined as the ratio of acoustical power W_s scattered by a bubble over all directions to the incident wave intensity I_i ,

$$\sigma_s = W_s/I_i = 4\pi R^2(I_s/I_i) \quad (11.1.14)$$

where $I_i = |p_i|^2/(2\varrho c)$ and $I_s = |p_s|^2/(2\varrho c)$ are the intensities of the incident and scattered waves, respectively, and c is the sound velocity. The dimension of σ_s is length squared.

By virtue of (11.1.1, 2, 11) we obtain

$$\sigma_s = 4\pi a^2 \{[(f_0/f)^2 - 1]^2 + (ka)^2\}^{-1}. \quad (11.1.15)$$

To reveal the physical meaning of σ_s , we rewrite (11.1.14) in the form

$$4\pi R^2 I_s = \sigma_s I_i.$$

Hence the acoustic power scattered by a bubble over all directions is equal to that transferred by an incident wave through the surface σ_s normal to the direction of the incident wave. In Fig. 11.1 the ratio of the scattering cross section to the geometrical one $\sigma_s/(\pi a^2)$ is shown as a function of ka . The peak corresponds to the resonance value of ka .

At resonance ($f = f_0$) we obtain from (11.1.15) for the scattering cross section

$$\sigma_s = 4\pi/k_0^2 = \lambda_0^2/\pi, \quad (11.1.16)$$

where $\lambda_0 = 2\pi/k_0$ is the resonance wavelength. Using (11.1.13) we find for a resonant bubble near the water surface

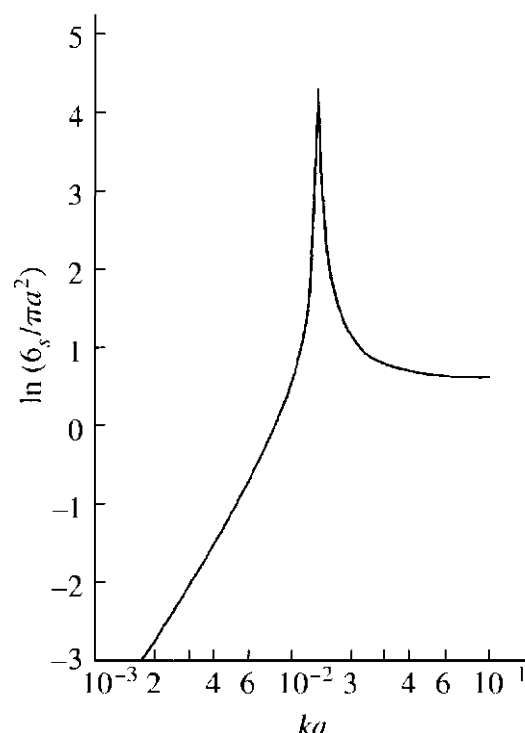
$$k_0 a = 0.0136. \quad (11.1.17)$$

Hence, for these bubbles our assumption that the bubble radius is small compared with the sound wavelength (in water and in air, as well) is confirmed.

Now we obtain from (11.1.16)

$$\sigma_s/(\pi a^2) \simeq 2.16 \cdot 10^4. \quad (11.1.18)$$

FIGURE 11.1. Dependence of the scattering cross section of an air bubble in water on ka . Only the losses due to radiation are taken into account



Thus, at resonance, the scattering cross section of a bubble is more than 20,000 times its geometrical one. Energy losses caused by shear viscosity and thermal conductivity somewhat decrease this value. Nevertheless, the sound scattering in the sea is for the most part due to resonant bubbles. The intensity of the scattered field rapidly decreases when the difference between the sound frequencies and the resonance frequency increases. The width of the resonance curve Δf determined at the level $\sigma_s/2$ is $\Delta f/f = k_0 a$.

According to (11.1.15), scattering at low frequencies ($f \ll f_0$) obeys the Rayleigh law.

$$\sigma_s = 4\pi a^2 (f/f_0)^4. \quad (11.1.19)$$

At high frequencies ($f \gg f_0$ but $ka \ll 1$) we have

$$\sigma_s = 4\pi a^2. \quad (11.1.20)$$

In this case σ_s does not depend upon frequency and is 4 times as great as the geometrical cross section of a bubble.

11.2 Scattering and Absorption of Sound by a Real Bubble

The scattering intensity of resonant bubbles was somewhat overestimated in the previous section since only radiation losses were taken into account. There are also additional losses due to the shear viscosity of sea water and the heat exchange between the air in a bubble and the surrounding water. As can be shown, the shear viscosity of air within a bubble can be neglected.

In a viscous medium a shear viscous stress acts at the surface of the bubble in the radial direction,

$$-2\eta \left[\frac{\partial}{\partial R} (v_s + v_i) \right]_{R=a} \simeq -2\eta \left(\frac{\partial v_s}{\partial R} \right)_{R=a} \quad (11.2.1)$$

where η is the dynamic viscosity of the water. As a result the boundary condition (11.1.7) must be replaced by

$$p_i + p_s - 2\eta \left(\frac{\partial v_s}{\partial R} \right) = p \quad \text{for } R = a. \quad (11.2.2)$$

Due to the thermal conductivity of water and air within the bubble, the bubble's oscillations are not purely adiabatic or isothermal. Obviously the ratio of the bubble radius a to λ_T , the temperature wavelength in air divided by 2π , determines how close oscillations are to one or another regime. The regime is adiabatic if $a \gg \lambda_T$, and isothermal if $a \ll \lambda_T$. For air $\lambda_T = 0.24 f^{-1/2}$ where f is the sound frequency [Hz]. Using (11.1.13) with $z = 0$, we obtain the condition that a bubble near the water surface oscillates adiabatically

$$a \gg (0.24)^2 / 327 \simeq 1.8 \cdot 10^{-4} \text{ cm.}$$

Let us now consider the oscillations of a real bubble more closely. Due to the heat exchange between air in a bubble and the surrounding water, variations of pressure and temperature in the bubble are somewhat behind the volume variation. For example, as the bubble volume decreases, the temperature increases, but due to some heat escaping into the environment the bubble begins to cool prior to expansion. As a consequence, at the minimum bubble volume the air temperature and pressure will already be below their maxima. Such a phase shift between the bubble volume and air pressure can be taken into account replacing γ in (11.1.3) by $\gamma = \gamma_1 - i\gamma_2$,

$$P V^{\gamma_1 - i\gamma_2} = \text{const.} \quad (11.2.3)$$

Then for the acoustic pressure in the bubble instead of (11.1.6) we obtain

$$p = \frac{3(\gamma_1 - i\gamma_2)P'_0}{ia\omega} v_R \quad (11.2.4)$$

where $P'_0 = P_0 + 2\alpha/a$, P_0 is the hydrostatic pressure at a depth of the bubble, and $2\alpha/a$ is the capillary pressure (α is the surface tension). The latter is significant only for bubbles of very small radii. For this reason this term was neglected when we earlier considered relatively big bubbles for which the adiabatic law is valid. For further calculations it is convenient to put $P'_0 = \varkappa P_0$, $\varkappa \equiv 1 + 2\alpha/aP_0$.

Substituting (11.1, 2, 4) into (11.2.2), taking into account, as above, that $v_R \simeq v_s$, and retaining only the main terms, we find

$$B = aA[(\hat{f}_0/f)^2 - 1 - i\delta]^{-1}, \quad (11.2.5)$$

where

$$\hat{f}_0 = (\gamma_1 \varkappa / \gamma)^{1/2} f_0 \quad (11.2.6)$$

is the resonant frequency of the bubble,

$$\delta = \delta_r + \delta_\eta + \delta_T = ka + 4\eta/(\rho\omega a^2) + (\tilde{f}_0/f)^2(\gamma_2/\gamma_1) \quad (11.2.7)$$

where δ_r , δ_η , and δ_T are the damping parameters due to reradiation, shear viscosity of sea water, and thermal conductivity between water and air in the bubble, respectively. Figure 11.2 shows the dependence of κ , γ_1/γ , and \tilde{f}_0/f_0 on the radius of the bubble at sea level, and Fig. 11.3 gives δ_r , δ_η , δ_T , and δ at resonant frequency as a function of \tilde{f}_0 . As follows from Fig. 11.2, the difference between \tilde{f}_0 and f_0 is less than 8% for air bubbles of radius greater than $2 \cdot 10^{-4}$ cm at sea level.

The scattering cross section is now

$$\sigma_s = 4\pi a^2(D^2 + \delta^2)^{-1} \quad (11.2.8)$$

where $D \equiv (\tilde{f}_0/f)^2 - 1$. The difference between (11.2.8) and (11.1.15) is only that in the former we have δ instead of ka . This difference is only essential near resonance.

Besides the scattering, part of the acoustic energy is absorbed due to shear viscosity and thermal conductivity. This energy loss is characterized by the *absorption*

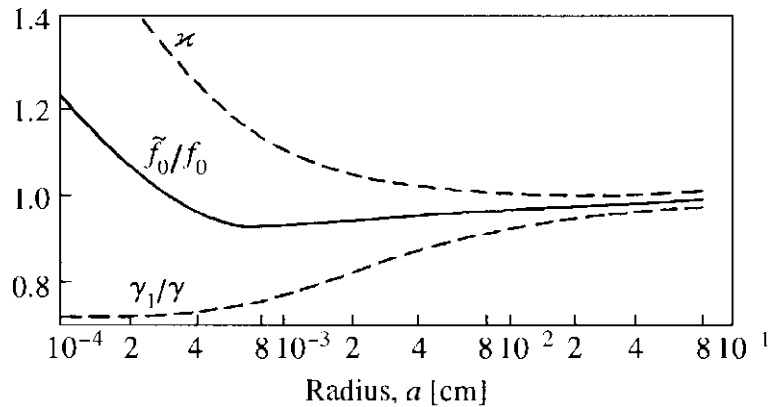


FIGURE 11.2. Dependence of the parameters κ , \tilde{f}_0/f_0 , and γ_1/γ on the radius a of an air bubble at sea level [11.1]

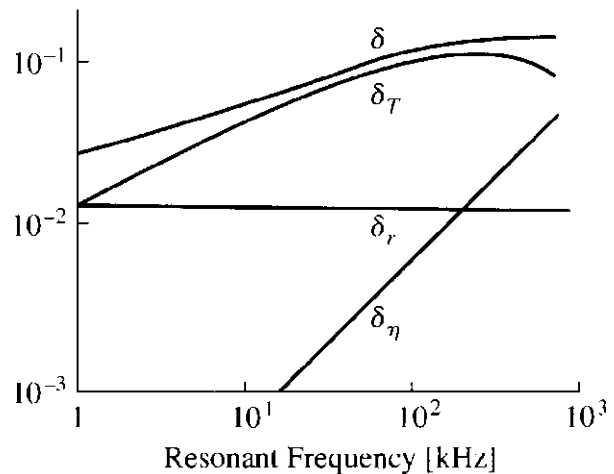


FIGURE 11.3. Resonance damping parameters for an air bubble at sea level [11.2]. Cited after [11.1]

cross section σ_a . Both scattering and absorption are responsible for the extinction of sound. Let $W_e = W_s + W_a$ be the sum of the acoustic power scattered (W_s) and absorbed (W_a). Then the *extinction cross section* is

$$\sigma_e = W_e/I_i, \quad (11.2.9)$$

where I_i is the intensity of the incident wave as before. W_e is equal to the rate at which work is done on the bubble by an incident pressure wave

$$W_e = -\frac{4\pi a^2}{T} \int_0^T \text{Re}\{p_i\} \text{Re}\{v_R\}_{R=a} dt, \quad (11.2.10)$$

where $T = 1/f$ is the wave period and $\text{Re}\{\dots\}$ denotes the real part. From (11.1.2) we obtain, since $ka \ll 1$,

$$(v_s)_{R=a} \simeq (v_R)_{R=a} = \frac{iB}{\omega \rho a^2} \exp(-i\omega t). \quad (11.2.11)$$

Substituting (11.1.1) and (11.2.11) into (11.2.10) and assuming for definiteness that A is a real quantity, we find

$$\sigma_e = 4\pi a^2 (\delta/ka) (D^2 + \delta^2)^{-1}. \quad (11.2.12)$$

From (11.2.8, 12) it follows that

$$\sigma_e/\sigma_s = \delta/ka.$$

The absorption cross section σ_a is obtained from the relation $\sigma_a = \sigma_e - \sigma_s$,

$$\sigma_a = 4\pi a^2 \left(\frac{\delta}{ka} - 1 \right) (D^2 + \delta^2)^{-1}. \quad (11.2.13)$$

Scattering by an Ensemble of Bubbles. Now let us consider the scattering of sound in water containing many bubbles spaced randomly with average distance l between them. If l is sufficiently large, so that $l \gg \max\{\lambda, \sqrt{\sigma_s}\}$, the interaction between bubbles can be neglected. Assume that in a unit volume there are n bubbles of radius a , n being generally a function of \mathbf{R} : $n = n(\mathbf{R})$. The acoustic power scattered by the unit volume will be

$$W_s = n\sigma_s I_i, \quad (11.2.14)$$

and the volume scattering coefficient (definition in Sect. 1.7)

$$m_v = n\sigma_s. \quad (11.2.15)$$

Usually m_v is given in units m^{-1} .

In fact, in sea water there are bubbles of different sizes. Let us denote a number of bubbles of radius between a and $a + da$ per unit volume by $n(a)da$. In the case of noninteracting bubbles the volume scattering coefficient can be obtained by integration of (11.2.8),

$$m_v = \int_0^\infty \sigma_s(a) n(a) da = 4\pi \int_0^\infty a^2 n(a) (D^2 + \delta^2)^{-1} da. \quad (11.2.16)$$

Due to scattering and absorption, the intensity of sound waves decreases by the value

$$dI = -\beta I dr \quad (11.2.17)$$

after propagating a distance dr . Assuming that only single scattering is essential, we obtain for the attenuation coefficient, using (11.2.12),

$$\beta = 4\pi \int_0^\infty a^2 n(a) (\delta/ka) (D^2 + \delta^2)^{-1} da. \quad (11.2.18)$$

The integration of (11.2.17) yields

$$I(r) = I(0) \exp(-\beta r). \quad (11.2.19)$$

11.3 Dispersion of Sound Velocity

In another extreme case, when the average distance between bubbles is small compared to the sound wavelength, the water with bubbles can be regarded for some purposes as a homogeneous medium but with properties different from those of pure water. Air bubbles markedly change the compressibility of water and, consequently, the sound velocity. Moreover, the sound velocity appears to be a function of frequency, i.e., such a medium is dispersive. The sound velocity is related to the compressibility K by the equation

$$c^2 = \frac{1}{\varrho K} \quad (11.3.1)$$

where ϱ is the density of sea water.

Following *Medwin* [11.3], we represent the compressibility in the form

$$K = K_0 + K_1 \quad (11.3.2)$$

where

$$K_0 = \frac{1}{\varrho c_0^2} \quad (11.3.3)$$

is the compressibility of "pure" bubble-free water, where the sound velocity is c_0 , and K_1 is the additional complex compressibility due to the bubbles. According to the definition of compressibility, we have

$$K_1 = -n S \xi / p_i \quad (11.3.4)$$

where n is the number of bubbles of radius a per unit volume, $S = 4\pi a^2$ is the surface of the bubble, ξ is the radial displacement of the bubble surface under the action of sound waves, and p_i the acoustic pressure in the latter. Substituting $\xi = (i/\omega)(v_R)_{R=a}$ where v_R is determined from (11.2.11) and considering (11.1.1) and (11.2.5), we find

$$K_1 = (4\pi a n / \varrho \omega^2) (D + i\delta) (D^2 + \delta^2)^{-1}. \quad (11.3.5)$$

For the sound velocity c we obtain

$$c = c_0[1 + (4\pi a n c_0^2 / \omega^2)(D + i\delta)(D^2 + \delta^2)^{-1}]^{-1/2}. \quad (11.3.6)$$

We have obtained the last expression under the assumption that the density of water with bubbles is the same as that of pure water, so that the bubble concentration cannot be too high.

For the case when relative changes of the sound velocity are also small, (11.3.6) can be expanded in a series. Retaining only the first term, we obtain for $c' = \text{Re}\{c\}$

$$c' = c_0\{1 - 3UZ^2 D[2k_0^2 a^2 (D^2 + \delta^2)]^{-1}\}, \quad (11.3.7)$$

where $U = (4/3)\pi n a^3$ is the volume of air in the unit volume of water, $Z = \tilde{f}_0/f$, $D = Z^2 - 1$, and $k_0 = 2\pi \tilde{f}_0/c_0$ is the wave number of the resonant frequency. In Fig. 11.4 the dependence of $\Delta c/c_0$ upon f/\tilde{f}_0 is shown, where $\Delta c = c' - c_0$. One can see that $\Delta c/c_0$ changes most markedly near the resonant frequency and has a minimum for $Z^2 = 1 + \delta$ and a maximum for $Z^2 = 1 - \delta$. Its values at these points are

$$\frac{\Delta c}{c_0} = \mp \frac{3U(1 \pm \delta)}{4k_0^2 a^2 \delta} \quad (11.3.8)$$

where the upper sign refers to the minimum, and the lower to the maximum.

At low frequency, $f \ll \tilde{f}_0$, we obtain from (11.3.7) approximately

$$\frac{\Delta c}{c_0} = -3U(2k_0^2 a^2)^{-1}. \quad (11.3.9)$$

We also have to note that wind waves at the ocean surface change the value of the hydrostatic pressure P_0 periodically in time and thus modulate the resonant frequency of bubbles. This, in its turn, produces temporary fluctuations of the sound velocity.

At high frequency, for $f \gg \tilde{f}_0$, we have

$$\frac{\Delta c}{c_0} = 3UZ^2[2k_0^2 a^2(1 + \delta^2)]^{-1} \simeq 0 \quad (11.3.10)$$

and, therefore, air bubbles do not affect the sound velocity in water.

Formula (11.3.7) can be easily generalized for the case of a mixture of bubbles of various sizes by changing U to $u(a)da$ which is the fractional volume for air contained in bubbles of radii from a to $a + da$, and integrating over a from

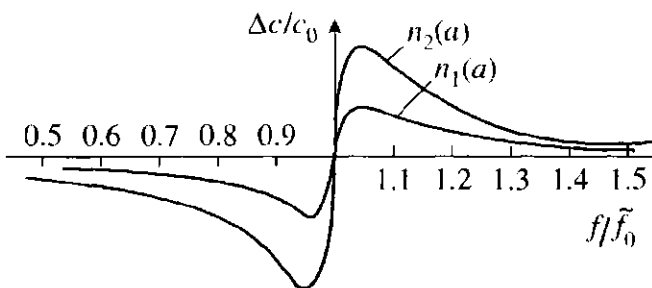


FIGURE 11.4. Dispersion of sound velocity in sea water for various concentrations of air bubbles of radius a [11.1]. $n_2(a) > n_1(a)$. For $f \ll \tilde{f}_0$, $\Delta c/c_0 \simeq U = (4/3)\pi n(a)a^3$

0 to ∞ ,

$$c' = c_0 \left\{ 1 - 3 \int_0^\infty u(a) Z^2 D [2k_0^2 a^2 (D^2 + \delta^2)]^{-1} da \right\}. \quad (11.3.11)$$

The presence of bubbles of different sizes leads to some “smearing” of the dispersion curve. Some new aspects of the problem of sound propagation in bubbly water are treated in [11.4].

11.4 Sound Scattering by an Air Bubble Near a Sea Surface

The acoustic behaviour of an air bubble near the sea surface was first considered by *Strasberg* [11.5], who has shown that the resonance frequency of a pulsating bubble at very small distances from the surface is higher than that at large depths. Using a perturbation method, *Ogus* and *Prosperetti* [11.6] have calculated the oscillation frequency of an air bubble near a slightly rough sea surface. *Guanaurd* and *Huang* [11.7] presented the exact solution of the scattering problem for the air bubble in the vicinity of the free surface, which is valid for the wide range of scattering angles, frequencies, and distances from the surface. *Ye* and *Feuillade* [11.8], using the combination of the method of image sources and the self-consistent method, have investigated in detail the scattering of low-frequency sound by the air bubble near the plane free surface. A great advantage of such an approach is its simplicity and physical clearness of the results obtained.

Following [11.8], we briefly present the basic results referring to the resonance frequency, scattering amplitude, and damping factor of a spherical bubble located under the free surface at point $\mathbf{R}_1 = \{0, 0, -d\}$. Assume that the bubble is irradiated by a plane monochromatic wave whose propagation direction is defined by the unit vector \mathbf{e}_i . The free surface coincides with the plane $z = 0$ of the Cartesian coordinates; the z axis is directed upwards; the origin of the coordinate system is chosen on the plane $z = 0$. The incident plane wave is scattered by the bubble and reflected from the surface. The wave scattered by the bubble is reflected from the surface and the reflected wave is scattered by the bubble again. This process of re scattering and rereflection is repeated multiple times. The presence of the free surface can be taken into account a different way, namely, by introducing an image source (bubble) at point $\mathbf{R}_2 = \{0, 0, d\}$, which is obtained by the specular reflection of the real bubble in the water surface. To satisfy the boundary condition at the free surface, the incident wave must be added by its specular image that represents the reflection wave.

First consider the air bubble located at \mathbf{R}_1 . For $ka \ll 1$, where a is the bubble radius, the scattered wave can be written in the first approximation as a spherically symmetric wave (monopole) even in the presence of the surface [11.9]

$$P'_s(\mathbf{R}) = B p_i(\mathbf{R}_1) \exp(ikR')/R', \quad (11.4.1)$$

where B is the scattering amplitude, $p_i(\mathbf{R})$ is the total field incident on the bubble, and $R' = |\mathbf{R} - \mathbf{R}_1|$.

In the low-frequency approximation ($\kappa a \ll 1$), the scattering amplitude is determined by the expression

$$B = a[(f_0/f)^2 - 1 - i\delta]^{-1}, \quad (11.4.2)$$

which with an accuracy of a constant factor coincides with the scattering amplitude of the air bubble in a boundless water medium [see (11.1.11)]. The resonance frequency f_0 and damping factor δ are given by (11.1.12) and (11.2.7), respectively.

In the presence of the free-surface, bubble-scattered fields are written as

$$p'_s(\mathbf{R}) = C \exp(i\kappa R')/R' \quad (11.4.3)$$

for the real bubble and as

$$p''_s(\mathbf{R}) = -C \exp(ikR'')/R'' \quad (11.4.4)$$

for the bubble image. Here, $R'' = |\mathbf{R} - \mathbf{R}_2|$. The constant C is subject to the determination.

The total acoustic field incident on the bubble at point \mathbf{R}_1 is a sum of three components:

1. wave from the acoustic source

$$p_i^{(0)} = \exp(ik_i \mathbf{R}_1), \quad \mathbf{k}_i = k\mathbf{e}_i; \quad (11.4.5)$$

2. wave reflected from the free surface

$$p_r = -\exp(ik_r \mathbf{R}_1) \quad (11.4.6)$$

where $\mathbf{k}_r = k\mathbf{e}_r$, \mathbf{e}_r is the unit vector in the propagation direction of the reflected wave. The horizontal components of the vectors \mathbf{e}_i and \mathbf{e}_r coincide, but their vertical components have opposite signs;

3. wave p_m due to multiple rescattering between the bubble and surface. Setting $\mathbf{R} = \mathbf{R}_1$ in (11.4.4), we find

$$p_m = -C \exp(2ikd)/2d, \quad (11.4.7)$$

where $2d = |\mathbf{R}_1 - \mathbf{R}_2|$.

Substituting now the total incident field in (11.4.1), we obtain

$$p'_s(\mathbf{R}) = B[\exp(ik_i \mathbf{R}_1) - \exp(ik_r \mathbf{R}_1) - C \exp(2ikd)/2d] \exp(ikR')/R'. \quad (11.4.8)$$

The unknown constant C is determined by the self-consistent method [11.8, 10, 11] that requires the equality of expressions (11.4.8) and (11.4.3):

$$B[\exp(ik_i \mathbf{R}_1) - \exp(ik_r \mathbf{R}_1) - C \exp(2ikd)/2d] \exp(ikR')/R' = C \exp(ikR')/R'. \quad (11.4.9)$$

From (11.4.9), it follows that

$$C = \frac{B[\exp(ik_i \mathbf{R}_1) - \exp(ik_r \mathbf{R}_1)]}{1 + B \exp(2ikd)/2d}. \quad (11.4.10)$$

Now substituting B from (11.4.2), we find

$$C = \frac{a[\exp(ik_i R_1) - \exp(ik_r R_1)]}{(f_0/f)^2 - 1 - i\delta + (a/2d) \exp(2ikd)}. \quad (11.4.11)$$

At $d \rightarrow \infty$, we obtain

$$C = \frac{a[\exp(ik_i R_1) - \exp(ik_r R_1)]}{(f_0/f)^2 - 1 - i\delta}. \quad (11.4.12)$$

In this case the scattered field depends only on the incident and single-scattered waves.

When the air bubble is located in the vicinity of a pressure-release surface, the total scattered field equals the sum of waves scattered by the air bubble and its specular image

$$\hat{p}_s(R) = C[\exp(ikR')/R' - \exp(ikR'')/R'']. \quad (11.4.13)$$

In the far zone at $R \rightarrow \infty$, $R' \simeq R - e_s R_1$, $R'' \simeq R - e_s R_2$,

$$\hat{p}_s(\mathbf{R}) = C[\exp(ik_s R_1) - \exp(ik_s R_2)] \exp(ikR)/R, \quad (11.4.14)$$

where $e_s = \mathbf{R}/R$ is the unit vector in the scattering direction, $k_s = ke_s$ is the wave vector of the scattered wave.

In order to analyze the features of the scattered wave, it is pertinent to introduce the efficient scattering amplitude $B(e_i, e_s)$ (in the far zone) for the air bubble near a free surface as

$$\begin{aligned} \hat{p}_s(\mathbf{R}) &= B(e_i, e_s) \exp(ik_i R_1) \exp(ikR')/R' \\ &\simeq B(e_i, e_s) \exp[i(k_i - k_s) R_1] \exp(ikR)/R. \end{aligned} \quad (11.4.15)$$

Equating (11.4.15) to (11.4.14) and taking into account the explicit form C , we find

$$\begin{aligned} B(e_i, e_s) &= a[(f_0/f)^2 - 1 - i\delta + (a/2d) \exp(2ikd)] \\ &\quad \times (1 - \exp[ik_s(\mathbf{R}_1 - \mathbf{R}_2)](1 - \exp[i(k_r - k_i) R_1])). \end{aligned} \quad (11.4.16)$$

The presence of the nearby pressure-release surface substantially alters the scattering amplitude, resonance frequency f_s , and damping factor. The resonance frequency is determined by equating the real part of the denominator to zero in (11.4.16):

$$f_s = f_0[1 - (a/2d) \cos(4\pi f_s d/c)]^{-1/2}, \quad (11.4.17)$$

For $2kd \ll 1$, the root of this equation in the first order in kd equals

$$f_s = f_0[1 - (a/2d)]^{-1/2}, \quad (11.4.18)$$

which coincides with an approximate formula obtained by *Strasberg* [11.5]. As $a/d \rightarrow 0$, the resonance frequency f_s tends to f_0 , the resonance frequency of the air bubble in a boundless water medium. At $d = a$ when the bubble directly adjoins to a free surface, its resonance frequency increases by a factor $\sqrt{2}$, $f_s/f_0 = \sqrt{2}$. For $d = 25a$, $f_s/f_0 = 1.01$, i.e., the influence of the surface almost vanishes.

In the presence of the surface, the new damping factor is given by

$$\delta_s = \delta - (a/2d) \sin(2kd). \quad (11.4.19)$$

If one takes into account only the radiation damping ($\delta = ka$), then in the first approximation in the small parameter $2kd$, $\delta_s = 0$, i.e., the radiation damping is completely compensated by the effect of the free surface. Allowing for the second term in the expansion $\sin(2kd)$ yields $\delta_s = [2(kd)^2/3]ka$, which is always less than ka for $kd \ll 1$.

Now we present the expression for the effective backscattered amplitude. Let the initial wave be incident on the surface at the angle of incidence θ in the plane xz . In this case $\mathbf{e}_i = \{\sin \theta, 0, \cos \theta\}$, $\mathbf{e}_r = \{\sin \theta, 0, -\cos \theta\}$, $\mathbf{e}_s = -\mathbf{e}_i$, and taking into account that $\mathbf{R}_1 = \{0, 0, -d\}$ and $\mathbf{R}_2 = \{0, 0, d\}$, we obtain

$$B(\mathbf{e}_i, -\mathbf{e}_i) = a[(f_0/f)^2 - 1 - i\delta + (a/2d) \exp(2ikd)]^{-1} [1 - \exp(2ikd \cos \theta)]^2. \quad (11.4.20)$$

For numerical calculations, it is more convenient to deal with the modulus of the normalized scattering amplitude

$$|B(\mathbf{e}_i, -\mathbf{e}_i)|/a = 4 \sin^2(kd \cos \theta) \{[(f_0/f)^2 + (a/2d) \cos(2kd) - 1]^2 + [\delta - (a/2d) \sin(2kd)]^2\}^{-1}. \quad (11.4.21)$$

The numerator in (11.4.21) coincides with the squared directional pattern of a system spherical source plus its specular image [see (4.1.15)]. In this case the factor $\sin^2(kd \cos \theta)$ describes interference of incident and reflected waves. Zeros of the interference pattern in (11.4.21) are at frequencies $f_n = nc/2d \cos \theta$ where $n = 1, 2, 3, \dots$; separations between zeros equal $c/2d \cos \theta$.

At resonance the scattering amplitude is given by

$$\frac{|B(\mathbf{e}_i, -\mathbf{e}_i)|}{a} = \frac{4 \sin^2(kd \cos \theta)}{\delta - (a/2d) \sin(2kd)}. \quad (11.4.22)$$

The results of numerical calculations from formula (11.4.22) show that the resonance frequency of the bubble increases as the bubble approaches the surface, while its scattering amplitude at resonance decreases [11.8]. As the bubble is moved away from the surface, the frequency dependence of the scattering amplitude takes the oscillatory character due to interference between scattered and reflected waves, the period of oscillations being smaller the farther the bubble is located from the surface.

11.5 Collective Bubble Oscillations

Air bubbles in a subsurface layer of the ocean generally occur as plumes and clouds of various forms and dimensions. Such clouds consist of many tiny air bubbles and vibrate like a system of coupled oscillators, which has natural frequencies much lower than those of each individual oscillator [11.12, 13]. An acoustically compact cloud can approximately be considered as a fluid sphere of density and

sound velocity different from those of the outer medium. The density of the air-water mixture within the cloud is then determined by a well-known law [11.14]

$$\rho_m = \rho(1 - U) + \rho_a U, \quad (11.5.1)$$

where ρ is the density of pure bubble-free water, ρ_a is the air density, and U is the void fraction—the ratio of the volume of air within the cloud to the total volume of the cloud (for definition U , see Sect. 11.3). Here and below, index m refers to properties of the air-water mixture. Since measured values U are of an order of 10^{-5} – 10^{-6} [11.12], the cloud density is almost the same as that of pure bubble-free water, i.e., $\rho_m \simeq \rho$.

The sound velocity within the cloud can be estimated from Wood's formula [11.14]

$$c_m = c \left[\frac{U}{\rho_a} \left(\frac{c}{c_a} \right)^2 + \frac{1}{\rho} (1 - U) \right]^{-1/2} [\rho(1 - U) + \rho_a U]^{-1/2}, \quad (11.5.2)$$

where c_m is the sound velocity of the air-water mixture, c_a is the sound velocity in air, and c is the sound velocity in water. Setting $\rho_a = 1.3 \cdot 10^{-3} \text{ g/cm}^3$, $\rho = 1 \text{ g/cm}^3$, $c_a = 333 \text{ m/s}$, $c = 1500 \text{ m/s}$, and $U = 10^{-5}$, we find $c_m = 1395 \text{ m/s}$, i.e., $c_m = 0.93c$.

The analysis of the sound scattering by a fluid sphere is a classic problem of the diffraction theory [11.15]. Its exact solution is represented as an infinite series in spherical wave functions. The coefficients of this series are found from the boundary conditions at the surface (conceptual) of the sphere. Below we present only expressions for the resonance frequency and relative backscattered intensity.

The fundamental resonance frequency of a spherical cloud in the boundless water medium is given by [11.12, 16]

$$f_R \simeq (2\pi R)^{-1} (3\gamma P_0 / \rho U)^{1/2}, \quad (11.5.3)$$

where R is the bubble cloud radius. For the present case of the cloud, one should set $\gamma = 1$ for isothermal conditions, while $\gamma = 1.4$ is used for the individual bubble oscillations (see Sect. 11.1). Comparing (11.5.3) with (11.1.12), one can see that the resonance frequency of the bubble cloud is significantly affected by the void fraction and the dimension of the cloud. Setting the cloud radius $R = 1 \text{ m}$ and the void fraction $U = 10^{-5}$, we obtain $f_R = 872 \text{ Hz}$. This value is 37.5 times lower than that for a single bubble of radius $a = 0.01 \text{ cm}$ [see (11.1.13)].

The ratio of the backscattered intensity I_s to the incident intensity I_i is given by [11.17, 18]

$$\frac{I_s}{I_i} = \frac{(kR)^6}{9(kr)^2} \frac{[1 - (x/x_m)]^2}{[1 - (x/x_m)(kR)^2/3]^2 + [(x/x_m)(kR)^3/3]^2}, \quad (11.5.4)$$

where k is the acoustic wave number, $x = \rho c^2$, $x_m = \rho_m c_m^2$, and r is the distance between the cloud and the receiver. From (11.5.4) it follows that the scattered intensity depends mainly on the ratio c/c_m and the acoustic wavelength. At

resonance, the relative intensity can be approximated by [11.18]

$$\left(\frac{I_s}{I_i}\right)_0 = \left(\frac{x_m}{x} - 1\right)^2 (k_0 r)^{-2} \simeq \left(\frac{c_m^2}{c^2} - 1\right)^2 (k_0 r)^{-2}, \quad (11.5.5)$$

where the subscript 0 refers to quantities at cloud resonance. For $R = 1$ m and $U = 10^{-5}$, we obtain $(I_s/I_i)_0 \sim 0.1$ for $r = 1$ m.

When a bubble cloud is near the pressure-release surface, the scattering problem becomes much more complicated due to cloud interactions with the sea surface. For the smooth sea surface these interactions can be taken into account with the method of images. Some numerical results are presented in [11.12] for the differential cross section and resonance frequency of a spherical cloud at various depths. The results are compared with those obtained in the absence of the surface. The main conclusion is that the backscattering cross section greatly increases when the cloud is near the surface. It is of interest to note that sometimes a deeper cloud exhibits a larger increase of the scattering intensity than clouds just in contact with the surface.

References

Chapter 1

- [1.1] H. Medwin: J. Acoust. Soc. Am. 58, 1318–1319 (1975)
- [A.1.1] O.P. Galkin, L.V. Shvachko: Akust. Zh. 47, 320–329 (2001) [Acoust. Phys. 47, 268–276 (2001)]
- [1.2] W.H. Munk, R.C. Spindel, A. Baggeroer, and T.G. Birdsall: J. Acoust. Soc. Am. 96, 2330–2342 (1994)
- [1.3] A.N. Guthrie, R.M. Fitzgerald, D.A. Nuttle, J.D. Shaffer: J. Acoust. Soc. Am. 56, 58–69 (1974)
- [1.4] H.M. Marsh, M. Schulkin: J. Acoust. Soc. Am. 34, 864–865 (1962)
- [1.5] W.H. Thorp, D.G. Browning: J. Sound Vib. 26, 576–578 (1973)
- [1.6] M. Schulkin, H.M. Marsh: J. Acoust. Soc. Am. 63, 43–48 (1978)
- [1.7] J.R. Lovett: J. Acoust. Soc. Am. 65, 253–254 (1979)
- [1.8] A.C. Kibblewhite, L.D. Hampton: J. Acoust. Soc. Am. 67, 147–157 (1980)
- [1.9] C. Levenson, K.A. Doblar: J. Acoust. Soc. Am. 59, 1134–1141 (1976)
- [1.10] L.M. Brekhovskikh, G.N. Ivanov-Frantskevich, M.N. Koshlyakov, K.N. Fedorov, L.M. Fomin, A.D. Yampolsky: Izv. Akad. Nauk SSSR Fiz. Atmos. Okeana 7, 511–527 (1971) [English transl.: Izv. Acad. Sci. USSR Atmos. Oceanic Phys. 7, 339–343 (1971)]
- [1.11] A.C. Vastano, G.E. Owens: J. Phys. Oceanogr. 3, 470–478 (1973)
- [1.12] G.E. Stanford: J. Acoust. Soc. Am. 55, 968–977 (1974)
- [1.13] R.P. Porter: “Acoustic Probing of Space-Time Scales in the Ocean”, in *Ocean Acoustics*, ed. by J.A. DeSanto, Topics in Current Physics, Vol. 8 (Springer, Berlin, Heidelberg, New York 1979) pp. 243–278
- [1.14] F. Dyson, W. Munk, B. Zetler: J. Acoust. Soc. Am. 59, 1121–1133 (1976)
- [1.15] V.A. Polyanskaya: Akust. Zh. 20, 95–102 (1974) [English transl.: Sov. Phys. Acoust. 20, 55–59 (1974)]
- [1.16] K.N. Fedorov: Vestn. Akad. Nauk SSSR (1978) 3–9
- [1.17] V.M. Zhurbas, R.V. Ozmudov: Okeanologiya 24, 197–203 (1984)
- [1.18] K.N. Fedorov: “Tonkaya struktura gidrofizicheskikh poлей v okeane” (Fine Structure of Hydrophysical Fields in the Ocean), in *Fizika Okeana* (Ocean Physics), ed. by V.K. Kamenkovich, A.S. Monin (Nauka, Moscow 1978) Vol. 1, pp. 113–147
- [1.19] T.B. Sanford: J. Acoust. Soc. Am. 56, 1118–1121 (1974)
- [1.20] T.E. Ewart: J. Acoust. Soc. Am. 60, 46–59 (1976)

- [1.21] R.F. Shvachko: "Rasseyaniye na sluchainykh neodnorodnostyakh i zvukoviye polya v okeane" (Scattering on Random Inhomogeneities and Sound Fields in the Ocean), in *Akustika okeana* (Ocean Acoustics), ed. by L.M. Brekhovskikh (Nauka, Moscow 1974) pp. 559–581
- [1.22] B. Kinsman: *Wind Waves* (Prentice-Hall, Englewood Cliffs, NJ, 1965)
- [1.23] O.M. Phillips: *The Dynamics of the Upper Ocean* (Cambridge University Press, Cambridge, 1966)
- [1.24] C.S. Cox, W.H. Munk: *J. Mar. Res.* 13, 198–227 (1954)
- [1.25] W.J. Pierson, L. Moskowitz: *J. Geophys. Res.* 69, 5181–5190 (1964)
- [1.26] S.A. Kitaigorodskii: *Physika vsaimodeystviya atmosfery i okeana* (Physics of Ocean–Atmosphere Interaction) (Gidrometeoizdat, Leningrad 1970)
- [1.27] E.P. Gul'in: *Dokl. Akad. Nauk SSSR* 212, 1082–1085 (1973) [English transl.: *Sov. Phys. Dokl.* 18, 647–649 (1973)]
- [1.28] N.N. Galubin: *Akust. Zh.* 22, 343–350 (1976) [English transl.: *Sov. Phys. Acoust.* 22, 193–197 (1976)]
- [1.29] S.D. Chuprov: *Akust. Zh.* 24, 116–124 (1978) [English transl.: *Sov. Phys. Acoust.* 24, 62–67 (1978)]
- [1.30] P.A. Kolobaev: *Okeanologiya* 15, 1013–1017 (1975)
- [1.31] P.A. Kolobaev: *Voprosy Sudostroenia. Ser. Acoust.* (1977) 58–66
- [1.32] J.B. Andreeva, L.M. Brekhovskikh: *Priroda Moscow* (1976) 34–43
- [1.33] R.P. Chapman, O.Z. Bluy, R.H. Adlington, A.E. Robinson: *J. Acoust. Soc. Am.* 56, 1722–1734 (1974)
- [1.34] T. Akal: *Mar. Geol.* 13, 251–266 (1972)
- [1.35] T. Akal: "Acoustical Characteristics of the Sea Floor," in *Physics of Sound in Marine Sediments*, ed. by L. Hampton (Research Centre, La Spezia, Italy 1974) pp. 447–480
- [1.36] V.I. Volovov, Yu.Yu. Zhitkovskii: "Otrazheniye i rasseyaniye zvuka dnom okeana" (Reflection and Scattering of Sound from the Ocean Bottom), in *Akustika okeana* (Ocean Acoustics), ed. by L.M. Brekhovskikh (Nauka, Moscow 1974) pp. 395–490
- [1.37] G.M. Wenz: *J. Acoust. Soc. Am.* 34, 1936–1956 (1962)
- [1.38] A.V. Furduev: "Shumy okeana" (Ocean Noise) in *Akustika okeana* (Ocean Acoustics) ed. by L.M. Brekhovskikh (Nauka, Moscow 1974) pp. 615–691
- [1.39] Yu.Yu. Jitkovskii: *Akust. Zh.* 40, 145–146 (1994) [*Acoust. Phys.* 40, 130–131 (1994)]
- [1.40] N.E. Mal'tsev, K.D. Sabinin, and A.V. Furduev: *Akust. Zh.* 36, 86–93 (1990) [*Sov. Phys. Acoust.* 36, 46–50 (1990)]
- [1.41] K.D. Sabinin, M.G. Deev: *Okeanologiya* 31, 714–719 (1991)
- [1.42] Yu.P. Lysanov, A.M. Plotkin, and G.I. Shapiro: *Izv. Acad. Sci. USSR Atmos. Oceanic Phys.* 25, 1272–1280 (1989)

Chapter 2

- [2.1] L.A. Chernov: *Waves in a Random Medium* (McGraw-Hill, New York 1960)
- [2.2] M.A. Pedersen: *J. Acoust. Soc. Am.* 33, 465–474 (1961)
- [2.3] D.A. Raphael: *J. Acoust. Soc. Am.* 48, 1249–1256 (1970)
- [2.4] H. Weinberg: *J. Acoust. Soc. Am.* 50, 975–984 (1971)
- [2.5] L.M. Brekhovskikh: *Waves in Layered Media*, 2nd ed. (Academic, New York 1980)

- [2.6] V.I. Smirnov: *Kurs vyeshey matematiki*, 3rd ed. (GITTL, Moscow 1953) pp. 447–451 [English transl.: *A Course of Higher Mathematics*, Vol. 4. Integral Functions and Partial Differential Equations (Pergamon, New York 1964)]
- [2.7] Yu.A. Kravtsov: *Akust. Zh.* 14, 1–24 (1968) [English transl.: *Sov. Phys. Acoust.* 14, 1–17 (1968)]
- [2.8] R.F. Henrick, H.S. Burkon: *J. Acoust. Soc. Am.* 73, 173–182 (1983)
- [2.9] W. Munk, C. Wunsch: *Deep Sea Res. A* 26, 123–161 (1979)
- [2.10] P.N. Mikhalevsky, A.N. Gavrilov, and A.B. Baggerocr: *IEEE J. Ocean Eng.* 24, 183–201 (1999)
- [2.11] B.D. Dushaw, B.M. Howe, J.A. Mercer, R.C. Spindel: *IEEE J. Ocean Eng.* 24, 202–214 (1999)
- [2.12] G.I. Kozubskaya, V.M. Kudryashov, and K.D. Sabinin: *Akust. Zh.* 45, 250–257 (1999) [*Acoust. Phys.* 45, 217–223 (1999)]
- [2.13] V.V. Goncharov, V.Yu. Zaitsev, V.M. Kurtepov, A.G. Nechaev, and A.I. Hil'ko: *Akusticheskaya tomografiya okeana* (Ocean Acoustic Tomography) (Institute Prikladnoy Fiziki, Nizhnii Novgorod 1997)
- [2.14] V.V. Goncharov, V.M. Kurtepov: "Uspekhi i problemy akusticheskoi tomographii okeana" (Advances and Problems of Ocean Acoustic Tomography), in *Akusticheskie volny v okeane* (Acoustic Waves in the Ocean), ed. by L.M. Brekhovskikh and I.B. Andreeva (Nauka, Moscow 1987) pp. 15–24
- [2.15] A.I. Hil'ko, J.W. Caruthers, and N.A. Sidorovskaia: *Ocean Acoustic Tomography*. A review with emphasis on the Russian approach (Institute of Applied Physics, Nizhnii Novgorod 1998)
- [2.16] W. Munk, C. Wunsch: *Res. Geophys. and Space Phys.* 21, 777–793 (1983)
- [2.17] L.Ya. Lubavin, A.G. Nechev: *Akust. Zh.* 35, 703–709 (1989) [*Sov. Phys. Acoust.* 35, 406–409 (1989)]
- [2.18] B. Cornuelle, W. Munk, and P. Worcester: *J. Geophys. Res.* 24, 6232–6250 (1989)
- [2.19] D.Yu. Mikhin, O.A. Godin, Yu.A. Chepurin, V.V. Goncharov, S.V. Burenkov, D.L. Aleinik, and V.V. Pislakov: "Dinamicheskaya tomografiya Sredizemnogo morya" (Dynamic Tomography of the Mediterranean Sea), in *Akustika okeana* (Ocean Acoustics) (Geos, Moscow 1989)
- [2.20] W. Munk, P. Worcester, and C. Wunsch: *Ocean Acoustic Tomography* (Cambridge University Press, New York 1995)
- [2.21] L.M. Brekhovskikh, V.V. Goncharov, C.A. Dremuchev, V.M. Kurtepov, and Yu.A. Chepurin: *Akust. Zh.* 36, 824–831 (1990) [*Acoust. Phys.* 36, 461–465 (1990)]
- [2.22] L.M. Brekhovskikh, V.V. Goncharov, C.A. Dremuchev, V.M. Kurtepov, V.G. Selivanov, and Yu.A. Chepurin: "Akusticheskie eksperimenty po rasprostraneniyu zvuka cheres vnutrithermoklennuyu linzu i na dvukh protyazhennykh trassakh" (Acoustical Experiments on Sound Propagation Through an Intrathermocline Lens and at Two Extended Tracks) in *Okeanologicheskaya akustika* (Oceanological Acoustics) ed. by L.M. Brekhovskikh and Yu.P. Lysanov (Nauka, Moscow 1993) pp. 21–34
- [2.23] V.V. Goncharov, V.M. Kurtepov: *Akust. Zh.* 40, 773–781 (1994) [*Acoust. Phys.* 40, 685–692 (1994)]
- [2.24] I.P. Smirnov, J.W. Caruthers, and A.I. Hil'ko: *Izv. Vyssh. Uchebn. Zaved.* 42, 982–991

Chapter 3

- [3.1] K.V. Mackenzie: *J. Acoust. Soc. Am.* 32, 221–231 (1960)
- [3.2] L.M. Brekhovskikh: *Waves in Layered Media*, 2nd ed. (Academic, New York 1980)
- [3.3] L.D. Landau, E.M. Lifshitz: *Teoriya uprugosti* (Nauka, Moscow 1965) [English transl.: *A Course of Theoretical Physics*, Vol. 7, Elasticity Theory, 2nd ed. (Pergamon, New York 1970)]
- [3.4] B.D. Tartakovskii: *Zh. Tech. Fiz.* 21, 1194–1201 (1951)

Chapter 4

- [4.1] G.N. Watson: *A Treatise on the Theory of Bessel Functions* (Cambridge University Press, Cambridge 1945)
- [4.2] H. Hönl, A.W. Maue, K. Westpfahl: “Theorie der Beugung,” in *Crystal Optics, Diffraction*, Encyclopedia of Physics, Vol. XXV/1 (Springer, Berlin, Göttingen, Heidelberg 1961)
- [4.3] L.M. Brekhovskikh: *Waves in Layered Media*, 2nd ed. (Academic, New York 1980)
- [4.4] H.K.V. Lotsch: *Optik Stuttgart* 32, 116–137; 189–204; 299–319; 553–569 (1970)
- [4.5] L.M. Brekhovskikh, O.A. Godin: *Acoustics of Layered Media II. Point Sources and Bounded Beams*, 2nd ed. (Springer, Berlin 1999)
- [4.6] L.B. Felsen, N. Marcuvitz: *Radiation and Scattering of Waves* (Prentice-Hall, Englewood Cliffs, NJ 1973)
- [4.7] V. Cerveny, R. Ravindra: *Theory of Seismic Head Waves* (Univ. Toronto Press, Toronto 1971)

Chapter 5

- [5.1] A. Zygmund: *Trigonometric Series* (Cambridge University Press, Cambridge 1959) Vol. 1
- [5.2] I.S. Gradshteyn, I.M. Ryzhik: *Table of Integrals, Series and Products* (Academic, New York 1965)
- [5.3] L.M. Brekhovskikh: *Waves in Layered Media*, 2nd ed. (Academic, New York 1980)
- [5.4] J.A. DeSanto: “Theoretical Methods in Ocean Acoustics,” in *Ocean Acoustics*, ed. by J.A. DeSanto, Topics in Current Physics, Vol. 8 (Springer, Berlin, Heidelberg, New York 1979) pp. 7–77
- [5.5] C.L. Pekeris: “Theory of Propagation of Explosive Sound in Shallow Water,” in *Propagation of Sound in the Ocean* (Geological Soc. Am., Boulder, CO 1948) pp. 1–117
- [5.6] L.M. Brekhovskikh: “Elementi teorii zvukovogo polya v okeane” (Elements of Sound Field Theory in the Ocean), in *Akustika okeana* (Ocean Acoustics), ed. by L.M. Brekhovskikh (Nauka, Moscow 1974) pp. 79–162
- [5.7] P.W. Smith, Jr.: *J. Acoust. Soc. Am.* 55, 1197–1204 (1974)
- [5.8] L.M. Brekhovskikh: *Waves in Layered Media* (Academic, New York 1960)
- [5.9] D.E. Weston: *J. Acoust. Soc. Am.* 68, 269–281, 282–286, 287–296 (1980)

Chapter 6

- [6.1] M.A. Pedersen, D.W. White: *J. Acoust. Soc. Am.* 48, 1219–1245 (1970)
- [6.2] L.M. Brekhovskikh: *Dokl. Akad. Nauk SSSR* 69, 157–160 (1949)

- [6.3] L.D. Rozenberg: Dokl. Akad. Nauk SSSR 69, 175–176 (1949)
- [6.4] W.H. Munk: J. Acoust. Soc. Am. 55, 220–226 (1974)
- [6.5] W.H. Munk, C. Wunsch: Deep Sea Res. 26A, 123–161 (1979)
- [6.6] N.S. Ageeva: “Zvukovoye pole sosredotochennogo istochnika v okeane” (The Sound Field of a Concentrated Source in the Ocean), in *Akustika okeana* (Ocean Acoustics), ed. by L.M. Brekhovskikh (Nauka, Moscow 1974) pp. 163–229
- [6.7] F.E. Hale: J. Acoust. Soc. Am. 33, 456–464 (1961)
- [6.8] D.S. Ahluwalia, J.B. Keller: “Exact and Asymptotic Representations of the Sound Field in a Stratified Ocean,” in *Wave Propagation and Underwater Acoustics*, ed. by J.B. Keller, J.S. Papadakis, Lecture Notes in Physics, Vol. 70 (Springer, Berlin, Heidelberg, New York 1977) pp. 14–84
- [6.9] V.A. Fock: *Electromagnetic Diffraction and Propagation Problems* (Pergamon, New York 1965)
- [6.10] H. Jeffreys, B. Swirles: *Methods of Mathematical Physics*, 3rd ed. (Cambridge University Press, Cambridge 1966)
- [6.11] A.C. Kibblewhite, R.H. Denham: J. Acoust. Soc. Am. 38, 63–71 (1965)
- [6.12] L.M. Brekhovskikh: *Waves in Layered Media*, 2nd ed. (Academic, New York 1980)
- [6.13] C.T. Tindle, K.M. Guthrie: J. Sound Vib. 34, 291–295 (1974)
- [6.14] S. Choudhary, L.B. Felsen: J. Acoust. Soc. Am. 63, 661–666 (1978)
- [6.15] J.M. Arnold, L.B. Felsen: J. Acoust. Soc. Am. 67, 757–763 (1980)
- [6.16] V.M. Kudryashov: Akust. Zh. 22, 724–729 (1976)
- [6.17] L.B. Felsen: J. Acoust. Soc. Am. 69, 352–361 (1981)
- [6.18] S.D. Chuprov: “Interferentsionnaya struktura zvukovogo polya v sloistom okeane” (Interference Structure of a Sound Field in a Layered Ocean), in *Akustika Okeana. Sovremennoe sostoyanie* (Ocean Acoustics. Current State), ed. by L.M. Brekhovskikh, I.B. Andreevoi (Nauka, Moscow 1982) pp. 71–91
- [6.19] G.K. Ivanova: Akust. Zh. 30, 490–494 (1984) [English transl.: Sov. Phys. Acoust. 30, 293–296 (1984)]
- [6.20] S.D. Chuprov, N.E. Mal'tsev: Dokl. Akad. Nauk SSSR 257, 475–479 (1981)
- [6.21] V.A. Zverev, E.F. Orlov (eds.): “Interferentsiya shirokopolosnogo zvuka v okeane” (Interference of Wide-Band Sound in the Ocean). (Institut prikladnoi fiziki, Gorky, 1988) 185 pp.
- [6.22] G.L. D'Spain, W.A. Kuperman: J. Acoust. Soc. Am. 106, 2454–2468 (1999)

Chapter 7

- [7.1] B.Z. Katzenelenbaum: *Teoriya neregulyarnykh volnovodov s medlenno menyayushimisya parametrami* (Theory of Irregular Waveguides with Slowly Varying Parameters) (Izd. Akad. Nauk SSSR, Moscow 1961)
- [7.2] A.D. Pierce: J. Acoust. Soc. Am. 37, 19–27 (1965)
- [7.3] D.M. Milder: J. Acoust. Soc. Am. 46, 1259–1263 (1969)
- [7.4] F.S. Chwieroth, R.D. Graves, A. Nagl, H. Uberall, G.L. Zarur: J. Acoust. Soc. Am. 64, 1105–1112 (1978)
- [7.5] D.E. Weston: Proc. Phys. Soc. London 73, 365–384 (1959)
- [7.6] A.V. Vagin, N.V. Gorskaya, A.V. Mikrykov: Voprosy Sudostroenia. Ser. Acoust. (1978) 20–28
- [7.7] C.H. Harrison: J. Acoust. Soc. Am. 62, 1382–1388 (1977)
- [7.8] L.M. Brekhovskikh: *Waves in Layered Media*, 2nd ed. (Academic, New York 1980)

- [7.9] R. Burridge, H. Weinberg: "Horizontal Rays and Vertical Modes," in *Wave Propagation and Underwater Acoustics*, ed. by J.B. Keller, J.S. Papadakis, Lecture Notes in Physics, Vol. 70 (Springer, Berlin, Heidelberg, New York 1977) pp. 86–152
- [7.10] C.H. Harrison: *J. Acoust. Soc. Am.* 65, 56–61 (1979)
- [7.11] M.A. Leontovich, V.A. Fock: *Zh. Eksp. Teor. Fiz.* 16, 557–573 (1946) [English transl.: *J. Phys. USSR* 10, 13–24 (1946)]
- [7.12] F.D. Tappert: "The Parabolic Approximation Method," in *Wave Propagation and Underwater Acoustics*, ed. by J.B. Keller, J.S. Papadakis, Lecture Notes in Physics, Vol. 70 (Springer, Berlin, Heidelberg, New York, 1977), pp. 224–284
- [7.13] S.T. McDaniel: *J. Acoust. Soc. Am.* 57, 307–311 (1975)
- [7.14] J.A. DeSanto: *J. Acoust. Soc. Am.* 62, 295–297 (1977)
- [7.15] J.A. DeSanto, R.H. Baer: "Probability Distribution of Intensity for Acoustic Propagation," Meeting on Sound Propagation and Underwater Systems, Inst. of Acoustics, London 1978 pp. 10–11
- [7.16] J.A. DeSanto, J.S. Perkins, R.H. Baer: *J. Acoust. Soc. Am.* 64, 1664–1666 (1978)
- [7.17] E.A. Polyanski: *Akust. Zh.* 20, 142–143 (1974)
- [7.18] J.A. DeSanto: "Theoretical Methods in Ocean Acoustics," in *Ocean Acoustics*, ed. by J.A. DeSanto, Topics in Current Physics, Vol. 8 (Springer, Berlin, Heidelberg, New York 1979) pp. 7–77
- [7.19] I.S. Gradshtein, I.M. Ryzhik: *Table of Integrals, Series and Products* (Academic, New York 1965)
- [A.7.1] S.T. McDaniel: *J. Acoust. Soc. Am.* 72, 916–923 (1982)

Chapter 8

- [8.1] B.D. Seckler, J.B. Keller: *J. Acoust. Soc. Am.* 31, 206–216 (1959)
- [8.2] L.M. Brekhovskikh: *Waves in Layered Media*, 2nd ed. (Academic, New York 1980)
- [8.3] M. Abramovitz, I.A. Stegun (eds.): *Handbook of Mathematical Functions with Formulas, Graphs and Mathematical Tables*, Applied Mathematics Series. 55 (National Bureau of Standards, Washington, DC 1964)
- [8.4] A.E. Karbowiak: *Proc. Inst. Electr. Eng.* 111, 1781–1788 (1964)
- [8.5] L.B. Felsen: "Quasi-Optic Diffraction," *Proc. Symp. on Quasi-Optics*, ed. by J. Fox (Polytechnic, New York 1964) pp. 1–40
- [8.6] V.M. Kurtepov: *Akust. Zh.* 15, 560–566 (1969) [English transl.: *Sov. Phys. Acoust.* 15, 484–489 (1970)]
- [8.7] J.A. DeSanto: "Theoretical Methods in Ocean Acoustics," in *Ocean Acoustics*, ed. by J.A. DeSanto, Topics in Current Physics, Vol. 8 (Springer, Berlin, Heidelberg, New York 1979) pp. 7–77

Chapter 9

- [9.1] J.W.S. Rayleigh: *Sci. Pap. Mag.* 6, 388–404 (1907)
- [9.2] J.W.S. Rayleigh: *The Theory of Sound*, Vol. 2 (Dover, New York 1945)
- [9.3] E.L. Feinberg: *Rasprostraneniye radiovoln vdol zemnoy poverkhnosti* (Propagation of Radiowaves Along the Earth's Surface) (Izd. Akad. Nauk SSSR, Moscow 1961)
- [9.4] F.G. Bass, I.M. Fuks: *Rasseyaniye voln na statisticheski nerovnoy poverkhnosti* (Nauka, Moscow 1972) [English transl.: *Wave Scattering from Statistically Rough Surfaces* (Pergamon, New York 1978)]

- [9.5] S.M. Rytov, Yu.A. Kravtsov, V.I. Tatarskii: *Vvedeniye v statisticheskuyu radiofiziku* (Nauka, Moscow 1978) Pt. 2 [English transl.: *Introduction of Statistical Radiophysics*, Sluchainye Polya, Vol. 3 (Springer, Berlin, Heidelberg, 1989)]
- [9.6] Yu.P. Lysanov: "Rasseyaniye zvuka nerovnimi poverkhnostyami" (Scattering of Sound by Rough Surfaces), in *Akustika okeana* (Ocean Acoustics), ed. by L.M. Brekhovskikh (Nauka, Moscow 1974) pp. 231–330
- [9.7] S.A. Kitaigorodskii: *Physika vsaimodeystviya atmosfery i okeana* (Physics of Ocean-Atmosphere Interaction) (Gidrometeoizdat, Leningrad 1970)
- [9.8] T.P. Barnett, J.C. Wilkerson: *J. Mar. Res.* 25, 292–328 (1967)
- [9.9] W.J. Pierson: *Adv. Geophys.* (1955) 93–176
- [9.10] W.J. Pierson, L. Moskowitz: *J. Geophys. Res.* 69, 5181–5190 (1964)
- [9.11] A.V. Belousov, E.A. Kopyl, Yu.P. Lysanov: *Akust. Zh.* 35, 223–228 (1989)
- [9.12] L.I. Mandel'shtam, G.S. Landsberg: "Novoye yavleniye pri rasseyanii sveta" (A New Phenomenon in Light Scattering), in *Polnoye sobraniye trudov* (Complete Collected Works of L.I. Mandel'shtam) (Izd. Akad. Nauk SSSR, Moscow 1948) Vol. 1, pp. 293–296
- [9.13] L.M. Brekhovskikh: *Zh. Eksp. Teor. Fiz.* 23, 275–288 (1952)
- [9.14] P.M. Morse, H. Feshbach: *Methods of Theoretical Physics* (McGraw-Hill, New York 1953) Vol. I
- [9.15] L.M. Brekhovskikh: *Dokl. Akad. Nauk SSSR* 79, 585–588 (1951)
- [9.16] L.M. Brekhovskikh: *Zh. Eksp. Teor. Fiz.* 23, 289–304 (1952)
- [9.17] M.A. Issakovich: *Zh. Eksp. Teor. Fiz.* 23, 305–314 (1952)
- [9.18] J.A. DeSanto: "Coherent Multiple Scattering from Rough Surfaces," in *Multiple Scattering and Waves in Random Media*, ed. by P.L. Chow, W.E. Kohler, G.C. Papanicolaou (North-Holland, Amsterdam 1981)
- [9.19] C.S. Cox, W.H. Munk: *J. Opt. Soc. Am.* 44, 838–850 (1954)
- [9.20] B.F. Kur'yanov: *Akust. Zh.* 8, 325–333 (1962) [English transl.: *Sov. Phys. Acoust.* 8, 252–257 (1962)]
- [9.21] I.M. Fuks: *Akust. Zh.* 20, 458–468 (1974) [English transl.: *Sov. Phys. Acoust.* 20, 276–281 (1974)]
- [9.22] W. Meecham: *Rpt. PQ-25, Int. Congr. on Acoustics, Tokyo 1968*
- [9.23] F.I. Kryazhev, V.M. Kudryashov, N.A. Petrov: *Akust. Zh.* 22, 377–384 (1976) [English transl.: *Sov. Phys. Acoust.* 22, 211–215 (1976)]
- [9.24] A. Bellis, F.D. Tappert: *J. Acoust. Soc. Am.* 66, 311–326 (1979)
- [9.25] M.T. Sheehy, R. Halley: *J. Acoust. Soc. Am.* 29, 464–469 (1975)
- [9.26] L.M. Brekhovskikh, Yu.P. Lysanov, N.V. Studenichnik: *Dokl. Akad. Nauk SSSR* 239, 211–214 (1978)
- [9.27] A.G. Voronovich: *Dokl. Akad. Nauk SSSR* 272, 1351–1355 (1983)
- [9.28] A.G. Voronovich: *Zh. Eksp. Teor. Fiz.* 89, 116–125 (1985)
- [9.29] A.G. Voronovich: "O dvukh novykh podkhodakh v teorii rasseyaniya voln na nerovnykh poverkhnostyakh" (On Two New Approaches in the Wave Scattering Theory by Rough Surfaces), in *Akusticheskie volny in okeane* (Acoustic Waves in the Ocean), ed. by L.M. Brekhovskikh, I.B. Andreeva (Nauka, Moscow 1987) pp. 121–130
- [9.30] A.G. Voronovich: *Wave Scattering from Rough Surfaces* (Springer, New York 1993)
- [9.31] L.N. Deryugin: *Dokl. Akad. Nauk SSSR* 87, 913–916 (1952)
- [9.32] R.F. Miller: *Proc. Cambridge Phil. Soc.* 65, 773–791 (1969)
- [9.33] A.G. Voronovich: *Dokl. Akad. Nauk SSSR* 273, 85–89 (1983)

- [9.34] E.P. Kuznetsova: *Akust. Zh.* 32, 271–274 (1986) [*Sov. Phys. Acoust.* 32, 165–166 (1986)]
- [9.35] M.Yu. Galaktionov: *Akust. Zh.* 37, 270–276 (1991) [*Sov. Phys. Acoust.* 37, 136–139 (1991)]

Chapter 10

- [10.1] V.I. Tatarskii: *Rasprostraneniye voln v turbulentnoy atmosfere* (Nauka, Moscow 1967) [English transl.: *The Effects of the Turbulent Atmosphere on Wave Propagation*, TT68-50464 (U.S. Dept. of Commerce, NTIS, Springfield, VA 1971); *Wave Propagation in a Turbulent Medium*, 1st ed. (McGraw-Hill, New York 1961)]
- [10.2] L.A. Chernov: *Volni v sluchaino-neodnorodnykh sredakh*, 2nd ed. (Nauka, Moscow 1975) [English transl.: *Waves in a Random Medium*, 1st ed. (McGraw-Hill, New York 1960)]
- [10.3] S.M. Rytov, Yu.A. Kravtsov, V.I. Tatarskii: *Vvedeniye v statisticheskuyu radiofiziku* (Nauka, Moscow 1978) Pt. 2 [English transl.: *Introduction to Statistical Radiophysics*, *Sluchainye Polya* Vol. 3 (Springer, Berlin, Heidelberg, 1989)]
- [10.4] S.M. Flatto (ed.): *Sound Transmission Through a Fluctuating Ocean* (Cambridge University Press, Cambridge 1979).
- [10.5] J.B. Keller, J.S. Papadakis (eds.): *Wave Propagation and Underwater Acoustics*, *Lecture Notes in Physics*, Vol. 70 (Springer, Berlin, Heidelberg, New York 1977)
- [10.6] J.W. Strohbehn (ed.): *Laser Beam Propagation in a Turbulent Medium*, *Topics in Applied Physics*, Vol. 25 (Springer, Berlin, Heidelberg, New York 1978)
- [10.7] W.H. Munk, F. Zachariasen: *J. Acoust. Soc. Am.* 59, 818–838 (1976)
- [10.8] P.M. Morse, H. Feshbach: *Methods of Theoretical Physics* (McGraw-Hill, New York 1953) Vol. 1
- [10.9] K.N. Fedorov: “Tonkaya struktura gidrofizicheskikh poley v okeane” (Fine Structure of Hydrophysical Fields in the Ocean), in *Physika okeana* (Ocean Physics), ed. by V.M. Kamenkovich, A.S. Monin (Nauka, Moscow 1978) Vol. 1, pp. 113–147
- [10.10] A.N. Kolmogorov: *Dokl. Akad. Nauk SSSR* 30, 299–303 (1941)
- [10.11] A.M. Obukhov: *Izv. Akad. Nauk SSSR, Ser. Geogr. Geofiz.* 13, 58–69 (1949)
- [10.12] W.H. Munk: *J. Acoust. Soc. Am.* 55, 220–226 (1974)
- [10.13] C.J.R. Garrett, W.H. Munk: *J. Geophys. Res.* 80, 291–297 (1975)
- [10.14] E.P. Gulín: *Akust. Zh.* 21, 721–731 (1975) [English transl.: *Sov. Phys. Acoust.* 21, 445–450 (1975)]
- [10.15] F. Dyson, W.H. Munk, B. Zetler: *J. Acoust. Soc. Am.* 59, 1121–1131 (1976)
- [10.16] R. Dashen, W. Munk, K.M. Watson, R. Zachariasen: In Ref. 10.4
- [A.10.1] Yu.P. Lysanov, I.A. Sazonov: *Akust. Zh.* 39, 697–702 (1993) [*Acoust. Phys.* 39, 366–369 (1998)]
- [A.10.2] Yu.P. Lysanov, L.M. Lyamshev: *Akust. Zh.* 44, 506–509 (1998) [*Acoust. Phys.* 44, 434–436 (1998)]
- [A.10.3] V.V. Zosimov, L.M. Lyamshev: *Akust. Zh.* 40, 709–737 (1994) [*Acoust. Phys.* 40, 627–653 (1994)]
- [A.10.4] J. Feder: *Fractals* (Plenum Press, New York 1988)
- [A.10.5] M. Stiasnie, Y. Agnon, and L. Shemer: *Physica D. Nonlinear Phenomena* 47, 341–352 (1991)
- [A.10.6] N.G.E. Henschel, I. Procaccia: *Phys. Rev. A* 29, 1461–1479 (1988)
- [A.10.7] B.B. Mandelbrot: *The Fractal Geometry of Nature* (Freeman, New York 1983)

- [A.10.8] R.A. Vadov: "Zatukhanie nizkochastotnogo zvuka v okeane" (Attenuation of Low-Frequency Sound in the Ocean), in *Problemy akustiki okeana* (Problems of Ocean Acoustics) ed. by L.M. Brekhovskikh and I.B. Andreeva (Nauka, Moscow 1984) pp. 31–42
- [A.10.9] M.T. Sheehy, R. Halley: J. Acoust. Soc. Am. 29, 464–469 (1957)
- [A.10.10] A.C. Kibblewhite, R.H. Lenham, and P.H. Barber: J. Acoust. Soc. Am. 38 629–643 (1965)
- [A.10.11] V.S. Gostev, N.G. Potylitsyn, and R.F. Shvachko: Proc. XI All-Union Acoust. Conf. (AKIN, Moscow 1991)

Chapter 11

- [11.1] C.S. Clay, H. Medwin: *Acoustical Oceanography* (Wiley, New York 1977)
- [11.2] C. Devin: J. Acoust. Soc. Am. 31, 1654–1667 (1959)
- [11.3] H. Medwin: J. Acoust. Soc. Am. 56, 1100–1104 (1974)
- [11.4] W. Lauterborn (ed.): *Cavitation and Inhomogeneities in Underwater Acoustics*, Springer Series in Electrophysics, Vol. 4 (Springer, Berlin, Heidelberg, New York 1980)
- [11.5] M. Strasberg: J. Acoust. Soc. Am. 25, 536–537 (1953)
- [11.6] H.N. Ogus, A. Prosperetti: J. Acoust. Soc. Am. 87, 2085–2092 (1990)
- [11.7] G.C. Gaunaurd, H. Huang: IEEE J. Ocean Eng. 20, 285–292 (1995)
- [11.8] Z. Ye, C. Feuilade: J. Acoust. Soc. Am. 102, 797–805 (1997)
- [11.9] Z. Ye: J. Acoust. Soc. Am. 101, 1945–1952 (1997)
- [11.10] L.L. Foldy: Phys. Rev. 67, 107–119 (1945)
- [11.11] A. Ishimaru: *Wave Propagation and Scattering in Random Media* (Academic, New York, 1979)
- [11.12] G.C. Gaunaurd, H. Huang: J. Acoust. Soc. Am. 107, 95–102 (2000)
- [11.13] S.W. Yoon, L.A. Crum, A. Prosperetti, and N.Q. Lu: J. Acoust. Soc. Am. 89, 700–706 (1991)
- [11.14] A.B. Wood: *A Textbook of Sound* (Macmillan, New York 1955)
- [11.15] P.M. Morse, K.U. Ingard: *Theoretical Acoustics* (Princeton University Press, Princeton 1968)
- [11.16] A. Prosperetti, N.Q. Lu, and H.S. Kim: J. Acoust. Soc. Am. 92, 2993–2996 (1992)
- [11.17] R.A. Roy, W. Carey, M. Nicholas, J. Schindall, and L.A. Crum: J. Acoust. Soc. Am. 92, 2993–2996 (1992)
- [11.18] P.A. Hwang, R.A. Roy, and L.A. Crum: *Sea Surface Sound '94*, ed. by M.J. Buckingham and J.R. Potter (World Scientific, Singapore 1994) pp. 270–289

Index

- Absorption
 - by air bubbles 253
 - cross section of bubble 255
 - in sea water 10
 - in sediments 28
- Acoustic pressure 36, 47, 61, 80, 101, 129, 167
- Adiabatic approximation 151
 - conditions for validity 157
 - equation 251
- Air bubble under sea surface 24
 - resonant frequency of 24, 252, 254, 261, 263
- Airy function 46, 99, 133, 169
- Ambient noise 30
- Angular distribution of sea wave energy 22, 193
- Anomaly of sound intensity 121, 122
- Antiwaveguide 9, 169
 - symmetric 172, 179
- Approximation
 - adiabatic 151, 157
 - of Kirchhoff (tangent plane) 201
 - of small slope 221
 - of Wentzel-Kramers-Brillouin 79, 137
- Attenuation coefficient
 - by bubbles 257
 - of normal modes 171
 - of quasi-modes 178
 - along ray 216
 - in water 10
- Averaged decay law 113
 - for coherent field 216
- Axial ray 125, 245
- Biological noise 31
- Bragg's law 186, 189
- Brunt-Väisälä frequency 243
- Caustic 46, 86, 97
 - equation of 97
- Characteristic function (rough surface) 204, 206
- Coherence parameter 22
- Coherent reflection coefficient 22, 199, 204
- Collective bubble behavior 262
- Convergence zone 4, 125
- Coriolis parameter 244
- Correlation function
 - for amplitude fluctuation 233
 - for Cartesian (quadratic) components of sound field 247
 - for phase fluctuation 228
 - for refractive index fluctuations 228, 238
 - spatial, for rough surface 187
 - spatial, for scattered field 189
 - temporal, for scattered field 196
- Critical (cutoff) frequency 106, 112
- Cross section
 - for absorption 256
 - for extinction 255
 - for scattering 252, 255
- Currents 12
 - effect on sound propagation 19
- Cutoff (critical) frequency 106, 112
- Damping parameters 255
- Decay law
 - averaged 113
 - for a coherent field 217
- Diffraction rays 171
- Dipole effect 83, 108

- Dispersion 257
 - in bubbly water 258
 - waveguide (geometric) 107
- Dispersion relation
 - for internal waves 244
 - for normal waves 105, 111, 129, 131, 134, 138, 152, 170, 175
 - for surface waves 192
- Displacement
 - of frequency 198, 211
 - of ray at reflection 91, 95
- Distribution
 - of bubble radii 25
 - of sea surface displacement 20, 205
 - of sea surface slopes 20, 207, 213
- Eddies, synoptic 13
- Eikonal 47
 - equation of 47, 228
- Excitation function of modes 108, 129
- Extinction cross section of bubble 255
- Far zone for scattered field 187, 209, 237
- Fine structure of water 17
- Fluctuations
 - of amplitude level 231
 - of arrival angle of ray 231
 - in multipath propagation 247
 - of phase 228, 247
- Focusing factor 45, 96
 - near caustic 46
 - in convergence zone 128
- Fore-reverberation 218
- Fraunhofer zone 82
- Frequency spectrum
 - of rough sea surface 21, 193
 - of scattered sound field 24, 196, 198, 210
- Frontal zone 12
- Garrett-Munk spectrum 244
- Green's formula 202
- Green's function 235
- Group velocity 107, 135
- Half-wave layer 71
- Helmholtz equation 37, 47, 80, 101, 128, 150, 185, 234
- Hydrostatic pressure
 - effect on resonant frequency of air bubble 251, 254
 - effect on sound attenuation 10
 - effect on sound velocity 1
- Images sources 81, 101
 - and normal modes 109
- Impedance
 - input 70
 - of layer 71
 - for solid halfspace 75
- Inertial frequency 244
- Inhomogeneities
 - anisotropic 239
 - effect of transmission 228
 - isotropic 238
- Integral representation of field
 - in layer 103
 - in underwater sound channel 130
- Integral scale of inhomogeneities 230
- Intensity
 - acoustic 43
 - anomaly of 126, 128
 - average, of scattered field 186, 188, 206, 235
 - relation between incident and transmission waves 62
- Interference
 - constructive 141
 - of modes in waveguide 108, 143
 - pattern 81, 143
 - pattern invariant 146
- Internal waves 15
 - effect on sound propagation 242
 - spectrum of 243
- Intrathermocline lenses
 - effect on sound field 33
- Kirchhoff approximation 201
- Kolmogorov-Obukhov law 19, 238
- Lambert's law 29
- Lamé parameters 72
- Layers
 - deep scattering 26
 - half wave 71
 - in microstructure 17
 - for ray tracing 42
 - reflection at 71
- Leakages 8
- Length of ray cycle 108, 114, 120, 124
- Long-range sound propagation 4, 118
- Method
 - of parabolic equation 163
 - ray-mode 142
 - reference waveguide 150
 - small perturbation 184, 234

- small slope 221
- stationary phase 89
- tangent plane 201
- Noise
 - ambient 30
 - biological 31
- Normal modes
 - coupled 159
 - in almost-stratified medium 149
 - in the ocean with perfectly rigid bottom 105
 - transformation of integral representation into 131
 - in two-layered liquid 110
 - in underwater sound channel 128
- Ocean acoustic tomography 52
- Ocean bottom 28
 - scattering at 30, 192
 - two-scale model of 212
- Parabolic equation 164
 - method of 163
- Pattern function 44
- Phase integral 138, 152
- Phase velocity of normal modes 107, 135
- Pierson-Moscovitz spectrum 193
- Pierson-Neumann spectrum 193
- Plane wave 38, 61, 74, 86, 103, 185, 203
- Potential
 - scalar 37, 73
 - vector 73
 - of velocity 37
- Power flux 66, 84
- Power of radiation 84
- Propagation
 - antiwaveguide 9, 169, 172, 179
 - in coastal wedge 154, 161
 - across cyclonic ring 14
 - across Gulf Stream 13
 - long-range 4, 118
 - multipath 4, 120
 - in shallow water 9, 101
 - waveguide 3, 118
- Quadratic (Cartesian) components 15, 247
- Quasi-modes 172, 178
- Radiation power 84
- Ray
 - axial 124, 246
 - curvature 40, 245
 - diagram 3, 4, 5–10, 116, 120, 124, 155, 162, 172, 178, 179
 - distance, travel time 41
 - equation of 41, 48, 120, 140, 142
 - in horizontal plane 161
 - invariant 146, 148
 - for range-dependent ocean 148
 - refraction of 38
- Ray theory 35
 - condition for validity 91
- Rayleigh law 238, 253
- Rayleigh parameter 23, 183, 200, 205, 216
- Rayleigh wave 76
- Reference waveguide method 150
- Reflection coefficient
 - coherent 23, 200, 205
 - at liquid-liquid interface 61
 - at liquid-solid interface 75
 - for multiple layers 71
 - for plane wave 61, 174
 - for rough sea surface, 200, 205
- Refraction
 - of rays 38
 - three-dimensional 47
- Relaxation frequency 9
 - dependence on temperature 9
- Resonant frequency
 - for air bubble 25, 252, 254
 - for swim bladders 27
- Salinity, effect
 - on sound attenuation 10
 - on sound velocity 1
- Scale of inhomogeneities
 - external 19, 238
 - integral 230
 - internal 19, 238
- Scattered field, average 203
- Scattering
 - by bubbles 25
 - combination 197
 - by fish 26
 - by ocean bottom 28
 - pattern for rough surface 217
 - by random inhomogeneities 234
 - with fractal spectrum 239
 - resonance (selective) 189, 237
 - by sea surface 22
 - by surface with two scale of roughness 212
- Scattering coefficient
 - of bubble 25, 256
 - for ocean surface 24, 193, 205, 213

- Scattering coefficient (*cont.*)
 - by random inhomogeneities 237
 - by rough surface 187
- Shadow zone 4, 9, 125
- Small perturbation method 184, 235
- Small-slope approximation 221
- Snell's law 39, 118, 119, 141, 153
 - for range-dependent ocean 50
- Sound field
 - in shadow zone 99, 171
 - in underwater sound channel 129
 - zonal structure 4, 125
- Sound potential 37
- Sound velocity 1
 - in bubbly water 258
 - at channel's axis 3
 - depth dependence of 3, 4, 6–9, 18, 124, 126
 - gradient of 2
 - in sea water 2
 - in sediments 28
- Source
 - image 81, 101
 - impulsive 102
 - point 80
- Spectrum
 - of Cartesian (quadratic) pressure component 15, 247
 - fractal 239
 - frequency, of rough sea surface 22
 - of Garrett-Munk 244
 - of Pierson-Moscovitz 193
 - of Pierson-Neumann 193
 - of random inhomogeneities 237, 239
 - of refractive index fluctuations 244
 - of scattered field 23, 196, 197, 210
 - spatial, of rough surface 187, 197, 213
- Spherical wave 38, 90
 - expansion into plane waves 85
- Stationary phase method 89
- Stonely wave 76
- Structure constant 19, 239
- Structure function 19, 231
- Surface channel
 - with rough boundary 215
 - underwater 6, 158
- Synoptic eddies 13
- Tangent plane method (Kirchhoff approximation) 201
- Temperature
 - effect on absorption 10
 - effect on sound velocity 2
 - fine structure of field of 17
- Time
 - signal spreading 123
 - travel over ray 41, 121, 124
- Transmission coefficient for plane wave 62, 174
 - from water into air and vice versa 65
- Transport equation 47, 232
- Trapping coefficient, for sound channel 118
- Turbulence 18, 238
- Underwater sound channel 2, 118
 - canonical 123
 - hydrostatic 3
 - integral representation of field in 103, 130
 - linear model of 119
 - surface 6, 158
 - thermal 3
 - two-axial 8
- Velocity
 - group, of modes 107, 135
 - particle 35
 - phase, of modes 107, 135
 - volume 38
- Wave
 - equation 35
 - internal 15
 - lateral 91, 179
 - normal (mode) 105, 110, 128, 131, 149
 - plane 38, 61, 74, 86, 103, 185, 203
 - Rayleigh surface 76
 - in solid 72
 - spherical 38, 88, 90
 - Stonely surface 76
- Waveguide
 - linear 119, 132
 - range-dependent 150
 - reference 150
- Weakly divergent bundles of rays 56
- Whispering gallery 121

Active Noise Control Primer, by Scott D. Snyder
The Science and Applications of Acoustics, by Daniel R. Raichel
Random Signals for Engineers Using MATLAB[®] and Mathcad[®],
by Richard C. Jaffe
Fundamentals of Ocean Acoustics, 3rd ed., by L.M. Brekhovskikh and
Yu.P. Lysanov
Cochlear Implants, by Graeme Clark



Fundamentals of Ocean Acoustics Third Edition

L.M. Brekhovskikh • Yu.P. Lysanov

This book provides an up-to-date introduction to the theory of sound propagation in the ocean. The text treats both ray and wave propagation and pays considerable attention to stochastic problems such as the scattering of sound at rough surfaces and random inhomogeneities. An introductory chapter that discusses the basic experimental data complements the following theoretical chapters.

New material has been added throughout for this third edition. New topics covered include

- interthermocline lenses and their effect on sound fields
- weakly divergent bundles of rays
- ocean acoustic tomography
- coupled modes
- sound scattering by anisotropic volume inhomogeneities with fractal spectra
- Voronovich's approach to sound scattering from the rough sea surface.

In addition, the list of references has been brought up to date, and the latest experimental data have been included.



Springer

ISBN 0-387-95467-8
www.springer-ny.com



**AIP
PRESS**